

DE GRUYTER

Shinsaku Fujita

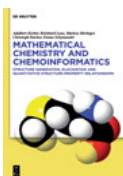
MATHEMATICAL STEREOCHEMISTRY



Fujita

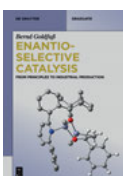
Mathematical Stereochemistry

Also of interest



Mathematical Chemistry and Chemoinformatics: Structure Generation, Elucidation and Quantitative Structure-Property Relationships

Kerber, Laue, Meringer, Rücker, Schymanski, 2013
ISBN 978-3-11-030007-9, e-ISBN 978-3-11-025407-5



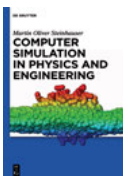
Enantioselective Catalysis: From Principles to Industrial Production
Goldfuß, 2015

ISBN 978-3-11-034040-2, e-ISBN 978-3-11-034041-9



Scientific Computing: For Scientists and Engineers

Heister, Rebholz, 2015
ISBN 978-3-11-035940-4, e-ISBN 978-3-11-035942-8



Computer Simulation in Physics and Engineering

Steinhauser, 2012
ISBN 978-3-11-025590-4, e-ISBN 978-3-11-025606-2



Chemical Sciences: Zeitschrift für Naturforschung B

G. Müller (Managing Editor)
ISSN 0932-0776, e-ISSN 1865-7117

Shinsaku Fujita

Mathematical Stereochemistry

—

DE GRUYTER

Author

Shinsaku Fujita
Shonan Institute of Chemoinformatics and Mathematical Chemistry
Kaneko 479-7
258-0019 Kanagawa-ken
Japan
shinsaku_fujita@nifty.com

ISBN 978-3-11-037197-0
e-ISBN (PDF) 978-3-11-036669-3
e-ISBN (EPUB) 978-3-11-038637-0
Set-ISBN 978-3-11-036670-9

Library of Congress Cataloging-in-Publication Data

A CIP catalog record for this book has been applied for at the Library of Congress.

Bibliographic information published by the Deutsche Nationalbibliothek

The Deutsche Nationalbibliothek lists this publication in the Deutsche Nationalbibliografie; detailed bibliographic data are available on the Internet at <http://dnb.dnb.de>.

© 2015 Walter de Gruyter GmbH, Berlin/Boston
Printing and binding: CPI books GmbH, Leck
♻️ Printed on acid-free paper
Printed in Germany

www.degruyter.com

Preface

Modern stereochemistry is based on an accumulated set of terms which do not always stem from mathematical foundations. The accumulated set of terms has *seemingly* worked well to discuss various aspects of stereochemistry in a qualitative fashion. However, the insufficient mathematical foundations have provided us with serious confusion even in qualitative discussions, whether or not we are aware of such insufficiency. The confusion has its sources in the most fundamental concepts and terminology of modern stereochemistry as follows:

1. **Misleading Dichotomy Between Enantiomers and Diastereomers:** The term ‘diastereomers’ is defined by the well-known (but misleading) dichotomy in modern stereochemistry: “Diastereomers are stereoisomers other than enantiomers.” However, diastereomers are incapable of constructing a definite set of molecular entities. On the other hand, a pair of enantiomers constructs a definite set of molecular entities, which is categorized to be an equivalence class, mathematically speaking. As a result, the expression of the dichotomy consists of such terms as belonging to different categories. Moreover, it does not refer to achiral molecules. Hence, the dichotomy is concluded to be misleading even though it works as a key concept supporting the theoretical foundations of modern stereochemistry. Unfortunately, all of the textbooks on organic chemistry and on stereochemistry adopt the misleading dichotomy so as to reproduce and spread unconscious confusion.
2. **Confusion of Reflections with Permutations:** In modern stereochemistry, there appears frequently such an expression as “The regular tetrahedron of the point group T_d functions as a permutation center or skeleton with four equivalent sites, and models of stereoisomers are generated by permutation of the ligands among these sites.” This expression unconsciously causes the confusion of reflections (contained in the point group T_d) with permutations (of ligands). Strictly speaking, such permutations are controlled by the symmetric group of degree 4 ($S^{[4]}$), which is a kind of permutation group isomorphic to the point group T_d . The regular tetrahedron belongs to the symmetric group $S^{[4]}$ as well as to the point group T_d . Thereby, the two groups $S^{[4]}$ and T_d have been frequently mixed up with each other in modern stereochemistry.
3. **Misleading Concepts of ‘Stereogenic Units’, ‘Chirality Units’, and ‘Pseudoasymmetric Units’:** To specify absolute configurations, the Cahn-Ingold-Prelog (CIP) system of stereochemical notation claims that ‘stereogenic units’ for assigning R/S -stereodescriptors consist of ‘chirality units’ and ‘pseudoasymmetric units’. Thus, R/S -stereodescriptors are assigned both to enantiomers (‘chirality units’ specified by uppercase labels ‘ R ’ and ‘ S ’) and diastereomers (‘pseudoasymmetric units’ specified by lowercase labels ‘ r ’ and ‘ s ’). This means that the assignment of R/S -stereodescriptors does not obey a single criterion so long as we obey the-state-of-the-art terminology of the CIP system. The term ‘stereogenic units’ (= ‘chirality units’ plus ‘pseudoasymmetric units’), which is considered to generate stereoisomerism, has been coined to rationalize as if the assignment of R/S -stereodescriptors would obey a single crite-

tion. Thereby, stereogenicity is misleadingly presumed to connote chirality, whereas stereogenicity and chirality should be independent of each other. As a result, the relationship between stereogenicity and chirality has not been fully demonstrated in modern stereochemistry.

4. **Misleading Presumption of a Single Pair of Chirality/Achirality:** The CIP system for specifying absolute configurations presumes a single pair of chirality/achirality and disregards the presence of pairwise properties of other types. As a result, a pair of *R/S*-stereodescriptors is misleadingly claimed to be assigned to a pair of enantiomers with opposite chirality senses, where ‘pseudoasymmetric units’ are regarded as exceptional cases without considering such pairwise properties of other types. Although ‘pseudoasymmetric units’ as diastereomers (\subset ‘stereogenic units’) are implicitly paired during the naming process of the CIP system, the use of the term ‘reflection-invariant’ for a lowercase label (‘*r*’ or ‘*s*’) forces us to focus our attention on the pairing of enantiomers. Note that diastereomers are not always paired in general.
5. **Misleading Terms of ‘Stereoheterotopic’, ‘Enantiotopic’, and ‘Diastereotopic’:** In order to specify intramolecular environments, *pro-R/pro-S*-descriptors are assigned to ‘enantiotopic’ and ‘diastereotopic’ positions, just as *R/S*-stereodescriptors are assigned to enantiomers (‘chirality units’) and diastereomers (‘pseudoasymmetric units’). Hence, this assignment does not obey a single criterion. To claim that this assignment is seemingly done in a single criterion, the term ‘stereoheterotopic’ has been coined by means of the term ‘enantiotopic’ plus the term ‘diastereotopic’. As a result, prostereoisomerism and prochirality are confused in the assignment of *pro-R/pro-S*-descriptors, just as stereoisomerism (stereogenicity) and chirality are confused in the assignment of *R/S*-stereodescriptors.

These matters should be replaced by a more reasonable set of terms for the purpose of understanding stereochemistry comprehensively, as introduced detailedly in *Chapter 1*. Keep in mind that these matters are concerned with the most fundamental terminology of modern stereochemistry. This fundamental terminology stems from the theoretical foundations of modern stereochemistry, which have long been developed rather qualitatively without mathematical basis since the beginning of stereochemistry by van’t Hoff and Le Bel. As a result, an ad-hoc remedy without mathematical formulations would repeat the history, so as to provide no substantial solutions. Hence, the task of aiming at a true remedy inevitably requires the restructuring of the theoretical foundations, which results in the renewal of the fundamental terminology of modern stereochemistry. In particular, the restructuring should be based on mathematical formulations, not on qualitative substitutions of words, nor on non-mathematical coinage of terms. Such a true remedy is the target of the remaining chapters of this book entitled *Mathematical Stereochemistry*.

Chapters 2 is devoted to the solution of the first matter described above, where the importance of equivalence relationships and equivalence classes is emphasized. In particular, a new flowchart for classifying various kinds of isomers is developed on the basis of equivalence classes, i.e., isomers as an equivalence class under an isomeric relationship,

isoskeletomers as an equivalence class under an isoskeletomeric relationship, stereoisomers as an equivalence class under a stereoisomeric relationship, and (self-)enantiomers as an equivalence class under an enantiomeric relationship.

Chapter 3 aims at the solution of the first and second matters described above, where the point-group theory is adopted as a mathematical device after developing the proligand-promolecule model based on a skeleton. Thereby, we are able to replace the misleading dichotomy (the first matter described above) with a new viewpoint: “The set of stereoisomers consists of definite pairs of (self)-enantiomers, where the relationship between two pairs of (self)-enantiomers is regarded as being diastereomeric.” Note that a pair of self-enantiomers indicates an achiral molecule. Mathematically speaking, each pair of (self)-enantiomers is an equivalence class under the action of the point group of a skeleton. Each set of stereoisomers is an equivalence class of another kind under the action of a stereoisomeric group. The proligand-promolecule model is useful to avoid the confusion of reflections with permutations, which has been pointed out as the second matter described above.

It should be emphasized that even the newly-defined diastereomeric relationship described in the preceding paragraph does not construct equivalence classes. Without defining such a stereoisomeric group, however, it is possible to solve the first and second matters to a great extent by taking account of the point group of the skeleton. In other words, geometric aspects can be discussed by using point groups, apart from stereoisomeric aspects. This course is pursued in *Chapter 4* to *Chapter 8*.

According to the point-group theory and the new viewpoint described in the preceding paragraph, I have developed **the unit-subduced-cycle-index (USCI) approach** for combinatorial enumeration of molecules as 3D structures. I have already published two monographs concerning this topic (S. Fujita, *Symmetry and Combinatorial Enumeration in Chemistry*, Springer-Verlag, Berlin Heidelberg, 1991; and S. Fujita, *Diagrammatical Approach to Molecular Symmetry and Enumeration of Stereoisomers*, Mathematical Chemistry Monographs Series Vol. 4, Univ. Kragujevac, Kragujevac, 2007).

The USCI approach is based on the concepts of sphericities and chirality fittingness (CF), which are assigned to equivalence classes (orbits) governed by coset representations. *Chapter 4* is devoted to an introduction to these concepts and to such related topics as the purely-geometric concept of prochirality.

After foundations of enumeration under point groups are introduced in *Chapter 5*, the USCI approach for symmetry-itemized enumeration under point groups is demonstrated in *Chapter 6*. The USCI approach supports four methods of combinatorial enumeration, which are based on unit subduced cycle indices without or with chirality fittingness (USCIs or USCIs-CFs). The USCIs or USCIs-CFs are calculated algebraically by starting from the subduction of coset representations. The concept of chirality fittingness (CF), which is derived from the concept of sphericities (homospheric, enantiospheric, and hemispheric), controls the modes of accommodating chiral and achiral proligands for producing promolecules. The USCI approach works well in quantitative and qualitative discussions to understand stereochemistry from the new viewpoint combined with point groups.

As a promising method for gross enumeration under point groups, I have developed **the proligand method**, where the concept of sphericities of cycles is devised as a substantial extension of the concept of sphericities of orbits in the USCI approach. I have already published a monograph on the proligand method and related methods developed by myself (S. Fujita, *Combinatorial Enumeration of Graphs, Three-Dimensional Structures, and Chemical Compounds*, Mathematical Chemistry Monographs Series Vol. 15, Univ. Kragujevac, Kragujevac, 2013). This monograph is a successor to Pólya-Read's monograph (G. Pólya and R. C. Read, *Combinatorial Enumeration of Groups, Graphs, and Chemical Compounds*, Springer-Verlag, New York, 1987), where graphs of Pólya-Read's monograph are substantially extended to three-dimensional structures of Fujita's monograph on the basis of the extended concept of sphericities of cycles. *Chapter 7* is devoted to an introduction of the proligand method. The proligand method is capable of recursive calculation, as discussed in *Chapter 8* for enumeration of alkanes as 3D structures.

To avoid the confusion of reflections with permutations (the second matter described above), we should examine permutation groups in comparison with point groups. *Chapter 9* aims at demonstrating how permutation groups have been mixed up with point groups in modern stereochemistry. The concept of *RS*-permutation groups isomorphic to point groups is introduced to settle the misleading situations of modern stereochemistry.

To solve the third matter described above, I have developed **the stereoisogram approach**, where point groups and *RS*-permutation groups are integrated to create *RS*-stereoisomeric groups. Note that usual permutation groups are restricted to *RS*-permutation groups, which are selected to be isomorphic to the corresponding point groups. As shown in *Chapter 10*, I have devised stereoisograms as diagrammatic expressions of such *RS*-stereoisomeric groups. Each stereoisogram consists of a quadruplet of promolecules, which are correlated by three relationships, i.e., enantiomeric (due to point groups), *RS*-diastereomeric (due to *RS*-permutation groups), and holantimeric ones (due to ligand-reflection groups). Thereby, such stereoisograms are categorized into five types (type I–type V), so that quadruplets of types I, III, and V are concluded to replace such conventional terms as 'stereogenic units', 'chirality units', and 'pseudoasymmetric units'. To show the usefulness of the stereoisogram approach, *Chapter 11* deals with stereoisograms for tetrahedral derivatives, while *Chapter 12* deals with stereoisograms for allene derivatives.

The crux of the stereoisogram approach (Chapter 10 to Chapter 12) is the rational introduction of three pairs of attributes, i.e., chirality/achirality, *RS*-stereogenicity/*RS*-astereogenicity, and sclerality/asclerality, which correspond to the three relationships contained in a stereoisogram. These three pairs of attributes are independent of each other, but may coalesce according to respective stereoisograms of five types. This is sharp contrast to the fact that modern stereochemistry presumes a single pair of attributes, i.e., chirality/achirality, and lacks the other pairs of attributes. The limitations of modern stereochemistry are concluded to come from misleading rationalization by means of chirality/achirality as a single pair, as pointed out as the fourth matter describe above.

Chapter 13 deals with stereochemical nomenclature, where the original foundations of the CIP system for assigning *R/S*-stereodescriptors (the third matter described above) are

clarified to be misleading, so that they should be replaced by new foundations originated from the stereoisogram approach. Among the three pairs of attributes established by the stereoisogram approach, a pair of *RS*-stereogenicity/*RS*-astereogenicity is concerned with the foundations of the CIP system. In fact, a pair of chirality/achirality (the fourth matter described above) has nothing to do with the assignability of *R/S*-stereodescriptors in the CIP system. It follows that a pair of *R/S*-stereodescriptors is given to a pair of *RS*-diastereomers (but not to a pair of enantiomers).

The stereoisogram approach is also effective to solve the fifth matter described above. As discussed in *Chapter 14*, the terms *enantiotopic*, *RS*-*diastereotopic*, and *holantitopic* have been coined by the stereoisogram approach, so that the conventional set of terms ‘stereoheterotopic’, ‘enantiotopic’, and ‘diastereotopic’ should be abandoned. This is parallel to the remedy that the present set of terms *RS*-*stereoisomeric*, *enantiomeric*, *RS*-*diastereomeric*, and *holantimeric* should replace the conventional set of terms ‘stereoisomeric’, ‘enantiomeric’, and ‘diastereomeric’. Finally, *Chapter 15* summarizes the perspectives of mathematical stereochemistry, which would be brought about on the basis of the stereoisogram approach.

An additional aim of this book is to give a field test of the X^YM_TE_X system, which has been developed by myself as a software for drawing structural formulas. I have released Version 5.01 of the X^YM_TE_X system in 2013. The X^YM_TE_X system is attached by an online manual of about 800 pages: S. Fujita, X^YM_TE_X: *Reliable Tool for Drawing Chemical Structural Formulas*, which is available from the following Web sites:

<http://xymtex.com/fujitas3/xymtex/xym501/manual/xymtex-manualPS.pdf> and

<http://www.ctan.org/tex-archive/macros/latex/contrib/xymtex/doc/XyMTeX-manual.pdf>

Because all of the structural formulas appearing in this book have been drawn by using the X^YM_TE_X system, the usefulness of the X^YM_TE_X system is clearly demonstrated.

Before closing the preface, it is worthwhile to emphasize the conceptual importance of the stereoisogram approach from a historical point of view.

- Fujita’s stereoisogram approach creates the intermediate concept of *RS*-stereoisomers, which mediates between enantiomers and stereoisomers. Such an intermediate concept brings about a paradigm shift, so that modern stereochemistry has been restructured substantially on the basis of mathematical formulations. This fact is parallel to the historical event that Avogadro’s theory has brought about a paradigm shift in chemistry by creating the intermediate concept of *molecule* (e.g., H₂O), which mediates between atoms (e.g., hydrogen atoms and oxygen atoms) and substances (e.g., water).
- As a result, Fujita’s stereoisogram approach has stopped the long-standing gap between van’t Hoff’s way (emphasizing asymmetry and stereoisomerism) and Le Bel’s way (emphasizing dissymmetry or chirality initiated by Pasteur), which has continuously puzzled organic chemists from the beginning of stereochemistry over 140 years.

About the author:

Shinsaku Fujita was born in Kita-Kyushu City, Japan in 1944. He received his undergraduate training at Kyoto University. After earning a Master's degree in 1968, he started as a research instructor and received a Dr. Eng. degree at Kyoto University under the guidance of Prof. Hitosi Nozaki. In 1972, he joined Ashigara Research Laboratories, Fuji Photo Film Co., Ltd., where he was engaged in the R&D of organic compounds for instant color photography and in the R&D of the organic reaction database until 1997. From 1997 to 2007, he has been Professor of Information Chemistry and Materials Technology at the Kyoto Institute of Technology. In 2007, he has started Shonan Institute of Chemoinformatics and Mathematical Chemistry as a private laboratory. He was awarded the Synthetic Organic Chemistry Award in 1982 and the Society of Computer Chemistry Japan Award in 2002. His research interests have included reactive intermediates (nitrenes), synthetic organic chemistry (cyclophanes, strained heterocycles, and organic compounds for photography), organic photochemistry, organic stereochemistry (theoretical approach), mathematical organic chemistry (combinatorial enumeration), and the organic reaction database (imaginary transition structures). He is the sole author of *Symmetry and Combinatorial Enumeration in Chemistry* (Springer-Verlag, 1991), *X²MT_EX—Typesetting Chemical Structural Formulas* (Addison-Wesley Japan, 1997), *Computer-Oriented Representation of Organic Reactions* (Yoshioka Shoten, 2001), *Organic Chemistry of Photography* (Springer-Verlag, 2004), *Diagrammatical Approach to Molecular Symmetry and Enumeration of Stereoisomers*, Mathematical Chemistry Monographs Series Vol. 4 (Kragujevac, 2007), *Combinatorial Enumeration of Graphs, Three-Dimensional Structures, and Chemical Compounds*, Mathematical Chemistry Monographs Series Vol. 15 (Kragujevac, 2013), and several books on T_EX/L^AT_EX. His homepage on World Wide Web is located at <http://xymtex.com/>.



Contents

1.	Introduction — 1
1.1	Two-Dimensional versus Three-Dimensional Structures — 1
1.1.1	Two-Dimensional Structures in Early History of Organic Chemistry — 1
1.1.2	Three-Dimensional Structures After Beginning of Stereochemistry — 2
1.1.3	Arbitrary Switching Between 2D-Based and 3D-Based Concepts — 2
1.2	Problematic Methodology for Categorizing Isomers and Stereoisomers — 4
1.2.1	Same or Different — 5
1.2.2	Dual Definition of Isomers — 6
1.2.3	Positional Isomers as a Kind of Constitutional Isomers — 9
1.3	Problematic Methodology for Categorizing Enantiomers and Diastereomers — 10
1.3.1	Enantiomers — 10
1.3.2	Diastereomers — 11
1.3.3	Chirality and Stereogenicity — 16
1.4	Total Misleading Features of the Traditional Terminology on Isomers — 16
1.4.1	Total Misleading Flowcharts — 17
1.4.2	Another Flowchart With Partial Solutions — 18
1.4.3	More Promising Way — 20
1.5	Isomer Numbers — 20
1.5.1	Combinatorial Enumeration as 2D Structures — 21
1.5.2	Importance of the Proligand-Promolecule Model — 21
1.5.3	Combinatorial Enumeration as 3D Structures — 22
1.6	Stereoisograms — 23
1.6.1	Stereoisograms as Diagrammatic Expressions of <i>RS</i> -Stereoisomeric Groups — 23
1.6.2	Theoretical Foundations and Group Hierarchy — 23
1.6.3	Avoidance of Misleading Standpoints of <i>R/S</i> -Stereodescriptors — 24
1.6.4	Avoidance of Misleading Standpoints of <i>pro-R/pro-S</i> -Descriptors — 25
1.6.5	Global Symmetries and Local Symmetries — 25
1.6.6	Enumeration under <i>RS</i> -Stereoisomeric Groups — 28
1.7	Aims of Mathematical Stereochemistry — 28
	References — 29

2. Classification of Isomers — 35

- 2.1 Equivalence Relationships of Various Levels of Isomerism — **35**
- 2.1.1 Equivalence Relationships and Equivalence Classes — **35**
- 2.1.2 Enantiomers, Stereoisomers, and Isomers — **36**
- 2.1.3 Inequivalence Relationships — **40**
- 2.1.4 Isoskeletonomers as a Missing Link for Consistent Terminology — **42**
- 2.1.5 Constitutionally-Anisomeric Relationships vs. Constitutionally-Isomeric Relationships — **45**
- 2.2 Revised Flowchart for Categorizing Isomers — **46**
- 2.2.1 Design of a Revised Flowchart for Categorizing Isomers — **46**
- 2.2.2 Illustrative Examples — **48**
- 2.2.3 Restriction of the Domain of Isomerism — **49**
- 2.2.4 Harmonization of 3D-Based Concepts with 2D-Based Concepts — **50**
- References — **52**

3. Point-Group Symmetry — 53

- 3.1 Stereoskeletons and the Proligand-Promolecule Model — **53**
- 3.1.1 Configuration and Conformation — **53**
- 3.1.2 The Proligand-Promolecule Model — **53**
- 3.2 Point Groups — **56**
- 3.2.1 Symmetry Axes and Symmetry Operations — **56**
- 3.2.2 Construction of Point Groups — **59**
- 3.2.3 Subgroups of a Point Group — **60**
- 3.2.4 Maximum Chiral Subgroup of a Point Group — **62**
- 3.2.5 Global and Local Point-Group Symmetries — **63**
- 3.3 Point-Group Symmetries of Stereoskeletons — **67**
- 3.3.1 Stereoskeletons of Ligancy 4 — **67**
- 3.3.2 Stereoskeletons of Ligancy 6 — **72**
- 3.3.3 Stereoskeletons of Ligancy 8 — **73**
- 3.3.4 Stereoskeletons Having Two or More Orbits — **74**
- 3.4 Point-Group Symmetries of (Pro)molecules — **77**
- 3.4.1 Derivation of Molecules from a Stereoskeleton via Promolecules — **77**
- 3.4.2 Orbits in Molecules and Promolecules Derived from Stereoskeletons — **78**
- 3.4.3 The SCR Notation — **82**
- 3.4.4 Site Symmetries vs. Coset Representations for Symmetry Notations — **83**
- References — **85**

4.	Sphericities of Orbits and Prochirality — 87
4.1	Sphericities of Orbits — 87
4.1.1	Orbits of Equivalent Proligands — 87
4.1.2	Three Kinds of Sphericities — 88
4.1.3	Chirality Fittingness for Three Modes of Accommodation — 89
4.2	Prochirality — 92
4.2.1	Confusion on the Term ‘Prochirality’ — 92
4.2.2	Prochirality as a Geometric Concept — 95
4.2.3	Enantiospheric Orbits vs. Enantiotopic Relationships — 98
4.2.4	Chirogenic Sites in an Enantiospheric Orbit — 100
4.2.5	Prochirality Concerning Chiral Proligands in Isolation — 107
4.2.6	Global Prochirality and Local Prochirality — 109
	References — 113
5.	Foundations of Enumeration Under Point Groups — 115
5.1	Orbits Governed by Coset Representations — 115
5.1.1	Coset Representations — 115
5.1.2	Mark Tables — 118
5.1.3	Multiplicities of Orbits — 120
5.2	Subduction of Coset Representations — 122
5.2.1	Subduced Representations — 123
5.2.2	Unit Subduced Cycle Indices (USCIs) — 127
	References — 130
6.	Symmetry-Itemized Enumeration Under Point Groups — 131
6.1	Fujita’s USCI Approach — 131
6.1.1	Historical Comments — 131
6.1.2	USCI-CFs for Itemized Enumeration — 131
6.1.3	Subduced Cycle Indices for Itemized Enumeration — 138
6.2	The FPM Method of Fujita’s USCI Approach — 140
6.2.1	Fixed-Point Vectors (FPVs) and Multiplicity Vectors (MVs) — 140
6.2.2	Fixed-Point Matrices (FPMs) and Isomer-Counting Matrices (ICMs) — 141
6.2.3	Practices of the FPM Method — 143
6.3	The PCI Method of Fujita’s USCI Approach — 149
6.3.1	Partial Cycle Indices With Chirality Fittingness (PCI-CFs) — 149
6.3.2	Partial Cycle Indices Without Chirality Fittingness (PCIs) — 151
6.3.3	Practices of the PCI Method — 151
6.4	Other Methods of Fujita’s USCI Approach — 164
6.4.1	The Elementary-Superposition Method — 164
6.4.2	The Partial-Superposition Method — 165
6.5	Applications of Fujita’s USCI Approach — 165

6.5.1	Enumeration of Flexible Molecules —	165
6.5.2	Enumeration of Molecules Interesting Stereochemically —	166
6.5.3	Enumeration of Inorganic Complexes —	168
6.5.4	Enumeration of Organic Reactions —	169
	References —	170
7.	Gross Enumeration Under Point Groups —	173
7.1	Counting Orbits —	173
7.2	Pólya's Theorem of Counting —	174
7.3	Fujita's Proligand Method of Counting —	177
7.3.1	Historical Comments —	177
7.3.2	Sphericities of Cycles —	178
7.3.3	Products of Sphericity Indices —	180
7.3.4	Practices of Fujita's Proligand Method —	183
7.3.5	Enumeration of Achiral and Chiral Promolecules —	187
	References —	191
8.	Enumeration of Alkanes as 3D Structures —	193
8.1	Surveys With Historical Comments —	193
8.2	Enumeration of Alkyl Ligands as 3D Planted Trees —	195
8.2.1	Enumeration of Methyl Proligands as Planted Promolecules —	195
8.2.2	Recursive Enumeration of Alkyl ligands as Planted Promolecules —	200
8.2.3	Functional Equations for Recursive Enumeration of Alkyl ligands —	202
8.2.4	Achiral Alkyl Ligands and Pairs of Enantiomeric Alkyl Ligands —	207
8.3	Enumeration of Alkyl Ligands as Planted Trees —	208
8.3.1	Alkyl Ligands or Monosubstituted Alkanes as Graphs —	208
8.3.2	3D Structures vs. Graphs for Characterizing Alkyl Ligands or Monosubstituted Alkanes —	210
8.4	Enumeration of Alkanes (3D-Trees) as 3D-Structural Isomers —	212
8.4.1	Alkanes as Centroidal and Bicentroidal 3D-Trees —	212
8.4.2	Enumeration of Centroidal Alkanes (3D-Trees) as 3D-Structural Isomers —	214
8.4.3	Enumeration of Bicentroidal Alkanes (3D-Trees) as 3D-Structural Isomers —	217
8.4.4	Total Enumeration of Alkanes as 3D-Trees —	222
8.5	Enumeration of Alkanes (3D-Trees) as Steric Isomers —	224
8.5.1	Centroidal Alkanes (3D-Trees) as Steric Isomers —	224
8.5.2	Bicentroidal Alkanes (3D-Trees) as Steric Isomers —	224
8.5.3	Total Enumeration of Alkanes (3D-Trees) as Steric Isomers —	226

- 8.6 Enumeration of Alkanes (Trees) as Graphs or Constitutional Isomers — 226
- 8.6.1 Alkanes as Centroidal and Bicentroidal Trees — 226
- 8.6.2 Enumeration of Centroidal Alkanes (Trees) as Constitutional Isomers — 227
- 8.6.3 Enumeration of Bicentroidal Alkanes (Trees) as Constitutional Isomers — 228
- 8.6.4 Total Enumeration of Alkanes (Trees) as Graphs or Constitutional Isomers — 231
- References — 231

9. Permutation-Group Symmetry — 233

- 9.1 Historical Comments — 233
- 9.2 Permutation Groups — 235
- 9.2.1 Permutation Groups as Subgroups of Symmetric Groups — 235
- 9.2.2 Permutations vs. Reflections — 236
- 9.3 *RS*-Permutation Groups — 238
- 9.3.1 *RS*-Permutations and *RS*-Diastereomeric Relationships — 238
- 9.3.2 *RS*-Permutation Groups vs. Point Groups — 239
- 9.3.3 Formulation of *RS*-Permutation Groups — 244
- 9.3.4 Action of *RS*-Permutation Groups — 245
- 9.3.5 Misleading Features of the Conventional Terminology — 248
- 9.4 *RS*-Permutation Groups for Skeletons of Ligancy 4 — 252
- 9.4.1 *RS*-Permutation Group for a Tetrahedral Skeleton — 252
- 9.4.2 *RS*-Permutation Group for an Allene Skeleton — 261
- 9.4.3 *RS*-Permutation Group for an Ethylene Skeleton — 265
- References — 271

10. Stereoisograms and *RS*-Stereoisomers — 273

- 10.1 Stereoisograms as Integrated Diagrammatic Expressions — 273
- 10.1.1 Elementary Stereoisograms of Skeletons with Position Numbering — 273
- 10.1.2 Stereoisograms Based on Elementary Stereoisograms — 280
- 10.2 Enumeration Under *RS*-Stereoisomeric Groups — 287
- 10.2.1 Subgroups of the *RS*-Stereoisomeric Group $C_{3v\hat{\sigma}i}$ — 287
- 10.2.2 Coset Representations — 290
- 10.2.3 Mark Table and its Inverse — 291
- 10.2.4 Subduction for *RS*-Stereoisomeric Groups — 292
- 10.2.5 USCI-CFs for *RS*-Stereoisomeric Groups — 294
- 10.2.6 SCI-CFs for *RS*-Stereoisomeric Groups — 297
- 10.2.7 The PCI Method for *RS*-Stereoisomeric Groups — 297
- 10.2.8 Type-Itemized Enumeration by the PCI Method — 301

10.2.9	Gross Enumeration Under <i>RS</i> -Stereoisomeric Groups —	303
10.3	Comparison with Enumeration Under Subgroups —	305
10.3.1	Comparison with Enumeration Under Point Groups —	305
10.3.2	Comparison with Enumeration Under <i>RS</i> -Permutation Groups —	307
10.3.3	Comparison with Enumeration Under Maximum-Chiral Point Subgroups —	309
10.4	<i>RS</i> -Stereoisomers as Intermediate Concepts —	311
	References —	312

11. Stereoisograms for Tetrahedral Derivatives — 313

11.1	<i>RS</i> -Stereoisomeric Group $T_{d\hat{\sigma}i}$ and Elementary Stereoisogram —	313
11.2	Stereoisograms of Five Types for Tetrahedral Derivatives —	315
11.2.1	Type-I Stereoisograms of Tetrahedral Derivatives —	315
11.2.2	Type-II Stereoisograms of Tetrahedral Derivatives —	317
11.2.3	Type-III Stereoisograms of Tetrahedral Derivatives —	318
11.2.4	Type-IV Stereoisograms of Tetrahedral Derivatives —	319
11.2.5	Type-V Stereoisograms of Tetrahedral Derivatives —	320
11.3	Enumeration Under the <i>RS</i> -Stereoisomeric Group $T_{d\hat{\sigma}i}$ —	322
11.3.1	Non-Redundant Set of Subgroups and Five Types of Subgroups —	322
11.3.2	Subduction of Coset Representations —	325
11.3.3	The PCI Method for the <i>RS</i> -Stereoisomeric Group $T_{d\hat{\sigma}i}$ —	327
11.3.4	Type-Itemized Enumeration by the PCI Method —	332
11.4	Comparison with Enumeration Under Subsymmetries —	334
11.4.1	Enumeration of Tetrahedral Promolecules Under the Point-Group Symmetry —	334
11.4.2	Enumeration of Tetrahedral Promolecules Under the <i>RS</i> -Permutation-Group Symmetry —	336
11.4.3	Comparison with Enumeration Under Maximum-Chiral Point Subgroups —	338
11.4.4	Confusion Between the Point-Group Symmetry and the <i>RS</i> -Permutation-Group Symmetry —	339
	References —	340

12. Stereoisograms for Allene Derivatives — 341

12.1	<i>RS</i> -Stereoisomeric Group $D_{2d\hat{\sigma}i}$ and Elementary Stereoisogram —	341
12.2	Stereoisograms of Five Types for Allene Derivatives —	343
12.2.1	Type-I Stereoisograms of Allene Derivatives —	343
12.2.2	Type-II Stereoisograms of Allene Derivatives —	345
12.2.3	Type-III Stereoisograms of Allene Derivatives —	347

12.2.4	Type-IV Stereoisograms of Allene Derivatives —	349
12.2.5	Type-V Stereoisograms of Allene Derivatives —	350
12.3	Enumeration Under the <i>RS</i> -Stereoisomeric Group $D_{2d\bar{\sigma}i}$ —	352
12.3.1	Non-Redundant Set of Subgroups and Five Types of Subgroups —	352
12.3.2	Subduction of Coset Representations —	355
12.3.3	The PCI Method for the <i>RS</i> -Stereoisomeric Group $D_{2d\bar{\sigma}i}$ —	355
12.3.4	Type-Itemized Enumeration by the PCI Method —	360
12.4	Comparison with Enumeration Under Subsymmetries —	362
12.4.1	Enumeration of Allene Promolecules Under the Point-Group Symmetry —	362
12.4.2	Enumeration of Allene Promolecules Under the <i>RS</i> -Permutation-Group Symmetry —	363
References —		364

13. Stereochemical Nomenclature — 365

13.1	Absolute Configuration —	365
13.1.1	Single Pair of Attributes ‘Chirality/Achirality’ in Modern Stereochemistry —	365
13.1.2	Three Pairs of Attributes in Fujita’s Stereoisogram Approach —	366
13.1.3	Three Aspects of Absolute Configuration —	367
13.2	Quadruplets of <i>RS</i> -Stereoisomers as Equivalence Classes —	368
13.2.1	Three Types of Pairwise Relationships in a Quadruplet of <i>RS</i> -Stereoisomers —	368
13.2.2	Formulation of Stereoisograms as Quadruplets of <i>RS</i> -Stereoisomers —	370
13.3	Inner Structures of Promolecules —	370
13.3.1	Inner Structures of <i>RS</i> -Stereogenic Promolecules —	371
13.3.2	Inner Structures of <i>RS</i> -Astereogenic Promolecules —	374
13.4	Assignment of Stereochemical Nomenclature —	376
13.4.1	Single Criterion for Giving <i>RS</i> -Stereodescriptors —	377
13.4.2	<i>RS</i> -Diastereomers: the CIP Priority System —	378
13.4.3	<i>R/S</i> -Stereodescriptors and Stereoisograms —	380
13.4.4	Chirality Faithfulness —	382
13.4.5	Stereochemical Notations for Other Skeletons —	384
References —		385

14. Pro-*RS*-Stereogenicity Based on Orbits — 387

14.1	Prochirality vs. Pro- <i>RS</i> -Stereogenicity —	387
14.1.1	Prochirality as a Geometric Concept —	387
14.1.2	Pro- <i>RS</i> -Stereogenicity as a Stereoisomeric Concept —	388

14.1.3	Prochirality and Pro- <i>RS</i> -Stereogenicity for Tetrahedral Derivatives —	388
14.2	Orbits under <i>RS</i> -Permutation Groups —	388
14.2.1	<i>RS</i> -Tropicity —	388
14.2.2	Pro- <i>RS</i> -Stereogenicity as a Stereoisomeric Concept —	390
14.3	<i>pro-R/pro-S</i> -Descriptors —	392
14.3.1	<i>RS</i> -Diastereotopic Relationships —	392
14.3.2	Single Criterion for Giving <i>pro-R/pro-S</i> -descriptors —	393
14.3.3	Probe Stereoisograms for Assigning <i>pro-R/pro-S</i> -Descriptors —	394
14.3.4	Misleading Interpretation of 'Prochirality' in Modern Stereochemistry —	396
14.4	Pro- <i>RS</i> -Stereogenicity Distinct From Prochirality —	398
14.4.1	Simultaneity of Prochirality and Pro- <i>RS</i> -Stereogenicity in a Type-IV Promolecule —	398
14.4.2	Coincidence of Prochirality and Pro- <i>RS</i> -stereogenicity —	400
14.4.3	Prochiral (but Already <i>RS</i> -Stereogenic) Promolecules —	402
14.5	Pro- <i>RS</i> -Stereogenicity for <i>pro-R/pro-S</i> -Descriptors —	403
	References —	404
15.	Perspectives —	405
15.1	Enumeration of Highly Symmetric Molecules —	405
15.2	Interaction of Orbits of Different Kinds —	405
15.3	Correlation Diagrams of Stereoisograms —	406
15.4	Group Hierarchy —	407
15.5	Non-Rigid Molecules and Conformations —	409
15.6	Interdisciplinary Nature of Mathematical Stereochemistry —	409
15.6.1	Mathematical and Stereochemical Barriers In Practical Levels —	410
15.6.2	Mathematical and Stereochemical Barriers In Conceptual Levels —	411
15.7	Reorganizing the Theoretical Foundations of Stereochemistry and Stereoisomerism —	411
	References —	412
	Index —	415

1 Introduction

1.1 Two-Dimensional versus Three-Dimensional Structures

1.1.1 Two-Dimensional Structures in Early History of Organic Chemistry

Organic-structural theory has been established by Kekulé [1] and Couper [2] in 1858, soon after Frankland [3] proposed the concept of valency in 1852. The development of the organic-structural theory has been reinforced by structural formulas named *graphic notation*, which has been proposed by Crum Brown [4,5] in 1864/1865. The invaluable potentialities of structural formulas have been early pointed out by Frankland in his textbook published in 1870 [6, Chapter III]: “Graphic Notation.—This mode of notation, although far too cumbrous for general use, is invaluable for clearly showing the arrangement of the individual atoms of a chemical compound. . . . It is also of especial value in rendering strikingly evident the causes of isomerism in organic bodies.”

In fact, Kekulé’s discussions on the number of isomeric dibromobenzenes [7] can be expressed by the structural formulas shown in Fig. 1.1, where each benzene ring is presumed to have delocalized double bonds so as to give a regular hexagonal skeleton. These three isomers are now designated as *ortho* (**1-1**), *meta* (**1-2**), and *para* (**1-3**), respectively. For the historical details, see Ihde’s book [8, Chapter 12].

Such structural formulas are two-dimensional (2D) or graphic expressions of molecular entities, which actually have three-dimensional (3D) structures. In spite of this limitation, 2D-structural formulas enable us to communicate essential properties of the molecules effectively, e.g., atom compositions and their connectivities. As a result, they are widely used nowadays as a versatile device for investigation and communication in organic chemistry.

The term *graph* has been imported into mathematics by Sylvester [9], so that graph theory has started as a field of mathematics, as summarized in a book [10, Chapter 4].

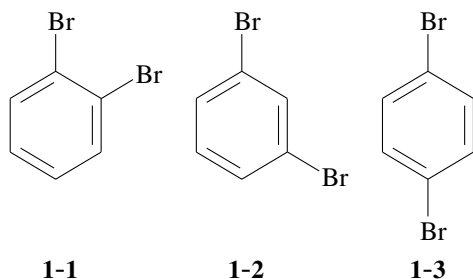


Fig. 1.1. Isomeric dibromobenzenes

1.1.2 Three-Dimensional Structures After Beginning of Stereochemistry

Stereochemistry has been founded by van't Hoff [11–13] and Le Bel [14,15] in the 1870s, where their standpoints were different, as pointed out by several reviews [16–18].

The standpoint of van't Hoff [11–13] stems from the concept of *asymmetric carbons*, which are regarded as conditions for exhibiting optical activity and for generating at most 2^n isomers (n : the number of asymmetric carbons) [11,13]. For example, an asymmetric carbon (*) with achiral ligands A, B, X, and Y is detected by means of a 2D-structural formula (1-5), which is then extended into 3D-structural formulas (1-4 and 1-6), as shown in Fig. 1.2. Strictly speaking, this process does not require reflection operations, so that a pair of enantiomers (mirror-image entities) are considered to be generated by a stereoisomerization process (e.g., an inversion or a pseudorotation). A reflection is subsidiarily used to judge whether or not the 3D-structural formulas (1-4 and 1-6) are mirror images of each other.

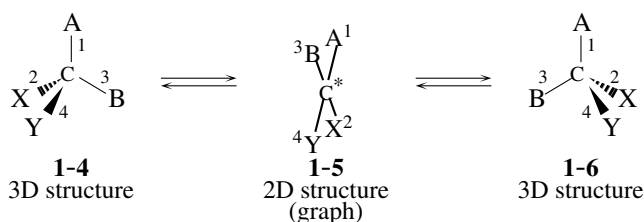


Fig. 1.2. Asymmetric carbon (*) of a 2D structure and the resulting 3D structures.

On the other hand, the standpoint of Le Bel [14,15] emphasizes spacial symmetries succeeding to Pasteur's concept of *dissymmetry* [19] (i.e., *chirality* due to Kelvin [20]). A molecular entity (1-4 or 1-6) as a 3D structure is treated as it is, where such a 2D structure as 1-5 is not always required. Thus the chirality of a molecular entity as a 3D structure is judged by a reflection operation, which is applied to examine whether or not the mirror image of 1-4 is superposable to 1-6.

The history of stereochemistry indicates that the concept of *asymmetric carbons* due to van't Hoff has overwhelmed the concept of *dissymmetry* due to Le Bel's theory. It follows that the process shown in Fig. 1.2 is erroneously regarded as equivalent to a reflection operation. This fact is frequently overlooked in modern stereochemistry, so that van't Hoff's theory and Le Bel's theory are now believed to be integrated into a unified theory. However, the unification is so seeming as to cause serious confusion in modern stereochemistry.

1.1.3 Arbitrary Switching Between 2D-Based and 3D-Based Concepts

Organic chemistry has adopted both 2D structures (graphs) and 3D structures, where these are linked mainly by applying van't Hoff's theory. This is a result of the history of organic

chemistry developed from 2D structures to 3D structures, although actual organic compounds are now decided to have 3D structures. Thus, most textbooks on organic chemistry first describe organic compounds as 2D structures and later introduce stereochemical aspects of 3D structures on the basis of van't Hoff's theory. It follows that concepts based on 2D structures (2D-based concepts) and concepts based on 3D structures (3D-based concepts) are mixed in the terminology of organic chemistry. They are switched in a rather arbitrary fashion to meet molecular entities to be considered, although the molecular entities have 3D structures in the real world.

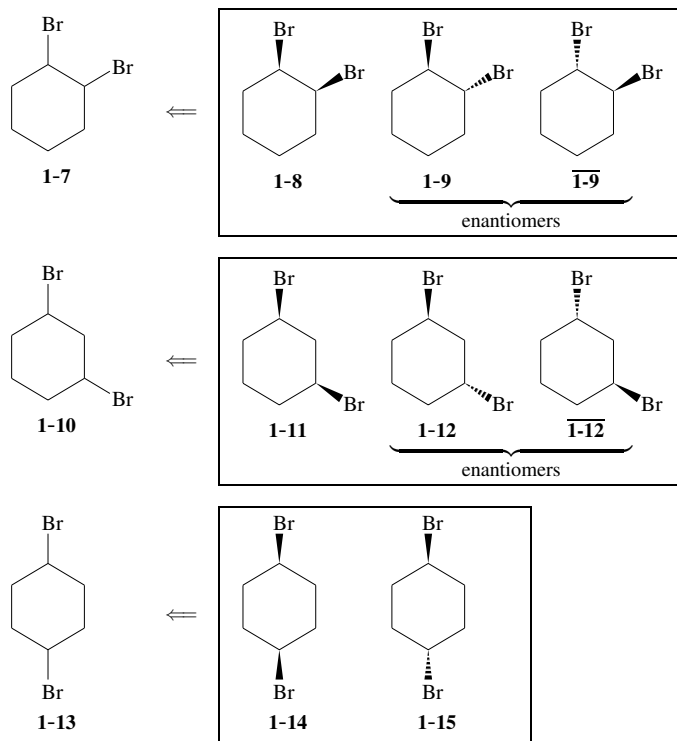


Fig. 1.3. Isomeric dibromocyclohexanes.

For example, dibromobenzenes shown in Fig. 1.1 can be discussed with the scope of 2D structures. The three dibromobenzenes (**1-1**, **1-2**, and **1-3**) are frequently referred to as 'positional isomers', which are based on 2D structures (graphs). Note that 'positional isomers' are concerned with different constitutions (due to 2D structures), because they are regarded as one of 'constitutional isomers'.

If exhaustive hydrogenation of a benzene ring is conducted (even if hypothetical), the resulting dibromocyclohexanes may be discussed in terms of 'positional isomers' as 2D structures (**1-7**, **1-10**, and **1-13**), as shown in Fig. 1.3. However, the dibromocyclohexanes

themselves are 3D-structural molecular entities (**1-8**, **1-9**, and $\overline{\mathbf{1-9}}$; **1-11**, **1-12**, and $\overline{\mathbf{1-12}}$; as well as **1-14** and **1-15**),¹ not 2D-structural ones (**1-7**, **1-10**, and **1-13**). The definition of the term ‘positional isomers’ as based on 2D structures cannot be directly applied to the 3D dibromocyclohexanes. The application of the term ‘positional isomers’ requires the conversion of the 3D structures into 2D structures. Thus, the set of 3D structures as stereoisomers (**1-8**, **1-9**, and $\overline{\mathbf{1-9}}$) is converted into the 2D structure **1-7**; the set of 3D structures as stereoisomers (**1-11**, **1-12**, and $\overline{\mathbf{1-12}}$) is converted into the 2D structure **1-10**; and the set of 3D structures as stereoisomers (**1-14** and **1-15**) is converted into the 2D structure **1-13**, respectively. When we say, for example, that **1-8** and **1-11** are positional isomers, we implicitly refer to the corresponding 2D structures **1-7** and **1-10** after conversion. These implicit conversions are conducted by means of the intuition or experience of organic chemists.

On the other hand, the examination of the 3D structures as they are is necessary to discuss stereoisomeric relationships between them. Thus, the 3D structure **1-8** is compared with a set of **1-9** and $\overline{\mathbf{1-9}}$, so that the former is determined to be a *cis*-isomer and the latter set is determined to be *trans*-isomers. This comparison is considered to be based on a *cis/trans*-isomerization (an epimerization) of **1-8** into **1-9** (or $\overline{\mathbf{1-9}}$).

Further, the 3D structure **1-8** is determined to be achiral, while the set of **1-9** and $\overline{\mathbf{1-9}}$ is determined to be a pair of enantiomers. These determinations require reflection operations.

The mixed situations of 2D- and 3D-based concepts may be overcome by the intuition or experience of organic chemists within the scope of modern stereochemistry. However, this approach has proved to have limitations, because it has been so qualitative and descriptive as to provide unconscious confusion, as summarized in reviews [21–23]. Even now, the standard theory of organic chemistry is influenced by the mixed situations of 2D- and 3D-based concepts, as discussed in the next section. It follows that such intuition or experience of organic chemists should be replaced by a more systematic procedure stemming from rational theoretical basis.

1.2 Problematic Methodology for Categorizing Isomers and Stereoisomers²

The arbitrary switching between 2D structures and 3D structures in organic chemistry provides the terminology of isomerism and stereoisomerism with unconscious confusion.

¹ In this discussion, a cyclohexane ring is tentatively drawn as a planar hexagonal diagram. Although this type of diagram is permitted in accord with stereochemical conventions, conformational changes of a cyclohexane ring should be considered in more detailed discussions. Thus, two chair-form conformers should be considered as extreme cases, which are interconverted through boat-form conformers. This book adopts the proligand-promolecule model based on a rigid skeleton. It follows that the effects of conformational changes are not treated in this book, so as to be open to further publications.

² This section is based on S. Fujita, “Misleading Classification of Isomers and Stereoisomers in Organic Chemistry”, *Bull. Chem. Soc. Jpn.*, **87**, 1367–1378 (2014).

1.2.1 Same or Different

There are many terms having the prefix *iso-* (Greek: *isos* equal) in scientific fields, especially in chemistry [8,24]. We are able to obtain a brief list if we glance over an appropriate dictionary, e.g., isomerism, isomorphism, isotope, isotactic, isotherm, and isotropic, along with such derivative terms as isopentyl, isobutyl, and stereoisomerism.

These terms have a common feature that each term denotes a set of objects having the *same* property in common but *different* in another property. Note that either the same property or the different property is sometimes omitted if it is obvious from the context. For example, the term *isomeric* (*iso-*, Greek: *isos* equal; *-mer*, Greek: *méros* part) coined by Berzelius in 1830 [25] means the relationship between two objects (molecules or related entities) which have the same molecular formula but different chemical or physical properties (or different three-dimensional (3D) structural formulas, structural-chemically speaking, cf. Def. 2.6 on page 39).

After the development of stereochemistry, we use a derivative term *stereoisomeric* (*stereo-*, Greek *stereós* solid, hard) to mean the relationship between two objects (molecules or related entities) which have the same constitution but different 3D-structural formulas (cf. Def. 2.5 on page 38). To hold the terminology to be consistent, the term ‘constitutionally isomeric’ was coined to denote the relationship between two objects which have the same molecular formula but different constitutions (represented by graphs or 2D-structural formulas, cf. Def. 2.4 on page 38).

As a result, the isomeric relationship turns out to be composed of the stereoisomeric relationship (a 3D-based concept) and the constitutionally-isomeric relationship (a 2D-based concept), as shown in Fig. 1.4(a). Obviously, the 2D-based concept and the 3D-based concept are misleadingly placed on the same level of Fig. 1.4(a).

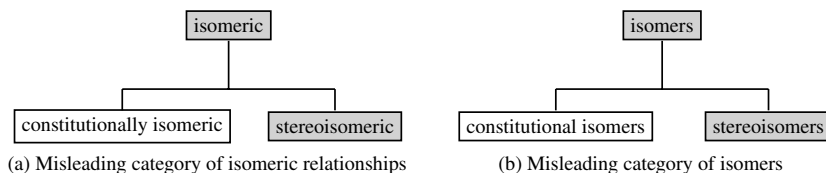


Fig. 1.4. Misleading category of isomeric relationships and the related category of isomers. A gray box represents an equivalence relationship or an equivalence class, which has been overlooked in modern stereochemistry.

The misleading category of isomeric relationships (Fig. 1.4(a)) is frequently applied to give the related category of isomers shown in Fig. 1.4(b), which is also misleading. The misleading features of Fig. 1.4(b) can be also demonstrated by comparing constitutional isomers as a 2D-based concept with stereoisomers as a 3D-based concept.

1.2.2 Dual Definition of Isomers

To demonstrate the misleading features of the scheme Fig. 1.4, we should examine the state-of-the-art definitions of terms on isomerism, which are summarized in Table 1.1 [26]. According to IUPAC Recommendations 1996 [27], the term *isomers* is defined as follows:

C-Definition I1 “molecular entities (or chemical species, or other equivalent expressions) which have the same molecular formula but differ in constitutional formulas or stereochemical formulas”,

where the term *constitution* is defined as “the description of the identity and connectivity (and corresponding bond multiplicities) of the atoms in a molecular entity (omitting any distinction arising from their arrangement)” and the term *stereochemical formula* is defined as “a three-dimensional (3D) view of a molecule either as such or in a projection”. On the other hand, *stereoisomers* are defined as

C-Definition S1 “isomers that possess identical constitution, but which differ in the arrangement of their atoms in space”.

Then, isomers are subdivided into stereoisomers and constitutional isomers [28], where *constitutional isomers* are defined as

C-Definition C1 “isomers which differ in constitution”.

Note that the expression ‘C-Definition’ means a conventional definition. The conventional definitions described above are summarized in Table 1.1.³

Table 1.1. Criteria for Conventional Classification of Isomers [26]

	classification	same	different	set of entities
C-Def. I1	isomer	molecular formula	2D- or 3D-structural formula	2D or 3D structures
C-Def. C1	constitutional isomer	molecular formula	2D-structural formula (constitution, graph)	2D structures (graphs)
C-Def. S1	stereoisomer	2D-structural formula (constitution, graph)	3D-structural formula	3D structures

As found in Table 1.1, the conventional definition of *isomers* (C-Def. I1) is dual with respect to criteria for difference as well as with respect to sets of entities. Hence, C-Def. I1 is concluded to be ambiguous, because the difference in constitutional formulas (2D-structural formulas) does not mean the same effects as the difference in stereochemical formulas (3D-structural formulas).

To show the duality of C-Def. I1 more clearly, let us examine isomeric butanols shown in Fig. 1.5. If C-Def. I1 is based on the difference in constitutional formulas (2D-structural

³ Table 1 of [26] is cited after slight modification.

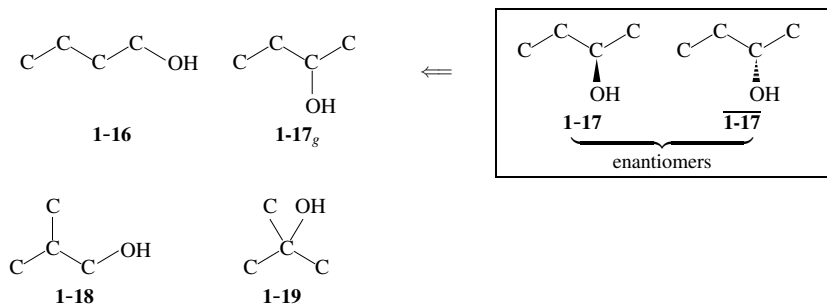


Fig. 1.5. Isomeric butanols with C₄H₁₀O, where hydrogens on carbons are omitted.

formulas), the following set of 2D structures is regarded as a set of isomers:

$$\left(\mathbf{1-16} \quad \mathbf{1-17}_g \quad \mathbf{1-18} \quad \mathbf{1-19} \right), \quad (1.1)$$

where **1-16**, **1-17_g**, **1-18**, and **1-19** are regarded as 2D structures (graphs).⁴ On the other hand, if C-Def. II is based on the difference in stereochemical formulas (3D-structural formulas), the following set of 3D structures is regarded as a set of isomers:

$$\left(\mathbf{1-16} \quad \mathbf{1-17} \quad \overline{\mathbf{1-17}} \quad \mathbf{1-18} \quad \mathbf{1-19} \right), \quad (1.2)$$

where **1-16**, **1-17**, $\overline{\mathbf{1-17}}$, **1-18**, and **1-19** are regarded as 3D structures.⁵ Because the set of isomers represented by Eq. 1.1 is different from the set of isomers represented by Eq. 1.2, the conventional definition of isomers (C-Def. II) is concluded to exhibit dual-purpose supporting both Eq. 1.1 and Eq. 1.2.

In fact, the dual definition of isomers (C-Def. II) aims at justifying both C-Def. C1 and C-Def. S1. The first meaning of C-Def. II, which results in Eq. 1.1, aims at justifying the definition of constitutional isomers (C-Def. C1). Thus, the set represented by Eq. 1.1 is a set of constitutional isomers in terms of C-Def. C1, so that the application of C-Def. C1 (constitutional isomers) provides the same set as generated by the first meaning of C-Def. II (isomers). Note that the set of constitutional isomers (Eq. 1.1) has nothing to do with stereoisomers (C-Def. S1).

On the other hand, the second meaning of C-Def. II, which results in Eq. 1.2, aims at justifying C-Def. S1. By the application of C-Def. S1 to the set represented by Eq. 1.2, the butanols **1-17** and $\overline{\mathbf{1-17}}$ are recognized to be stereoisomers with the same constitution:

$$\langle \mathbf{1-17} \quad \overline{\mathbf{1-17}} \rangle, \quad (1.3)$$

⁴ Strictly speaking, the subscript *g* should be added so as to express **1-16_g**, **1-18_g**, and **1-19_g** in a similar way to **1-17_g**. However, the subscript *g* is omitted for the sake of simplicity.

⁵ Strictly speaking, the structural formulas of **1-16**, **1-18**, and **1-19** should be drawn by adding bold wedges and hashed wedges to specify their 3D structures. Because of achirality, however, these butanols in Fig. 1.5 are drawn without such stereochemical conventions for the sake of simplicity.

where the pair of angle brackets contains stereoisomers detected. The set of stereoisomers represented by Eq. 1.3 is linked with the graph **1-17_g** contained in Eq. 1.1.

As found in the discussions in the preceding paragraphs, the set of constitutional isomers (Eq. 1.1) due to C-Def. C1 is concerned with 2D structures (graphs), while the set of stereoisomers (Eq. 1.3) selected from Eq. 1.2 by means of C-Def. S1 is concerned with 3D structures. They are distinct concepts, where the linkage between ‘isomers’ and ‘constitutional isomers’ (C-Def. C1 due to the first meaning of C-Def. I1) is conceptually different from the linkage between ‘isomers’ and ‘stereoisomers’ (C-Def. S1 due to the second meaning of C-Def. I1). It follows that the schemes shown in Fig. 1.4 are misleading, because such distinct concepts are placed on the same level as indicating the dichotomy of isomers.

To develop a rational remedy for revising the misleading schemes of Fig. 1.4 as well as for avoiding the duality in the definition of isomers (C-Def. I1), more implications in the methodology of modern stereochemistry should be examined. Strictly speaking, **1-16**, **1-18**, and **1-19** in Eq. 1.2 (other than **1-17** and $\overline{\mathbf{1-17}}$) are not characterized by C-Def. S1, because C-Def. S1 is concerned with a relationship among two or more 3D structures.⁶ However, they can be correlated to the counterpart graphs in Eq. 1.1, just as Eq. 1.3 is correlated to the graph **1-17_g**. As a result, Eq. 1.2 is converted into the following set of 3D structures:

$$\left(\mathbf{1-16} \quad \langle \mathbf{1-17} \quad \overline{\mathbf{1-17}} \rangle \quad \mathbf{1-18} \quad \mathbf{1-19} \right), \quad (1.4)$$

which is partially divided by means of C-Def. S1.

The methodology of modern stereochemistry is based on the presumption that the set represented by Eq. 1.1 (for graphs) corresponds to the set represented by Eq. 1.4 (for 3D structures) in a one-to-one fashion, where, in particular, the detected set of stereoisomers, $\langle \mathbf{1-17} \quad \overline{\mathbf{1-17}} \rangle$, is regarded as a graph **1-17_g**. Although these two sets (Eq. 1.1 and Eq. 1.4) are conceptually different (2D vs. 3D), they are forced to be regarded as the same thing by devising C-Def-I1 of dual-purpose. A more reasonable or mathematical rationalization for the correspondence between Eq. 1.1 and Eq. 1.4 should be developed in order to reorganizing the methodology of modern stereochemistry.



Exercise 1.1.

- Apply C-Def. I1, C-Def. C1, and C-Def. S1 to the set of butanols (Fig. 1.5) after adding isomeric ethers ($\text{CH}_3\text{CH}_2\text{-O-CH}_2\text{CH}_3$, $\text{CH}_3\text{CH}_2\text{CH}_2\text{-O-CH}_3$, and $(\text{CH}_3)_2\text{CH-O-CH}_3$).
- Discuss the merits of omitting such isomeric ethers so as to restrict the domain of thinking to the set of butanols (Fig. 1.5).

⁶ In other words, C-Def. S1 does not define a *self-stereoisomeric relationship*, which is concerned with a relationship between a 3D structure and itself. For a revision of C-Def. S1, see Def. 2.5 on page 38.



Exercise 1.2.

- Apply C-Def. C1 to the set of dibromocyclohexanes as 2D structures listed in Fig. 1.3:

$$\left(\mathbf{1-7 \ 1-10 \ 1-13} \right) \quad (1.5)$$

- Confirm that C-Def. C1 cannot be applied to the comparison between **1-8** and **1-9**.
- Apply C-Def. S1 to the set of dibromocyclohexanes as 3D structures listed in Fig. 1.3:

$$\left(\mathbf{1-8 \ 1-9 \ \overline{1-9} \ 1-11 \ 1-12 \ \overline{1-12} \ 1-14 \ 1-15} \right) \quad (1.6)$$

- Discuss the correspondence between the set of Eq. 1.5 and the set of Eq. 1.6.

1.2.3 Positional Isomers as a Kind of Constitutional Isomers

Positional isomers are defined as

C-Definition P1 “constitutional isomers that have the same carbon skeleton and the same functional groups but differ from each other in the location of the functional groups on or in the carbon chain” [29].

Because positional isomers are a kind of constitutional isomers of 2D-basis, they are also categorized to be a 2D-based concept.

The definition of C-Def. P1 is applied to the set of butanols represented by Fig. 1.5, where a straight chain $\text{CH}_3\text{CH}_2\text{CH}_2\text{CH}_3$ and a branched chain $(\text{CH}_3)_2\text{CHCH}_3$ are adopted as a set of skeletons to be considered.⁷ Thereby, the set of Eq. 1.1 is converted into the following divided set:

$$\left(\left\{ \mathbf{1-16 \ 1-17_g} \right\} \left\{ \mathbf{1-18 \ 1-19} \right\} \right), \quad (1.7)$$

where each pair of braces consists of positional isomers to be detected.

The definition of C-Def. P1 cannot be applied directly to the set of Eq. 1.2. Instead, the set of Eq. 1.2 is first converted by means of C-Def. S1 into the set of Eq. 1.4, which corresponds to Eq. 1.1. Then, the set of Eq. 1.4 is treated by C-Def. P1 to give the following set of 3D structures:

$$\left(\left\{ \mathbf{1-16 \ \langle 1-17 \ \overline{1-17} \rangle} \right\} \left\{ \mathbf{1-18 \ 1-19} \right\} \right), \quad (1.8)$$

which corresponds to Eq. 1.7 for 2D structures (graphs). If 3D structures such as Eq. 1.2 are taken into consideration, the test (C-Def. S1) for stereoisomers is prerequisite to the test (C-

⁷ Because discussions on ‘positional isomers’ require a beforehand selection of skeletons, they are not so well differentiated from so-called ‘skeletal isomers’. This means that ‘positional isomers’ and ‘skeletal isomers’ should be discussed in an integrated fashion. See Def. 2.10 on page 43 for defining isoskeletal relationships and isoskeletonomers.

Def. P1) for positional isomers (constitutional isomers). So long as modern stereochemistry remains within a limit of Eq. 1.7 for graphs, it lacks analytical methods for deriving Eq. 1.8 for 3D structures. At present, the linkage of Eq. 1.7 for graphs with Eq. 1.8 for 3D structures depends upon the intuition or academic training of organic chemists, but not upon a reliable systematic method based on mathematical formulations.



Exercise 1.3.

- Apply C-Def. P1 to the set represented by Eq. 1.5 of Exercise 1.2.
- Compare this result with the result obtained by applying C-Def. C1 (Exercise 1.2).
- Confirm that C-Def. P1 cannot be applied to the comparison between **1-8** and **1-9** (Fig. 1.3)

1.3 Problematic Methodology for Categorizing Enantiomers and Diastereomers⁸

This section is devoted to demonstrating the misleading dichotomy between enantiomers and diastereomers.

1.3.1 Enantiomers

According to the IUPAC Recommendations 1996 [27], the term *enantiomer* is defined as

C-Definition E1 “one of a pair of molecular entities which are mirror images of each other and non-superposable”.

Let us apply C-Def. E1 to the butanols listed in Fig. 1.5, which are collected in the set represented by Eq. 1.2 for 3D structures. Thereby, we detect a pair of enantiomers **1-17/1-17** to give the following division:

$$\left(\mathbf{1-16} \quad [\mathbf{1-17} \quad \overline{\mathbf{1-17}}] \quad \mathbf{1-18} \quad \mathbf{1-19} \right), \quad (1.9)$$

where a pair of square brackets consists of a pair of enantiomers.

Strictly speaking, the definition of C-Def. E1 is ineffective to detect the achirality of **1-16**, **1-18**, or **1-19**, because C-Def. E1 is concerned with the relationship between a pair of molecular entities. As discussed later (cf. Def. 2.3 on page 36), an enantiomeric relationship due to C-Def. E1 is not an equivalence relationship. Hence, the detection of the achirality of **1-16**, **1-18**, or **1-19** implicitly depends on a reflection operation for superposability, which cannot be properly treated by C-Def. E1.

⁸ See Footnote 2.

1.3.2 Diastereomers

Dichotomy between Enantiomers and Diastereomers

On the other hand, the term *diastereomers* is defined subsidiarily by starting from stereoisomers and enantiomers as follows:

C-Definition D1 “stereoisomers that are not enantiomers are termed diastereomers”.

Mislow’s review [23] has revealed the historical situations of the coinage of the term *diastereomers* from a viewpoint of “chemical philology”. As a result, stereoisomers are subdivided into *enantiomers* and *diastereomers*. Various expressions have appeared to define the dichotomy between enantiomeric relationships and diastereomeric relationships in IUPAC rules and in textbooks:

Remark 1.1 (Diastereomeric Relationships and Misleading Dichotomy).

- IUPAC Recommendations 1996 [27, page 2205]: “Diastereoisomerism: *Stereoisomerism* other than *enantiomerism*. Diastereoisomers (or diastereomers) are stereoisomers not related as mirror images.” Note that the terms ‘stereoisomerism’, ‘enantiomerism’, and ‘diastereomerism’ have phenomenological meanings, which are related to stereoisomeric relationships, enantiomeric relationships, and diastereomeric relationships.
- IUPAC Recommendations 2005 [30, page 175]: “Stereoisomers that are mirror images of one another are called enantiomers (sometimes these have been called optical isomers), while those that are not are called diastereoisomers (or geometrical isomers).”
- Mislow’s textbook [28, page 51]: “Stereoisomers which are related as object and nonsuperimposable mirror image are called *enantiomers* or *antipodes*, whereas those which are not so related are called *diastereomers*.” Note that the term ‘antipodes’ is now obsolete.
- Eliel’s textbook [31, page 1208]: “Stereoisomers: Isomers of identical constitution but different in the arrangement of their atoms in space. Subclasses are Enantiomers and Diastereomers.”
- Zelewsky’s textbook [32, page 49]: “Stereoisomers can be sharply divided into two subsets, namely into *enantiomers* and *diastereomers* (or *diastereoisomers*).”
- North’s textbook [33, page 17]: “By definition, any pair of stereoisomers which are not enantiomers of one another are called diastereomers.”
- Morris’ textbook [34, page 38]: “Diastereomers are stereoisomers that are not enantiomers.”

The statements collected in Remark 1.1 can be summarized into two distinct schemes, as illustrated by Fig. 1.6(a) (cf. [35]) or Fig. 1.6(b) (cf. [32, 36–39]). These schemes are

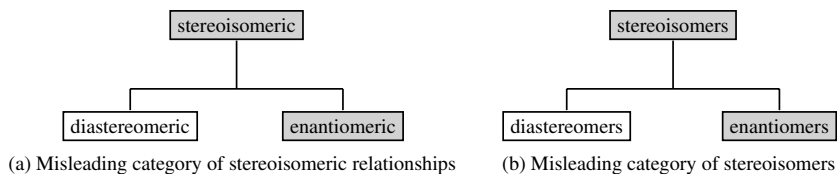


Fig. 1.6. Misleading category of stereoisomeric relationships and related category of stereoisomers. A gray box represents an equivalence relationship or an equivalence class, which has been overlooked in modern stereochemistry.

conceptually different from each other, where the former is concerned with relationships, while the latter is concerned with molecular entities.

Counter-Examples against the Dichotomy

Restricted rotation around a double bond can result in the formation of enantiomers, which are referred to as ‘geometric enantiomers’. For example, the oximation of *meso*-2,6-diphenyl-1-methyl-4-piperidone **1-20**, which is achiral because of intramolecular compensation of opposite chirality senses, results in the formation of oximes **1-21** and **1-22**, as shown in Fig. 1.7 [40,41]. These oximes are *Z/E*-isomers (‘diastereomers’) to each other, because they are interchangeable by the permutation (*syn/anti*-isomerization) of the hydroxyl group. At the same time, they are enantiomeric to each other because they are mirror images under reflection (C-Def. E1), i.e., **1-22** = $\overline{\mathbf{1-21}}$ (mirror image). The absolute configuration of (+)-1-methyl-2,6-diphenyl-4-piperidone oxime is determined to be assigned to **1-21** [42].

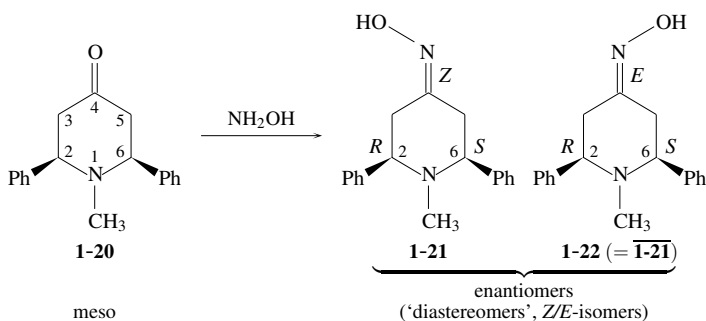


Fig. 1.7. ‘Genometric enantiomerism’ for oximes.

So long as we obey C-Def. D1, we are unable to adopt the *Z/E*-isomerism (the ‘diastereomeric’ relationship) between the oximes **1-21** and **1-22** (= $\overline{\mathbf{1-21}}$), so that we are forced to say that they are solely enantiomeric to each other (C-Def. E1). However, this assignment

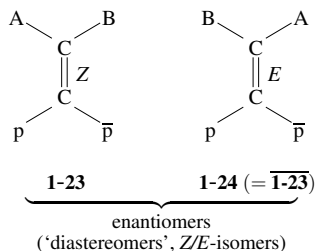


Fig. 1.8. ‘Geometric enantiomerism’ for double bonds. The symbols A and B represent achiral ligands in isolation, while the symbols p and \bar{p} represent a pair of enantiomeric ligands in isolation. The priority sequence is presumed to be $A > B > p > \bar{p}$.

due to the dichotomy (C-Def. D1) is unbalanced, because the identification of **1-21** requires the label Z for the oxime double bond as well as the label R at the position 2 and the label S at the position 6. The necessity of the label Z indicates that the Z/E-isomerism of **1-21** should be determined in order to assure the differentiation from **1-22** ($= \overline{\text{1-21}}$) with the label E. This case provides a counter-example to C-Def. D1.

A more general example of ‘geometric enantiomers’ is shown in Fig. 1.8, where the symbols A and B represent achiral ligands in isolation, while the symbols p and \bar{p} represent a pair of enantiomeric ligands in isolation. The ethylene derivatives **1-23** and **1-24** are Z/E-isomers to each other, because the exchange between A and B (or between p and \bar{p}) causes *cis/trans*-isomerization between them. Note that the permutation of p and \bar{p} (even of A and B) does not contain reflections (mirror-image formations) of p and \bar{p} (even A and B). To assign the labels Z and E, the priority sequence is presumed to be $A > B > p > \bar{p}$. At the same time, they are enantiomeric to each other, because they are mirror images to each other under reflection (C-Def. E1). This case provides a counter-example to C-Def. D1 in general.

‘Geometric enantiomers’ are also found in the series of cyclobutane derivatives, as shown in Fig. 1.9 [43]. The cyclobutanes **1-25** and $\overline{\text{1-25}}$ are enantiomeric because a mirror plane can be selected to contain the cyclobutane ring (C-Def. E1). At the same time, they are ‘diastereomeric’ (Z/E-isomeric) because the permutation (epimerization) of A and B (or p and \bar{p}) brings about a Z/E- or *cis/trans*-isomerization between **1-25** and $\overline{\text{1-25}}$. Although the latter permutation of p and \bar{p} (even of A and B) does not contain reflections (mirror-image formations) of p and \bar{p} (even A and B), it causes the conversion of **1-25** into $\overline{\text{1-25}}$, which corresponds to an enantiomeric relationship. This case provides a further counter-example to C-Def. D1.

The counter-examples shown in Figs. 1.7–1.9 indicate that the dichotomy due to C-Def. D1 should be abandoned, even though the various descriptions listed in Remark 1.1 and the schemes of Fig. 1.6 have been misleadingly widespread. A balanced viewpoint is that *enantiomeric relationships and ‘diastereomeric’ relationships are independent concepts,*

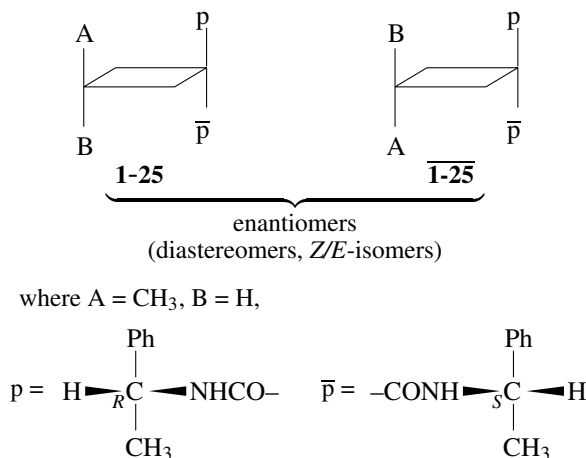


Fig. 1.9. ‘Geometric enantiomers’ of cyclobutane derivatives. The cyclobutane ring is presumed to be planar without losing generality.

which may be coincident with each other. Such coincident cases as Figs. 1.7–1.9 should be more properly taken into consideration than they are.⁹

More Essential Counter-Examples Against the Dichotomy

More cumbersome but essential situations than the counter-examples shown in Figs. 1.7–1.9 occur in tetrahedral molecular entities. For example, let us examine **1-26** and **1-27** shown in Fig. 1.10, where each central carbon atom is attached by a pair of enantiomeric ligands p and $\bar{\text{p}}$ in isolation as well as another pair of enantiomeric ligands q and $\bar{\text{q}}$ in isolation.

By applying C-Def. E1, the tetrahedral molecular entities **1-26** and **1-27** (= $\bar{\mathbf{1-26}}$) are determined to be enantiomeric each other. During the application of C-Def. E1, a reflection operation works to accomplish the conversion (reflection) of p into $\bar{\text{p}}$ (and $\bar{\text{p}}$ into p) as well as the conversion of q into $\bar{\text{q}}$ (and $\bar{\text{q}}$ into q) in addition to the reflection at the center of the tetrahedral skeleton. As a result, there occurs the conversion of **1-26** into its mirror image $\bar{\mathbf{1-26}}$ (= **1-27**).

So long as we obey the dichotomy (C-Def. D1), we are forced to conclude that **1-26** and **1-27** (= $\bar{\mathbf{1-26}}$) are in an enantiomeric relationship, not in a ‘diastereomeric’ relationship. If we keep in mind the counter-examples shown in Figs. 1.7–1.9, there appears a question whether this conclusion is acceptable or not.

To solve this question, let us apply van’t Hoff’s theory (Fig. 1.2) to **1-26** and **1-27** (= $\bar{\mathbf{1-26}}$), as shown in Fig. 1.11, although van’t Hoff’s theory has originally taken account of

⁹ In this book, the terms *coincidence*, *coalescence*, and *confluence* (and the related terms) are used in the same meaning for convenience’ sake.

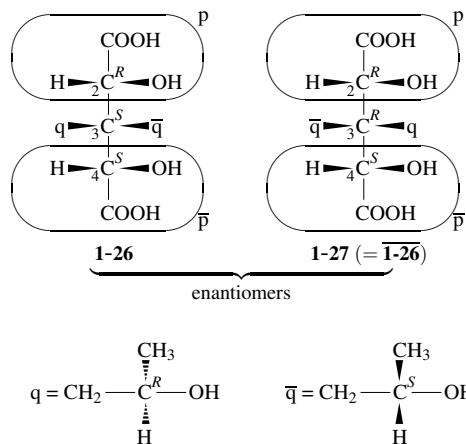


Fig. 1.10. Coalescence of an enantiomeric relationship and a 'diastereomeric' relationship.

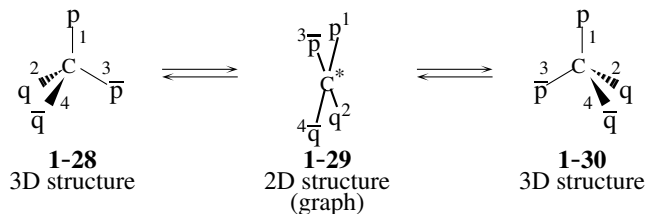


Fig. 1.11. Application of van't Hoff's theory to an asymmetric carbon (*) of a 2D structure with a set of ligands, p , \bar{p} , q , and \bar{q} , where the symbols p and \bar{p} (or q and \bar{q}) represent a pair of enantiomeric ligands in isolation (when detached).

achiral ligands only. The 2D structure 1-29 is concerned with the central atom, where each of p , \bar{p} , q , and \bar{q} represents an abstract ligand with a chirality sense.

The interconversion between 1-28 (for 1-26) and 1-30 (for 1-27 (= 1-26)) via 1-29 is not accompanied by the mirror-image formation of ligands. In other words, there occurs no reflection of p into \bar{p} (and \bar{p} into p), nor of q into \bar{q} (and \bar{q} into q), so that the process of converting 1-28 into 1-30 is regarded as the exchange of two ligands (e.g., q and \bar{q}). The exchange of two ligands (e.g., q and \bar{q}) is essentially the same as the permutations presumed in Figs. 1.7–1.9. Because each of the permutations of Figs. 1.7–1.9 is correlated to a 'diastereomeric' relationship, the relationship between 1-28 and 1-30 is also determined to be a 'diastereomeric' relationship.

Remember that 1-28 and 1-30 is enantiomeric to each other at the same time. Hence, the enantiomeric relationship between 1-28 and 1-30 (or between 1-26 and 1-27 (= 1-26)) is coincident with the 'diastereomeric' relationship between them. So long as we obey the dichotomy (C-Def. D1), however, we are forced to conclude that 1-28 and 1-30 (= 1-28) are in an enantiomeric relationship, not in a 'diastereomeric' relationship.



Exercise 1.4.

- Apply van't Hoff's theory (Fig. 1.2) to a central carbon of a 2D structure with a set of ligands, A, B, p, and \bar{p} , where A and B are achiral ligands and p and \bar{p} represent a pair of enantiomeric ligands in isolation.
- Compare this result with Fig. 1.11.
- Apply C-Def. D1 to the resulting molecular entities, which are referred to under the term 'pseudoasymmetry'.

1.3.3 Chirality and Stereogenicity

The relational term *enantiomeric* (C-Def. E1) is closely related to the attributive terms *chirality/achirality*. The relational term 'diastereomeric' (C-Def. D1) is closely related to the attributive term *stereogenicity*. It should be emphasized that *modern stereochemistry presumes a single pair of attributive terms chirality/achirality*. The attributive term *stereogenicity* has no definite counterpart, which would be named *non-stereogenicity* (or *asterogenicity*) if such a counterpart is possible. However, modern stereochemistry lacks the term *non-stereogenicity*, so that such non-stereogenic cases have not yet been targets of discussions.

Historically speaking, the introduction of the term *stereogenicity* has aimed at the revision [44] of the Cahn-Ingold-Prelog (CIP) system, which was originally based on chirality [45]. Thereby, the *R/S*-stereodescriptors of the CIP system has been changed to be based on stereogenicity. The term *chirality* linked with the term *enantiomeric* (C-Def. E1) specifies a definite pair of enantiomers (two mirror images). In contrast, the term *stereogenicity* linked with the term 'diastereomeric' (C-Def. D1) is incapable of specifying any definite pair, because two *or more* molecular entities may be diastereomeric to one another. To avoid this paradoxical situation, a pair of *R/S*-stereodescriptors of the CIP system is still presumed to be assigned to a pair of enantiomers, where 'chirality centers' etc. are categorized as 'stereogenic units' to be specified by *R/S*-stereodescriptors [44]. Hence, chirality and stereogenicity are not well discriminated in modern stereochemistry, although several attempts have appeared [46,47].

1.4 Total Misleading Features of the Traditional Terminology on Isomers¹⁰

The misleading features of Fig. 1.4 and Fig. 1.6 accumulate in practical judgements on categories of isomers and stereoisomers.

¹⁰ See Footnote 2.

1.4.1 Total Misleading Flowcharts

By combining Fig. 1.4 with Fig. 1.6, we obtain total misleading flowcharts, as shown in Fig. 1.12.

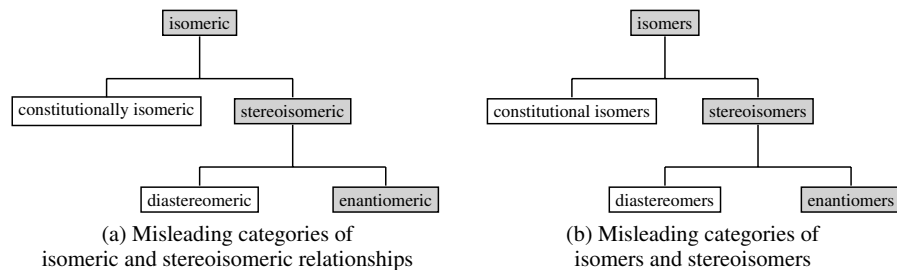


Fig. 1.12. Misleading categories of isomeric and stereoisomeric relationships as well as the related categories of isomers and stereoisomers. A gray box represents an equivalence relationship or an equivalence class, which has been overlooked in modern stereochemistry.

In the above discussions, we have used the relational schemes (Fig. 1.4(a), Fig. 1.6(a), and Fig. 1.12(a)) and the attributive schemes (Fig. 1.4(b), Fig. 1.6(b), and Fig. 1.12(b)) in an arbitrary or rather loose fashion. However, they should be differentiated more strictly in further discussions. In the next chapters, more mathematical treatments will be developed after the introduction of the concepts of *equivalence relationships* and *equivalence classes*.

As found in the above discussions, modern stereochemistry suffers from the following essential drawbacks:

1. Differentiation of relational terms (e.g., isomeric and stereoisomeric) from attributive terms (e.g., isomers and stereoisomers) is insufficient.
2. Relational terms are used to differentiate between only two molecular entities, where the concept of *equivalence relationships* is not taken into consideration. As a result, the schemes based on relational terms (Fig. 1.4(a), Fig. 1.6(a), and Fig. 1.12(a)) are misleadingly extended to the schemes based on attributive terms (Fig. 1.4(b), Fig. 1.6(b), and Fig. 1.12(b)).
3. A set of two or more molecular entities cannot be systematically discussed by means of the schemes based on attributive terms (Fig. 1.4(b), Fig. 1.6(b), and Fig. 1.12(b)), because the lack of the concept of equivalence classes inhibits proper discussions on classification of isomers.
4. 2D-based concepts (e.g., constitutional isomers) and 3D-based concepts (e.g., stereoisomers) are mixed without mathematical formulations. The misleading dichotomy between constitutional isomers and stereoisomers should be replaced by a more rational scheme.
5. Coincidence between enantiomeric relationships and diastereomeric relationships has been nullified by presuming the misleading dichotomy between enantiomers and di-

astereomers. For a remedy against the misleading dichotomy, see a recent review [48, Chapter 9].

6. The concept of chirality is not fully distinguished from the concept of stereogenicity in the CIP system.
7. Because of lacking the concept of equivalence classes in Fig. 1.12(b), the number of such equivalence classes cannot be evaluated. Hence, modern stereochemistry is incapable of the combinatorial enumeration of isomers, so long as it obeys the schemes of Fig. 1.12.

These essential drawbacks have caused serious confusion, which could not be avoided so long as modern stereochemistry adopts qualitative or descriptive approaches. The aims of the present book are to specify such serious confusion and to give rational solutions by developing mathematical formulations for avoiding the essential drawbacks.

1.4.2 Another Flowchart With Partial Solutions

After Mislow pointed out the drawback of such a flowchart as Fig. 1.12(a) [35], he has proposed another flowchart shown in Fig. 1.13 on the basis of an isometry. However, the proposed remedy by this flowchart [35,46] did not fully solve the misleading features described above.

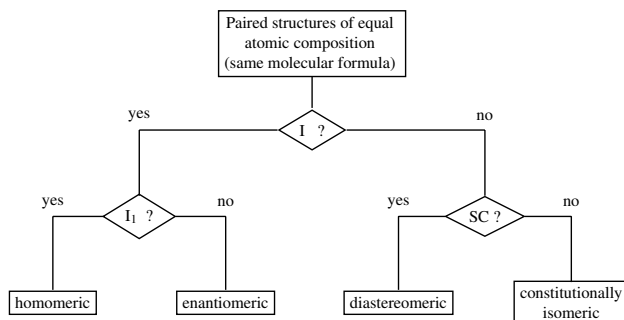


Fig. 1.13. Flowchart for classifying pairwise relationships: I = isometric; I_1 = related by an isometry of the first kind; SC = same constitution [35]. This flowchart lacks the definition of a stereoisomeric relationship as well as the concepts of equivalence relationships and equivalence classes.

1. Mislow and Siegel [46] has properly pointed out that the geometric attribute of chirality (e.g., ‘local symmetry’) and the stereoisomerism (e.g., ‘stereogenicity’) are conceptually distinct but they may interact. However, their discussions on the interaction are qualitative and afford no integrated foundation of mathematical basis. In fact, Fig. 1.13 emphasizes the the geometric attribute of chirality by the selection of the top judgement

- (‘I?’) due to an isometry, so that the term ‘stereoisomeric’ does not appear in the right branch of Fig. 1.13 [35].
2. The flowchart of Fig. 1.13 emphasizes relational terms (e.g., enantiomeric and diastereomeric) and makes light of attributive terms (e.g., enantiomers and diastereomers). For example, the application of Fig. 1.13 to the set represented by Eq. 1.2 (Fig. 1.5) arrives at the result that the two achiral molecular entities of the same 3D structure (e.g., {**1-16**, **1-16**}) are determined to be homomeric, just as the two chiral molecular entities of the same 3D structure (e.g., {**1-17**, **1-17**}) are determined to be homomeric. However, this judgement does not aim at partition for constructing equivalence classes, because the flowchart of Fig. 1.13 lacks the concept of equivalence relationships and the homomeric relationship is not recognized as an equivalence relationship.
 3. Because of lacking the concept of equivalence classes, the flowchart of Fig. 1.13 is silent about the results of its application to a set of *more than two* molecular entities. It follows that the flowchart does not aim at classifying *more than two* molecular entities into sets of stereoisomers or pairs of enantiomers as equivalence classes.
 4. Because of lacking the concept of equivalence classes, the flowchart of Fig. 1.13 is insufficient to evaluate the number of such equivalence classes which are inequivalent to each other (isomer number). In other words, the flowchart of Fig. 1.13 does not support combinatorial enumeration of isomers.
 5. The flowchart of Fig. 1.13 does not permit coincidence between enantiomeric relationships and diastereomeric relationships, so that the interaction between the geometric attribute of chirality (e.g., ‘local symmetry’) and the stereoisomerism (e.g., ‘stereogenicity’) is not properly estimated. Thus, the ‘I?’ judgement due to an isometry in Fig. 1.13 characterizes the relationship between an object (e.g., **1-4** in Fig. 1.2) and its mirror image ($\overline{\mathbf{1-4}} = \mathbf{1-6}$) by means of a reflection. However, the interconversion between them can alternatively occur by the process without a reflection (Fig. 1.2), which is regarded as one embodiment of stereoisomerism (a diastereomeric relationship). The flowchart of Fig. 1.13 results in the nullification of the process of Fig. 1.2 (a diastereomeric relationship), even though the latter is specified by the attributive term ‘stereogenic’ in place of the relational term ‘diastereomeric’ [46].

!
Remark 1.2 (Essential Viewpoints of Fig. 1.12(a) and Fig. 1.13). The scheme of Fig. 1.12(a) separates the term ‘stereoisomeric’ (a 3D-based concept) from the term ‘constitutionally isomeric’ (a 2D-based concept) at the top judgement. This scheme suffers from the duality of the definition of an isomeric relationship (C-Def. I1 in Table 1.1). On the other hand, the flowchart shown in Fig. 1.13 separates the term ‘diastereomeric’ (a 3D-based concept) from the term ‘constitutionally isomeric’ (a 2D-based concept) at the ‘SC?’ judgement. Although the top ‘I?’ judgement due to an isometry is concerned with 3D structures, the ‘no’ branch of the ‘I?’ judgement contains the term ‘constitutionally isomeric’ (a 2D-based concept) and the term ‘diastereomeric’

(a 3D-based concept). To avoid this inconsistency, the term ‘constitutionally isomeric’ (a 2D-based concept) should be temporarily regarded as a 3D-based concept at the ‘I?’ judgement. This is an example of the arbitrary switching between 2D-based and 3D-based concepts, which has been discussed in Subsection 1.1.3.

1.4.3 More Promising Way

In contrast to the flowchart of Fig. 1.13 [35], the present approach lays stress on 3D-based concepts and on equivalence classes produced by an equivalence relationship even for the purpose of investigating the geometric attribute of chirality [49]. Thus, an achiral molecular entity is characterized by a one-membered equivalence class (e.g., [1-16], [1-18], or [1-19] for Fig. 1.5), while a chiral molecular entity and its mirror image are characterized by a two-membered equivalence class (e.g., [1-17] $\overline{[1-17]}$). Thereby, the set of Eq. 1.2 is partitioned as follows:

$$\left([1-16] \quad [1-17] \quad \overline{[1-17]} \quad [1-18] \quad [1-19] \right), \quad (1.10)$$

which are counted to be equal to 4 by means of the proligand method [49, Table 12.1], as described below (cf. Section 1.5 and Subsection 2.1.2).

Moreover, Eq. 1.10 is further partitioned via Eq. 1.8 so as to give the following classification of equivalence classes of various levels:

$$\left(\{ \{ [1-16] \} \} \quad \{ \{ [1-17] \quad \overline{[1-17]} \} \} \quad \{ \{ [1-18] \} \quad \{ [1-19] \} \} \right), \quad (1.11)$$

which meets qualitative and quantitative purposes. Such equivalence classes of various levels will be discussed later. The partition of Eq. 1.11 is further revised by the stereoisogram approach, as described below.

Because of lacking the concept of equivalence classes, the flowchart of Fig. 1.13 for classifying pairwise relationships does not aim at such partitions as Eq. 1.10 and Eq. 1.11. This means that even the flowchart of Fig. 1.13 adopts a qualitative or descriptive approach without the concepts of equivalence relationships and equivalence classes, just as Fig. 1.12 of modern stereochemistry has adopted.

1.5 Isomer Numbers

The flowcharts shown in Fig. 1.12 mainly aim at qualitative discussions on the the geometric attribute of chirality and stereoisomerism. On the other hand, the flowchart shown in Fig. 1.13 is focused on qualitative discussions about the geometric attribute of chirality. These flowcharts of two different types commonly emphasize relationships (not equivalence relationships), so that they make light of equivalence classes, which are important for

such quantitative purposes as the evaluation of isomer numbers. Even the sets appearing in Fig. 1.12(b) (e.g., isomers and stereoisomers) are not regarded as equivalence classes in the state-of-the-art methodology of modern stereochemistry. For the purpose of combinatorial enumeration, such equivalence classes are counted after developing quantitative formulations based on mathematics.

1.5.1 Combinatorial Enumeration as 2D Structures

The graph theory has provided organic chemistry with quantitative devices for evaluating isomer numbers. Pólya has developed a powerful theorem referred to under his name [50–52]. By means of Pólya's theorem, he has counted benzene derivatives [50,51] as well as alkanes and substituted alkanes with higher carbon contents [52]. For example, alkanols with the molecular formulas $C_nH_{2n+2}O$ are counted as 2D structures (graphs, constitutional isomers) by recursive applications of Pólya's theorem [52], where the number of alkanols with $n = 4$ (i.e., butanols) has been combinatorially enumerated to be 4. This result is consistent with the manual enumeration listed in Fig. 1.5, which corresponds to the set represented by Eq. 1.1.

The unchanged importance of Pólya's theorem is obvious by the fact that his paper published in 1937 [52] was translated into English after 50 years [53]. For an introductory description on the enumeration of benzenes, see his own textbook [54, Chapter 6]. Interaction between organic chemistry and graph theory has proved to be successful, as summarized in reviews [55–58] and books [59–62].

1.5.2 Importance of the Proligand-Promolecule Model

The methodology implied in Le Bel's theory may be useful to treat 3D structures as they are. However, Le Bel himself [14] has stated that “In the reasoning which follows, we shall ignore the asymmetries (*originally dissymmetries*) which might arise from the arrangement in space possessed by the atoms and univalent radicals; but shall consider them as spheres or material points, which will be equal if the atoms or radicals are equal, and different if they are different. This restriction is justified by the fact, that, up to the present time, it has been possible to account for all the cases of isomerism observed without recourse to such arrangement, and the discussion at the end of the paper will show that the appearance of the rotatory power can be equally well foreseen without the aid of the hypothesis of which we have just spoken.” (cited from an English translation [15] where the italicized words are added). Contrary to Le Bel's statement, the ignorance of the inner arrangement and the presumption of spheres or material points have caused serious confusion, as found in the later history of stereochemistry.

Fujita has avoided the ignorance of the inner arrangement of Le Bel's theory by introducing the *proligand-promolecule model* [63], where a molecular entity with rotatable

ligands is treated as a *promolecule* with *proligands*, which are regarded as abstract ligands with chirality or achirality. Thereby, the systematic characterization of the global symmetry and local symmetries of a molecular entity is accomplished, where the inner arrangement due to a local symmetry is ascribed to each proligand, which is clarified to be controlled by *subduction of coset representations* [64–66]. The importance of the proligand-promolecule model has been confirmed by using skeletons of high point-group symmetries, e.g., octahedral complexes [67], prismane derivatives [68,69], and adamantane derivatives [70].

1.5.3 Combinatorial Enumeration as 3D Structures

After introducing the concepts of *sphericities* and *chirality fittingness* coupled with the proligand-promolecule model, Fujita has developed the *Unit-Subduced-Cycle-Index (USCI) approach* in order to accomplish symmetry-itemized enumeration of chemical compounds as 3D structures [71,72]. Among the four methods of Fujita's USCI approach, the fixed-point-matrix (FPM) method [73], the partial-cycle-index (PCI) method [74], and the elementary-superposition (ES) method [75] have recently been applied to symmetry-itemized enumeration of cubane derivatives.

To survey gross features without symmetry-itemization, a more simplified approach is desirable. *Fujita's proligand method* has been developed for the purpose of gross enumerations of 3D structures [76–78], where the basis of the concepts of sphericities and chirality fittingness is changed from equivalence classes (orbits) in Fujita's USCI approach to cycles in Fujita's proligand method. From the viewpoint of 2D- vs. 3D-based concepts, Pólya's theorem for graph enumeration is regarded as a degenerate case of Fujita's proligand method for 3D-structural enumeration [49].

For example, alkanols with the molecular formulas $C_nH_{2n+2}O$ are counted as 3D structures by recursive applications of Fujita's proligand method [79]. Thereby, the number of alkanols with $n = 4$ (i.e., butanols) has been combinatorially enumerated to be 4, which is partially itemized by chirality/achirality, i.e., three achiral butanols and one pair of enantiomeric butanols. This result is consistent with the manual enumeration listed in Fig. 1.5, which corresponds to the set represented by Eq. 1.4 or more strictly to the set represented by Eq. 1.9. Compare Eq. 1.4 (or Eq. 1.9) with Eq. 1.1.

By revising the concepts of sphericities and chirality fittingness, Fujita has developed related methods of gross enumeration [80–82], where various mathematical concepts (e.g., characters and double cosets) for cyclic groups are linked with the concepts of sphericities and chirality fittingness [49]. Among them, Fujita's proligand method [83], the markaracter method [84], the characteristic-monomial method [85], the extended-superposition method [86], and the double-coset-representation method [87] have recently been applied to gross enumeration of cubane derivatives.

The comparison between Pólya's theorem and Fujita's proligand method has been discussed in reviews [88,89] and Fujita's recent book [49]. For comparison using alkanes of high carbon contents (up to 100), see Refs. [90–92] and [49, Chapter 13].

1.6 Stereoisograms

1.6.1 Stereoisograms as Diagrammatic Expressions of *RS*-Stereoisomeric Groups

To avoid the drawbacks pointed out in Section 1.4 as well as to cover combinatorial enumeration described in Section 1.5, integrated discussions on stereogenicity and chirality are necessary after developing theoretical or mathematical tools for investigation. Fujita has developed the *stereoisogram approach*, where the concept of stereogenicity is restricted to the concept of *RS-stereogenicity*, which is integrated with the concept of chirality [93–95]. The key of this integration is the concepts of *RS-diastereomers* and *holantimers*, which are combined with *enantiomers*. These components are controlled by an *RS*-stereoisomeric group, so that the corresponding stereoisogram is devised as its diagrammatic expression.

For example, the pair of **1-4** and **1-6** in Fig. 1.2 is regarded as being *RS*-diastereomeric to each other, where **1-4** is regarded as a reference promolecule. Note that the term *promolecule* is used to denote an abstract molecular entity which is substituted by proligands as abstract ligands with chirality/achirality. The pair of *RS*-diastereomers **1-4** and **1-6** is placed in the horizontal direction of Fig. 1.14(a). The enantiomer $\overline{\mathbf{1-4}}$ generated by a reflection from the reference promolecule **1-4** is placed in the vertical direction of Fig. 1.14(a). Finally, the reference promolecule **1-4** is converted into its holantimer $\overline{\mathbf{1-6}}$ (= **1-4**), where the tetrahedral skeleton of Fig. 1.2 is maintained and the four ligands are converted into mirror images. The holantimer $\overline{\mathbf{1-6}}$ is placed in the diagonal direction of Fig. 1.14(a). The resulting quadruplet of promolecules are linked with equality symbols or double-headed arrows, so that there appears a stereoisogram of type I, as discussed later in detail.

In a similar way, by selecting **1-28** of Fig. 1.11 as a reference promolecule, there appear a stereoisogram of type I, as shown in Fig. 1.14(b).

The horizontal directions of each stereoisogram (Fig. 1.14(a) or (b)) are concerned with *RS*-diastereomeric relationships (attribute: *RS*-stereogenicity); the vertical directions of each stereoisogram are concerned with enantiomeric relationships (attribute: chirality); and the diagonal directions of each stereoisogram are concerned with holantimeric relationships (attribute: sclerality).

Each of the two stereoisograms shown in Fig. 1.14 is characterized by the presence of equality symbols along the diagonal directions, each of which is referred to as a self-holantimeric relationship or an ascleral attribute. Thereby, the *RS*-diastereomeric relationship is concluded to be coincident with the enantiomeric relationship in Fig. 1.14(a) or (b).

1.6.2 Theoretical Foundations and Group Hierarchy

Each stereoisogram is controlled by an *RS*-stereoisomeric group, which is derived from a point group of a stereoskeleton at issue. Thereby, a general proof for the existence of five types of stereoisograms (type I to type V) has been obtained on the basis of the existence

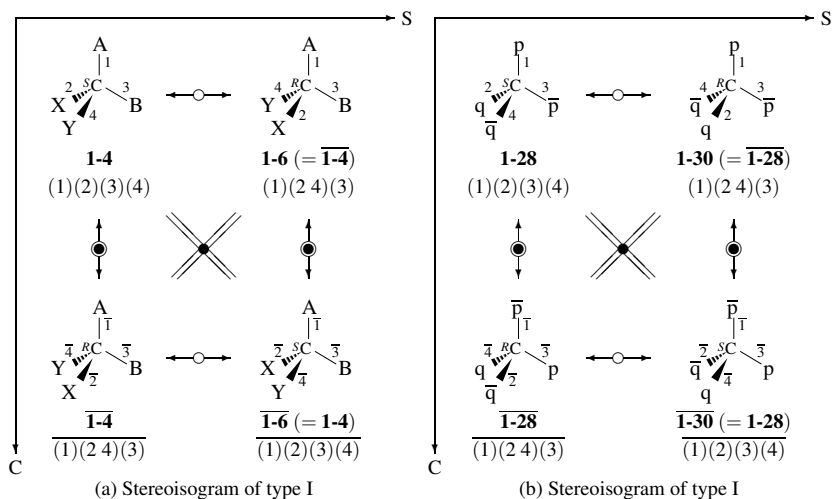


Fig. 1.14. Stereoisograms of type I for demonstrating the coincidence between an enantiomeric relationship (along the vertical direction) and an *RS*-diastereomeric relationship (along the horizontal direction).

of five types of subgroups of the *RS*-stereoisomeric group [96]. The group hierarchy has been formulated to be composed of point groups, *RS*-stereoisomeric groups, stereoisomeric groups, and isoskeletal groups by using an allene skeleton [97,98], an ethylene skeleton [99], and a square planar skeleton [100].

Stereoisograms of various skeletons of high symmetries have been discussed from a viewpoint that chirality and *RS*-stereogenicity are free from the conventional 'chirality' and 'stereogenicity', e.g., trigonal bipyramidal compounds [101,102], prismane derivatives [68, 69], and octahedral complexes [103–105].

Theoretical foundations of Fujita's stereoisogram approach have been discussed for the purpose of providing a new scheme for investigating geometric and stereoisomeric features in stereochemistry [106], for the purpose of developing theory of organic stereoisomerism in harmony with molecular symmetry [107], as well as for the purpose of demonstrating three aspects of absolute configuration [108]. Among the three aspects of absolute configuration, modern stereochemistry is clarified to emphasize the chiral aspect and to overlook the *RS*-stereogenic aspect and the scleral aspect.

1.6.3 Avoidance of Misleading Standpoints of *R/S*-Stereodescriptors

According to Fujita's stereoisogram approach, the basis of *R/S*-stereodescriptors of the CIP system is changed from 'stereogenicity' to *RS*-stereogenicity as a more definite concept, which is a common characteristic of type-I, type-III, and type-V stereoisograms [109,110]. As a result, a pair of *RS*-stereodescriptors is assigned to a pair of *RS*-diastereomers (e.g.,

1-4/1-6 or $\overline{1-4/1-6}$, not to a pair of enantiomers (e.g., **1-4/1-4** or **1-6/1-6**). In other words, the assignment of *R/S*-stereodescriptors is based on the *RS*-stereogenic aspect of absolute configuration, not to the chiral aspect of absolute configuration [108]. Coincidence between an *RS*-stereogenic relationship and an enantiomeric relationship has been discussed in such cases as Fig. 1.14, which work as counter-examples against the misleading dichotomy between enantiomeric and ‘diastereomeric’ relationships (see Section 1.3). The concept of *chirality (un)faithfulness* has been proposed for the purpose that *R/S*-stereodescriptors determined originally by *RS*-stereogenicity are interpreted as if they were assigned by chirality [110]. Thereby, misleading standpoints for *R/S*-stereodescriptors of the CIP system are rationally avoided [111], where the conventional terminology has been entirely replaced by the terminology based on Fujita’s stereoisogram approach. In particular, the ‘stereogenic centers and axes’ of the CIP system (e.g., ‘chirality centers’ and ‘pseudosymmetric centers’) are replaced by *promolecules characterized by type-I, type-III, or type-V stereoisograms* [111].

1.6.4 Avoidance of Misleading Standpoints of *pro-R/pro-S*-Descriptors

Long-standing confusion on the term ‘prochirality’ in stereochemistry has been avoided by Fujita’s stereoisogram approach [112], where the concept of *pro-R/S*-Stereogenicity has been proposed to accomplish integrated treatment with prochirality redefined. Thereby, *pro-R/pro-S*-descriptors have been clarified to be specified by *RS*-diastereotopic relationships, not by stereoheterotopic relationships [113,114]. The scope of the concepts of holantimers contained in stereoisograms has been discussed [70,115], where rational avoidance of misleading standpoints for *pro-R/pro-S*-descriptors has been accomplished. See also a recent review [116, Chapter 10]. As a result, the conventional terminology on so-called ‘prochirality’ has been entirely replaced by the terminology based on Fujita’s stereoisogram approach [115,117].

1.6.5 Global Symmetries and Local Symmetries

Global Symmetries in the Assignment of *R/S*-Stereodescriptors

According to Fujita’s stereoisogram approach, the conventional term ‘chiral center’ or ‘stereogenic center’ is replaced by the term *RS-stereoisomeric center*, which has three aspects, i.e., *RS*-stereogenic, chiral, scleral aspects. When we discuss the assignment of *R/S*-stereodescriptors, we should focus our attention on the *RS*-stereogenic aspect. For this purpose, such an *RS*-stereoisomeric center is called an *RS-stereogenic center* in a more distinctive fashion.

When a molecule has one *RS*-stereogenic center, its global symmetry and its local symmetry can be discussed commonly by examining ligands around the *RS*-stereogenic center. Thereby, either one of *R/S*-stereodescriptors is assigned to specify the *RS*-stereogenic aspect

of absolute configuration. Note that the term *symmetry* is used to denote chirality/achirality, *RS*-stereogenicity/*RS*-astereogenicity, and sclerality/asclerality, collectively.

Local Symmetries in the Assignment of *R/S*-Stereodescriptors

When a molecule has two or more *RS*-stereogenic centers, its global symmetry and its local symmetry should be discussed separately. For the purpose of discussing the assignment of *RS*-stereodescriptors, the local symmetry of each *RS*-stereogenic center should be discussed by examining ligands around the *RS*-stereogenic center.

Let us examine *meso*-2,6-diphenyl-1-methyl-4-piperidone **1-20** shown in Fig. 1.7. The global symmetry is characterized by a type-IV stereoisogram, i.e., achiral, *RS*-astereogenic and ascleral. Note that modern stereochemistry emphasizes only the achirality.

To examine the local symmetry at the 2-position of **1-20** (marked by a solid circle), the following four ligands are selected around the 2-position: a phenyl ligand, a hydrogen atom, a ring branch $p = -N(CH_3)-CH(Ph)-CH_2-C(=O)-CH_2-$ (along positions 1-6-5-4-3-2), and another ring branch $q = CH_2-C(=O)-CH_2-CH(Ph)-N(CH_3)-$ (along positions 3-4-5-6-1-2). Thereby, we obtain a promolecule **1-20**₂ as a reference promolecule, which generates a quadruplet of promolecules so as to give a type-III stereoisogram shown in Fig. 1.15(b). Because of the type-III stereoisogram of Fig. 1.15(b), the local symmetry at the 2-position is concluded to be chiral, *RS*-stereogenic, and scleral.

Although modern stereochemistry takes account of local chirality (under the introduction of the term ‘chirotopic’ [46]) as well as of ‘stereogenicity’ (under the introduction of the term ‘stereogenic units’ [44]), the latter concept of ‘stereogenicity’ is not restricted to the present concept *RS*-stereogenicity. Moreover, the concept of ‘stereogenicity’ is solely used during the selection of ‘stereogenic units’, but it turns out to be forgotten during the process of assigning *RS*-stereodescriptors. This means that a pairwise feature of the term *RS*-stereogenicity is overlooked by the conventional term ‘stereogenicity’. In fact, the CIP system first takes account of **1-20**₂ (labelled ‘*R*’ due to the priority sequence $p > Ph > q > H$) and then its enantiomer $\overline{\mathbf{1-20}}_2$ (labelled ‘*S*’ due to the priority sequence $\overline{p} > Ph > \overline{q} > H$) during the process of assigning *RS*-stereodescriptors, where the difference between the priority sequences is nullified in terms of ‘hierarchical digraph’ [44]. Thus the CIP system implicitly emphasizes the pair of **1-20**₂/ $\overline{\mathbf{1-20}}_2$ (an enantiomeric pair) and overlooks the pair of **1-20**₂/**1-31**₂ (an *RS*-diastereomeric pair), even though the CIP system adopts the term ‘stereogenic units’.

The misleading standpoints of *RS*-stereodescriptors described in the preceding paragraph are more clearly demonstrated by translating Fig. 1.15(b) into a stereoisogram using 3D-structural formulas, as illustrated in Fig. 1.15(a). The reference promolecule **1-20**₂ of Fig. 1.15(b) corresponds to the reference **1-20**₂ of Fig. 1.15(a), the 2-position of which is attached by a solid circle in order to emphasize an *RS*-stereogenic center to be examined. The *RS*-diastereomeric promolecule **1-31**₂ of Fig. 1.15(b) is translated into **1-31**₂ of Fig. 1.15(a). The *RS*-diastereomeric relationship between **1-20**₂ and **1-31**₂ corresponds to the epimerization of **1-20**₂ into **1-31**₂, where there occurs a permutation between a phenyl lig-

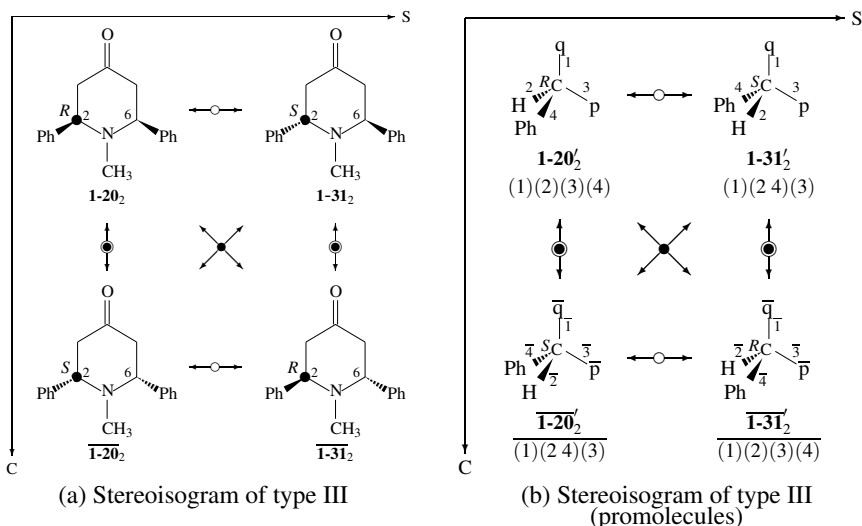


Fig. 1.15. Stereoisograms of type III for demonstrating local symmetries. (a) The 2-position of *meso*-2,6-diphenyl-1-methyl-4-piperidone **1-20**₂ is attached by a solid circle to emphasize an *RS*-stereogenic center to be examined. (b) A promolecule **1-20**'₂ is produced as a reference, where the two ring moieties centered at the 2-position are regarded as chiral proligands *p* and *q* as well as the substituents Ph and H are regarded as additional proligands.

and a hydrogen atom at the 2-position. The stereoisogram of Fig. 1.15(a) indicates that a pair of *R/S*-stereodescriptors is assigned to the pair of *RS*-diastereomers **1-20**₂/**1-31**₂ (due to the common priority sequence $p > \text{Ph} > q > \text{H}$), not to the pair of enantiomers **1-20**₂/**1-20**₂ (due to the different priority sequences $p > \text{Ph} > q > \text{H}$ and $\bar{p} > \text{Ph} > \bar{q} > \text{H}$). Note that a mirror plane is selected as containing the tentative plane of a six-membered ring. It should be emphasized that the pair of enantiomers **1-20**₂/**1-20**₂ is concerned only with the local symmetry at the 2-position, because **1-20** itself is achiral from the viewpoint of the global symmetry.

Exercise 1.5.

- Draw a type-IV stereoisogram for characterizing *meso*-2,6-diphenyl-1-methyl-4-piperidone **1-20**. Compare the resulting diagram with the type-III stereoisogram shown in Fig. 1.15.
- Assign *R/S*-stereodescriptors to the 6-position of **1-20** by drawing a stereoisogram concerned with **1-20**₆.
- Compare the label *S* assigned to **1-20**₆ with the label *S* assigned to **1-20**₂.

Correlation Diagrams of Stereoisograms

To comprehend global symmetries and local symmetries, Fujita has developed the concept of *correlation diagrams of stereoisograms* [118–120], where the global symmetry of a molecular entity and the local symmetries of the positions of the molecular entity are separately characterized by respective stereoisograms, which are correlated with one another in terms of correlation diagrams of stereoisograms. Such correlation diagrams are diagrammatic expression for the theory of organic stereoisomerism in harmony with molecular symmetry [107]. They provide us with a powerful device for reorganizing the theoretical foundations of stereochemistry and stereoisomerism [111].

1.6.6 Enumeration under *RS*-Stereoisomeric Groups

As an extension of Fujita's USCI approach under the action of point groups (see Section 1.5), quadruplets of *RS*-stereoisomers have been counted under the action of *RS*-stereoisomeric groups [121,122], where the isomer numbers are itemized according to type-I to type-V stereoisograms. More detailed enumerations of quadruplets of *RS*-stereoisomers have been conducted [123,124]. The isomer numbers derived from a tetrahedral skeleton are itemized according to the subgroups of *RS*-stereoisomeric groups, where the fixed-point-matrix (FPM) method and the partial-cycle-index (PCI) method of Fujita's USCI approach are extended so as to be combined with Fujita's stereoisogram approach. These procedures have been applied to count isomers based on an allene skeleton [125,126]. These results of enumeration have been discussed from a viewpoint of reorganizing the theoretical foundations of stereochemistry and stereoisomerism [127].

1.7 Aims of Mathematical Stereochemistry

The theoretical foundations of modern stereochemistry have descriptive nature without mathematical formulations, where they are intended to aim at investigating qualitative subjects. Even in qualitative investigations on geometric properties, however, the theoretical foundations of modern stereochemistry have inherent difficulties. Such difficulties are amplified more and more in qualitative investigations on stereoisomerism, as shown in Sections 1.2–1.4.

On the other hand, combinatorial enumeration of compounds as one of quantitative investigations on geometric properties have been investigated in terms of mathematical formulations based on group theory, as discussed in Section 1.5. As such quantitative investigations, I have published monographs on Fujita's USCI approach for symmetry-itemized combinatorial enumeration [71], on the mandala concept to comprehend intra- and intermolecular stereochemistry [72], and on Fujita's proligand method for gross combinatorial enumeration [49]. The mathematical formulations developed for Fujita's USCI approach are capable of supporting investigations on geometric properties, both quantitative and qualita-

tive, as discussed also in these books [71–49]. However, they are still insufficient to qualitative and quantitative investigations on stereoisomerism.

To support qualitative and quantitative investigations on stereoisomerism, I have later developed Fujita's stereoisogram approach, as shown in Section 1.6. The concept of stereoisograms based on mathematical formulations works as a linkage between geometric properties (chirality) and stereoisomerism (*RS*-stereogenicity). Thereby, unconscious confusion in modern stereochemistry [21–23] has been avoided in a qualitative fashion, as described in reviews [48,116,117]. Moreover, quantitative investigations on stereoisograms have been recently started as discussed in Subsection 1.6.6.

Mathematical stereochemistry is a new discipline of stereochemistry, which is based on theoretical foundations due to mathematical formulations. According to Fujita's stereoisogram approach as one of the fields of mathematical stereochemistry, the conventional terminology of modern stereochemistry is thoroughly revised to cover both geometric properties and stereoisomerism and both qualitative investigations and quantitative ones

References

- [1] F. A. Kekulé, *Liebigs Ann. Chem.*, **106**, 129–159 (1858).
- [2] A. S. Couper, *Annales de chimie et de physique*, **53**, 469–489 (1858).
- [3] E. Frankland, *Phil. Trans. Roy. Soc.*, **142**, 417–444 (1852).
- [4] A. Crum Brown, *Trans. Royal Soc. Edinburgh*, **23**, 707–719 (1864).
- [5] A. Crum Brown, *J. Chem. Soc.*, **18**, 230–245 (1865).
- [6] E. Frankland, "Lecture Notes for Chemical Students. Vol. I. Inorganic Chemistry", 2nd ed., John van Voorst, London (1870).
- [7] F. A. Kekulé, *Liebigs Ann. Chem.*, **137**, 129–196 (1866).
- [8] A. J. Ihde, "The Development of Modern Chemistry", Dover, New York (1984).
- [9] J. J. Sylvester, *Nature*, **17**, 284 (1877-8).
- [10] N. L. Biggs, E. K. Lloyd, and R. J. Wilson, "Graph Theory 1736–1936", Oxford Univ. Press, Oxford (1976).
- [11] J. H. van't Hoff, *Archives Néerlandaises des Sciences exactes et naturelles*, **9**, 445–454 (1874).
- [12] J. H. van't Hoff, A Suggestion Looking to the Extension into Space of the Structural Formulas at Present Used in Chemistry. And a Note Upon the Relation Between the Optical Activity and the Chemical Constitution of Organic Compounds, in "Foundations of Stereochemistry, Memoirs of Pasteur, van't Hoff, Le Bel and Wislicenus", ed. by G. M. Richardson, American Book Co., New York (1901) pp 35–46.
- [13] J. H. van't Hoff, "La Chimie Dans L'Espace", P. M. Bazendijk, Rotterdam (1875).

- [14] J. A. Le Bel, *Bull. Soc. Chim. Fr.* (2), **22**, 337–347 (1874).
- [15] J. A. Le Bel, On the Relations Which Exist Between the Atomic Formulas of Organic Compounds and the Rotatory Power of Their Solutions, in “Foundations of Stereochemistry, Memoirs of Pasteur, van’t Hoff, Le Bel and Wislicenus”, ed. by G. M. Richardson, American Book Co., New York (1901) pp 47–60, <https://archive.org/details/foundationsofste00richrich>.
- [16] R. G. Riddell and M. J. T. Robinson, *Tetrahedron*, **30**, 2001–2007 (1974).
- [17] R. B. Grossman, *J. Chem. Educ.*, **66**, 30–33 (1989).
- [18] A. M. Rouhi, *Chem & Eng. News*, **September 6**, 28–32 (1999).
- [19] L. Pasteur, in “Œuvre de Pasteur”, ed. by P. Vallery-Radot, Masson et C^{ie}, Paris (1922) Vol. 1 pp 314–344.
- [20] W. Thomson and (Lord Kelvin), “The Molecular Tactics of a Crystal”, Clarendon, Oxford (1894).
- [21] E. L. Eliel, *Chirality*, **9**, 428–430 (1997).
- [22] G. Helmchen, *Enantiomer*, **2**, 315–318 (1997).
- [23] K. Mislow, *Chirality*, **14**, 126–134 (2002).
- [24] M. P. Crosland, “Historical Studies in the Language of Chemistry”, Dover, Mineola New York (1978).
- [25] J. J. Berzelius, *Ann. Phys. Chem.*, **19**, 305–335 (1830).
- [26] S. Fujita, *Bull. Chem. Soc. Jpn.*, **87**, 1367–1378 (2014).
- [27] IUPAC Organic Chemistry Division, *Pure Appl. Chem.*, **68**, 2193–2222 (1996).
- [28] K. Mislow, “Introduction to Stereochemistry”, Benjamin, New York (1965).
- [29] G. Gunawardena, *OChemPal* (2009),
<http://science.uvu.edu/ochem/index.php/alphabeteal/o-p/positional-isomers/>.
- [30] N. G. Connelly, T. Damhus, R. M. Hartshorn, A. T. Hutton, and IUPAC, “Nomenclature of Inorganic Chemistry, IUPAC Recommendations 2005”, RSC Publishing, Cambridge (2005).
- [31] E. L. Eliel and S. H. Wilen, “Stereochemistry of Organic Compounds”, John Wiley & Sons, New York (1994).
- [32] A. von Zelewsky, “Stereochemistry of Coordination Compounds”, John Wiley & Sons, Chichester (1996).
- [33] N. North, “Principles and Applications of Stereochemistry”, Stanley Thornes, Cheltenham (1998).
- [34] D. G. Morris, “Stereochemistry”, Royal Soc. Chem., Cambridge (2001).
- [35] K. Mislow, *Bull. Soc. Chim. Belg.*, **86**, 595–601 (1977).
- [36] H. Hirschmann and K. R. Hanson, *Eur. J. Biochem.*, **22**, 301–309 (1971).

- [37] E. L. Eliel, *Top. Curr. Chem.*, **105**, 1–76 (1982).
- [38] T. W. G. Solomons, “Organic Chemistry”, 3rd ed., John Wiley & Sons, New York (1984).
- [39] K. P. C. Vollhardt and N. E. Schore, “Organic Chemistry. Structure and Function”, 4th ed., Freeman, New York (2003).
- [40] R. E. Lyle and G. G. Lyle, *J. Org. Chem.*, **22**, 856–856 (1957).
- [41] R. E. Lyle and G. G. Lyle, *J. Org. Chem.*, **24**, 1679–1684 (1959).
- [42] G. G. Lyle and E. T. Pelosi, *J. Am. Chem. Soc.*, **88**, 5276–5279 (1966).
- [43] V. Prelog, J. Thix, and T. Srikrishnan, *Helv. Chim. Acta*, **65**, 2622–2644 (1982).
- [44] V. Prelog and G. Helmchen, *Angew. Chem. Int. Ed. Eng.*, **21**, 567–583 (1982).
- [45] R. S. Cahn, C. K. Ingold, and V. Prelog, *Angew. Chem. Int. Ed. Eng.*, **5**, 385–415 (1966).
- [46] K. Mislow and J. Siegel, *J. Am. Chem. Soc.*, **106**, 3319–3328 (1984).
- [47] G. Helmchen, A. General Aspects. 1. Nomenclature and Vocabulary of Organic Stereochemistry, in “Stereochemical Synthesis. Methods of Organic Chemistry (Houben-Weyl). Workbench Edition E21”, 4 ed., ed. by G. Helmchen, R. W. Hoffmann, J. Mulzer, and E. Schaumann, Georg Thieme, Stuttgart New York (1996) Vol. 1 pp 1–74.
- [48] S. Fujita, Stereoisograms: A Remedy Against Oversimplified Dichotomy between Enantiomers and Diastereomers in Stereochemistry, in “Chemical Information and Computational Challenge in the 21st Century”, ed. by M. V. Putz, Nova, New York (2012) Chapter 9, pp 223–242.
- [49] S. Fujita, “Combinatorial Enumeration of Graphs, Three-Dimensional Structures, and Chemical Compounds”, University of Kragujevac, Faculty of Science, Kragujevac (2013).
- [50] G. Pólya, *Compt. Rend.*, **201**, 1167–1169 (1935).
- [51] G. Pólya, *Helv. Chim. Acta*, **19**, 22–24 (1936).
- [52] G. Pólya, *Acta Math.*, **68**, 145–254 (1937).
- [53] G. Pólya and R. C. Read, “Combinatorial Enumeration of Groups, Graphs, and Chemical Compounds”, Springer-Verlag, New York (1987).
- [54] G. Pólya, R. E. Tarjan, and D. R. Woods, “Notes on Introductory Combinatorics”, Birkhäuser, Boston (1983).
- [55] H. Hosoya, *Kagaku no Ryoiki*, **26**, 989–1001 (1972).
- [56] D. H. Rouvray, *Chem. Soc. Rev.*, **3**, 355–372 (1974).
- [57] O. E. Polansky, *MATCH Commun. Math. Comput. Chem.*, **1**, 11–31 (1975).
- [58] K. Balasubramanian, *Chem. Rev.*, **85**, 599–618 (1985).

- [59] F. Harary and E. M. Palmer, “Graphical Enumeration”, Academic Press, New York (1973).
- [60] A. T. Balaban, ed., “Chemical Applications of Graph Theory”, Academic Press, London (1976).
- [61] D. Bonchev and D. H. Rouvray, eds., “Chemical Graph Theory. Introduction and Fundamentals”, Gordon & Breach, Yverdon Switzerland (1991).
- [62] N. Trinajstić, “Chemical Graph Theory”, 2nd ed., CRC Press, Boca Raton (1992).
- [63] S. Fujita, *Tetrahedron*, **47**, 31–46 (1991).
- [64] S. Fujita, *Theor. Chim. Acta*, **76**, 247–268 (1989).
- [65] S. Fujita, *Bull. Chem. Soc. Jpn.*, **63**, 315–327 (1990).
- [66] S. Fujita, *J. Am. Chem. Soc.*, **112**, 3390–3397 (1990).
- [67] S. Fujita, *Polyhedron*, **12**, 95–110 (1993).
- [68] S. Fujita, *J. Math. Chem.*, **50**, 2202–2222 (2012).
- [69] S. Fujita, *J. Math. Chem.*, **50**, 2168–2201 (2012).
- [70] S. Fujita, *Tetrahedron: Asymmetry*, **23**, 623–634 (2012).
- [71] S. Fujita, “Symmetry and Combinatorial Enumeration in Chemistry”, Springer-Verlag, Berlin-Heidelberg (1991).
- [72] S. Fujita, “Diagrammatical Approach to Molecular Symmetry and Enumeration of Stereoisomers”, University of Kragujevac, Faculty of Science, Kragujevac (2007).
- [73] S. Fujita, *Bull. Chem. Soc. Jpn.*, **84**, 1192–1207 (2011).
- [74] S. Fujita, *Bull. Chem. Soc. Jpn.*, **85**, 793–810 (2012).
- [75] S. Fujita, *Bull. Chem. Soc. Jpn.*, **85**, 811–821 (2012).
- [76] S. Fujita, *Theor. Chem. Acc.*, **113**, 73–79 (2005).
- [77] S. Fujita, *Theor. Chem. Acc.*, **113**, 80–86 (2005),
- [78] S. Fujita, *Theor. Chem. Acc.*, **115**, 37–53 (2006).
- [79] S. Fujita, *Theor. Chem. Acc.*, **117**, 353–370 (2007).
- [80] S. Fujita, *Theor. Chim. Acta*, **91**, 315–332 (1995).
- [81] S. Fujita, *Theor. Chem. Acc.*, **99**, 224–230 (1998).
- [82] S. Fujita, *J. Math. Chem.*, **42**, 215–263 (2007).
- [83] S. Fujita, *MATCH Commun. Math. Comput. Chem.*, **67**, 5–24 (2012).
- [84] S. Fujita, *MATCH Commun. Math. Comput. Chem.*, **67**, 25–54 (2012).
- [85] S. Fujita, *MATCH Commun. Math. Comput. Chem.*, **67**, 649–668 (2012).
- [86] S. Fujita, *MATCH Commun. Math. Comput. Chem.*, **67**, 669–686 (2012).
- [87] S. Fujita, *MATCH Commun. Math. Comput. Chem.*, **67**, 687–712 (2012).

- [88] S. Fujita, *Croat. Chem. Acta*, **79**, 411–427 (2006).
- [89] S. Fujita, *Bull. Chem. Soc. Jpn.*, **83**, 1–18 (2010).
- [90] S. Fujita, *Theor. Chem. Acc.*, **117**, 339–351 (2007).
- [91] S. Fujita, *MATCH Commun. Math. Comput. Chem.*, **57**, 265–298 (2007).
- [92] S. Fujita, *MATCH Commun. Math. Comput. Chem.*, **57**, 299–340 (2007).
- [93] S. Fujita, *J. Org. Chem.*, **69**, 3158–3165 (2004).
- [94] S. Fujita, *J. Math. Chem.*, **35**, 265–287 (2004).
- [95] S. Fujita, *Tetrahedron*, **60**, 11629–11638 (2004).
- [96] S. Fujita, *MATCH Commun. Math. Comput. Chem.*, **54**, 39–52 (2005).
- [97] S. Fujita, *MATCH Commun. Math. Comput. Chem.*, **52**, 3–18 (2004).
- [98] S. Fujita, *Memoirs of the Faculty of Engineering and Design, Kyoto Institute of Technology*, **53**, 19–38 (2005).
- [99] S. Fujita, *J. Chem. Inf. Comput. Sci.*, **44**, 1719–1726 (2004).
- [100] S. Fujita, *MATCH Commun. Math. Comput. Chem.*, **53**, 147–159 (2005).
- [101] S. Fujita, *J. Math. Chem.*, **50**, 1791–1814 (2012).
- [102] S. Fujita, *J. Math. Chem.*, **50**, 1815–1860 (2012).
- [103] S. Fujita, *MATCH Commun. Math. Comput. Chem.*, **71**, 511–536 (2014).
- [104] S. Fujita, *MATCH Commun. Math. Comput. Chem.*, **71**, 537–574 (2014).
- [105] S. Fujita, *MATCH Commun. Math. Comput. Chem.*, **71**, 575–608 (2014).
- [106] S. Fujita, *Tetrahedron*, **65**, 1581–1592 (2009).
- [107] S. Fujita, *J. Math. Chem.*, **49**, 95–162 (2011).
- [108] S. Fujita, *J. Math. Chem.*, **52**, 1514–1534 (2014).
- [109] S. Fujita, *MATCH Commun. Math. Comput. Chem.*, **61**, 11–38 (2009).
- [110] S. Fujita, *J. Comput. Aided Chem.*, **10**, 16–29 (2009).
- [111] S. Fujita, *Tetrahedron: Asymmetry*, **25**, 1169–1189 (2014).
- [112] S. Fujita, *Tetrahedron*, **62**, 691–705 (2006).
- [113] S. Fujita, *MATCH Commun. Math. Comput. Chem.*, **61**, 39–70 (2009).
- [114] S. Fujita, *J. Comput. Aided Chem.*, **10**, 76–95 (2009).
- [115] S. Fujita, *Tetrahedron: Asymmetry*, **25**, 1190–1204 (2014).
- [116] S. Fujita, Prochirality and Pro-*RS*-Stereogenicity. Stereoisogram Approach Free from the Conventional “Prochirality” and “Prostereogenicity”, in “Carbon Bonding and Structures. Advances in Physics and Chemistry”, ed. by M. V. Putz, Springer-Verlag, Dordrecht Heidelberg London (2011), Vol. 5 of Carbon Materials: Chemistry and Physics, Chapter 10, pp 227–271.

- [117] S. Fujita, *Yuki Gosei Kagaku Kyokai-Shi/J. Synth. Org. Chem. Jpn.*, **66**, 995–1004 (2008).
- [118] S. Fujita, *MATCH Commun. Math. Comput. Chem.*, **63**, 3–24 (2010).
- [119] S. Fujita, *MATCH Commun. Math. Comput. Chem.*, **63**, 25–66 (2010).
- [120] S. Fujita, *J. Math. Chem.*, **47**, 145–166 (2010).
- [121] S. Fujita, *MATCH Commun. Math. Comput. Chem.*, **58**, 611–634 (2007).
- [122] S. Fujita, *MATCH Commun. Math. Comput. Chem.*, **61**, 71–115 (2009).
- [123] S. Fujita, *J. Math. Chem.*, **52**, 508–542 (2014).
- [124] S. Fujita, *J. Math. Chem.*, **52**, 543–574 (2014).
- [125] S. Fujita, *J. Math. Chem.*, **52**, 1717–1750 (2014).
- [126] S. Fujita, *J. Math. Chem.*, **52**, 1751–1793 (2014).
- [127] S. Fujita, *Tetrahedron: Asymmetry*, **25**, 1153–1168 (2014).

2 Classification of Isomers¹

2.1 Equivalence Relationships of Various Levels of Isomerism

The methodology of modern stereochemistry has an unconscious tendency to make light of equivalence relationships and to emphasize inequivalence relationships too much. For the purpose of realizing problematic situations in isomerism and stereoisomerism, it is important to examine whether a relationship specifies equivalence or inequivalence.

2.1.1 Equivalence Relationships and Equivalence Classes

The misleading features of Figs. 1.12(a) and (b) (page 17) as well as the lack of equivalence classes (orbits) for Fig. 1.13 (page 18) will be discussed detailedly in this subsection after the introduction of equivalence relationships and equivalence classes.

Let us consider a set of elements (or objects):

$$\mathbf{X} = \{\dots, a, \dots, b, \dots, c, \dots\}, \quad (2.1)$$

where the finite number of elements (a, b, c , etc.) are identified under a first given criterion. Chemically speaking, for example, the elements a, b, c , etc. are molecular entities, each of which is characterized by a 3D structure as such a first given criterion. For the simplicity's sake, the set \mathbf{X} (Eq. 2.1) is presumed to exhibit no redundancy, so that it contains no duplication under the first given criterion.² Suppose that they are classified by another given criterion, which is called here *an equivalence relationship*.

According to Def. 4.2 of Ref.[1], an equivalence relationship and an equivalence class are defined as follows:

Definition 2.1 (Equivalence Relationship). Suppose that a relationship \sim defined between arbitrary two elements (a and b) of a given set \mathbf{X} satisfies either of two cases, i.e., $a \sim b$ or $a \not\sim b$. If the relationship satisfies (1) $a \sim a$ (reflective); (2) $a \sim b$ then $b \sim a$ (symmetric); and (3) $a \sim b, b \sim c$, then $b \sim c$ (transitive), then this relationship is called an *equivalence relationship*.

Definition 2.2 (Equivalence Classes and Partition). By collecting elements equivalent under the equivalence relationship (Def. 2.1), we can construct a subset of \mathbf{X} , which is called an *equivalence class*. The set \mathbf{X} is classified into equivalence classes under the equivalence relationship (Def. 2.1). This classification is called a *partition* in terms of the equivalence relationship (Def. 2.1).

¹ This chapter is based on S. Fujita, "Misleading Classification of Isomers and Stereoisomers in Organic Chemistry", *Bull. Chem. Soc.*, **87**, 1367–1378 (2014).

² Two elements (objects) of \mathbf{X} (Eq. 2.1) may be homomeric. Note that a homomeric relationship depends on proper rotations belonging to a chiral point group (cf. Remark 2.2).

Chemically speaking, an equivalence relationship defined by Def. 2.1 aims at the classification of molecular entities (as elements of \mathbf{X}), so that the resulting partition concerning equivalence classes (Def. 2.2) is interpreted to be the taxonomy of molecular entities under the equivalence relationship. The reflective nature $a \sim a$ for Def. 2.1 permits a single membership of an equivalence class.

An equivalence class is often called *an orbit*, which is distinct from the chemical term *orbital*. Note that the term *orbital* is an abbreviation of the term *orbital function*, which is used in quantum chemistry. In this book, the term *orbit* is mainly used to refer to an equivalence class of (pro)ligands.

Suppose that the equivalence relationship of Def. 2.1 is applied to the set of Eq. 2.1 to give the following partition:

$$\{\{a b c \dots\} \quad \{a' b' c' \dots\} \quad \dots\}, \quad (2.2)$$

where the set $\{a b c \dots\}$ is an equivalence class, while the other set $\{a' b' c' \dots\}$ is another equivalence class. The two equivalence classes are *inequivalent* to each other under the equivalence relationship of Def. 2.1.

2.1.2 Enantiomers, Stereoisomers, and Isomers

Enantiomeric Relationships as Equivalence Relationships

The conventional definition of an enantiomeric relationship (C-Def. E1 on page 10 in Section 1.3) is incapable of generating an equivalence relationship. As a result, for example, the application of C-Def. E1 to the butanols listed in Fig. 1.5 (page 7) results in Eq. 1.9 (page 10), in which each achiral molecular entity is not detected as an equivalence class. To avoid this fault, the following definition is devised according to Def. 2.1:

Definition 2.3 (Enantiomeric Relationship, Chirality/Achirality). The relationship between an object³ and its mirror image is called an *enantiomeric* relationship, where the object and the mirror image may be superimposable on each other. If they are not superimposable on each other, they are referred to as being *chiral*, so as to generate a pair of *enantiomers* as a two-membered equivalence class. If they are superimposable on each other, they are in a *self-enantiomeric* relationship, so as to generate a single *achiral* object as a one-membered equivalence class.

The term *object* is a molecular entity, if Def. 2.3 is used in chemistry. The term *molecular entity* is used to refer to a molecule or a related object such as a ligand.

Because Def. 2.3 defines an enantiomeric relationship as an equivalence relationship, an achiral molecular entity as a one-membered equivalence class can be discussed in the same level as a pair of enantiomeric molecular entities, which is regarded as a two-membered equivalence class.

³ The term *object* is used here in place of the mathematical term *element* in Eq. 2.1, because the latter is frequently used to denote a chemical element (H, He, etc.).

Rule 2.1 (Terminology on Enantiomeric Relationships). Note that Def. 2.3 permits a self-enantiomeric case to designate an achiral molecular entity. To avoid confusion, the relationship due to Def. 2.3 is referred to as being (*self-*)*enantiomeric*, if necessary. The plural form *enantiomers* may be used to refer to a pair of chiral objects which are enantiomeric. The singular form *enantiomer* may be used to refer to one of a pair of enantiomers, if the other of the pair is obvious [2].

The application of Def. 2.3 to the butanols listed in Fig. 1.5 (page 7) results in the following partition:

$$\left([1-16] \quad [1-17 \quad \overline{1-17}] \quad [1-18] \quad [1-19] \right), \quad (2.3)$$

where a pair of square brackets consists of a pair of (self-)enantiomers. Thus, there appear three one-membered equivalence classes (i.e., three achiral molecular entities) and one two-membered equivalence class (a pair of enantiomers). These are inequivalent under an enantiomeric relationship (Def. 2.3), as counted to be equal to 4. This partition is identical with Eq. 1.10 (page 20).

The application of Def. 2.3 to a set of isomeric 2,3,4-trihydroxyglutaric acids shown in Fig. 2.1 generates the following partition:

$$\left([2-1] \quad [2-2] \quad [2-3 \quad \overline{2-3}] \right). \quad (2.4)$$

Thus, there appear two one-membered equivalence classes and one two-membered equivalence class, where each equivalence class is surrounded by a pair of square brackets. Each of the one-membered equivalence classes corresponds to an achiral molecule [2-1] or [2-2], while the two-membered equivalence class corresponds to a pair of enantiomers [2-3 $\overline{2-3}$].

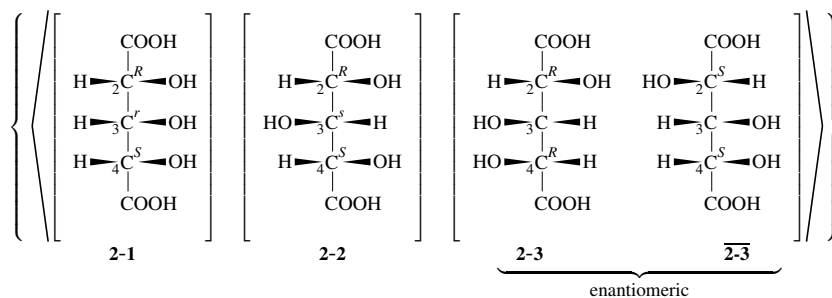


Fig. 2.1. Classification of Isomeric 2,3,4-trihydroxyglutaric acids into two achiral isomers and one pair of enantiomers. A pair of square brackets contains a pair of (self-)enantiomers, a pair of angle brackets contains an equivalence class of stereoisomers, and a pair of braces contains an equivalence class of isoskeletomers.

Stereoisomeric Relationships as Equivalence Relationships

The term *constitution* is defined as a criterion for defining a stereoisomeric relationship in accord with the IUPAC Recommendation 1996 [2].

Definition 2.4 (Constitution). The constitution of a molecular entity describes the identification of atoms (as a molecular formula) and their connectivity (and corresponding bond multiplicities) in the molecular entity (omitting any description arising from their spatial arrangement).

In other words, the constitution of a molecular entity can be regarded as a 2D structure (or a graph including bond multiplicities on its edges).

Thereby, a stereoisomeric relationship is defined as producing a set of stereoisomers as an equivalence class.

Definition 2.5 (Stereoisomeric Relationship). The relationship between a molecular entity and a counterpart molecular entity having an identical constitution is called a *stereoisomeric* relationship. The molecular entity and the counterpart may be identical with each other. The multiple application of stereoisomeric relationships produces a distinct set of molecular entities as an equivalence class, the members of which are called *stereoisomers*.

The expression ‘the identical constitution’ means that the molecular formula, the connectivity, and the bond multiplicity are identical according to Def. 2.4 (cf. Def. 2.9) and can be replaced by ‘the identical 2D structure’ or ‘the identical graph’. Compare this definition with the conventional definition (C-Def. S1) described in Subsection 1.2.2 on page 6.

The application of Def. 2.5 to the butanols listed in Fig. 1.5 (page 7) results in the following partition:

$$\left(\langle \mathbf{1-16} \rangle \quad \langle \mathbf{1-17} \quad \overline{\mathbf{1-17}} \rangle \quad \langle \mathbf{1-18} \rangle \quad \langle \mathbf{1-19} \rangle \right), \quad (2.5)$$

where a pair of angle brackets indicates an equivalence class. Thus, there appear three one-membered equivalence classes and one two-membered equivalence classes. Each equivalence class represents a set of stereoisomers. Compare the partition represented by Eq. 2.5 with the partition represented by Eq. 1.4 (page 8) which has been partially divided by means of C-Def. S1.

The application of Def. 2.5 to a set of isomeric 2,3,4-trihydroxyglutaric acids shown in Fig. 2.1 generates the following partition:

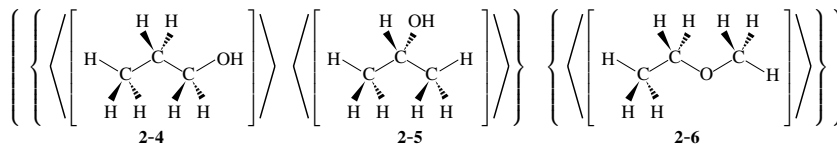
$$\left(\langle \mathbf{2-1} \quad \mathbf{2-2} \quad \mathbf{2-3} \quad \overline{\mathbf{2-3}} \rangle \right), \quad (2.6)$$

where a pair of angle brackets represents an equivalence class of stereoisomers. Thus, all of the 2,3,4-trihydroxyglutaric acids (Fig. 2.1) are classified into a single equivalence class of stereoisomers.

Isomeric Relationships as Equivalence Relationships

A molecule has a definite molecular formula, which serves as a criterion for determining isomeric relationships:

(a) 3D-Based Expressions



(b) 2D-Based Expressions (Graphs)

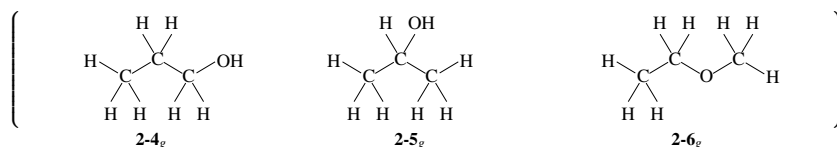


Fig. 2.2. Classification of molecules with the molecular formula C_3H_8O . (a) 3D-based expressions: A pair of square brackets contains a pair of (self)-enantiomers, a pair of angle brackets contains an equivalence class of stereoisomers, a pair of braces contains an equivalence class of isoskeletonomers, and a pair of bold parentheses contains an equivalence class of isomers. (b) 2D-based expressions (graphs).

Definition 2.6 (Isomeric Relationships, Isomers). The term *isomeric relationship* is defined as a relationship between two molecules (or related entities) which have the same molecular formula but are not superimposable as 3D structures. The plural form *isomers* can be used to denote a definite set (equivalence class) of molecules in an isomeric relationship or any set of molecules in an isomeric relationship if a fixed reference molecule is considered.

The expression ‘not superimposable’ means having different 3D structural formulas, structural-chemically speaking; or having different properties, organo-chemically speaking.

It should be noted that Def. 2.6 is capable of avoiding the dual definition (C-Def. II) described in Table 1.1 (page 6).

The definition of an isomeric relationship (Def. 2.6) is an equivalence relationship, so that a one-membered equivalence class is permitted in terms of a self-isomeric relationship. For example, an equivalence class of isomers with the molecular formula CH_4O consists of a single molecule (methanol, (CH_3OH)). On the other hand, an equivalence class of isomers with the molecular formula C_2H_6O consists of ethanol and dimethyl ether, i.e., $(C_2H_5OH \ CH_3OCH_3)$.

As for isomers with the molecular formula C_3H_8O , there appear three isomers listed in Fig. 2.2. The application of Def. 2.6 generates a three-membered equivalence class of isomers:

$$\mathbf{(2-4 \ 2-5 \ 2-6)}, \quad (2.7)$$

where a pair of bold parentheses represents a equivalence class of isomers.

Remark 2.1 (Same or different). The three molecules (2-4, 2-5, and 2-6) listed in Eq. 2.7 should be referred to as being equivalent (same, equal) under an isomeric

relationship (Def. 2.6), although organic chemists tend to lay stress on the difference between them.

2.1.3 Inequivalence Relationships

Diastereomeric Relationships as Inequivalence Relationships

The conventional definition of ‘diastereomeric relationship’ or ‘diastereomer’ (C-Def. D1) described in Subsection 1.3.2 is revised to meet the revised definition of an enantiomeric relationship as an equivalence relationship (Def. 2.3).

Definition 2.7 (Diastereomeric Relationships). The term *diastereomeric relationship* is defined as a relationship between two equivalence classes of (self-)enantiomers, where these two equivalence classes are contained in an equivalence class of stereoisomers and inequivalent under an enantiomeric relationship (Def. 2.3).

The diastereomeric relationship (Def. 2.7) is not an equivalence relationship, so that it is incapable of generating equivalence classes.

For example, the successive applications of Def. 2.5 (a stereoisomeric relationship) and Def. 2.3 (an enantiomeric relationship) result in the combination of Eq. 2.6 with Eq. 2.4 as follows:

$$\left(\langle [2-1] \quad [2-2] \quad [2-3 \quad \overline{2-3}] \rangle \right), \quad (2.8)$$

which shows that three pairs of (self-)enantiomers construct an equivalence class of stereoisomers. Note that any two pairs of (self-)enantiomers in Eq. 2.8 are in a diastereomeric relationship according to Def. 2.7. Hence, a diastereomeric relationship refers to the fact that two pairs of (self-)enantiomers in Eq. 2.8 are inequivalent under the action of an enantiomeric relationship (but equivalent under the action of a stereoisomeric relationship).

Constitutionally-Anisomeric Relationships as Inequivalence Relationships

The conventional definition of ‘constitutionally-isomeric relationship’ or ‘constitutional isomer’ (C-Def. C1) described in Subsection 1.2.2 is revised to meet the revised definition of a stereoisomeric relationship as an equivalence relationship (Def. 2.5). The term *constitutionally-anisomeric relationship* is coined because it is an inequivalence relationship.

Definition 2.8 (Constitutionally-anisomeric Relationships). The term *constitutionally-anisomeric relationship* is defined as a relationship between two equivalence classes of stereoisomers, where these two equivalence classes are contained in an equivalence class of isomers and inequivalent under a stereoisomeric relationship (Def. 2.5).

The constitutionally-anisomeric relationship (Def. 2.8) is not an equivalence relationship, so that it is incapable of generating equivalence classes.

The isomers listed in Fig. 2.2 (with the molecular formula C_3H_8O) is determined to generate an equivalence class shown in Eq. 2.7 under an isomeric relationship (Def. 2.6). By applying a further application of a stereoisomeric relationship (Def. 2.5), the set represented by Eq. 2.7 is divided to give the following partition:

$$\left(\langle \mathbf{2-4} \rangle \langle \mathbf{2-5} \rangle \langle \mathbf{2-6} \rangle \right), \quad (2.9)$$

where a pair of angle brackets represents an equivalence class of stereoisomers. Two equivalence classes of stereoisomers (e.g., $\langle \mathbf{2-4} \rangle$ and $\langle \mathbf{2-5} \rangle$) are constitutionally-anisomeric to each other according to Def. 2.8.

By applying a further application of an enantiomeric relationship (Def. 2.3), the set represented by Eq. 2.9 is divided to give the following partition:

$$\left(\langle \langle \mathbf{2-4} \rangle \rangle \langle \langle \mathbf{2-5} \rangle \rangle \langle \langle \mathbf{2-6} \rangle \rangle \right), \quad (2.10)$$

where a pair of square brackets represents an equivalence class of (self-)enantiomers.

Constitutionally-Isomeric Relationships as a 2D-Based Concept

By starting from the term *constitution* (Def. 2.4), the term ‘constitutional isomerism’ is defined in IUPAC Recommendations 1996 [2] (cf. C-Def. C1 in Subsection 1.2.2). This term is adopted for the sake of convenience, although it is a 2D-based concept.

Definition 2.9 (Constitutional Isomerism as a 2D-based Concept [2]). *Constitutional isomerism* is defined as isomerism between structures differing in constitution and described by different line formula, e.g. CH_3OCH_3 and CH_3CH_2OH .

This definition means that a constitutionally-isomeric relationship (i.e., constitutional isomerism) is based on the examination of graphs (2D-structural formulas after omitting any description arising from their spatial arrangement), as discussed in Subsection 1.2.2. As a result, ‘constitutional isomers’ are defined as compounds that have the same molecular formula but different graphs (constitutions or 2D structures). In other words, the meaning of ‘isomeric’ in the term ‘constitutionally-isomeric’ (Def. 2.9) depends on Def. 2.6. See Table 1.1 (page 6). In contrast, the meaning of ‘anisomeric’ in the term ‘constitutionally-anisomeric’ (Def. 2.8) depends on Def. 2.5.

Exercise 2.1. Discuss the difference between the term *constitutionally-anisomeric* (Def. 2.8) and the term *constitutionally-isomeric* (Def. 2.9). See Subsection 2.1.5.

For example, the isomers listed in Fig. 2.2 (with the molecular formula C_3H_8O) is determined to be a set of graphs:

$$\left(\mathbf{2-4}_g \mathbf{2-5}_g \mathbf{2-6}_g \right), \quad (2.11)$$

where each symbol represents a graph corresponding to the 3D structure listed in Fig. 2.2. The set of graphs (Eq. 2.11) corresponds to the set of equivalence classes of stereoisomers

(Eq. 2.9) in a one-to-one fashion: $2-4_g \rightarrow \langle 2-4 \rangle$, $2-5_g \rightarrow \langle 2-5 \rangle$, and $2-6_g \rightarrow \langle 2-6 \rangle$. Such a one-to-one correspondence (bijection) between a set of constitutional isomers (due to Def. 2.9) and an equivalence class of stereoisomers (due to Def. 2.5) holds true in general.

Theorem 2.1. A set of constitutional isomers due to Def. 2.9 corresponds to a set of equivalence classes of stereoisomers due to Def. 2.5 in a one-to-one fashion.

The conventional definition of an isomeric relationship exhibits dual nature as summarized in Table 1.1 (page 6). This conventional definition of an isomeric relationship can be replaced by Def. 2.6 (an isomeric relationship) because of Theorem 2.1, where the conventional 2D-based definition (Def. 2.9) is successfully linked to the present 3D-based definition of a stereoisomeric relationship (Def. 2.5). Thereby, the dual nature (Table 1.1) is avoided rationally. Note that such an equivalence class of stereoisomers is based on 3D structures, where both Def. 2.5 (a stereoisomeric relationship) and Def. 2.6 (an isomeric relationship) are based on 3D structures.



Exercise 2.2.

- Confirm Theorem 2.1 by using a set of stereoisomers shown in Fig. 2.1 (**2-1**, **2-2**, **2-3**, and **2-3**). See Eq. 2.6.
- Confirm Theorem 2.1 by using the butanols listed in Fig. 1.5 on page 7 (**1-16**, **1-17**, **1-17**, **1-18**, and **1-19**). See Eq. 2.5.

2.1.4 Isoskeletonomers as a Missing Link for Consistent Terminology

As discussed in Subsection 1.2.3, ‘positional isomers’ are regarded as a kind of constitutional isomers (Def. 2.9). This means that the term ‘positional isomers’ expresses a 2D-based concept. To avoid the dual features summarized in Table 1.1 and to develop consistent terminology, the 2D-based term ‘positional isomers’ should be replaced by a more promising term of 3D basis.

A hint for carrying out the mission described in the preceding paragraph is hidden in the history of organic structural chemistry [3,4]. Kekulé [5] discussed the usage of ‘rational formulas’, which correspond to C_2H_5OH , $C_2H_5NH_2$, etc. in the modern mode of representations. These ‘rational formulas’ represent types of compounds, where C_2H_5OH stems from the linkage between a unit C_2H_5 and another unit OH. Thus, the rational formulas originally aimed at the taxonomy of organic compounds, which has been later accomplished by more informative formulas, i.e., 2D-structural formulas, although they are still used under the name *condensed structural formulas*. Now, the taxonomy of organic compounds is represented by linking 2D-structural formulas with compound types (e.g., alkanols and alkylamines), where the linkage has overwhelmed the usage of rational formulas. However, the methodology based on the usage of rational formula has survived even under the link-

age, because any parts of a 2D-structural formula can be regarded as units represented by a rational formula.

By keeping in mind the history described above, let us consider *o*-, *m*- and *p*-dibromobenzenes (**1-1**, **1-2**, and **1-3**), which have been shown in Fig. 1.1 (page 1) of Section 1.1. They are traditionally called ‘positional isomers’ with no explicit mention of a benzene ring as a common skeleton (see Subsection 1.2.3). By inverting the viewpoint of the term, we lay stress on the benzene skeleton according to the taxonomy of organic chemistry, because the positional isomers are regarded as molecules derived from a benzene skeleton. This inverted viewpoint is extended to more general cases as follows:

Definition 2.10 (Isoskeletomeric relationship, Isoskeletomers). A skeleton is selected as a meaningful substructure of a 3D-structural formula to be examined. An *isoskeletomeric* relationship is defined as a relationship between two molecular entities which contain the same skeleton and have the same molecular formula. An expression *self-isoskeletomeric* is permitted, so that the isoskeletomeric relationship is an equivalence relationship. Then, the resulting molecular entities called *isoskeletomers* construct an equivalence class.

The term *isoskeletomer* is coined on the basis of iso- (Greek: *isos* equal), skeleto- (Greek: *skeletós* withered, dried up) and -mer (Greek: *méros* part). The expression ‘meaningful’ is used to emphasize that such a skeleton can be selected according to the aim of discussions at issue. There are several cases which require two or more related skeletons to categorize isomers.

Exercise 2.3.



- Examine isoskeletomeric relationships of molecules having the molecular formula $C_6H_4Br_2$, where a benzene skeleton, a prismane skeleton, and a Dewar-benzene skeleton are selected as skeletons described in Def. 2.10
- Compare the sets of isoskeletomers with the set of Fig. 1.1 by focusing attention on equivalence classes. Show that the relationship between these sets obey the constitutional isomerism defined by Def. 2.9.
- Confirm stereoisomeric relationships by applying Def. 2.5. Show that the relationship between the resulting sets obey the constitutional isomerism defined by Def. 2.9. For enumeration of prismane derivatives, see [6,7].
- Finally, discuss the misleading features of Fig. 1.12 (page 17).

To differentiate equivalence classes of isoskeletomers, the term *skeletally-anisomeric* is adopted to emphasize the inequivalence under Def. 2.10:

Definition 2.11 (Skeletally-anisomeric relationship). The term *skeletally-anisomeric relationship* is defined as a relationship between two equivalence classes of isoskeletomers, which are inequivalent under an isoskeletomeric relationship (Def. 2.10).

A skeletally-anisomeric relationship is an inequivalent relationship.

The isomers listed in Fig. 2.2 (with the molecular formula C_3H_8O) generates an equivalence class shown in Eq. 2.7 under an isomeric relationship (Def. 2.6). After we select

skeletons to be 3D structures corresponding to $\text{CH}_3\text{CH}_2\text{CH}_3$ and $\text{CH}_3\text{CH}_2\text{OCH}_3$, we apply an isoskeletomeric relationship (Def. 2.10) to the set represented by Eq. 2.7. Thereby the set is divided to give the following partition:

$$\left(\{2-4 \ 2-5\} \ \{2-6\} \right), \quad (2.12)$$

where a pair of braces represents an equivalence class of isoskeletomers under an isoskeletomeric relationship represented by Def. 2.10. The resulting two equivalence classes of isoskeletomers, $\{2-4 \ 2-5\}$ and $\{2-6\}$, are determined to be skeletally-anisomeric according to Def. 2.11.

Successive applications of a stereoisomeric relationship (Def. 2.5) and an enantiomeric relationship (Def. 2.3) convert Eq. 2.12 into the following partition (cf. Eq. 2.9 and Eq. 2.10):

$$\left(\{ \langle [2-4] \rangle \ \langle [2-5] \rangle \} \ \{ \langle [2-6] \rangle \} \right), \quad (2.13)$$

which is depicted in Fig. 2.2(a).

If we select 2D-based skeletons in place of the 3D-base skeletons of Def. 2.10, the set of graphs represented by Eq. 2.11 can be divided into the following set:

$$\left(\{2-4_g \ 2-5_g\} \ \{2-6_g\} \right), \quad (2.14)$$

which is a 2D-based expression for representing ‘positional isomers’ of the conventional terminology. Note that Eq. 2.14 of 2D basis corresponds to Eq. 2.12 of 3D basis.

Thus, the 3D-structural formula to be examined may be a graph (a 2D-structural formula) or other formulas (e.g., a rational formula), if the examination has a specific purpose. The 15CI Index Guide, 2004 of Chemical Abstracts [8, Appendix IV-B] collects such skeletons under the name *molecular skeletons*, e.g., methane, 3,6,9,12-tetraoxatetradecane, benzene, pyrrolidine, 9H-fluorene, and bicyclo[2.2.1]hept-2-ene.



Exercise 2.4.

- Examine isoskeletomeric relationships of butanols having the molecular formula $\text{C}_4\text{H}_{10}\text{O}$ (Fig. 1.5 on page 7), where a butane skeleton and a 2-methylpropane skeleton are selected as skeletons described in Def. 2.10.
- Compare this result of 3D basis with the result due to the traditional term ‘positional isomers’ of 2D basis.
- Confirm stereoisomeric relationships by applying Def. 2.5.

The traditional methodology without isoskeletomeric relationships is examined by the following exercise. The comparison between Exercise 2.4 and Exercise 2.5 will clarify the effect of such an intermediate isoskeletomeric relationship.



Exercise 2.5.

- Examine the same problem of Exercise 2.4 without considering the skeletons described above. Thus, enumerate isomers of $C_4H_{10}O$ directly.
- Confirm stereoisomeric relationships by applying Def. 2.5. See Eq. 2.3.

2.1.5 Constitutionally-Anisomeric Relationships vs. Constitutionally-Isomeric Relationships

It is worthwhile to compare the term *constitutionally-anisomeric* of 3D basis (Def. 2.8) with the term *constitutionally-isomeric* of 2D basis (Def. 2.9) by using illustrative examples.

Let us examine dichloroethylenes with the molecular formula $C_2H_2Cl_2$ (Fig. 2.3) by selecting an ethylene skeleton. According to Def. 2.10, the set of isoskeletonomers:

$$\{\mathbf{2-7} \ \mathbf{2-8} \ \mathbf{2-9}\} \quad (2.15)$$

is obtained as an equivalence class. Then, Def. 2.5 is applied to the set of isoskeletonomers (Eq. 2.15). Thereby, the set is subdivided into two sets, i.e., a two-membered set of stereoisomers $\langle \mathbf{2-7} \ \mathbf{2-8} \rangle$ and a one-membered set $\langle \mathbf{2-9} \rangle$, each of which is an equivalence class, because it has an identical graph (an identical constitution):

$$\{\langle \mathbf{2-7} \ \mathbf{2-8} \rangle \ \langle \mathbf{2-9} \rangle\}. \quad (2.16)$$

The relationship between **2-7** and **2-8** in the equivalence class $\langle \mathbf{2-7}, \mathbf{2-8} \rangle$ is determined to be stereoisomeric, more specifically, *cis/trans*-isomeric or ‘diastereomeric’.

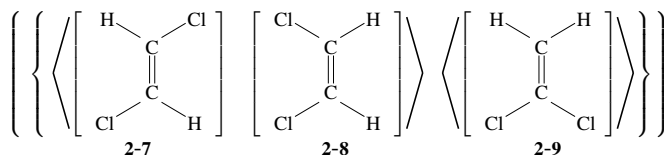


Fig. 2.3. Isoskeletonomers of dichloroethylene. They are subdivided into two sets of stereoisomers. A pair of square brackets contains a pair of (self)-enantiomers, a pair of angle brackets contains an equivalence class of stereoisomers, a pair of braces contains an equivalence class of isoskeletonomers, and a pair of bold parentheses contains an equivalence class of isomers.

From a 3D-based viewpoint, Eq. 2.16 of 3D basis indicates that the set $\langle \mathbf{2-7} \ \mathbf{2-8} \rangle$ and the set $\langle \mathbf{2-9} \rangle$ are inequivalent to each other under the stereoisomeric relationship defined by Def. 2.5. In other words, the two sets as equivalence classes of stereoisomers are constitutionally-anisomeric to each other according to Def. 2.8.

In contrast, from a 2D-based viewpoint, the set $\langle \mathbf{2-7} \ \mathbf{2-8} \rangle$ degenerates into a single graph $\mathbf{2-7}_g$, which corresponds to a constitution represented by $C(HCl)=CHCl$. Hence, Fig. 2.3 is rerepresented by the following 2D-based set:

$$\{\mathbf{2-7}_g \ \mathbf{2-9}_g\}, \quad (2.17)$$

which is regarded as a set of constitutional isomers according to Def. 2.9. The two graphs $\mathbf{2-7}_g$ and $\mathbf{2-9}_g$ are constitutionally-isomeric, where the term *constitutionally-isomeric* is a 2D-based concept. Note that Eq. 2.16 of 3D basis corresponds to Eq. 2.17 of 2D basis in a one-to-one fashion.



Exercise 2.6.

- Examine isoskeletomeric relationships of molecules having the molecular formula C_4H_8 , where butene skeletons, a cyclopropane skeleton, and a cyclobutane skeleton are selected as skeletons described in Def. 2.10.
- Compare the sets of isoskeletomers by focusing attention on equivalence classes. Apply a skeletally-anisomeric relationship defined by Def. 2.11.
- Confirm stereoisomeric relationships by applying Def. 2.5. Apply Def. 2.8 and discuss constitutionally-anisomeric relationships.
- Discuss constitutional isomerism as a 2D-based concept (Def. 2.9).
- Discuss the misleading features of Fig. 1.12 (page 17).

2.2 Revised Flowchart for Categorizing Isomers

2.2.1 Design of a Revised Flowchart for Categorizing Isomers

As discussed in Chapter 1, such wide-spread flowcharts as Fig. 1.12 (page 17) and Fig. 1.13 (page 18) more or less suffer from the arbitrary switching between 2D-based and 3D-based concepts (cf. Subsection 1.1.3 and Remark 1.2 on page 19). To avoid the mixing of 2D- and 3D-based concepts, a flowchart to be designed should be throughout based on 3D-based concepts, because all molecular entities have 3D structures.

A revised flowchart for categorizing isomers and stereoisomers (Fig. 2.4) is obtained by emphasizing the following items [9]:

- the explicit consideration to equivalence relationships, which generate equivalence classes.
- the intermediacy of an isoskeletomeric relationship as an equivalence relationship, which generates a set of isoskeletomers as an equivalence class.

The respective judgements of the revised flowchart (Fig. 2.4) adopt equivalence relationships defined in the preceding section, i.e., an isomeric relationship (Def. 2.6), an isoskeletomeric relationship (Def. 2.10), a stereoisomeric relationship (Def. 2.5), and an

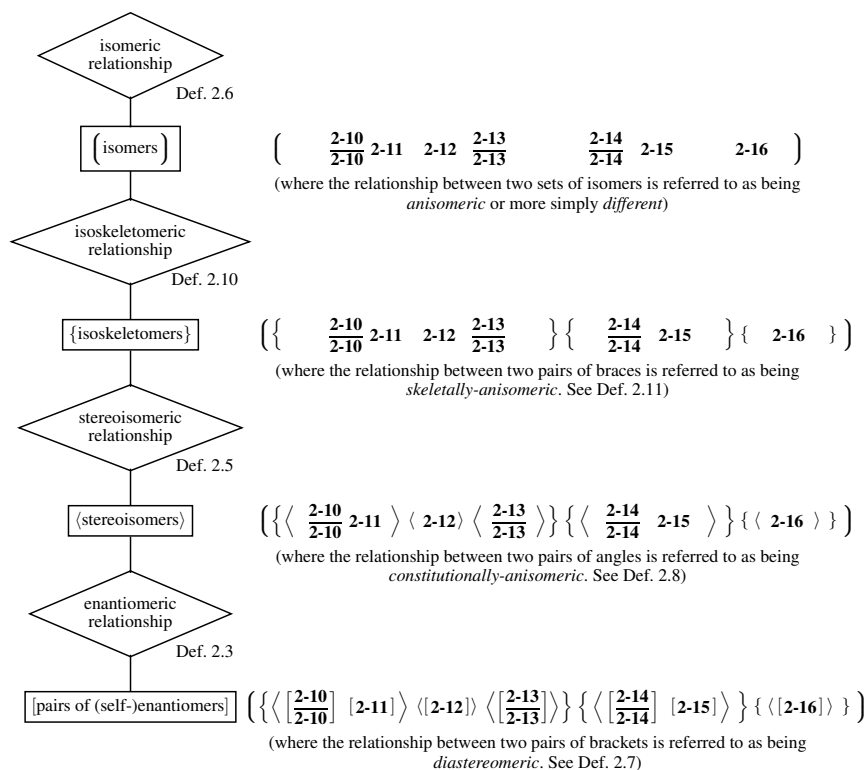


Fig. 2.4. Flowchart for classifying various kinds of isomers on the basis of equivalence classes. A pair of bold parentheses represents isomers as an equivalence class under an isomeric relationship (Def. 2.6). A pair of braces represents isoskeletalomers as an equivalence class under an isoskeletalomeric relationship (Def. 2.10), a pair of angle brackets represents stereoisomers as an equivalence class under a stereoisomeric relationship (Def. 2.5), and a pair of square brackets represents (self)-enantiomers as an equivalence class under an enantiomeric relationship (Def. 2.3).

enantiomeric relationship (Def. 2.3) in a successive fashion. The resulting equivalence classes in each level are differentiated by an inequivalence relationship, i.e., an anisomeric relationship, a skeletally-anisomeric relationship (Def. 2.11), a constitutionally-anisomeric relationship (Def. 2.8), or a diastereomeric relationship (Def. 2.7).

It should be noted that all of the terms adopted in Fig. 2.4 are 3D-based concepts. Such 2D-based terms as ‘constitutionally-isomeric’ (Def. 2.9) and ‘positionally isomeric’ (C-Def. P1 in Subsection 1.2.3) are not adopted in Fig. 2.4. Thus, the term ‘constitutionally-isomeric’ of 2D basis is related to the term *constitutionally-anisomeric* of 3D basis and the term ‘positionally isomeric’ of 2D basis is related to the term *skeletally-anisomeric* of 3D basis.

2.2.2 Illustrative Examples

Let us examine the effects of the flowchart of Fig. 2.4 by using the set of cyclic ethers collected in Fig. 2.5. Successive subdivisions produced by applying the respective equivalence relationships to the set shown in Fig. 2.5 are illustrated in the right column of Fig. 2.4.

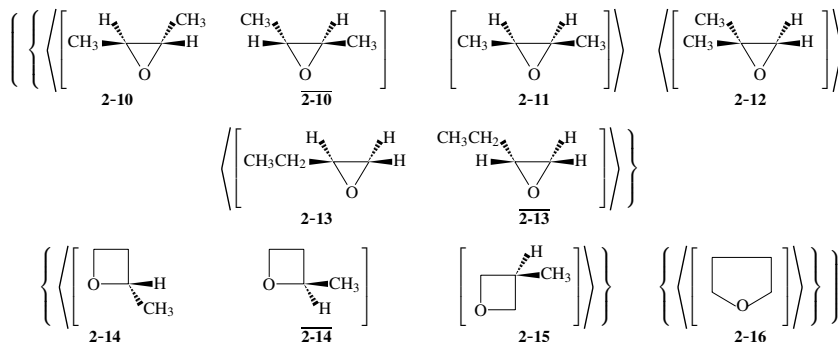


Fig. 2.5. Cyclic ethers with the molecular formula C_4H_8O . A pair of square brackets contains a pair of (self)-enantiomers, a pair of angle brackets contains an equivalence class of stereoisomers, and a pair of braces contains an equivalence class of isoskeletons.

The cyclic ethers **2-10–2-16** have the same molecular formula C_4H_8O . It follows that they are isomeric by applying Def. 2.6, so as to generate an equivalence class as surrounded by a pair of bold parentheses $\{\dots\}$. Each pair of isomers selected from the set of isomers as an equivalence class is referred to as being *isomeric*. The relationship between the set of isomers having C_4H_8O and another set of isomers having the other molecular formula is referred to being *anisomeric* or simply being *different* to each other.

An isoskeletal relationship (Def. 2.10) is applied to the set of isomers having the same molecular formula C_4H_8O , where an oxirane skeleton, an oxetane skeleton, and a tetrahydrofuran skeleton are successively selected as skeletons for Def. 2.10. Thereby, the set of isomers is subdivided into sets of isoskeletons, each set of which is surrounded by a pair of braces $\{\dots\}$. That is to say, a set of oxiranes $\{2-10, \overline{2-10}, 2-11, 2-12, 2-13, \text{ and } \overline{2-13}\}$, a set of oxetanes $\{2-14, \overline{2-14}, \text{ and } 2-15\}$, and a one-membered set of tetrahydrofuran $\{2-16\}$ are equivalence classes under Def. 2.10.

Two molecules selected from each set (e.g., **2-10** and **2-11** from the set of oxiranes) is referred to as being isoskeletal. The relationship between a set surrounded by a pair of braces (e.g., the set of oxiranes) and another set surrounded by a pair of braces (e.g., the set of oxetanes) are referred to as being *skeletally-anisomeric*.

A stereoisomeric relationship (Def. 2.5) is applied to each of the resulting sets of isoskeletons. Thereby each set surrounded by a pair of braces is subdivided into sets

of stereoisomers, each set of which is surrounded by a pair of angle brackets $\langle \dots \rangle$. For example, the set represented by $\langle \mathbf{2-10} \overline{\mathbf{2-10}} \mathbf{2-11} \rangle$ is an equivalence class of stereoisomers.

Two molecules selected from each set (e.g., $\mathbf{2-10}$ and $\mathbf{2-11}$) is referred to as being stereoisomeric. The relationship between a set surrounded by a pair of angle brackets (e.g., $\langle \mathbf{2-10} \overline{\mathbf{2-10}} \mathbf{2-11} \rangle$) and another set surrounded by a pair of angle brackets (e.g., $\langle \mathbf{2-12} \rangle$) is referred to as being *constitutionally-anisomeric*.

An enantiomeric relationship (Def. 2.3) is applied to each of the resulting sets of stereoisomers. Thereby each set surrounded by a pair of angle brackets is subdivided into sets of (self-)enantiomers, each set of which is surrounded by a pair of square brackets $[\dots]$. Two molecules selected from each set is referred to as being enantiomeric (e.g., $\mathbf{2-10}$ and $\overline{\mathbf{2-10}}$ from the set $[\mathbf{2-10} \overline{\mathbf{2-10}}]$). If the set is one-membered (e.g., $[\mathbf{2-11}]$), it is referred to as being self-enantiomeric (or achiral). The relationship between a set surrounded by a pair of square brackets (e.g., $[\mathbf{2-10} \overline{\mathbf{2-10}}]$) and another set surrounded by a pair of square brackets (e.g., $[\mathbf{2-11}]$) is referred to as being *diastereomeric*, even if these sets are chiral or achiral.

The resulting categories are illustrated in Fig. 2.5, where a pair of square brackets $[\dots]$ contains a pair of (self-)enantiomers, a pair of angle brackets $\langle \dots \rangle$ contains an equivalence class of stereoisomers, and a pair of braces $\{ \dots \}$ contains an equivalence class of isoskeletoomers.

Exercise 2.7. Consider acyclic compounds of the molecular formula C_4H_8O : a ketone ($CH_3CH_2COCH_3$), an aldehyde ($CH_3CH_2CH_2CHO$), and alcohols ($CH_2=CHCH(OH)CH_3$, $CH_3CH=CHCH_2OH$, and $CH_3CH=CHCH_2OH$). After they are added to the set of molecule collected in Fig. 2.5, categorize the resulting set of isomers in accord with the flowchart of Fig. 2.4.

2.2.3 Restriction of the Domain of Isomerism

The domain of isomerism to be examined by the flowchart of Fig. 2.4 can be restricted appropriately according to the target of our discussions. For example, Exercise 2.7 indicates that we are able to discuss cyclic ethers shown in Fig. 2.5 without considering isomeric acyclic compounds.

As an extreme case, the set of oxiranes may be beforehand selected as a starting set:

$$\{ \mathbf{2-10} \overline{\mathbf{2-10}} \mathbf{2-11} \mathbf{2-12} \mathbf{2-13} \overline{\mathbf{2-13}} \}. \quad (2.18)$$

Thereby, the judgement due to the isoskeletomeric relationship is implicitly accomplished beforehand.

Moreover, the judgement of a stereoisomeric relationship (Def. 2.5) can be omitted if we aim at discussing geometric attributes of stereochemistry. For example, the direct application of an enantiomeric relationship (Def. 2.3) to the set represented by Eq. 2.18

results in the following subdivision:

$$\{ [2-10 \overline{2-10}] [2-11] [2-12] [2-13 \overline{2-13}] \}, \quad (2.19)$$

where each two-membered equivalence class indicates a pair of enantiomers and each one-membered equivalence class indicates an achiral molecule. As a result, the set of Eq. 2.18 contains four (self-)enantiomers, which are categorized into two enantiomeric pairs and two achiral molecules. In other words, the geometric attributes (in particular, the number of (self-)enantiomers) have been specified by Eq. 2.19 without considering stereoisomerism.

The process from Eq. 2.18 to Eq. 2.19 provides us with a manual solution of the following enumeration problem:



Exercise 2.8. Consider an oxirane skeleton substituted by alkyl ligands (CH_3 and CH_3CH_2). How many are there chiral or achiral oxirane derivatives of the molecular formula $\text{C}_4\text{H}_8\text{O}$?

2.2.4 Harmonization of 3D-Based Concepts with 2D-Based Concepts

It is worthwhile to mention again that the 2D-based term ‘constitutionally-isomeric’ (Def. 2.9) corresponds to the 3D-based term *constitutionally-anisomeric* (Def. 2.8), which is correlated to the 3D-based term *stereoisomeric* (Def. 2.5). See Subsection 2.1.5. A 3D-based set of equivalence classes which are inequivalent under the stereoisomeric relationship (Def. 2.5) corresponds to a set of 2D-based set of ‘constitutional isomers’, where each equivalence class of stereoisomers (a 3D-basis concept) corresponds to each ‘constitutional isomer’ (a 2D-based concept) in a one-to-one fashion. The flowchart of Fig. 2.4 is throughout based on the terms of 3D basis, so that it provides us with the following merits for harmonizing 3D-based concepts with 2D-based concepts:

- The duality of the conventional definition of the term ‘isomeric’ (Table 1.1) and the misleading features of Fig. 1.12(a) and (b) (cf. Remark 1.2) are avoided rationally.
- The arbitrary switching between 2D-based and 3D-based concepts, which is inherent to the flowchart of Fig. 1.13 (cf. Remark 1.2), is rationally avoided by the flowchart of Fig. 2.4.

It is convenient to give an appropriate name to a set of equivalence classes of molecules which are inequivalent under an equivalence relationship. This is because the number of such inequivalent orbits of molecules, i.e., the size of such a set, is a target of combinatorial enumeration.

Rule 2.2 (Terminology on *Isomers*).

- A set of *steric isomers*⁴ is defined as a set of molecules inequivalent under a homomeric relationship (due to proper rotations belonging to a chiral point group). For example, each molecule contained in the set represented by Eq. 2.18 has a molecular formula C_4H_8O and constructs a one-membered equivalence class under the chiral point group C_2 . The six molecules are inequivalent to each other under the chiral point group C_2 , so that they are regarded as *steric isomers*. Then we are permitted to say that there are six steric isomers.
- A set of *3D-structural isomers* is defined as a set of equivalence classes which are inequivalent under an enantiomeric relationship (an achiral point group). For example, the molecules with C_4H_8O in Eq. 2.18 are divided into four pairs of (self-)enantiomers as equivalence classes (Eq. 2.19). The four pairs of (self-)enantiomers are inequivalent to each other under an enantiomeric relationship (an achiral point group C_{2v}). They are regarded as *3D-structural isomers*. Then we are permitted to say that there are four 3D-structural isomers.
- A set of *constitutional isomers* is defined as a set of equivalence classes which are inequivalent under a stereoisomeric relationship (cf. Def. 2.9).⁵ For example, the molecules with C_4H_8O in Eq. 2.18 are divided in three sets of stereoisomers:

$$\{ \langle \overline{2-10} \ 2-10 \ 2-11 \rangle \ \langle 2-12 \rangle \ \langle \overline{2-13} \ 2-13 \rangle \} \quad (2.20)$$

under a stereoisomeric relationship. The three sets of stereoisomers (as equivalence classes) are inequivalent to each other under a stereoisomeric relationship. They are regarded as *constitutional isomers*. Then we are permitted to say that there are three constitutional isomers.

A set of *steric isomers*, a set of *3D-structural isomers*, or a set of *constitutional isomers* is concerned with a set of equivalence classes of molecules which have *3D structures* (not 2D structures) and are inequivalent under each equivalence relationship (a homomeric relation-

⁴ In this book, the term *steric isomers* is used in place of the term *configurational isomers*. As defined in [10, Rule E-1.4(b)], “molecules differing in configuration are termed configurational isomers”, where the term *configuration* is concerned with enantiomeric relationships and diastereomeric relationships (containing *cis/trans*-isomerism). In other words, the term *configurational isomers* is based on the preliminary determination of stereoisomers, while the term *steric isomers* (also the term *3D-structural isomers*) is independent of stereoisomers. Note that various definitions have been propounded to differentiate configurations from conformations, as discussed in [10, Appendix 1]. On the other hand, the term *steric isomer* is adopted in this book because of the proligand-promolecule model based on a rigid stereoskeleton, where conformational isomerism is excluded rationally. This book emphasizes the term *absolute configuration* rather than the term of a broader meaning containing *cis/trans*-isomers. In particular, three aspects of absolute configuration will be introduced, where the chiral aspect of absolute configuration (or an enantiomeric relationship) is differentiated from the *RS*-stereogenic aspect of absolute configuration (or an *RS*-diastereomeric relationship).

⁵ Although Def. 2.9 is a 2D-based definition, the present definition is a 3D-based definition. These two definitions correspond to each other in a one-to-one fashion.

ship, an enantiomeric relationship, or a stereoisomeric relationship). It follows that the same set of isomers can be discussed from a viewpoint of steric isomers, 3D-structural isomers, or constitutional isomers.

References

- [1] S. Fujita, “Symmetry and Combinatorial Enumeration in Chemistry”, Springer-Verlag, Berlin-Heidelberg (1991).
- [2] IUPAC Organic Chemistry Division, *Pure Appl. Chem.*, **68**, 2193–2222 (1996).
- [3] O. Shimamura (Chem. Soc. Japan), ed., “Kagaku no Genten 10, Yukikagaku-Kozo-Ron [Classics of Chemistry, Vol. 10, Organic Structural Theory]”, Gakkai Shuppan Center, Tokyo (1976).
- [4] M. P. Crosland, “Historical Studies in the Language of Chemistry”, Dover, Mineola New York (1978).
- [5] F. A. Kekulé, *Liebigs Ann. Chem.*, **106**, 129–159 (1858).
- [6] S. Fujita, *J. Math. Chem.*, **50**, 2202–2222 (2012).
- [7] S. Fujita, *J. Math. Chem.*, **50**, 2168–2201 (2012).
- [8] Chemical Abstracts Service, “15CI Index Guide, 2004”, American Chemical Society, Columbus (2004).
- [9] S. Fujita, *Bull. Chem. Soc. Jpn.*, **87**, 1367–1378 (2014).
- [10] The Commission on the Nomenclature of Organic Chemistry of IUPAC, *Pure and App. Chem.*, **45**, 11–30 (1976).

3 Point-Group Symmetry

3.1 Stereoskeletons and the Proligand-Promolecule Model

3.1.1 Configuration and Conformation

In modern stereochemistry, the structure of a molecular entity is characterized successively as follows:

1. As discussed in Chapter 2, a molecular entity is characterized first by its *constitution* (Def. 2.4 on page 38), which specifies atoms and their connectivity in the form of a 2D structure (a graph).
2. Then, the molecular entity is characterized to be a 3D structure by means of the term *stereoisomer*. Such a 3D structure is characterized by the term *configuration* as a 3D-based concept, which is used to designate the arrangements of atoms of a molecular entity in 3D space without considering differences due to its conformation. The term *configuration* is usually used in the form of *absolute configuration* or *relative configuration*.
3. A rotation around a bond is characterized to be one of dynamic properties of the molecular entity by the term *conformation*. Other dynamic properties such as inversion at nitrogen and valence tautomerism are characterized in additional processes.

If we take account of conformation, the characterization of a molecular entity as a single definite entity would be difficult, because such a molecular entity may have the infinite number of conformers at most.¹ It follows that our discussions of the first stage should be restricted to the domain of thinking that avoids the influence of conformational changes. Then, the influence of conformational changes will be taken into consideration during subsequent stages of discussions. In other words, the steps 1 and 2 described above are the main targets of this book and the step 3 will be later investigated in virtue of the results of the precedent steps 1 and 2.

3.1.2 The Proligand-Promolecule Model

To discuss a molecular entity as a single definite entity having a 3D structure, we adopt the proligand-promolecule model [1]. By starting from the term *ligand*, the term *proligand* is defined as a more abstract term as follows:

Definition 3.1 (Proligand). A *proligand* is an abstract ligand which has chirality or achirality, but no concrete 3D structure.

¹ If a rotation around a single bond is energetically forbidden (e.g., a sterically-hindered biphenyl), such a fixed molecular entity is considered to be a rigid skeleton.

For the sake of convenience, achiral proligands are represented by uppercase letters (A, B, X, Y, etc.), while pairs of proligands with opposite chirality senses are represented by pairs of lowercase letters without and with an overbar (p/\bar{p} , q/\bar{q} , etc.).



Remark 3.1 (Ligands and Proligands). The term *ligand* defined by the IUPAC Nomenclature of Inorganic Chemistry, Recommendations 1990 [2], i.e., “the atoms or groups joined to the central atom in an inorganic coordination entity”, can be easily extended to connote organic compounds, i.e., “the term ‘ligand’ is defined as atoms or groups joined to a given skeleton, which may be an organic or inorganic entity”. The term *proligand* is defined here on the basis of the extended term *ligand*. The word ‘group’ in the expression ‘atom or group’ would bring about confusion because of the wide-spread term *group* of the group theory, although the expression is recommended by the IUPAC Provisional Recommendations 2004 [3, Rule P-91.1.1].

The expression ‘a given skeleton’ in Remark 3.1 is redefined to give a more definite concept by presuming the rigidity of a skeleton as follows:

Definition 3.2 (Stereoskeletons). A *stereoskeleton* (or shortly *skeleton*) is a rigid 3D entity with a finite number of substitution positions.

The resulting stereoskeleton is characterized by a point group.²

The combination of Def. 3.1 with Def. 3.2 gives the following definition of promolecules:

Definition 3.3 (Promolecule). A *promolecule* is a 3D molecular entity in which the substitution positions of a given stereoskeleton (Def. 3.2) are occupied by a set of proligands.

The resulting promolecule is a rigid entity, the symmetry of which can be characterized by a subgroup of the point group of the stereoskeleton at issue.³

For example, let us examine achiral 2,3,4-trihydroxyglutaric acids, the 3D structures of which are depicted in Fig. 3.1 in the form of Fischer-like projections, **3-1** and **3-2**. We focus our attention on the central carbon atom at the 3-position of each molecule, so that a tetrahedral skeleton **3-5** and four ligands are extracted. Among the four ligands, chiral ligands CH(OH)–COOH (labelled ‘R’) and C(OH)H–COOH (labelled ‘S’) are regarded as proligands represented by the lowercase letters p and \bar{p} , while achiral ligands OH and H are regarded as proligands represented by uppercase letters A and B. Finally, these proligands

² The rigidity of a skeleton is not a drawback in further discussions, because the flexibility of a skeleton can be discussed by presuming interconversion among two or more rigid skeletons.

³ The prefix *pro-* of the terms *proligand* and *promolecule* is used in the sense ‘before’, because a proligand is a precursor of a ligand and a promolecule is a precursor of a molecule [4, Chapter 21].

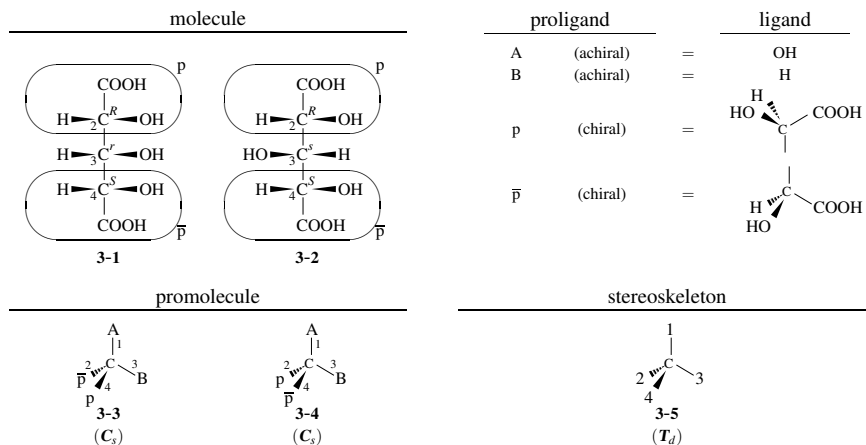


Fig. 3.1. The proligand-promolecule model for 2,3,4-trihydroxyglutaric acids.

are placed on the four positions of the tetrahedral skeleton **3-5** to give promolecules **3-3** and **3-4** according to Def. 3.3.

As found easily, the promolecule **3-3** (or **3-4**) has a mirror plane containing a A—C—B plane, so that it is concluded to be achiral. The achirality of the molecule **3-1** (or **3-2**) remains unchanged in the corresponding promolecule **3-3** (or **3-4**). This result holds true in general so as to give the following theorem of *conservation of chirality/achirality*:

Theorem 3.1 (Conservation of Chirality/Achirality). The chirality/achirality of a given molecule remains unchanged in the corresponding promolecule.

On the other hand, the point-group symmetry of the promolecule **3-3** (or **3-4**) is determined to be C_s , which is a subgroup of T_d of the tetrahedral skeleton **3-5**. This property holds true in general so as to give the following theorem:

Theorem 3.2. The point-group symmetry of a promolecule is a subgroup of the corresponding skeleton from which the promolecule is derived.

On the same line, the point-group symmetry of a molecule is a subgroup of the corresponding skeleton from which the promolecule is derived.

Exercise 3.1.

- Examine the promolecule corresponding to pentaerythritol $C(CH_2OH)_4$, which belongs to the point group D_{2d} .
- Confirm that this molecule is a mismatched molecule discussed below. See [4, Section 21.4].

It should be noted that the point-group symmetry (highest-attainable symmetry) of a molecule is not always the same as that of the corresponding promolecule. Such an excep-

tional case is called a *mismatched molecule* [4, Section 21.4]. Even in such an exceptional case, Theorem 3.1 assures a geometric relationship between a molecule and the corresponding promolecule.

3.2 Point Groups

3.2.1 Symmetry Axes and Symmetry Operations

The geometric symmetry of a molecular entity (molecule, promolecule, ligand, proligand, or others) is characterized by a point group, which consists of symmetry operations (rotations and/or reflections). Each of the operations converts the molecular entity into its homomer (a superposable entity) or its enantiomer (a mirror-image entity), where at least one point is fixed during the conversion.

Rotation Axes and Rotation Operations

One of representative symmetry operations is a rotation operation, which moves a molecular entity by a given degree around an axis so as to give its homomeric molecular entity. The term *homomeric* means that the original molecular entity and the rotated one are identical with each other, where they are superimposable on each other with rotations and without (roto)reflection operations.

For example, suppose that the tetrahedral skeleton **3-5** is rotated by 120° around the C—1 bond (Fig. 3.2). This operation is called a *three-fold rotation*, which is designated by an italic symbol $C_{3(1)}$. The C—1 bond is regarded as a *three-fold (rotation) axis* denoted by a roman-type symbol $C_{3(1)}$. Thereby, the original skeleton **3-5** is converted into the corresponding homomer **3-5'**, as shown in Fig. 3.2.

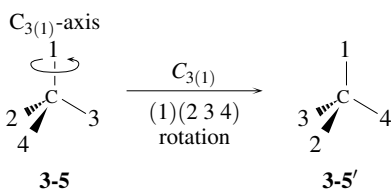


Fig. 3.2. Rotation around a $C_{3(1)}$ -axis along the C—1 bond. A numbered tetrahedral skeleton **3-5** is converted into its homomeric skeleton **3-5'** by a three-fold rotation operation $C_{3(1)}$.

The effect of the rotation $C_{3(1)}$ on the four positions of **3-5** is represented by a permutation, which is interpreted to be a product of cycles as follows:

$$C_{3(1)} \sim \begin{pmatrix} 1 & 2 & 3 & 4 \\ 1 & 3 & 4 & 2 \end{pmatrix} = (1)(2\ 3\ 4), \quad (3.1)$$

where the symbol \sim indicates the correspondence between a symmetry operation and a permutation (a product of cycles). Note that the 1-position is fixed as denoted by a 1-cycle (i.e., (1)), while the other three positions are transformed successively $2 \leftarrow 3 \leftarrow 4 \leftarrow 2$ in a cyclic manner, as denoted by a 3-cycle (i.e., (2 3 4)).

Mirror-Planes for Reflections and Rotoreflection Axes for Rotoreflections

A reflection is an operation which generates the mirror image of an original molecular entity. If the original molecular entity is superposable on the mirror-image, it is concluded to be achiral. Such an achiral molecular entity has a *mirror plane*, which contains fixed points during the reflection at issue.

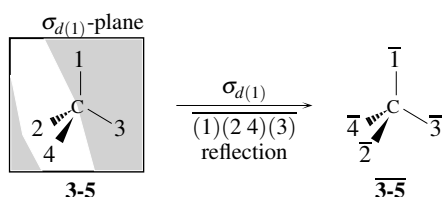


Fig. 3.3. Reflection by a mirror plane for demonstrating chirality/achirality. A numbered tetrahedral skeleton **3-5** is converted into a mirror-numbered skeleton **$\bar{3}\text{-}\bar{5}$** by a reflection operation concerning a mirror plane.

To demonstrate chirality/achirality clearly, we introduce a *mirror-numbered skeleton* (e.g., **$\bar{3}\text{-}\bar{5}$**), which is obtained from a numbered skeleton (e.g., **3-5**) by a reflection operation, as illustrated in Fig. 3.3.

Definition 3.4 (Numbered Skeleton and Mirror-Numbered Skeletons). Suppose that a given skeleton has n substitution positions, which are numbered sequentially from 1 to n . A reflection operation acts on the skeleton to give its mirror image, where each of the n positions is locally reflected in accord with the global reflection of the skeleton. Such a local reflection is represented by a sequential number with an overbar, i.e., $\bar{1}$ to \bar{n} . The resulting mirror image is called a *mirror-numbered skeleton*.

It should be emphasized that a reflection operation causes the formation of a global mirror image as well as local mirror images.

For example, let examine a mirror plane which contains a plane of 1—C—3 (denoted as $\sigma_{d(1)}$ by shadowing) in the tetrahedral skeleton **3-5**. The reflection concerning the mirror plane $\sigma_{d(1)}$ converts **3-5** into the corresponding mirror image **$\bar{3}\text{-}\bar{5}$** , as shown in Fig. 3.3.

According to Def. 3.4, the original tetrahedral skeleton **3-5** with positions numbered from 1 to 4 is converted into its mirror image **$\bar{3}\text{-}\bar{5}$** named a *mirror-numbered skeleton*, which represents the global reflection (i.e., the reflection of the original skeleton with respect to the central carbon atom) as well as the local reflection (i.e., the reflection of each substitution position attached by a number with an overbar ($\bar{1}\text{-}\bar{4}$)).

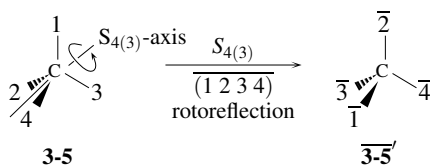


Fig. 3.4. Rotoreflexion around an $S_{4(3)}$ -axis which bisects the 1—C—3 angle. A numbered tetrahedral skeleton **3-5** is converted into its mirror-image skeleton $\overline{3-5'}$ by a four-fold rotoinversion operation $S_{4(3)}$.

The effect of the reflection $\sigma_{d(1)}$ on the four positions of **3-5** is represented by a permutation, which is interpreted to be a product of cycles as follows:

$$\sigma_{d(1)} \sim \left(\begin{array}{cccc} 1 & 2 & 3 & 4 \\ \overline{1} & \overline{4} & \overline{3} & \overline{2} \end{array} \right) = \overline{(1)(2\ 4)(3)}. \quad (3.2)$$

Note that the 1- or 3-position is fixed but its chirality sense is converted into the opposite one, as denoted by a 1-cycle with an overbar (i.e., $\overline{1}$ or $\overline{3}$). On the other hand, the 2- and 4-positions are transformed successively $2 \leftarrow 4 \leftarrow 2$ in a cyclic manner, where their chirality senses are changed, as denoted by a 2-cycle with an overbar (i.e., $\overline{(2\ 4)}$).

A rotoinversion is a combined operation of a rotation around an axis and a reflection about a plane, where there appears the mirror image of an original molecular entity. If the original molecular entity is superposable on the mirror image, it is concluded to be achiral.

For example, let examine an axis bisecting the angle of 1—C—3, which is denoted by the symbol $S_{4(3)}$, as shown in the tetrahedral skeleton **3-5** of Fig. 3.4. The rotation by 90° around the $S_{4(3)}$ -axis and the successive reflection about the mirror plane perpendicular to the $S_{4(3)}$ -axis is collectively called a *four-fold rotoinversion*, which is denoted by the symbol $S_{4(3)}$. The action of $S_{4(3)}$ on the tetrahedral skeleton **3-5** results in the formation of the corresponding mirror image $\overline{3-5'}$ with mirror-numbered positions.

The effect of the rotoinversion $S_{4(3)}$ on the four positions of **3-5** is represented by a permutation, which is interpreted to be a product of cycles as follows:

$$\sigma_{d(1)} \sim \left(\begin{array}{cccc} 1 & 2 & 3 & 4 \\ \overline{2} & \overline{3} & \overline{4} & \overline{1} \end{array} \right) = \overline{(1\ 2\ 3\ 4)}. \quad (3.3)$$

Note that the 1- to 4-positions are transformed successively $1 \leftarrow 2 \leftarrow 3 \leftarrow 4 \leftarrow 1$ in a cyclic manner, where their chirality senses are changed, as denoted by a 4-cycle with an overbar (i.e., $\overline{(1\ 2\ 3\ 4)}$).

In this book, the term *reflection* is used to refer collectively to both the terms *reflection* and *rotoinversion* for the sake of simplicity. The expression (*roto*)*reflection* is used if necessary.

Remark 3.2 (Importance of Mirror-Numbered Skeletons). A mirror-numbered skeleton (Def. 3.4) is important to specify the effect of reflections. If the four positions of a tetrahedral skeleton are controlled by the point group T_d , such a mirror-numbered skeleton is so essential as to be taken into consideration. On the other hand, if the same four positions are controlled by the symmetric group of degree 4 ($S^{[4]}$), such a mirror-numbered skeleton is not taken into consideration, although $S^{[4]}$ is isomorphic to T_d . In this book, $S^{[4]}$ is regarded as being isomorphic to the RS -permutation group $T_{\bar{\sigma}}$, the properties of which will be examined in Chapter 9.

3.2.2 Construction of Point Groups

A set of symmetry operations (rotations and (roto)reflections) can be generated by examining the symmetry elements (rotation axes, mirror planes, and roto-reflection axes).

For example, the tetrahedral skeleton **3-5** has symmetry elements shown in Fig. 3.5 (rotation axes, mirror planes, and roto-reflection axes).

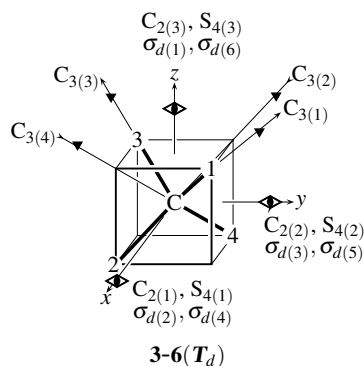


Fig. 3.5. Rotation axes and mirror planes in the tetrahedral skeleton of T_d -symmetry [5].

1. The three-fold rotations $C_{3(i)}$ ($i = 1, 2, 3, 4$) represents a clockwise rotation by 120° around the respective three-fold axes (i.e., $C_{3(i)}$ for $i = 1, 2, 3, 4$) which run from the center to the respective positions (numbered as $i = 1, 2, 3, 4$). Among them, the $C_{3(1)}$ -rotation is explained in Fig. 3.2.
2. A pair of mirror planes ($\sigma_{d(2)}/\sigma_{d(4)}$, $\sigma_{d(3)}/\sigma_{d(5)}$, or $\sigma_{d(1)}/\sigma_{d(6)}$) located at the x - y -, or z -axis represents a perpendicular set of planes containing the respective axis. The six mirror planes exhibit the following features: $\sigma_{d(2)}$ (containing the 3-C-4 plane) and $\sigma_{d(4)}$ (containing the 1-C-2 plane) intersect each other perpendicularly at the x -axis; $\sigma_{d(3)}$ (containing the 2-C-3 plane) and $\sigma_{d(5)}$ (containing the 1-C-4 plane) intersect each

other perpendicularly at the y -axis; and $\sigma_{d(1)}$ (containing the 2-C-4 plane) and $\sigma_{d(6)}$ (containing the 1-C-3 plane) intersect each other perpendicularly at the z -axis. Among them, the $\sigma_{d(1)}$ -plane has been explained in Fig. 3.3

3. The three two-fold axes ($C_{2(1)}$, $C_{2(2)}$, and $C_{2(3)}$) and the three four-fold rotoreflection axes ($S_{4(1)}$, $S_{4(2)}$, and $S_{4(3)}$) run through x -, y -, and z -coordinate axes, respectively. Among them, the $S_{4(3)}$ -axis has been explained in Fig. 3.4.

These symmetry elements (Fig. 3.5) are accompanied by respective symmetry operations, so that there appear 12 rotations and 12 (roto)reflections. The total 24 symmetry operations construct the point group T_d for characterizing the tetrahedral skeleton **3-5**.⁴ The operations of the point group T_d are collected in Table 3.1. The multiplication table of the point group T_d has once been reported [5, Table 2.2].

In similar ways to Eqs. 3.1–3.3, a set of permutations of degree 4 corresponding to respective operations are obtained diagrammatically. The resulting product of cycles is collected in the $T_d(/C_{3v})$ -column of Table 3.1. The set of permutations is alternatively obtained by calculating the coset representation $T_d(/C_{3v})$ algebraically [4]. See Subsection 3.2.5.

3.2.3 Subgroups of a Point Group

A subset of a point group may construct a group, which is called a *subgroup* [4, Chapters 3 and 4]. Among such subgroups, a set of conjugate subgroups is collectively represented by a representative subgroup selected appropriately from the set. For example, the point group T_d is characterized by a set of eleven subgroups up to conjugacy:

$$C_1 = \{I\} \quad (3.4)$$

$$C_2 = \{I, C_{2(1)}\} \quad (3.5)$$

$$C_s = \{I, \sigma_{d(1)}\} \quad (3.6)$$

$$C_3 = \{I, C_{3(1)}, C_{3(1)}^2\} \quad (3.7)$$

$$S_4 = \{I, S_{4(1)}, C_{2(1)}, S_{4(1)}^3\} \quad (3.8)$$

$$D_2 = \{I, C_{2(1)}, C_{2(2)}, C_{2(3)}\} \quad (3.9)$$

$$C_{2v} = \{I, C_{2(3)}, \sigma_{d(1)}, \sigma_{d(6)}\} \quad (3.10)$$

$$C_{3v} = \{I, C_{3(1)}, C_{3(1)}^2, \sigma_{d(1)}, \sigma_{d(2)}, \sigma_{d(3)}\} \quad (3.11)$$

$$D_{2d} = \{I, C_{2(1)}, C_{2(2)}, C_{2(3)}, \sigma_{d(1)}, \sigma_{d(2)}, S_{4(3)}, S_{4(3)}^3\} \quad (3.12)$$

$$T = \{I, C_{2(1)}, C_{2(2)}, C_{2(3)},$$

⁴ In this book, each symmetry element is represented by an upshape capital letter (e.g., C_3) or a Greek letter (e.g., σ_v); each symmetry operation is represented by a italicized capital letter (e.g., C_3) or a Greek letter (e.g., σ_v); and each point group is represented by a bold-faced italicized capital letter (e.g., C_3), which is based on the Schönflies symbol.

Table 3.1. Operations of T_d and Coset Representation T_d/C_{3v}

reference number*	operation $g \in T_d$	T_d/C_{3v} (product of cycles)	PSI (product of sphericity indices)	cycle term
1	I	(1)(2)(3)(4)	b_1^4	s_1^4
2	$C_{2(1)}$	(1 2)(3 4)	b_2^2	s_2^2
3	$C_{2(2)}$	(1 4)(2 3)	b_2^2	s_2^2
4	$C_{2(3)}$	(1 3)(2 4)	b_2^2	s_2^2
5	$C_{3(1)}$	(1)(2 3 4)	$b_1 b_3$	$s_1 s_3$
6	$C_{3(3)}$	(1 2 4)(3)	$b_1 b_3$	$s_1 s_3$
7	$C_{3(2)}$	(1 4 3)(2)	$b_1 b_3$	$s_1 s_3$
8	$C_{3(4)}$	(1 3 2)(4)	$b_1 b_3$	$s_1 s_3$
9	$C_{3(1)}^2$	(1)(2 4 3)	$b_1 b_3$	$s_1 s_3$
10	$C_{3(4)}^2$	(1 2 3)(4)	$b_1 b_3$	$s_1 s_3$
11	$C_{3(3)}^2$	(1 4 2)(3)	$b_1 b_3$	$s_1 s_3$
12	$C_{3(2)}^2$	(1 3 4)(2)	$b_1 b_3$	$s_1 s_3$
13	$\sigma_{d(1)}$	$\overline{(1)(2 4)(3)}$	$a_1^2 c_2$	$s_1^2 s_2$
16	$\sigma_{d(6)}$	$\overline{(1 3)(2)(4)}$	$a_1^2 c_2$	$s_1^2 s_2$
17	$\sigma_{d(2)}$	$\overline{(1)(2)(3 4)}$	$a_1^2 c_2$	$s_1^2 s_2$
18	$\sigma_{d(4)}$	$\overline{(1 2)(3)(4)}$	$a_1^2 c_2$	$s_1^2 s_2$
21	$\sigma_{d(3)}$	$\overline{(1)(2 3)(4)}$	$a_1^2 c_2$	$s_1^2 s_2$
23	$\sigma_{d(5)}$	$\overline{(1 4)(2)(3)}$	$a_1^2 c_2$	$s_1^2 s_2$
14	$S_{4(3)}$	$\overline{(1 2 3 4)}$	c_4	s_4
15	$S_{4(3)}^3$	$\overline{(1 4 3 2)}$	c_4	s_4
19	$S_{4(1)}$	$\overline{(1 4 2 3)}$	c_4	s_4
20	$S_{4(1)}^3$	$\overline{(1 3 2 4)}$	c_4	s_4
22	$S_{4(2)}$	$\overline{(1 2 4 3)}$	c_4	s_4
24	$S_{4(2)}$	$\overline{(1 3 4 2)}$	c_4	s_4

* The reference number corresponds to that of the multiplication table of T_d reported in [5, Table 2.2].

$$C_{3(1)}, C_{3(1)}^2, C_{3(2)}, C_{3(2)}^2, C_{3(3)}, C_{3(3)}^2, C_{3(4)}, C_{3(4)}^2 \} \quad (3.13)$$

$$T_d = \{\mathbf{A}, \mathbf{B}\}, \quad (\text{cf. Table 3.1}) \quad (3.14)$$

where a representative subgroup is selected from a set of conjugate subgroups. For example, the subgroup C_{3v} is a representative of the following conjugate subgroups:

$$C_{3v(1)} = \{I, C_{3(1)}, C_{3(1)}^2, \sigma_{d(1)}, \sigma_{d(2)}, \sigma_{d(3)}\} = C_{3v} \quad (3.15)$$

$$C_{3v(2)} = \{I, C_{3(2)}, C_{3(2)}^2, \sigma_{d(2)}, \sigma_{d(5)}, \sigma_{d(6)}\} \quad (3.16)$$

$$C_{3v(3)} = \{I, C_{3(3)}, C_{3(3)}^2, \sigma_{d(1)}, \sigma_{d(4)}, \sigma_{d(5)}\} \quad (3.17)$$

$$C_{3v(4)} = \{I, C_{3(4)}, C_{3(4)}^2, \sigma_{d(3)}, \sigma_{d(4)}, \sigma_{d(6)}\}. \quad (3.18)$$

Such non-redundant subgroups as Eqs. 3.4–3.14 are aligned in an ascending order of their orders to give the following set:

$$SSG_{T_d} = \{C_1, C_2, C_s, C_3, S_4, D_2, C_{2v}, C_{3v}, D_{2d}, T, T_d\}, \quad (3.19)$$

which is called a *non-redundant set of subgroups* (SSG) for the point group T_d .

In general, a non-redundant set of subgroups (SSG) for a given point group G is obtained as follows:

$$SSG_G = \{G_1 (= C_1), G_2, \dots, G_i, \dots, G_s (= G)\}, \quad (3.20)$$

where the symbol G_i denotes a representative of conjugate subgroups under the action of G [4, Chapter 2]. For the detailed discussion, see the next chapter.

3.2.4 Maximum Chiral Subgroup of a Point Group

An achiral point group G_Y is divided into a set G_C of rotations and another set of (roto)reflections. The set G_C of rotations is a subgroup of the original point group G_Y , where $|G_C| = |G_Y|/2$. The G_C is called the *maximum chiral subgroup* of the point group G_Y . Then, the point group G_Y is decomposed into two *cosets* as follows:

$$G_Y = G_C + G_C\sigma, \quad (3.21)$$

where the operation σ is selected appropriately from the set of (roto)reflections. Then, all of the (roto)reflections are contained in the coset $G_C\sigma$.

Let us select an element g from G_C ($g \in G_C$). Then, we obtain $G_Cg = G_C$. This means that the coset $G_C (= G_C I)$ is fixed under the action of $g \in G_C$. On the other hand, σg is a (roto)reflection, i.e., $\sigma g \in G_C\sigma$. This means that $G_C\sigma g = G_C\sigma$. The coset $G_C\sigma$ is fixed under the action of $g \in G_C$.

Chemically speaking, a given molecular entity A as a reference corresponds to the coset $G_C (= G_C I)$, while its enantiomeric entity \bar{A} corresponds to the other coset $G_C\sigma$. The number $|G_C|$ of entities corresponding to the coset G_C are homomeric to the reference molecule A under the action of G_C . The number $|G_C|$ of entities corresponding to the coset $G_C\sigma$ are homomeric to the reference molecule \bar{A} under the action of G_C .

This holds true for a numbered skeleton and the corresponding mirror-numbered skeleton.

Theorem 3.3 (Homomeric Relationship under Point Groups). Suppose that a given numbered skeleton belongs to an achiral point group. Then the numbered skeleton is fixed (or converted into a homomer) under the action of the maximum chiral point group. The corresponding mirror-numbered skeleton (Def. 3.4) is also fixed (or converted into a homomer) under the action of the maximum chiral point group.

This theorem gives the mathematical foundation of the term *homomeric*.

For example, the point group T_d (order: $|T_d| = 24$) has the maximum chiral subgroup T (order: $|T| = 12$), which is contained in the upper part of Table 3.1, as designated by a large gray letter **A**. Thereby, the following coset decomposition is obtained:

$$T_d = T + T\sigma_{d(1)}, \quad (3.22)$$

where the second coset corresponds to the lower part of Table 3.1, as designated by a large gray letter **B**.

Exercise 3.2. Confirm Theorem 3.3 by using the data of Table 3.1. See Fig. 3.2 and Eq. 3.1 for the application of the operation $C_{3(1)}$.

3.2.5 Global and Local Point-Group Symmetries

Diagrammatic Meaning of Orbits

The tetrahedral skeleton **3-5** belongs to the point group T_d , which is called the *global point-group symmetry* of **3-5**. Some pieces of information on orbits of **3-5** are shown in the diagrams **3-7** and **3-8** of Fig. 3.6.

Let us focus our attention on the 1-position of **3-5**, which is fixed under the subgroup C_{3v} represented by Eq. 3.11. Mathematically speaking, the subgroup $C_{3v(1)}$ is the *stabilizer* of the 1-position, where the symbol (1) in the subscript $3v(1)$ indicates the 1-position. Chemically speaking, on the other hand, the subgroup $C_{3v(1)}$ is referred to as the *local point-group symmetry* of the 1-position of **3-5**. The right diagram **3-8** shown in Fig. 3.6 is the top view of **3-5** through the 1—C bond, which is the $C_{3(1)}$ -axis of the stabilizer $C_{3v(1)}$.

There are four conjugate subgroups with respect to C_{3v} (Eq. 3.11), as shown in Eqs. 3.15–3.18. The subgroup $C_{3v(1)}$ ($= C_{3v}$) of Eq. 3.15 fixes the 1-position, as shown in the top view **3-8**. Similarly, the subgroup $C_{3v(2)}$ of Eq. 3.16 fixes the 2-position, the subgroup $C_{3v(3)}$ of Eq. 3.17 fixes the 3-position, and the subgroup $C_{3v(4)}$ of Eq. 3.18 fixes the 4-position. The conjugacy of these four subgroups assures that the four positions are equivalent under the global point-group symmetry T_d . In other words, the four positions construct an equivalence class (orbit) as shown in Fig. 3.6,⁵ where the local point-group symmetries $C_{3v(i)}$ ($i = 1-4$) are expressed collectively by the representative subgroup C_{3v} contained in the SSG of the global point-group symmetry T_d (Eq. 3.19).

The four-membered orbit surrounded by a gray double circle in **3-7** is designated by the symbol $T_d(/C_{3v})$, which has been coined by combining the global point-group symmetry (T_d) and the representative local point-group symmetry C_{3v} [6]. The algebraic meaning of

⁵ In this book, an equivalence class of positions or proligands in a molecular entity is called *an orbit* for the sake of simplicity.

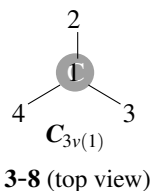
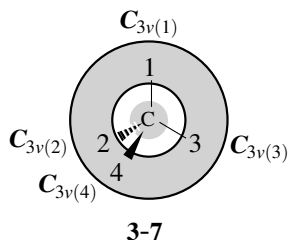


Fig. 3.6. Local point-group symmetries and orbits for a tetrahedral skeleton (left). The subgroups $C_{3v(i)}$ ($i = 1-4$) are the local point-group symmetries of the i -positions, where they are conjugate to one another. The top view (right) through the 1—C bond (the $C_{3v(1)}$ -axis) indicates the local point-group symmetry $C_{3v(1)}$ of the 1-position. The four positions 1–4 construct an orbit governed by the coset representation T_d/C_{3v} .

the symbol T_d/C_{3v} will be later discussed in detail. The number of positions (the size of the orbit) is calculated to be $|T_d|/|C_{3v}| = 24/6 = 4$.

The central carbon of **3-7** constructs a one-membered orbit governed by the coset representation T_d/T_d , where the size of the orbit is calculated $|T_d|/|T_d| = 24/24 = 1$.

As found in Fig. 3.6, an orbit of substitution positions can be characterized diagrammatically by the combination of a global point-group symmetry and a local point-group symmetry. This procedure is summarized as a theorem:

Theorem 3.4 (Orbits Due to Global and Local Point-Group Symmetries). The global point-group symmetry G of a molecular entity and the local point-group symmetry G_i ($\subseteq G$) of a position in the molecular entity indicate the presence of an orbit of equivalent positions, which is expressed by the symbol G/G_i . The size of the orbit is calculated to be $|G|/|G_i|$.

Algebraic Meaning of Orbits

According to the Chapter 5 of [4], the coset decomposition (strictly the right coset decomposition) of T_d by its subgroup C_{3v} is obtained as follows:⁶

$$T_d = C_{3v} + C_{3v}C_{2(1)} + C_{3v}C_{2(3)} + C_{3v}C_{2(2)}, \quad (3.23)$$

1
2
3
4

where the sequential numbers attached to the respective cosets correspond to the positions of a tetrahedral skeleton **3-6** shown in Fig. 3.5. The stabilizers of the respective cosets are calculated to be $I^{-1}C_{3v}I = C_{3v} = C_{3v(1)}$, $C_{2(1)}^{-1}C_{3v}C_{2(1)} = C_{3v(2)}$, $C_{2(3)}^{-1}C_{3v}C_{2(3)} = C_{3v(3)}$,

⁶ For the purpose of using the multiplication table of T_d reported in [5, Table 2.2], the right coset decomposition is used here, where the symbol T_d/C_{3v} is used to designate the coset representation based on the right coset decomposition. Note that Eq. 3.23 is equivalent to the left coset decomposition: $T_d = C_{3v} + C_{2(1)}^{-1}C_{3v} + C_{2(3)}^{-1}C_{3v} + C_{2(2)}^{-1}C_{3v}$, where $C_{2(1)}^{-1}$ etc. represent the inverse element of $C_{2(1)}$ etc.

and $C_{2(2)}^{-1} C_{3v} C_{2(2)} = C_{3v(4)}$, which fix the respective positions of **3-6**, as confirmed diagrammatically (cf. Eqs. 3.15–3.18).

The cosets appearing in the right-hand side of Eq. 3.23 are gathered to give a set of cosets denoted by the symbol T_d/C_{3v} as follows:

$$T_d/C_{3v} = \left\{ \begin{array}{c} C_{3v} \\ 1 \end{array}, \begin{array}{c} C_{3v}C_{2(1)} \\ 2 \end{array}, \begin{array}{c} C_{3v}C_{2(3)} \\ 3 \end{array}, \begin{array}{c} C_{3v}C_{2(2)} \\ 4 \end{array} \right\}, \quad (3.24)$$

$$\left\{ \begin{array}{ccc} \mathbf{1} & 5 & 9 \\ 13 & 17 & 21 \end{array} \right\} \left\{ \begin{array}{ccc} \mathbf{2} & 6 & 10 \\ 14 & 18 & 22 \end{array} \right\} \left\{ \begin{array}{ccc} \mathbf{4} & 8 & 12 \\ 16 & 20 & 24 \end{array} \right\} \left\{ \begin{array}{ccc} \mathbf{3} & 7 & 11 \\ 15 & 19 & 23 \end{array} \right\}$$

where a pair of braces below each coset represents operations contained in the coset by using the reference numbers listed in the leftmost column of Table 3.1.

The action of the operation $C_{3(1)}$ from the right-hand side of each coset contained in Eq. 3.24 results in the set T_d/C_{3v} into a permuted one:

$$T_d/C_{3v}|_{C_{3(1)}} = \left\{ \begin{array}{c} C_{3v} \\ 1 \end{array}, \begin{array}{c} C_{3v}C_{2(3)} \\ 3 \end{array}, \begin{array}{c} C_{3v}C_{2(2)} \\ 4 \end{array}, \begin{array}{c} C_{3v}C_{2(1)} \\ 2 \end{array} \right\}. \quad (3.25)$$

$$\left\{ \begin{array}{ccc} \mathbf{5} & 9 & 1 \\ 17 & 21 & 13 \end{array} \right\} \left\{ \begin{array}{ccc} \mathbf{8} & 12 & 4 \\ 20 & 24 & 16 \end{array} \right\} \left\{ \begin{array}{ccc} \mathbf{7} & 11 & 3 \\ 19 & 23 & 15 \end{array} \right\} \left\{ \begin{array}{ccc} \mathbf{6} & 10 & 2 \\ 18 & 22 & 14 \end{array} \right\}$$

The operations of each coset is concurrently permuted as found in the a pair of braces below the coset. The representative of each coset is converted into a permuted one, i.e., $C_{3v} = C_{3v}C_{3(1)} (C_{3(1)}: \mathbf{5})$, $C_{3v}C_{2(3)} = C_{3v}C_{3(4)} (C_{3(4)}: \mathbf{8})$, $C_{3v}C_{2(2)} = C_{3v}C_{3(2)} (C_{3(2)}: \mathbf{7})$, or $C_{3v}C_{2(1)} = C_{3v}C_{3(3)} (C_{3(3)}: \mathbf{6})$, where there appears no alternation of the chirality sense of each position.

Exercise 3.3.

- Confirm the following multiplications:

$$1C_{3(1)} = C_{3(1)}, \quad C_{2(1)}C_{3(1)} = C_{3(4)}, \quad C_{2(3)}C_{3(1)} = C_{3(2)}, \quad C_{2(2)}C_{3(1)} = C_{3(3)}. \quad (3.26)$$

$$\begin{array}{ccc} 1 & 5 & \\ & 5 & \\ 2 & 5 & \\ & 8 & \\ 4 & 5 & \\ & 7 & \\ 3 & 5 & \\ & 6 & \end{array}$$

For the multiplication table of T_d , see [5, Table 2.2].

- Examine $C_{3(1)}$ (**5**), $C_{3(4)}$ (**8**), $C_{3(2)}$ (**7**), and $C_{3(3)}$ (**6**) by considering which cosets in Eq. 3.24 contain them.
- Confirm $C_{3v} = C_{3v}C_{3(1)} (C_{3(1)}: \mathbf{5})$, $C_{3v}C_{2(3)} = C_{3v}C_{3(4)} (C_{3(4)}: \mathbf{8})$, etc. to generate Eq. 3.25.

Because the three-fold rotation $C_{3(1)}$ brings about the conversion of the set T_d/C_{3v} into the other set $T_d/C_{3v}|_{C_{3(1)}}$, the following permutation is assigned to the operation $C_{3(1)}$:

$$C_{3(1)} \sim \left(\begin{array}{c} T_d/C_{3v} \\ T_d/C_{3v}|_{C_{3(1)}} \end{array} \right) = \left(\begin{array}{cccc} 1 & 2 & 3 & 4 \\ 1 & 3 & 4 & 2 \end{array} \right) = (1)(2\ 3\ 4). \quad (3.27)$$

This permutation is consistent with Eq. 3.1, which is obtained by a diagrammatic derivation depicted in Fig. 3.2.

On the other hand, the action of the reflection $\sigma_{d(1)}$ from the right-hand side of each coset contained in Eq. 3.24 results in the set T_d/C_{3v} into another permuted one:

$$T_d/C_{3v}|_{\sigma_{d(1)}} = \left\{ \begin{array}{c} C_{3v} \\ \bar{1} \end{array}, \begin{array}{c} C_{3v}C_{2(2)} \\ \bar{4} \end{array}, \begin{array}{c} C_{3v}C_{2(3)} \\ \bar{3} \end{array}, \begin{array}{c} C_{3v}C_{2(1)} \\ \bar{2} \end{array} \right\}, \quad (3.28)$$

$$\left\{ \begin{array}{ccc} \bar{13} & 21 & 17 \\ 1 & 9 & 5 \end{array} \right\} \left\{ \begin{array}{ccc} \bar{15} & 23 & 19 \\ 3 & 11 & 7 \end{array} \right\} \left\{ \begin{array}{ccc} \bar{16} & 24 & 20 \\ 4 & 12 & 8 \end{array} \right\} \left\{ \begin{array}{ccc} \bar{14} & 22 & 18 \\ 2 & 10 & 6 \end{array} \right\}$$

The operations of each coset is concurrently permuted as found in the a pair of braces below the coset, where the upper row and the lower row are interchanged. The representative of each coset is converted into a permuted one, i.e., $C_{3v} = C_{3v}\sigma_{d(1)}$ ($\sigma_{d(1)}$: $\bar{13}$), $C_{3v}C_{2(3)} = C_{3v}S_{4(3)}^3$ ($S_{4(3)}^3$: $\bar{15}$), $C_{3v}C_{2(2)} = C_{3v}\sigma_{d(6)}$ ($\sigma_{d(6)}$: $\bar{16}$), or $C_{3v}C_{2(1)} = C_{3v}S_{4(3)}$ ($S_{4(3)}$: $\bar{14}$), where there occurs the alternation of the chirality sense of each position. This alternation is emphasized by an overbar over the sequence number for each coset.



Exercise 3.4.

- Confirm the following multiplications:

$$I\sigma_{d(1)} = \sigma_{d(1)}, C_{2(1)}\sigma_{d(1)} = S_{4(3)}^3, C_{2(3)}\sigma_{d(1)} = \sigma_{d(6)}, C_{2(2)}\sigma_{d(1)} = S_{4(3)}. \quad (3.29)$$

$$\begin{array}{ccccc} 1 & 13 & 13 & 2 & 13 \\ & & & 15 & \\ & & & 4 & 13 \\ & & & 16 & 3 & 13 & 14 \end{array}$$

For the multiplication table of T_d , see [5, Table 2.2].

- Examine $\sigma_{d(1)}$ ($\bar{13}$), $S_{4(3)}^3$ ($\bar{15}$), $\sigma_{d(6)}$ ($\bar{16}$), and $S_{4(3)}$ ($\bar{14}$) by considering which cosets in Eq. 3.24 contain them.
- Confirm $C_{3v} = C_{3v}\sigma_{d(1)}$ ($\sigma_{d(1)}$: $\bar{13}$), $C_{3v}C_{2(3)} = C_{3v}S_{4(3)}^3$ ($S_{4(3)}^3$: $\bar{15}$), etc. to generate Eq. 3.28.

Because the reflection $\sigma_{d(1)}$ converts the set T_d/C_{3v} into the other set $T_d/C_{3v}|_{\sigma_{d(1)}}$, the following permutation is assigned to the reflection $\sigma_{d(1)}$:

$$\sigma_{d(1)} \sim \left(\begin{array}{c} T_d/C_{3v} \\ T_d/C_{3v}|_{\sigma_{d(1)}} \end{array} \right) = \left(\begin{array}{cccc} 1 & 2 & 3 & 4 \\ \bar{1} & \bar{4} & \bar{3} & \bar{2} \end{array} \right) = \overline{(1)(2\ 4)(3)}, \quad (3.30)$$

where an overbar over each number represents the alternation of the chirality sense of each position. This permutation is consistent with Eq. 3.2, which is obtained by a diagrammatic derivation depicted in Fig. 3.3.

The procedures illustrated in the derivation of Eqs. 3.27 and 3.30 are repeated to cover all of the operations of T_d . The resulting set of permutations is called a *coset representation*, which is denoted by the symbol $T_d(/C_{3v})$.⁷ The obtained permutations (products of cycles) are identical with those listed in the $T_d(/C_{3v})$ -column of Table 3.1, which have been alternatively obtained diagrammatically.

⁷ The term *permutation representation* is widely used in group theory. The present book adopts the term *coset representation* to denote a transitive permutation representation and to emphasize the alternation of ligand chirality sense.

Exercise 3.5. Apply the procedures illustrated in the derivation of Eqs. 3.27 and 3.30 to all of the operations of T_d by referring to the multiplication table of T_d [5, Table 2.2].

By comparing the present algebraic derivation with the diagrammatic one described above, the coset representation $T_d(/C_{3v})$ reveals that the global symmetry T_d and the local symmetry C_{3v} can be discussed by relying on the concept of an orbit (an equivalence class) and the corresponding coset representation.

In general, a given group G and its subgroup G_i generates a coset representation $G(/G_i)$, which is used to characterize an orbit (equivalence class) of positions with the local point-group symmetry G_i [4,7]. Thereby, we arrive at an algebraic formulation of Theorem 3.4, which has been obtained diagrammatically.

According to the SSG shown in Eq. 3.20, the corresponding *set of coset representations* (SCR) is obtained as follows:

$$\text{SCR}_G = \{G(/G_1), G(/G_2), \dots, G(/G_i), \dots, G(/G_s)\}, \quad (3.31)$$

where $G_1 = C_1$ (the identity group) and $G_s = G$. This SCR will be again discussed in detail in Chapter 5 (Eq. 5.8 on page 116). For a more detailed discussion, see [4, Chapter 5].

3.3 Point-Group Symmetries of Stereoskeletons

3.3.1 Stereoskeletons of Ligancy 4

Stereoskeletons of ligancy 4 listed in Fig. 3.7 are important to discuss stereochemistry and stereoisomerism. In particular, a tetrahedral skeleton **3-5** and an allene skeleton **3-9** are bases for assigning *R/S*-stereodescriptors, while an ethylene skeleton **3-10** is a basis for assigning *Z/E*-descriptors.

Coset Representations of Stereoskeletons of Ligancy 4

As discussed in the preceding section, a tetrahedral skeleton **3-5** belongs to the point group T_d (order 24). The four positions of **3-5** construct an equivalence class (orbit) governed by a coset representation $T_d(/C_{3v})$, the degree of which is calculated to be $|T_d|/|C_{3v}| = 24/6 = 4$ [8]. See Table 3.1.⁸

An allene skeleton **3-9** belongs to the point group D_{2d} (order 8), where each of the four positions belongs to the local point-group symmetry C_s or its conjugate subgroup. Hence, the four positions of **3-9** construct an equivalence class (orbit) governed by a coset representation $D_{2d}(/C_s)$. The degree of $D_{2d}(/C_s)$ is calculated to be $|D_{2d}|/|C_s| = 8/2 = 4$,

⁸ For the data of T_d applied to adamantane derivatives see [9]. For the data of T_d applied to edge derivatives of a tetrahedron, see [10]. See also Appendices of [4].

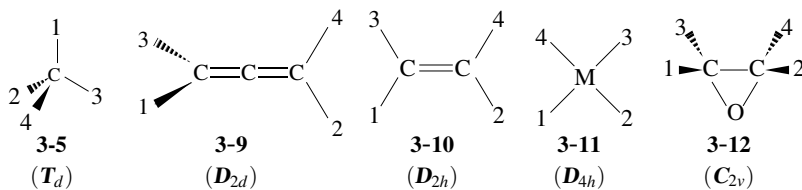


Fig. 3.7. Stereoskeletons of ligancy 4.

Table 3.2. Operations of D_{2d} and Coset Representation D_{2d}/C_s

operation $g \in D_{2d}$	D_{2d}/C_s (product of cycles)	PSI (product of sphericity indices)	cycle term
I	(1)(2)(3)(4)	b_1^4	s_1^4
$C_{2(1)}$	(1 2)(3 4)	b_2^2	s_2^2
$C_{2(2)}$	(1 4)(2 3)	b_2^2	s_2^2
$C_{2(3)}$	(1 3)(2 4)	b_2^2	s_2^2
$\sigma_{d(1)}$	$\overline{(1)(2\ 4)(3)}$	$a_1^2 c_2$	$s_1^2 s_2$
$\sigma_{d(2)}$	$\overline{(1\ 3)(2)(4)}$	$a_1^2 c_2$	$s_1^2 s_2$
S_4	$\overline{(1\ 2\ 3\ 4)}$	c_4	s_4
S_4^3	$\overline{(1\ 4\ 3\ 2)}$	c_4	s_4

where $C_s = \{I, \sigma_{d(1)}\}$ [8,11]. The concrete form of the coset representation D_{2d}/C_s is collected in Table 3.2 in the form of products of cycles.⁹

The two carbon atoms of **3-9**, each of which attached by two substitution positions, belong to a two-membered orbit governed by the coset representation D_{2d}/C_{2v} . The local point-group symmetry of each carbon is determined to be $C_{2v} = \{I, C_{2(3)}, \sigma_{d(1)}, \sigma_{d(2)}\}$, which is a subgroup of the global point-group symmetry D_{2d} (cf. Table 3.2). Note that each carbon of the two carbons is fixed under the action of the subgroup C_{2v} . The size of the orbit is calculated to be $|D_{2d}|/|C_{2v}| = 8/4 = 2$.

The central atom of the allene skeleton **3-9** belongs to a one-membered orbit governed by the coset representation D_{2d}/D_{2d} , because the central atom is fixed under all of the operation of D_{2d} .

An ethylene skeleton **3-10** belongs to the point group D_{2h} (order 8). The local point-group symmetry of the 1-position is determined to be $C_s'' = \{I, \sigma_h\}$ [11,15]. Hence, the four positions of **3-10** construct an equivalence class (orbit) governed by a coset representation

⁹ For the data of D_{2d} applied to adamantane-2,6-dione derivatives see [12–14]. See also Appendices of [4].

Table 3.3. Operations of D_{2h} and Coset Representation $D_{2h}(/C_s'')$

operation $g \in D_{2h}$	$D_{2h}(/C_s'')$ (product of cycles)	PSI (product of sphericity indices)	cycle term
I	(1)(2)(3)(4)	b_1^4	s_1^4
$C_{2(1)}$	(1 2)(3 4)	b_2^2	s_2^2
$C_{2(2)}$	(1 4)(2 3)	b_2^2	s_2^2
$C_{2(3)}$	(1 3)(2 4)	b_2^2	s_2^2
σ_h	$\overline{(1)(2)(3)(4)}$	a_1^4	s_1^4
i	$\overline{(1 4)(2 3)}$	c_2^2	s_2^2
$\sigma_{d(1)}$	$\overline{(1 2)(3 4)}$	c_2^2	s_2^2
$\sigma_{d(2)}$	$\overline{(1 3)(2 4)}$	c_2^2	s_2^2

$D_{2h}(/C_s'')$, the degree of which is calculated to be $|D_{2h}|/|C_s''| = 8/2 = 4$. The concrete form of the coset representation $D_{2h}(/C_s'')$ is collected in Table 3.2 in the form of products of cycles.¹⁰

The two carbon atoms of **3-10** belong to a two-membered orbit governed by the coset representation $D_{2h}(/C_{2v}')$. The local point-group symmetry of each carbon is determined to be $C_{2v}' = \{I, C_{2(3)}, \sigma_h, \sigma_{d(2)}\}$, which is a subgroup of the global point-group symmetry D_{2h} (cf. Table 3.3). Note that each of the two carbons is fixed under the action of C_{2v}' . The size of the orbit is calculated to be $|D_{2h}|/|C_{2v}'| = 8/4 = 2$.

A square planar skeleton **3-11** belongs to the point group D_{4h} (order 16). The local point-group symmetry of the 1-position is determined to be $C_{2v}'' = \{I, C_{2(1)}, \sigma_h, \sigma_{v(1)}\}$. Hence, the four positions of **3-11** construct an equivalence class (orbit) governed by a coset representation $D_{4h}(/C_{2v}'')$, the degree of which is calculated to be $|D_{4h}|/|C_{2v}''| = 16/4 = 4$.¹¹ The concrete form of the coset representation $D_{4h}(/C_{2v}'')$ is collected in Table 3.4 in the form of products of cycles.

An oxirane skeleton **3-12** belongs to the point group C_{2v} (order 4). The local point-group symmetry of the 1-position is determined to be $C_1 = \{I\}$. Hence, the four positions of **3-12** construct an equivalence class (orbit) governed by a coset representation $C_{2v}(/C_1)$, the degree of which is calculated to be $|C_{2v}|/|C_1| = 4/1 = 4$ [8]. The concrete form of the coset representation $C_{2v}(/C_1)$ is collected in Table 3.5 in the form of products of cycles.

¹⁰ For the data of D_{2h} applied to edge derivatives of tricyclodecanes, see [10].

¹¹ For the data of the point group D_{4h} applied to square planar complexes, see [16].

Table 3.4. Operations of D_{4h} and Coset Representation $D_{4h}/(C_{2v}'')$

operation $g \in D_{4h}$	$D_{4h}/(C_{2v}'')$ (product of cycles)	PSI (product of sphericity indices)	cycle term
I	(1)(2)(3)(4)	b_1^4	s_1^4
$C_{2(3)}$	(1 3)(2 4)	b_2^2	s_2^2
$C_{2(1)}'$	(1 2)(3 4)	b_2^2	s_2^2
$C_{2(2)}'$	(1 4)(2 3)	b_2^2	s_2^2
$C_{2(1)}$	(1)(2 4)(3)	$b_1^2 b_2$	$s_1^2 s_2$
$C_{2(2)}$	(1 3)(2)(4)	$b_1^2 b_2$	$s_1^2 s_2$
C_4	(1 2 3 4)	b_4	s_4
C_4^3	(1 4 3 2)	b_4	s_4
σ_h	$\overline{(1)(2)(3)(4)}$	a_1^4	s_1^4
i	$\overline{(1 3)(2 4)}$	c_2^2	s_2^2
$\sigma_{d(1)}$	$\overline{(1 2)(3 4)}$	c_2^2	s_2^2
$\sigma_{d(2)}$	$\overline{(1 4)(2 3)}$	c_2^2	s_2^2
$\sigma_{v(1)}$	$\overline{(1)(2 4)(3)}$	$a_1^2 c_2$	$s_1^2 s_2$
$\sigma_{v(2)}$	$\overline{(1 3)(2)(4)}$	$a_1^2 c_2$	$s_1^2 s_2$
S_4	$\overline{(1 2 3 4)}$	c_4	s_4
S_4^3	$\overline{(1 4 3 2)}$	c_4	s_4

Table 3.5. Operations of C_{2v} and Coset Representation $C_{2v}/(C_1)$

operation $g \in C_{2v}$	$C_{2v}/(C_1)$ (product of cycles)	PSI (product of sphericity indices)	cycle term
I	(1)(2)(3)(4)	b_1^4	s_1^4
C_2	(1 4)(2 3)	b_2^2	s_2^2
$\sigma_{v(1)}$	$\overline{(1 2)(3 4)}$	c_2^2	s_2^2
$\sigma_{v(2)}$	$\overline{(1 3)(2 4)}$	c_2^2	s_2^2

Regular Representations of a Stereoskeleton of C_{2v}

If the local point-group symmetry is an identity group $C_1 = \{I\}$, the corresponding coset representation G/C_1 is called a *regular representation*. For detailed discussions of regular representations, see [5, Section 6.4 and Chapter 7].

Such a regular representation is obtained directly by starting from the multiplication table of G . Note that each coset ($\{I\}g = \{g\}$, $g \in G$) appearing in the set of cosets G/C_1 derived from the coset decomposition consists of a single operation g ($\in G$) at issue.

As an example, let us obtain the regular representation C_{2v}/C_1 . The multiplication table of C_{2v} is shown in Table 3.6. For the sake of convenience, the multiplication table of C_{2v} (Table 3.6) contains serial numbers for representing operations. The number 4 at the intersection between $\sigma_{v(1)}$ -row and $\sigma_{v(2)}$ -row column represents $\sigma_{v(2)}\sigma_{v(1)} = C_2$, where the successive action of $\sigma_{v(2)}$ (3) and $\sigma_{v(1)}$ (2) results in the same effect of C_2 (4).

Table 3.6. Multiplication Table of the Point Group C_{2v}

		the 1st operation			
		I	$\sigma_{v(1)}$	$\sigma_{v(2)}$	C_2
the 2nd operation	I	1	2	3	4
	$\sigma_{v(1)}$	2	1	4	3
	$\sigma_{v(2)}$	3	4	1	2
	C_2	4	3	2	1

The regular representation C_{2v}/C_1 is obtained from the multiplication table of C_{2v} shown in Table 3.6. The $\sigma_{v(1)}$ -row of Table 3.6 corresponds to the following permutation:

$$\sigma_{v(1)} \sim \left(\begin{array}{cccc} 1 & 2 & 3 & 4 \\ \bar{2} & \bar{1} & \bar{4} & \bar{3} \end{array} \right) = \overline{(1\ 2)(3\ 4)}, \quad (3.32)$$

which is identical with the product of cycles in the $\sigma_{v(1)}$ -row of Table 3.5. Note that an overbar attached to each number represents a mirror-image formation locally at the numbered position, while the global mirror-image formation of the oxirane skeleton is represented by the permuted sequence of the numbers.

The action of the reflection $\sigma_{v(1)}$ on a numbered skeleton **3-12** is illustrated in Fig. 3.8. Because the reflection $\sigma_{v(1)}$ is a mirror-image formation on the basis of a mirror plane bisecting the oxirane ring perpendicularly through the midpoint of the C—C bond and the oxygen atom, the action of $\sigma_{v(1)}$ generates a mirror-numbered skeleton $\overline{\mathbf{3-12}}$. This result is consistent with the correspondence between $\sigma_{v(1)}$ and the permutation $\overline{(1\ 2)(3\ 4)}$ (Eq. 3.32). It should be emphasized that such a reflection as $\sigma_{v(1)}$ results in the local mirror-image formation of the (pro)ligands along with the global mirror-image formation of the oxirane skeleton.

The two carbon atoms of the oxirane skeleton **3-12** belong to a two-membered orbit governed by the coset representation C_{2v}/C'_s . The local point-group symmetry of each

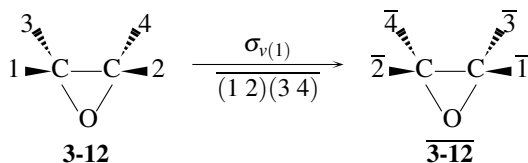


Fig. 3.8. Action of a reflection on an oxirane skeleton to generate a mirror-numbered skeleton. The position number with an overbar represents the reverse of chirality sense at the position.

carbon is determined to be $C'_s = \{I, \sigma_{v(2)}\}$, which is a subgroup of the global point-group symmetry C_{2v} (cf. Table 3.5). Note that each of the two carbons is fixed under the action of C'_s . The size of the orbit is calculated to be $|C_{2v}|/|C'_s| = 4/2 = 2$.



Exercise 3.6.

- In the continuation of Eq. 3.32, calculate the coset representation $C_{2v}/(C_1)$ by using the multiplication table (Table 3.6). Confirm that the result is identical with the data collected in Table 3.5.
- Calculate the coset representation $C_{2v}/(C'_s)$, where $C'_s = \{I, \sigma_{v(2)}\}$. Confirm that the two carbon atoms of the oxirane skeleton **3-12** construct a two-membered $C_{2v}/(C'_s)$ -orbit.

The oxygen atom of the oxirane skeleton **3-12** belongs to a one-membered orbit governed by the coset representation $C_{2v}/(C_{2v})$. The local point-group symmetry of the oxygen atom is determined to be C_{2v} , which is identical with the global point-group symmetry C_{2v} (cf. Table 3.5). Note that the oxygen atom is fixed under the action of C_{2v} . The size of the orbit is calculated to be $|C_{2v}|/|C_{2v}| = 4/4 = 1$.

3.3.2 Stereoskeletons of Ligancy 6

Representative stereoskeletons of ligancy 6 are listed in Fig. 3.9.

An octahedral skeleton **3-13** appears in inorganic octahedral complexes. Each coordination bond is represented by a thick line between a central metal M and a vertex of the octahedral complex. The vertices are linked with thin lines to visualize the edges of the octahedron to be examined.

The six positions (vertices) of **3-13** belong to a six-membered orbit governed by the coset representation $O_h/(C_{4v})$. The local point-group symmetry of each position is determined to be C_{4v} of order 8, which is a subgroup of the global point-group symmetry O_h of order 48. Note that each of the six vertices is fixed under the action of C_{4v} or its conjugate subgroup. The size of the orbit is calculated to be $|O_h|/|C_{4v}| = 48/8 = 6$.¹²

¹² For the data of the point group O_h applied to octahedral complexes, see [17–21].

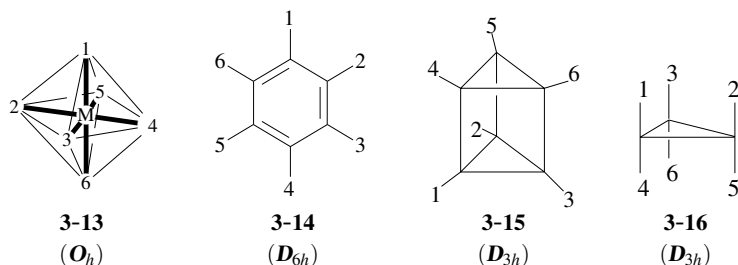


Fig. 3.9. Stereoskeletons of ligancy 6.

A benzene skeleton **3-14** belongs to the point group D_{6h} of order 24. The three double bonds depicted tentatively are delocalized to cover all of the bonds of the benzene ring so as to exhibit the global point-group symmetry D_{6h} .¹³ The six positions of **3-13** belong to a six-membered orbit governed by the coset representation $D_{6h}/(C'_{2v})$. The local point-group symmetry of each position is determined to be C'_{2v} , of order 4, which is a subgroup of the global point-group symmetry D_{6h} . Note that each of the six positions is fixed under the action of C'_{2v} or its conjugate subgroup. The size of the orbit is calculated to be $|D_{6h}|/|C'_{2v}| = 24/4 = 6$.

A prismane skeleton **3-15** belongs to the point group D_{3h} of order 12. The six positions of **3-15** belong to a six-membered orbit governed by the coset representation $D_{3h}/(C_s)$. The local point-group symmetry of each position is determined to be C_s of order 2, which is a subgroup of the global point-group symmetry D_{3h} . Note that each of the six positions is fixed under the action of C_s or its conjugate subgroup. The size of the orbit is calculated to be $|D_{3h}|/|C_s| = 12/2 = 6$.¹⁴

A cyclopropane skeleton **3-16** belongs to the point group D_{3h} of order 12. The six positions of **3-16** belong to a six-membered orbit governed by the coset representation $D_{3h}/(C_s)$. The size of the orbit is calculated to be $|D_{3h}|/|C_s| = 12/2 = 6$.¹⁵

3.3.3 Stereoskeletons of Ligancy 8

Representative stereoskeletons of ligancy 8 are listed in Fig. 3.10.

A cubane skeleton **3-17** with eight positions belongs to the point group O_h of order 48, which is the same as the point group for characterizing the octahedral skeleton **3-13** with six positions. The eight positions of **3-17** belong to an eight-membered orbit governed by the coset representation $O_h/(C_{3v})$. The local point-group symmetry of each position is determined to be C_{3v} of order 6, which is a subgroup of the global point-group symmetry

¹³ The data of D_{6h} applied to benzene derivatives have been reported [22].

¹⁴ For the data of the point group D_{3h} applied to prismane derivatives, see [23–25].

¹⁵ For the data of the point group D_{3h} applied to cyclopropane derivatives, see [8,23].

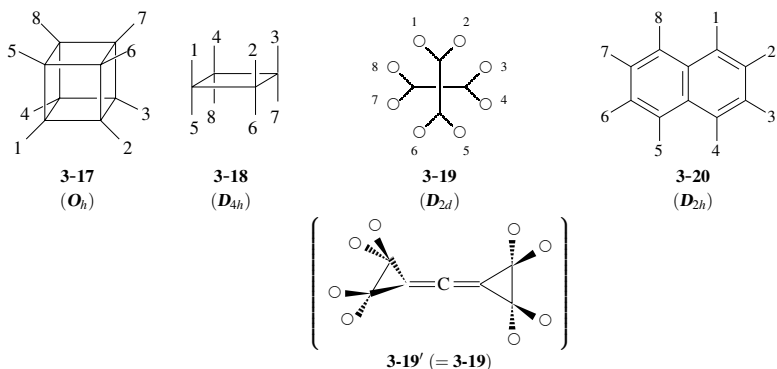


Fig. 3.10. Stereoskeletons of ligancy 8.

O_h . Note that each of the eight positions is fixed under the action of C_{3v} or its conjugate subgroup. The size of the orbit is calculated to be $|O_h|/|C_{3v}| = 48/6 = 8$.¹⁶

A cyclobutane skeleton **3-18** with eight positions belongs to the point group D_{4h} of order 16, which is the same as the point group for characterizing the square planar skeleton **3-11** with four positions. The eight positions of **3-18** belong to an eight-membered orbit governed by the coset representation $D_{4h}/(C_s)$. The local point-group symmetry of each position is determined to be C_s of order 2, which is a subgroup of the global point-group symmetry D_{4h} . Note that each of the eight positions is fixed under the action of C_s or its conjugate subgroup. The size of the orbit is calculated to be $|D_{4h}|/|C_s| = 16/2 = 8$.¹⁷

A dicyclopropylidene skeleton **3-19** with eight positions belongs to the point group D_{2d} of order 8, which is the same as the point group for characterizing the allene skeleton **3-9** with four positions. Note that this diagram is a top view of the allene derivative with two cyclopropane rings **3-19'**. The eight positions of **3-19** belong to an eight-membered orbit governed by the coset representation $D_{2d}/(C_1)$. Because the local point-group symmetry of each position is determined to be C_1 , the coset representation $D_{2d}/(C_1)$ is a regular representation. The size of the orbit is calculated to be $|D_{2d}|/|C_1| = 8/1 = 8$.¹⁸

3.3.4 Stereoskeletons Having Two or More Orbits

Naphthalene Skeleton

A naphthalene skeleton **3-20** with eight positions belongs to the point group D_{2h} of order 8. The action of D_{2h} on the eight positions generates a *permutation representation* denoted by

¹⁶ For the data of the point group O_h applied to cubane derivatives, see [26–33].

¹⁷ For the data of the point group D_{4h} applied to cyclobutane derivatives, see [34,35]. See also [16].

¹⁸ For the data of the point group D_{2d} applied to dicyclopropylidene, see [7,36–38]. See also [5, Chapters 6–8].

$\mathbf{P}_{D_{2h}}$ of degree 8 in a similar way to the construction of Table 3.3.¹⁹ For example, the action of the two-fold rotation $C_{2(3)}$ on **3-20** generates a permutation $C_{2(3)} \sim (1\ 5)(4\ 8)|(2\ 8)(3\ 7)$, where the two-fold axis $C_{2(3)}$ is perpendicular to the naphthalene ring and runs through the center of the central bond of **3-20**. The reflection $\sigma_{d(1)}$ on **3-20** generates a permutation $\sigma_{d(1)} \sim (1\ 4)(5\ 8)|(2\ 3)(7\ 8)$, where the mirror plane $\sigma_{d(1)}$ at issue is perpendicular to the naphthalene ring and bisects the bond attached by 2 and 3 as well as the bond attached by 7 and 8. Each of the resulting eight permutations is divided into two parts as designated by a vertical bar (|). As a result, the eight positions of **3-20** are divided into two four-membered orbits, i.e., $\{1, 4, 5, 8\}$ and $\{2, 3, 6, 7\}$. The local point-group symmetry of each position is determined to be $\mathbf{C}_s'' = \{I, \sigma_h\}$. Hence, each of the two orbits is governed by the coset representation $D_{2h}(/C_s'')$, which is the same as the coset representation for characterizing the ethylene skeleton **3-10** with four positions. The size of each orbit is calculated to be $|D_{2h}|/|C_s''| = 8/2 = 4$. The above discussion is summarized into the following equation:

$$\mathbf{P}_{D_{2h}} = 2D_{2h}(/C_s''). \quad (3.33)$$

Adamantane and Related Skeletons

As more complex stereoskeletons, Fig. 3.11 shows an adamantane skeleton **3-21** of T_d , an adamantane-2,6-dione skeleton **3-22** of D_{2d} , and an adamantane-2-one skeleton **3-23** of C_{2v} .²⁰

An adamantane skeleton **3-21** of T_d has two sets of positions, i.e., a twelve-membered set of bridge positions $\{1, 2, \dots, 12\}$ and a four-membered set of bridgehead positions $\{1', 2', 3', 4'\}$. The former twelve-membered set constructs an equivalence class (orbit), which is governed by the coset representation $T_d(/C_s)$ of degree 12 ($= |T_d|/|C_s| = 24/2$), because each of the positions is fixed under the subgroup C_s or its conjugate subgroup. On the other hand, the latter four-membered set constructs an equivalence class (orbit), which is governed by the coset representation $T_d(/C_{3v})$ of degree 4 ($= |T_d|/|C_{3v}| = 24/6$), because each of the positions is fixed under the subgroup C_{3v} or its conjugate subgroup. When the total 16 positions are considered to be represented by a permutation representation \mathbf{P}_{T_d} , they are divided into two orbits according to the following equation:

$$\mathbf{P}_{T_d} = T_d(/C_s) + T_d(/C_{3v}), \quad (3.34)$$

where the first term of the right-hand side is concerned with the twelve-membered orbit of bridge positions and the second term is concerned with the four-membered orbit of bridgehead positions.

¹⁹ For the sake of simplicity, such a permutation representation is referred to as a permutation group, if it does not degenerate.

²⁰ Strictly speaking, even a tetrahedral skeleton **3-5** of ligancy 4 has another one-membered orbit of a central carbon, which is governed by the coset representation $T_d(/T_d)$. To discuss derivatives of **3-5**, we are able to focus on the coset representation $T_d(/C_{3v})$ for the four substitution positions.

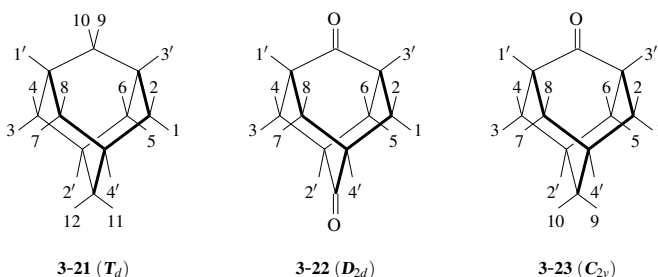


Fig. 3.11. Orbits in an adamantane skeleton, an adamantane-2,6-dione skeleton, and an adamantane-2-one skeleton.

An adamantane-2,6-dione skeleton **3-22** of D_{2d} has two sets of positions, i.e., an eight-membered set of bridge positions $\{1, 2, \dots, 8\}$ and a four-membered set of bridgehead positions $\{1', 2', 3', 4'\}$. The former eight-membered set constructs an equivalence class (orbit), which is governed by the coset representation $D_{2d}/(C_1)$ of degree 8 ($= |D_{2d}|/|C_1| = 8/1$), because each of the positions is fixed under the subgroup C_1 . On the other hand, the latter four-membered set constructs an equivalence class (orbit), which is governed by the coset representation $D_{2d}/(C_s)$ of degree 4 ($= |D_{2d}|/|C_s| = 8/2$), because each of the positions is fixed under the subgroup C_s or its conjugate subgroup. When the total 12 positions are considered to be represented by a permutation representation $P_{D_{2d}}$, they are divided into two orbits according to the following equation:

$$P_{D_{2d}} = D_{2d}/(C_1) + D_{2d}/(C_s), \quad (3.35)$$

where the first term of the right-hand side is concerned with the eight-membered orbit of bridge positions and the second term is concerned with the four-membered orbit of bridgehead positions.

An adamantane-2-one skeleton **3-23** of C_{2v} has a four-membered orbit of bridge positions $\{1, 3, 5, 7\}$ belonging to the coset representation $C_{2v}/(C_1)$, another four-membered orbit of bridge positions $\{2, 4, 6, 8\}$ belonging to the coset representation $C_{2v}/(C_1)$, a two-membered orbit of bridge positions $\{9, 10\}$ belonging to the coset representation $C_{2v}/(C'_s)$, a two-membered orbit of bridgehead positions $\{1', 3'\}$ belonging to the coset representation $C_{2v}/(C'_s)$, and another two-membered orbit of bridgehead positions $\{2', 4'\}$ belonging to the coset representation $C_{2v}/(C_s)$. When the total 14 positions are considered to be represented by a permutation representation $P_{C_{2v}}$, they are divided into five orbits according to the following equation:

$$P_{C_{2v}} = 2C_{2v}/(C_1) + C_{2v}/(C_s) + 2C_{2v}/(C'_s), \quad (3.36)$$

where the total value 14 can be calculated from the data of the right-hand side, i.e., $2|C_{2v}|/|C_1| + |C_{2v}|/|C_s| + 2|C_{2v}|/|C'_s| = 2 \times \frac{4}{1} + \frac{4}{2} + 2 \times \frac{4}{2} = 14$.

3.4 Point-Group Symmetries of (Pro)molecules

3.4.1 Derivation of Molecules from a Stereoskeleton via Promolecules

The positions of a given stereoskeleton (Def. 3.2) accommodate a set of proligands (Def. 3.1) to generate a promolecule (Def. 3.3) according to the proligand-promolecule model. For example, the four positions of a tetrahedral skeleton **3-5** accommodate a set of achiral proligands ABX^2 to generate a promolecule **3-24**, where the T_d -symmetry of the skeleton **3-5** is restricted to the C_s -symmetry of **3-24**, as shown in the top row of Fig. 3.12. By placing $A = Cl$, $B = Br$, and $X = H$, the promolecule **3-24** is converted into bromochloromethane **3-25** as a molecule of the same C_s -symmetry.

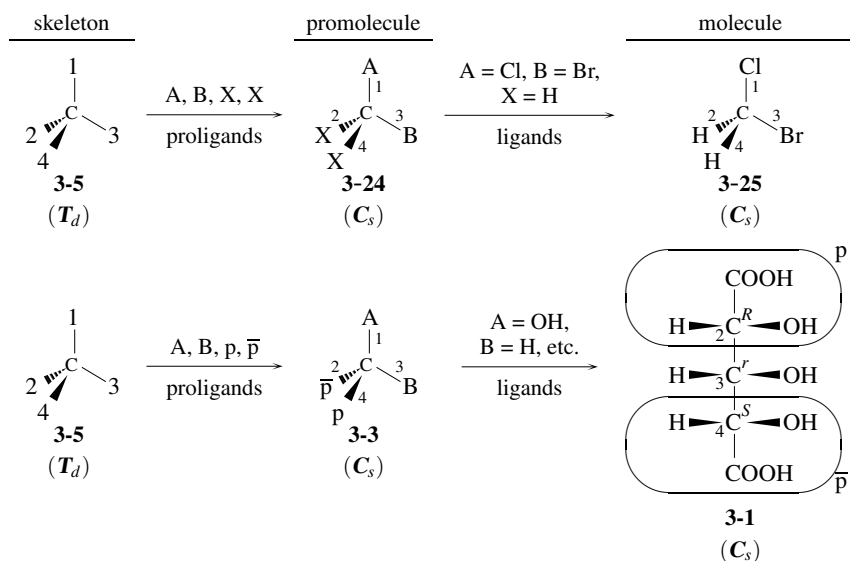


Fig. 3.12. Derivation of molecules from a stereoskeleton via promolecules (the proligand-promolecule model).

On the other hand, suppose that the four positions of a tetrahedral skeleton **3-5** accommodate a set of proligands $ABp\bar{p}$ (the bottom row of Fig. 3.12), where the symbols A and B represent achiral proligands in isolation and the symbols p and \bar{p} represent a pair of enantiomeric proligands in isolation.²¹ The accommodation results in the generation

21 According to the IUPAC Recommendations 1996 [39], the term *enantiomorphic* is applied to a mirror image related to groups within a molecular entity. However, this book adopts the term *enantiomeric* (*in isolation*), because a (pro)ligand may be incorporated within a (pro)molecule or detached from a (pro)molecule. When detached, a (pro)ligand may be regarded as a kind of molecular entity with a vacant bond.

of a promolecule **3-3**, where the T_d -symmetry of the skeleton **3-5** is restricted to the C_s -symmetry of **3-3**, as shown in the bottom row of Fig. 3.12. By placing $A = \text{OH}$, $B = \text{H}$, $p = \text{CH(OH)-COOH}$, and $\bar{p} = \text{C(OH)H-COOH}$, the promolecule **3-3** is converted into an achiral 2,3,4-trihydroxyglutaric acid **3-1** as a molecule of the same C_s -symmetry.

3.4.2 Orbits in Molecules and Promolecules Derived from Stereoskeletons

Orbits of Equivalent Ligands

The above procedure of deriving promolecules and molecules (Fig. 3.12) can be applied to respective stereoskeletons discussed in Section 3.3. As a result of such derivation, the point-group symmetry of each stereoskeleton (Section 3.3) is restricted to its subgroup during the derivation.

Several derivatives based on a tetrahedral skeleton **3-5** of T_d -symmetry are illustrated in Fig. 3.13, where ligands are selected from hydrogen and halogen atoms (chlorine, bromine, and fluorine). Their point-group symmetries are subgroups of the point group T_d .

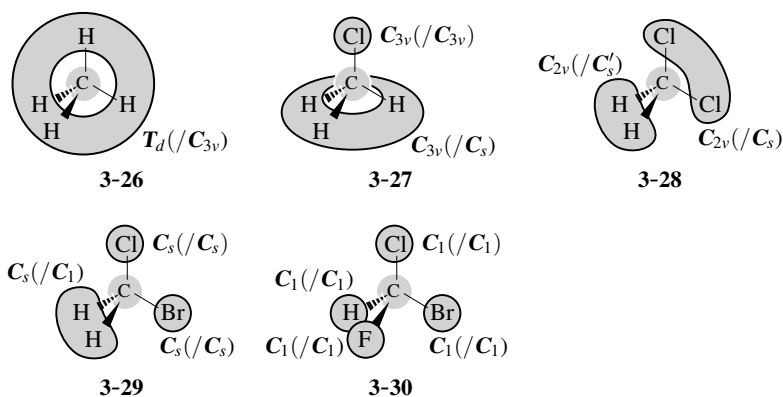


Fig. 3.13. Orbits in methane derivatives based on a tetrahedral skeleton. Each orbit governed by a coset representation is designated by a gray solid circle or a shadowed round frame.

According to the subgroup of each derivative, the four points of the original tetrahedral skeleton **3-5** are divided into several sets of equivalent ligands, where each set constructs an equivalence class (orbit) in a similar way to the set of four positions in the tetrahedral skeleton **3-5** (cf. Fig. 3.6). As a rather trivial example, methane **3-26** with four hydrogen atoms belongs to the point group T_d , so that the four hydrogens as ligands construct an equivalence class (orbit) governed by the coset representation $T_d(/C_{3v})$, just as the tetrahedral skeleton has a $T_d(/C_{3v})$ -orbit.

By placing a set of three hydrogen atoms and one chlorine atom on the four positions of **3-5**, there appears chloromethane **3-27**, as shown in Fig. 3.13. The molecule of

chloromethane **3-27** belongs to the point group C_{3v} (Eq. 3.11), which is a subgroup of T_d . Note that the three-fold axis (C_3) runs along the C—Cl bond.

Determination of Orbits

From a viewpoint of Fujita's unit-subduced-cycle-index (USCI) approach [4], there are two ways of discussing the point-group symmetries of (pro)molecules:

1. (Methodology 1: without subduction) The resulting chloromethane molecule **3-27** can be considered as it is, without referring to the tetrahedral skeleton **3-5**. Suppose that a set of four positions with three hydrogens and one chlorine is represented by a permutation representation $\mathbf{P}_{C_{3v}}$, because **3-27** belongs to the point group C_{3v} . The three hydrogen atoms of **3-27** are equivalent to construct an orbit governed by the coset representation $C_{3v}/(C_s)$, because each hydrogen atom is fixed under the action of the point group C_s , which is a subgroup of C_{3v} . The one chlorine atom belongs to the local point-group symmetry C_{3v} , so that the one-membered orbit of the chlorine atom is governed by the coset representation $C_{3v}/(C_{3v})$. It follows that we obtain the following equation:

$$\mathbf{P}_{C_{3v}} = C_{3v}/(C_s) + C_{3v}/(C_{3v}). \quad (3.37)$$

In general, suppose that the positions of a given molecule (or promolecule) belonging to the point-group symmetry \mathbf{G} is characterized by a permutation representation $\mathbf{P}_{\mathbf{G}}$. Then, the permutation representation $\mathbf{P}_{\mathbf{G}}$ is divided into a sum of coset representations of \mathbf{G} [4,8]:

$$\mathbf{P}_{\mathbf{G}} = \sum_{i=1}^s \alpha_i \mathbf{G}/(\mathbf{G}_i), \quad (3.38)$$

where the subgroup \mathbf{G}_i ($i = 1, 2, \dots, s$) covers the SSG of \mathbf{G} (Eq. 3.20), the coset representation $\mathbf{G}/(\mathbf{G}_i)$ covers the SCR of \mathbf{G} (Eq. 3.31), and the integer α_i represents the multiplicity of the coset representation $\mathbf{G}/(\mathbf{G}_i)$.

2. (Methodology 2: via subduction) The molecule of chloromethane **3-27** is alternatively interpreted by referring to the tetrahedral skeleton **3-5** (cf. Fig. 3.12). Then, the coset representation $T_d/(C_{3v})$ of the tetrahedral skeleton **3-5** is divided into the cosets representations $C_{3v}/(C_s)$ and $C_{3v}/(C_{3v})$ under the restriction to C_{3v} . This process is symbolically represented by the following equation:

$$T_d/(C_{3v}) \downarrow C_{3v} = C_{3v}/(C_s) + C_{3v}/(C_{3v}), \quad (3.39)$$

which is called the *subduction* of the coset representation $T_d/(C_{3v})$ by C_{3v} [4,7]. Note that the sum of the sizes of orbits appearing in the right-hand side ($|C_{3v}|/|C_s| = 6/2 = 3$ and $|C_{3v}|/|C_{3v}| = 6/6 = 1$) is equal to the size of an orbit appearing in the left-hand side ($|T_d|/|C_{3v}| = 24/6 = 4$).

In general, let us consider a given stereoskeleton of the point group \mathbf{G} , where the coset representation $\mathbf{G}/(\mathbf{G}_i)$ governs the $|\mathbf{G}|/|\mathbf{G}_i|$ positions of the stereoskeleton. Supposed that the point-group symmetry \mathbf{G} of the skeleton is restricted to the subgroup \mathbf{G}_j . Then

the positions of the skeleton are divided into a set of orbits in a product molecule of the point group G_j . The process of the division is called a *subduction* [4, Chapter 9], which obeys the following equation:

$$G(/G_i) \downarrow G_j = \sum_{k=1}^{v_j} \beta_k^{(ij)} G_j(/H_k^{(j)}) \quad (3.40)$$

for $i = 1, 2, \dots, s$ and $j = 1, 2, \dots, s$, where the subgroup $H_k^{(j)}$ covers the SSG of G_j and the coset representation $G_j(/H_k^{(j)})$ covers the SCR of G_j .

Mathematically speaking, Eq. 3.37 does not take account of the concept of subduction, while Eq. 3.39 takes account of the concept of subduction. Chemically speaking, Eq. 3.37 does not take account of the original skeleton **3-5**, while Eq. 3.39 takes account of the original skeleton **3-5** explicitly.

As found by comparing between the right-hand side of Eq. 3.37 (Methodology 1) and that of Eq. 3.39 (Methodology 2), these two methodologies are essentially equivalent from the viewpoint of coset representations to be considered. In particular, both methodologies are commonly effective to qualitative discussions. However, quantitative applications such as combinatorial enumerations require Methodology 2 (Eq. 3.40) which explicitly takes account of stereoskeletons for the proligand-promolecule model.

The following discussions will adopt the second way (Methodology 2) via the concept of subduction, because the first way (Methodology 1) is easily derived from the second way, as exemplified by the derivation from Eq. 3.39 to Eq. 3.37. Although the following procedure is concerned with a stereoskeleton with one orbit of positions, it can easily be extended to cover a stereoskeleton with two or more orbits of positions:

i

Rule 3.1. Procedure for Determining Orbits (Methodology 2).

1. Consider a stereoskeleton having n positions which are equivalent under the global point-group symmetry G of the stereoskeleton.
2. Determine the stabilizer G_i of one position selected appropriately from the n positions (cf. Subsection 3.2.5). The group G_i is a subgroup of G and fixes the selected position. Thereby, the n -positions construct an equivalence class (orbit) governed by the coset representation $G(/G_i)$.
3. Place a set of ligands (or proligands) on the n positions of the skeleton. Determine the global point-group symmetry G_j of the resultant product. This process is regarded as the restriction of G to G_j , which is represented by a subduction $G(/G_i) \downarrow G_j$.
4. Select a set of equivalent ligands (or proligands) under G_j so as to generate an equivalence class (orbit). Determine the stabilizer $H_k^{(j)}$ of one ligand (or proligand) selected appropriately from the orbit. Thereby this orbit is governed by the coset representation $G_j(/H_k^{(j)})$.
5. The preceding step is repeated to cover all sets of equivalent ligands (or proligands). The resultant coset representations $G_j(/H_k^{(j)})$ are collected to give Eq. 3.40.

Dichloromethane **3-28** shown in Fig. 3.13 is produced by placing a set of ligands (two chlorine atoms and two hydrogen atoms) on the four positions of **3-5**. The dichloromethane **3-28** belongs to the point group C_{2v} (Eq. 3.10), which is a subgroup of T_d . Note that there appears a two-fold axis ($C_{2(3)}$) bisects the angle of Cl—C—Cl and two mirror planes $\sigma_{d(1)}$ and $\sigma_{d(6)}$, if the point group C_{2v} is selected as a subgroup of T_d (cf. Table 3.1). The two chlorine atoms of **3-28** are equivalent to construct an orbit governed by the coset representation $C_{2v}/(C_s)$, because each chlorine atom is fixed under the action of the point group $C_s = \{I, \sigma_{d(1)}\}$ (Eq. 3.6), which is a subgroup of C_{2v} ($\subset T_d$). The two hydrogen atoms of **3-28** are equivalent to construct another orbit governed by the coset representation $C_{2v}/(C'_s)$, because each hydrogen atom is fixed under the action of the point group $C'_s = \{I, \sigma_{d(6)}\}$, which is a subgroup of C_{2v} ($\subset T_d$).

In summary, the derivation of dichloromethane **3-28** (C_{2v}) from the tetrahedral skeleton **3-5** (T_d) is symbolically represented by the following subduction:

$$T_d/(C_{3v}) \downarrow C_{2v} = C_{2v}/(C_s) + C_{2v}/(C'_s), \quad (3.41)$$

where the sum of the sizes of orbits appearing in the right-hand side ($|C_{2v}|/|C_s| + |C_{2v}|/|C'_s| = 4/2 + 4/2 = 4$) is equal to the size of an orbit appearing in the left-hand side ($|T_d|/|C_{3v}| = 24/6 = 4$). It should be noted that the two groups $C_s = \{I, \sigma_{d(1)}\}$ and $C'_s = \{I, \sigma_{d(6)}\}$ are conjugate within T_d but not conjugate within C_{2v} .

Bromochloromethane **3-29** shown in Fig. 3.13 is produced by placing a set of ligands (two hydrogens, one bromine, and one chlorine) on the four positions of **3-5**. The molecule of bromochloromethane **3-29** belongs to the point group C_s , which is a subgroup of T_d . Note that there appears a mirror plane containing the plane of Cl—C—Br. The two hydrogen atoms of **3-29** are equivalent to construct an orbit governed by the coset representation $C_s/(C_1)$, because each hydrogen atom is fixed under the action of the point group C_1 , which is a subgroup of C_s ($\subset T_d$). The chlorine atom (or the bromine atom) constructs a one-membered $C_s/(C_s)$ -orbit, because it is fixed by the mirror plane due to the local point-group symmetry C_s .

As a result, the derivation of bromochloromethane **3-29** (C_s) from the tetrahedral skeleton **3-5** (T_d) is symbolically represented by the following subduction:

$$T_d/(C_{3v}) \downarrow C_s = C_s/(C_1) + 2C_s/(C_s), \quad (3.42)$$

where the sum of the sizes of orbits appearing in the right-hand side ($|C_s|/|C_1| + 2 \times |C_s|/|C_s| = 2 + 2 \times 2/2 = 4$) is equal to the size of an orbit appearing in the left-hand side ($|T_d|/|C_{3v}| = 24/6 = 4$).

Bromochlorofluoromethane **3-30** shown in Fig. 3.13 is produced by placing a set of ligands (hydrogen, one fluorine, one bromine, and one chlorine) on the four positions of **3-5**. The molecule of bromochlorofluoromethane **3-30** belongs to the point group C_1 , which is a subgroup of T_d . Each of the atoms in **3-30** constructs a one-membered orbit governed by the coset representation $C_1/(C_1)$, because each atom is fixed under the action of the point group C_1 , which is a subgroup of the global symmetry C_1 .

The derivation of bromochlorofluoromethane **3-30** (C_1) from the tetrahedral skeleton **3-5** (T_d) is symbolically represented by the following subduction:

$$T_d(/C_{3v}) \downarrow C_1 = 4C_1(/C_1), \quad (3.43)$$

where the sum of the sizes of orbits appearing in the right-hand side ($4 \times |C_1|/|C_1| = 4 \times 1/1 = 4$) is equal to the size of an orbit appearing in the left-hand side ($|T_d|/|C_{3v}| = 24/6 = 4$).

3.4.3 The SCR Notation

The set of coset representations (SCR) discussed in Methodology 1 (Eq. 3.38) and the subduction of coset representations due to Methodology 2 (Eq. 3.40) can be applied to detailed specification of point-group symmetries of molecules [8,40].

The SCR Notation of Methodology 1

Methodology 1 discussed on page 79 (Eq. 3.38) does not take account of a stereoskeleton. If the number $|G|/|G_i|$ of (pro)ligands $A^{(i)}$ occupy the positions governed by the coset representation $G(/G_i)$, the resulting (pro)molecule is represented by the following *SCR notation* (due to Methodology 1) [8]:²²

$$G[\dots; /G_i(A_{|G|/|G_i|}^{(i)}); \dots]. \quad (3.44)$$

The molecules listed in Fig. 3.13 are characterized by the following SCR notations, where the SCR and accommodated atoms for each molecule are aligned according to Eq. 3.44:

$$\mathbf{3-26} \quad T_d[/C_{3v}(H_4); /T_d(C)] \quad (3.45)$$

$$\mathbf{3-27} \text{ (Eq. 3.37)} \quad C_{3v}[/C_s(H_3); 2/C_{3v}(C, Cl)] \quad (3.46)$$

$$\mathbf{3-28} \text{ (Eq. 3.41)} \quad C_{2v}[/C_s(Cl_2); /C'_s(H_2); /C_{2v}(C)] \quad (3.47)$$

$$\mathbf{3-29} \text{ (Eq. 3.42)} \quad C_s[/C_1(H_2); 3/C_s(C, Cl, Br)] \quad (3.48)$$

$$\mathbf{3-30} \text{ (Eq. 3.43)} \quad C_1[5/C_1(C, H, F, Cl, Br)], \quad (3.49)$$

Central carbon atoms are also specified by the respective SCR notations. Note that the number before a slash is the multiplicity of the coset representations at issue. For example, the term $2/C_{3v}(C, Cl)$ in Eq. 3.46 is an abbreviated form of $/C_{3v}(C); /C_{3v}(Cl)$, which are the same kind of coset representations, but exhibit different modes of accommodation (the central carbon atom and the chlorine atom) in chloromethane **3-27**.

²² The original notation of case 1 [8] is adopted after renamed *the SCR notation of Methodology 1*.

The SCR Notation of Methodology 2

Methodology 2 discussed on page 79 (Eq. 3.40) takes account of a stereoskeleton. The subduction of coset representation of the skeleton (Eq. 3.40) is explicitly characterized in the SCR notation of Methodology 2 [8]:²³

$$\mathbf{G}(\dots | / \mathbf{G}_i | \dots) \downarrow \mathbf{G}_j = \mathbf{G}_j[\dots | \dots; / \mathbf{H}_k^{(ij)} (A_{|\mathbf{G}_j|/|\mathbf{H}_k^{(ij)}|}^{(k(ij))}); \dots | \dots], \quad (3.50)$$

where the coset representation $\mathbf{G}(/ \mathbf{G}_i)$ of the skeleton is subduced into the \mathbf{G}_j -symmetry of the (pro)molecule to be specified. Then, the $\mathbf{G}_j(\mathbf{H}_k^{(ij)})$ -orbit of the (pro)molecule accommodates the number $|\mathbf{G}_j|/|\mathbf{H}_k^{(ij)}|$ of (pro)ligands represented by $A^{(k(ij))}$.

The molecules listed in Fig. 3.13 are characterized by the following SCR notations of Methodology 2. After the subduction of the tetrahedral skeleton into its subgroup, the resulting SCR and accommodated atoms for each molecule are aligned according to Eq. 3.50:

$$\mathbf{3-26} \quad \mathbf{T}_d(/ \mathbf{C}_{3v} | / \mathbf{T}_d) \downarrow \mathbf{T}_d[/ \mathbf{C}_{3v}(\text{H}_4) | / \mathbf{T}_d(\text{C})] \quad (3.51)$$

$$\mathbf{3-27} \text{ (Eq. 3.39)} \quad \mathbf{T}_d(/ \mathbf{C}_{3v} | / \mathbf{T}_d) \downarrow \mathbf{C}_{3v}[/ \mathbf{C}_s(\text{H}_3); / \mathbf{C}_{3v}(\text{Cl}) | / \mathbf{C}_{3v}(\text{C})] \quad (3.52)$$

$$\mathbf{3-28} \text{ (Eq. 3.41)} \quad \mathbf{T}_d(/ \mathbf{C}_{3v} | / \mathbf{T}_d) \downarrow \mathbf{C}_{2v}[/ \mathbf{C}_s(\text{Cl}_2); / \mathbf{C}'_s(\text{H}_2) | / \mathbf{C}_{2v}(\text{C})] \quad (3.53)$$

$$\mathbf{3-29} \text{ (Eq. 3.42)} \quad \mathbf{T}_d(/ \mathbf{C}_{3v} | / \mathbf{T}_d) \downarrow \mathbf{C}_s[/ \mathbf{C}_1(\text{H}_2); 2 / \mathbf{C}_s(\text{Cl}, \text{Br}) | / \mathbf{C}_s(\text{C})] \quad (3.54)$$

$$\mathbf{3-30} \text{ (Eq. 3.43)} \quad \mathbf{T}_d(/ \mathbf{C}_{3v} | / \mathbf{T}_d) \downarrow \mathbf{C}_1[4 / \mathbf{C}_1(\text{H}, \text{F}, \text{Cl}, \text{Br}) | / \mathbf{C}_1(\text{C})] \quad (3.55)$$

For example, the four positions of the tetrahedral skeleton is subduced according to Eq. 3.39, while the local point-group symmetry of the central carbon atom is subduced according to $\mathbf{T}_d(/ \mathbf{T}_d) \downarrow \mathbf{C}_{3v} = \mathbf{C}_{3v}(/ \mathbf{C}_{3v})$. The total feature is expressed by the symbol $\mathbf{T}_d(/ \mathbf{C}_{3v} | / \mathbf{T}_d) \downarrow \mathbf{C}_{3v}$. The resulting chloromethane **3-27** is characterized by the SCR notation of Methodology 2 shown in Eq. 3.52.

3.4.4 Site Symmetries vs. Coset Representations for Symmetry Notations

It is worthwhile here to point out the merits of the SCR notation [8] in comparison with other methods for differentiating molecules with the same point-group symmetry. Let us examine the point group \mathbf{C}_{2v} for characterizing dichloromethane (CH_2Cl_2 , **3-28**) based on a tetrahedral skeleton (cf. Eq. 3.47 and Eq. 3.53). A notation assigned to dichloromethane should be different from those assigned to other \mathbf{C}_{2v} -molecules, e.g., water molecule (H_2O) as a planar molecule and adamantan-2-one based on the skeleton **3-23**.²⁴

1. Pople's method is based on 'framework groups' [41], which assigns the notation

$$\mathbf{C}_{2v}[\mathbf{C}_2(\text{C}), \sigma_v(\text{Cl}_2), \sigma'_v(\text{Cl}_2)]$$

to dichloromethane, where each atom is characterized

²³ The original notation of case 2 [8] is slightly modified and renamed *the SCR notation of Methodology 2*.

²⁴ For additional examples of the SCR notations of \mathbf{C}_{2v} -molecules, see [8, Table 8]. In addition, the SCR notations of \mathbf{D}_{3h} -, \mathbf{T}_d -, \mathbf{D}_{2d} -, \mathbf{D}_{2d} -, and \mathbf{D}_{2h} -molecules have also been reported [8].

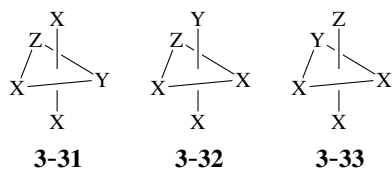


Fig. 3.14. Three trigonal bipyramidal derivatives with the composition X^3YZ . A central atom (P) is omitted for the sake of simplicity.

by a framework group. Because the relationship between such a framework group and a global symmetry is not fully clarified, this notation has drawbacks in the application to trigonal bipyramidal complexes, as pointed out by Brocas [42]. In addition, the formulations due to framework groups have not reached the concepts of coset representations, their subductions, and orbits. Fujita's SCR notation [8] is successfully applied to trigonal bipyramidal complexes [40].

2. Flurry's method is based on site symmetries [43], which are used to assign the notation [$C_{2v}(C)$, $C_s(Cl_2)$, $C'_s(H_2)$] to dichloromethane. The term 'site symmetries' corresponds to the term *local point-group symmetries* in the present context. Because Flurry's notation has emphasized site symmetries, it has not reached the concepts of coset representations, their subductions, and orbits.
3. Fujita's SCR (set-of-coset-representation) notation is based on coset representations and their subductions [8,40]. As discussed above, the SCR notation of Methodology 1 [8] adopts the data of a set of coset representations, where the SCR notation shown in Eq. 3.47 is assigned to dichloromethane. The SCR notation of Methodology 2 [8] adopts the subduction data (e.g., Eq. 3.41), where the SCR notation shown in Eq. 3.53 is assigned to dichloromethane. The concept of site symmetries (local point-group symmetries) for Flurry's method has been incorporated into the concept of coset representations for Fujita's SCR notation, as discussed in our book [4, Chapter 7].²⁵

Brocas [42] has pointed out that three isomers (**3-31**, **3-32**, and **3-33**) having the composition PX^3YZ , which are derived from a trigonal bipyramidal skeleton of D_{3h} , have the same framework group, i.e., $C_s[\sigma(PXYZ), X(X_2)]$ (Fig. 3.14) according to Pople's method. Flurry's method also gives the same notation [$C_s(PXYZ)$, $C_1(X_2)$] to the three isomers. To differentiate them, Brocas [42] has proposed the modified Schönflies symbols, i.e., C_{3h} for **3-31** as well as C_{sv} for **3-32** and **3-33**. However, **3-32** and **3-33** have the same modified Schönflies symbol C_{sv} yet.

Fujita has discussed the orbits of a trigonal bipyramidal skeleton and their subduction in detail [8]. The five positions of the skeleton are divided into two orbits, where three

²⁵ For site symmetries applied to the construction of symmetry adapted functions, see [44]. For coset representations applied to the same purpose, see [45].

equatorial positions construct a $D_{3h}(/C_{2v})$ -orbit ($|D_{3h}|/|C_{2v}| = 12/4 = 3$), while two axial positions construct a $D_{3h}(/C_{3v})$ -orbit ($|D_{3h}|/|C_{3v}| = 12/6 = 2$). In addition, a central phosphorus atom constructs a $D_{3h}(/D_{3h})$ -orbit ($|D_{3h}|/|D_{3h}| = 12/12 = 1$). These orbits are subdivided into suborbitals during the derivation of **3-31**, **3-32**, and **3-33**. According to Fujita's SCR notation, the modes of subdivision are specified by the following SCR notations [8]:

$$\mathbf{3-31} \quad D_{3h}(/C_{2v} \mid /C_{3v} \mid /D_{3h}) \downarrow C'_s[3/C_s(X, Y, Z) \mid /C_1(X_2) \mid /C_s(P)] \quad (3.56)$$

$$\mathbf{3-32} \quad D_{3h}(/C_{2v} \mid /C_{3v} \mid /D_{3h}) \downarrow C_s[/C_1(X_2), /C_s(Z) \mid 2/C_s(X, Y) \mid /C_s(P)] \quad (3.57)$$

$$\mathbf{3-33} \quad D_{3h}(/C_{2v} \mid /C_{3v} \mid /D_{3h}) \downarrow C_s[/C_1(X_2), /C_s(Y) \mid 2/C_s(X, Z) \mid /C_s(P)] \quad (3.58)$$

The comparison between Eq. 3.57 and Eq. 3.58 indicates that three $C_s(/C_s)$ -orbits in **3-32** exhibit different modes of separation from those in **3-33**, where the difference stems from the axial and equatorial positions of the skeleton.

References

- [1] S. Fujita, *Tetrahedron*, **47**, 31–46 (1991).
- [2] IUPAC, “Nomenclature of Inorganic Chemistry, Recommendations 1990”, Blackwell Scientific, Oxford (1990).
- [3] IUPAC Chemical Nomenclature and Structure Representation Division, *Provisional Recommendations. Nomenclature of Organic Chemistry* (2004), http://old.iupac.org/reports/provisional/abstract04/favre_310305.html.
cf. H. A. Favre, W. H. Powell, “Nomenclature of Organic Chemistry. IUPAC Recommendations and Preferred Names 2013”, The Royal Society of Chemistry, Cambridge (2013).
- [4] S. Fujita, “Symmetry and Combinatorial Enumeration in Chemistry”, Springer-Verlag, Berlin-Heidelberg (1991).
- [5] S. Fujita, “Diagrammatical Approach to Molecular Symmetry and Enumeration of Stereoisomers”, University of Kragujevac, Faculty of Science, Kragujevac (2007).
- [6] S. Fujita, *Theor. Chim. Acta*, **76**, 247–268 (1989).
- [7] S. Fujita, *J. Am. Chem. Soc.*, **112**, 3390–3397 (1990).
- [8] S. Fujita, *Bull. Chem. Soc. Jpn.*, **63**, 315–327 (1990).
- [9] S. Fujita, *Bull. Chem. Soc. Jpn.*, **63**, 203–215 (1990).
- [10] S. Fujita, *Tetrahedron*, **46**, 365–382 (1990).
- [11] S. Fujita, *J. Math. Chem.*, **33**, 113–143 (2003).
- [12] S. Fujita, *Bull. Chem. Soc. Jpn.*, **63**, 2770–2775 (1990).
- [13] S. Fujita, *Bull. Chem. Soc. Jpn.*, **64**, 3313–3323 (1991).

- [14] S. Fujita, *Theor. Chim. Acta*, **82**, 473–498 (1992).
- [15] S. Fujita, *J. Math. Chem.*, **32**, 1–17 (2002).
- [16] S. Fujita, *Helv. Chim. Acta*, **85**, 2440–2457 (2002).
- [17] S. Fujita, *Polyhedron*, **12**, 95–110 (1993).
- [18] S. Fujita and N. Matsubara, *Internet Electronic Journal of Molecular Design*, **2**, 224–241 (2003).
- [19] S. Fujita, *MATCH Commun. Math. Comput. Chem.*, **71**, 511–536 (2014).
- [20] S. Fujita, *MATCH Commun. Math. Comput. Chem.*, **71**, 537–574 (2014).
- [21] S. Fujita, *MATCH Commun. Math. Comput. Chem.*, **71**, 575–608 (2014).
- [22] S. Fujita, *J. Chem. Inf. Comput. Sci.*, **39**, 151–163 (1999).
- [23] S. Fujita, *Bull. Chem. Soc. Jpn.*, **63**, 1876–1883 (1990).
- [24] S. Fujita, *J. Math. Chem.*, **50**, 2202–2222 (2012).
- [25] S. Fujita, *J. Math. Chem.*, **50**, 2168–2201 (2012).
- [26] S. Fujita, *Bull. Chem. Soc. Jpn.*, **84**, 1192–1207 (2011).
- [27] S. Fujita, *MATCH Commun. Math. Comput. Chem.*, **67**, 5–24 (2012).
- [28] S. Fujita, *MATCH Commun. Math. Comput. Chem.*, **67**, 25–54 (2012).
- [29] S. Fujita, *MATCH Commun. Math. Comput. Chem.*, **67**, 649–668 (2012).
- [30] S. Fujita, *MATCH Commun. Math. Comput. Chem.*, **67**, 669–686 (2012).
- [31] S. Fujita, *MATCH Commun. Math. Comput. Chem.*, **67**, 687–712 (2012).
- [32] S. Fujita, *Bull. Chem. Soc. Jpn.*, **85**, 793–810 (2012).
- [33] S. Fujita, *Bull. Chem. Soc. Jpn.*, **85**, 811–821 (2012).
- [34] S. Fujita, *J. Math. Chem.*, **47**, 145–166 (2010).
- [35] S. Fujita, *J. Math. Chem.*, **49**, 95–162 (2011).
- [36] S. Fujita, *MATCH Commun. Math. Comput. Chem.*, **54**, 251–300 (2005).
- [37] S. Fujita, *MATCH Commun. Math. Comput. Chem.*, **55**, 5–38 (2006).
- [38] S. Fujita, *MATCH Commun. Math. Comput. Chem.*, **55**, 237–270 (2006).
- [39] IUPAC Organic Chemistry Division, *Pure Appl. Chem.*, **68**, 2193–2222 (1996).
- [40] S. Fujita, *Memoirs of the Faculty of Engineering and Design, Kyoto Institute of Technology*, **47**, 111–126 (1999).
- [41] J. A. Pople, *J. Am. Chem. Soc.*, **102**, 4615–4622 (1980).
- [42] J. Brocas, *J. Am. Chem. Soc.*, **108**, 1135–1145 (1986).
- [43] R. L. Flurry, Jr., *J. Am. Chem. Soc.*, **103**, 2901–2902 (1981).
- [44] R. L. Flurry, Jr., *Theor. Chim. Acta*, **31**, 221–230 (1973).
- [45] S. Fujita, *Theor. Chim. Acta*, **78**, 45–63 (1990).

4 Sphericities of Orbits and Prochirality¹

4.1 Sphericities of Orbits

This section introduces the concept of *sphericities* and the related concept *chirality fittingness* [1,2], which are defined to characterize equivalence classes (orbits).

4.1.1 Orbits of Equivalent Proligands

As discussed in Chapter 3 (Subsection 3.4.2), point-group symmetries of promolecules can be investigated by Methodology 1 (Eq. 3.38 on page 79) and Methodology 2 (Eq. 3.40 on page 80), just as point-group symmetries of molecules have been discussed by these methods [1]. These methods are based on a common foundation due to a set of orbits contained in molecules or promolecules. The following theorem is obvious because of the proligand-promolecule model (Defs. 3.1–3.3 on pages 53–54):

Theorem 4.1 (Conservation of Orbits). A set of orbits in a molecule is maintained in the corresponding promolecule, although the point group of the molecule may be different from that of the promolecule.

The case in which the molecule and the corresponding promolecule belong to different point groups is referred to as a *mismatched case* (cf. Subsection 3.1.2). Theorem 4.1 is related to Theorem 3.1 (page 55).

For example, the two-membered $C_s(/C_1)$ -orbit accommodating two hydrogens and the one-membered $C_s(/C_s)$ -orbits accommodating respectively a chlorine atom and a bromine atom in the molecule **3-29** (Fig. 3.13) remain unchanged in the corresponding promolecule **4-1**, where we place A = Cl, B = Br, and X = H, as shown in Fig. 4.1. Because both the molecule **3-29** and the promolecule **4-1** belong to the same point group C_s , the coset representations $C_s(/C_1)$ and $C_s(/C_s)$ are also maintained during the process of interconversion between **3-29** and **4-1**.

On the other hand, the highest-attainable symmetry of pentaerythritol **4-3** is determined to be D_{2d} , as shown in a top view of Fig. 4.1. Note that the occupation of a tetrahedral

¹ This chapter is based on S. Fujita, "Chirality fittingness of an orbit governed by a coset representation. Integration of point-group and permutation-group theories to treat local chirality and prochirality", *J. Am. Chem. Soc.*, **112**, 3390–3397 (1990); S. Fujita, "Stereochemistry and Stereoisomerism Characterized by the Sphericity Concept", *Bull. Chem. Soc. Jpn.*, **74**, 1585–1603 (2001); S. Fujita, "Prochirality Revisited. An Approach for Restructuring Stereochemistry by Novel Terminology", *J. Org. Chem.*, **67**, 6055–6063 (2002); S. Fujita, "Sphericity Governs Both Stereochemistry in a Molecule and Stereoisomerism Among Molecules", *Chem. Rec.*, **2**, 164–176 (2002); S. Fujita, "Sphericity Beyond Topicity in Characterizing Stereochemical Phenomena. Novel Concepts Based on Coset Representations and Their Subductions", *Bull. Chem. Soc. Jpn.*, **75**, 1863–1883 (2002).

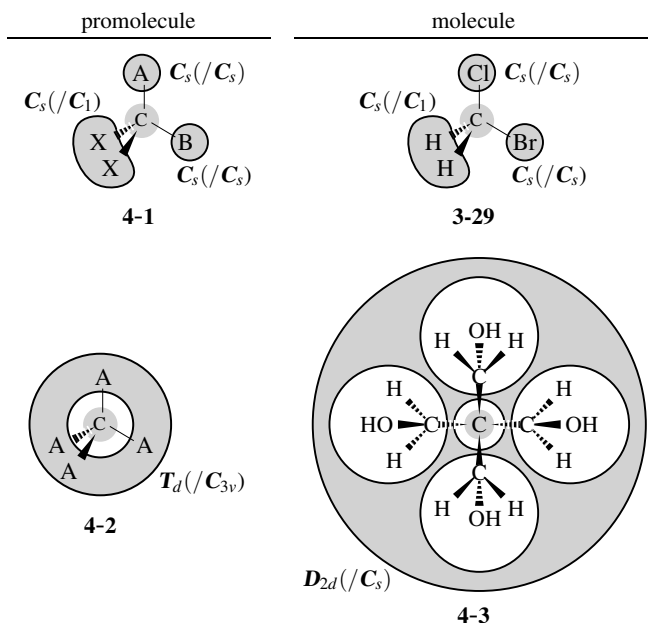


Fig. 4.1. Orbits in promolecules and molecules for characterizing chlorobromomethane (a matched case) and pentaerythritol (a mismatched case).

skeleton by four hydroxymethyl ligands results in the symmetry restriction from T_d to D_{2d} , because each hydroxymethyl ligand (CH_2OH) belongs to the point group C_s . The four hydroxymethyl ligands construct an orbit governed by the coset representation $D_{2d}(/C_s)$, where the size of the orbit is calculated to be $|D_{2d}(/C_s)| = 8/2 = 4$.

By placing $A = \text{CH}_2\text{OH}$, the molecule **4-3** of D_{2d} is converted into the corresponding promolecule **4-2** of T_d . The four-membered $D_{2d}(/C_s)$ -orbit of **4-3** is converted into the four-membered $T_d(/C_{3v})$ -orbit of **4-2**, where the size of the orbit is unchanged to be $|T_d(/C_{3v})| = 24/6 = 4$. Theorem 4.1 permits such a case that the point group of the molecule is different from that of the promolecule. This case is an example of mismatched case.

It should be noted that the promolecule **4-2** is also obtained by starting from methane **3-26** (Fig. 3.13 on page 78) by placing $A = \text{H}$. This case is a matched case, because the four-membered $T_d(/C_{3v})$ -orbit of the methane molecule **3-26** is unchanged to give the four-membered $T_d(/C_{3v})$ -orbit of the promolecule **4-2** in accord with Theorem 4.1.

4.1.2 Three Kinds of Sphericities

The next task is to formulate *sphericities* and *chirality fittingness* as common properties for characterizing an orbit of a molecule (e.g., **3-29** and **4-3** in Fig. 4.1) and the corresponding orbit of the derived promolecule (e.g., **4-1** and **4-2** in Fig. 4.1).

A coset representation $G(/G_i)$ is classified into three cases according to whether the global point-group symmetry G and the local point-group symmetry G_i are achiral or chiral. The terms concerning *sphericity* have been coined by Fujita to refer to the three cases as follows [1,2]:

Definition 4.1 (Sphericities for Characterizing Coset Representations and Orbits).

- **(Homosphericity)** If both the global point-group symmetry G and the local point-group symmetry G_i are achiral, the coset representation $G(/G_i)$ is defined as being *homospheric*. The corresponding orbit of size $|G|/|G_i|$ is referred to as a *homospheric orbit*.
- **(Enantiosphericity)** If the global point-group symmetry G is achiral but the local point-group symmetry G_i is chiral, the coset representation $G(/G_i)$ is defined as being *enantiospheric*. The corresponding orbit of size $|G|/|G_i|$ is referred to as an *enantiospheric orbit*, which is divided into two halves of size $|G|/2|G_i|$ under the maximum chiral subgroup of G .
- **(Hemisphericity)** If both the global point-group symmetry G and the local point-group symmetry G_i are chiral, the coset representation $G(/G_i)$ is defined as being *hemispheric*. The corresponding orbit of size $|G|/|G_i|$ is referred to as a *hemispheric orbit*.

Exercise 4.1.



- Assign sphericities to the orbits appearing in the molecules (3-29 and 4-3) and the promolecules (4-1 and 4-2) listed in Fig. 4.1 (page 88).
 - Compare the sphericity of an orbit in each molecule with the sphericity of the corresponding orbit in the derived promolecule.
-

4.1.3 Chirality Fittingness for Three Modes of Accommodation

The sphericities defined by Def. 4.1 specify the modes of accommodation in the corresponding orbits. The term *chirality fittingness* is coined by Fujita to refer to the mode of accommodation which is specified by the sphericity of each orbit [1,2]. Such modes of accommodation are summarized in Fig. 4.2.

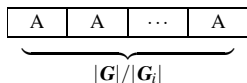
Chirality Fittingness of Homospheric Orbits

Because the local point-group symmetry G_i of a homospheric orbit $G(/G_i)$ -orbit is achiral according to Def. 4.1, the following theorem is obvious.

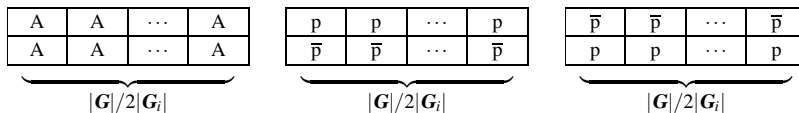
Theorem 4.2 (Chirality Fittingness of a Homospheric Orbit). A homospheric $G(/G_i)$ -orbit is capable of accommodating the number $|G|/|G_i|$ of achiral ligands (or proligands) of the same kind.

The mode of accommodation due to Theorem 4.2 is illustrated in Fig. 4.2(a), where the homospheric orbit consists of $|G|/|G_i|$ frames, each of which accommodates an achiral proligand A in isolation.

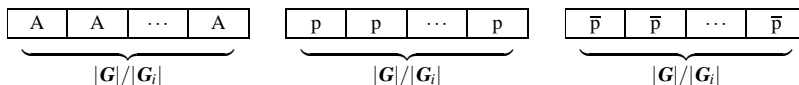
(a) Chirality fittingness of a homospheric orbit



(b) Chirality fittingness of an enantiospheric orbit



(c) Chirality fittingness of a hemispheric orbit

**Fig. 4.2.** Chirality fittingness of orbits of three kinds of sphericities.

The restriction of a homospheric orbit to the maximum chiral subgroup G_C (cf. Subsection 3.2.4) results in no division, so as to give the following subduction of $G(/G_i)$:

$$G(/G_i) \downarrow G_C = G_C(/G_{(C)_i}), \quad (4.1)$$

where the achiral subgroup G_i of G is restricted to a chiral subgroup $G_{(C)_i}$ of the maximum chiral subgroup G_C , where the size of the orbit remain unchanged, i.e., $|G_C|/|G_{(C)_i}| = |G|/|G_i|$.

As found in Fig. 3.13 (page 78), the $T_d(/C_{3v})$ -orbit of **3-26**, the $C_{3v}(/C_{3v})$ - and $C_{3v}(/C_s)$ -orbit of **3-27**, and the $C_{2v}(/C_s)$ - and $C_{2v}(/C'_s)$ -orbit of **3-28** are homospheric according to Def. 4.1. The $D_{2d}(/C_s)$ -orbit of **4-3** (Fig. 4.1) is also homospheric according to Def. 4.1. According to Eq. 4.1, we obtain $T_d(/C_{3v}) \downarrow T = T(/C_3)$, $C_{3v}(/C_{3v}) \downarrow C_3 = C_3(/C_3)$, $C_{3v}(/C_s) \downarrow C_3 = C_3(/C_1)$, and so on. Each of these homospheric orbits accommodates achiral ligands of the same kinds (hydrogens, chlorines, or hydroxymethyls). The corresponding promolecules have homospheric orbits, each of which accommodates achiral proligands of the same kind, e.g., the achiral proligand A or B in the $C_s(/C_s)$ -orbit of **4-1** as well as the four achiral A's in the $T_d(/C_{3v})$ -orbit of **4-2** (Fig. 4.1). These results hold true in general, so as to give Theorem 4.2 and the illustration of Fig. 4.2(a).

Chirality Fittingness of Enantiospheric Orbits

An enantiospheric $G(/G_i)$ -orbit of size $|G|/|G_i|$ (Def. 4.1) is divided into two halves of size $|G|/2|G_i|$ under the maximum chiral subgroup G_C of G (cf. Subsection 3.2.4). Note that the two halves become equivalent by reflection operations which are not contained in the maximum chiral group ($G - G_C$). It follows that the restriction to the maximum chiral subgroup G_C results in the following subduction of $G(/G_i)$ [3]:

$$G(/G_i) \downarrow G_C = 2G_C(/G_i), \quad (4.2)$$

where the chiral subgroup G_i of G is also a subgroup of the maximum chiral subgroup G_C , or in several cases,

$$G(/G_i) \downarrow G_C = G_C(/G_i) + G_C(/G'_i), \quad (4.3)$$

where G_i and G'_i are conjugate under G but not conjugate under G_C . Because of $|G_C| = |G|/2$, the size $|G_C|/|G_i|$ (or $|G_C|/|G'_i|$) is equal to $|G|/2|G_i|$.

In order that the two halves are equivalent by reflection operations ($G - G_C$), a set of ligands (or proligands) contained in one half should be a mirror image of another set of ligands (or proligands) contained in the other half. This requirement affords the following theorem:

Theorem 4.3 (Chirality Fittingness of an Enantiospheric Orbit). An enantiospheric $G(/G_i)$ -orbit is divided into two halves, where one half is capable of accommodating achiral or chiral ligands (or proligands) of same kind, and the other half is capable of accommodating achiral ligands (or proligands) of the same kind as the original half or chiral ligands (or proligands) of the opposite chirality sense to the original half.

The mode of accommodation due to Theorem 4.3 is illustrated in Fig. 4.2(b), where the enantiospheric orbit is divided into two halves, each of which has $|G|/2|G_i|$ frames. The two sets of frames are filled by achiral proligands A or pairs of chiral proligands p/\bar{p} in a manner that the global point-group symmetry G is maintained. Even in the cases of accommodating achiral proligands A's, one half of A's is the mirror image of the other half of A's.

The $C_s(/C_1)$ -orbit of the promolecule **4-1** (or the molecule **3-29**) is a two-membered enantiospheric orbit, which accommodates two achiral proligands X's (or hydrogen atoms as achiral ligands) according to Theorem 4.3 and the first illustration of Fig. 4.2(b). It should be noted that an achiral proligand X (or an achiral ligand H) in isolation is restricted to be locally chiral after it is incorporated into either half of the $C_s(/C_1)$ -orbit of **4-1** (or **3-29**). It is a mirror image of another achiral proligand X (or another achiral ligand H) which is incorporated into the other half of the $C_s(/C_1)$ -orbit.

The $C_s(/C_1)$ -orbit of a promolecule **4-4** (Fig. 4.3) exhibits one mode of accommodation of a pair of chiral proligands p/\bar{p} , where one half of the $C_s(/C_1)$ -orbit accommodates the proligand p and the other half accommodates the counterpart proligand \bar{p} according to the second (or the third) illustration of Fig. 4.2(b). The mode of accommodation can be also applied to the molecule **4-5**.

As found in the $C_s(/C_1)$ -orbit of another achiral promolecule **4-6** (Fig. 4.3), an opposite packing is possible according to the third (or second) illustration of Fig. 4.2(b). This mode of accommodation can be also applied to the molecule **4-7**.

The relationship between **4-4** and **4-6** (or between **4-5** and **4-7**) is referred to as being 'diastereomeric' due to modern stereochemistry, or more definitely, as being *RS*-diastereomeric due to Fujita's stereoisogram approach [4-6]. The central atoms of **4-4** and **4-6** (or **4-5** and **4-7**) are frequently called 'pseudoasymmetric atoms'.

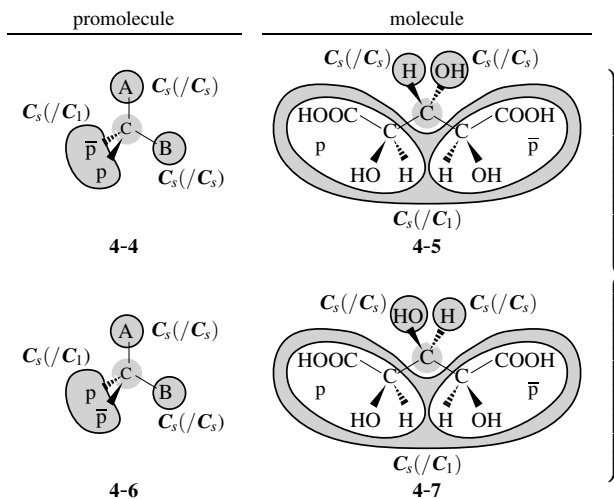


Fig. 4.3. Orbits in promolecules and molecules for characterizing achiral 2,3,4-trihydroxyglutaric acids. The two modes of packing are controlled by the chirality fittingness of an enantiospheric $C_s(/C_1)$ -orbit.

Chirality Fittingness of Hemispheric Orbits

According to Def. 4.1, a chiral promolecule (or a chiral molecule) has hemispheric orbits, but no homospheric nor enantiospheric orbits. The following theorem holds true obviously:

Theorem 4.4 (Chirality Fittingness of a Hemispheric Orbit). A hemispheric $G(/G_i)$ -orbit is capable of accommodating the number $|G|/|G_i|$ of achiral or chiral ligands (or proligands) of the same kind.

The modes of accommodation are illustrated in Fig. 4.2(c).

All of the $C_1(/C_1)$ -orbits appearing in bromochlorofluoromethane **3-30** (Fig. 3.13 on page 78) are determined to be hemispheric, where each $C_1(/C_1)$ -orbit accommodates an atom H, Cl, Br, or F as an achiral ligand in isolation. Each mode of accommodation obeys the first illustration of of Fig. 4.2(c). When incorporated, the local point-group symmetry of each atom (or each achiral ligand) is restricted to be chiral. It should be noted that there is an enantiomeric counterpart of **3-30**, where it exhibits the same point-group symmetric properties except optical rotations.

4.2 Prochirality

4.2.1 Confusion on the Term ‘Prochirality’

The term ‘prochirality’ has been originally proposed by Hanson to support *pro-R/pro-S*-descriptors [7]. The term ‘prochirality’ for supporting *pro-R/pro-S*-descriptors has caused continuous confusion, as found in later discussions without mathematical foundations [8–

12]. This type of confusion is parallel to the confusion on the term ‘chirality’ for supporting *R/S*-stereodescriptors of Cahn-Ingold-Prelog (CIP) system [13,14]. Such entangled discussions that have attempted to justify the ‘prochirality’ for supporting *pro-R/pro-S*-descriptors should be totally abandoned,² because it is difficult to select proper and rational parts from the accumulated discussions.

In fact, the IUPAC Recommendations 1974 [16] has given a polysemous definition of the term ‘prochirality’ as follows:

- E-4.12(a) [defining the term ‘prochirality’ as a geometric concept]: “An achiral object having at least one pair of features that can be distinguished only by reference to a chiral object or to a chiral reference frame is said to be prochiral, and the property of having such a pair of features is termed prochirality. A consequence is that, if one of the features of the pair in a prochiral object is considered to differ from the other feature, the resultant object is chiral.”
- E-4.12(b) [defining the term ‘prochirality’ for supporting *pro-R/pro-S*-descriptors by Hanson [7]]: “In a molecule an achiral center or atom is said to be prochiral if it would be held to be chiral when two attached atoms or groups, that taken in isolation are indistinguishable, are considered to be differ.”

The IUPAC Recommendations 1974 [16] has mainly given examples due to Rule E-4.12(b). For example, Rule E-4.13 of [16] has exemplified *pro-R/pro-S*-descriptors by using the methylene carbon atom of D-(+)-glyceraldehyde $\text{CH}_2(\text{OH})\text{--CH}(\text{OH})\text{--CHO}$, which was described in Hanson’s paper [7]. It follows that Rule E-4.12(b) as well as Hanson’s definition permits the presence of a ‘prochiral center’ in such a chiral molecule as D-(+)-glyceraldehyde, so that this example is contradictory to Rule E-4.12(a). Note that the prefix *pro-* of the term prochiral stems from Greek *pró-* (before in time or place) so as to support E-4.12(a) rather than E-4.12(b). In this meaning, Rule E-4.12(b) as well as Hanson’s definition of ‘prochirality’ has nothing to do with chirality as a geometric concept and should be abandoned.

From the viewpoint of orbits, the methylene carbon atom of D-(+)-glyceraldehyde **4-9** has four ligands, each of which belongs to a one-membered hemispheric C_1 ($/\text{C}_1$)-orbit, as shown in Fig. 4.4. A proligand A or B in the corresponding promolecule **4-8** is achiral in isolation (when detached) but becomes locally chiral after accommodated in a one-membered hemispheric C_1 ($/\text{C}_1$)-orbit. The two A’s in **4-8** (as well as two H’s in **4-9**) are geometrically different from each other, so that they are differentiated energetically even under achiral

² The IUPAC Recommendations 1996 [15] has referred to the term ‘prochirality’ as “This term is used in different, sometimes contradictory ways; four are listed below.” After the terms ‘stereoheterotopic’, ‘enantiotopic’, and ‘diastereotopic’ were introduced [8,11], the term ‘stereoheterotopic’ has been misleadingly used for the purpose of rationalize Hanson’s ‘prochirality’ [7]. However, the misleading usage of the term ‘stereoheterotopic’ for this purpose is strongly discouraged, as pointed out by the IUPAC Recommendations 1996 [15].

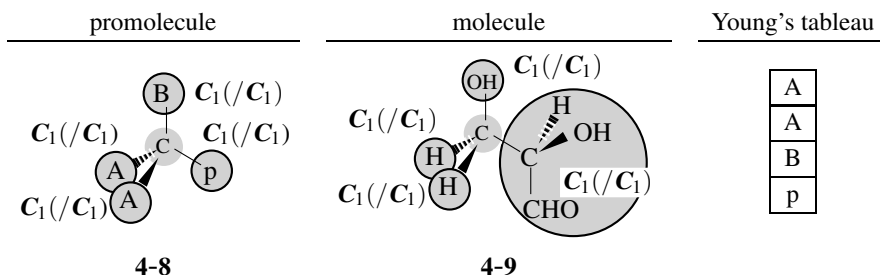


Fig. 4.4. Orbits in glyceraldehyde under the point group C_1

conditions. Moreover, the methylene carbon atom belongs to a one-membered hemispheric $C_1(/C_1)$ -orbit. The corresponding Young's tableau shown in the rightmost part of Fig. 4.4 clearly demonstrates the inequivalence of the four proligands (two A's, B and p).

If we obey E-4.12(b) due to Hanson's definition [7], we are forced to say that the methylene carbon atom is an achiral center or atom, even though it is locally chiral because it belongs to the one-membered hemispheric $C_1(/C_1)$ -orbit. Hence, the terminology concerning 'prochirality' described in E-4.12(b) (due to Hanson's definition [7]) is misleading from a geometric point of view and should be abandoned.

Another confusion has appeared when Hirschmann [11, page 67] claimed that *meso*-tartaric acid, which exhibits prochirality due to Rule E-4.12(a) (cf. [17, page 3326]), should not be called 'a prochiral compound' according to Rule E-4.12(b): "In contrast to citric acid, however, this compound (*meso*-tartaric acid) contains no prochiral centers since both C-2 and C-3 are chiral centers with inverse configurations." In a textbook on biochemistry by Bentley [18, page 182], on the other hand, *meso*-tartaric acid was referred to as being 'prochiral' by applying Hirschmann's superposition test [19]. To avoid this inconsistency, Hirschmann [11] followed Hanson's recommendation that "prochirality should be regarded as an attribute of steric elements and not of the complete molecule", so that his adopted way was to nullify Rule E-4.12(a). This way is misleading because, logically speaking, there should appear local prochirality and global prochirality, just as there appear local chirality and global chirality.

Even under Rule E-4.12(b) for supporting *pro-R/pro-S*-descriptors by Hanson [7], the bond between C-2 and C-3 in *meso*-tartaric acid (in place of "a prochiral center") can be regarded as a basis of 'prochirality' by considering the mathematical concept of *centroid* and *bicentroid* by Jordan [20]. However, this way causes a further inconsistency, because chiral tartaric acids are forced to be 'prochiral' according to Rule E-4.12(b).

The inconsistency concerning the term 'prochiral' due to Rule E-4.12(b) has once been discussed by Mislow and Siegel [17], where they stated "This problem (the above inconsistency) can be easily avoided if the usage of 'prochirality' with reference to prostereoisomerism is altogether abandoned, and such a course of action seems at least worthy of consid-

eration.” The concept of sphericities of orbits proposed by Fujita [1,2] has supported a more fundamental discussion on *meso*-tartaric acid [21], as discussed below (see page 108).

A definite solution to such entangled situations has been provided by introducing new terminology on *prochirality*, which is based on the concept of sphericities [1,22]. This book emphasizes the term *prochirality* based on the concept of sphericities [1,22], although the new terminology has not so well-known to organic chemists, except that it has been recently cited in a textbook on organic chemistry [23, page 173].

4.2.2 Prochirality as a Geometric Concept

In this book, the concept of *prochirality* is definitely used to specify geometric features of stereochemistry [1,22]. The theoretical foundation of *prochirality* has been discussed in terms of G_j -blocks (or G_j -ligands) contained in an enantiospheric $G(/G_i)$ -orbit [3]. Moreover, the stereoisogram approach developed recently by Fujita [4–6] is capable of settling long-standing confusion on the term ‘prochirality’ in stereochemistry [24], where the concept of *pro-RS*-stereogenicity has been proposed to accomplish integrated treatment with prochirality redefined in this section (Def. 4.2). A recent article by Fujita [25] has discussed rational avoidance of misleading standpoints of the conventional term ‘prochirality’ for supporting *pro-R/pro-S*-descriptors.

According to Def. 4.1, an enantiospheric $G(/G_i)$ -orbit has two halves that are equivalent under the global point-group symmetry G but inequivalent under the maximum chiral subgroup $G_C (C G)$. Thereby, the term *prochirality* is defined as follows [1]:

Definition 4.2 (Prochirality). A *prochiral* molecule or promolecule is defined as an achiral molecule or promolecule that has at least one enantiospheric orbit (cf. Def. 4.1).

According to Def. 4.2, the following theorem is obvious:

Theorem 4.5 (Single-Step Synthesis). A prochiral (pro)molecule defined by Def. 4.2 can be converted into a chiral (pro)molecule or its mirror-image counterpart (enantiomer) by a single-step synthesis.

The expression “by a single-step synthesis” in Theorem 4.5 is essential to develop further discussions. Such a single-step synthesis that differentiates the two halves of an enantiospheric orbit (Def. 4.1 and Fig. 4.2(b)) is traditionally called ‘asymmetric synthesis’, but is referred to as a *chiral synthesis* in this book.

The key of determining prochirality is to specify the enantiosphericity of a coset representation $G(/G_i)$, as summarized in the following procedure:

Rule 4.1. Procedure for Determining Prochirality.

1. Determine a stereoskeleton and ligands to characterize a given molecule according to the purpose of your discussion.

- The detected ligands are transformed into the corresponding proligands (cf. Def. 3.1 on page 53), so that the molecule is converted into the corresponding promolecule (cf. Def. 3.3 on page 54).
- Determine the global point-group symmetry G (or simply the global achirality or chirality) of the promolecule.
- Classify proligands into equivalence classes (orbits) by gathering proligands convertible under the global point-group symmetry G . See Subsection 3.4.2.
- Determine the local point-group symmetry G_i , which fixes any proligand of each equivalence class (orbit). Or simply determine whether G_i is achiral or chiral.
- Examine and classify $G(/G_i)$ to be homospheric, enantiospheric, or hemispheric (cf. Def. 4.1)
- If at least one enantiospheric orbit is present, the promolecule (and the molecule) is determined to be prochiral (Def. 4.2).

For example, the two proligands X's in the promolecule **4-1** as well as the two hydrogens in the molecule **3-29** (Fig. 4.1) are accommodated in an enantiospheric $C_s(/C_1)$ -orbit. Thereby, **4-1** (or **3-29**) is concluded to be a prochiral promolecule (or a prochiral molecule) according to Def. 4.2.

Either one of the two hydrogens in **3-29** (Fig. 4.1) is substituted for a fluorine atom, the resultant molecule CHFClBr is chiral so as to exemplifying Theorem 4.5. Either one of the two X's in **4-1** is substituted for an achiral proligand Y in isolation, the resultant promolecule CABXY is chiral so as to exemplify Theorem 4.5.

By placing four hydrogens on the four positions of an oxirane skeleton **3-12** of C_{2v} -symmetry (Fig. 3.7 on page 68), we obtain oxirane **4-10** with the molecular formula C_2H_4O (Fig. 4.5). The four hydrogens $\{1, 2, 3, 4\}$ of **4-10** construct an orbit governed by a coset representation $C_{2v}/(C_1)$, which is determined to be enantiospheric. Oxirane **4-10** is concluded to be prochiral according to Def. 4.2. The four-membered enantiopheric orbit $\{1, 2, 3, 4\}$ is divided into two orbits $\{1, 4\}$ and $\{2, 3\}$ under the maximum chiral subgroup C_2 . Thereby, a single-step chiral synthesis is possible according to Theorem 4.5.

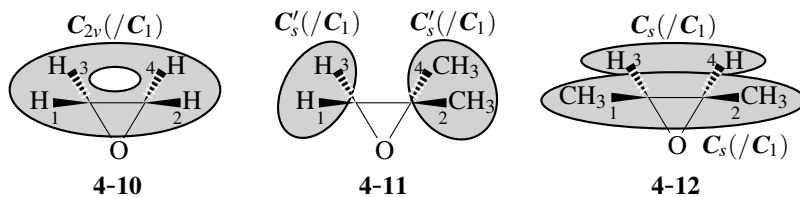


Fig. 4.5. Prochiral oxirane derivatives having enantiospheric orbits.

**Exercise 4.2.**

- Depict a pair of enantiomeric *E*-oxiranes with the composition H^2X^2 which are generated from oxirane **4-10**.
- Compare enantiosphericity (as an attribute of an orbit) with enantiotopic relationships by considering the four-membered $C_{2v}/(C_1)$ -orbit of **4-10**.

2,2-Dimethyloxirane **4-11** is characterized by two two-membered enantiospheric $C'_s/(C_1)$ -orbits, which accommodate two hydrogens and two methyl ligands respectively (Fig. 4.5). 2,2-Dimethyloxirane **4-11** is concluded to be prochiral according to Def. 4.2. The two-membered enantiopheric orbit $\{1,3\}$ with two hydrogens is divided into two one-membered orbits $\{1\}$ and $\{3\}$ under the maximum chiral subgroup C_1 . Similarly, the two-membered enantiopheric orbit $\{2,4\}$ with two methyl ligands is divided into two one-membered orbits $\{2\}$ and $\{4\}$ under the maximum chiral subgroup C_1 . Thereby, a single-step chiral synthesis is possible according to Theorem 4.5.

cis-2,3-Dimethyloxirane **4-12** is characterized by two two-membered enantiospheric $C_s/(C_1)$ -orbits, which accommodate two hydrogens and two methyl ligands respectively (Fig. 4.5). Hence, *cis*-2,3-dimethyloxirane **4-12** is concluded to be prochiral according to Def. 4.2. The two-membered enantiopheric orbit $\{3,4\}$ with two hydrogens is divided into two one-membered orbits $\{3\}$ and $\{4\}$ under the maximum chiral subgroup C_1 . Similarly, the two-membered enantiopheric orbit $\{1,2\}$ with two methyl ligands is divided into two one-membered orbits $\{1\}$ and $\{2\}$ under the maximum chiral subgroup C_1 . Thereby, a single-step chiral synthesis is possible according to Theorem 4.5.

The prochirality of *cis*-2,3-dimethyloxirane **4-12** is based on an oxirane skeleton, which is in sharp contrast to ‘a prochiral center’ emphasized by Rule E-4.12(b) of the IUPAC Recommendations 1974 [16]. In other words, the prochirality of **4-12** due to enantiosphericity has nothing to do with the assignability of *pro-R/pro-S*-descriptors. This means that the *prochirality* based on the concept of sphericities is conceptually distinct from the ‘prochirality’ defined in Rule E-4.12(b) of the IUPAC Recommendations 1974 [16] for supporting *pro-R/pro-S*-descriptors by Hanson [7]. The former *prochirality* should be adopted and the latter ‘prochirality’ should be abandoned after the term *pro-RS-stereogenicity* proposed by Fujita is introduced (cf. Chapter 14).

**Exercise 4.3.**

- Assign an *R/S*-stereodescriptor to each carbon atoms of *cis*-2,3-dimethyloxirane **4-12**.
- Discuss the similarity between *cis*-2,3-dimethyloxirane **4-12** and *meso*-tartaric acid from a viewpoint of the assignability of *R/S*-stereodescriptors.
- Discuss the similarity between the ring C—C bond of **4-12** and the central C—C bond of *meso*-tartaric acid from the viewpoint of prochirality.

4.2.3 Enantiospheric Orbits vs. Enantiotopic Relationships

The attributive term *enantiospheric* characterizes the property (attribute) of an orbit of molecular entities. In contrast, modern stereochemistry has traditionally relied on a relational term *enantiotopic*, which characterizes the relationship between pairwise entities. For the purpose of assuring the compatibility of the present approach with the traditional way of modern stereochemistry, it is convenient to define the relational term *enantiotopic* by starting from the attributive term *enantiospheric*.

Because an enantiospheric $G(/G_i)$ -orbit is divided into two halves as illustrated in Fig. 4.2(b), the relationship between the two halves is characterized by the term *enantiotopic* defined as follows [1,2,26]:

Definition 4.3 (Enantiotopic Relationship as One Extreme Case (Membership Criterion)). An *enantiotopic* relationship (as one extreme case) is defined as a relationship between one half and the other half of an enantiospheric orbit (cf. Def. 4.1).

The two halves are separated under internal or external chiral conditions according to Eq. 4.2 or Eq. 4.3. Such an internal chiral condition is accomplished, for example, by a tentative linkage of a chiral component (cf. Prelog's rule [27]), while such an external chiral condition is provided, for example, by the attack of chiral reagents (cf. BINAP [28]).

As an example, let us examine an octachloro derivative **4-13** of the adamantane-2,6-dione skeleton **3-22** of D_{2d} -symmetry (Fig. 3.11 on page 76). As shown in Fig. 4.6, **4-13** belongs to the point group D_{2d} . According to Def. 4.2, the octachloro derivative **4-13** is prochiral, because there is an enantiospheric $D_{2d}(/C_1)$ -orbit of eight chlorine atoms (numbered from 1 to 8). The eight-membered enantiospheric $D_{2d}(/C_1)$ -orbit is divided into two halves, i.e., {1, 2, 3, 4} (shadowed) and {5, 6, 7, 8}, which are equivalent under D_{2d} but inequivalent under D_2 . When the halves {1, 2, 3, 4} and {5, 6, 7, 8} are regarded as blocks in the enantiospheric $D_{2d}(/C_1)$ -orbit, each of the blocks is fixed by the subgroup D_2 . Hence, the local point-group symmetry of each block (named D_2 -block) is determined to be D_2 , so that a set of the two D_2 -blocks (two halves) can be regarded as a two-membered orbit governed by the coset representation $D_{2d}(/D_2)$, which is again enantiospheric. According to Def. 4.3, one half {1, 2, 3, 4} (shadowed) and the other half {5, 6, 7, 8} in **4-13** are enantiotopic to each other.

The membership criterion for the term *enantiotopic* (Def. 4.3) stems from the fact that the two D_2 -blocks of in the $D_{2d}(/C_1)$ -orbit of **4-13** ({1, 2, 3, 4} (shadowed) and {5, 6, 7, 8}) are equivalent under D_{2d} but inequivalent under D_2 . This fact provides us with an alternative definition of the term *enantiotopic* (symmetry criterion):

Definition 4.4 (Enantiotopic Relationship as One Extreme Case (Symmetry Criterion)). Two blocks equivalent under an achiral group G but inequivalent under its maximum chiral subgroup G_C are defined as being enantiotopic.

The membership criterion for the term *enantiotopic* (Def. 4.3) gives a basis of a further definition of the term *enantiotopic*, as shown in Fig. 4.6. If the shadowed **4-13** is regarded as a product of a hypothetical chiral labelling, the alternative labelling gives **4-13'**. The

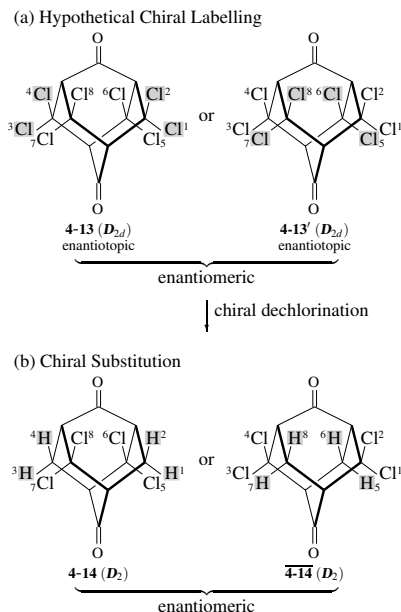


Fig. 4.6. An octachloro derivative of D_{2d} and tetrachloro derivatives of D_2 , which are derived from an adamantane-2,6-dione skeleton.

hypothetically labeled species, **4-13** and **4-13'**, are recognized to be enantiomeric to each other. Hence, we arrive at an additional criterion for the term *enantiotopic*, i.e., substitution criterion:

Definition 4.5 (Enantiotopic Relationship as One Extreme Case (Substitution Criterion)). Two blocks capable of producing enantiomeric molecular entities by hypothetical chiral labelling are defined as being *enantiotopic*.

Suppose that the chlorine atoms of the shadowed block in **4-13** (or **4-13'**) are substituted by hydrogens under chiral conditions (e.g. the attack of chiral reagents). Thereby, a tetrachloro derivative **4-14** of D_2 (or $\overline{\mathbf{4-14}}$ of D_2) is generated, where **4-14** and $\overline{\mathbf{4-14}}$ are enantiomeric to each other. The conversion of **4-13** of D_{2d} into **4-14** of D_2 (or $\overline{\mathbf{4-14}}$ of D_2) can be regarded as a chiral synthesis, which consists of a single step. Hence, a prochiral molecule defined by Def. 4.2 is capable of producing chiral molecules by a single step. The single step is represented by the following subductions concerning the $D_{2d}(/C_1)$ -orbit for each C_1 -member and the $D_{2d}(/D_2)$ -orbit for each D_2 -block.

$$D_{2d}(/C_1) \downarrow D_2 = 2D_2(/C_1) \quad (4.4)$$

$$D_{2d}(/D_2) \downarrow D_2 = 2D_2(/D_2). \quad (4.5)$$

As an alternative extreme, each member of an enantiospheric $G(/G_i)$ -orbit has a local point-group symmetry G_i . If we focus our attention to each member, we obtain the following definition:

Definition 4.6 (Enantiotopic Relationship as the Other Extreme Case (Membership Criterion)).

An *enantiotopic* relationship (as the other extreme case) is defined as a relationship between any one (pro)ligand in one half and any one (pro)ligand in the other half of an enantiospheric orbit (Def. 4.1).

Let us examine a chlorine atom at the 1-position of the D_{2d}/C_1 -orbit, as shadowed in **4-13₁** (Fig. 4.7). The shadowed species **4-13₁** is regarded as a reference. By applying the respective operations of D_2 to the reference **4-13₁**, there appear four homomeric species, **4-13₁**, **4-13₂**, **4-13₃**, and **4-13₄**, which are equivalent under D_2 .³ On the other hand, a hypothetical chiral labelling produces a shadowed species **4-13'₅** as another reference, as shown in the right of Fig. 4.7(a). By applying the respective operations of D_2 to the reference **4-13'₅**, there appear four homomeric species, **4-13'₅**, **4-13'₆**, **4-13'₇**, and **4-13'₈**. Note that **4-13'₅** can be produced from **4-13₁** by applying reflection operations ($\in D_{2d} - D_2$),⁴ so that **4-13₁** and **4-13'₅** are enantiomeric to each other, if our discussions are restricted to point-group symmetries.

By applying Def. 4.6, there appear four enantiotopic relationships, i.e., between 1-Cl and 5-Cl (**4-13₁** and **4-13'₅**), between 1-Cl and 6-Cl (**4-13₁** and **4-13'₆**), between 1-Cl and 7-Cl (**4-13₁** and **4-13'₇**), as well as between 1-Cl and 8-Cl (**4-13₁** and **4-13'₈**), if a pair of reference species is selected to be a pair of **4-13₁** and **4-13'₅**. These enantiotopic relationships correspond to the enantiomeric relationships due to hypothetical chiral labelling shown in Fig. 4.7(a).

Suppose that the chlorine atom of each shadowed block is substituted by hydrogen under chiral conditions (e.g. the attack of chiral reagents). Thereby, there emerges a heptachloro derivative **4-15** or $\overline{\mathbf{4-15}}$, where **4-15** and $\overline{\mathbf{4-15}}$ are enantiomeric to each other. The conversion of **4-13** of D_{2d} into **4-15** of C_1 (or $\overline{\mathbf{4-15}}$ of C_1) can be regarded as a chiral synthesis, which consists of a single step. Hence, **4-13** is capable of producing chiral molecules by a single step, so that the prochirality due to Def. 4.2 corresponds to a single-step chiral synthesis. The single step is represented by the following subduction concerning the D_{2d}/C_1 -orbit for each C_1 -member:

$$D_{2d}/C_1 \downarrow C_1 = 8C_1/C_1, \quad (4.6)$$

which shows each of the remaining seven chlorine atoms or the hydrogen atom belongs to a one-membered C_1/C_1 -orbit.

4.2.4 Chirogenic Sites in an Enantiospheric Orbit

One extreme case defined by Def. 4.3 is concerned with a G/G_C -orbit derived from a G/G_i -orbit, while the other extreme case defined by Def. 4.6 is concerned with the

³ Strictly speaking, the renumbering of positions is necessary in accord with the operations of D_2 .

⁴ Strictly speaking, the renumbering of positions is necessary in accord with the reflections.

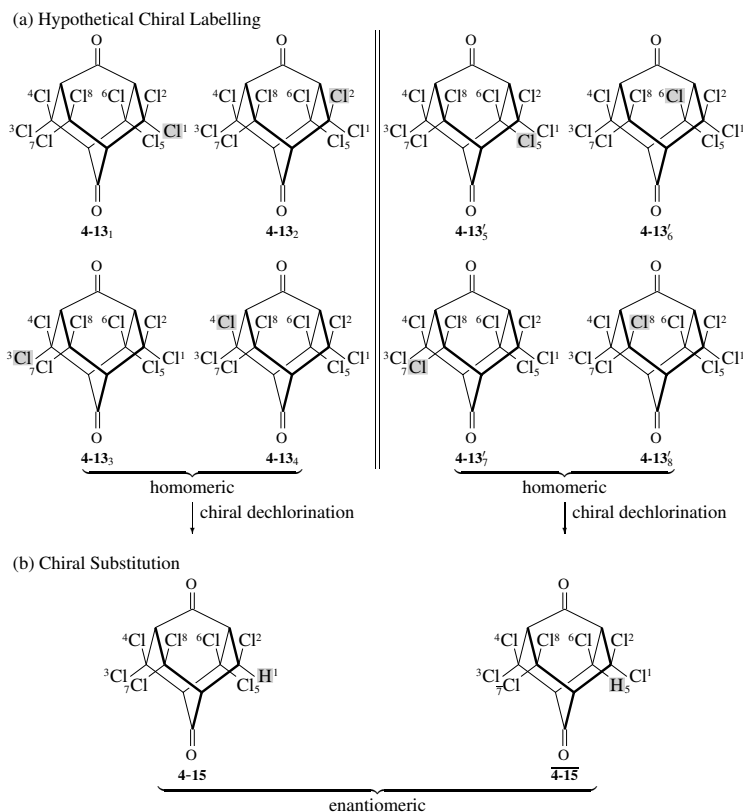


Fig. 4.7. An octachloro derivative of D_{2d} and heptachloro derivatives of C_1 , which are derived from an adamantane-2,6-dione skeleton.

$G(/G_i)$ -orbit itself. The former differentiates a block of G_C -symmetry (e.g., a D_2 -block) from the $G(/G_C)$ -orbit so as to yield a G_C -molecule (e.g., a D_2 -molecule from $D_{2d}/(D_2)$ in Fig. 4.6). The latter differentiates a block of G_i -symmetry from the $G(/G_i)$ -orbit so as to yield a G_i -molecule (e.g., a C_1 -molecule from $D_{2d}/(C_1)$ in Fig. 4.7). To refer to these cases, a G_C -chirogenic site for the former and a G_i -chirogenic site for the latter are used according to the following definition [3]:

Definition 4.7 (*H-Chirogenic Sites*). A block selected from either half of a $G(/G_i)$ -orbit is called a *H-chirogenic site*, if the differentiation of the block from the remaining part of the orbit produces a (pro)molecule of a chiral point group H .

This definition stems from the following theorem:

Theorem 4.6 (*Presence of Chirogenic Site*). Any block in one half of an enantiospheric $G(/G_i)$ -orbit possesses the counterpart in the other half, where the two blocks are equivalent under the group G but inequivalent under the maximum chiral point group G_C . Each of the blocks is called a *chirogenic site*.

The relationship between the two chirogenic sites of Theorem 4.6 are referred to as being *enantiotopic* in a general fashion:

Definition 4.8 (Enantiotopic Relationship as a General Case (Membership Criterion)). An *enantiotopic* relationship (as a general case) is defined as a relationship between a chirogenic site in one half and the counterpart chirogenic site in the other half of an enantiospheric orbit (cf. Def. 4.1).

Any block in one half of an enantiospheric $G(/G_i)$ -orbit is a chirogenic site described in Theorem 4.6. The point-group symmetry H of the chirogenic site is not so easily specified in order to apply Def. 4.7. However, it can be specified in several cases, as described above.

The case described in Fig. 4.7 is generalized to give the following theorem:

Theorem 4.7. Each G_i -block in a $G(/G_i)$ -orbit is a G_i -chirogenic site.

This has once been reported as Corollary 2 of [3]. This theorem shows that Def. 4.6 is one extreme case of Def. 4.8.

The case described in Fig. 4.6 is generalized to give the following theorem:

Theorem 4.8. Each of the two halves of a $G(/G_i)$ -orbit is a G_C -chirogenic site, where G_C is the maximum chiral subgroup of G .

This is once reported as Theorem 7 of [3]. This theorem shows that Def. 4.3 is the other extreme case of Def. 4.8.

A regular representation $G(/C_1)$ has special properties, as described in Chapter 7 of [2] and Section 6.4 of [29]. By applying the idea supporting Lemma 7.1 of [2], we are able to derive the following theorem:

Theorem 4.9. An orbit governed by a regular representation $G(/C_1)$ has a chirogenic site that corresponds to every subgroup.

This is once reported as Theorem 8 of [3].

Let us examine Theorem 4.9 by using the octachloro derivatives of the adamantane-2,6-dione skeleton. Because the coset representation $D_{2d}(/C_1)$ is a regular representation, the C'_2 -block $\{1, 2\}$ is a C'_2 -chirogenic site according to Theorem 4.9 ($C'_2 \subset D_{2d}$), as shown in Fig. 4.8. The shadowed species **4-13**₁₂ produced by a hypothetical chiral labelling is selected as a reference. Then there appears a homomeric **4-13**₃₄ under the action of the maximum chiral subgroup D_2 . On the other hand, another reference **4-13'**₅₆ can be selected to produce homomeric species, **4-13'**₅₆ and **4-13'**₇₈ under the action of D_2 . A pair of shadowed references, **4-13**₁₂ and **4-13'**₅₆, can be regarded as a pair of enantiomers, if the action of reflections is considered under point-group symmetries. Note that the four blocks of **4-13**₁₂, i.e., $\{1, 2\}$, $\{3, 4\}$, $\{5, 6\}$, and $\{7, 8\}$, construct an enantiospheric four-membered orbit governed by the coset representation $D_{2d}(/C'_2)$. Theorem 4.7 indicates the presence of a C'_2 -chirogenic site. Note that the relationship between $\{1, 2\}$ and $\{5, 6\}$ as well as between $\{1, 2\}$ and $\{7, 8\}$ is enantiotopic to each other according to Def. 4.8.

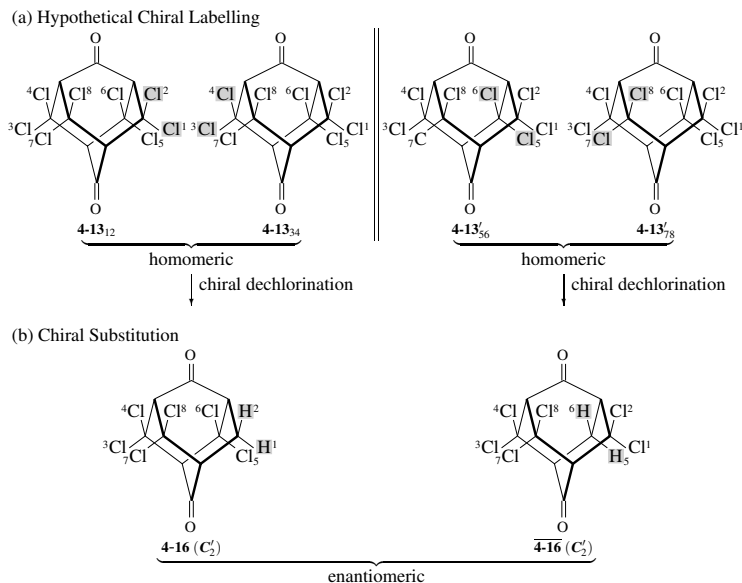


Fig. 4.8. An octachloro derivative of D_{2d} and hexachloro derivatives of C'_2 , which are derived from an adamantane-2,6-dione skeleton.

As shown in Fig. 4.8, the shadowed chlorine atoms are converted into hydrogens under chiral conditions to give either one of C'_2 -molecules, **4-16** and $\overline{\mathbf{4-16}}$, which are enantiomeric to each other.

On the other hand, the C_2 -block $\{1,3\}$ in the $D_{2d}/(C_1)$ -orbit of the octachloro-adamantane-2,6-dione is a C_2 -chirogenic site according to Theorem 4.9 ($C_2 \subset D_{2d}$), as shown in Fig. 4.9. The shadowed species **4-13**₁₃ produced by a hypothetical chiral labelling is selected as a reference. Then there appears a homomeric **4-13**₂₄ under the action of the maximum chiral subgroup D_2 . Another reference **4-13'**₅₇ can be selected to give homomeric species, **4-13'**₅₇ and **4-13'**₆₈. A pair of shadowed references **4-13**₁₃ and **4-13'**₅₇ can be regarded as being enantiomeric. Note that the four blocks of **4-13**₁₃, i.e., $\{1,3\}$, $\{2,4\}$, $\{5,7\}$, and $\{6,8\}$, construct an enantiospheric four-membered orbit governed by the coset representation $D_{2d}/(C_2)$. Theorem 4.7 indicates the presence of a C_2 -chirogenic site. Note that the relationship between $\{1,3\}$ and $\{5,7\}$ as well as between $\{1,3\}$ and $\{6,8\}$ is enantiotopic to each other according to Def. 4.8.

As shown in Fig. 4.9, the shadowed chlorine atoms are converted into hydrogens under chiral conditions to give either one of C_2 -molecules, **4-17** and $\overline{\mathbf{4-17}}$, which are enantiomeric to each other.

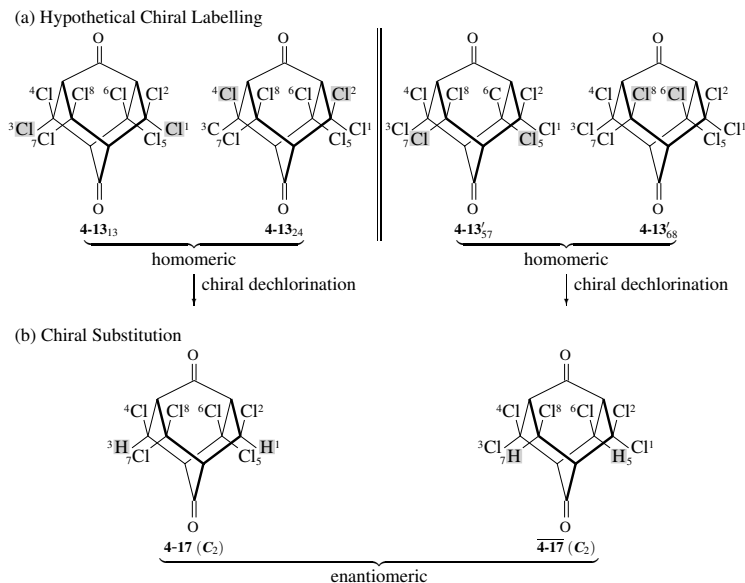


Fig. 4.9. An octachloro derivative of D_{2d} and hexachloro derivatives of C_2 , which are derived from an adamantane-2,6-dione skeleton.



Exercise 4.4.

- Examine adamantane-2,6-dione derivatives shown in Fig. 4.10 to determine orbits contained in them.
- Confirm that **4-18** and **4-19** are prochiral.
- Apply Theorem 4.7 to **4-18** and **4-19**.
- Apply Theorem 4.8 to **4-18** and **4-19**.

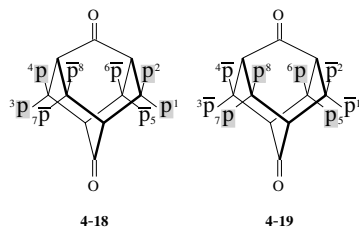


Fig. 4.10. Adamantane-2,6-dione derivatives with an enantiospheric orbit. The symbols p and \bar{p} represent a pair of enantiomeric proligands in isolation.

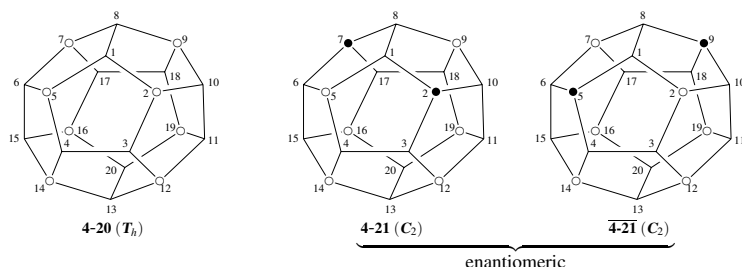


Fig. 4.11. Eight-membered enantiospheric $T_h(/C_3)$ -orbit derived from a dodecahedrane skeleton and its desymmetrization into C_2 -molecules.

Dodecahedrane⁵ with the molecular formula $C_{20}H_{20}$ can be regarded as a stereoskeleton of the point group I_h . Combinatorial enumeration based on the dodecahedrane skeleton has been investigated by Fujita [31–34]. Among the enumerated derivatives [31], there appears an octa-substituted derivative **4-20** of T_h -symmetry, where eight achiral substituents represented by an open circle construct an enantiospheric orbit governed by the coset representation $T_h(/C_3)$. By using this derivative, let us examine a C_2 -chirogenic site appearing in an enantiospheric $T_h(/C_3)$ -orbit [3]. This examination provides us with an example of Theorem 4.6 and Def. 4.7.

Suppose that an open circle in **4-20** represents a chlorine atom. The set of eight chlorine atoms $\{2, 5, 7, 9, 12, 14, 16, 19\}$ constructs an enantiospheric $T_h(/C_3)$ -orbit ($|T_h|/|C_3| = 24/3 = 8$), because each chlorine atom is fixed by the local point-group C_3 . One half $\{2, 7, 14, 19\}$ and the other half $\{5, 9, 12, 16\}$ are equivalent under the point group T_h , but inequivalent under the maximum chiral point group T .

According to Theorem 4.6, a block $\{2, 7\}$ can be selected as a chirogenic site from one half $\{2, 7, 14, 19\}$. Then, the mirror-image counterpart is determined to be $\{5, 9\}$ selected from the other half $\{5, 9, 12, 16\}$. The local point-group symmetry of the block $\{2, 7\}$ is determined to be C_2 , because the hypothetical moiety 2—1—8—7 (containing the block $\{2, 7\}$) is fixed by the two-fold axis bisecting the bond 1–8 (and the bond 13–20). The block $\{2, 7\}$ generates homotopic or enantiotopic chirogenic sites under the action of T_h . Thus, such homotopic chirogenic sites as generated by rotations ($\in T$) are determined to be $\{2, 7\}$, $\{2, 14\}$, $\{2, 19\}$, $\{7, 14\}$, $\{7, 19\}$, and $\{14, 19\}$, which are selected from one half $\{2, 7, 14, 19\}$ of the $T_h(/C_3)$ -orbit. Such enantiotopic chirogenic sites as generated by reflections ($\in T_h - T$) are determined to be $\{5, 9\}$, $\{5, 12\}$, $\{5, 16\}$, $\{9, 12\}$, $\{9, 16\}$, and $\{12, 16\}$, which are selected from the other half $\{5, 9, 12, 16\}$ of the $T_h(/C_3)$ -orbit. The resulting homotopic or enantiotopic chirogenic sites construct an orbit governed by a coset representation $T_h(/C_2)$ (the size: $|T_h|/|C_2| = 24/2 = 12$), because each chirogenic site is fixed by C_2 or its conjugate subgroups.

⁵ Total synthesis of dodecahedrane is extensively studied by Paquette and his coworkers [30].

According to Theorem 4.7, the block $\{2,7\}$ belonging to the coset representation $T_h(/C_2)$ is concluded to be a C_2 -chirogenic site. In fact, the substitution of the chlorine atoms of the block $\{2,7\}$ by hydrogens (represented by a solid circle) generates a C_2 -molecule **4-21**, as shown in Fig. 4.11. The counterpart synthesis concerning the block $\{5,9\}$ generates another C_2 -molecule **4-21**, which is enantiomeric to **4-21**.



Exercise 4.5. cf. [3].

- Apply Theorem 4.7 to **4-20** with a $T_h(/C_3)$ -orbit in order to generate C_3 -derivatives, which are enantiomeric to each other.
- Apply Theorem 4.8 to **4-20** with a $T_h(/C_3)$ -orbit in order to generate T -derivatives, which are enantiomeric to each other. Note that T is the maximum chiral subgroup of T_h .



*Remark 4.1 (Relational Term *enantiotopic* vs. Attributive Term *enantiospheric*).*

- The term *enantiotopic* has been originally coined by Mislow and Raban [35], where the symmetry criterion and the substitution criterion were proposed to specify enantiotopicity. The symmetry criterion is that “Groups are said to be enantiotopic by internal comparison if they can be interchanged only by a rotation-reflection operations (S_n), and not simply by a rotation [C_n ($n > 1$)], to give a structure indistinguishable from the original.” The substitution criterion is that “If the structures resulting from substitution of the achiral G groups by an achiral G' group are enantiomers, the groups themselves are enantiotopic.” The term *enantiotopic* is a relational term, which specifies a relationship between paired objects. It makes light of the concept of equivalence classes (orbits).
- The term *enantiospheric* has been originally coined by Fujita [1] on the basis of the concept of equivalence classes (orbits), where the membership criterion (Def. 4.8) is proposed for defining the relational term *enantiotopic*. The term *enantiospheric* is an attributive term, which specifies the property (or attribute) of an equivalence class (orbit).
- The attributive term *enantiospheric* is capable of deducing the relational term *enantiotopic*, as found in Def. 4.3 (as one extreme case), Def. 4.6 (as the other extreme case), and Def. 4.8 (as a general case). But the reverse deduction is not so easy, in particular, without the concept of orbits.



Remark 4.2 (Chirotopic vs. Chirogenic).

- The term *chirotopic* has originally been coined by Mislow and Siegel [17] to characterize local chirality. Thus, “any atom, and, by extension, any point or seg-

ment of the molecular model, chirotopic, whether occupied by an atomic nucleus or not, that resides within a chiral environment” is characterized as *chirotopic*. This means that the term *chirotopic* is an attributive term. Note that the suffix ‘-topic’ is commonly used in a natural extension of the previous and generally accepted terminology concerning *enantiotopic* [35], although the term *enantiotopic* is a relational term. It is desirable to differentiate between attributive terms and relational terms without using such a common suffix.

- Because an chirotopic atom may be present in both achiral and chiral molecular models, the term *chirotopic* is not directly related to the term *prochirality*. From the present viewpoint of considering equivalence classes (orbits), the term *chirotopic* is concerned with both an enantiospheric orbit and a hemispheric orbit. In this book, we use the term *locally chiral* is used in place of the term *chirotopic* to characterize one half of an enantiospheric orbit as well as the whole of a hemispheric orbit.
- The term *chirogenic* has originally been coined by Fujita [3] to characterize the local chirality of an enantiospheric orbit, not of a hemispheric orbit. Thereby, the term *chirogenic* is directly related to the term *prochirality*.

4.2.5 Prochirality Concerning Chiral Proligands in Isolation

The chirality fittingness of an enantiospheric orbit shown in Fig. 4.2(b) indicates that a set of chiral prolignds (p) and another same-sized set of enantiomeric prolignds (\bar{p}) in isolation can be accommodated in the two halves of an enantiospheric orbit. A molecular entity having such an enantiospheric orbit as filled by p 's and \bar{p} 's is characterized to be prochiral according to Def. 4.2. One half filled by p 's and the other half filled by \bar{p} 's are enantiotopic to each other according to Def. 4.3. A chirogenic site can be selected from either one of the two halves to generate chiral molecular entities under chiral conditions (cf. Exercise 4.4 and Fig. 4.10).

Let us examine the two-membered enantiospheric orbit $\{p, \bar{p}\}$ of **4-4** (Fig. 4.3), where the prolignd p and the other prolignd \bar{p} are enantiotopic to each other. If a selective chiral attack on the prolignd p in **4-4** with the composition $ABp\bar{p}$ generates another chiral prolignd q , there appears a chiral promolecule **4-22** with the composition $ABq\bar{p}$, as shown in Fig. 4.12. If an opposite chiral attack on the prolignd \bar{p} in **4-4** with the composition $ABp\bar{p}$ generates another chiral prolignd \bar{q} , there appears another chiral promolecule $\overline{\mathbf{4-22}}$ with the composition $AB\bar{q}p$, as shown in Fig. 4.12. The product promolecules **4-22** and $\overline{\mathbf{4-22}}$ are enantiomeric to each other. These results indicate the prochirality of **4-4**. Note that the conversion of the prolignd p into q (or \bar{p} into \bar{q}) in the promolecule **4-4** corresponds, for example, to the esterification of either ligand COOH into COOCH_3 in the 2,3,4-trihydroxyglutaric acid **4-5** (Fig. 4.3).

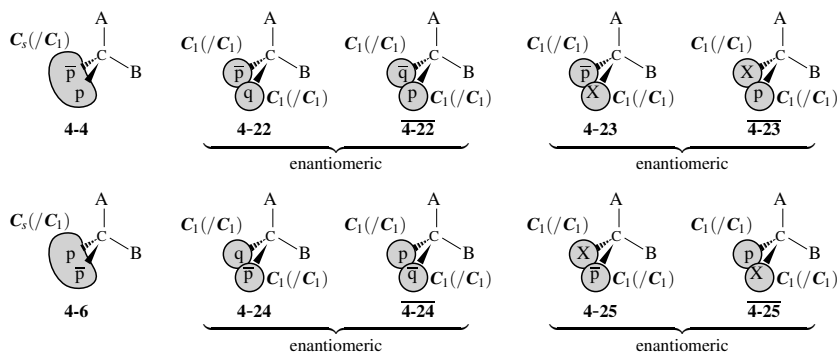


Fig. 4.12. Prochirality concerning chiral proligands in isolation.

If a selective chiral attack on the proligand p in **4-4** with the composition $ABp\bar{p}$ generates an achiral proligand X , there appears a chiral promolecule **4-23** with the composition $ABX\bar{p}$, as shown in Fig. 4.12. If an opposite chiral attack on the proligand \bar{p} in **4-4** with the composition $ABp\bar{p}$ generates an achiral proligand X ($\bar{X} = X$), there appears another chiral promolecule **4-23** with the composition $ABXp$, as shown in Fig. 4.12. The product promolecules **4-23** and **4-23** are enantiomeric to each other. These results indicate the prochirality of **4-4**. Note that the conversion of the proligand p into X (or \bar{p} into X) in the promolecule **4-4** corresponds, for example, to the oxidation of either ligand $CH(OH)-COOH$ into $CO-COOH$ in the molecule **4-5**.

The two-membered enantiospheric orbit $\{p, \bar{p}\}$ of **4-6** (Fig. 4.3) exhibits similar behaviors so as to generate **4-24** and **4-24** (or **4-25** and **4-25**), which are enantiomeric to each other. These results indicate the prochirality of **4-6**.

The troublesome case of *meso*-tartaric acid described on page 94 is clearly demonstrated as a prochiral molecule by means of the presence of an enantiospheric orbit (Fig. 4.13). The molecule **4-28** of *meso*-tartaric acid is generated from two chiral ligands of opposite chirality senses in isolation (p and \bar{p}), which are linked through a single bond. The highest-attainable symmetry of **4-28** is determined to be C_s , so that the two ligands construct a two-membered orbit governed by $C_s(/C_1)$, which is enantiospheric. Note that a mirror plane for the point group C_s is perpendicular to the central $C2-C3$ bond and runs through its midpoint. Each ligand is fixed under the identity group C_1 , which is regarded as the local point-group symmetry. The presence of an enantiospheric orbit indicates the prochirality of **4-28**.

Another viewpoint is possible by taking account of an orbit of two carboxyl groups ($COOH$), an orbit of two hydroxyl groups (OH), and an orbit of two hydrogen atoms (H). Each of these orbits is governed by a coset representation $C_s(/C_1)$, which is enantiospheric. The presence of enantiospheric orbits indicates the prochirality of **4-28**.

A further viewpoint should be added. Suppose that the two chiral ligands are interpreted as a pair of proligands p and \bar{p} , which are placed on a dumbbell skeleton **4-26**. Thereby, there appears a promolecule **4-27**. The pair of p and \bar{p} in **4-27** constructs a two-membered

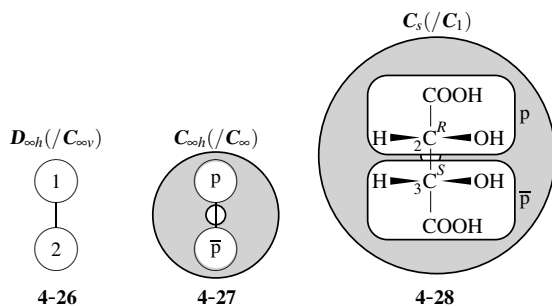


Fig. 4.13. Prochiral promolecule derived from a dumbbell skeleton for characterizing *meso*-tartaric acid.

$C_{\infty h}(/C_{\infty})$ -orbit, which is determined to be enantiospheric. Note that a mirror plane for the global point-group symmetry $C_{\infty h}$ is perpendicular to the central bond and runs through its midpoint. Each proligand is fixed under the infinite rotatory group C_{∞} , which is regarded as the local point-group symmetry. The presence of an enantiospheric orbit indicates the prochirality of **4-27**.

It is worthwhile to point out the importance of the dumbbell skeleton **4-26** in discussing molecules with two carbon centers. Mathematically (graph-theoretically) speaking, acyclic molecules are regarded as trees, which are categorized into *centroidal* and *bicentroidal trees* according to Jordan [20]. Hanson's *pro-R/pro-S*-descriptors [7] as well as Cahn-Ingold-Prelog's *R/S*-stereodescriptors [13,14] have laid stress on 'prochiral centers' or 'chiral centers', where each molecule is factorized into centroidal trees. However, the above discussion on *meso*-tartaric acid indicates that such molecules with two carbon centers should be regarded as bicentroidal trees, if global point-group symmetry is taken into consideration.

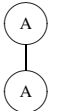
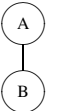
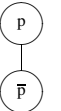
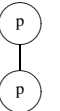
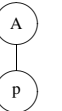

This approach emphasizing bicentroidal properties has been developed by Fujita [21, 36], where a dumbbell skeleton of $D_{\infty h}$ -symmetry is used as a stereoskeleton. By placing two proligands (A, B: achiral; p, \bar{p} , q: chiral) on the two positions governed by a coset representation $D_{\infty h}(/C_{\infty v})$, there appear six promolecules listed in Table 4.1, which summarizes the subduction of $D_{\infty h}(/C_{\infty v})$. Among them, only **4-32** is concluded to be globally prochiral because it has an enantiospheric $C_{\infty h}(/C_{\infty})$ -orbit.

4.2.6 Global Prochirality and Local Prochirality

As found in the preceding discussions, prochirality (*global prochirality*) appears in an achiral promolecule (or molecule) having at least an enantiospheric orbit (Def. 4.2). Such global prochirality is characterized by an enantiospheric orbit governed by $G(/G_i)$, where the achiral promolecule (or molecule) belongs to the global symmetry G and the local symmetry G_i is a chiral subgroup of G .

Table 4.1. Subduction of $D_{\infty h}(/C_{\infty v})$ [21]

subduction of $D_{\infty h}(/C_{\infty v})$	generated coset representation	sphericity
$D_{\infty h}(/C_{\infty v}) \downarrow D_{\infty h}$	$D_{\infty h}(/C_{\infty v})$	homospheric
$D_{\infty h}(/C_{\infty v}) \downarrow C_{\infty v}$	$2C_{\infty v}(/C_{\infty v})$	homospheric
$D_{\infty h}(/C_{\infty v}) \downarrow C_{\infty h}$	$C_{\infty h}(/C_{\infty})$	enantiospheric
$D_{\infty h}(/C_{\infty v}) \downarrow D_{\infty}$	$D_{\infty}(/C_{\infty})$	hemispheric
$D_{\infty h}(/C_{\infty v}) \downarrow C_{\infty}$	$2C_{\infty}(/C_{\infty})$	hemispheric

					
4-29($D_{\infty h}$)	4-30($C_{\infty v}$)	4-31($D_{\infty h}$)	4-32($C_{\infty h}$)	4-33(C_{∞})	4-34(C_{∞})

If an achiral proligand in a homospheric orbit has an inner structure, it may possess an enantiospheric suborbit, which exhibits *local prochirality*. Such local prochirality is characterized by an enantiospheric orbit governed by $G_j(/G_k^{(j)})$, where G_j is an achiral subgroup of the global symmetry G , while $G_k^{(j)}$ is a chiral subgroup of G_j .

Let us consider a homospheric $G(/G_j)$ -orbit. This is combined with an enantiospheric $G_j(/G_k^{(j)})$ -suborbit, so as to generate $G(/G_k^{(j)})$, which is determined to be enantiospheric. The $G(/G_k^{(j)})$ -orbit results in global prochirality.

Let us examine succinic acid **4-36** shown in Fig. 4.14. The two achiral hydroxymethyl ligands in the molecule **4-36** construct an orbit governed by $C_{2v}(/C_s)$, which is determined to be homospheric. The corresponding dumbbell-type promolecule **4-35** with two proligands (A's) has a homospheric $D_{\infty h}(/C_{\infty v})$ -orbit $\{A, A\}$, which is determined to be homospheric.

Because each proligand A has an inner structure, the two hydrogen atoms of A (= CH₂OH) construct a suborbit $\{H_\alpha, H_\beta\}$, governed by a coset representation $C_s(/C_1)$, where the local symmetry C_s appears in a coset representation $C_{2v}(/C_s)$ in a nested fashion. By focusing our attention on the 2-carbon, we obtain the promolecule **4-37**, where the $C_s(/C_1)$ -suborbit of the two hydrogens $\{H_\alpha, H_\beta\}$ is explicitly illustrated by surrounding in a gray box (A = CH₂OH and B = COOH). Because the $C_s(/C_1)$ -suborbit is enantiospheric, it brings about local prochirality at the 2-position.

The successive (nested) appearance of $C_{2v}(/C_s)$ and $C_s(/C_1)$ results in a coset representation $C_{2v}(/C_1)$, which governs a four-membered orbit of hydrogens $\{H_{\alpha 2}, H_{\beta 2}, H_{\alpha 3}, H_{\beta 3}\}$ contained in **4-36** (the subscript numbers 2 and 3 represent the 2- and 3-carbon). The enantiospheric $C_{2v}(/C_1)$ -orbit indicates that the orbit of the four hydrogens at the 2-carbon and 3-carbon brings about global prochirality.

Let us next examine glycerol **4-39** shown in Fig. 4.15, where its highest-attainable symmetry is determined to be C_s . The two hydroxymethyl ligands construct an orbit governed by an enantiospheric coset representation $C_s(/C_1)$. If we place X = CH₂OH, A = H, and B

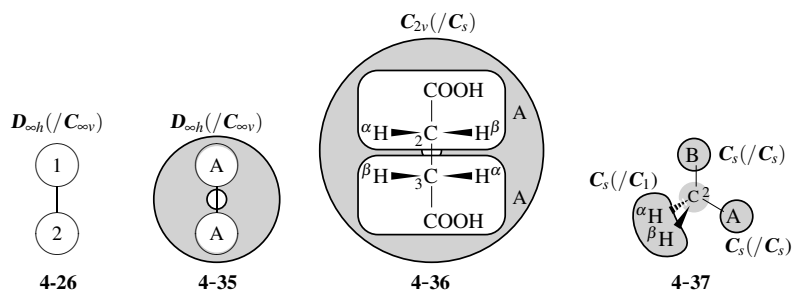


Fig. 4.14. Global prochirality and local prochirality in succinic acid. The promolecule **4-35** exhibits homosphericity, while the molecule **4-36** exhibits enantiosphericity globally and locally. The promolecule **4-37** ($A = \text{CH}_2\text{OH}$ and $B = \text{COOH}$) illustrates the local prochirality at the 2-position.

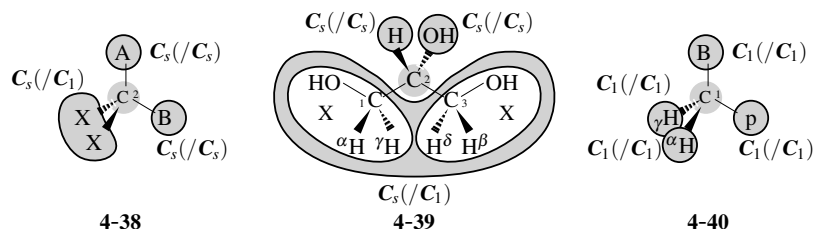


Fig. 4.15. Global prochirality and no local prochirality in glycerol. The promolecule **4-38** ($A = \text{H}$ and $B = \text{OH}$) exhibits enantiosphericity, while the molecule **4-39** exhibits enantiosphericity globally. The promolecule **4-40** ($p = \text{CH}(\text{OH})\text{CH}_2\text{OH}$ and $B = \text{OH}$) illustrates no local prochirality at the 1-position.

$= \text{OH}$, we obtain the corresponding promolecule **4-38**. The two achiral proligands $\{X, X\}$ construct an enantiospheric $C_s(/C_1)$ -orbit. Hence, the molecule **4-39** and the promolecule **4-38** are determined to be prochiral with respect to these enantiospheric orbits.

If we consider the inner structure of **4-39**, an orbit of two hydroxyl ligands, an orbit of two hydrogens $\{H_\alpha, H_\beta\}$ and another orbit of two hydrogens $\{H_\gamma, H_\delta\}$ are all determined to be enantiospheric because of their coset representation $C_s(/C_1)$. These results are parallel to the enantiospheric $C_s(/C_1)$ -orbit of $\{X, X\}$ in the promolecule **4-38**.

If we focus our attention to the 1-position of **4-39**, we obtain the promolecule **4-40**, which belongs to C_1 . Note that we place $p = \text{CH}(\text{OH})\text{CH}_2\text{OH}$ (a chiral proligand in isolation) and $B = \text{OH}$. The promolecule **4-40** contains no enantiospheric orbits and by no means exhibits prochirality. In particular, the two hydrogens in **4-40** are inequivalent under the local symmetry C_1 , so that H_α belongs to a one-membered $C_1(/C_1)$ -orbit and H_γ belongs to another one-membered $C_1(/C_1)$ -orbit.

Consider the molecule **4-42** of 2,4-dihydroxyglutaric acid. The highest-attainable symmetry of **4-42** is determined to be C_s , as shown in Fig. 4.16. The local point-group symmetry at the 2-position (or 4-position) is restricted to C_1 , because the 2-position (or 4-position) is fixed under C_1 . It follows that the two ligands p and \bar{p} ($= \text{CH}(\text{OH})\text{COOH}$) are fixed under

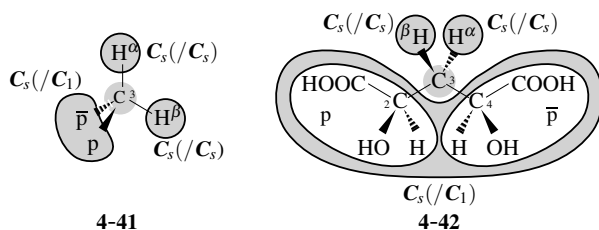


Fig. 4.16. Global prochirality in 2,4-dihydroxyglutaric acid. The promolecule **4-41** as well as the molecule **4-42** has an enantiospheric $C_s(/C_1)$ -orbit of $\{p, \bar{p}\}$. The two hydrogens H_α and H_β separately belong to one-membered homospheric $C_s(/C_s)$ -orbits.

C_1 but interchangeable under C_s , so as to construct an enantiospheric $C_s(/C_1)$ -orbit. The global prochirality is deduced by the presence of the enantiospheric $C_s(/C_1)$ -orbit of $\{p, \bar{p}\}$.

The discussion described in the preceding paragraph holds true for the prochirality of the corresponding promolecule **4-41**. It should be emphasized that the prochirality of **4-41** as well as of **4-42** (concerning the enantiospheric $C_s(/C_1)$ -orbit of $\{p, \bar{p}\}$) essentially exhibits the same characteristics as the prochirality of the promolecule **4-4** as well as **4-6** (or the prochirality of the molecule **4-5** as well as **4-7**), which have been examined in Fig. 4.12.

The two hydrogens H_α and H_β in **4-42** as well as in **4-41** separately belong to one-membered homospheric $C_s(/C_s)$ -orbits. Although H_α and H_β represent the same hydrogen atom when detached, they are geometrically different from each other under the accommodated conditions in **4-42** as well as in **4-41**. In other words, H_α and H_β are not interchangeable under the global symmetry C_s .



Remark 4.3 (Misleading Standpoints for So-Called ‘Factorization’). The so-called ‘factorization’ into ‘chiral centers’ and ‘prochiral centers’ [7] is misleading from the purely-geometric point of view, because both ‘chiral centers’ [13,14] and ‘prochiral centers’ [7] are not based on the purely-geometric concepts of chirality and achirality. Because of the following misleading features, the ‘factorization’ by Hanson [7] should be abandoned.

- If we obey the so-called ‘factorization’ [7, Model V], we are forced to see that there are ‘two chiral centers’ (the 2- and 4-carbon atoms) and ‘one prochiral center’ (the 3-carbon atom) in 2,4-dihydroxyglutaric acid **4-42**. As a result of the ‘factorization’, the ‘two chiral centers’ (concerning the two ligands $\{p, \bar{p}\}$) are excluded from our domain of thinking throughout the subsequent discussions on ‘prochirality’. From the present purely-geometric viewpoint, in contrast, the set $\{p, \bar{p}\}$ constructs a two-membered equivalence class (orbit), which is governed by an enantiospheric coset representation $C_s(/C_1)$, as discussed in Fig. 4.16. Hence, **4-42** is prochiral with respect to the enantiospheric $C_s(/C_1)$ -orbit $\{p, \bar{p}\}$.

- As a result of the ‘factorization’ [7, Model V], the ‘one prochiral center’ (the 3-carbon atom) in 2,4-dihydroxyglutaric acid **4-42** is concerned with two hydrogens (H_α and H_β). Note that achiral 2,4-dihydroxyglutaric acid **4-42** is converted into either one of achiral 2,3,4-trihydroxyglutaric acids **4-5** ($H_\alpha \rightarrow OH$) or **4-7** ($H_\beta \rightarrow OH$) (compare Fig. 4.16 with Fig. 4.3). It is misleading geometrically to use the term ‘prochiral’ for the purpose of indicating the process of converting an achiral molecule into another achiral molecule. Moreover, the resultant **4-5** and **4-7** are not enantiomeric, but ‘diastereomeric’ to each other. This fact is inconsistent to the original aim of coinage of the term ‘prochirality’.

From the viewpoint of Fujita’s stereoisogram approach [4–6], Cahn-Ingold-Prelog’s ‘chiral centers’ [13,14] is not based on the purely-geometric concept of chirality as well as Hanson’s ‘prochiral centers’ [7] is not based on the purely-geometric concept of prochirality. Just as Cahn-Ingold-Prelog’s ‘chiral centers’ [13,14] should be replaced by a newly-defined *RS*-stereogenic centers [37] (cf. Chapter 13), Hanson’s ‘prochirality’ [7] should be replaced by a newly-defined pro-*RS*-stereogenicity [25] (cf. Chapter 14).

References

- [1] S. Fujita, *J. Am. Chem. Soc.*, **112**, 3390–3397 (1990).
- [2] S. Fujita, “Symmetry and Combinatorial Enumeration in Chemistry”, Springer-Verlag, Berlin-Heidelberg (1991).
- [3] S. Fujita, *Bull. Chem. Soc. Jpn.*, **64**, 3313–3323 (1991).
- [4] S. Fujita, *J. Org. Chem.*, **69**, 3158–3165 (2004).
- [5] S. Fujita, *J. Math. Chem.*, **35**, 265–287 (2004).
- [6] S. Fujita, *Tetrahedron*, **60**, 11629–11638 (2004).
- [7] K. R. Hanson, *J. Am. Chem. Soc.*, **88**, 2731–2742 (1966).
- [8] H. Hirschmann and K. R. Hanson, *Eur. J. Biochem.*, **22**, 301–309 (1971).
- [9] H. Hirschmann and K. R. Hanson, *J. Org. Chem.*, **36**, 3293–3306 (1971).
- [10] H. Hirschmann and K. R. Hanson, *Tetrahedron*, **30**, 3649–3656 (1974).
- [11] H. Hirschmann, *Trans. N. Y. Acad. Sci. Ser. II*, **41**, 61–69 (1983).
- [12] E. L. Eliel, *Top. Curr. Chem.*, **105**, 1–76 (1982).
- [13] R. S. Cahn, C. K. Ingold, and V. Prelog, *Angew. Chem. Int. Ed. Eng.*, **5**, 385–415 (1966).
- [14] V. Prelog and G. Helmchen, *Angew. Chem. Int. Ed. Eng.*, **21**, 567–583 (1982).

- [15] IUPAC Organic Chemistry Division, *Pure Appl. Chem.*, **68**, 2193–2222 (1996).
- [16] The Commission on the Nomenclature of Organic Chemistry of IUPAC, *Pure and App. Chem.*, **45**, 11–30 (1976).
- [17] K. Mislow and J. Siegel, *J. Am. Chem. Soc.*, **106**, 3319–3328 (1984).
- [18] R. Bentley, “Molecular Asymmetry in Biology”, Vol. 1, Academic Press, New York (1969).
- [19] H. Hirschmann, The Structural Basis for the Differentiation of Identical Groups in Asymmetric Reactions, in “Essays in Biochemistry”, ed. by S. Graff, Wiley, New York (1956) pp 156–174.
- [20] C. Jordan, *J. Reine Angew. Math.*, **70**, 185–190 (1869).
- [21] S. Fujita, *J. Chem. Inf. Comput. Sci.*, **32**, 354–363 (1992).
- [22] S. Fujita, *J. Org. Chem.*, **67**, 6055–6063 (2002).
- [23] M. B. Smith, “March’s Advanced Organic Chemistry: Reactions, Mechanisms, and Structure”, 7th ed., Wiley, New York (2013), lines 1–5 on page 173.
- [24] S. Fujita, *Tetrahedron*, **62**, 691–705 (2006).
- [25] S. Fujita, *Tetrahedron: Asymmetry*, **25**, 1190–1204 (2014).
- [26] S. Fujita, *Tetrahedron*, **56**, 735–740 (2000).
- [27] V. Prelog, *Helv. Chim. Acta*, **36**, 308–319 (1953).
- [28] R. Noyori, T. Ohkuma, M. Kitamura, H. Takaya, N. Sato, H. Kumobayashi, and S. Akutagawa, *J. Am. Chem. Soc.*, **109**, 5856–5858 (1987).
- [29] S. Fujita, “Diagrammatical Approach to Molecular Symmetry and Enumeration of Stereoisomers”, University of Kragujevac, Faculty of Science, Kragujevac (2007).
- [30] L. A. Paquette, R. J. Ternansky, D. W. Balogh, and G. Kentgen, *J. Am. Chem. Soc.*, **105**, 5446–5450 (1983).
- [31] S. Fujita, *Bull. Chem. Soc. Jpn.*, **63**, 2759–2769 (1990).
- [32] S. Fujita, *Bull. Chem. Soc. Jpn.*, **85**, 439–449 (2012).
- [33] S. Fujita, *J. Comput. Chem. Jpn.*, **11**, 131–139 (2012).
- [34] S. Fujita, *J. Comput. Chem. Jpn.*, **11**, 140–148 (2012).
- [35] K. Mislow and M. Raban, *Top. Stereochem.*, **1**, 1–38 (1967).
- [36] S. Fujita, *J. Chem. Inf. Comput. Sci.*, **40**, 426–437 (2000).
- [37] S. Fujita, *Tetrahedron: Asymmetry*, **25**, 1169–1189 (2014).

5 Foundations of Enumeration Under Point Groups

5.1 Orbits Governed by Coset Representations

The algebraic meaning of orbits described preliminarily in Subsection 3.2.5 is here demonstrated in a more general fashion according to Chapter 5 of [1]. Thereby, the procedure for determining orbits (Rule 3.1 on page 80) is restated algebraically.

5.1.1 Coset Representations

A group \mathbf{G} is decomposed by its subgroup \mathbf{G}_i into a sum of cosets:

$$\mathbf{G} = \mathbf{G}_i g_1 + \mathbf{G}_i g_2 + \cdots + \mathbf{G}_i g_\ell + \cdots + \mathbf{G}_i g_n, \quad (5.1)$$

where each representative g_ℓ ($\ell = 1, 2, \dots, n$, where $g_1 = I$) is selected arbitrarily from the corresponding coset and $n = |\mathbf{G}|/|\mathbf{G}_i|$. This process is called *a coset decomposition*. The stabilizer of each coset $\mathbf{G}_i g_\ell$ is represented by $g_\ell^{-1} \mathbf{G}_i g_\ell$, which is conjugate to \mathbf{G}_i . Let us collect the cosets appearing in the right-hand side of Eq. 5.1 to give an ordered set of cosets:

$$\mathbf{G}/\mathbf{G}_i = \{ \mathbf{G}_i g_1, \mathbf{G}_i g_2, \cdots, \mathbf{G}_i g_\ell, \cdots, \mathbf{G}_i g_n \}, \quad (5.2)$$

where the sequential numbers are attached below the respective cosets.

Suppose that an element g of \mathbf{G} acts on each coset $\mathbf{G}_i g_\ell$ to give $\mathbf{G}_i g_\ell g$. Then, there appears another ordered set as follows:

$$\mathbf{G}/\mathbf{G}_i|_g = \{ \mathbf{G}_i g_1 g, \mathbf{G}_i g_2 g, \cdots, \mathbf{G}_i g_\ell g, \cdots, \mathbf{G}_i g_n g \} \quad (5.3)$$

for $g \in \mathbf{G}_C$, where \mathbf{G}_C denotes the maximum chiral subgroup of \mathbf{G} if the group \mathbf{G} represents an achiral point group.¹ The sequential numbers $1^g, 2^g$, etc. represent that the cosets numbered by 1, 2, etc. are converted into the cosets numbered by $1^g, 2^g$, etc. on the action of g . If g represents a reflection ($g \in \mathbf{G} - \mathbf{G}_C$), the resulting set is differentiated from Eq. 5.3 by attaching a sequential number with an overbar:

$$\mathbf{G}/\mathbf{G}_i|_g = \{ \mathbf{G}_i g_1 g, \mathbf{G}_i g_2 g, \cdots, \mathbf{G}_i g_\ell g, \cdots, \mathbf{G}_i g_n g \} \quad (5.4)$$

¹ The propositions of this chapter hold true for groups in general, although the discussions on them are restricted to point groups. For example, \mathbf{G} can be selected to be an extended group derived by adding a reflection operation to the symmetric group of degree n (S^n).

for $g \in \mathbf{G} - \mathbf{G}_C$. The conversion of \mathbf{G}/\mathbf{G}_i (Eq. 5.2) into $\mathbf{G}/\mathbf{G}_i|_g$ (Eq. 5.3 or Eq. 5.4) is denoted by a permutation as follows:

$$\begin{aligned} \pi_g &= \begin{pmatrix} \mathbf{G}/\mathbf{G}_i \\ \mathbf{G}/\mathbf{G}_i|_g \end{pmatrix} = \begin{pmatrix} \mathbf{G}_i g_1 & \mathbf{G}_i g_2 & \cdots & \mathbf{G}_i g_\ell & \cdots & \mathbf{G}_i g_n \\ \mathbf{G}_i g_1 g & \mathbf{G}_i g_2 g & \cdots & \mathbf{G}_i g_\ell g & \cdots & \mathbf{G}_i g_n g \end{pmatrix} \\ &= \begin{cases} \begin{pmatrix} 1 & 2 & \cdots & \ell & \cdots & n \\ 1^g & 2^g & \cdots & \ell^g & \cdots & n^g \end{pmatrix} & \text{for } g \in \mathbf{G}_C \\ \begin{pmatrix} 1 & 2 & \cdots & \ell & \cdots & n \\ \bar{1}^g & \bar{2}^g & \cdots & \bar{\ell}^g & \cdots & \bar{n}^g \end{pmatrix} & \text{for } g \in \mathbf{G} - \mathbf{G}_C. \end{cases} \end{aligned} \tag{5.5}$$

The permutations π_g for all elements g 's of \mathbf{G} are gathered to give the following set called a *coset representation*:

$$\mathbf{G}(/ \mathbf{G}_i) = \{ \pi_g \mid \forall g \in \mathbf{G} \}, \tag{5.6}$$

where the symbol $\mathbf{G}(/ \mathbf{G}_i)$ is coined by Fujita to emphasize the correspondence between the global symmetry \mathbf{G} and the local symmetry \mathbf{G}_i in the action of the point group \mathbf{G} [2,3].²

A given group \mathbf{G} contains a set of subgroups. After a representative is selected from each set of conjugate subgroups, such representatives are collected to give a *non-redundant set of subgroups* (SSG):

$$\text{SSG}_{\mathbf{G}} = \{ \mathbf{G}_1, \mathbf{G}_2, \cdots, \mathbf{G}_i, \cdots, \mathbf{G}_s \}, \tag{5.7}$$

where the subgroups are ordered in an ascending order of subgroups, $\mathbf{G}_1 = \mathbf{C}_1$ (the identity group), and $\mathbf{G}_s = \mathbf{G}$. See the preliminary discussion on Eq. 3.20 (page 62) and the examples demonstrated therein.

According to Eq. 5.6 for each subgroup selected from $\text{SSG}_{\mathbf{G}}$ (Eq. 5.7), we obtain the following *set of coset representations* up to conjugacy:

$$\text{SCR}_{\mathbf{G}} = \{ \mathbf{G}(/ \mathbf{G}_1), \mathbf{G}(/ \mathbf{G}_2), \cdots, \mathbf{G}(/ \mathbf{G}_i), \cdots, \mathbf{G}(/ \mathbf{G}_s) \}. \tag{5.8}$$

See the preliminary discussion on Eq. 3.31 (page 67) and the examples demonstrated therein. For a more detailed discussion, see [1, Chapter 5].

As an example of obtaining coset representations, let us reexamine Exercise 3.6 (page 72). The SSG of \mathbf{C}_{2v} is obtained as follows:

$$\text{SSG}_{\mathbf{C}_{2v}} = \{ \mathbf{C}_1, \mathbf{C}_2, \mathbf{C}_s, \mathbf{C}'_s, \mathbf{C}_{2v} \}, \tag{5.9}$$

² A coset representation is called a *transitive permutation representation* in a mathematical context. The term *coset representation* and the symbol $\mathbf{G}(/ \mathbf{G}_i)$ are adopted in this book for the purpose of emphasizing the correspondence between algebraic formulations and geometric embodiments through the concept of equivalence classes (orbits). Note that a coset representation $\mathbf{G}(/ \mathbf{G}_i)$ corresponds to an equivalence class (orbit) in a one-to-one fashion.

Table 5.1. Coset Representations of C_{2v}

C_{2v}	C_{2v}/C_1	C_{2v}/C_2	C_{2v}/C_s	C_{2v}/C'_s	C_{2v}/C_{2v}
I	$(1)(2)(3)(4)$	$(1)(2)$	$(1)(2)$	$(1)(2)$	(1)
C_2	$(1\ 4)(2\ 3)$	$(1)(2)$	$(1\ 2)$	$(1\ 2)$	(1)
$\sigma_{v(1)}$	$(1\ 2)(3\ 4)$	$(1\ 2)$	$(1)(2)$	$(1\ 2)$	(1)
$\sigma_{v(2)}$	$(1\ 3)(2\ 4)$	$(1\ 2)$	$(1\ 2)$	$(1)(2)$	(1)

where $C_2 = \{I, C_2\}$, $C_s = \{I, \sigma_{v(1)}\}$, and $C'_s = \{I, \sigma_{v(2)}\}$. Note that the number attached to each operation corresponds to the sequential number of the multiplication table of C_{2v} (Table 3.6 on page 71). The coset decomposition of C_{2v} by C_2 is obtained as follows:

$$C_{2v} = C_2 + C_2 \sigma_{v(1)} \quad (5.10)$$

$$\begin{matrix} 1 & 2 \\ \{1\ 4\} & \{2\ 3\} \end{matrix}$$

Thereby, a set of cosets C_{2v}/C_2 is obtained according to Eq. 5.2:

$$C_{2v}/C_2 = \{ C_2, C_2 \sigma_{v(1)} \} \quad I \sim (1)(2), \quad (5.11)$$

$$\begin{matrix} 1 & 2 \\ \{1\ 4\} & \{2\ 3\} \end{matrix}$$

which gives a permutation $I \sim (1)(2)$ by applying Eqs. 5.4 and 5.5. This procedure based on Eqs. 5.4 and 5.5 is repeated to cover all the operations of C_{2v} , so that the following permutations are obtained:

$$C_{2v}/C_2|_{C_2} = \{ C_2 C_2, C_2 \sigma_{v(2)} \} \quad C_2 \sim (1)(2) \quad (5.12)$$

$$\begin{matrix} 1 & 2 \\ \{4\ 1\} & \{3\ 2\} \end{matrix}$$

$$C_{2v}/C_2|_{\sigma_{v(1)}} = \{ C_2 \sigma_{v(1)}, C_2 \} \quad \sigma_{v(1)} \sim \overline{(1\ 2)} \quad (5.13)$$

$$\begin{matrix} 2 & 1 \\ \{2\ 3\} & \{1\ 4\} \end{matrix}$$

$$C_{2v}/C_2|_{\sigma_{v(2)}} = \{ C_2 \sigma_{v(2)}, C_2 C_2 \} \quad \sigma_{v(2)} \sim \overline{(1\ 2)} \quad (5.14)$$

$$\begin{matrix} 2 & 1 \\ \{3\ 2\} & \{4\ 1\} \end{matrix}$$

The resultant permutations construct a coset representation C_{2v}/C_2 , which is collected in the C_{2v}/C_2 -column of Table 5.1.

Similarly, the coset representations of C_{2v} are obtained by using the multiplication table shown in Table 3.6. They are collected in Table 5.1.

Exercise 5.1.

- Compare the coset decomposition represented by Eq. 3.23 of the point group T_d (on page 64) with Eq. 5.1 of general cases.
 - Examine T_d/C_{3v} (Eq. 3.24) and $T_d/C_{3v}|_{C_{3(1)}}$ (Eq. 3.25) as examples of Eq. 5.2 and Eq. 5.3.
 - Examine the permutations represented by Eq. 3.27 and Eq. 3.30 as examples of Eq. 5.5.
-



5.1.2 Mark Tables

In general, a permutation representation is represented by a sum of coset representations (cf. Subsections 3.3.4 and 3.4.2). According to Burnside [4, Definition 180], the *mark* m of a permutation representation \mathbf{P}_{G_i} of \mathbf{G} is defined as the number of n symbols which are left unchanged by every element of \mathbf{G}_j . The application of the concept of marks has been described in Chapter 5 of [1], which provides us with a basis of this section.

According to Def. 5.2 of [1], let the symbol m_{ij} be the mark of \mathbf{G}_j in the coset representation \mathbf{G}/\mathbf{G}_i . Then, a set of marks m_{ij} for \mathbf{G}_j ($j = 1, 2, \dots, s$) is obtained definitely to construct a \mathbf{G}/\mathbf{G}_i -row of a table called a *table of marks* or a *mark table*, as shown in Table 5.2. The mark tables of representative point groups have been reported by Fujita’s monograph [1, Appendix A].

Table 5.2. Mark table of the group \mathbf{G} (M_G)

coset representation	marks of \mathbf{G}_j					
	\mathbf{G}_1	\mathbf{G}_2	...	\mathbf{G}_i	...	\mathbf{G}_s
\mathbf{G}/\mathbf{G}_1	m_{11}	0	...	0	...	0
\mathbf{G}/\mathbf{G}_2	m_{21}	m_{22}	...	0	...	0
⋮	⋮	⋮	⋮	⋮	⋮	⋮
\mathbf{G}/\mathbf{G}_i	m_{i1}	m_{i2}	...	m_{ii}	...	0
⋮	⋮	⋮	⋮	⋮	⋮	⋮
\mathbf{G}/\mathbf{G}_s	1	1	...	1	...	1

The coset representations of \mathbf{C}_{2v} shown in Table 5.1 are used to calculate marks of each coset representation by paying attention to 1-cycles. For example, the $\mathbf{C}_{2v}/\mathbf{C}_2$ -column of Table 5.1 gives the following set of subgroups:

$$\mathbf{C}_1 = \{I\} \sim \{(1)(2)\} \quad 2 \quad (5.15)$$

$$\mathbf{C}_2 = \{I, C_2\} \sim \{(1)(2), (1)(2)\} \quad 2 \quad (5.16)$$

$$\mathbf{C}_s = \{I, \sigma_{v(1)}\} \sim \{(1)(2), \overline{(1\ 2)}\} \quad 0 \quad (5.17)$$

$$\mathbf{C}'_s = \{I, \sigma_{v(2)}\} \sim \{(1)(2), \overline{(1\ 2)}\} \quad 0 \quad (5.18)$$

$$\mathbf{C}_{2v} = \{I, C_2, \sigma_{v(1)}, \sigma_{v(2)}\} \sim \{(1)(2), (1)(2), \overline{(1\ 2)}, \overline{(1\ 2)}\} \quad 0 \quad (5.19)$$

The mark of each subgroup is shown at the rightmost part of each line. The resultant row vector $(2, 2, 0, 0, 0)$ appears in the $\mathbf{C}_{2v}/\mathbf{C}_2$ -row of Table 5.3. This process is repeated to cover all of the coset representations of Table 5.1. The results are collected in Table 5.3 [1, Table A.5]. This process is essentially equivalent to the subduction $\mathbf{C}_{2v}/\mathbf{C}_2 \downarrow \mathbf{G}_j$ ($\mathbf{G}_j \subset \mathbf{G}$), as described below.

Table 5.3. Mark table of the group $C_{2v} (M_{C_{2v}})$

coset representation	marks of G_j				
	C_1	C_2	C_s	C'_s	C_{2v}
$C_{2v}/(C_1)$	4	0	0	0	0
$C_{2v}/(C_2)$	2	2	0	0	0
$C_{2v}/(C_s)$	2	0	2	0	0
$C_{2v}/(C'_s)$	2	0	0	2	0
$C_{2v}/(C_{2v})$	1	1	1	1	1

Table 5.4. Inverse mark table of the group $G (M_G^{-1})$

G_j	coset representation						$\sum_i \bar{m}_{ji}$
	$G/(G_1)$	$G/(G_2)$	\dots	$G/(G_j)$	\dots	$G/(G_s)$	
G_1	\bar{m}_{11}	0	\dots	0	\dots	0	$\sum_i \bar{m}_{1i}$
G_2	\bar{m}_{21}	\bar{m}_{22}	\dots	0	\dots	0	$\sum_i \bar{m}_{2i}$
\vdots	\vdots	\vdots	\ddots	\vdots	\ddots	\vdots	\vdots
G_j	\bar{m}_{j1}	\bar{m}_{j2}	\dots	\bar{m}_{jj}	\dots	0	$\sum_i \bar{m}_{ji}$
\vdots	\vdots	\vdots	\ddots	\vdots	\ddots	\vdots	\vdots
G_s	\bar{m}_{s1}	\bar{m}_{s2}	\dots	\bar{m}_{sj}	\dots	\bar{m}_{ss}	$\sum_i \bar{m}_{si}$

Table 5.5. Inverse mark table of the group $C_{2v} (M_{C_{2v}}^{-1})$

G_j	coset representation					$\sum_i \bar{m}_{ji}$
	$C_{2v}/(C_1)$	$C_{2v}/(C_2)$	$C_{2v}/(C_s)$	$C_{2v}/(C'_s)$	$C_{2v}/(C_{2v})$	
C_1	$\frac{1}{4}$	0	0	0	0	$\frac{1}{4}$
C_2	$-\frac{1}{4}$	$\frac{1}{2}$	0	0	0	$\frac{1}{4}$
C_s	$-\frac{1}{4}$	0	$\frac{1}{2}$	0	0	$\frac{1}{4}$
C'_s	$-\frac{1}{4}$	0	0	$\frac{1}{2}$	0	$\frac{1}{4}$
C_{2v}	$\frac{1}{2}$	$-\frac{1}{2}$	$-\frac{1}{2}$	$-\frac{1}{2}$	1	0

Because the mark table of G is an $s \times s$ square matrix M_G , there exists the corresponding inverse matrix M_G^{-1} in general. It can be generally proved that the inverse mark table M_G^{-1} is also an $s \times s$ lower triangular matrix, as shown in Table 5.4.

The inverse mark table M_G^{-1} plays an important role in combinatorial enumeration. The properties of the inverse mark table M_G^{-1} have been discussed in detail in Fujita’s monograph [5, Appendix B]. Among such properties, the sum of each row $\sum_i \bar{m}_{ji}$ should be noted because it has positive values for a cyclic subgroup, but vanishes to zero for a non-cyclic subgroup in general.

Table 5.5 shows the inverse mark table $M_{C_{2v}}^{-1}$ of C_{2v} , which can be directly calculated from the mark table shown in Table 5.3.

The mark tables of several point groups and their inverses have been collected in Fujita’s monograph [1, Appendices A and B].

5.1.3 Multiplicities of Orbits

The mark table is regarded as an $s \times s$ lower triangular matrix,

$$M_{\mathbf{G}} = (m_{ij}) = \begin{matrix} \mathbf{G}/\mathbf{G}_1 \\ \mathbf{G}/\mathbf{G}_2 \\ \vdots \\ \mathbf{G}/\mathbf{G}_i \\ \vdots \\ \mathbf{G}/\mathbf{G}_s \end{matrix} \begin{pmatrix} m_{11} & 0 & \cdots & 0 & \cdots & 0 \\ m_{21} & m_{22} & \cdots & 0 & \cdots & 0 \\ \vdots & \vdots & \ddots & \vdots & \ddots & \vdots \\ m_{i1} & m_{i2} & \cdots & m_{ii} & \cdots & 0 \\ \vdots & \vdots & \ddots & \vdots & \ddots & \vdots \\ 1 & 1 & \cdots & 1 & \cdots & 1 \end{pmatrix}, \quad (5.20)$$

where $m_{ij} = 0$ for $j > i$, $m_{i1} = |\mathbf{G}|/|\mathbf{G}_i|$ for all i (the first column), and $m_{sj} = 1$ for all j (the last row). Each row of the mark table (Table 5.2) or the corresponding *mark matrix* (Eq. 5.20) is regarded as a row vector called a *fixed-point vector* (FPV) of the coset representation, which is represented as follows:

$$\text{FPV}_{\mathbf{G}/\mathbf{G}_i} = (m_{i1}, m_{i2}, \dots, m_{ij}, \dots, m_{is}) \quad (5.21)$$

for $i = 1, 2, \dots, s$.

Let us consider a permutation representation $\mathbf{P}_{\mathbf{G}}$, which contains the coset representation \mathbf{G}/\mathbf{G}_i of multiplicity α_i (for $i = 1, 2, \dots, s$). The permutation representation is represented as follows:

$$\mathbf{P}_{\mathbf{G}} = \sum_{i=1}^s \alpha_i \mathbf{G}/\mathbf{G}_i, \quad (5.22)$$

where $\alpha_i \geq 0$. This equation has once been noted as Eq. 3.38 (page 79). Let the symbol μ_j be the mark of \mathbf{G}_j in $\mathbf{P}_{\mathbf{G}}$. The mark μ_j is obtained by examining the number of 1-cycles in the permutations of \mathbf{G}_j . Thereby, we obtain an FPV of $\mathbf{P}_{\mathbf{G}}$ as a row vector:

$$\text{FPV}_{\mathbf{P}_{\mathbf{G}}} = (\mu_1, \mu_2, \dots, \mu_j, \dots, \mu_s). \quad (5.23)$$

According to Eq. 5.22, the $\text{FPV}_{\mathbf{P}_{\mathbf{G}}}$ is obtained by summing up $\alpha_i \times \text{FPV}_{\mathbf{G}/\mathbf{G}_i}$ (Eq. 5.21), as represented by the following equation:

$$\text{FPV}_{\mathbf{P}_{\mathbf{G}}} = \sum_{i=1}^s \alpha_i \text{FPV}_{\mathbf{G}/\mathbf{G}_i}. \quad (5.24)$$

The sum represented by Eq. 5.24 is rewritten by combining the elements of Eq. 5.23 with those of Eq. 5.21. Thereby, each mark μ_j is obtained according to the following equation:

$$\mu_j = \alpha_1 m_{1j} + \alpha_2 m_{2j} + \cdots + \alpha_i m_{ij} + \cdots + \alpha_s m_{sj} = \sum_{i=1}^s \alpha_i m_{ij} \quad (5.25)$$

for $j = 1, 2, \dots, s$. Note that the marks appearing in the right-hand side of Eq. 5.25 are contained in the j -th column of the mark matrix (Eq. 5.20) or the mark table (Table 5.2), i.e., m_{ij} for $i = 1, 2, \dots, s$, where \mathbf{G}_j is tentatively fixed.

To memorize the heart of the above derivations, let the symbol $MV_{\mathbf{P}_G}$ be a multiplicity vector of coset representations in the permutation representation:

$$MV_{\mathbf{P}_G} = (\alpha_1, \alpha_2, \dots, \alpha_i, \dots, \alpha_s). \quad (5.26)$$

Thereby, Eq. 5.25 is rewritten in the form of vectors and a matrix as follows:

$$FPV_{\mathbf{P}_G} = MV_{\mathbf{P}_G} \times M_G \quad (5.27)$$

or more visually in the following equivalent equation:

$$(\mu_1, \mu_2, \dots, \mu_j, \dots, \mu_s) = (\alpha_1, \alpha_2, \dots, \alpha_i, \dots, \alpha_s) M_G. \quad (5.28)$$

Because our target is to obtain the $MV_{\mathbf{P}_G}$, these equations are transformed into the following equation:

$$MV_{\mathbf{P}_G} = FPV_{\mathbf{P}_G} \times M_G^{-1} \quad (5.29)$$

or more visually into the following equivalent form:

$$(\alpha_1, \alpha_2, \dots, \alpha_i, \dots, \alpha_s) = (\mu_1, \mu_2, \dots, \mu_j, \dots, \mu_s) M_G^{-1}. \quad (5.30)$$

The symbol M_G^{-1} represents the inverse matrix of the mark matrix M_G . The inverse is an $s \times s$ lower triangular matrix:

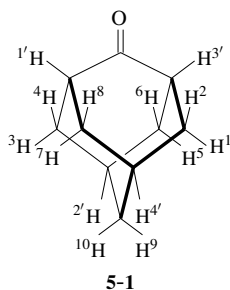
$$M_G^{-1} = (\bar{m}_{ji}) = \begin{pmatrix} \mathbf{G}/(\mathbf{G}_1) & \mathbf{G}/(\mathbf{G}_2) & \cdots & \mathbf{G}/(\mathbf{G}_j) & \cdots & \mathbf{G}/(\mathbf{G}_s) \\ \bar{m}_{11} & 0 & \cdots & 0 & \cdots & 0 \\ \bar{m}_{21} & \bar{m}_{22} & \cdots & 0 & \cdots & 0 \\ \vdots & \vdots & \ddots & \vdots & \ddots & \vdots \\ \bar{m}_{j1} & \bar{m}_{j2} & \cdots & \bar{m}_{jj} & \cdots & 0 \\ \vdots & \vdots & \ddots & \vdots & \ddots & \vdots \\ \bar{m}_{s1} & \bar{m}_{s2} & \cdots & \bar{m}_{sj} & \cdots & \bar{m}_{ss} \end{pmatrix}. \quad (5.31)$$

The inverse mark tables of representative point groups have been reported by Fujita's monograph [1, Appendix B]. Now, the diagrammatic procedure for determining orbits (Rule 3.1 on page 80) is rationalized algebraically by Eq. 5.29 (or Eq. 5.30).

As shown in Fig. 5.1, adamantan-2-one **5-1** derived from the adamantan-2-one skeleton **3-23** (page 76) belongs to C_{2v} , because the substitution of 14 hydrogens does not change the symmetry C_{2v} of the skeleton (cf. Fig. 3.11 on page 76). The 14 hydrogens of **5-1** are governed by a permutation representation $\mathbf{P}_{C_{2v}, \mathbf{5-1}}$ shown in the right part of Fig. 5.1. The permutation representation is identical with that of the skeleton **3-23**, which has been determined diagrammatically to be the sum of coset representations represented by Eq. 3.36 on page 76 (cf. Rule 3.1 on page 80).

Each subgroup of $SSG_{C_{2v}}$ (Eq. 5.9) is operated to **5-1** to count a mark (the number of fixed points). Thereby, the following FPV is obtained with respect of the 14 hydrogens:

$$FPV_{\mathbf{P}_{C_{2v}, \mathbf{5-1}}} = (14, 0, 2, 4, 0). \quad (5.32)$$



C_{2v}	$P_{C_{2v},5-1}$				
$I \sim$	$(1)(3)(5)(7)$	$(2)(4)(6)(8)$	$(9)(10)$	$(1')(3')$	$(2')(4')$
$C_2 \sim$	$(1\ 3)(5\ 7)$	$(2\ 4)(6\ 8)$	$(9\ 10)$	$(1'\ 3')$	$(2'\ 4')$
$\sigma_{v(1)} \sim$	$(1\ 7)(3\ 5)$	$(2\ 8)(4\ 6)$	$(9\ 10)$	$(1'\ 3')$	$(2')(4')$
$\sigma_{v(2)} \sim$	$(1\ 5)(3\ 7)$	$(2\ 6)(4\ 8)$	$(9)(10)$	$(1')(3')$	$(2'\ 4')$
	$C_{2v}/(C_1)$	$C_{2v}/(C_1)$	$C_{2v}/(C'_2)$	$C_{2v}/(C'_2)$	$C_{2v}/(C_s)$

Fig. 5.1. Adamantan-2-one of C_{2v} and a permutation representation for characterizing 14 hydrogens. The permutation representation $P_{C_{2v},5-1}$ is represented by the sum of coset representations shown in the bottom row.

According to Eq. 5.29 (or Eq. 5.30), the multiplicity vector $MV_{C_{2v},5-1}$ is obtained as follows:

$$\begin{aligned}
 MV_{C_{2v},5-1} &= FPVP_{C_{2v},5-1} \times M_{C_{2v}}^{-1} \\
 &= (14, 0, 2, 4, 0) \begin{pmatrix} \frac{1}{4} & 0 & 0 & 0 & 0 \\ -\frac{1}{4} & \frac{1}{2} & 0 & 0 & 0 \\ -\frac{1}{4} & 0 & \frac{1}{2} & 0 & 0 \\ -\frac{1}{4} & 0 & 0 & \frac{1}{2} & 0 \\ \frac{1}{2} & -\frac{1}{2} & -\frac{1}{2} & -\frac{1}{2} & 1 \end{pmatrix} \\
 &= (2, 0, 1, 2, 0).
 \end{aligned} \tag{5.33}$$

The inverse mark table $M_{C_{2v}}^{-1}$ is calculated from the mark table shown in Table 5.3. The $MV_{C_{2v},5-1}$ derived algebraically (Eq. 5.33) corresponds to the following set of coset representations:

$$P_{C_{2v},5-1} = 2C_{2v}/(C_1) + C_{2v}/(C_s) + 2C_{2v}/(C'_2), \tag{5.34}$$

which is consistent with Eq. 3.36 (page 76) derived diagrammatically.

5.2 Subduction of Coset Representations

The concept of *subduction of coset representations* has been proposed by Fujita [2], where the terms *subduction* and *subduced representation* have been introduced to emphasize the difference from the term *restriction of an irreducible representation*. The subduction concept has been preliminarily described on page 79 (Eq. 3.40), where it has been introduced diagrammatically. This section is devoted to a mathematical description on the subduction concept according to Chapter 9 of [1].³

³ The subduction of coset representations is alternatively formulated in term of *double cosets*. For the correspondence between the subduction of coset representations and double cosets, see Chapter 9 of [5].

5.2.1 Subduced Representations

From the permutations contained in the coset representation $\mathbf{G}(/G_i)$ (Eq. 5.6), let us select the permutations corresponding to all of the elements of a subgroup $\mathbf{G}_j \in \text{SSG}_{\mathbf{G}}$ (Eq. 5.7). This process is called a *subduction of the coset representation* and denoted by the symbol $\mathbf{G}(/G_i) \downarrow \mathbf{G}_j$, which is coined by Fujita [2,3]. The resulting representation is called a *subduced representation*, which is represented as follows:

$$\mathbf{G}(/G_i) \downarrow \mathbf{G}_j = \{ \pi_g \mid \forall g \in \mathbf{G}_j \}. \quad (5.35)$$

Note that the subduced representation is not always transitive, although the coset representation $\mathbf{G}(/G_i)$ is transitive.⁴

A subduced representation $\mathbf{G}(/G_i) \downarrow \mathbf{G}_j$ as a non-transitive representation is divided into a sum of coset representations of \mathbf{G}_j . As a result, the original orbit governed by $\mathbf{G}(/G_i)$ is divided into a set of suborbits governed by the coset representations of \mathbf{G}_j .

Suppose that the subgroup \mathbf{G}_j is characterized by the following SSG:

$$\text{SSG}_{\mathbf{G}_j} = \{ \mathbf{H}_1^{(ij)}, \mathbf{H}_2^{(ij)}, \dots, \mathbf{H}_k^{(ij)}, \dots, \mathbf{H}_{v_j}^{(ij)} \}, \quad (5.36)$$

where each $\mathbf{H}_k^{(ij)}$ is equal to a subgroup contained in the $\text{SSG}_{\mathbf{G}}$ (Eq. Eq. 5.7) or to its conjugate subgroup. Then, the subduced representation (Eq. 5.35) is divided into a sum of coset representations of \mathbf{G}_j as follows:

$$\mathbf{G}(/G_i) \downarrow \mathbf{G}_j = \sum_{k=1}^{v_j} \beta_k^{(ij)} \mathbf{G}_j(/H_k^{(j)}) \quad (5.37)$$

for $i = 1, 2, \dots, s$ and $j = 1, 2, \dots, s$, where the subgroup $\mathbf{H}_k^{(j)}$ covers the SSG of \mathbf{G}_j (Eq. 5.36) with the multiplicity $\beta_k^{(ij)}$. This equation has been already introduced as Eq. 3.40 (page 80), where the multiplicity $\beta_k^{(ij)}$ has been evaluated diagrammatically. Now, our target is to calculate the multiplicity $\beta_k^{(ij)}$ algebraically.

Each $\mathbf{G}(/G_i)$ -row of the mark matrix $M_{\mathbf{G}}$ (Eq. 5.20) (or equivalently the mark table shown in Table 5.2) is denoted by $\text{FPV}_{\mathbf{G}(/G_i)}$ (Eq. 5.21), which is regarded as a fixed-point vector (FPV). From the elements of $\text{FPV}_{\mathbf{G}(/G_i)}$ (Eq. 5.21), we select the elements corresponding to the subgroup \mathbf{G}_j as follows:

$$\text{FPV}_{\mathbf{G}(/G_i) \downarrow \mathbf{G}_j} = (\mu_1^{(ij)}, \mu_2^{(ij)}, \dots, \mu_\ell^{(ij)}, \dots, \mu_{v_j}^{(ij)}), \quad (5.38)$$

which can be regarded as a fixed point vector as denoted by the symbol $\text{FPV}_{\mathbf{G}(/G_i) \downarrow \mathbf{G}_j}$. If a subgroup of $\text{SSG}_{\mathbf{G}}$ (Eq. 5.7) is separated into two or more subgroups of $\text{SSG}_{\mathbf{G}_j}$ (Eq. 5.36),

⁴ A transitive representation governs one equivalence class (orbit). A non-transitive representation governs two or more equivalence classes (orbits).

the corresponding mark due to conjugacy in $\text{FPV}_{\mathbf{G}/(\mathbf{G}_i)}$ (Eq. 5.21) is used multiply in Eq. 5.38.

Let $\beta_k^{(ij)}$ be the multiplicity of $\mathbf{G}_j/(\mathbf{H}_k^{(j)})$ in $\mathbf{G}/(\mathbf{G}_i) \downarrow \mathbf{G}_j$, as shown in Eq. 5.37. Then, we define the corresponding multiplicity vector (MV):

$$\text{MV}_{\mathbf{G}/(\mathbf{G}_i) \downarrow \mathbf{G}_j} = (\beta_1^{(ij)}, \beta_2^{(ij)}, \dots, \beta_k^{(ij)}, \dots, \beta_{v_j}^{(ij)}) \tag{5.39}$$

In a similar way to the derivation of Eq. 5.29, we obtain:

$$\text{MV}_{\mathbf{G}/(\mathbf{G}_i) \downarrow \mathbf{G}_j} = \text{FPV}_{\mathbf{G}/(\mathbf{G}_i) \downarrow \mathbf{G}_j} \times M_{\mathbf{G}_j}^{-1}, \tag{5.40}$$

which can be represented more visually in the following equivalent form:

$$(\beta_1^{(ij)}, \beta_2^{(ij)}, \dots, \beta_k^{(ij)}, \dots, \beta_{v_j}^{(ij)}) = (\mu_1^{(ij)}, \mu_2^{(ij)}, \dots, \mu_\ell^{(ij)}, \dots, \mu_{v_j}^{(ij)}) M_{\mathbf{G}_j}^{-1}. \tag{5.41}$$

The symbol $M_{\mathbf{G}_j}^{-1}$ represents the inverse matrix of the mark matrix of \mathbf{G}_j denoted by the symbol $M_{\mathbf{G}_j}$. The inverse is a $v_j \times v_j$ lower triangular matrix:

$$M_{\mathbf{G}_j}^{-1} = (\overline{m}_{\ell k}^{(j)}) = \begin{pmatrix} \mathbf{G}_j/(\mathbf{H}_1^{(j)}) & \mathbf{G}_j/(\mathbf{H}_2^{(j)}) & \dots & \mathbf{G}_j/(\mathbf{H}_\ell^{(j)}) & \dots & \mathbf{G}_j/(\mathbf{H}_{v_j}^{(j)}) \\ \overline{m}_{11}^{(j)} & 0 & \dots & 0 & \dots & 0 \\ \overline{m}_{21}^{(j)} & \overline{m}_{22}^{(j)} & \dots & 0 & \dots & 0 \\ \vdots & \vdots & \ddots & \vdots & \ddots & \vdots \\ \overline{m}_{\ell 1}^{(j)} & \overline{m}_{\ell 2}^{(j)} & \dots & \overline{m}_{\ell \ell}^{(j)} & \dots & 0 \\ \vdots & \vdots & \ddots & \vdots & \ddots & \vdots \\ 1 & 1 & \dots & 1 & \dots & 1 \end{pmatrix}. \tag{5.42}$$

The equivalent result to Eq. 5.40 (or Eq. 5.41) has been reported [1, Lemma 9.1].

As found in the preceding paragraphs, Eq. 5.37 (or Eq. 3.40) has now been derived algebraically by using the mark table of \mathbf{G} and the inverse mark table \mathbf{G}_j . When \mathbf{G}_j runs over the $\text{SSG}_{\mathbf{G}}$ (Eq. 5.7) and independently, \mathbf{G}_i of $\mathbf{G}/(\mathbf{G}_i)$ runs over the $\text{SSG}_{\mathbf{G}}$ (Eq. 5.7) ($i = 1, 2, \dots, s$ and $j = 1, 2, \dots, s$), we obtain a *subduction table* of \mathbf{G} , as shown in Table 5.6. Representative subduction tables have been reported as Appendix C of [1].

As an example, let us obtain the \mathbf{C}_2 -column of the subduction table of \mathbf{C}_{2v} . The mark table (mark matrix) and its inverse are obtained as follows (cf. Appendices A and B of [1]):

$$M_{\mathbf{C}_2} = \begin{pmatrix} 2 & 0 \\ 1 & 1 \end{pmatrix} \quad M_{\mathbf{C}_2}^{-1} = \begin{pmatrix} \frac{1}{2} & 0 \\ -\frac{1}{2} & 1 \end{pmatrix}. \tag{5.43}$$

The \mathbf{C}_1 -, and \mathbf{C}_2 -columns of the mark table of the group \mathbf{C}_{2v} (Eq. 5.3) are collected to give fixed-point vectors (FPVs) as a 5×2 matrix, each row of which represents $\text{FPV}_{\mathbf{C}_{2v}/(\mathbf{G}_i) \downarrow \mathbf{C}_2}$ ($i = 1, 2, \dots, s$) according to Eq. 5.38. The calculation by Eq. 5.40 is con-

Table 5.6. Subduction Table of G

	$G(/G_i) \downarrow G_j \ (j = 1, 2, \dots, s)$		
	...	$\downarrow G_j$...
$G(/C_1)^*$...	$\frac{ G }{ G_j } G_j(/C_1)$...
\vdots	\vdots	\vdots	\vdots
$G(/G_i)$...	$\sum_{k=1}^{v_j} \beta_k^{(ij)} G_j(/H_k^{(j)})$...
\vdots	\vdots	\vdots	\vdots
$G(/G)^*$...	$G_j(/G_j)$...

* $G_1 = C_1$ and $G_s = G$

Table 5.7. Subduction Table of C_{2v}

	$\downarrow C_1$	$\downarrow C_2$	$\downarrow C_s$	$\downarrow C'_s$	$\downarrow C_{2v}$
$C_{2v}(/C_1)$	$4C_1(/C_1)$	$2C_2(/C_1)$	$2C_s(/C_1)$	$2C'_s(/C_1)$	$C_{2v}(/C_1)$
$C_{2v}(/C_2)$	$2C_1(/C_1)$	$2C_2(/C_2)$	$C_s(/C_1)$	$C'_s(/C_1)$	$C_{2v}(/C_2)$
$C_{2v}(/C_s)$	$2C_1(/C_1)$	$C_2(/C_1)$	$2C_s(/C_s)$	$C'_s(/C_1)$	$C_{2v}(/C_s)$
$C_{2v}(/C'_s)$	$2C_1(/C_1)$	$C_2(/C_1)$	$C_s(/C_1)$	$2C'_s(/C'_s)$	$C_{2v}(/C'_s)$
$C_{2v}(/C_{2v})$	$C_1(/C_1)$	$C_2(/C_2)$	$C_s(/C_s)$	$C'_s(/C'_s)$	$C_{2v}(/C_{2v})$

ducted in the following matrix multiplication:

$$\begin{matrix}
 C_{2v}(/C_1) \downarrow C_2 \\
 C_{2v}(/C_2) \downarrow C_2 \\
 C_{2v}(/C_s) \downarrow C_2 \\
 C_{2v}(/C'_s) \downarrow C_2 \\
 C_{2v}(/C_{2v}) \downarrow C_2
 \end{matrix}
 \begin{matrix}
 C_1 & C_2 \\
 \left(\begin{matrix} 4 & 0 \\ 2 & 2 \\ 2 & 0 \\ 2 & 0 \\ 1 & 1 \end{matrix} \right) \\
 \text{FPVs}
 \end{matrix}
 \begin{matrix}
 \left(\begin{matrix} \frac{1}{2} & 0 \\ -\frac{1}{2} & 1 \end{matrix} \right) \\
 \\
 \\
 \\
 \\
 \text{MVs}
 \end{matrix}
 =
 \begin{matrix}
 /C_1 & /C_2 \\
 \left(\begin{matrix} 2 & 0 \\ 0 & 2 \\ 1 & 0 \\ 1 & 0 \\ 0 & 1 \end{matrix} \right) \\
 \\
 \\
 \\
 \\
 \text{MVs}
 \end{matrix}
 \begin{matrix}
 2C_2(/C_1) \\
 2C_2(/C_2) \\
 C_2(/C_1) \\
 C_2(/C_1) \\
 C_2(/C_2)
 \end{matrix}
 , \quad (5.44)$$

where each row of the resulting 5×2 matrix represents $MV_{C_{2v}(/G_i) \downarrow C_2}$, which corresponds to each subduction listed in the rightmost column of Eq. 5.44.

The process of evaluating subductions is repeated to cover all of the subgroups of $SSG_{C_{2v}}$. The results are summarized in Table 5.7. The result of Eq. 5.44 appears in the $\downarrow C_2$ -column of Table 5.7.

Exercise 5.2.

- Apply Eq. 5.35 to the data of Table 5.1. Thus, construct subduced representations $C_{2v}(/G_i) \downarrow C_2$ by selecting permutations corresponding to $C_2 = \{I, C_2\}$.
- Evaluate FPVs by counting the number of 1-cycles contained in each subduction. Compare this result with Eq. 5.44.




Exercise 5.3.

- Confirm that the four positions denoted by a solid circle in adamantan-2-one **5-2** (Fig. 5.2) construct an orbit governed by the coset representation $C_{2v}/(C_1)$.
- Discuss the chirality fittingness of the enantiospheric $C_{2v}/(C_1)$ -orbit in **5-2**. Thereby, confirm the prochirality of **5-2** with respect to the $C_{2v}/(C_1)$ -orbit.
- Confirm that dioxo derivatives, **5-3** and $\overline{\mathbf{5-3}}$, are enantiomeric to each other.
- Discuss the derivation of **5-3** and $\overline{\mathbf{5-3}}$ from **5-2** on the basis of the subduction $C_{2v}/(C_1) \downarrow C_2$ (Eq. 5.44 and Table 5.7).
- Confirm that oxa derivatives, **5-4** and $\overline{\mathbf{5-4}}$, are enantiomeric to each other.
- Discuss the derivation of **5-4** and $\overline{\mathbf{5-4}}$ from **5-2** on the basis of the subduction $C_{2v}/(C_1) \downarrow C_1$ (the first column of Table 5.7).

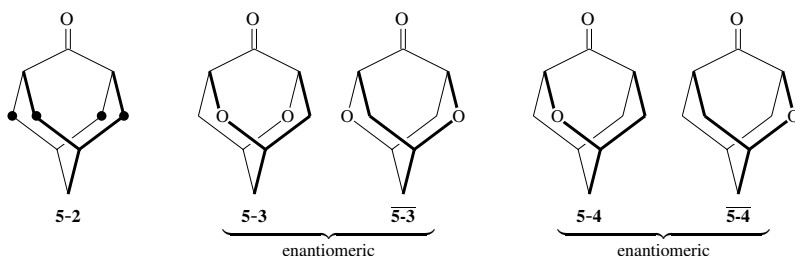


Fig. 5.2. Adamantan-2-one, dioxo derivatives, and oxa derivatives. See Exercise 5.3.


Exercise 5.4.

- In a continuation of Exercise 5.3, confirm that the four positions denoted by a solid circle in adamantane-2,6-dione **5-5** (Fig. 5.3) construct an orbit governed by the coset representation $D_{2d}/(C_2')$. See Fig. 10.3 of [1].
- Discuss the chirality fittingness of the enantiospheric $D_{2d}/(C_2')$ -orbit in **5-5**. Thereby, confirm the prochirality of **5-5** with respect to the $D_{2d}/(C_2')$ -orbit.
- Confirm that dioxo derivatives, **5-6** and $\overline{\mathbf{5-6}}$, are enantiomeric to each other.
- Discuss the derivation of **5-6** and $\overline{\mathbf{5-6}}$ from **5-5** on the basis of the following subduction:

$$D_{2d}/(C_2') \downarrow D_2 = D_2/(C_2') + D_2/(C_2''), \quad (5.45)$$

which has been once noted in [1, Eq. 10.13].

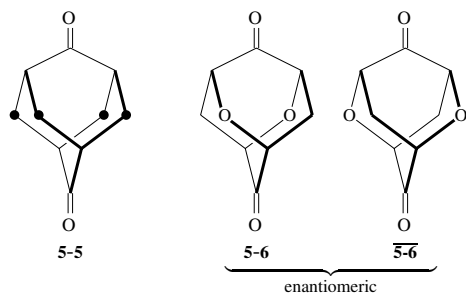


Fig. 5.3. Adamantane-2,6-dione and dioxo derivatives. See Exercise 5.4.

5.2.2 Unit Subduced Cycle Indices (USCIs)

USCIs With Chirality Fittingness

Let the symbols a_d , c_d , and b_d denote *sphericity indices* for characterizing homospheric, enantiospheric, or hemispheric coset representations or the corresponding orbits (cf. Def. 4.1 on page 89) [1,3]:

Definition 5.1 (Sphericity Indices for Characterizing Coset Representations and Orbits).

- **(Sphericity index a_d for a homospheric orbit)** The sphericity index a_d is assigned to a homospheric $G/(G_i)$ -orbit (G : achiral; and G_i : achiral).
- **(Sphericity index c_d for an enantiospheric orbit)** The sphericity index c_d is assigned to an enantiospheric $G/(G_i)$ -orbit (G : achiral; and G_i : chiral).
- **(Sphericity index b_d for a hemispheric orbit)** The sphericity index b_d is assigned to a hemispheric $G/(G_i)$ -orbit (G : chiral; and G_i : chiral).

The subscript d of a_d , c_d , or b_d represents the size of the orbit, i.e., $d = |G|/|G_i|$.

According to Def. 4.1 (Subsection 4.1.2), each coset representation $G_j/(H_k^{(j)})$ contained in the right-hand side of Eq. 5.37 is categorized to be homospheric, enantiospheric, or hemispheric. Then, a unit subduced cycle index with chirality faithfulness (USCI-CF) is defined on the basis of Eq. 5.37, which represents the subduction $G/(G_i) \downarrow G_j$ [1, Def. 9.3]:

Definition 5.2 (Unit Subduced Cycle Indices with Chirality Fittingness (USCI-CFs)). The coset representation $G_j/(H_k^{(j)})$ contained in the right-hand side of Eq. 5.37 is characterized by a sphericity index $\$_{d_{jk}}$ ($\$ = a, c, \text{ or } b$) defined in Def. 5.1. Then, a unit subduced cycle index with chirality fittingness (USCI-CF) is defined on the basis of Eq. 5.37 as follows:

$$\text{USCI-CF}(G/(G_i) \downarrow G_j; \$_d) = \prod_{k=1}^{v_j} \$_{d_{jk}}^{\beta_k^{(ij)}}, \quad (5.46)$$

where $\$_{d_{jk}}$ is equal to $a_{d_{jk}}$, $c_{d_{jk}}$, or $b_{d_{jk}}$ according to the sphericity of $G_j/(H_k^{(j)})$ and the subscript is calculated to be

$$d_{jk} = \frac{|G_j|}{|H_k^{(j)}|}. \quad (5.47)$$

By starting from the data collected in the subduction table of G (Table 5.6), the whole set of USCI-CFs for G is obtained easily, which is collected as a USCI-CF table of G (Table 5.8).

Table 5.8. USCI-CF Table of G

	$G(/G_i) \downarrow G_j \ (j = 1, 2, \dots, s)$		
	\dots	$\downarrow G_j$	\dots
$G(/C_1)$	\dots	$\$ \frac{ G }{ G_j }$	\dots
\vdots	\vdots	\vdots	\vdots
$G(/G_i)$	\dots	$\sum_{k=1}^{v_j} \$ d_{jk}^{\beta_k^{(ij)}}$	\dots
\vdots	\vdots	\vdots	\vdots
$G(/G)$	\dots	$\$ 1$	\dots

Table 5.9. USCI-CF Table of C_{2v}

	$\downarrow C_1$	$\downarrow C_2$	$\downarrow C_s$	$\downarrow C'_s$	$\downarrow C_{2v}$
$C_{2v}(/C_1)$	b_1^4	b_2^2	c_2^2	c_2^2	c_4
$C_{2v}(/C_2)$	b_1^2	b_1^2	c_2	c_2	c_2
$C_{2v}(/C_s)$	b_1^2	b_2	a_1^2	c_2	a_2
$C_{2v}(/C'_s)$	b_1^2	b_2	c_2	a_1^2	a_2
$C_{2v}(/C_{2v})$	b_1	b_1	a_1	a_1	a_1
Σ	$\frac{1}{4}$	$\frac{1}{4}$	$\frac{1}{4}$	$\frac{1}{4}$	0

For example, the data collected in the subduction table of C_{2v} (Table 5.7) can be converted into the corresponding USCI-CF table of C_{2v} shown in Table 5.9. Note that the Σ -row of Table 5.9 collects the row sums of the inverse mark table (the $\sum_i \bar{m}_{ji}$ -column of Table 5.5).

The USCI-CF tables for representative point groups have been collected as Appendix E of Fujita's monograph [1].

USCIs Without Chirality Fittingness

If no chiral proligands are taken into consideration, chirality fittingness is unnecessary to be considered. Hence, the sphericity indices $\$ d_{jk}$ in the USCI-CF (Eq. 5.46 of Def. 5.2) degenerate into a single dummy variable $s_{d_{jk}}$ ($s_{d_{jk}} = a_{d_{jk}} = c_{d_{jk}} = b_{d_{jk}}$), so that the following definition of a unit subduced cycle index (USCI without chirality fittingness) is obtained [1, Def. 9.2]:

Definition 5.3 (Unit Subduced Cycle Indices (USCIs)). A unit subduced cycle index (USCI without chirality fittingness) is defined on the basis of Eq. 5.37 as follows:

$$\text{USCI}(G(/G_i) \downarrow G_j; s_d) = \prod_{k=1}^{v_j} s_{d_{jk}}^{\beta_k^{(ij)}} \quad (5.48)$$

where the subscript of the dummy variable $s_{d_{jk}}$ is calculated to be

$$d_{jk} = \frac{|G_j|}{|H_k^{(j)}|}. \quad (5.49)$$

By placing $s_{d_{jk}} = \$_{d_{jk}} = a_{d_{jk}} = c_{d_{jk}} = b_{d_{jk}}$ according to Def. 5.48, Table 5.8 degenerates to give the USCI table of \mathbf{G} shown in Table 5.10.

Table 5.10. USCI Table of \mathbf{G}

	$\mathbf{G}(/ \mathbf{G}_i) \downarrow \mathbf{G}_j \ (j = 1, 2, \dots, s)$		
	...	$\downarrow \mathbf{G}_j$...
$\mathbf{G}(/ \mathbf{C}_1)$...	$s \frac{ \mathbf{G}/\mathbf{G}_j }{ \mathbf{G}_j }$...
\vdots	\vdots	\vdots	\vdots
$\mathbf{G}(/ \mathbf{G}_i)$...	$\sum_{k=1}^{v_j} s_{d_{jk}}^{(ij)}$...
\vdots	\vdots	\vdots	\vdots
$\mathbf{G}(/ \mathbf{G})$...	s_1	...

By placing $s_{d_{jk}} = a_{d_{jk}} = c_{d_{jk}} = b_{d_{jk}}$ according to Def. 5.48, Table 5.9 degenerates to give the USCI table of \mathbf{C}_{2v} shown in Table 5.11. Note that the Σ -row of Table 5.11 collects the row sums of the inverse mark table (the $\sum_i \bar{m}_{ji}$ -column of Table 5.5).

Table 5.11. USCI Table of \mathbf{C}_{2v}

	$\downarrow \mathbf{C}_1$	$\downarrow \mathbf{C}_2$	$\downarrow \mathbf{C}_s$	$\downarrow \mathbf{C}'_s$	$\downarrow \mathbf{C}_{2v}$
$\mathbf{C}_{2v}(/ \mathbf{C}_1)$	s_1^4	s_2^2	s_2^2	s_2^2	s_4
$\mathbf{C}_{2v}(/ \mathbf{C}_2)$	s_1^2	s_1^2	s_2	s_2	s_2
$\mathbf{C}_{2v}(/ \mathbf{C}_s)$	s_1^2	s_2	s_1^2	s_2	s_2
$\mathbf{C}_{2v}(/ \mathbf{C}'_s)$	s_1^2	s_2	s_2	s_1^2	s_2
$\mathbf{C}_{2v}(/ \mathbf{C}_{2v})$	s_1	s_1	s_1	s_1	s_1
Σ	$\frac{1}{4}$	$\frac{1}{4}$	$\frac{1}{4}$	$\frac{1}{4}$	0

The USCI tables for representative point groups have been collected as Appendix D of Fujita's monograph [1].

Exercise 5.5.

- Show that the power of a_1 or b_1 appearing in each USCI-CF (Table 5.9) is equal to each mark (Table 5.3).
- Show that the power of s_1 of each USCI (Table 5.11) is equal to each mark (Table 5.3).
- Confirm that these results hold true in general.

References

- [1] S. Fujita, “Symmetry and Combinatorial Enumeration in Chemistry”, Springer-Verlag, Berlin-Heidelberg (1991).
- [2] S. Fujita, *Theor. Chim. Acta*, **76**, 247–268 (1989).
- [3] S. Fujita, *J. Am. Chem. Soc.*, **112**, 3390–3397 (1990).
- [4] W. Burnside, “Theory of Groups of Finite Order”, 2nd ed., Cambridge University Press, Cambridge (1911).
- [5] S. Fujita, “Combinatorial Enumeration of Graphs, Three-Dimensional Structures, and Chemical Compounds”, University of Kragujevac, Faculty of Science, Kragujevac (2013).

6 Symmetry-Itemized Enumeration Under Point Groups

6.1 Fujita's USCI Approach

6.1.1 Historical Comments

A characteristic of Fujita's USCI (unit-subduced-cycle-index) approach [1] is the effective application of USCI-CFs (*unit subduced cycle indices with chirality fittingness*), which are algebraically derived from the concept of *subduction* applied to mark tables in combination with the concepts of *sphericities* and *chirality fittingness*.

It is worthwhile to refer to several pioneering works for enumeration, although they did not reach the concept of USCI-CFs. Sheehan [2] proposed a method based on mark tables in counting graphs with a given automorphism group. Sheehan's method can be regarded as a degenerate enumeration without chirality fittingness from the viewpoint of Fujita's USCI approach. Hässelbarth [3] reported a pioneering work based on mark tables in chemical enumeration. Related methods based on double cosets were proposed by Ruch et al. [4,5] and Brocas [6]. Mead [7,8] pointed out the relationship between mark tables and double cosets in isomer counting. These pioneering works did not reach the concept of USCI-CFs, which in turn requires the development of subduction of coset representations, sphericities, and chirality fittingness.

As for Fujita's USCI approach, subduction of coset representations for deriving USCIs has been proposed by Fujita [9]. Correlation of USCIs to Pólya's cycle indices has been clarified by Fujita [10]. The concept of sphericities applied to the derivation of USCI-CFs has been reported by Fujita [11,12]. Subduction of coset representations has been applied to systematic classification of molecular symmetry [13] and to integration of point-group and permutation-group theories [14]. Related topics have been summarized as a monograph by Fujita [1]. The importance of the concept of sphericities has been emphasized to discuss stereochemistry in a molecule and stereoisomerism among molecules [15] as well as to discuss sphericity beyond topicity in characterizing stereochemical phenomena [16].

6.1.2 USCI-CFs for Itemized Enumeration

A promolecule (or molecule) of \mathbf{G}_j derived from a stereoskeleton of \mathbf{G} is characterized by the sum of suborbits represented by Eq. 3.40 (obtained diagrammatically in Subsection 3.4.2) and equivalently by Eq. 5.37 (obtained algebraically in Subsection 5.2.1). Each sub-orbit of the size $d_{jk} = |\mathbf{G}_j|/|\mathbf{H}_k^{(j)}|$ is governed by a coset representation $\mathbf{G}_j(/ \mathbf{H}_k^{(j)})$, which accommodates a set of d_{jk} proligands (or ligands) according to the chirality fittingness specified by the sphericity of $\mathbf{G}_j(/ \mathbf{H}_k^{(j)})$. According to Def. 5.1 (page 127), the chirality fitting-

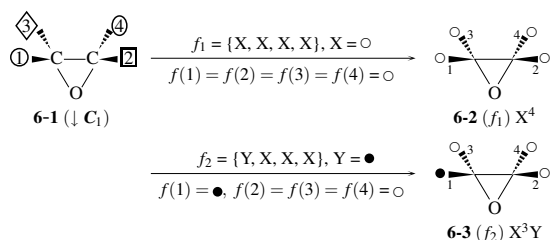


Fig. 6.1. Modes of packing due to the subduction $C_{2v}(/C_1) \downarrow C_1$ for generating oxirane derivatives.

ness is represented systematically by the sphericity index $\$d_{jk}$ ($a_{d_{jk}}$, $c_{d_{jk}}$, or $b_{d_{jk}}$), which decides the packing of the $G_j(/H_k^{(j)})$ -suborbit as shown in Fig. 4.2 (page 90).

To grasp the total features of derivation due to subduction of coset representations, let us examine the derivation based on the oxirane skeleton **3-12** (Fig. 3.7 on page 68), the four positions of which belong to a four-membered enantiospheric $C_{2v}(/C_1)$ -orbit.

The mode of derivation is represented by a function f :

$$f : \{f(1), f(2), f(3), f(4)\}, \quad (6.1)$$

in which the component $f(i)$ ($i = 1, 2, 3, 4$) represents a substituent accommodated at the i -position of the numbered skeleton.

First, four substituents are selected from the following ligand inventory:

$$L_1 = \{X, Y\}, \quad (6.2)$$

where the symbols X and Y represent achiral proligands in isolation.

As a result of the subduction $C_{2v}(/C_1) \downarrow C_1$, the four positions are divided into four one-membered orbits ($4C_1(/C_1)$, USCI-CF: b_1^4), which are differentiated from one another, as surrounded with different frames in **6-1** (Fig. 6.1). Each position of **6-1** as a one-membered orbit accommodates X or Y independently. For example, the functions $f_1: \{X, X, X, X\}$ and $f_2: \{Y, X, X, X\}$ generate **6-2** (composition: X^4) and **6-3** (composition: X^3Y), respectively.

This process is repeated by noting that each position of **6-1** accommodates X or Y independently, so that the derivatives f_1 to f_{16} collected in Fig. 6.2 are obtained. Because each position of **6-1** accommodates X or Y independently, we are safe to place $b_1 = X + Y$. Thereby, the numbers of f_1 to f_{16} collected in Fig. 6.2 are evaluated with respect to the compositions (X^4 , X^3Y , etc.) to give the following generating function:

$$b_1^4 : \quad (X + Y)^4 = X^4 + 4X^3Y + 6X^2Y^2 + 4XY^3 + Y^4. \quad (6.3)$$

The coefficients appearing in the right-hand side are shown in the C_1 -column in the right part of Fig. 6.2.

As a result of the subduction $C_{2v}(/C_1) \downarrow C_s$, the four positions are divided into two two-membered orbits ($2C_s(/C_1)$, USCI-CF: c_2^2), which are differentiated from one another

	C_1	C_2	C_s	C'_s	C_{2v}	
	b_1^4	b_2^2	c_2^2	c_2^2	c_4	
X^4 6-2 (f_1)	1	1	1	1	1	$C_{2v}/(C_{2v})$
X^3Y 6-3 (f_2) 6-4 (f_3) 6-5 (f_4) 6-6 (f_5)	4	0	0	0	0	$C_{2v}/(C_1)$
X^2Y^2 6-7 (f_6) 6-8 (f_7)	2	2	0	0	0	$C_{2v}/(C_2)$
X^2Y^2 6-9 (f_8) 6-10 (f_9)	2	0	2	0	0	$C_{2v}/(C_s)$
X^2Y^2 6-11 (f_{10}) 6-12 (f_{11})	2	0	0	2	0	$C_{2v}/(C'_s)$
XY^3 6-13 (f_{12}) 6-14 (f_{13}) 6-15 (f_{14}) 6-16 (f_{15})	4	0	0	0	0	$C_{2v}/(C_1)$
Y^4 6-17 (f_{16})	1	1	1	1	1	$C_{2v}/(C_{2v})$

$(X^4 + Y^4)$
 $(X^2 + Y^2)^2$
 $(X^2 + Y^2)^2$
 $(X^2 + Y^2)^2$
 $(X^4 + Y^4)$

Fig. 6.2. Orbits of promolecules based on an oxirane skeleton and their fixed-point vectors (vectors of marks). An open circle represents an achiral proligand X in isolation, while a solid circle represents another achiral proligand Y in isolation. Each row of the right-hand part should be compared with the corresponding row of the mark table of C_{2v} (Table 5.3 on page 119).

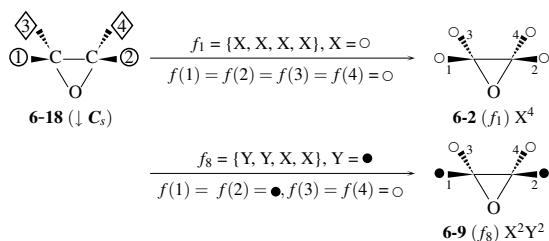


Fig. 6.3. Modes of packing due to the subduction $C_{2v}/(C_1) \downarrow C_s$ for generating oxirane derivatives.

as surrounded with different frames in **6-18** (Fig. 6.3). Each orbit of **6-18** accommodates X^2 or Y^2 independently. For example, the functions $f_1: \{X, X, X, X\}$ and $f_8: \{Y, Y, X, X\}$ generate **6-2** (composition: X^4) and **6-9** (composition: X^2Y^2), respectively.

This process is repeated by noting that each position of **6-18** accommodates X^2 or Y^2 independently, so that the derivatives f_1 , f_8 , f_9 , and f_{16} are obtained, as collected in Fig. 6.2. Because each position of **6-18** accommodates X^2 or Y^2 independently, we are safe to

place $c_2 = X^2 + Y^2$. Thereby, the numbers of f_1, f_8, f_9 , and f_{16} are evaluated with respect to the compositions (X^4 and X^2Y^2) to give the following generating function:

$$c_2^2: \quad (X^2 + Y^2)^2 = X^4 + 2X^2Y^2 + Y^4. \tag{6.4}$$

The coefficients appearing in the right-hand side are shown in the C_s -column in the right part of Fig. 6.2.

Similarly, the generating functions for the subduction of $C_{2v}/(C_1)$ by other subgroups are calculated, as collected in the right part of Fig. 6.2. The results are summarized as a fixed-point matrix (FPM) (Eq. 6.5).

$$\text{FPM}_{3-12} = \begin{matrix} X^4 \\ X^3Y \\ X^2Y^2 \\ XY^3 \\ Y^4 \end{matrix} \begin{matrix} C_1 & C_2 & C_s & C'_s & C_{2v} \\ \left(\begin{array}{ccccc} 1 & 1 & 1 & 1 & 1 \\ 4 & 0 & 0 & 0 & 0 \\ 6 & 2 & 2 & 2 & 0 \\ 4 & 0 & 0 & 0 & 0 \\ 1 & 1 & 1 & 1 & 1 \end{array} \right) \end{matrix}. \tag{6.5}$$

The 16 derivatives collected in Fig. 6.2 can be characterized in an alternative viewpoint. Let the symbol \mathbf{F}_{3-12} represent the set of the 16 derivatives:

$$\mathbf{F}_{3-12} = \{f_1, f_2, f_3, f_4, f_5, f_6, f_7, f_8, f_9, f_{10}, f_{11}, f_{12}, f_{13}, f_{14}, f_{15}, f_{16}\}, \tag{6.6}$$

The four positions of the skeleton **3-12** are permuted on the action of C_{2v} in terms of the coset representation $C_{2v}/(C_1)$. According to the permutations of the four positions, the set \mathbf{F}_{3-12} is transformed on the action of C_{2v} as follows:

$$\begin{matrix} \mathbf{F}_{3-12}|_I = & \left\{ \begin{array}{c} f_1, \\ \surd \end{array} \right\} & \left\{ \begin{array}{c} f_2, f_3, f_4, f_5, \\ \surd \ \surd \ \surd \ \surd \end{array} \right\} & \left\{ \begin{array}{c} f_6, f_7, \\ \surd \ \surd \end{array} \right\} & \left\{ \begin{array}{c} f_8, f_9, \\ \surd \ \surd \end{array} \right\} & \left\{ \begin{array}{c} f_{10}, f_{11}, \\ \surd \ \surd \end{array} \right\} & \left\{ \begin{array}{c} f_{12}, f_{13}, f_{14}, f_{15}, \\ \surd \ \surd \ \surd \ \surd \end{array} \right\} & \left\{ \begin{array}{c} f_{16} \\ \surd \end{array} \right\} \\ \mathbf{F}_{3-12}|_{C_2} = & \left\{ \begin{array}{c} f_1, \\ \surd \end{array} \right\} & \left\{ \begin{array}{c} f_5, f_4, f_3, f_2, \\ \surd \ \surd \end{array} \right\} & \left\{ \begin{array}{c} f_6, f_7, \\ \surd \ \surd \end{array} \right\} & \left\{ \begin{array}{c} f_9, f_8, \\ \surd \ \surd \end{array} \right\} & \left\{ \begin{array}{c} f_{11}, f_{10}, \\ \surd \ \surd \end{array} \right\} & \left\{ \begin{array}{c} f_{15}, f_{14}, f_{13}, f_{12}, \\ \surd \ \surd \ \surd \ \surd \end{array} \right\} & \left\{ \begin{array}{c} f_{16} \\ \surd \end{array} \right\} \\ \mathbf{F}_{3-12}|_{\sigma_{(1)}} = & \left\{ \begin{array}{c} f_1, \\ \surd \end{array} \right\} & \left\{ \begin{array}{c} f_3, f_2, f_5, f_4, \\ \surd \ \surd \end{array} \right\} & \left\{ \begin{array}{c} f_7, f_6, \\ \surd \ \surd \end{array} \right\} & \left\{ \begin{array}{c} f_8, f_9, \\ \surd \ \surd \end{array} \right\} & \left\{ \begin{array}{c} f_{11}, f_{10}, \\ \surd \ \surd \end{array} \right\} & \left\{ \begin{array}{c} f_{13}, f_{12}, f_{15}, f_{14}, \\ \surd \ \surd \ \surd \ \surd \end{array} \right\} & \left\{ \begin{array}{c} f_{16} \\ \surd \end{array} \right\} \\ \mathbf{F}_{3-12}|_{\sigma_{(2)}} = & \left\{ \begin{array}{c} f_1, \\ \surd \end{array} \right\} & \left\{ \begin{array}{c} f_4, f_5, f_2, f_3, \\ \surd \ \surd \end{array} \right\} & \left\{ \begin{array}{c} f_7, f_6, \\ \surd \ \surd \end{array} \right\} & \left\{ \begin{array}{c} f_9, f_8, \\ \surd \ \surd \end{array} \right\} & \left\{ \begin{array}{c} f_{10}, f_{11}, \\ \surd \ \surd \end{array} \right\} & \left\{ \begin{array}{c} f_{13}, f_{12}, f_{15}, f_{14}, \\ \surd \ \surd \ \surd \ \surd \end{array} \right\} & \left\{ \begin{array}{c} f_{16} \\ \surd \end{array} \right\} \\ & X^4 & X^3Y & X^2Y^2 & XY^3 & Y^4 \\ & [\theta]_1 & [\theta]_2 & [\theta]_3 & [\theta]_4 & [\theta]_5 \end{matrix} \tag{6.7}$$

where the symbol \surd corresponds to a 1-cycle (a fixed derivative) appearing in a permutation representation.

The right-hand sides of these equations are divided into five parts according to the compositions (X^4, X^3Y , etc.), which are represented by the partition $[\theta]$ (e.g., $[\theta]_1 = [4, 0; 0, 0]$ and $[\theta]_2 = [3, 1; 0, 0]$). Each division is represented by the following permutations:

$$\lambda_g^{[\theta]} = \left(\begin{array}{c} \mathbf{F}_{3-12}^{[\theta]} \\ \mathbf{F}_{3-12}^{[\theta]}|_g \end{array} \right) \text{ for } g \in C_{2v}, \tag{6.8}$$

which construct a permutation representation:

$$A_{C_{2v}, \mathbf{F}_{3-12}}^{[\theta]} = \left\{ \lambda_g^{[\theta]} \mid \forall g \in C_{2v} \right\} \tag{6.9}$$

The permutation representation may not be transitive, so that it is divided into a sum of coset representations as follows:

$$A_{C_{2v}, F_{3-12}}^{[\theta]} = \sum_{G_i} A_{\theta_i} C_{2v}(/G_i), \quad (6.10)$$

where the summation runs over $G_i \in \text{SSG}_{C_{2v}}$ and the integer A_{θ_i} represents the multiplicity of each coset representation. It should be noted that the coset representation $C_{2v}(/G_i)$ governs an orbit of promolecules (derivatives) of G_i . Hence, the subduction $C_{2v}(/G_i) \downarrow G_j$ gives the corresponding mark (the number of fixed promolecules). For example, the first X^2Y^2 -row of Fig. 6.2 is concerned with an orbit of C_2 -promolecules, which indicates the marks for $C_{2v}(/C_2) \downarrow G_j$. Hence, each row of the FPM (Eq. 6.5) can be regarded as a fixed-point vector (FPV) to evaluate the coefficient A_{θ_i} .

Let us collect the coefficients A_{θ_i} to give a 5×5 matrix called an *isomer-counting matrix* (ICM):

$$\text{ICM}_{3-12} = (A_{\theta_i}) \quad (6.11)$$

By using the FPM (Eq. 6.5), the ICM (Eq. 6.11) is calculated as follows:

$$\text{ICM}_{3-12} = \text{FPM}_{3-12} \times M_{C_{2v}}^{-1} = \begin{matrix} X^4 \\ X^3Y \\ X^2Y^2 \\ XY^3 \\ Y^4 \end{matrix} \begin{pmatrix} C_1 & C_2 & C_s & C'_s & C_{2v} \\ 0 & 0 & 0 & 0 & 1 \\ 1 & 0 & 0 & 0 & 0 \\ 0 & 1 & 1 & 1 & 0 \\ 1 & 0 & 0 & 0 & 0 \\ 0 & 0 & 0 & 0 & 1 \end{pmatrix} \quad (6.12)$$

Each element of ICM_{3-12} indicates the number of derivatives in which an achiral promolecule or a pair of enantiomeric promolecules is counted once. For example, the value 1 at the intersection between the X^2Y^2 -row and the C_2 column indicates the presence of one pair of enantiomers of C_2 with the composition X^2Y^2 , i.e., an enantiomeric pair of **6-7** and **6-8** in Fig. 6.2.

Exercise 6.1.

- Classify the 16 derivatives listed in Fig. 6.2 in terms of homomeric and enantiomeric relationships.
 - Then, confirm the data of ICM_{3-12} (Eq. 6.12).
-

Let us now examine the effect of chiral proligands, where four substituents are selected from the following ligand inventory:

$$L_2 = \{p, \bar{p}\}. \quad (6.13)$$

The symbols p and \bar{p} represent an enantiomeric pair of chiral proligands in isolation. In a similar way to Fig. 6.2 based on the ligand inventory L_1 , there appear 16 derivatives based

on the ligand inventory L_2 , where the symbol \odot represents p , while the symbol \bullet represents \bar{p} .

The USCI-CF b_1^4 for the subduction $C_{2v}(/C_1) \downarrow C_1$ means that the four positions as four one-membered orbits ($4C_1(/C_1)$) independently accommodate a proligand p or \bar{p} . By placing $b_1 = p + \bar{p}$ for such a hemispheric orbit as $C_1(/C_1)$, the following generating function is obtained:

$$\begin{aligned} b_1^4: \quad (p + \bar{p})^4 &= p^4 + 4p^3\bar{p} + 6p^2\bar{p}^2 + 4p\bar{p}^3 + \bar{p}^4 \\ &= 2 \times \frac{1}{2}(p^4 + \bar{p}^4) + 8 \times \frac{1}{2}(p^3\bar{p} + p\bar{p}^3) + 6p^2\bar{p}^2 \end{aligned} \quad (6.14)$$

The coefficients appearing in the right-hand side are shown in the C_1 -column in the right part of Fig. 6.4. Because a pair of enantiomers is counted once in the present enumeration, the term $\frac{1}{2}(p^4 + \bar{p}^4)$ corresponds to one pair of enantiomers, where a proligand with the composition p^4 is enantiomeric to the counterpart with the composition \bar{p}^4 .

The USCI-CF c_2^2 for the subduction $C_{2v}(/C_1) \downarrow C_s$ means that each of the two-membered enantiospheric orbits ($2C_s(/C_1)$) accommodate a pair of proligands p/\bar{p} in accord to the chirality fittingness shown in Fig. 4.2(b). Because there are two modes of packing, we are able to place $c_2 = 2p\bar{p}$. As a result, we obtain the following generating function:

$$c_2^2: \quad (2p\bar{p})^2 = 4p^2\bar{p}^2. \quad (6.15)$$

The coefficients appearing in the right-hand side are shown in the C_s -column in the right part of Fig. 6.4, where the number 4 is factorized into 1, 1, and 2. Note that a pair of p/\bar{p} is accommodated in one $C_s(/C_1)$ -orbit, independent of another pair of p/\bar{p} accommodated in the other $C_s(/C_1)$ -orbit (cf. 6-29 or 6-30).

Similarly, the generating functions for the subduction of $C_{2v}(/C_1)$ by other subgroups are calculated, as collected in the right part of Fig. 6.4. The results are summarized as a fixed-point matrix (Eq. 6.16).

$$\text{FPM}'_{3-12} = \begin{matrix} \frac{1}{2}(p^4 + \bar{p}^4) \\ \frac{1}{2}(p^3\bar{p} + p\bar{p}^3) \\ p^2\bar{p}^2 \end{matrix} \begin{pmatrix} C_1 & C_2 & C_s & C'_s & C_{2v} \\ 2 & 2 & 0 & 0 & 0 \\ 8 & 0 & 0 & 0 & 0 \\ 6 & 2 & 4 & 4 & 2 \end{pmatrix}. \quad (6.16)$$

Note that the values in the C_1 -column stem from Eq. 6.14, while the values in the C_s -column stem from Eq. 6.15.

In place of FPM'_{3-12} (Eq. 6.16), an alternative form of FPM is convenient for further algebraic derivation:

$$\text{FPM}''_{3-12} = \begin{matrix} p^4 \\ p^3\bar{p} \\ p^2\bar{p}^2 \\ p\bar{p}^3 \\ \bar{p}^4 \end{matrix} \begin{pmatrix} C_1 & C_2 & C_s & C'_s & C_{2v} \\ 1 & 1 & 0 & 0 & 0 \\ 4 & 0 & 0 & 0 & 0 \\ 6 & 2 & 4 & 4 & 2 \\ 4 & 0 & 0 & 0 & 0 \\ 1 & 1 & 0 & 0 & 0 \end{pmatrix} \quad (6.17)$$

	C_1	C_2	C_s	C'_s	C_{2v}						
	b_1^4	b_2^2	c_2^2	c_2^2	c_4						
$\frac{1}{2}(p^4 + \bar{p}^4)$						2	2	0	0	0	$C_{2v}(/C_2)$
$\frac{1}{2}(p^3\bar{p} + p\bar{p}^3)$						4	0	0	0	0	$C_{2v}(/C_1)$
$\frac{1}{2}(p^3\bar{p} + p\bar{p}^3)$						4	0	0	0	0	$C_{2v}(/C_1)$
$p^2\bar{p}^2$						1	1	1	1	1	$C_{2v}(/C_{2v})$
$p^2\bar{p}^2$						1	1	1	1	1	$C_{2v}(/C_{2v})$
$p^2\bar{p}^2$						2	0	0	2	0	$C_{2v}(/C'_s)$
$p^2\bar{p}^2$						2	0	2	0	0	$C_{2v}(/C_s)$
											$(p + \bar{p})^4$ $(p^2 + \bar{p}^2)^2$ $(2p\bar{p})^2$ $(2p\bar{p})^2$ $(2p\bar{p}^2)$

Fig. 6.4. Orbits of promolecules based on an oxirane skeleton and their fixed-point vectors (vectors of marks). The symbol \odot represents a chiral proligand p in isolation, while the symbol \bullet represents its enantiomeric proligand \bar{p} in isolation. Each row of the right-hand part should be compared with the corresponding row of the mark table of C_{2v} (Table 5.3 on page 119).

Let the symbol \mathbf{F}'_{3-12} represent the set of the 16 derivatives collected in Fig. 6.4:

$$\mathbf{F}'_{3-12} = \{f_1, f_2, f_3, f_4, f_5, f_6, f_7, f_8, f_9, f_{10}, f_{11}, f_{12}, f_{13}, f_{14}, f_{15}, f_{16}\}, \quad (6.18)$$

This set can be treated along a similar line to the set \mathbf{F}_{3-12} (Eq. 6.6) for Fig. 6.2. Hence, in a parallel way to Eq. 6.12, the FPM (Eq. 6.16) generates the following ICM:

$$\text{ICM}'_{3-12} = \text{FPM}'_{3-12} \times M_{C_{2v}}^{-1} = \begin{matrix} \frac{1}{2}(p^4 + \bar{p}^4) \\ \frac{1}{2}(p^3\bar{p} + p\bar{p}^3) \\ p^2\bar{p}^2 \end{matrix} \begin{pmatrix} C_1 & C_2 & C_s & C'_s & C_{2v} \\ 0 & 1 & 0 & 0 & 0 \\ 2 & 0 & 0 & 0 & 0 \\ 0 & 0 & 1 & 1 & 2 \end{pmatrix}. \quad (6.19)$$

The alternative FPM represented by Eq. 6.17 generates an alternative ICM as a more convenient form for algebraic derivation:

$$\text{ICM}_{3-12}'' = \text{FPM}_{3-12}'' \times M_{C_{2v}}^{-1} = \begin{matrix} p^4 \\ p^3\bar{p} \\ p^2\bar{p}^2 \\ p\bar{p}^3 \\ \bar{p}^4 \end{matrix} \begin{pmatrix} C_1 & C_2 & C_s & C_s' & C_{2v} \\ 0 & \frac{1}{2} & 0 & 0 & 0 \\ 1 & 0 & 0 & 0 & 0 \\ 0 & 0 & 1 & 1 & 2 \\ 1 & 0 & 0 & 0 & 0 \\ 0 & \frac{1}{2} & 0 & 0 & 0 \end{pmatrix} \quad (6.20)$$

The C_1 -column of Eq. 6.20 contains the value 1 for $p^3\bar{p}$ and the value 1 for $p\bar{p}^3$. These values corresponds to the value 2 in the C_1 -column of Eq. 6.19 because of $2 \times \frac{1}{2}(p^3\bar{p} + p\bar{p}^3)$. On the other hand, the C_2 -column of Eq. 6.20 contains the value $\frac{1}{2}$ for p^4 and the value $\frac{1}{2}$ for \bar{p}^4 . These values corresponds to the value 1 in the C_2 -column of Eq. 6.19 because of $1 \times \frac{1}{2}(p^4 + \bar{p}^4)$.



Exercise 6.2.

- Classify the 16 derivatives listed in Fig. 6.4 in terms of homomeric and enantiomeric relationships.
- Then, confirm the data of ICM_{3-12}' (Eq. 6.19) or of ICM_{3-12}'' (Eq. 6.20).

It should be emphasized that orbits among promolecules can be abstractly discussed in a parallel fashion to orbits within a promolecule. As found in Figs. 6.2 and 6.4, a set of homomers (or enantiomers) of each promolecule to be counted is regarded as an orbit, whose local symmetry represents the point-group symmetry of the promolecule. For example, the set of enantiomers **6-7** (f_6) and **6-8** (f_7) in Fig. 6.2 can be regarded as an orbit governed by $C_{2v}/(C_2)$, where the local symmetry C_2 is the point-group symmetry of **6-7** and **6-8**. The enantiomeric pair of **6-7** and **6-8** is counted once under the action of C_{2v} . Note that each row shown in the right-hand part of Fig. 6.2 (and Fig. 6.4) is identical with the corresponding row of the mark table of C_{2v} (Table 5.3 on page 119).

6.1.3 Subduced Cycle Indices for Itemized Enumeration

Subduced Cycle Indices with Chirality Fittingness (SCI-CFs)

Suppose that the substitution positions of a stereoskeleton are controlled by a permutation representation \mathbf{P}_G . Thereby, the substitution positions are divided into a set of orbits according to Eq. 5.22 (page 120), where each coset representation $\mathbf{G}/(\mathbf{G}_i)$ is contained with multiplicity α_i . Because each coset representation $\mathbf{G}/(\mathbf{G}_i)$ is subduced according to Eq. 5.37

(page 123), the permutation representation \mathbf{P}_G (Eq. 5.22) is subduced into \mathbf{G}_j according to the following equation:

$$\begin{aligned}\mathbf{P}_G \downarrow \mathbf{G}_j &= \sum_{i=1}^s \alpha_i \mathbf{G}(/G_i) \downarrow \mathbf{G}_j \\ &= \sum_{i=1}^s \alpha_i \sum_{k=1}^{v_j} \beta_k^{(ij)} \mathbf{G}_j(/H_k^{(j)})\end{aligned}\quad (6.21)$$

Thereby, subduced cycle indices with chirality fittingness (SCI-CFs) are defined as follows:

Definition 6.1 (Subduced Cycle Indices with Chirality Fittingness (SCI-CFs)). When a permutation representation \mathbf{P}_G for controlling the substitution positions of a stereoskeleton is represented by Eq. 6.21, the corresponding subduced cycle index with chirality fittingness (SCI-CF) is defined as follows:

$$\begin{aligned}\text{SCI-CF}_{\mathbf{P}_G}(\mathbf{G}_j; \mathcal{S}_{d_{jk}}) &= \prod_{i=1}^s (\text{USCI-CF}(\mathbf{G}(/G_i) \downarrow \mathbf{G}_j; \mathcal{S}_d))^{\alpha_i} \\ &= \prod_{i=1}^s \left(\prod_{k=1}^{v_j} \mathcal{S}_{d_{jk}}^{\beta_k^{(ij)}} \right)^{\alpha_i}\end{aligned}\quad (6.22)$$

where $\mathcal{S}_{d_{jk}}$ is equal to $a_{d_{jk}}$, $c_{d_{jk}}$, or $b_{d_{jk}}$ according to the sphericity of $\mathbf{G}_j(/H_k^{(j)})$ and the subscript is calculated to be

$$d_{jk} = \frac{|\mathbf{G}_j|}{|\mathbf{H}_k^{(j)}|}.\quad (6.23)$$

This definition is a simplified form of Def. 19.3 of Fujita's monograph [1].

Subduced Cycle Indices Without Chirality Fittingness (SCIs)

The sphericity indices $\mathcal{S}_{d_{jk}}$ in Def. 6.1 degenerate into a dummy variable $s_{d_{jk}}$, so as to give the following definition of SCIs:

Definition 6.2 (Subduced Cycle Indices without Chirality Fittingness (SCIs)). When a permutation representation \mathbf{P}_G for controlling the substitution positions of a stereoskeleton is represented by Eq. 6.21, the corresponding subduced cycle index (SCI) is defined as follows:

$$\begin{aligned}\text{SCI}_{\mathbf{P}_G}(\mathbf{G}_j; s_{d_{jk}}) &= \prod_{i=1}^s (\text{USCI-CF}(\mathbf{G}(/G_i) \downarrow \mathbf{G}_j; s_d))^{\alpha_i} \\ &= \prod_{i=1}^s \left(\prod_{k=1}^{v_j} s_{d_{jk}}^{\beta_k^{(ij)}} \right)^{\alpha_i}\end{aligned}\quad (6.24)$$

where the subscript is calculated to be

$$d_{jk} = \frac{|\mathbf{G}_j|}{|\mathbf{H}_k^{(j)}|}.\quad (6.25)$$

This definition is a simplified form of Def. 15.1 of Fujita's monograph [1].

6.2 The FPM Method of Fujita's USCI Approach

6.2.1 Fixed-Point Vectors (FPVs) and Multiplicity Vectors (MVs)

Consider a stereoskeleton belonging to point-group symmetry \mathbf{G} , where its substitution positions are controlled by a permutation representation $\mathbf{P}_{\mathbf{G}}$ (cf. Eq. 5.22 on page 120). Suppose that the substitution positions accommodate proligands selected from a ligand inventory:

$$\mathbf{L} = \{X_1, \dots, X_n; p_1, \bar{p}_1, \dots, p_{n'}, \bar{p}_{n'}\}, \quad (6.26)$$

where the symbols $X_1, \dots,$ and X_n represent achiral proligands in isolation, while the paired symbols $p_1/\bar{p}_1, \dots,$ and $p_{n'}/\bar{p}_{n'}$ represent pairs of enantiomeric proligands in isolation. A resulting promolecule has the following composition:

$$W_{\theta} = X_1^{x_1} \cdots X_n^{x_n} p_1^{p_1} \bar{p}_1^{\bar{p}_1} \cdots p_{n'}^{p_{n'}} \bar{p}_{n'}^{\bar{p}_{n'}}, \quad (6.27)$$

where the sum of the exponents is equal to the number of the substitution positions (or equivalently to the degree of the permutation representation $\mathbf{P}_{\mathbf{G}}$). The composition can be alternatively represented by the following partition:

$$[\theta] = [x_1, \dots, x_n; p_1, \bar{p}_1, \dots, p_{n'}, \bar{p}_{n'}]. \quad (6.28)$$

For the sake of simplicity, we presume $x_1 \geq \dots \geq x_n; p_1 \geq \bar{p}_1, \dots, p_{n'} \geq \bar{p}_{n'};$ and $p_1 \geq \dots \geq p_{n'}$ without losing generality.

Just as $\mathbf{F}_{3,12}$ (Eq. 6.6) and $\mathbf{F}'_{3,12}$ (Eq. 6.18) of the oxirane skeleton of \mathbf{C}_{2v} are discussed separately with respect of partitions $[\theta]$ (cf. Eq. 6.7), the present cases of the stereoskeleton of \mathbf{G} can be discussed by focusing our attention on respective partitions $[\theta]$. Hence, we are able to treat functions with $[\theta]$ separately:

$$\mathbf{F}^{[\theta]} = \{f_1^{[\theta]}, f_2^{[\theta]}, \dots, f_{|\mathbf{F}^{[\theta]}|}^{[\theta]}\}, \quad (6.29)$$

which contains homomeric or enantiomeric promolecules of each promolecule with the partition $[\theta]$ to be counted once. In a similar way to Eq. 6.8 for \mathbf{C}_{2v} , the set of functions (Eq. 6.29) generates a permutation $\lambda_g^{[\theta]}$ on the action of $g \in \mathbf{G}$:

$$\lambda_g^{[\theta]} = \left(\begin{array}{c} \mathbf{F}^{[\theta]} \\ \mathbf{F}^{[\theta]} \Big|_g \end{array} \right) \text{ for } g \in \mathbf{G}. \quad (6.30)$$

In a similar way to Eq. 6.9 for \mathbf{C}_{2v} , the permutation $\lambda_g^{[\theta]}$ constructs a permutation representation $\Lambda_{\mathbf{G}}^{[\theta]}$, when g runs over the point group \mathbf{G} :

$$\Lambda_{\mathbf{G}}^{[\theta]} = \left\{ \lambda_g^{[\theta]} \mid \forall g \in \mathbf{G} \right\}. \quad (6.31)$$

The permutation representation $\Lambda_{\mathbf{G}}^{[\theta]}$ is intransitive in general, so that it is divided into a set of coset representations. In a similar way to Eq. 6.10 for \mathbf{C}_{2v} , such a set of coset representations

can be represented as follows:

$$\Lambda_{\mathbf{G}}^{[\theta]} = \sum_{\mathbf{G}_i} A_{\theta_i} \mathbf{G}(/ \mathbf{G}_i), \quad (6.32)$$

where the symbol A_{θ_i} denotes the multiplicity of the $\mathbf{G}(/ \mathbf{G}_i)$ -orbit, which represents the number of inequivalent promolecules with the partition $[\theta]$ under the action of \mathbf{G} .

The division represented by Eq. 6.32 is parallel to the division of Eq. 5.22 (page 120), although the former is concerned with orbits of promolecules, while the latter concerned with orbits within a promolecule. Hence, the multiplicity vector $\text{MVP}_{\mathbf{P}_{\mathbf{G}}}$ (Eq. 5.26 on page 121) for characterizing substitution positions can be rewritten to give a vector called *an isomer-counting vector* (ICV) $\mathbf{A}^{[\theta]}$ for characterizing promolecules:

$$\mathbf{A}^{[\theta]} = (A_{\theta_1}, \dots, A_{\theta_j}, \dots, A_{\theta_s}). \quad (6.33)$$

In a similar way to $\text{FPV}_{\mathbf{P}_{\mathbf{G}}}$ (Eq. 5.23 on page 120) for the permutation representation $\mathbf{P}_{\mathbf{G}}$, an FPV for the permutation representation $\Lambda_{\mathbf{G}}^{[\theta]}$ is represented by the symbol $\mathbf{R}^{[\theta]}$ as follows:

$$\mathbf{R}^{[\theta]} = (\rho_{\theta_1}, \dots, \rho_{\theta_j}, \dots, \rho_{\theta_s}), \quad (6.34)$$

where the symbol ρ_{θ_j} is used to denote the mark (the number of fixed points) with \mathbf{G}_j and $[\theta]$. In a similar way to Eq. 5.27 (page 121) and Eq. 5.28 (page 121) for $\mathbf{P}_{\mathbf{G}}$, the following equations are obtained to characterize the present case of $\Lambda_{\mathbf{G}}^{[\theta]}$:

$$\mathbf{R}^{[\theta]} = \mathbf{A}^{[\theta]} \times M_{\mathbf{G}} \quad (6.35)$$

$$(\rho_{\theta_1}, \dots, \rho_{\theta_j}, \dots, \rho_{\theta_s}) = (A_{\theta_1}, \dots, A_{\theta_j}, \dots, A_{\theta_s}) M_{\mathbf{G}}. \quad (6.36)$$

Our target of counting inequivalent promolecules under the action of \mathbf{G} is now translated to obtain the isomer-counting vector $\mathbf{A}^{[\theta]}$, which is obtained by Eq. 6.35 or Eq. 6.36. For this purpose, it is necessary to evaluate the FPV $\mathbf{R}^{[\theta]}$ represented by Eq. 6.34.

6.2.2 Fixed-Point Matrices (FPMs) and Isomer-Counting Matrices (ICMs)

Recent advances of computer hardware and software (in particular, computer algebra systems such as Mathematica and Maple) enable us to treat generating functions more and more easily. As a result, the fixed-point-matrix (FPM) method and the the partial-cycle-index (PCI) method of USCI approach, both of which are based on generating functions, become more and more accessible than the early years of the development of the USCI approach. It follows that the discussions below will mainly depend on the methods based on generating functions.

Let us construct a matrix called *an isomer-counting matrix* (ICM) by collecting the isomer-counting vectors $\mathbf{A}^{[\theta]}$ (Eq. 6.33), where $[\theta]_1, [\theta]_2, \dots, [\theta]_{\theta}, \dots, [\theta]_{|\theta]}$ are considered as possible partitions. This means that the permutation representation $\Lambda_{\mathbf{G}}^{[\theta]}$ (Eq. 6.31: $[\theta]$ covers possible partitions) runs to cover the whole of the permutation representation $\mathbf{P}_{\mathbf{G}}$:

Definition 6.3 (Isomer-Counting Matrix (ICM) for Itemized Enumeration).

$$\text{ICM}_{\mathbf{P}_G} = \begin{pmatrix} A_{11} & \cdots & A_{1j} & \cdots & A_{1s} \\ A_{21} & \cdots & A_{2j} & \cdots & A_{2s} \\ \vdots & & \vdots & & \vdots \\ A_{\theta 1} & \cdots & A_{\theta j} & \cdots & A_{\theta s} \\ \vdots & & \vdots & & \vdots \\ A_{|\theta|1} & \cdots & A_{|\theta|j} & \cdots & A_{|\theta|s} \end{pmatrix}. \quad (6.37)$$

The fixed-point matrices (FPMs) introduced for C_{2v} (Eq. 6.5 and Eq. 6.17) can be easily generalized to define an FPM of G . The FPV (Eq. 6.34) for $A_G^{[\theta]}$ is used to specify each row, which contains $\rho_{\theta j}$ as an element for characterizing the number of fixed points with G_j and $[\theta]$:

Definition 6.4 (Fixed-Point Matrix (FPM) for Itemized Enumeration).

$$\text{FPM}_{\mathbf{P}_G} = \begin{pmatrix} \rho_{11} & \cdots & \rho_{1j} & \cdots & \rho_{1s} \\ \rho_{21} & \cdots & \rho_{2j} & \cdots & \rho_{2s} \\ \vdots & & \vdots & & \vdots \\ \rho_{\theta 1} & \cdots & \rho_{\theta j} & \cdots & \rho_{\theta s} \\ \vdots & & \vdots & & \vdots \\ \rho_{|\theta|1} & \cdots & \rho_{|\theta|j} & \cdots & \rho_{|\theta|s} \end{pmatrix}. \quad (6.38)$$

The j -th column of $\text{FPM}_{\mathbf{P}_G}$ (Eq. 6.38) is concerned with the subduction by the subgroup G_j , which corresponds to the SCI defined by Def. 6.1 (Eq. 6.22). The sphericity index $\$_{d_{jk}}$ specifies the mode of packing according to the sphericity at issue, as shown in Fig. 4.2 (page 90). Hence, the following theorem for evaluating the j -th column of $\text{FPM}_{\mathbf{P}_G}$ (Eq. 6.38) is obtained:

Theorem 6.1. Suppose that the substitution positions of a stereoskeleton of G accommodate promolecules selected from a ligand inventory \mathbf{L} (Eq. 6.26) to give promolecules with the composition W_θ . A generating function for evaluating the mark $\rho_{\theta j}$ (the number of fixed promolecules with G_j and $[\theta]$) is obtained to be:

$$\sum_{[\theta]} \rho_{\theta j} W_\theta = \text{SCI-CF}_{\mathbf{P}_G}(\mathbf{G}_j; \$_{d_{jk}}) \Big|_{\$_{d_{jk}} = \Sigma \mathbf{L}} \quad (6.39)$$

for $j = 1, 2, \dots, s$, where the symbol W_θ denotes the composition represented by Eq. 6.27 and the symbol $\$_{d_{jk}} = \Sigma \mathbf{L}$ denotes the introduction of a ligand-inventory function into the sphericity index $\$_{d_{jk}}$ as follows:

$$a_{d_{jk}} = \sum_{\ell=1}^n X_\ell^{d_{jk}} \quad (6.40)$$

$$c_{d_{jk}} = \sum_{\ell=1}^n X_\ell^{d_{jk}} + 2 \sum_{\ell=1}^{n'} P_\ell^{d_{jk}/2} \overline{P}_\ell^{d_{jk}/2} \quad (6.41)$$

$$b_{d_{jk}} = \sum_{\ell=1}^n X_\ell^{d_{jk}} + \sum_{\ell=1}^{n'} P_\ell^{d_{jk}} + \sum_{\ell=1}^{n'} \overline{P}_\ell^{d_{jk}} \quad (6.42)$$

This theorem has been reported in Fujita's monograph [1, Lemma 19.2].

In a similar way to Eq. 6.12 or Eq. 6.20 for C_{2v} , we are able to obtain an ICM for G by using Eq. 6.37 (Def. 6.3) and Eq. 6.38 (Def. 6.4) as follows:

Theorem 6.2 (The FPM Method of Fujita's USCI Approach). By starting from FPM_{P_G} (Eq. 6.38) evaluated by Theorem 6.1, the number A_{θ_j} of promolecules with the point-group symmetry G_j and the composition W_θ is obtained in the form of the isomer-counting matrix ICM_{P_G} (Eq. 6.37) as follows:

$$ICM_{P_G} = FPM_{P_G} \times M_G^{-1}, \quad (6.43)$$

where the inverse mark table M_G^{-1} is given in Eq. 5.31 (page 121).

This theorem has been reported in Fujita's monograph [1, Theorem 19.4]. To memorize Eq. 6.43 intuitively, its concrete matrix form is given as follows:

$$\begin{pmatrix} A_{11} & \cdots & A_{1j} & \cdots & A_{1s} \\ A_{21} & \cdots & A_{2j} & \cdots & A_{2s} \\ \vdots & & \vdots & & \vdots \\ A_{\theta 1} & \cdots & A_{\theta j} & \cdots & A_{\theta s} \\ \vdots & & \vdots & & \vdots \\ A_{|\theta|1} & \cdots & A_{|\theta|j} & \cdots & A_{|\theta|s} \end{pmatrix} = \begin{pmatrix} \rho_{11} & \cdots & \rho_{1j} & \cdots & \rho_{1s} \\ \rho_{21} & \cdots & \rho_{2j} & \cdots & \rho_{2s} \\ \vdots & & \vdots & & \vdots \\ \rho_{\theta 1} & \cdots & \rho_{\theta j} & \cdots & \rho_{\theta s} \\ \vdots & & \vdots & & \vdots \\ \rho_{|\theta|1} & \cdots & \rho_{|\theta|j} & \cdots & \rho_{|\theta|s} \end{pmatrix} \times M_G^{-1}. \quad (6.44)$$

On the other hand, subdued cycle indices without chirality fittingness (SCIs) represented by Eq. 6.24 (Def. 6.2) can be regarded as a degenerate case of SCI-CFs. It follows that Theorem 6.1 can be simplified by replacing ligand-inventory functions ($a_{d_{jk}}$, $c_{d_{jk}}$, and $b_{d_{jk}}$) into a ligand-inventory function of a single degenerate form:

$$s_{d_{jk}} = \sum_{\ell=1}^n X_\ell^{d_{jk}}. \quad (6.45)$$

This has been once reported as Lemmas 15.2 and 15.3 in Fujita's monograph [1]. Theorem 6.2 holds true for the degenerate case, as once reported in [1, Theorem 15.4]

6.2.3 Practices of the FPM Method

Procedure of Enumeration Based on the FPM Method

For the purpose of doing well to solve practical problems of enumeration, we could forget the proof of Theorems 6.1 and 6.2 for the time being. The following procedure for practical enumeration is helpful to 'digest' the theorems by chewing on a few examples.

Rule 6.1. Procedure of Enumeration Based on the FPM Method.

1. Determine the point group G of a stereoskeleton to be considered. See Section 3.3.
2. Divide the substitution positions of the skeleton into orbits. See Subsection 3.3.4.



3. Assign a coset representation to each of the orbits in the form of Eq. 5.22.
 - For a diagrammatical method, see the procedure for determining orbits (Rule 3.1 on page 80).
 - For an algebraic method based on the mark table of G , see Subsection 5.1.3.
4. Necessary data for characterizing the point group G (a mark table, an inverse mark table, and a USCI-CF table) should be collected.
5. Calculate an SCI-CF for each subgroup by using Eq. 6.22 (Def. 6.1).
6. Evaluate an FPM by using Eq. 6.39 (Theorem 6.1).
7. Calculate an ICM by using Eq. 6.43 (Theorem 6.2).

As a practical example of the above procedure, a Maple programming code for generating the FPM and the ICM has been reported [17], where cubane derivatives are enumerated on the basis of the point group O_h .

FPM Method Applied to Adamantan-2-one Derivatives

To exemplify the procedure for enumeration based on the FPM method (Rule 6.1), let us enumerate derivatives of adamantan-2-one, which has once been examined in Exercise 5.3 (Fig. 5.2 on page 126).

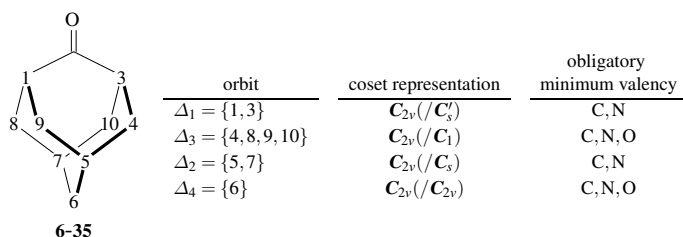


Fig. 6.5. Adamantan-2-one skeleton for polyaza, polyoxa-derivatives.

Suppose that the nine skeletal positions of the adamantan-2-one skeleton **6-35** (Fig. 6.5) are substituted by a set of carbons, nitrogens, and oxygens to produce polyoxa, polyaza-derivatives.

1. The skeleton **6-35** is determined to belong to the point group C_{2v} by examining its symmetry elements according to Section 3.3 (Step 1 of Rule 6.1). As for the symmetry elements of C_{2v} , remember Table 3.5 (page 70) and Eqs. 5.15–5.19 (page 118).
2. The nine skeletal positions (the 2-position is excluded) are divided into bridgehead $\{1, 3, 5, 7\}$ and bridge positions $\{4, 6, 8, 9, 10\}$. By glancing at the skeleton **6-35** according to Subsection 3.3.4, these positions are found to be further divided into four orbits, which are determined to belong to the following coset representations (Steps 2

and 3 of Rule 6.1). The four bridgehead positions are divided into two orbits, i.e., a two-membered homospheric orbit $\Delta_1 = \{1, 3\}$ belonging to $C_{2v}/(C'_s)$ (degree: $|C_{2v}|/|C'_s| = 4/2 = 2$) and another two-membered homospheric orbit $\Delta_2 = \{5, 7\}$ belonging to $C_{2v}/(C_s)$ (degree: $|C_{2v}|/|C_s| = 4/2 = 2$). The five bridge positions are divided into two orbits, i.e., a four-membered enantiospheric orbit $\Delta_3 = \{4, 8, 9, 10\}$ belonging to $C_{2v}/(C_1)$ (degree: $|C_{2v}|/|C_1| = 4/1 = 4$) and a one-membered homospheric orbit $\Delta_4 = \{6\}$ belonging to $C_{2v}/(C_{2v})$ (degree: $|C_{2v}|/|C_{2v}| = 4/4 = 1$). As for the coset representations of C_{2v} , see Table 5.1 (page 117).

3. The mark table of C_{2v} (Table 5.3 on page 119), the inverse mark table of C_{2v} (Table 5.5 on page 119), and the USCI-CF table of C_{2v} (Table 5.9 on page 128) have already discussed (Step 4 of Rule 6.1).
4. In order to place carbons, nitrogens, and oxygens on the skeletal positions of **6-35**, it is necessary to take account of obligatory minimum valencies (OMVs) [1, Chapter 14]. Each bridgehead position (in Δ_1 and Δ_2) has the OMV of 3, which permits the substitution of an atom with valency 3 or more. This means that the corresponding ligand inventory is selected as $L_1 = \{C, N\}$. Hence, a ligand-inventory function is selected as follows:

$$a_d = b_d = c_d = C^d + N^d. \quad (6.46)$$

On the other hand, each bridge position (in Δ_3 and Δ_4) has the OMV of 2, which permits the substitution of an atom with valency 2 or more. This means that the corresponding ligand inventory is selected as $L_2 = \{C, N, O\}$. Hence, a ligand-inventory function is selected as follows:

$$\acute{a}_d = \acute{b}_d = \acute{c}_d = C^d + N^d + O^d, \quad (6.47)$$

where an acute accent is attached to designate the difference in the mode of substitution.

5. Each SCI-CF (Step 5 of Rule 6.1) should take such OMVs into consideration. Hence, each SCI-CF is composed of two parts surrounded by pairs of parentheses, where one part is calculated from the USCI-CFs of Δ_1 and Δ_2 , while the other part is calculated from the USCI-CFs of Δ_3 and Δ_4 (for the USCI-CF table of C_{2v} , see Table 5.9):

$$\text{SCI-CF}(C_1)_{\mathbf{6-35}} = (b_1^4)(\acute{b}_1^5) = (C+N)^4(C+N+O)^5 \quad (6.48)$$

$$\text{SCI-CF}(C_2)_{\mathbf{6-35}} = (b_2^2)(\acute{b}_1\acute{b}_2^2) = (C^2+N^2)^2(C+N+O)(C^2+N^2+O^2)^2 \quad (6.49)$$

$$\begin{aligned} \text{SCI-CF}(C_s)_{\mathbf{6-35}} &= (a_1^2c_2)(\acute{a}_1\acute{c}_2^2) = (C+N)^2(C^2+N^2) \\ &\quad \times (C+N+O)(C^2+N^2+O^2)^2 \end{aligned} \quad (6.50)$$

$$\begin{aligned} \text{SCI-CF}(C'_s)_{\mathbf{6-35}} &= (a_1^2c_2)(\acute{a}_1\acute{c}_2^2) = (C+N)^2(C^2+N^2) \\ &\quad \times (C+N+O)(C^2+N^2+O^2)^2 \end{aligned} \quad (6.51)$$

$$\text{SCI-CF}(C_{2v})_{\mathbf{6-35}} = (a_2^2)(\acute{a}_1\acute{c}_4) = (C^2+N^2)^2(C+N+O)(C^4+N^4+O^4). \quad (6.52)$$

6. After Eqs. 6.46 and 6.47 are introduced into the respective SCI-CFs, the resulting functions represented by Eqs. 6.48–6.52 are expanded to give generating functions. The

coefficients of respective terms $C^kN^lO^m$ are collected to generate an FPM (see Eq. 6.39 of Theorem 6.1). As an example of such an FPM, several values are collected to give the following FPM (Step 6 of Rule 6.1):

$$\text{FPM}_{3-12} = \begin{matrix} & C_1 & C_2 & C_s & C'_s & C_{2v} \\ \begin{matrix} C^9 \\ C^8N \\ C^8O \\ C^7N^2 \\ C^7O^2 \\ C^7NO \\ C^6N^3 \\ C^6O^3 \\ C^6N^2O \\ C^6NO^2 \end{matrix} & \left(\begin{matrix} 1 & 1 & 1 & 1 & 1 \\ 9 & 1 & 3 & 3 & 1 \\ 5 & 1 & 1 & 1 & 1 \\ 36 & 4 & 6 & 6 & 2 \\ 10 & 2 & 2 & 2 & 0 \\ 40 & 0 & 2 & 2 & 0 \\ 84 & 4 & 10 & 10 & 2 \\ 10 & 2 & 2 & 2 & 0 \\ 140 & 4 & 4 & 4 & 2 \\ 70 & 2 & 6 & 6 & 0 \end{matrix} \right) \end{matrix} \quad (6.53)$$

7. According to Eq. 6.43 (Theorem 6.2), the FPV (Eq. 6.53) is multiplied by the inverse mark table of C_{2v} ($M_{C_{2v}}^{-1}$, Table 5.5) to give the corresponding ICM (Step 7 of Rule 6.1). The resulting ICM (Eq. 6.54) contains the coefficient of the term $C^kN^lO^m$ at the intersection between the $C^kN^lO^m$ -row and the sub-group-column to be obtained.

$$\text{ICM}_{3-12} = \text{FPM}_{3-12} \times M_{C_{2v}}^{-1} = \begin{matrix} & C_1 & C_2 & C_s & C'_s & C_{2v} \\ \begin{matrix} C^9 \\ C^8N \\ C^8O \\ C^7N^2 \\ C^7O^2 \\ C^7NO \\ C^6N^3 \\ C^6O^3 \\ C^6N^2O \\ C^6NO^2 \end{matrix} & \left(\begin{matrix} 0 & 0 & 0 & 0 & 1 \\ 1 & 0 & 1 & 1 & 1 \\ 1 & 0 & 0 & 0 & 1 \\ 6 & 1 & 2 & 2 & 2 \\ 1 & 1 & 1 & 1 & 0 \\ 9 & 0 & 1 & 1 & 0 \\ 16 & 1 & 4 & 4 & 2 \\ 1 & 1 & 1 & 1 & 0 \\ 33 & 1 & 1 & 1 & 2 \\ 14 & 1 & 3 & 3 & 0 \end{matrix} \right) \end{matrix} \quad (6.54)$$

Note that a pair of enantiomers or an achiral derivative is counted once under the point group C_{2v} .

The C^8N -row of the ICM (Eq. 6.54) indicates the presence of one pair of C_1 -derivatives (**6-36** and $\overline{\mathbf{6-36}}$), one C_s -derivative (**6-37**), one C'_s -derivative (**6-38**), and one C_{2v} -derivative (**6-39**). They are depicted in Fig. 6.6.

On the other hand, the C^7N^2 -row of the ICM (Eq. 6.54) indicates that there are six pairs of enantiomers of C_1 (**6-40**/ $\overline{\mathbf{6-40}}$, **6-41**/ $\overline{\mathbf{6-41}}$, **6-42**/ $\overline{\mathbf{6-42}}$, **6-43**/ $\overline{\mathbf{6-43}}$, **6-44**/ $\overline{\mathbf{6-44}}$, and **6-45**/ $\overline{\mathbf{6-45}}$), one pair of enantiomers of C_2 (**6-46**/ $\overline{\mathbf{6-46}}$), two C_s -derivatives (**6-47** and **6-48**), two C'_s -derivatives (**6-49** and **6-50**), and two C_{2v} -derivatives (**6-51** and **6-52**). They are also depicted in Fig. 6.6.

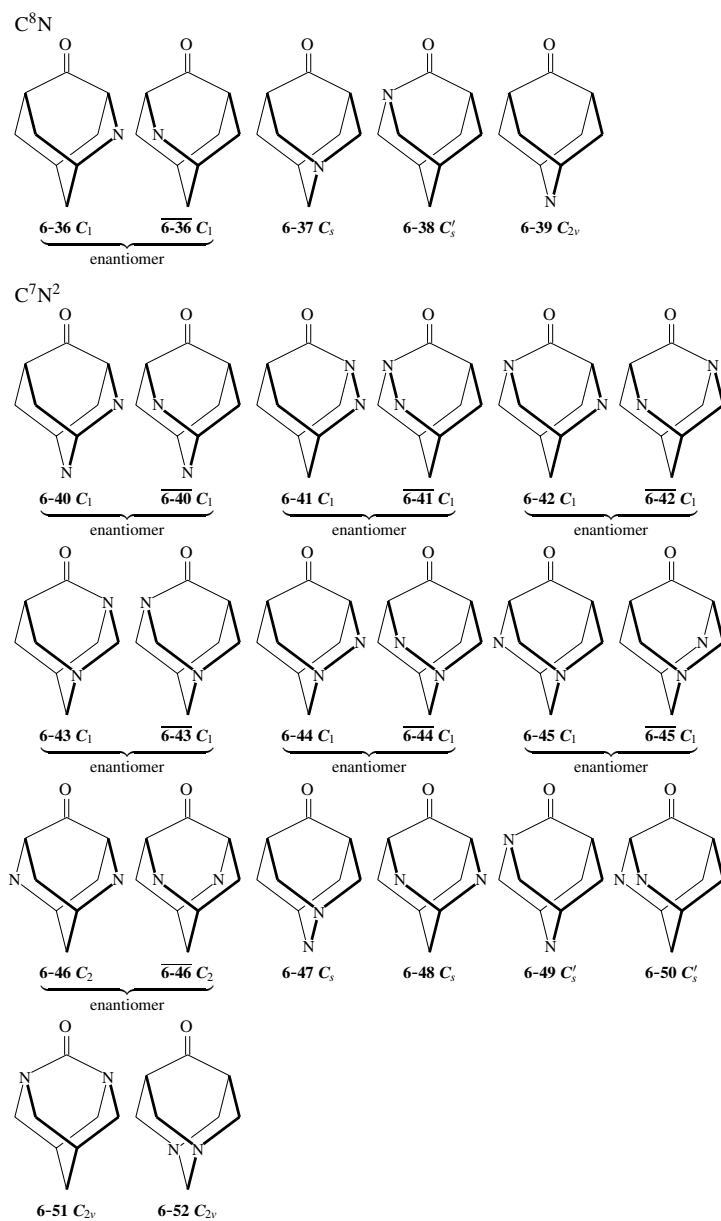


Fig. 6.6. Monoaza- or diazaadamantan-2-ones of various point-group symmetries. A vacant vertex indicates the substitution of a carbon atom omitted for the sake of simplicity.

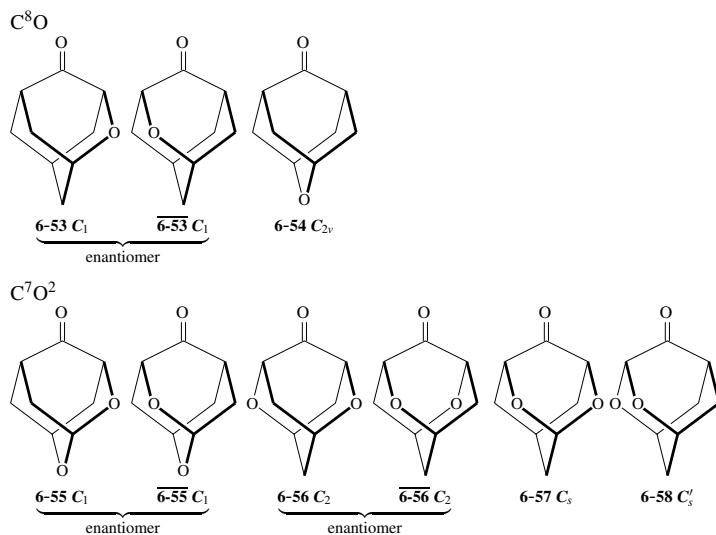


Fig. 6.7. Mono- or dioxadadamantan-2-ones of various point-group symmetries. A vacant vertex indicates the substitution of a carbon atom omitted for the sake of simplicity.

The C^8O -row of the ICM (Eq. 6.54) indicates the presence of one pair of C_1 -derivatives ($6-53$ and $\overline{6-53}$) and one C_{2v} -derivative ($6-54$). They are shown in the first row of Fig. 6.7.

The C^7O^2 -row of the ICM (Eq. 6.54) indicates the presence of one pair of C_1 -derivatives ($6-55$ and $\overline{6-55}$), one pair of C_2 -derivatives ($6-56$ and $\overline{6-56}$), one C_s -derivative ($6-57$), and one C'_s -derivative ($6-58$). They are shown in the second row of Fig. 6.7.

The comparison between Fig. 6.6 and Fig. 6.7 illustrates the effect of OMVs. Remember that each bridgehead position (OMV = 3) does not permit the substitution of a divalent oxygen atom.



Exercise 6.3. The ligand inventories for enumerating oxirane derivatives, L_1 (Eq. 6.2) and L_2 (Eq. 6.13), are combined to give a single ligand inventory:

$$L = \{X, Y, p, \overline{p}\}. \quad (6.55)$$

Then, enumerate oxirane derivatives with compositions $X^x Y^y p^p \overline{p}^{\overline{p}}$ according to the procedure shown above (Rule 6.1).



Exercise 6.4. Depict aza-oxa-derivatives by referring to the C^7NO -row of the ICM represented by Eq. 6.54. Compare these structures with those having C^7N^2 (Fig. 6.6) and those having C^7O^2 (Fig. 6.7).

Tables of Supporting Data

For Step 4 of the above procedure (Rule 6.1), the data of C_2 , C_s , C_3 , S_4 , C_{2v} , D_2 , C_{3v} , D_{2d} , T , T_d , C_{3h} , D_3 , and D_{3h} (mark tables, inverse mark tables, subduction tables, USCI tables, and USCI-CF tables) are collected in Fujita's monograph [1, Appendices A–E]. Additional data have been reported: C_5 (mark table, inverse mark table, USCI table) [18], C_{5v} (mark table, inverse mark table) [19], D_5 (mark table, inverse mark table, USCI table) [18], I (mark table, inverse mark table, USCI table) [18], D_{2h} (inverse mark table, USCI table) [20], D_{4h} (mark table) [21], T_h (mark table, inverse mark table, subduction table) [22], I_h (inverse mark table, USCI-CF table¹) [23] and (subduction table) [22], O_h (mark table, inverse mark table, enumeration of octahedron complexes) [24] and (mark table, inverse mark table, USCI-CF table, enumeration of cubane derivatives) [17], $S^{[5]}$ (inverse mark table, USCI table) [25], and D_{6h} (inverse mark table, USCI table) [26].

6.3 The PCI Method of Fujita's USCI Approach

6.3.1 Partial Cycle Indices With Chirality Fittingness (PCI-CFs)

After respective rows of the matrices of Eq. 6.44 are multiplied by the composition W_θ , they are summed up to give an alternative expression for enumeration:

$$\begin{aligned} & \left(\sum_{[\theta]} A_{\theta 1} W_\theta, \dots, \sum_{[\theta]} A_{\theta i} W_\theta, \dots, \sum_{[\theta]} A_{\theta s} W_\theta \right) \\ &= \left(\sum_{[\theta]} \rho_{\theta 1} W_\theta, \dots, \sum_{[\theta]} \rho_{\theta j} W_\theta, \dots, \sum_{[\theta]} \rho_{\theta s} W_\theta \right) M_G^{-1}, \end{aligned} \quad (6.56)$$

where the subscripts i and j are adjusted in terms of the vector multiplication of the right-hand side. Each element of these formal vectors is a generating function concerning the composition W_θ . Each element $\sum_{[\theta]} \rho_{\theta j} W_\theta$ ($j = 1, 2, \dots, s$) in the right-hand side of Eq. 6.56 has already been evaluated by Eq. 6.39 of Theorem 6.1. This evaluation for giving the generating functions can be delayed after the formal summation of SCI-CFs.

¹ The USCI-CF table of [23, Table 3] contains several misprints. The intersection between the $I_h(/C_2)$ -row and the C_3 -column: b_2^{30} should be read as b_3^{20} ; the intersection between the $I_h(/C_s)$ -row and the C_5 -column: b_5^{15} should be read as b_5^{12} ; the intersection between the $I_h(/C_s)$ -row and the D_{2h} -column: $a_4^3 c_6^8$ should be read as $a_4^3 c_6^6$; the intersection between the $I_h(/C_{3i})$ -row and the C_{3i} -column: $a_1^2 c_3^6$ should be read as $a_1^2 a_3^6$; the intersection between the $I_h(/C_{5v})$ -row and the C_{3v} -column: c_3^4 should be read as a_3^4 ; the intersection between the $I_h(/C_{5v})$ -row and the D_{5d} -column: $a_2 c_{10}$ should be read as $a_2 a_{10}$; the intersection between the $I_h(/D_{3d})$ -row and the C_{3i} -column: $a_1 c_3^3$ should be read as $a_1 a_3^3$; and the intersection between the $I_h(/D_{5d})$ -row and the C_{5i} -column: $a_1 c_5$ should be read as $a_1 a_5$.

To conduct the formal summation of SCI-CFs (Eq. 6.22 of Def. 6.1) beforehand, we first define a formal row vector of SCI-CFs:

$$\begin{aligned} & \text{V-SCI-CF}_{\mathbf{P}_G} \\ &= \left(\text{SCI-CF}_{\mathbf{P}_G}(\mathbf{G}_1; \$_{d_{1k}}), \dots, \text{SCI-CF}_{\mathbf{P}_G}(\mathbf{G}_j; \$_{d_{jk}}), \dots, \text{SCI-CF}_{\mathbf{P}_G}(\mathbf{G}_s; \$_{d_{sk}}) \right) \\ &= \left(\prod_{i=1}^s \left(\prod_{k=1}^{v_1} \$_{d_{1k}}^{\beta_k^{(i1)}} \right)^{\alpha_i}, \dots, \prod_{i=1}^s \left(\prod_{k=1}^{v_j} \$_{d_{jk}}^{\beta_k^{(ij)}} \right)^{\alpha_i}, \dots, \prod_{i=1}^s \left(\prod_{k=1}^{v_s} \$_{d_{sk}}^{\beta_k^{(is)}} \right)^{\alpha_i} \right) \end{aligned} \quad (6.57)$$

Thereby, *partial cycle indices with chirality fittingness* (PCI-CFs) for respective subgroups \mathbf{G}_i are defined in the form of multiplication of the formal vector by the inverse mark table M_G^{-1} as follows:

$$\begin{aligned} & \left(\text{PCI-CF}_{\mathbf{P}_G}(\mathbf{G}_1; \$_d), \dots, \text{PCI-CF}_{\mathbf{P}_G}(\mathbf{G}_i; \$_d), \dots, \text{PCI-CF}_{\mathbf{P}_G}(\mathbf{G}_s; \$_d) \right) \\ &= \text{V-SCI-CF}_{\mathbf{P}_G} \times M_G^{-1}, \end{aligned} \quad (6.58)$$

where the sphericity index $\$_{d_{jk}}$ is replaced by $\$_d$ because the products concerning j and k have been calculated in the right-hand side. The vector calculation is alternatively expressed by picking up each $\text{PCI-CF}_{\mathbf{P}_G}(\mathbf{G}_i; \$_d)$ to give the following definition:

Definition 6.5 (Partial Cycle Indices With Chirality Fittingness (PCI-CFs)). A *partial cycle index with chirality fittingness* (PCI-CF) is defined by the following equation:

$$\begin{aligned} \text{PCI-CF}_{\mathbf{P}_G}(\mathbf{G}_i; \$_d) &= \sum_{j=1}^s \bar{m}_{ji} \text{SCI-CF}_{\mathbf{P}_G}(\mathbf{G}_j; \$_{d_{jk}}) = \sum_{j=1}^s \bar{m}_{ji} \prod_{i=1}^s \left(\text{USCI-CF}(G(\mathbf{G}_i) \downarrow \mathbf{G}_j; \$_{d_{jk}}) \right)^{\alpha_i} \\ &= \sum_{j=1}^s \bar{m}_{ji} \left(\prod_{i=1}^s \left(\prod_{k=1}^{v_j} \$_{d_{jk}}^{\beta_k^{(ij)}} \right)^{\alpha_i} \right) \end{aligned} \quad (6.59)$$

for $i = 1, 2, \dots, s$, where $\text{SCI-CF}_{\mathbf{P}_G}$ comes from Eq. 6.22 of Def. 6.1.

This definition is a simplified form of Def. 19.6 of Fujita's monograph [1].

According to Eq. 6.56, the PCI-CFs defined in Def. 6.5 give generating functions for giving the numbers of promolecules $A_{\theta i}$ with \mathbf{G}_i and $[\theta]$:

Theorem 6.3. Suppose that the substitution positions of a stereoskeleton of \mathbf{G} accommodate proligands selected from a ligand inventory \mathbf{L} (Eq. 6.26) to give promolecules with the composition W_θ . A generating function for evaluating the number of promolecules $A_{\theta i}$ with \mathbf{G}_i and $[\theta]$ is obtained to be:

$$\sum_{[\theta]} A_{\theta i} W_\theta = \text{PCI-CF}_{\mathbf{P}_G}(\mathbf{G}_i; \$_d) \Big|_{\$_d = \Sigma_{\mathbf{L}}} \quad (6.60)$$

for $j = 1, 2, \dots, s$, where the symbol W_θ denotes the composition represented by Eq. 6.27 and the symbol $\$_d = \Sigma_{\mathbf{L}}$ denotes the introduction of a ligand-inventory function to the sphericity index $\$_d$ as follows:

$$a_d = \sum_{\ell=1}^n X_\ell^d \quad (6.61)$$

$$c_d = \sum_{\ell=1}^n X_\ell^d + 2 \sum_{\ell=1}^{n'} p_\ell^{d/2} p_\ell^{d/2} \quad (6.62)$$

$$b_d = \sum_{\ell=1}^n X_{\ell}^d + \sum_{\ell=1}^{n'} p_{\ell}^d + \sum_{\ell=1}^{n'} \bar{p}_{\ell}^d. \quad (6.63)$$

This theorem has been reported in Fujita's monograph [1, Lemma 19.7]. Note that the ligand-inventory functions Eqs. 6.61–6.63 obey the modes of accommodation due to chirality fittingness, which have been illustrated in Fig. 4.2 (page 90).

6.3.2 Partial Cycle Indices Without Chirality Fittingness (PCIs)

When the sphericity indices $\$d_{jk}$ in Def. 6.5 degenerate into a dummy variable $s_{d_{jk}}$, the following definition of PCIs is obtained:

Definition 6.6 (Partial Cycle Indices Without Chirality Fittingness (PCIs)). A *partial cycle index* (PCI) is defined by the following equation:

$$\begin{aligned} \text{PCI}_{\mathbf{P}_{\mathbf{G}}}(G_i; s_{d_{jk}}) &= \sum_{j=1}^s \bar{m}_{ji} \text{SCLP}_{\mathbf{G}}(G_j; s_{d_{jk}}) = \sum_{j=1}^s \bar{m}_{ji} \prod_{i=1}^s (\text{USCI}(G(/G_i) \downarrow G_j; s_d))^{\alpha_i} \\ &= \sum_{j=1}^s \bar{m}_{ji} \left(\prod_{i=1}^s \left(\prod_{k=1}^{v_j} s_{d_{jk}}^{\beta_k^{(ij)}} \right)^{\alpha_i} \right) \end{aligned} \quad (6.64)$$

for $i = 1, 2, \dots, s$, where $\text{SCLP}_{\mathbf{G}}$ comes from Eq. 6.24 of Def. 6.2.

This definition succeeds Defs. 16.3 and 16.4 of Fujita's monograph [1].

Partial cycle indices without chirality fittingness (PCIs) represented by Eq. 6.64 (Def. 6.6) can be regarded as a degenerate case of PCI-CFs. It follows that Theorem 6.3 can be simplified by replacing ligand-inventory functions ($a_{d_{jk}}$, $c_{d_{jk}}$, and $b_{d_{jk}}$) into a ligand-inventory function of a single degenerate form:

$$s_{d_{jk}} = \sum_{\ell=1}^n X_{\ell}^{d_{jk}}. \quad (6.65)$$

This has been once reported as Theorem 16.3 and Corollary 16.1 of Fujita's monograph [1].

6.3.3 Practices of the PCI Method

Procedure of Enumeration Based on the PCI Method

The procedure for enumeration based on the PCI method can be described in a parallel way to the procedure for enumeration based on the FPM method (Rule 6.1 on page 143). Even if we forget the proof of Theorem 6.3 for the time being, we are able to do well in practical enumeration.

Rule 6.2. Procedure of Enumeration Based on the PCI Method. Step 1–Step 5 of Rule 6.1 on page 143 are followed. Then,

6. Calculate PCI-CFs for the respective subgroups by applying Def. 6.5 to the SCI-CFs obtained by Step 5.
7. Calculate generating functions by introducing ligand-inventory functions according to Theorem 6.3.

As a practical example of the above procedure, a Maple programming code for the PCI method has been reported [27], where cubane derivatives are enumerated on the basis of the point group O_h .

PCI Method Applied to Oxirane Derivatives

To exemplify the above procedure of the PCI method (Rule 6.2), let us revisit oxirane derivatives based on the skeleton **3-12** (page 68). The previous discussion on oxirane derivatives (Figs. 6.2 and 6.4) is concerned with the case that USCI-CFs are regarded as SCI-CFs because of the presence of one orbit of substitution positions. As a result, the previous discussion can be recognized as an embodiment of Step 1 to Step 5 from the present point of view. Hence, the collection of USCI-CFs shown at the top of Fig. 6.2 (or Fig. 6.4) can generate a formal row vector of SCI-CFs (Eq. 6.57), which is represented by

$$\text{V-SCI-CF}_{\mathbf{P}_{C_{2v}}} = (b_1^4, b_2^2, c_2^2, c_2^2, c_4). \quad (6.66)$$

The formal row vector is multiplied by the inverse mark table $M_{C_{2v}}^{-1}$ (Table 5.5) according to Eq. 6.58, so as to give the following expression of PCI-CFs (Step 6 of Rule 6.2):

$$\begin{aligned} & (\text{PCI-CF}_{\mathbf{3-12}}(C_1), \text{PCI-CF}_{\mathbf{3-12}}(C_2), \text{PCI-CF}_{\mathbf{3-12}}(C_s), \text{PCI-CF}_{\mathbf{3-12}}(C'_s), \text{PCI-CF}_{\mathbf{3-12}}(C_{2v})) \\ &= (b_1^4, b_2^2, c_2^2, c_2^2, c_4) \begin{pmatrix} \frac{1}{4} & 0 & 0 & 0 & 0 \\ -\frac{1}{4} & \frac{1}{2} & 0 & 0 & 0 \\ -\frac{1}{4} & 0 & \frac{1}{2} & 0 & 0 \\ -\frac{1}{4} & 0 & 0 & \frac{1}{2} & 0 \\ \frac{1}{2} & -\frac{1}{2} & -\frac{1}{2} & -\frac{1}{2} & 1 \end{pmatrix}. \end{aligned} \quad (6.67)$$

By means of formal vector calculations, we obtain the following set of PCI-CFs:

$$\text{PCI-CF}_{\mathbf{3-12}}(C_1) = \frac{1}{4}b_1^4 - \frac{1}{4}b_2^2 - \frac{1}{2}c_2^2 + \frac{1}{2}c_4 \quad (6.68)$$

$$\text{PCI-CF}_{\mathbf{3-12}}(C_2) = \frac{1}{2}b_2^2 - \frac{1}{2}c_4 \quad (6.69)$$

$$\text{PCI-CF}_{\mathbf{3-12}}(C_s) = \frac{1}{2}c_2^2 - \frac{1}{2}c_4 \quad (6.70)$$

$$\text{PCI-CF}_{\mathbf{3-12}}(C'_s) = \frac{1}{2}c_2^2 - \frac{1}{2}c_4 \quad (6.71)$$

$$\text{PCI-CF}_{\mathbf{3-12}}(C_{2v}) = c_4. \quad (6.72)$$

Suppose that the four positions of the skeleton **3-12** accommodate a set of four proligands, which is selected from the following ligand inventory:

$$\mathbf{L} = \{A, B, X, Y; p, \bar{p}, q, \bar{q}, r, \bar{r}, s, \bar{s}\}, \quad (6.73)$$

where the symbols A, B, X, and Y denote achiral proligands, while a pair of p/\bar{p} , q/\bar{q} , r/\bar{r} , or s/\bar{s} denote a pair of chiral proligands with opposite chirality senses. By applying Eqs. 6.61–6.63, the following ligand-inventory functions are obtained:

$$a_d = A^d + B^d + X^d + Y^d \quad (6.74)$$

$$c_d = A^d + B^d + X^d + Y^d + 2 \left(p^{d/2} \bar{p}^{d/2} + q^{d/2} \bar{q}^{d/2} + r^{d/2} \bar{r}^{d/2} + s^{d/2} \bar{s}^{d/2} \right) \quad (6.75)$$

$$b_d = A^d + B^d + X^d + Y^d + p^d + \bar{p}^d + q^d + \bar{q}^d + r^d + \bar{r}^d + s^d + \bar{s}^d. \quad (6.76)$$

The ligand-inventory functions (Eqs. 6.74–6.76) are introduced into the PCI-CFs (Eqs. 6.68–6.72) according to Theorem 6.3. The resulting equations are expanded to give the following generating functions:

$$\begin{aligned} f_{\mathbf{3-12}}(\mathbf{C}_1) = & \{A^3B + \dots\} + \left\{ 2 \times \frac{1}{2} (A^3p + A^3\bar{p}) + \dots \right\} \\ & + \left\{ \frac{1}{2} (A^2p^2 + A^2\bar{p}^2) + \dots \right\} + \{3A^2BX + \dots\} \\ & + \left\{ 6 \times \frac{1}{2} (A^2Bp + A^2B\bar{p}) + \dots \right\} + \{A^2p\bar{p} + \dots\} + \\ & + \left\{ 6 \times \frac{1}{2} (A^2pq + A^2\bar{p}\bar{q}) + \dots \right\} + 6ABXY + \\ & + \left\{ 12 \times \frac{1}{2} (ABXp + ABX\bar{p}) + \dots \right\} + \left\{ 6 \times \frac{1}{2} (ABp^2 + AB\bar{p}^2) + \dots \right\} \\ & + \{6ABp\bar{p} + \dots\} + \left\{ 12 \times \frac{1}{2} (ABpq + AB\bar{p}\bar{q}) + \dots \right\} \\ & + \left\{ 2 \times \frac{1}{2} (Ap^3 + A\bar{p}^3) + \dots \right\} \\ & + \left\{ 6 \times \frac{1}{2} (Ap^2\bar{p} + A\bar{p}p^2) + \dots \right\} + \left\{ 6 \times \frac{1}{2} (Ap^2q + A\bar{p}^2\bar{q}) + \dots \right\} \\ & + \left\{ 12 \times \frac{1}{2} (Ap\bar{p}q + A\bar{p}p\bar{q}) + \dots \right\} + \left\{ 12 \times \frac{1}{2} (Apqr + A\bar{p}\bar{q}\bar{r}) + \dots \right\} \\ & + \left\{ 2 \times \frac{1}{2} (p^3\bar{p} + p\bar{p}^3) + \dots \right\} + \left\{ 2 \times \frac{1}{2} (p^3q + p\bar{p}^3\bar{q}) + \dots \right\} \\ & + \left\{ 6 \times \frac{1}{2} (p^2\bar{p}q + p\bar{p}^2\bar{q}) + \dots \right\} + \left\{ 2 \times \frac{1}{2} (p^2q^2 + p\bar{p}^2\bar{q}^2) + \dots \right\} \\ & + \left\{ 6 \times \frac{1}{2} (p^2q\bar{q} + p\bar{p}^2q\bar{q}) + \dots \right\} + \left\{ 6 \times \frac{1}{2} (p^2qr + p\bar{p}^2\bar{q}\bar{r}) + \dots \right\} \\ & + \{2p\bar{p}q\bar{q} + \dots\} \\ & + \left\{ 12 \times \frac{1}{2} (p\bar{p}qr + p\bar{p}\bar{q}\bar{r}) + \dots \right\} + \left\{ 12 \times \frac{1}{2} (pqrs + \bar{p}\bar{q}\bar{r}\bar{s}) + \dots \right\} \quad (6.77) \end{aligned}$$

$$f_{\mathbf{3-12}}(\mathbf{C}_2) = \{A^2B^2 + \dots\} + \left\{ \frac{1}{2} (A^2p^2 + A^2\bar{p}^2) + \dots \right\}$$

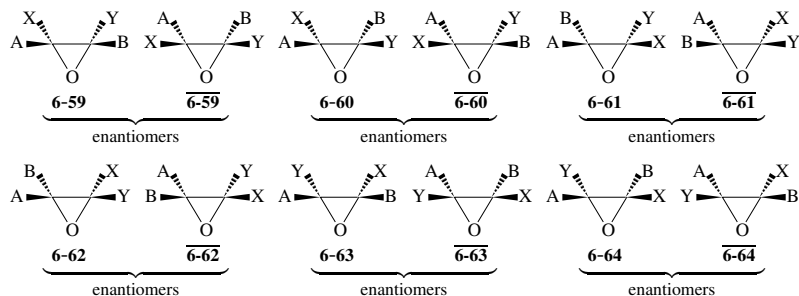


Fig. 6.8. Six pairs of enantiomeric oxiranes with the composition ABXY. All of these oxirane derivatives belong to the point group C_1 .

$$+ \left\{ \frac{1}{2}(p^4 + \bar{p}^4) + \dots \right\} + \left\{ 2 \times \frac{1}{2}(p^2q^2 + \bar{p}^2\bar{q}^2) + \dots \right\} \quad (6.78)$$

$$\begin{aligned} f_{3-12}(C_s) &= f_{3-12}(C'_s) \\ &= \{A^2B^2 + \dots\} + \{2A^2p\bar{p} + \dots\} + \{p^2\bar{p}^2 + \dots\} + \{4p\bar{p}q\bar{q} + \dots\} \end{aligned} \quad (6.79)$$

$$f_{3-12}(C_{2v}) = \{A^4 + \dots\} + \{2p^2\bar{p}^2 + \dots\}, \quad (6.80)$$

where each pair of braces contains a representative of terms of the same type, e.g., the representative A^4 correspond to A^4 , B^4 , X^4 , and Y^4 . These generating functions contain the data of the ICMs which have been obtained by the FPM method (Eq. 6.12 and Eq. 6.20; the symbols X and Y correspond to A and B). It should be noted the present enumeration counts a pair of enantiomers or an achiral derivative once. For example, the term $6ABXY$ of $f_{3-12}(C_1)$ (Eq. 6.77) represents the presence of six pairs of enantiomers, which are depicted in Fig. 6.8.



Exercise 6.5.

- Depict 12 enantiomeric pairs corresponding to the term $12 \times \frac{1}{2}(pqrs + \overline{pqrs})$ of Eq. 6.77.
- Compare these 12 pairs with the six pairs collected in Fig. 6.8. Note that the difference between them will be discussed in terms of type-I and type-III stereoisograms.

PCI Method Applied to Tetrahedral Derivatives

As a more complicated example of the procedure of the PCI method (Rule 6.2 on page 151), let us examine a tetrahedral skeleton **3-5** (Fig. 3.7 on page 68). As found in the discussion described there, the tetrahedral skeleton **3-5** belongs to the point group T_d , which is characterized by eleven subgroups listed in the SSG represented by Eq. 3.19 on page 62 (Steps 1 and 2 of Rule 6.2). The four positions of **3-5** construct a four-membered orbit governed by the coset representation T_d/C_{3v} (Table 3.1 on page 61), which is regarded as a permutation representation P_{T_d} (Step 3 of Rule 6.2). The USCI-CF table and the inverse mark table ($M_{T_d}^{-1}$) have been listed in Fujita's monograph [1, Table E.10 and Table B.10] (Step 4

of Rule 6.2). Thereby, we are able to obtain a formal vector of SCI-CFs as follows (Step 5 of Rule 6.2):

$$\text{V-SCI-CF}_{\mathbf{P}_{T_d}} = (b_1^4, b_2^2, a_1^2 c_2, b_1 b_3, c_4, b_4, a_2^2, a_1 a_3, a_4, b_4, a_4). \quad (6.81)$$

The formal row vector is multiplied by the inverse mark table $M_{T_d}^{-1}$ according to Eq. 6.58, so as to give the following expression of PCI-CFs (Step 6 of Rule 6.2):

$$\begin{aligned} & (\text{PCI-CF}_{3.5}(\mathbf{C}_1), \text{PCI-CF}_{3.5}(\mathbf{C}_2), \dots, \text{PCI-CF}_{3.5}(\mathbf{T}_d)) \\ & = \text{V-SCI-CF}_{\mathbf{P}_{T_d}} \times M_{T_d}^{-1}. \end{aligned} \quad (6.82)$$

By means of formal vector calculations, we obtain the following set of PCI-CFs:

$$\begin{aligned} \text{PCI-CF}_{3.5}(\mathbf{C}_1) &= \frac{1}{24}b_1^4 - \frac{1}{8}b_2^2 - \frac{1}{4}a_1^2 c_2 - \frac{1}{6}b_1 b_3 + \frac{1}{4}b_4 \\ &+ \frac{1}{4}a_2^2 + \frac{1}{2}a_1 a_3 - \frac{1}{2}a_4 \end{aligned} \quad (6.83)$$

$$\text{PCI-CF}_{3.5}(\mathbf{C}_2) = \frac{1}{4}b_2^2 - \frac{1}{4}c_4 - \frac{1}{4}b_4 - \frac{1}{4}a_2^2 + \frac{1}{2}a_4 \quad (6.84)$$

$$\text{PCI-CF}_{3.5}(\mathbf{C}_s) = \frac{1}{2}a_1^2 c_2 - \frac{1}{2}a_2^2 - a_1 a_3 + a_4; \quad (6.85)$$

$$\text{PCI-CF}_{3.5}(\mathbf{C}_3) = \frac{1}{2}b_1 b_3 - \frac{1}{2}a_1 a_3 - \frac{1}{2}b_4 + \frac{1}{2}a_4 \quad (6.86)$$

$$\text{PCI-CF}_{3.5}(\mathbf{S}_4) = \frac{1}{2}c_4 - \frac{1}{2}a_4 \quad (6.87)$$

$$\text{PCI-CF}_{3.5}(\mathbf{D}_2) = 0 \quad (6.88)$$

$$\text{PCI-CF}_{3.5}(\mathbf{C}_{2v}) = \frac{1}{2}a_2^2 - \frac{1}{2}a_4 \quad (6.89)$$

$$\text{PCI-CF}_{3.5}(\mathbf{C}_{3v}) = a_1 a_3 - a_4 \quad (6.90)$$

$$\text{PCI-CF}_{3.5}(\mathbf{D}_{2d}) = 0 \quad (6.91)$$

$$\text{PCI-CF}_{3.5}(\mathbf{T}) = \frac{1}{2}b_4 - \frac{1}{2}a_4 \quad (6.92)$$

$$\text{PCI-CF}_{3.5}(\mathbf{T}_d) = a_4. \quad (6.93)$$

These PCI-CFs have been once noted in the articles by the author [15,28].

The four positions of the tetrahedral skeleton **3-5** are substituted by proligands selected from the proligand inventory **L** (Eq. 6.73). Theorem 6.3 permits us to adopt the same set of ligand-inventory functions listed in Eqs. 6.74–6.76, which are introduced into the PCI-CFs (Eqs. 6.83–6.93). After expansion (Step 7 of Rule 6.2), we obtain the following generating functions [15,28]:

$$\begin{aligned} f_{3.5}(\mathbf{C}_1) &= \left\{ 2 \times \frac{1}{2} (\text{ABXp} + \text{ABX}\bar{\text{p}}) + \dots \right\} + \left\{ 2 \times \frac{1}{2} (\text{ABpq} + \text{AB}\bar{\text{p}}\bar{\text{q}}) + \dots \right\} \\ &+ \left\{ 2 \times \frac{1}{2} (\text{Ap}\bar{\text{p}}\bar{\text{q}} + \text{Ap}\bar{\text{p}}\text{q}) + \dots \right\} + \left\{ 2 \times \frac{1}{2} (\text{Apqr} + \text{Ap}\bar{\text{q}}\bar{\text{r}}) + \dots \right\} \end{aligned}$$

$$\begin{aligned}
& + \left\{ 2 \times \frac{1}{2} (\overset{[\theta]_{30}}{pqrs} + \overline{pqrs}) + \dots \right\} + \left\{ 2 \times \frac{1}{2} (\overset{[\theta]_{29}}{p\overline{p}qr} + \overline{p\overline{p}qr}) + \dots \right\} \\
& + \left\{ \frac{1}{2} (A^2 B p + A^2 B \overline{p}) + \dots \right\} + \left\{ \frac{1}{2} (A B p^2 + A B \overline{p}^2) + \dots \right\} \\
& + \left\{ \frac{1}{2} (A^2 p q + A^2 \overline{p} \overline{q}) + \dots \right\} + \left\{ \frac{1}{2} (A p^2 \overline{p} + A p \overline{p}^2) + \dots \right\} \\
& + \left\{ \frac{1}{2} (A p^2 q + A \overline{p}^2 \overline{q}) + \dots \right\} + \left\{ \frac{1}{2} (p^2 \overline{p} q + p \overline{p}^2 \overline{q}) + \dots \right\} \\
& + \left\{ \frac{1}{2} (p^2 q \overline{q} + \overline{p}^2 q \overline{q}) + \dots \right\} + \left\{ \frac{1}{2} (p^2 q r + \overline{p}^2 q \overline{r}) + \dots \right\} \\
& + \left\{ p \overline{p} q \overline{q} + p \overline{p} r \overline{r} + \dots \right\} + \left\{ A B X Y \right\} \tag{6.94}
\end{aligned}$$

$$f_{3-5}(C_2) = \left\{ \frac{1}{2} (A^2 p^2 + A^2 \overline{p}^2) + \dots \right\} + \left\{ \frac{1}{2} (p^2 q^2 + \overline{p}^2 \overline{q}^2) + \dots \right\} \tag{6.95}$$

$$\begin{aligned}
f_{3-5}(C_s) & = \left\{ 2 A B p \overline{p} + 2 A B q \overline{q} + \dots \right\} + \left\{ A^2 p \overline{p} + \dots \right\} \\
& + \left\{ A^2 B X + A^2 B Y + \dots \right\} \tag{6.96}
\end{aligned}$$

$$\begin{aligned}
f_{3-5}(C_3) & = \left\{ \frac{1}{2} (A^3 p + A^3 \overline{p}) + \dots \right\} + \left\{ \frac{1}{2} (A p^3 + A \overline{p}^3) + \dots \right\} \\
& + \left\{ \frac{1}{2} (p^3 q + \overline{p}^3 \overline{q}) + \dots \right\} + \left\{ \frac{1}{2} (p^3 \overline{p} + p \overline{p}^3) + \dots \right\} \tag{6.97}
\end{aligned}$$

$$f_{3-5}(S_4) = \{ p^2 \overline{p}^2 + q^2 \overline{q}^2 + r^2 \overline{r}^2 + s^2 \overline{s}^2 \} \tag{6.98}$$

$$f_{3-5}(C_{2v}) = \{ A^2 B^2 + A^2 X^2 + A^2 Y^2 + \dots \} \tag{6.99}$$

$$f_{3-5}(C_{3v}) = \{ A^3 B + A^3 X + A^3 Y + \dots \} \tag{6.100}$$

$$f_{3-5}(T) = \left\{ \frac{1}{2} (p^4 + \overline{p}^4) + \dots \right\} \tag{6.101}$$

$$f_{3-5}(T_d) = \{ A^4 + B^4 + X^4 + Y^4 \} \tag{6.102}$$

In these generating functions, the coefficient of the term $A^a B^b X^c Y^d p^p \overline{p}^q q^r \overline{q}^s r^t \overline{r}^u s^v \overline{s}^w$ indicates the number of inequivalent (self-)enantiomeric pairs to be counted. Note that such a term as $\frac{1}{2} (A B X p + A B X \overline{p})$ indicates the presence of one enantiomeric pair of promolecules under the point-group symmetry. The enumeration results represented by the generating functions (Eqs. 6.94–6.102) are consistent with the data listed in Tables 4 and 5 of [28] (and Table 21.1 of [1]) as tabular forms.

The results shown in Eqs. 6.94–6.102 are illustrated in Fig. 6.9, where a representative selected from each pair of braces is depicted. For example, **6-94** (T_d) with the composition A^4 is a representative for $\{A^4 + B^4 + X^4 + Y^4\}$ appearing in Eq. 6.102.

	<i>RS</i> -astereogenic	<i>RS</i> -stereogenic
chiral		<p style="text-align: center;">Type I</p> <hr/> <p style="text-align: center;">6-65 (C_1) 6-66 (C_1)</p>
	<p style="text-align: center;">Type II</p> <hr/>	<p style="text-align: center;">Type III</p> <hr/>
achiral	<p style="text-align: center;">Type IV</p> <hr/>	<p style="text-align: center;">Type V</p> <hr/>

Fig. 6.9. Tetrahedral promolecules enumerated under the point group T_d . The symbols A, B, X, and Y represent atoms or achiral ligands. The symbols p, q, r, and s represents chiral ligands, while each symbol with an overbar represents the corresponding chiral ligand with the opposite chirality. An arbitrary promolecule is depicted as a representative of each pair of enantiomers. Types I–V will be discussed later in terms of Fujita's stereoisogram approach.

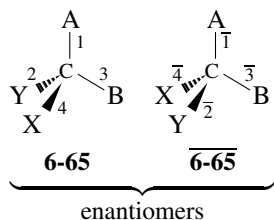


Fig. 6.10. One pair of enantiomeric tetrahedral derivatives with the composition ABXY. These derivatives belong to the point group C_1 . This case is categorized as type I in Fujita's stereoisogram approach, as discussed later.

Because the above PCI method counts once a pair of enantiomers or an achiral promolecule, an arbitrary promolecule is depicted as a representative of each pair of enantiomers in Fig. 6.9. For example, the term ABXY of $f_{3,5}(C_1)$ (Eq. 6.94) indicates the presence of one pair of enantiomers with the composition ABXY, i.e., **6-65** and $\overline{\mathbf{6-65}}$, which are depicted in Fig. 6.10. Among them, however, only **6-65** is adopted as a representative in Fig. 6.9. This case is frequently referred to as a so-called 'asymmetric carbon center' or 'chirality center'. Compare Fig. 6.10 with Fig. 6.8 from the viewpoint of stereoisomerism with respect to stereoskeletons of ligancy 4 (the oxirane skeleton **3-12** vs. the tetrahedral skeleton **3-5**). The case of Fig. 6.10 is categorized as type I in Fujita's stereoisogram approach, as discussed later.

On the other hand, the term $2 \times \frac{1}{2}(ABXp + ABX\bar{p})$ in Eq. 6.94 indicates the presence of two pairs of enantiomers. A representative of each pair (e.g., one with the composition ABXp) is depicted as **6-82** or **6-83** in Fig. 6.9. The pomolecule **6-82** (or **6-83**) is accompanied with the corresponding enantiomer $\overline{\mathbf{6-82}}$ (or $\overline{\mathbf{6-83}}$), as shown in Fig. 6.11. These two pairs are diastereomeric to each other in terms of Def. 2.7 (page 40).

Similar situations hold true for promolecules **6-84** and **6-85** (for the term $2 \times \frac{1}{2}(ABpq + AB\bar{p}\bar{q})$), **6-86** and **6-87** (for the term $2 \times \frac{1}{2}(Ap\bar{p}q + Ap\bar{p}\bar{q})$), **6-88** and **6-89** (for the term $2 \times \frac{1}{2}(Apqr + A\bar{p}\bar{q}\bar{r})$), **6-90** and **6-91** (for the term $2 \times \frac{1}{2}(p\bar{p}qr + p\bar{p}\bar{q}\bar{r})$), as well as **6-92** and **6-93** (for term $2 \times \frac{1}{2}(pqrs + \bar{p}\bar{q}\bar{r}\bar{s})$). These terms are gathered as the top six terms in the generating function of C_1 (Eq. 6.94). These cases exemplified by Fig. 6.11 are categorized as type III in Fujita's stereoisogram approach, as discussed later.

Note that the pomolecule **6-82** can be converted into **6-83** by exchanging the proligands X and p, where the combined process of detachment and reattachment or the inversion process via such a planar arrangement as shown in Fig. 1.2 (page 2) is plausible. However, the pair of **6-82**/ $\overline{\mathbf{6-82}}$ is independent of the other pair of **6-83**/ $\overline{\mathbf{6-83}}$, so long as the present enumeration is done under the point group T_d . They are counted separately as being inequivalent under the point group T_d , although they are counted together in terms of the term $2 \times \frac{1}{2}(ABXp + ABX\bar{p})$ in Eq. 6.94.

The term $2ABp\bar{p}$ in the generating function $f_{3,5}(C_s)$ (Eq. 6.96) indicates the presence of two achiral promolecules with the composition ABp \bar{p} and the point group C_s . These achiral promolecules are depicted as **6-100** and **6-101** in Fig. 6.9, which are diastereomeric

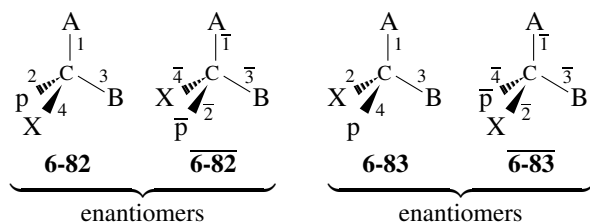


Fig. 6.11. Two pairs of enantiomeric tetrahedral derivatives with the composition $ABXp$ or $ABX\bar{p}$. These derivatives belong to the point group C_1 . These two pairs are diastereomeric to each other in terms of Def. 2.7. This case is categorized as type III in Fujita's stereoisogram approach, as discussed later.

to each other in terms of Def. 2.7 (page 40). This case is categorized as type V in Fujita's stereoisogram approach, as discussed later. Note again that the pomolecule **6-100** can be converted into **6-101** by exchanging the proligands p and \bar{p} , where the combined process of detachment and reattachment or the inversion process via such a planar arrangement as shown in Fig. 1.2 (page 2) is plausible. However, **6-100** is inequivalent to **6-101**, so long as the present enumeration is done under the point group T_d .

PCI Method Applied to Allene Derivatives

The procedure of the PCI method (Rule 6.2 on page 151) is also applied to an allene skeleton **3-9** (Fig. 3.7 on page 68), which belongs to the point group D_{2d} . The non-redundant set of subgroups (SSG) for the point group D_{2d} is found to be:

$$SSG_{D_{2d}} = \{C_1, C_2, C_2', C_s, S_4, C_{2v}, D_2, D_{2d}\}, \quad (6.103)$$

which contains subgroups up to conjugacy (Steps 1 and 2 of Rule 6.2).

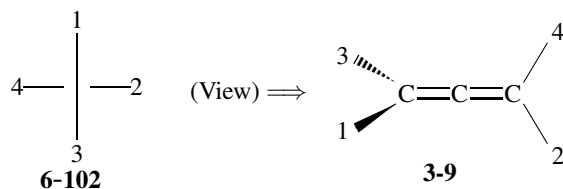


Fig. 6.12. Convention for drawing allene derivatives

A top view **6-102** shown in Fig. 6.12 is more convenient than the projection formula **3-9** in order to grasp symmetrical features of the allene skeleton. The four positions of **6-102** (= **3-9**) construct a four-membered orbit governed by the coset representation D_{2d}/C_s (Table 3.2 on page 68), which is regarded as a permutation representation $P_{D_{2d}}$ (Step 3 of

Rule 6.2). The USCI-CF table and the inverse mark table ($M_{D_{2d}}^{-1}$) have been listed in Fujita's monograph [1, Table E.8 and Table B.8] (Step 4 of Rule 6.2). Thereby, we are able to obtain a formal vector of SCI-CFs as follows (Step 5 of Rule 6.2):

$$\text{V-SCI-CF}_{P_{D_{2d}}} = (b_1^4, b_2^2, b_2^2, a_1^2 c_2, c_4, a_2^2, b_4, a_4). \quad (6.104)$$

This formal row vector is multiplied by the inverse mark table $M_{D_{2d}}^{-1}$ according to Eq. 6.58, so as to give the following expression of PCI-CFs (Step 6 of Rule 6.2):

$$\begin{aligned} & (\text{PCI-CF}_{3,9}(\mathbf{C}_1), \text{PCI-CF}_{3,9}(\mathbf{C}_2), \dots, \text{PCI-CF}_{3,9}(\mathbf{D}_{2d})) \\ &= \text{V-SCI-CF}_{P_{D_{2d}}} \times M_{D_{2d}}^{-1}. \end{aligned} \quad (6.105)$$

By means of formal vector calculations, we obtain the following set of PCI-CFs (Step 6 of Rule 6.2):

$$\text{PCI-CF}_{3,9}(\mathbf{C}_1) = \frac{1}{8}b_1^4 - \frac{1}{8}b_2^2 - \frac{1}{4}b_2^2 - \frac{1}{4}a_1^2 c_2 + \frac{1}{4}a_2^2 + \frac{1}{4}b_4 \quad (6.106)$$

$$\text{PCI-CF}_{3,9}(\mathbf{C}_2) = \frac{1}{4}b_2^2 - \frac{1}{4}c_4 - \frac{1}{4}a_2^2 - \frac{1}{4}b_4 + \frac{1}{2}a_4 \quad (6.107)$$

$$\text{PCI-CF}_{3,9}(\mathbf{C}'_2) = \frac{1}{2}b_2^2 - \frac{1}{2}b_4 \quad (6.108)$$

$$\text{PCI-CF}_{3,9}(\mathbf{C}_s) = \frac{1}{2}a_1^2 c_2 - \frac{1}{2}a_2^2 \quad (6.109)$$

$$\text{PCI-CF}_{3,9}(\mathbf{S}_4) = \frac{1}{2}c_4 - \frac{1}{2}a_4 \quad (6.110)$$

$$\text{PCI-CF}_{3,9}(\mathbf{C}_{2v}) = \frac{1}{2}a_2^2 - \frac{1}{2}a_4 \quad (6.111)$$

$$\text{PCI-CF}_{3,9}(\mathbf{D}_2) = \frac{1}{2}b_4 - \frac{1}{2}a_4 \quad (6.112)$$

$$\text{PCI-CF}_{3,9}(\mathbf{D}_{2d}) = a_4 \quad (6.113)$$

These PCI-CFs have been once noted in the article by Fujita [29].

The four positions of the allene skeleton **6-102** (=3-9) are substituted by proligands selected from the proligand inventory **L** (Eq. 6.73). According to Theorem 6.3, the same set of ligand-inventory functions as listed in Eqs. 6.74–6.76 are introduced into the PCI-CFs (Eqs. 6.106–6.113). After expansion (Step 7 of Rule 6.2), we obtain the following generating functions:

$$\begin{aligned} f_{3,9}(\mathbf{C}_1) &= \left\{ \frac{1}{2}(A^3 p + A^3 \bar{p}) + \dots \right\} + \{A^2 B X + \dots\} + \{A^2 p \bar{p} + \dots\} \\ &+ \left\{ 6 \times \frac{1}{2}(A B X p + A B X \bar{p}) + \dots \right\} + \{2 A B p \bar{p} + \dots\} \\ &+ \left\{ 6 \times \frac{1}{2}(A B p q + A B \bar{p} q) + \dots \right\} \\ &+ \left\{ 6 \times \frac{1}{2}(A p \bar{p} q + A p \bar{p} \bar{q}) + \dots \right\} + \left\{ 6 \times \frac{1}{2}(A p q r + A \bar{p} q r) + \dots \right\} \end{aligned}$$

$$\begin{aligned}
& + \{6 \times \frac{1}{2}(\text{pqrs} + \overline{\text{pqr}\overline{\text{s}}}) + \dots\} + \{6 \times \frac{1}{2}(\text{p}\overline{\text{p}}\text{qr} + \text{p}\overline{\text{p}}\overline{\text{q}\overline{\text{r}}}) + \dots\} \\
& + \{3 \times \frac{1}{2}(\text{A}^2\text{Bp} + \text{A}^2\text{B}\overline{\text{p}}) + \dots\} + \{3 \times \frac{1}{2}(\text{ABp}^2 + \text{AB}\overline{\text{p}}^2) + \dots\} \\
& + \{3 \times \frac{1}{2}(\text{A}^2\text{pq} + \text{A}^2\overline{\text{p}\overline{\text{q}}}) + \dots\} + \{3 \times \frac{1}{2}(\text{Ap}^2\overline{\text{p}} + \text{Ap}\overline{\text{p}}^2) + \dots\} \\
& + \{\frac{1}{2}(\text{Ap}^3 + \text{A}\overline{\text{p}}^3) + \dots\} + \{3 \times \frac{1}{2}(\text{Ap}^2\text{q} + \text{A}\overline{\text{p}}^2\overline{\text{q}}) + \dots\} \\
& + \{\frac{1}{2}(\text{p}^3\overline{\text{p}} + \text{p}\overline{\text{p}}^3) + \dots\} + \{\frac{1}{2}(\text{p}^3\text{q} + \overline{\text{p}}^3\overline{\text{q}}) + \dots\} \\
& + \{3 \times \frac{1}{2}(\text{p}^2\overline{\text{p}}\text{q} + \text{p}\overline{\text{p}}^2\overline{\text{q}}) + \dots\} + \{3 \times \frac{1}{2}(\text{p}^2\text{q}\overline{\text{q}} + \overline{\text{p}}^2\text{q}\overline{\text{q}}) + \dots\} \\
& + \{3 \times \frac{1}{2}(\text{p}^2\text{qr} + \overline{\text{p}}^2\overline{\text{q}\overline{\text{r}}}) + \dots\} + \{3\text{p}\overline{\text{p}}\text{q}\overline{\text{q}} + \text{p}\overline{\text{p}}\overline{\text{r}} + \dots\} \\
& + \{3\text{ABXY}\} \tag{6.114}
\end{aligned}$$

$$f_{3.9}(\mathbf{C}_2) = \{\frac{1}{2}(\text{A}^2\text{p}^2 + \text{A}^2\overline{\text{p}}^2) + \dots\} + \{\frac{1}{2}(\text{p}^2\text{q}^2 + \overline{\text{p}}^2\overline{\text{q}}^2) + \dots\} \tag{6.115}$$

$$\begin{aligned}
f_{3.9}(\mathbf{C}'_2) &= \{\text{A}^2\text{B}^2 + \dots\} + \{2 \times \frac{1}{2}(\text{A}^2\text{p}^2 + \text{A}^2\overline{\text{p}}^2) + \dots\} \\
&+ \{\text{p}^2\overline{\text{p}}^2 + \dots\} + \{2 \times \frac{1}{2}(\text{p}^2\text{q}^2 + \overline{\text{p}}^2\overline{\text{q}}^2) + \dots\} \tag{6.116}
\end{aligned}$$

$$\begin{aligned}
f_{3.9}(\mathbf{C}_s) &= \{2\text{ABp}\overline{\text{p}} + 2\text{ABq}\overline{\text{q}} + \dots\} + \{\text{A}^2\text{p}\overline{\text{p}} + \dots\} \\
&+ \{\text{A}^2\text{BX} + \text{A}^2\text{BY} + \dots\} + \{\text{A}^3\text{B} + \text{A}^3\text{X} + \dots\} \tag{6.117}
\end{aligned}$$

$$f_{3.9}(\mathbf{S}_4) = \{\text{p}^2\overline{\text{p}}^2 + \text{q}^2\overline{\text{q}}^2 + \text{r}^2\overline{\text{r}}^2 + \text{s}^2\overline{\text{s}}^2\} \tag{6.118}$$

$$f_{3.9}(\mathbf{C}_{2v}) = \{\text{A}^2\text{B}^2 + \text{A}^2\text{X}^2 + \text{A}^2\text{Y}^2 + \dots\} \tag{6.119}$$

$$f_{3.9}(\mathbf{D}_2) = \{\frac{1}{2}(\text{p}^4 + \overline{\text{p}}^4) + \dots\} \tag{6.120}$$

$$f_{3.9}(\mathbf{D}_{2d}) = \{\text{A}^4 + \text{B}^4 + \text{X}^4 + \text{Y}^4\} \tag{6.121}$$

In these generating functions, the coefficient of the term $\text{A}^a\text{B}^b\text{X}^x\text{Y}^y\text{p}^p\overline{\text{p}}^{\overline{p}}\text{q}^q\overline{\text{q}}^{\overline{q}}\text{r}^r\overline{\text{r}}^{\overline{r}}\text{s}^s\overline{\text{s}}^{\overline{s}}$ indicates the number of inequivalent (self-)enantiomeric pairs to be counted.

The term 3ABXY of $f_{3.9}(\mathbf{C}_1)$ (Eq. 6.114) indicates the presence of three pairs of enantiomers with the composition ABXY . They are depicted in Fig. 6.13(a).² This case is frequently referred to as a so-called ‘chirality axis’. Compare this figure (three pairs of enan-

² The numbering of positions in Fig. 6.13 obeys the action of $\mathbf{S}^{[4]} \times \{1, \sigma\}$. This means that the reference promolecule **6-103** (or **6-106**) is permuted under the action of $\mathbf{S}^{[4]} \times \{1, \sigma\}$. This permutation is adopted for the purpose of examining the relationship between point-group symmetry and permutation-group symmetry as discussed later. If the action is restricted to that of \mathbf{D}_{2d} , on the other hand, the respective pairs **{6-103, $\overline{6-103}$ }**, **{6-104, $\overline{6-104}$ }**, **{6-105, $\overline{6-105}$ }** should be permuted separately under the action of \mathbf{D}_{2d} . In this permutation, the mode of position numbering for **{6-103, $\overline{6-103}$ }** should be used. For example, **6-104** is generated by placing $\{f(1) = \text{A}, f(2) = \text{B}, f(3) = \text{X}, f(4) = \text{Y}\}$ on the positions numbered for **{6-103, $\overline{6-103}$ }**. This is the way adopted in the USCI approach for combinatorial enumeration under the action of \mathbf{D}_{2d} . See the modes of numbering in Figs. 6.2 and 6.4 for the cases of an oxirane skeleton.

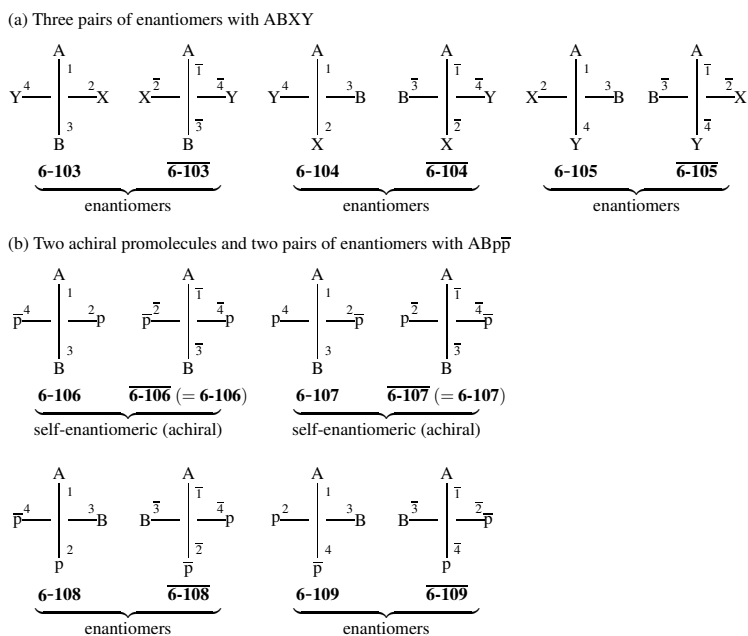


Fig. 6.13. Allene derivatives enumerated under the point group D_{2d} . (a) Three pairs of enantiomeric allene derivatives with the composition ABXY. These derivatives belong to the point group C_1 . (b) Two achiral promolecules of C_s , as well as two pairs of enantiomers of C_1 , where they have the composition ABp \bar{p} .

tiomers for allene derivatives) with Fig. 6.8 (six pairs of enantiomers for oxirane derivatives) and with Fig. 6.10 (one pair of enantiomers for tetrahedral derivatives) from the viewpoint of stereoisomerism with respect to stereoskeletons of liganacy 4.

The term $2ABp\bar{p}$ in the generating function $f_{3,9}(C_s)$ (Eq. 6.117) indicates the presence of two achiral promolecules of C_s , i.e., **6-106** and **6-107**, which are depicted in Fig. 6.13(b). Although the appearance of **6-106** and **6-107** seemingly suffers from the duplicated usage of the skeleton of the same numbering, it stems from two modes of packing of an enantiospheric orbit $\{2, 4\}$ of **6-102** (Fig. 6.12) by an enantiomeric pair of chiral proligands $p\bar{p}$ (cf. Fig. 4.2 on page 90). Thus, the function $\{f(1) = A, f(2) = p, f(3) = B, f(4) = \bar{p}\}$ is applied to give **6-106**, while the complementary function $\{f(1) = A, f(2) = \bar{p}, f(3) = B, f(4) = p\}$ is applied to give **6-107**.

The term $2ABp\bar{p}$ of $f_{3,9}(C_1)$ (Eq. 6.114) indicates the presence of two pairs of enantiomers with the composition ABp \bar{p} , i.e., a pair of **6-108** and **6-108** and another pair of **6-109** and **6-109**. These are depicted in the bottom row of Fig. 6.13(b).

It is worthwhile to compare Fig. 6.13(a) with Fig. 6.13(b) from a viewpoint of permutations (detachments and reattachments) of proligands. First, the enantiomers **6-103** and **6-103** are interchanged to each other by the permutation $(1)(3)(2\ 4)$ of the proligands X and Y.

In contrast, the permutation (1)(3)(2 4) of the proligands p and \bar{p} converts the achiral promolecule **6-106** into the other achiral promolecule **6-107**. Second, the enantiomers **6-104** and **6-104** are interchanged to each other by the permutation (1)(2)(3 4) of the proligands B and Y. In contrast, the permutation (1)(2)(3 4) of the proligands p and \bar{p} converts the chiral promolecule **6-108** into the other chiral promolecule **6-109**, where the former is not enantiomeric to the latter. Third, the enantiomers **6-105** and **6-105** are interchanged to each other by the permutation (1)(2 3)(4) of the proligands B and X. In contrast, the permutation (1)(2 3)(4) of the proligands p and \bar{p} converts the chiral promolecule **6-109** into the other chiral promolecule **6-108**, where the former is not enantiomeric to the latter.

These examples clearly demonstrate that the effects of permutations are different from the effects of reflections. Modern stereochemistry has adopted Fig. 6.13(a) as a standard and regarded Fig. 6.13(b) as an exception. It follows that modern stereochemistry has failed to integrate Fig. 6.13(a) and and Fig. 6.13(b).

PCI Method Applied to Adamantan-2-one Derivatives

As another example of the procedure of the PCI method (Rule 6.2 on page 151), let us re-examine the enumeration of polyaza, polyoxa-derivatives of the adamantan-2-one skeleton **6-35** (Fig. 6.5 on page 144). A formal row vector is generated by using the SCI-CFs (Eqs. 6.48–6.52) according to Eq. 6.57 and multiplied by the inverse mark table of C_{2v} ($M_{C_{2v}}^{-1}$, Table 5.5) according to Eq. 6.58. Thereby, the following PCI-CFs are obtained to meet Eq. 6.59 (Def. 6.5).

$$\begin{aligned} \text{PCI-CF}(C_1)_{6-35} &= \frac{1}{4}(b_1^4)(\hat{b}_1^5) - \frac{1}{4}(b_2^2)(\hat{b}_1\hat{b}_2^2) - \frac{1}{4}(a_1^2c_2)(\hat{a}_1\hat{c}_2^2) \\ &\quad - \frac{1}{4}(a_1^2c_2)(\hat{a}_1\hat{c}_2^2) + \frac{1}{2}(a_2^2)(\hat{a}_1\hat{c}_4) \end{aligned} \quad (6.122)$$

$$\text{PCI-CF}(C_2)_{6-35} = \frac{1}{2}(b_2^2)(\hat{b}_1\hat{b}_2^2) - \frac{1}{2}(a_2^2)(\hat{a}_1\hat{c}_4) \quad (6.123)$$

$$\text{PCI-CF}(C_s)_{6-35} = \frac{1}{2}(a_1^2c_2)(\hat{a}_1\hat{c}_2^2) - \frac{1}{2}(a_2^2)(\hat{a}_1\hat{c}_4) \quad (6.124)$$

$$\text{PCI-CF}(C'_s)_{6-35} = \frac{1}{2}(a_1^2c_2)(\hat{a}_1\hat{c}_2^2) - \frac{1}{2}(a_2^2)(\hat{a}_1\hat{c}_4) \quad (6.125)$$

$$\text{PCI-CF}(C_{2v})_{6-35} = \frac{1}{2}(a_2^2)(\hat{a}_1\hat{c}_4), \quad (6.126)$$

where each SCI-CF in the right-hand sides takes account of OMVs by using sphericity indices without (OMV = 3) and with acute accents (OMV = 2). The ligand-inventory functions represented by Eqs. 6.46 (OMV = 3) and 6.47 (OMV = 2) are introduced into Eqs. 6.122–6.126. Then, the resulting equations are expanded to give the following generating functions:

$$\begin{aligned} f_{6-35}(C_1) &= C^8N + C^8O + 6C^7N^2 + 9C^7NO + C^7O^2 \\ &\quad + 16C^6N^3 + 33C^6N^2O + 14C^6NO^2 + C^6O^3 \\ &\quad + 25C^5N^4 + 67C^5N^3O + 46C^5N^2O^2 + 13C^5NO^3 + C^5O^4 \end{aligned}$$

$$\begin{aligned}
& + 25C^4N^5 + 84C^4N^4O + 79C^4N^3O^2 + 33C^4N^2O^3 + 5C^4NO^4 \\
& + 16C^3N^6 + 67C^3N^5O + 79C^3N^4O^2 + 46C^3N^3O^3 + 11C^3N^2O^4 \\
& + 6C^2N^7 + 33C^2N^6O + 46C^2N^5O^2 + 33C^2N^4O^3 + 11C^2N^3O^4 \\
& + C^2N^2O^5 + CN^8 + 9CN^7O + 14CN^6O^2 + 13CN^5O^3 \\
& + 5CN^4O^4 + N^8O + N^7O^2 + N^6O^3 + N^5O^4
\end{aligned} \tag{6.127}$$

$$\begin{aligned}
f_{6-35}(C_2) &= C^7N^2 + C^7O^2 + C^6N^3 + C^6N^2O + C^6NO^2 + C^6O^3 \\
& + 2C^5N^4 + 3C^5N^2O^2 + 2C^4N^5 + 2C^4N^4O + 3C^4N^3O^2 + 3C^4N^2O^3 \\
& + C^3N^6 + 3C^3N^4O^2 + C^2N^7 + C^2N^6O + 3C^2N^5O^2 + 3C^2N^4O^3 \\
& + CN^6O^2 + N^7O^2 + N^6O^3
\end{aligned} \tag{6.128}$$

$$\begin{aligned}
f_{6-35}(C_s) &= C^8N + 2C^7N^2 + C^7NO + C^7O^2 + 4C^6N^3 + C^6N^2O + 3C^6NO^2 + C^6O^3 \\
& + 5C^5N^4 + 3C^5N^3O + 5C^5N^2O^2 + 2C^5NO^3 \\
& + 5C^4N^5 + 2C^4N^4O + 7C^4N^3O^2 + 3C^4N^2O^3 + C^4NO^4 \\
& + 4C^3N^6 + 3C^3N^5O + 7C^3N^4O^2 + 4C^3N^3O^3 + C^3N^2O^4 + C^3NO^5 \\
& + 2C^2N^7 + C^2N^6O + 5C^2N^5O^2 + 3C^2N^4O^3 + C^2N^3O^4 \\
& + CN^8 + CN^7O + 3CN^6O^2 + 2CN^5O^3 + CN^4O^4 + CN^3O^5 \\
& + N^7O^2 + N^6O^3
\end{aligned} \tag{6.129}$$

$$\begin{aligned}
f_{6-35}(C'_s) &= C^8N + 2C^7N^2 + C^7NO + C^7O^2 + 4C^6N^3 + C^6N^2O + 3C^6NO^2 + C^6O^3 \\
& + \dots \quad (\text{omitted, equal to } f_{C_s})
\end{aligned} \tag{6.130}$$

$$\begin{aligned}
f_{6-35}(C_{2v}) &= C^9 + C^8N + C^8O + 2C^7N^2 + 2C^6N^3 + 2C^6N^2O + 2C^5N^4 + C^5O^4 \\
& + 2C^4N^5 + 2C^4N^4O + C^4NO^4 + C^4O^5 + 2C^3N^6 + 2C^3N^2O^4 \\
& + 2C^2N^7 + 2C^2N^6O + 2C^2N^3O^4 + 2C^2N^2O^5 + CN^8 + CN^4O^4 \\
& + N^9 + N^8O + N^5O^4 + N^4O^5,
\end{aligned} \tag{6.131}$$

where the coefficient of the term $C^kN^lO^m$ represents the number of derivatives having the composition $C^kN^lO^m$ and the respective point-group symmetry. Several values in the right-hand sides have already appeared in the corresponding rows of the ICM represented by Eq. 6.54. See also Figs. 6.6 and 6.7 for examples of derivatives counted by Eqs. 6.127–6.131.

6.4 Other Methods of Fujita's USCI Approach

6.4.1 The Elementary-Superposition Method

The elementary-superposition method of Fujita's USCI approach [30,31] provides us with a procedure of evaluating each element ρ_{θ_j} of the FPV $\mathbf{R}^{|\theta|}$ (Eq. 6.34) without relying on generating functions. For the details of the elementary-superposition method (without chirality fittingness), see Chapter 18 of [1]. For recent results of cubane derivatives, see Ref. [32].

6.4.2 The Partial-Superposition Method

The partial-superposition method of Fujita's USCI approach [31] provides us with a procedure of evaluating each SCI-CF contained in a PCI-CF (Eq. 6.59 in Def. 6.5) without relying on generating functions. For the details of the partial-superposition method (without chirality fittingness), see Chapter 18 of [1]. Recent results of cubane derivatives by means of the elementary-superposition method [32] can be easily applied to the partial-superposition method.

6.5 Applications of Fujita's USCI Approach

6.5.1 Enumeration of Flexible Molecules

Bond Rotation

Fujita's USCI approach has been applied to the enumeration of isomers derived from a non-rigid parent molecule, the non-rigidity of which stems from bond rotations [12]. After the application of the proligand-promolecule model (cf. Section 3.1), the proligand is restored to a mobile ligand belonging to a given point group H . The point group G of the skeleton and the point group H of the mobile ligand are applied in a nested fashion. For example, a $T_d(/C_{3v})$ -orbit of a tetrahedral skeleton and a $C_{3v}(/C_s)$ -orbit of a methyl ligand is linked to give $T_d(/C_{3v})[C_{3v}(/C_s)]$. Such restored ligands can have different 3D structures (e.g., a methyl ligand and a phenyl ligand) in the enumeration of non-rigid molecules [33]. The methyl ligand of dimethyl ether, tetramethylallene, or 2,2-dimethylpropane is replaced by a substituted methyl ligand to aim at systematic enumeration of non-rigid isomers with given ligand symmetries [34]. Combinatorial enumeration of non-rigid isomers with given ligand symmetries has been accomplished on the basis of promolecules with a symmetry of $D_{\infty h}$ [35].

Ring Flipping

1,3,5-Trioxane derivatives have been enumerated by using a pseudo-point group \widehat{D}_{3h} , which is an extension of a point group C_{3v} for treating the ring flipping of a six-membered chair-form ring [36]. The pseudo-point group \widehat{D}_{3h} , which is isomorphic to the point group D_{3h} , is applicable to the enumeration of ammonia derivatives with N-inversion [36].

Cyclohexane derivatives have been enumerated on the basis of a pseudo-point group \widehat{D}_{6h} , which is an extension of a point group D_{3d} for treating the ring flipping of a six-membered chair-form ring [37]. Systematic design of highly-symmetric cyclohexane derivatives has been investigated by taking account of the pseudo-point group \widehat{D}_{6h} [38], where characterization of their energetic and symmetric equivalency has been discussed.

In a similar way, tetrahydropyran and 1,3-dioxane derivatives [39], 1,4-dioxane and 1,4-oxathiane derivatives [40], as well as spiro[5.5]undecane derivatives [41] have been enumerated under considering ring flipping.

The ring flipping and N-inversion of piperidine derivatives have been treated in an integrated fashion by presuming a quadruplet of conformers as a model [42], where an extended pseudo-point group has been defined.

6.5.2 Enumeration of Molecules Interesting Stereochemically

Ethylene Derivatives

Orbits of faces of ethylene derivatives have been discussed in terms of sphericities [43], where a two-membered enantiospheric orbit is concluded to exhibit prochirality. The attributive term *enantiospheric* assigned to such a two-membered orbit is compared with the relational term *enantiotopic*. The four positions of an ethylene skeleton **3-10** (page 68) have been discussed by means of a four-membered $D_{2h}(/C_s')$ -orbit [44]. The enumeration of derivatives under the point group D_{2h} is compared with the enumeration under the permutation group ($\subset S^{[4]}$).



Exercise 6.6.

- By referring to [44], apply the PCI method of the USCI approach to the four positions of the ethylene skeleton **3-10**, where they are substituted by proligands selected from the proligand inventory **L** (Eq. 6.73).
 - Discuss promolecules with the composition ABXY and with the composition ABp̄p̄. See Subsection 9.4.3.
-

Benzene Derivatives

Symmetry-itemized enumeration of benzene derivatives with achiral and chiral substituents and relevant derivatives derived from D_{6h} -skeletons (cf. **3-14** on page 73) has been discussed in terms of Fujita's USCI approach [26]. The restricted-subduced-cycle-index (RSCI) method has been proposed for the purpose of counting matchings of graphs [45]. The RSCI method has been applied to discussions on Z-counting polynomials and the Hosoya index as well as on matching polynomials [45]. Combinatorial enumeration based on $[2_6](1,2,3,4,5,6)$ cyclophane of D_{6h} -symmetry has been investigated by means of the PCI method [46], where the resulting derivatives have been discussed in terms of the SCR notation for systematic classification of molecular symmetries.

Prismane Derivatives

Enumeration of cage-shaped molecules derived from a prismane skeleton **3-15** (page 73) has been discussed in terms of an edge strategy [47]. The restricted-fixed-point-matrix (RFPM) method, which was developed as an extension of the FPM method of the USCI approach, has been applied to the enumeration of prismane derivatives under the restricted condition, where the occupation of a common vertex or the occupation of adjacent edges is avoided [48]. The restricted-partial-cycle-index (RPCI) method, which was developed by starting from the PCI method of Fujita's USCI approach, has been applied to the enumeration of prismane derivatives under the restricted condition [49].

Cubane Derivatives

The FPM method of Fujita's USCI approach has been applied to enumeration based on a cubane skeleton **3-17** (page 74), where a Maple programming code for generating the FPM and the ICM has been reported [17]. The PCI method of Fujita's USCI approach has been applied to enumeration based on a cubane skeleton **3-17** [27], where a Maple programming code for the PCI method has been reported. Symmetry-itemized enumeration of cubane derivatives as 3D entities has also been conducted by the elementary-superposition method of Fujita's USCI approach [32].

Adamantane Derivatives

Enumeration of cage-shaped molecules based on a tetrahedrane skeleton has been discussed [50], where adamantane **3-21** (page 76) is generated by expansion of the 6 edges of the tetrahedral skeleton. Skeletal isomers of adamantane with given symmetries has been systematically enumerated by Fujita's USCI approach [20]. An adamantane skeleton **3-21** has two types of substitution positions, i.e., four bridgeheads and 12 bridges. Enumeration based on **3-21** has been conducted systematically [51]. Subductive and inductive derivation for designing molecules of high symmetry has been formulated on the basis of an adamantane skeleton [52], where a regular representation $T_d(/C_1)$ plays a crucial role. Adamantane-2,6-dione as a D_{2d} -skeleton **3-22** (page 76) has been used to enumerate derivatives by the FPM method and the elementary-superposition method of Fujita's USCI approach [30]. The elementary-superposition method has been applied to SCI-CFs, PCI-CFs, and CI-CFs, where adamantane-2,6-dione **3-22** is used as a D_{2d} -skeleton [31].

Dodecahedrane Derivatives

The USCIs and USCI-CFs of the point group I_h group has been calculated and applied to systematic enumeration of dodecahedrane derivatives [23]. The restricted-subduced-cycle-index (RSCI) method for generating Z-counting polynomials and Z-indices as well as matching polynomials has been developed and applied to dodecahedrane [45]. The restricted-fixed-point-matrix (RFPM) method based on restricted subduced cycle indices

has been applied to enumeration of sterically hindered derivatives of dodecahedrane [53]. The restricted-partial-cycle-index (RPCI) method based on restricted subduced cycle indices (RSCIs) has been applied to enumeration of sterically hindered derivatives of dodecahedrane [54].

Icosahedral Derivatives

Enumeration of Fujita's USCI approach has been discussed by applying the point group I (or the alternating group $A^{[5]}$) to the 20 faces of icosahedron [18]. The restricted-partial-cycle-index (RPCI) method for treating steric hindrance due to monodentate and bidentate ligands has been applied to enumeration based on an icosahedral skeleton of I_h , where differences between unrestricted and restricted enumerations are discussed [55].

Fullerene Derivatives

Symmetry-itemized enumeration of fullerene derivatives by the FPM method has been investigated [56], where the desymmetrization lattice for the $I_h(/C_s)$ -orbit is given and the numbers of derivatives of $C_{60}X_nH_{60-n}$ ($n = 1-60$) are given in a tabular form. To evaluate bond-differentiating chiral reactions to give adducts of fullerene, the sphericity concept for an orbit of bonds is taken into consideration [22]. Thereby, symmetry-itemized enumeration of C_{60} -adducts have been conducted. The restricted-subduced-cycle-index (RSCI) method for symmetry-itemized enumeration of Kekulé structures has been applied to fullerene C_{60} [57]. The restricted-subduced-cycle-index (RSCI) method has been applied to restricted enumeration of Kekulé structures (perfect matchings of graphs) [58].

6.5.3 Enumeration of Inorganic Complexes

Octahedral Complexes

An octahedral skeleton **3-13** (page 73) belongs to the point group O_h . The six substitution positions of **3-13** construct a six-membered orbit governed by the coset representation $O_h(/C_{4v})$ ($|O_h|/|C_{4v}| = 48/8 = 6$). Symmetry-itemized enumeration based on **3-13** has been conducted by using the FPM method [24], where the resulting promolecules are categorized in terms of the subgroups of O_h . On the other hand, the 12 edges of **3-13** construct a twelve-membered orbit governed by the coset representation $O_h(/C_{2v}'')$ ($|O_h|/|C_{2v}''| = 48/4 = 12$). Symmetry-itemized enumeration based on **3-13** has been conducted by using the PCI method [59]. The resulting edge configurations are examined with respect to edge numbers and point-group symmetries, so as to show the modes of substitution of bidentate and terdentate ligands,

Ferrocene Derivatives

Ferrocene has a sandwich structure, where two cyclopentadienyl ligands are regarded as being rotatable from a viewpoint of stereoisomerism. To take account of such a sandwich structure, ferrocene derivatives have been enumerated by starting from a dumbbell skeleton of $D_{\infty h}$ (cf. Table 4.1 on page 110), where the two cyclopentadienyl ligands of C_{5v} -symmetry occupy the two positions of the dumbbell skeleton [19].

Trigonal Bipyramidal Derivatives

The SCR notation of trigonal bipyramidal derivatives has been discussed in detail (cf. Fig. 3.14 on page 84) [13]. The FPM method of Fujita's USCI approach has been applied to the enumeration of trigonal bipyramidal complexes [47], where the numbers of isomers with the composition $X^l Y^m Z^n$ are itemized with respect to subgroups of D_{3h} . For example, the [3,1,1]-row³ of Table 4 of [13] indicates there appear two C_s -derivatives, one C'_s -derivative, and one C_{3v} -derivative. As for the two C_s -derivatives and the one C'_s -derivative, see Fig. 3.14. A more elaborate enumeration taking account of both achiral and chiral proligands has been accomplished by using the PCI method [60]. This article contains the description on stereoisograms of trigonal bipyramidal compounds, where the pair of concepts *RS*-stereogenicity/*RS*-stereoisomerism is compared with the pair of concepts stereogenicity/stereoisomerism so as to propose a revised interpretation of Berry's pseudorotation.

Square Planar Complexes

The four positions of a square planar skeleton **3-11** (page 68) construct a four-membered orbit governed by the coset representation D_{4h}/C_{2v}'' ($|D_{4h}|/|C_{2v}''| = 16/4 = 4$). The PCI method of Fujita's USCI approach has been applied to enumeration of square planar complexes with both achiral and chiral proligands [21]. The effect of the point group D_{4h} has been compared with the effect of the symmetric group of degree 4 (S^4).

6.5.4 Enumeration of Organic Reactions

Fujita has proposed the concept of *imaginary transition structures* (ITSs) for representing organic reactions [61]. A series of articles on the ITS concept have appeared during the 1980s in *J. Chem. Inf. Comput. Sci.* [61–75], *J. Chem. Soc. Perkin II* [76], and *Bull. Chem. Soc. Jpn.* [77,78]. The accomplishments have been summarized in reviews [79–81] and Fujita's monograph [82]. Any subgraphs of ITSs represent reaction types for systematic classification of organic reactions [76], where there appears a hierarchy of subgraphs, i.e.,

³ The original partition [3,2,1] in the l, m, n -column of [13, Table 4] should be read as [3,1,1], which corresponds to the composition X^3YZ .

basic reaction graphs (BRGs) — reaction graphs (RGs) — reaction center graphs (RCGs) — imaginary transition structures (ITSs). After hexagonal RGs are enumerated on the basis of BRGs, the enumeration of hexagonal RCGs based on RGs have been investigated by the FPM method [83]. A reaction pair is defined as a pair of forward and reverse reactions. To enumerate reaction pairs, a pseudo-point group \widehat{D}_{6h} is constructed to characterize a skeleton for generating hexagonal reaction pairs. Then, enumeration of hexagonal reaction pairs has been conducted by counting the modes of edge substitution on the skeleton of \widehat{D}_{6h} [84].

References

- [1] S. Fujita, “Symmetry and Combinatorial Enumeration in Chemistry”, Springer-Verlag, Berlin-Heidelberg (1991).
- [2] J. Sheehan, *Canad. J. Math.*, **20**, 1068–1076 (1968).
- [3] W. Hässelbarth, *Theor. Chim. Acta*, **67**, 339–367 (1985).
- [4] E. Ruch, W. Hässelbarth, and B. Richter, *Theor. Chim. Acta*, **19**, 288–300 (1970).
- [5] E. Ruch and D. J. Klein, *Theor. Chim. Acta*, **63**, 447–472 (1983).
- [6] J. Brocas, *J. Am. Chem. Soc.*, **108**, 1135–1145 (1986).
- [7] C. A. Mead, *J. Am. Chem. Soc.*, **109**, 2130–2137 (1987).
- [8] C. A. Mead, *J. Am. Chem. Soc.*, **114**, 4018–4019 (1992).
- [9] S. Fujita, *Theor. Chim. Acta*, **76**, 247–268 (1989).
- [10] S. Fujita, *J. Math. Chem.*, **5**, 99–120 (1990).
- [11] S. Fujita, *J. Math. Chem.*, **5**, 121–156 (1990).
- [12] S. Fujita, *Theor. Chim. Acta*, **77**, 307–321 (1990).
- [13] S. Fujita, *Bull. Chem. Soc. Jpn.*, **63**, 315–327 (1990).
- [14] S. Fujita, *J. Am. Chem. Soc.*, **112**, 3390–3397 (1990).
- [15] S. Fujita, *Chem. Rec.*, **2**, 164–176 (2002).
- [16] S. Fujita, *Bull. Chem. Soc. Jpn.*, **75**, 1863–1883 (2002).
- [17] S. Fujita, *Bull. Chem. Soc. Jpn.*, **84**, 1192–1207 (2011).
- [18] S. Fujita, *J. Graph Theory*, **18**, 349–371 (1994).
- [19] S. Fujita, *Bull. Chem. Soc. Jpn.*, **72**, 2409–2416 (1999).
- [20] S. Fujita, *Tetrahedron*, **46**, 365–382 (1990).
- [21] S. Fujita, *Helv. Chim. Acta*, **85**, 2440–2457 (2002).
- [22] S. Fujita, *J. Chem. Inf. Comput. Sci.*, **36**, 270–285 (1996).
- [23] S. Fujita, *Bull. Chem. Soc. Jpn.*, **63**, 2759–2769 (1990).
- [24] S. Fujita, *Polyhedron*, **12**, 95–110 (1993).

- [25] S. Fujita, *J. Math. Chem.*, **12**, 173–195 (1993).
- [26] S. Fujita, *J. Chem. Inf. Comput. Sci.*, **39**, 151–163 (1999).
- [27] S. Fujita, *Bull. Chem. Soc. Jpn.*, **85**, 793–810 (2012).
- [28] S. Fujita, *Bull. Chem. Soc. Jpn.*, **74**, 1585–1603 (2001).
- [29] S. Fujita, *MATCH Commun. Math. Comput. Chem.*, **55**, 237–270 (2006).
- [30] S. Fujita, *Bull. Chem. Soc. Jpn.*, **63**, 2770–2775 (1990).
- [31] S. Fujita, *Theor. Chim. Acta*, **82**, 473–498 (1992).
- [32] S. Fujita, *Bull. Chem. Soc. Jpn.*, **85**, 811–821 (2012).
- [33] S. Fujita, *Bull. Chem. Soc. Jpn.*, **63**, 2033–2043 (1990).
- [34] S. Fujita, *J. Chem. Inf. Comput. Sci.*, **40**, 135–146 (2000).
- [35] S. Fujita, *J. Chem. Inf. Comput. Sci.*, **40**, 426–437 (2000).
- [36] S. Fujita, *Bull. Chem. Soc. Jpn.*, **67**, 2927–2934 (1994).
- [37] S. Fujita, *Bull. Chem. Soc. Jpn.*, **67**, 2935–2948 (1994).
- [38] S. Fujita, *MATCH Commun. Math. Comput. Chem.*, **46**, 25–44 (2002).
- [39] S. Fujita, *J. Chem. Soc. Faraday Trans.*, **94**, 2515–2523 (1998).
- [40] S. Fujita, *J. Chem. Inf. Comput. Sci.*, **38**, 876–884 (1998).
- [41] S. Fujita, *J. Chem. Soc. Faraday Trans.*, **94**, 3197–3205 (1998).
- [42] S. Fujita, *Bull. Chem. Soc. Jpn.*, **72**, 1759–1768 (1999).
- [43] S. Fujita, *J. Org. Chem.*, **67**, 6055–6063 (2002).
- [44] S. Fujita, *J. Math. Chem.*, **32**, 1–17 (2002).
- [45] S. Fujita, *Bull. Chem. Soc. Jpn.*, **85**, 439–449 (2012).
- [46] S. Fujita, *Memoirs of the Faculty of Engineering and Design, Kyoto Institute of Technology*, **47**, 111–126 (1999).
- [47] S. Fujita, *Bull. Chem. Soc. Jpn.*, **63**, 1876–1883 (1990).
- [48] S. Fujita, *MATCH Commun. Math. Comput. Chem.*, **69**, 291–310 (2013).
- [49] S. Fujita, *MATCH Commun. Math. Comput. Chem.*, **69**, 311–332 (2013).
- [50] S. Fujita, *Bull. Chem. Soc. Jpn.*, **62**, 3771–3778 (1989).
- [51] S. Fujita, *Bull. Chem. Soc. Jpn.*, **63**, 203–215 (1990).
- [52] S. Fujita, *J. Chem. Inf. Comput. Sci.*, **31**, 540–546 (1991).
- [53] S. Fujita, *J. Comput. Chem. Jpn.*, **11**, 131–139 (2012).
- [54] S. Fujita, *J. Comput. Chem. Jpn.*, **11**, 140–148 (2012).
- [55] S. Fujita, *MATCH Commun. Math. Comput. Chem.*, **69**, 263–290 (2013).
- [56] S. Fujita, *Bull. Chem. Soc. Jpn.*, **64**, 3215–3223 (1991).
- [57] S. Fujita, *Bull. Chem. Soc. Jpn.*, **85**, 282–304 (2012).

- [58] S. Fujita, *MATCH Commun. Math. Comput. Chem.*, **69**, 333–354 (2013).
- [59] S. Fujita and N. Matsubara, *Internet Electronic Journal of Molecular Design*, **2**, 224–241 (2003).
- [60] S. Fujita, *J. Math. Chem.*, **50**, 1815–1860 (2012).
- [61] S. Fujita, *J. Chem. Inf. Comput. Sci.*, **26**, 205–212 (1986).
- [62] S. Fujita, *J. Chem. Inf. Comput. Sci.*, **26**, 212–223 (1986).
- [63] S. Fujita, *J. Chem. Inf. Comput. Sci.*, **26**, 224–230 (1986).
- [64] S. Fujita, *J. Chem. Inf. Comput. Sci.*, **26**, 231–237 (1986).
- [65] S. Fujita, *J. Chem. Inf. Comput. Sci.*, **26**, 238–242 (1986).
- [66] S. Fujita, *J. Chem. Inf. Comput. Sci.*, **27**, 99–104 (1987).
- [67] S. Fujita, *J. Chem. Inf. Comput. Sci.*, **27**, 104–110 (1987).
- [68] S. Fujita, *J. Chem. Inf. Comput. Sci.*, **27**, 111–115 (1987).
- [69] S. Fujita, *J. Chem. Inf. Comput. Sci.*, **27**, 115–120 (1987).
- [70] S. Fujita, *J. Chem. Inf. Comput. Sci.*, **27**, 120–126 (1987).
- [71] S. Fujita, *J. Chem. Inf. Comput. Sci.*, **28**, 1–9 (1988).
- [72] S. Fujita, *J. Chem. Inf. Comput. Sci.*, **28**, 78–82 (1988).
- [73] S. Fujita, *J. Chem. Inf. Comput. Sci.*, **28**, 128–137 (1988).
- [74] S. Fujita, *J. Chem. Inf. Comput. Sci.*, **28**, 137–142 (1988).
- [75] S. Fujita, *J. Chem. Inf. Comput. Sci.*, **29**, 22–30 (1989).
- [76] S. Fujita, *J. Chem. Soc. Perkin II*, 597–616 (1988).
- [77] S. Fujita, *Bull. Chem. Soc. Jpn.*, **61**, 4189–5206 (1988).
- [78] S. Fujita, *Bull. Chem. Soc. Jpn.*, **62**, 662–667 (1989).
- [79] S. Fujita, *Yuki Gosei Kagaku Kyokai-Shi/J. Synth. Org. Chem. Jpn.*, **47**, 396–412 (1989).
- [80] S. Fujita, *Pure Appl. Chem.*, **61**, 605–608 (1989).
- [81] S. Fujita, *J. Chem. Ed.*, **67**, 290–293 (1990).
- [82] S. Fujita, “Computer-Oriented Representation of Organic Reactions”, Yoshioka-Shoten, Kyoto (2001).
- [83] S. Fujita, *J. Math. Chem.*, **7**, 111–133 (1991).
- [84] S. Fujita, *Theor. Chim. Acta*, **94**, 105–124 (1996).

7 Gross Enumeration Under Point Groups¹

7.1 Counting Orbits

In Subsection 5.1.3, we have discussed multiplicities of orbits, which are itemized in terms of coset representations, as exemplified by Eq. 5.34 (page 122) for characterizing adamantan-2-one **5-1** of C_{2v} (Fig. 5.1 on page 122). Thus, the 14 hydrogens of **5-1** are specified by two $C_{2v}/(C_1)$ -orbits, one $C_{2v}/(C_s)$ -orbits, and two $C_{2v}/(C'_s)$ -orbits (Eq. 5.34). According to our purposes, there would be some cases in which such specification is not necessary, but only the number of orbits, i.e., the value 5 ($= 2 + 1 + 2$), is required.

To accomplish this task, the Cauchy-Frobenius lemma (so-called Burnside's lemma) plays a crucial role. Let \mathbf{P}_G be a permutation representation of the point group G acting on a set Δ of positions (or other objects). The permutation representation \mathbf{P}_G is regarded as a permutation group of order $|\mathbf{P}_G|$ ($= |G|$), if there occurs no degeneration. Suppose that \mathbf{P}_G is divided into a set of coset representations, i.e., $\mathbf{P}_G = \sum_{i=1}^s \alpha_i G(/G_i)$ (Eq. 5.22 on page 120), where each coset representation $G(/G_i)$ governs an orbit Δ_i . Our task is to obtain the total number r represented by

$$r = \sum_{i=1}^s \alpha_i. \quad (7.1)$$

Let us examine an orbit Δ_i governed by $G(/G_i)$. The symbol $n_g^{(i)}$ is used to represent the number of fixed points under the action of g ($\in G$). Because such fixed points in Δ_i are concerned with g ($\in G_i$), they are counted to be equal to the size $|\Delta_i|$ multiplied by the number of operations of the stabilizer $|G_i|$. Hence, we obtain the following theorem:

$$\sum_{g \in G} n_g^{(i)} = \sum_{g \in G_i} n_g^{(i)} = |\Delta_i| \cdot |G_i| = |G|. \quad (7.2)$$

Note that the size of the $G(/G_i)$ -orbit is calculated to be $|\Delta_i| = |G|/|G_i|$. The total number of fixed points is calculated by summing up the numbers of Eq. 7.2 over Δ_i ($i = 1, 2, \dots, s$):

$$\sum_i \alpha_i \sum_{g \in G} n_g^{(i)} = \sum_i \alpha_i |G| = r |G|, \quad (7.3)$$

which is equal to $\sum_{g \in G} n_g$, where the symbol n_g represents the number of fixed points for each operation g . Hence we obtain a theorem:

¹ This chapter is based on S. Fujita, "Graphs to Chemical Structures 1. Sphericity Indices of Cycles for Stereochemical Extension of Pólya's Theorem", *Theor. Chem. Acc.*, **113**, 73–79 (2005); S. Fujita, "Graphs to Chemical Structures 2. Extended Sphericity Indices of Cycles for Stereochemical Extension of Pólya's Coronas", *Theor. Chem. Acc.*, **113**, 80–86 (2005); and S. Fujita, "Graphs to Chemical Structures 3. General Theorems with the Use of Different Sets of Sphericity Indices for Combinatorial Enumeration of Nonrigid Stereoisomers", *Theor. Chem. Acc.*, **115**, 37–53 (2006).

Theorem 7.1 (Cauchy-Frobenius).

$$r = \frac{1}{|\mathbf{G}|} \sum_{g \in \mathbf{G}} n_g. \quad (7.4)$$

For example, the application of each $g \in \mathbf{C}_{2v}$ to the 14 hydrogens of adamantan-2-one **5-1** gives the number of fixed hydrogen atoms, which is obtained by counting 1-cycles of each row collected in the right table of Fig. 5.1 (page 122). Because the 1-cycles are counted to give $n_I = 14$, $n_{C_2} = 0$, $n_{\sigma_{v(1)}} = 2$, and $n_{\sigma_{v(2)}} = 4$, Theorem 7.1 gives the number of orbits:

$$r = \frac{1}{4}(14 + 0 + 2 + 4) = 5, \quad (7.5)$$

which is consistent with Eq. 5.34 (page 122).



Exercise 7.1. Confirm Eqs. 7.2 and 7.3 by using the data collected in the right table of Fig. 5.1 (page 122).

7.2 Pólya's Theorem of Counting

Before discussing Fujita's proligand method, we set to work on Pólya's theorem of counting, where the difference between graphs (2D structures) and 3D structures is not taken into consideration. Pólya's theorem directly uses permutation groups, whereas Fujita's proligand method puts stress on point groups which are accompanied by permutation representations (or coset representations). The following discussion on Pólya's theorem is based on a compromise standpoint using permutation representations of point groups (not permutation groups) in order to assure an easy access to Fujita's proligand method.

Let us reexamine the enumeration based on the oxirane skeleton **3-12**, where the 16 derivatives have been listed in Fig. 6.2 (page 133). They are represented as the functions contained in \mathbf{F}_{3-12} shown by Eq. 6.6 (page 134). The action of $g \in \mathbf{C}_{2v}$ on \mathbf{F}_{3-12} is represented by a permutation $\lambda_g^{[\theta]}$ (Eq. 6.8 on page 134), which constructs a permutation representation $\Lambda_{\mathbf{C}_{2v}, \mathbf{F}_{3-12}}^{[\theta]}$ (Eq. 6.9 on page 134). The number of fixed derivatives (fixed functions) on the action of each permutation is obtained by counting functions checked by \surd in each row of Eq. 6.7 on page 134 (16, 4, 4, and 4). Hence, the number of derivatives inequivalent under the action of \mathbf{C}_{2v} is calculated to be equal to the number of orbits:

$$r = \frac{1}{4}(16 + 4 + 4 + 4) = 7 \quad (7.6)$$

by applying Theorem 7.1.

The result of Fujita's USCI approach in Fig. 6.2 (page 133) is reinterpreted to give Fig. 7.1 by means of Pólya's counting theorem based on Theorem 7.1.

The number of fixed derivatives under the action of each operation of \mathbf{C}_{2v} is evaluated by using the corresponding cycle term, which has been shown in the cycle-term column of

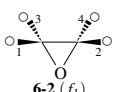
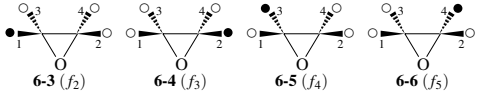
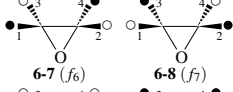
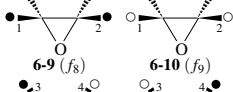
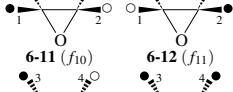
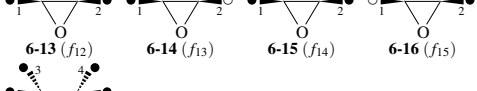
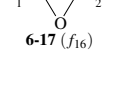
	Fujita's proligand method:	I	C_2	$\sigma_{v(1)}$	$\sigma_{v(2)}$	(PSI)
	Pólya's theorem:	b_1^4	b_2^2	c_2^2	c_2^2	(cycle term)
		s_1^4	s_2^2	s_2^2	s_2^2	
X^4		1	1	1	1	$C_{2v}/(C_{2v})$
X^3Y		4	0	0	0	$C_{2v}/(C_1)$
X^2Y^2		2	2	0	0	$C_{2v}/(C_2)$
X^2Y^2		2	0	2	0	$C_{2v}/(C_s)$
X^2Y^2		2	0	0	2	$C_{2v}/(C_4)$
XY^3		4	0	0	0	$C_{2v}/(C_1)$
Y^4		1	1	1	1	$C_{2v}/(C_{2v})$
		$r = \frac{1}{4} (\underbrace{16}_{(X+Y)^4} + \underbrace{4}_{(X^2+Y^2)^2} + \underbrace{4}_{(X^2+Y^2)^2} + \underbrace{4}_{(X^2+Y^2)^2}) = 7$				

Fig. 7.1. Orbits of promolecules based on an oxirane skeleton and their numbers of fixed points. An open circle represents an achiral proligand X in isolation, while a solid circle represents another achiral proligand Y in isolation.

Table 3.5 on page 70 (s_1^4 for an identity operation I and s_2^2 for C_2 , $\sigma_{v(1)}$, or $\sigma_{v(2)}$). Note that such a cycle term is determined by referring to each cycle structure (1^4) (four one-cycles for I) or (2^2) (two two-cycles for C_2 , $\sigma_{v(1)}$, or $\sigma_{v(2)}$), as found in Table 3.5. Because we use the ligand inventory $\mathbf{L}_1 = \{X, Y\}$ (Eq. 6.2 on page 132), we obtain the following generating functions for counting fixed derivatives (fixed functions):

$$s_1^4 \text{ for } I: \quad (X + Y)^4 = X^4 + 4X^3Y + 6X^2Y^2 + 4XY^3 + Y^4 \quad (7.7)$$

$$s_2^2 \text{ for } C_2, \sigma_{v(1)}, \sigma_{v(2)}: \quad (X^2 + Y^2)^2 = X^4 + 2X^2Y^2 + Y^4 \quad (7.8)$$

Each coefficient of X^xY^y appearing in the right-hand sides is equal to the number of functions with the composition $W_\theta = X^xY^y$, which are inequivalent under C_{2v} , as shown in the right part of Fig. 7.1. Theorem 7.1 is applied to the right-hand sides of Eqs. 7.7 and 7.8 ($\times 3$), which are summed up and divided by $|C_{2v}| = 4$. The resultant generating function has the coefficient A_θ of the term $W_\theta = X^xY^y$, which represents the number of derivatives

(functions) inequivalent under C_{2v} :

$$\begin{aligned} \sum_{[\theta]} A_{\theta} W_{\theta} &= \frac{1}{4} \{ (X + Y)^4 + 3(X^2 + Y^2)^2 \} \\ &= X^4 + X^3Y + 3X^2Y^2 + XY^3 + Y^4. \end{aligned} \quad (7.9)$$

According to Eq. 7.9, the 16 functions of Fig. 7.1 are categorized into seven orbits, each of which corresponds to a derivative to be counted once, as aligned in each row. Note that a pair of enantiomers or an achiral derivative is counted once, because they are regarded as graphs.

The order of the calculation processes for giving Eq. 7.9 can be reversed without losing generality. It follows that Theorem 7.1 is applied to the set of cycle terms $\{s_1^4, s_2^2, s_2^2, s_2^2\}$ in the first step, so as to give a *cycle index*:

$$CI(C_{2v}; s_d) = \frac{1}{4} (s_1^4 + 3s_2^2), \quad (7.10)$$

into which a ligand-inventory function $s_d = X^d + Y^d$ is introduced in the second step. This reverse procedure gives a generating function equivalent to Eq. 7.9.

The above discussions can be easily extended to a general case. For this purpose, we first define Pólya's cycle index:

Definition 7.1 (Pólya's Cycle Index). Let $\mathbf{P}_{\mathbf{G}}$ be a permutation representation of \mathbf{G} . Suppose that a permutation $p_g \in \mathbf{P}_{\mathbf{G}}$ has a cycle structure $(1^{v_1} 2^{v_2} \dots n^{v_n})^{(p_g)}$, where $\sum_{i=1}^n i v_i = n$. Then, Pólya's cycle index is defined as follows:

$$CI(\mathbf{P}_{\mathbf{G}}; s_d) = \frac{1}{|\mathbf{P}_{\mathbf{G}}|} \sum_{p_g \in \mathbf{P}_{\mathbf{G}}} (s_1^{v_1} s_2^{v_2} \dots s_n^{v_n})^{(p_g)}. \quad (7.11)$$

The ligand inventory \mathbf{L} (Eq. 6.26) is restricted to the set containing only achiral proligands:

$$\mathbf{L}' = \{X_1, \dots, X_m\}. \quad (7.12)$$

A resulting promolecule has the following composition:

$$W_{\theta} = X_1^{x_1} \dots X_m^{x_m}, \quad (7.13)$$

where the sum of the exponents is equal to the number of the substitution positions (or equivalently to the degree of the permutation representation $\mathbf{P}_{\mathbf{G}}$). The composition can be represented by

$$[\theta] : x_1 + x_2 + \dots + x_m = n. \quad (7.14)$$

Thereby, we arrive at Pólya's theorem of counting:

Theorem 7.2 (Pólya's Theorem of Counting). Let the symbol A_{θ} denote the number of derivatives (orbits) inequivalent under the action of $\mathbf{P}_{\mathbf{G}}$. A generating function for A_{θ} is represented by

$$\sum_{[\theta]} A_{\theta} W_{\theta} = CI(\mathbf{P}_{\mathbf{G}}; s_d) \Big|_{s_d = \Sigma_{\mathbf{L}'}} , \quad (7.15)$$

where the symbol $s_d = \sum_{\mathbf{L}'} \dots$ denotes the introduction of the following ligand-inventory function into a dummy variable s_d :

$$s_d = \sum_{i=1}^m X^d. \quad (7.16)$$

This theorem has been once explained in Fujita's monograph [1, Theorem 13.8].

7.3 Fujita's Proligand Method of Counting

7.3.1 Historical Comments

After Pólya's theorem for counting graphs (constitutions) non-equivalent with respect to a given permutation group was proposed in 1935–1937 [2–5], there have appeared many articles on its chemical applications, as summarized in books [6–8] and reviews [9–12].

The crux of Pólya's theorem (Theorem 7.2) is the restriction of (pro)ligands to achiral ones. That is to say, even if chiral (pro)ligands in isolation are considered, they are regarded as graphs (as if they were achiral (pro)ligands). This means that Pólya's theorem takes no account of the concept of sphericities, as pointed out in a review [13].

After modifying the concept of sphericities (cf. Chapter 4) substantially, Fujita has proposed the proligand method [14–16], where the combination of point groups and their permutation representations (or coset representations) is stressed instead of such direct usage of permutation groups as found in Pólya's theorem. For detailed discussions, see Chapter 7 of Fujita's monograph [17]. In particular, Pólya's theorem has been discussed as a degenerate case of Fujita's proligand method [17, Section 7.4].

The effects of the modified concept of sphericities for Fujita's proligand method are predominant in the enumeration of alkanes and monosubstituted alkanes, as summarized in Fujita's account [18]. Thus, combinatorial enumeration of monosubstituted alkanes as three-dimensional planted trees [19,20] and that of alkanes as centroidal and bicentroidal three-dimensional trees [21,22] have been investigated by means of Fujita's proligand method. Various types of enumeration based on Fujita's proligand method have been applied to alkanes and monosubstituted alkanes, e.g., enumeration of primary, secondary, and tertiary monosubstituted alkanes [23], enumeration by the combination of two dichotomies for three-dimensional trees [24], enumeration by dual recognition as uninuclear and binuclear promolecules [25], enumeration of monosubstituted alkanes [26] and alkanes [27] itemized with respect to numbers of asymmetric and pseudoasymmetric centers, as well as enumeration of monosubstituted alkanes [28] and alkanes [29] itemized with respect to internal branching.

7.3.2 Sphericities of Cycles

To take account of both chiral and achiral proligands in isolation, we should introduce the concept of *sphericities of cycles* in a parallel way to the concept of sphericities of orbits:

Definition 7.2 (Sphericities of Cycles). Suppose that $g \in G$ acts on the set of substitution positions Δ ($|\Delta| = n$), where the corresponding permutation $p_g \in \mathbf{P}_G$ has a cycle structure $(1^{v_1} 2^{v_2} \dots d^{v_d} \dots n^{v_n})$ ($\sum_{i=1}^n i v_i = n$). The sphericity of a d -cycle is defined as follows:

- **(Homospheric cycles)** A d -cycle in p_g is defined to be *homospheric*, if g is an improper rotation (reflection or rotoreflection) and d is odd.
- **(Enantiospheric cycles)** A d -cycle in p_g is defined to be *enantiospheric*, if g is an improper rotation (reflection or rotoreflection) and d is even.
- **(Hemispheric cycles)** A d -cycle in p_g is defined to be *hemispheric*, if g is a proper rotation and d is odd or even.

In a parallel way to the chirality fittingness introduced for characterizing orbits (cf. Fig. 4.2 on page 90 as well as Theorems 4.2, 4.3, and 4.4), each d -cycle has chirality fittingness according to its sphericity.

A homospheric d -cycle (d : odd) fixes an achiral promolecule having d -positions occupied by achiral proligands of the same kind (e.g., X's or Y's), because the action of a permutation due to the d -cycle causes a reflection to satisfy $\overline{X} = X$. Note that chiral proligands are not permitted because they cannot retain the achirality of the promolecule under the reflection (d is odd). Hence, we obtain the following theorem:

Theorem 7.3 (Chirality Fittingness of a Homospheric Cycle). A homospheric d -cycle is capable of acting on the number d of achiral ligands (or proligands) of the same kind.

This theorem corresponds to the chirality fittingness of a homospheric orbit on the action of a cyclic achiral group [17, Theorem 7.3] as well as to Theorem 4.2 (page 89) for the chirality fittingness of a homospheric orbit on the action of an achiral group. The mode of action due to Theorem 7.3 is parallel to the illustration shown in Fig. 4.2(a) on page 90.

An enantiospheric d -cycle (d : even) fixes an achiral promolecule having d -positions occupied by achiral proligands of the same kind (e.g., X's or Y's), because the action of a permutation due to the d -cycle causes a reflection to satisfy $\overline{X} = X$. In addition, such an enantiospheric d -cycle permits the number $d/2$ of chiral proligands of the same kind (e.g., p 's) and the same number $d/2$ of chiral proligands with opposite chirality sense (e.g., \overline{p} 's), because they are totally retain the achirality of the promolecule under the reflection (d is even). Hence, we obtain the following theorem:

Theorem 7.4 (Chirality Fittingness of an Enantiospheric Cycle). An enantiospheric d -cycle is capable of acting on the number d of achiral ligands (or proligands) of the same kind as well as on the number $d/2$ of chiral proligands of the same kind and the same number $d/2$ of chiral proligands with opposite chirality sense.

This theorem corresponds to the chirality fittingness of an enantiospheric orbit on the action of a cyclic achiral group [17, Theorem 7.1] as well as to Theorem 4.3 (page 91) for the

				Fujita's proligand method:					
				I	C_2	$\sigma_{v(1)}$	$\sigma_{v(2)}$	(PSI)	
				b_1^4	b_2^2	c_2^2	c_2^2		
$\frac{1}{2}(p^4 + \bar{p}^4)$				2	2	0	0	$C_{2v}/(C_2)$	
$\frac{1}{2}(p^3\bar{p} + p\bar{p}^3)$					4	0	0	0	$C_{2v}/(C_1)$
$\frac{1}{2}(p^3\bar{p} + p\bar{p}^3)$					4	0	0	0	$C_{2v}/(C_1)$
$p^2\bar{p}^2$				1	1	1	1	$C_{2v}/(C_{2v})$	
$p^2\bar{p}^2$				1	1	1	1	$C_{2v}/(C_{2v})$	
$p^2\bar{p}^2$				2	0	0	2	$C_{2v}/(C_s)$	
$p^2\bar{p}^2$				2	0	2	0	$C_{2v}/(C_s)$	
				$r = \frac{1}{4}(16 + 4 + 4 + 4) = 7$					
				$(p + \bar{p})^4$ $(p^2 + \bar{p}^2)^2$ $(2p\bar{p})^2$ $(2p\bar{p})^2$					

Fig. 7.2. Orbits of promolecules based on an oxirane skeleton and their numbers of fixed points. The symbol \odot represents a chiral proligand p in isolation, while the symbol \bullet represents its enantiomeric proligand \bar{p} in isolation.

chirality fittingness of an enantiospheric orbit on the action of an achiral group. The mode of action due to Theorem 7.4 is parallel to the illustration shown in Fig. 4.2(b) on page 90.

As examples of enantiospheric cycles with respect to chiral proligands, let us reexamine the oxirane derivatives collected in Fig. 6.4 (page 137), where the ligand inventory $L_2 = \{p, \bar{p}\}$ (Eq. 6.13 on page 135) is adopted. The reflection $\sigma_{v(1)}$ of the point group C_{2v} is represented by a permutation $(1\ 2)(3\ 4)$, which is characterized by a cycle structure (2^2) (Table 3.5 on page 70). According to Theorem 7.4, each 2-cycle is determined to be enantiospheric. As found in Fig. 7.2, the 2-cycle represented by $(1\ 2)$ (or $(3\ 4)$) fixes four functions, i.e., **6-29** (f_{11}), **6-30** (f_{12}), **6-33** (f_{15}), and **6-34** (f_{16}), each of which is composed of two pairs of enantiomeric proligands in isolation (the symbol \odot for p 's and the symbol \bullet for \bar{p} 's). The data are shown in the $\sigma_{v(1)}$ -column of Fig. 7.2.

As for examples of enantiospheric cycles with respect to achiral proligands, the data shown in the $\sigma_{v(1)}$ -column of Fig. 7.1 are also effective.

A hemispheric d -cycle (d : odd or even) fixes an achiral or a chiral promolecule having d -positions occupied by achiral or chiral proligands of the same kind (e.g., X's, Y's, p 's,

or \bar{p} 's), because the action of a permutation due to the d -cycle causes a rotation without mirror-image formation. Hence, we obtain the following theorem:

Theorem 7.5 (Chirality Fittingness of a Hemispheric Cycle). A hemispheric d -cycle is capable of acting on the number d of achiral or chiral ligands (or proligands) of the same kind.

This theorem corresponds to the chirality fittingness of a hemispheric orbit on the action of a cyclic chiral group [17, Theorem 7.5] as well as to Theorem 4.4 (page 92) for the chirality fittingness of a hemispheric orbit on the action of a chiral group. The mode of action due to Theorem 7.5 is parallel to the illustration shown in Fig. 4.2(c) on page 90.

As examples of hemispheric cycles with respect to chiral proligands, let us again examine Fig. 7.2. The two-fold rotation C_2 of the point group C_{2v} is represented by a permutation $(1\ 4)(2\ 3)$, which is characterized by a cycle structure (2^2) (Table 3.5 on page 70). According to Theorem 7.5, each 2-cycle is determined to be hemispheric. As found in Fig. 7.2, the 2-cycle represented by $(1\ 4)$ (or $(2\ 3)$) fixes four functions. Among the fixed functions, **6-19** (f_1) and **6-20** (f_2) are respectively composed of four p 's (the symbol \odot) and four \bar{p} 's (the symbol \ominus). On the other hand, **6-29** (f_{11}) and **6-30** (f_{12}) are respectively composed of two p 's and two \bar{p} 's. Note that the two 2-cycles $(1\ 4)$ and $(2\ 3)$ act independently on a set of two p 's and on another set of two \bar{p} 's, so that there appear four combinations, i.e., p^2/p^2 , \bar{p}^2/\bar{p}^2 , p^2/\bar{p}^2 , and \bar{p}^2/p^2 . The data are shown in the C_2 -column of Fig. 7.2.

As for examples of hemispheric cycles with respect to achiral proligands, the data shown in the C_2 -column of Fig. 7.1 are also effective.

7.3.3 Products of Sphericity Indices

To systematize the process of evaluating the number of fixed functions, we assign a sphericity index to each cycle according to the three types of sphericities defined by Def. 7.2 as follows:

Definition 7.3 (Sphericity Indices for Characterizing Cycles).

- **(Sphericity index a_d for a homospheric cycle)** The sphericity index a_d is assigned to a homospheric d -cycle.
- **(Sphericity index c_d for an enantiospheric cycle)** The sphericity index c_d is assigned to an enantiospheric d -cycle.
- **(Sphericity index b_d for a hemispheric cycle)** The sphericity index b_d is assigned to a hemispheric d -cycle.

Because each permutation has its cycle structure $(1^{v_1} 2^{v_2} \dots d^{v_d} \dots n^{v_n})$ ($\sum_{i=1}^n i v_i = n$) (cf. Def. 7.2), it is characterized by a product of sphericity indices (PSI):

Definition 7.4 (Products of Sphericity Indices (PSIs)). Suppose that a permutation p_g ($\in \mathbf{P}_G$) has a cycle structure $(1^{v_1} 2^{v_2} \dots d^{v_d} \dots n^{v_n})$ ($\sum_{i=1}^n i v_i = n$), as shown in Def. 7.2. Then, the corresponding *product of sphericity indices* is defined as a monomial term:

$$\text{PSI}(p_g; \$_d) = \$_1^{v_1} \$_2^{v_2} \dots \$_d^{v_d} \dots \$_n^{v_n}, \quad (7.17)$$

where $\$_d$ denotes a_d , c_d , or b_d according to Def. 7.3.

Let us return to Fig. 7.2. The PSIs for C_{2v} are collected in Table 3.5 (page 70). Because we use the ligand inventory $\mathbf{L}_2 = \{p, \bar{p}\}$ (Eq. 6.13), Theorems 7.3, 7.4, and 7.5 provide us with the following generating functions for counting fixed derivatives (fixed functions):

$$b_1^4 \text{ for } I: \quad (p + \bar{p})^4 = p^4 + 4p^3\bar{p} + 6p^2\bar{p}^2 + 4p\bar{p}^3 + \bar{p}^4 \quad (7.18)$$

$$b_2^2 \text{ for } C_2: \quad (p^2 + \bar{p}^2)^2 = p^4 + 2p^2\bar{p}^2 + \bar{p}^4 \quad (7.19)$$

$$c_2^2 \text{ for } \sigma_{v(1)}, \sigma_{v(2)}: \quad (2p\bar{p})^2 = 4p^2\bar{p}^2, \quad (7.20)$$

where a PSI (Def. 7.4) is shown at the top of each equation. Each coefficient of $p^p\bar{p}^{\bar{p}}$ appearing in the right-hand sides is equal to the number of functions with the composition $W_\theta = p^p\bar{p}^{\bar{p}}$, which are inequivalent under C_{2v} . These coefficients are collected in the respective columns of the right part of Fig. 7.2.

Theorem 7.1 is applied to the right-hand sides of Eqs. 7.18–7.20, which are summed up and divided by $|C_{2v}| = 4$. The resulting generating function has the coefficient A_θ of the term $W_\theta = p^p\bar{p}^{\bar{p}}$, which represents the number of derivatives (functions) inequivalent under C_{2v} :

$$\begin{aligned} \sum_{[\theta]} A_\theta W_\theta &= \frac{1}{4} \{ (p + \bar{p})^4 + (p^2 + \bar{p}^2)^2 + 2 \times (p^2 + \bar{p}^2)^2 \} \\ &= \frac{1}{2} (p^4 + \bar{p}^4) + 2 \times \frac{1}{2} (p^3\bar{p} + p\bar{p}^3) + 4p^2\bar{p}^2 \end{aligned} \quad (7.21)$$

According to Eq. 7.21, the 16 functions of Fig. 7.2 are categorized into seven orbits, each of which corresponds to a derivative to be counted once, as aligned in each row. Note that a pair of enantiomers ($\frac{1}{2}(p^4 + \bar{p}^4)$ or $\frac{1}{2}(p^3\bar{p} + p\bar{p}^3)$) or an achiral derivative ($p^2\bar{p}^2$) is counted once.

The order of the calculation processes of Eq. 7.21 can be reversed without losing generality. It follows that Theorem 7.1 is applied to the set of products of sphericity indices (PSIs) $\{b_1^4, b_2^2, c_2^2, c_2^2\}$ in the first step, so as to give a *cycle index with chirality fittingness* (CI-CF):

$$\text{CI-CF}(C_{2v}; \$d) = \frac{1}{4} (b_1^4 + b_2^2 + 2c_2^2), \quad (7.22)$$

into which ligand-inventory functions $b_d = p^d + \bar{p}^d$ and $c_d = 2p^{d/2}\bar{p}^{d/2}$ (as well as a_d if necessary) are introduced in the second step. This reverse procedure gives a generating function equivalent to Eq. 7.21.

The above discussions can be easily extended to a general case. For this purpose, we first define Fujita's cycle index with chirality fittingness (CI-CF) by starting the PSIs defined above (Def. 7.4):

Definition 7.5 (Fujita's Cycle Index With Chirality Fittingness (CI-CF)). Suppose that a permutation $p_g (\in \mathbf{P}_G)$ has a cycle structure $(1^{v_1} 2^{v_2} \dots d^{v_d} \dots n^{v_n})_{(p_g)}$ ($\sum_{i=1}^n i v_i = n$), as shown in Def. 7.2, and that the corresponding product of sphericity indices (PSIs) is defined as shown in Def. 7.4. Then, Fujita's *cycle index with chirality fittingness* (CI-CF) is defined as follows:

$$\text{CI-CF}(\mathbf{P}_G; \$d) = \frac{1}{|\mathbf{P}_G|} \sum_{p_g \in \mathbf{P}_G} \text{PSI}(p_g; \$d)$$

$$= \frac{1}{|\mathbf{P}_G|} \sum_{p_g \in \mathbf{P}_G} (\$1^{v_1} \$2^{v_2} \dots \$d^{v_d} \dots \$n^{v_n})^{(p_g)}, \quad (7.23)$$

where $\$d$ denotes a_d , c_d , or b_d according to Def. 7.3.

To apply Def. 7.5 to a general case, the ligand inventory \mathbf{L} (Eq. 6.26 on page 140) is used as it is. A resulting promolecule has the composition W_θ represented by Eq. 6.27 (page 140). The composition can be alternatively represented by the partition $[\theta]$ shown in Eq. 6.28 (page 140). As an extension of the procedure based on Eq. 7.22, the following theorem is obtained in general:

Theorem 7.6 (Fujita's Proligand Method of Counting). Suppose that the n positions of a given skeleton belongs to \mathbf{P}_G , where the CI-CF is shown in Def. 7.5. The ligand inventory \mathbf{L} (Eq. 6.26) is used to give derivatives with the composition W_θ . Let the symbol A_θ denote the number of such derivatives (orbits), which are inequivalent under the action of \mathbf{P}_G . A generating function for A_θ is represented as follows:

$$\sum_{[\theta]} A_\theta W_\theta = \text{CI-CF}(\mathbf{P}_G; \$d) \Big|_{\$d = \sum_{\mathbf{L}}}, \quad (7.24)$$

where the symbol $\$d = \sum_{\mathbf{L}}$ denotes the introduction of the following ligand-inventory functions into the respective sphericity indices $\$d$:

$$a_d = \sum_{\ell=1}^n X_\ell^d \quad (7.25)$$

$$c_d = \sum_{\ell=1}^n X_\ell^d + 2 \sum_{\ell=1}^{n'} p_\ell^{d/2} \bar{p}_\ell^{d/2} \quad (7.26)$$

$$b_d = \sum_{\ell=1}^n X_\ell^d + \sum_{\ell=1}^{n'} p_\ell^d + \sum_{\ell=1}^{n'} \bar{p}_\ell^d \quad (7.27)$$

This theorem with a more elaborate proof has been once described in Fujita's monograph [17, Theorem 7.21].



Exercise 7.2.

- The ligand inventories for enumerating oxirane derivatives (cf. Figs. 7.1 and 7.2), \mathbf{L}_1 (Eq. 6.2) and \mathbf{L}_2 (Eq. 6.13), are combined to give a single ligand inventory:

$$\mathbf{L} = \{X, Y; p, \bar{p}\}. \quad (7.28)$$

Then, enumerate oxirane derivatives with compositions $X^x Y^y p^p \bar{p}^{\bar{p}}$ according to Theorem 7.6 (cf. Eq. 7.22).

- Compare this result with Exercise 6.3 (page 148).

7.3.4 Practices of Fujita's Proligand Method

Procedure of Enumeration Based on Fujita's Proligand Method

To do well with practical problems of enumeration, we may forget the proof of Theorem 7.6 for the time being. What we should do is to obey the following procedure:

i

Rule 7.1. Procedure of Enumeration Based on Fujita's Proligand Method.

Step 1–Step 3 of Rule 6.1 on page 143 are followed. Then,

4. Construct a permutation representation \mathbf{P}_G by combining coset representations (cf. Eq. 5.22 on page 120). Otherwise, such a permutation representation \mathbf{P}_G can be diagrammatically obtained by applying each operation of G to the skeleton at issue, because Fujita's proligand method does not require the division of the substitution positions into orbits.
5. Assign a sphericity index (a_d , c_d , or b_d) to each cycle of a permutation of \mathbf{P}_G according to Def. 7.3.
6. Construct a product of sphericity indices (PSIs) to each permutation according to Def. 7.4.
7. Calculate a CI-CF by applying Def. 7.5 to the PSIs obtained above.
8. Calculate a generating function by introducing ligand-inventory functions according to Theorem 7.6.

As a practical example of the above procedure, cubane derivatives are recently enumerated on the basis of the point group \mathbf{O}_h [30], where the calculation processes have simply followed the utilities of the Maple system for algebraic calculations.

Proligand Method Applied to Tetrahedral Derivatives

As the first example of the procedure of Fujita's proligand method (Rule 7.1), let us examine a tetrahedral skeleton **3-5** (Fig. 3.7 on page 68). The skeleton **3-5** belongs to the point group \mathbf{T}_d (Step 1–Step 3 of Rule 7.1). The permutation representation $\mathbf{P}_{\mathbf{T}_d}$ for the four positions of **3-5** is identical with the coset representation $\mathbf{T}_d(/C_{3v})$, which has been collected in the $\mathbf{T}_d(/C_{3v})$ -column of Table 3.1 on page 61 (Step 4 of Rule 7.1). The assignment of SIs (Step 5 of Rule 7.1) and the construction of PSIs (Step 6 of Rule 7.1) produce the PSIs for respective operations, as summarized in the PSI-column of Table 3.1. Thereby, a CI-CF is calculated to be the sum of the PSIs divided by $|\mathbf{T}_d| = 24$ (Step 7 of Rule 7.1):

$$\text{CI-CF}(\mathbf{T}_d; \$_d) = \frac{1}{24}(b_1^4 + 3b_2^2 + 8b_1b_3 + 6a_1^2c_2 + 6c_4). \quad (7.29)$$

The CI-CF (Eq. 7.29) can be alternatively obtained by summing up the PCI-CFs represented by Eqs. 6.83–6.93 (page 155).

The four positions of the tetrahedral skeleton **3-5** are substituted by proligands selected from the proligand inventory \mathbf{L} (Eq. 6.73 on page 153). According to Theorem 7.6, the

same set of ligand-inventory functions as listed in Eqs. 6.74–6.76 (page 153) is introduced into the CI-CF (Eq. 7.29). After expansion (Step 8 of Rule 7.1), we obtain the following generating function for gross enumeration:

$$\begin{aligned}
 f_{3.5} = & \{A^4 + \dots\} + \{A^3B + \dots\} + \left\{\frac{1}{2}(A^3p + A^3\bar{p}) + \dots\right\} \\
 & + \{A^2B^2 + \dots\} + \left\{\frac{1}{2}(A^2p^2 + A^2\bar{p}^2) + \dots\right\} + \{A^2BX + \dots\} \\
 & + \left\{\frac{1}{2}(A^2Bp + A^2B\bar{p}) + \dots\right\} + \{A^2p\bar{p} + \dots\} + \left\{\frac{1}{2}(A^2pq + A^2\bar{p}\bar{q}) + \dots\right\} \\
 & + \{ABXY + \dots\} + \left\{2 \times \frac{1}{2}(ABXp + ABX\bar{p}) + \dots\right\} + \left\{\frac{1}{2}(ABp^2 + AB\bar{p}^2) + \dots\right\} \\
 & + \{2ABp\bar{p} + \dots\} + \left\{2 \times \frac{1}{2}(ABpq + AB\bar{p}\bar{q}) + \dots\right\} + \left\{\frac{1}{2}(Ap^3 + A\bar{p}^3) + \dots\right\} \\
 & + \left\{\frac{1}{2}(Ap^2\bar{p} + Ap\bar{p}^2) + \dots\right\} + \left\{\frac{1}{2}(Ap^2q + A\bar{p}^2\bar{q}) + \dots\right\} \\
 & + \left\{2 \times \frac{1}{2}(Ap\bar{p}q + Ap\bar{p}\bar{q}) + \dots\right\} + \left\{2 \times \frac{1}{2}(Apqr + A\bar{p}\bar{q}\bar{r}) + \dots\right\} \\
 & + \left\{\frac{1}{2}(p^4 + \bar{p}^4) + \dots\right\} + \left\{\frac{1}{2}(p^3\bar{p} + p\bar{p}^3) + \dots\right\} + \left\{\frac{1}{2}(p^3q + \bar{p}^3\bar{q}) + \dots\right\} \\
 & + \{p^2\bar{p}^2 + \dots\} + \left\{\frac{1}{2}(p^2\bar{p}q + p\bar{p}^2\bar{q}) + \dots\right\} + \left\{\frac{1}{2}(p^2q^2 + \bar{p}^2\bar{q}^2) + \dots\right\} \\
 & + \left\{\frac{1}{2}(p^2q\bar{q} + \bar{p}^2q\bar{q}) + \dots\right\} + \left\{\frac{1}{2}(p^2qr + \bar{p}^2\bar{q}\bar{r}) + \dots\right\} + \{p\bar{p}q\bar{q} + \dots\} \\
 & + \left\{2 \times \frac{1}{2}(p\bar{p}qr + p\bar{p}\bar{q}\bar{r}) + \dots\right\} + \left\{2 \times \frac{1}{2}(pqrs + \bar{p}\bar{q}\bar{r}\bar{s}) + \dots\right\}. \quad (7.30)
 \end{aligned}$$

The coefficients of the terms appearing in Eq. 7.30 are consistent with the list of promolecules of Fig. 6.9 (page 157), which has been obtained by the PCI method.

The generating function (Eq. 7.30) can be alternatively obtained by summing up the generating functions of the respective subgroups (Eqs. 6.94–6.102 on page 156), which are obtained by the PCI method. For example, the term ABXY in the gross generating function (Eq. 7.30) indicates the presence of one pair of enantiomers with the composition ABXY and corresponds to the term ABXY of $f_{3.5}(C_1)$ (Eq. 6.94). See Fig. 6.10 (page 158). The term $2 \times \frac{1}{2}(ABXp + ABX\bar{p})$ in Eq. 7.30 indicates the presence of two pairs of enantiomers (**6-82/6-82** and **6-83/6-83** in Fig. 6.11 on page 159), which are diastereomeric to each other. This term corresponds to the counterpart appearing in $f_{3.5}(C_1)$ (Eq. 6.94). The term $2ABp\bar{p}$ in Eq. 7.30 indicates the presence of two achiral promolecules with the composition $ABp\bar{p}$ and the point group C_s (**6-100** and **6-101** in Fig. 6.9 on page 157), which are diastereomeric to each other. The term $2ABp\bar{p}$ in Eq. 7.30 corresponds to the counterpart appearing in the generating function $f_{3.5}(C_s)$ (Eq. 6.96).

Proligand Method Applied to Allene Derivatives

As the second example, let us examine an allene skeleton **3-9** (Fig. 3.7 on page 68) by means of the above procedure (Rule 7.1). The skeleton **3-9** belongs to the point group D_{2d}

(Step 1–Step 3 of Rule 7.1). The permutation representation $\mathbf{P}_{D_{2d}}$ for the four positions of **3-12** is identical with the coset representation $\mathbf{D}_{2d}(/C_s)$, which has been collected in the $\mathbf{D}_{2d}(/C_s)$ -column of Table 3.2 on page 68 (Step 4 of Rule 7.1). The assignment of SIs (Step 5 of Rule 7.1) and the construction of PSIs (Step 6 of Rule 7.1) produce the PSIs for respective operations, as summarized in the PSI-column of Table 3.2. Thereby, a CI-CF is calculated to be the sum of the PSIs divided by $|D_{2d}| = 8$ (Step 7 of Rule 7.1):

$$\text{CI-CF}(\mathbf{D}_{2d}; \$d) = \frac{1}{8}(b_1^4 + 3b_2^2 + 2a_1^2c_2 + 2c_4). \quad (7.31)$$

The CI-CF (Eq. 7.31) can be alternatively obtained by summing up the PCI-CFs represented by Eqs. 6.106–6.113 (page 160).

The four positions of the allene skeleton **3-9** (= **6-102** as the top view, cf. Fig. 6.12 on page 159) are substituted by proligands selected from the proligand inventory \mathbf{L} (Eq. 6.73). According to Theorem 7.6, the same set of ligand-inventory functions as listed in Eqs. 6.74–6.76 (page 153) is introduced into the CI-CF (Eq. 7.31). After expansion (Step 8 of Rule 7.1), we obtain the following generating function for gross enumeration:

$$\begin{aligned} f_{3,9} = & \{A^4 + \dots\} + \{A^3B + \dots\} + \left\{ \frac{1}{2}(A^3p + A^3\bar{p}) + \dots \right\} \\ & + \{2A^2B^2 + \dots\} + \left\{ 3 \times \frac{1}{2}(A^2p^2 + A^2\bar{p}^2) + \dots \right\} + \{2A^2BX + \dots\} \\ & + \left\{ 3 \times \frac{1}{2}(A^2Bp + A^2B\bar{p}) + \dots \right\} + \{2A^2p\bar{p} + \dots\} \\ & + \left\{ 3 \times \frac{1}{2}(A^2pq + A^2p\bar{q}) + \dots \right\} + \{3ABXY + \dots\} \\ & + \left\{ 6 \times \frac{1}{2}(ABXp + ABX\bar{p}) + \dots \right\} + \left\{ 3 \times \frac{1}{2}(ABp^2 + AB\bar{p}^2) + \dots \right\} \\ & + \{4ABp\bar{p} + \dots\} + \left\{ 6 \times \frac{1}{2}(ABpq + ABp\bar{q}) + \dots \right\} + \left\{ \frac{1}{2}(Ap^3 + A\bar{p}^3) + \dots \right\} \\ & + \left\{ 3 \times \frac{1}{2}(Ap^2\bar{p} + Ap\bar{p}^2) + \dots \right\} + \left\{ 3 \times \frac{1}{2}(Ap^2q + A\bar{p}^2\bar{q}) + \dots \right\} \\ & + \left\{ 6 \times \frac{1}{2}(Ap\bar{p}q + Ap\bar{p}\bar{q}) + \dots \right\} + \left\{ 6 \times \frac{1}{2}(Apqr + A\bar{p}q\bar{r}) + \dots \right\} \\ & + \left\{ \frac{1}{2}(p^4 + \bar{p}^4) + \dots \right\} + \left\{ \frac{1}{2}(p^3\bar{p} + p\bar{p}^3) + \dots \right\} + \left\{ \frac{1}{2}(p^3q + \bar{p}^3\bar{q}) + \dots \right\} \\ & + \{2p^2\bar{p}^2 + \dots\} + \left\{ 3 \times \frac{1}{2}(p^2\bar{p}q + p\bar{p}^2\bar{q}) + \dots \right\} + \left\{ 3 \times \frac{1}{2}(p^2q^2 + \bar{p}^2\bar{q}^2) + \dots \right\} \\ & + \left\{ 3 \times \frac{1}{2}(p^2q\bar{q} + \bar{p}^2q\bar{q}) + \dots \right\} + \left\{ 3 \times \frac{1}{2}(p^2qr + \bar{p}^2q\bar{r}) + \dots \right\} + \{3p\bar{p}q\bar{q} + \dots\} \\ & + \left\{ 6 \times \frac{1}{2}(p\bar{p}qr + p\bar{p}q\bar{r}) + \dots \right\} + \left\{ 6 \times \frac{1}{2}(pqrs + \bar{p}q\bar{r}s) + \dots \right\}. \quad (7.32) \end{aligned}$$

The generating function (Eq. 7.32) can be alternatively obtained by summing up the symmetry-itemized generating functions represented by Eqs. 6.114–6.121 (page 161).

Proligand Method Applied to Ethylene Derivatives

Because the four positions of the ethylene skeleton **3-10** (Fig. 3.7 on page 68) construct an orbit governed by the coset representation D_{2h}/C_s'' (Steps 1–6 of Rule 7.1), the PSIs collected in Table 3.3 (page 69) are summed up and divided by 8 ($= |D_{2h}|$), so as to give the following CI-CF (Step 7 of Rule 7.1):

$$\text{CI-CF}(D_{2h}; \mathcal{S}_d) = \frac{1}{8}(b_1^4 + 3b_2^2 + a_1^4 + 3c_2^2). \quad (7.33)$$

Suppose that the four positions of the ethylene skeleton **3-10** (page 68) are substituted by proligands selected from the proligand inventory \mathbf{L} (Eq. 6.73 on page 153). According to Theorem 7.6, the same set of ligand-inventory functions as listed in Eqs. 6.74–6.76 (page 153) is introduced into the CI-CF (Eq. 7.33). After expansion (Step 8 of Rule 7.1), we obtain the following generating function for gross enumeration:

$$\begin{aligned} f_{\mathbf{3-10}} = & \{A^4 + \dots\} + \{A^3B + \dots\} + \left\{\frac{1}{2}(A^3p + A^3\bar{p}) + \dots\right\} \\ & + \{3A^2B^2 + \dots\} + \left\{3 \times \frac{1}{2}(A^2p^2 + A^2\bar{p}^2) + \dots\right\} + \{3A^2BX + \dots\} \\ & + \left\{3 \times \frac{1}{2}(A^2Bp + A^2B\bar{p}) + \dots\right\} + \{3A^2p\bar{p} + \dots\} \\ & + \left\{3 \times \frac{1}{2}(A^2pq + A^2\bar{p}\bar{q}) + \dots\right\} + \{6ABXY + \dots\} \\ & + \left\{6 \times \frac{1}{2}(ABXp + ABX\bar{p}) + \dots\right\} + \left\{3 \times \frac{1}{2}(ABp^2 + AB\bar{p}^2) + \dots\right\} \\ & + \{3ABp\bar{p} + \dots\} + \left\{6 \times \frac{1}{2}(ABpq + AB\bar{p}\bar{q}) + \dots\right\} + \left\{\frac{1}{2}(Ap^3 + A\bar{p}^3) + \dots\right\} \\ & + \left\{3 \times \frac{1}{2}(Ap^2\bar{p} + A\bar{p}p^2) + \dots\right\} + \left\{3 \times \frac{1}{2}(Ap^2q + A\bar{p}^2\bar{q}) + \dots\right\} \\ & + \left\{6 \times \frac{1}{2}(Ap\bar{p}q + A\bar{p}p\bar{q}) + \dots\right\} + \left\{6 \times \frac{1}{2}(Apqr + A\bar{p}\bar{q}\bar{r}) + \dots\right\} \\ & + \left\{\frac{1}{2}(p^4 + \bar{p}^4) + \dots\right\} + \left\{\frac{1}{2}(p^3\bar{p} + p\bar{p}^3) + \dots\right\} + \left\{\frac{1}{2}(p^3q + \bar{p}^3\bar{q}) + \dots\right\} \\ & + \{3p^2\bar{p}^2 + \dots\} + \left\{3 \times \frac{1}{2}(p^2\bar{p}q + p\bar{p}^2\bar{q}) + \dots\right\} + \left\{3 \times \frac{1}{2}(p^2q^2 + \bar{p}^2\bar{q}^2) + \dots\right\} \\ & + \left\{3 \times \frac{1}{2}(p^2q\bar{q} + \bar{p}^2q\bar{q}) + \dots\right\} + \left\{3 \times \frac{1}{2}(p^2qr + \bar{p}^2\bar{q}\bar{r}) + \dots\right\} + \{6p\bar{p}q\bar{q} + \dots\} \\ & + \left\{6 \times \frac{1}{2}(p\bar{p}qr + p\bar{p}\bar{q}\bar{r}) + \dots\right\} + \left\{6 \times \frac{1}{2}(pqrs + \bar{p}\bar{q}\bar{r}\bar{s}) + \dots\right\}. \quad (7.34) \end{aligned}$$

The coefficient of each term in Eq. 7.34 is consistent with the sum of the corresponding row of the tables obtained by the symmetry-itemized enumeration under the point group D_{2h} [31, Tables 3 and 4].

7.3.5 Enumeration of Achiral and Chiral Promolecules

Enumeration Under Maximum Chiral Point Groups

The maximum-chiral point group G_C of an achiral point group G is used to enumerate two chiral promolecules of an enantiomeric pair separately. Thereby, each promolecule, either chiral or achiral, is counted once under the action of G_C , where its *homomers* generated by G_C are regarded as being undistinguished. Thus, one promolecule is inequivalent to another promolecule under the action of G_C , so that each promolecule belongs to a one-membered orbit (equivalence class) under the action of G_C . For the sake of convenience, the set of inequivalent promolecules with the composition W_θ under the action of G_C is called *steric isomers*, although this terminology has somewhat ambiguous nature with respect to the term *isomer* (cf. Rule 2.2 on page 51).

Under the action of G , in contrast, an achiral promolecule belongs to a one-membered orbit, while a pair of enantiomeric chiral promolecules belongs to a two-membered orbit. For the sake of convenience, the set of inequivalent promolecules with the composition W_θ under the action of G is called *3D-structural isomers*, although this terminology also has somewhat ambiguous nature with respect to the term *isomer* (cf. Rule 2.2 on page 51).

The restriction of Def. 7.5 to G_C provides us with the following CI-CF for counting under the action of G_C :

Definition 7.6 (CI-CF for Counting Steric Isomers). Suppose that a permutation $p_g (\in \mathbf{P}_{G_C})$ has a cycle structure $(1^{v_1} 2^{v_2} \dots d^{v_d} \dots n^{v_n})^{(p_g)}$ ($\sum_{i=1}^n i v_i = n$), as shown in the hemispheric case of Def. 7.2. The CI-CF for counting steric isomers under the action of G_C is defined as follows:

$$\text{CI-CF}^{(C)}(\mathbf{P}_{G_C}; b_d) = \frac{1}{|\mathbf{P}_{G_C}|} \sum_{p_g \in \mathbf{P}_{G_C}} (b_1^{v_1} b_2^{v_2} \dots b_d^{v_d} \dots b_n^{v_n})^{(p_g)}. \quad (7.35)$$

To apply Def. 7.35 to a general case, the ligand inventory \mathbf{L} (Eq. 6.26 on page 140) is used as it is. A resulting promolecule has the composition W_θ represented by Eq. 6.27 (page 140). The composition can be alternatively represented by the partition $[\theta]$ shown in Eq. 6.28. Then, Theorem 7.6 is modified to meet G_C , so as to give the following theorem:

Theorem 7.7 (Fujita's Proligand Method of Counting Steric Isomers). Suppose that the n positions of a given skeleton belongs to \mathbf{P}_{G_C} , which is the maximum subgroup of \mathbf{P}_G . The CI-CF is shown in Eq. 7.35 of Def. 7.6. The ligand inventory \mathbf{L} (Eq. 6.26) is used to give derivatives with the composition W_θ . Let the symbol $A_\theta^{(C)}$ denote the number of such derivatives (orbits), which are inequivalent under the action of \mathbf{P}_{G_C} . A generating function for $A_\theta^{(C)}$ is represented as follows:

$$\sum_{[\theta]} A_\theta^{(C)} W_\theta = \text{CI-CF}^{(C)}(\mathbf{P}_{G_C}; b_d) \Big|_{b_d = \Sigma_{\mathbf{L}}}, \quad (7.36)$$

where the symbol $b_d = \Sigma_{\mathbf{L}}$ denotes the introduction of the following ligand-inventory function into the sphericity index b_d :

$$b_d = \sum_{\ell=1}^n X_\ell^d + \sum_{\ell=1}^{n'} p_\ell^d + \sum_{\ell=1}^{n''} \bar{p}_\ell^d. \quad (7.37)$$

Achiral and Chiral Promolecules

All of the rotations of a given point group \mathbf{G} are contained in its maximum-chiral subgroup \mathbf{G}_C , while all of the reflections (rotoreflections) are contained in the complementary set $\mathbf{G} - \mathbf{G}_C$. Hence, the summation in the right-hand side of Eq. 7.23 (Def. 7.5) is divided into two summations:

$$\begin{aligned} \text{CI-CF}(\mathbf{P}_G; \$_d) &= \frac{1}{|\mathbf{P}_G|} \sum_{p_g \in \mathbf{P}_{G_C}} (b_1^{v_1} b_2^{v_2} \dots b_d^{v_d} \dots b_n^{v_n})^{(p_g)} \\ &+ \frac{1}{|\mathbf{P}_G|} \sum_{p_g \in \mathbf{P}_{\mathbf{G}-\mathbf{P}_{G_C}}} (\$1^v \$2^v \dots \$d^v \dots \$n^v)^{(p_g)}, \end{aligned} \quad (7.38)$$

where the former summation is concerned with \mathbf{G}_C , while the latter summation is concerned with $\mathbf{G} - \mathbf{G}_C$. The former summation has the half value of the CI-CF represented by Eq. 7.35, because of $|\mathbf{P}_G| = 2|\mathbf{P}_{G_C}|$.

Let the symbol $A_\theta^{(a)}$ denote the number of achiral promolecules with the composition W_θ . Let the symbol $A_\theta^{(e)}$ denote the number of enantiomeric pairs of chiral promolecules with the composition W_θ . Because an achiral promolecule or a pair of enantiomers is counted once by Eq. 7.24 of Theorem 7.6, we obtain the following relationship:

$$\sum_{[\theta]} A_\theta W_\theta = \sum_{[\theta]} A_\theta^{(a)} W_\theta + \sum_{[\theta]} A_\theta^{(e)} W_\theta \quad (7.39)$$

On the other hand, because an achiral promolecule or each of enantiomers is counted once by Eq. 7.36 of Theorem 7.7, we obtain the following relationship:

$$\sum_{[\theta]} A_\theta^{(c)} W_\theta = \sum_{[\theta]} A_\theta^{(a)} W_\theta + 2 \sum_{[\theta]} A_\theta^{(e)} W_\theta \quad (7.40)$$

Thereby, we are able to evaluate $A_\theta^{(a)}$ and $A_\theta^{(e)}$ as follows:

$$\sum_{[\theta]} A_\theta^{(a)} W_\theta = 2 \sum_{[\theta]} A_\theta W_\theta - \sum_{[\theta]} A_\theta^{(c)} W_\theta \quad (7.41)$$

$$\sum_{[\theta]} A_\theta^{(e)} W_\theta = \sum_{[\theta]} A_\theta^{(c)} W_\theta - \sum_{[\theta]} A_\theta W_\theta \quad (7.42)$$

The evaluation of the right-hand side of Eq. 7.41 or Eq. 7.42 can be done by calculating the corresponding CI-CF preliminarily without the introduction of ligand-inventory functions. According to Eqs. 7.41 and 7.42, the CI-CF represented by Eq. 7.38 (equivalent to Eq. 7.23 of Def. 7.5) and the CI-CF represented by Eq. 7.35 are treated to give the following CI-CFs:

Definition 7.7 (CI-CFs for Counting Achiral Promolecules and Pairs of Enantiomers).

$$\begin{aligned} \text{CI-CF}^{(a)}(\mathbf{P}_G; \$_d) &= 2\text{CI-CF}(\mathbf{P}_G; \$_d) - \text{CI-CF}^{(c)}(\mathbf{P}_G; b_d) \\ &= \frac{2}{|\mathbf{P}_G|} \sum_{p_g \in \mathbf{P}_{\mathbf{G}-\mathbf{P}_{G_C}}} (\$1^v \$2^v \dots \$d^v \dots \$n^v)^{(p_g)} \end{aligned} \quad (7.43)$$

$$\begin{aligned}
 \text{CI-CF}^{(e)}(\mathbf{P}_G; \$_d) &= \text{CI-CF}^{(c)}(\mathbf{P}_G; b_d) - \text{CI-CF}(\mathbf{P}_G; \$_d) \\
 &= \frac{1}{|\mathbf{P}_G|} \left\{ \sum_{p_g \in \mathbf{P}_{G_C}} (b_1^{v_1} b_2^{v_2} \dots b_d^{v_d} \dots b_n^{v_n})^{(p_g)} \right. \\
 &\quad \left. - \sum_{p_g \in \mathbf{P}_G - \mathbf{P}_{G_C}} (\$_1^{v_1} \$_2^{v_2} \dots \$_d^{v_d} \dots \$_n^{v_n})^{(p_g)} \right\}. \tag{7.44}
 \end{aligned}$$

Note that $\text{CI-CF}^{(a)}(\mathbf{P}_G; \$_d)$ (Eq. 7.43) is two-times of the $(\mathbf{P}_G - \mathbf{P}_{G_C})$ -part of Eq. 7.38 (equivalent to Eq. 7.23 of Def. 7.5), while $\text{CI-CF}^{(e)}(\mathbf{P}_G; \$_d)$ (Eq. 7.44) is obtained by exchanging plus signs into minus signs with respect to the $(\mathbf{P}_G - \mathbf{P}_{G_C})$ -part of Eq. 7.38. Obviously, the sum of Eq. 7.43 and Eq. 7.44 is equal to Eq. 7.38 (equivalent to Eq. 7.23 of Def. 7.5).

By combining Eq. 7.41 with Eq. 7.43, we obtain the following theorem for counting achiral promolecules:

Theorem 7.8 (Fujita's Proligand Method of Counting Achiral Promolecules). As a continuation of Theorems 7.6 and 7.7, the number $A_\theta^{(a)}$ of achiral promolecules inequivalent under the action of \mathbf{P}_G is obtained by the following generating function:

$$\sum_{[\theta]} A_\theta^{(a)} W_\theta = \text{CI-CF}^{(a)}(\mathbf{P}_G; \$_d) \Big|_{\$_d = \Sigma_L}, \tag{7.45}$$

where the symbol $\$_d = \Sigma_L$ denotes the introduction of the following ligand-inventory functions into the respective sphericity indices $\$_d$ of Eq. 7.43:

$$a_d = \sum_{\ell=1}^n X_\ell^d \tag{7.46}$$

$$c_d = \sum_{\ell=1}^n X_\ell^d + 2 \sum_{\ell=1}^{n'} p_\ell^{d/2} \bar{p}_\ell^{d/2} \tag{7.47}$$

$$b_d = \sum_{\ell=1}^n X_\ell^d + \sum_{\ell=1}^{n'} p_\ell^d + \sum_{\ell=1}^{n'} \bar{p}_\ell^d \tag{7.48}$$

On the other hand, by combining Eq. 7.42 with Eq. 7.44, we obtain the following theorem for counting enantiomeric pairs of chiral promolecules:

Theorem 7.9 (Fujita's Proligand Method of Counting Pairs of Enantiomers). As a continuation of Theorems 7.6 and 7.7, the number $A_\theta^{(e)}$ of pairs of enantiomeric promolecules inequivalent under the action of \mathbf{P}_G is obtained by the following generating function:

$$\sum_{[\theta]} A_\theta^{(e)} W_\theta = \text{CI-CF}^{(e)}(\mathbf{P}_G; \$_d) \Big|_{\$_d = \Sigma_L}, \tag{7.49}$$

where the symbol $\$_d = \Sigma_L$ denotes the introduction of the following ligand-inventory functions into the respective sphericity indices $\$_d$ of Eq. 7.44:

$$a_d = \sum_{\ell=1}^n X_\ell^d \tag{7.50}$$

$$c_d = \sum_{\ell=1}^n X_\ell^d + 2 \sum_{\ell=1}^{n'} p_\ell^{d/2} \bar{p}_\ell^{d/2} \tag{7.51}$$

$$b_d = \sum_{\ell=1}^n X_{\ell}^d + \sum_{\ell=1}^{n'} p_{\ell}^d + \sum_{\ell=1}^{n'} \bar{p}_{\ell}^d \quad (7.52)$$

Examples of Enumerating Achiral and Chiral Promolecules

Achiral and Chiral Tetrahedral Promolecules

By starting from the CI-CF for the enumeration under T_d (Eq. 7.29), Eqs. 7.35, 7.43, and 7.44 are applied to the tetrahedral skeleton **3-5** (page 55) of T_d so as to give the following CI-CFs:

$$\text{CI-CF}^{(C)}(\mathbf{T}; b_d) = \frac{1}{12}(b_1^4 + 3b_2^2 + 8b_1b_3) \quad (7.53)$$

$$\text{CI-CF}^{(a)}(\mathbf{T}_d; \$_d) = \frac{1}{12}(6a_1^2c_2 + 6c_4) = \frac{1}{2}(a_1^2c_2 + c_4) \quad (7.54)$$

$$\text{CI-CF}^{(e)}(\mathbf{T}_d; \$_d) = \frac{1}{24}(b_1^4 + 3b_2^2 + 8b_1b_3 - 6a_1^2c_2 - 6c_4). \quad (7.55)$$

The ligand-inventory functions listed in Eqs. 6.74–6.76 are introduced into these CI-CFs. The expansions of the resulting equations give the respective generating functions in accord with Theorems 7.7 (steric isomers), 7.8 (achiral promolecules), and 7.9 (pairs of enantiomeric promolecules).



Exercise 7.3.

- Calculate the generating function obtained by introducing the ligand-inventory functions (Eqs. 6.74–6.76) into the CI-CFs (Eqs. 7.53–7.55).
- Compare the results with the data of the symmetry-itemized enumeration (Eqs. 6.94–6.102 on page 156) and with those of the gross enumeration (Eq. 7.30).

Achiral and Chiral Allene Derivatives

By starting from the CI-CF for the enumeration under D_{2d} (Eq. 7.31), Eqs. 7.35, 7.43, and 7.44 are applied to the allene skeleton **3-9** (= **6-102** on page 159) of D_{2d} so as to give the following CI-CFs:

$$\text{CI-CF}^{(C)}(\mathbf{D}_2; b_d) = \frac{1}{4}(b_1^4 + 3b_2^2) \quad (7.56)$$

$$\text{CI-CF}^{(a)}(\mathbf{D}_{2d}; \$_d) = \frac{1}{4}(2a_1^2c_2 + 2c_4) = \frac{1}{2}(a_1^2c_2 + c_4) \quad (7.57)$$

$$\text{CI-CF}^{(e)}(\mathbf{D}_{2d}; \$_d) = \frac{1}{8}(b_1^4 + 3b_2^2 - 2a_1^2c_2 - 2c_4). \quad (7.58)$$

The ligand-inventory functions listed in Eqs. 6.74–6.76 are introduced into these CI-CFs. The expansions of the resulting equations give the respective generating functions in accord with Theorems 7.7 (steric isomers), 7.8 (achiral promolecules), and 7.9 (pairs of enantiomeric promolecules).



Exercise 7.4.

- Calculate the generating function obtained by introducing the ligand-inventory functions (Eqs. 6.74–6.76) into the CI-CFs (Eqs. 7.56–7.58).
 - Compare the results with the data of the symmetry-itemized enumeration (Eqs. 6.114–6.121 on page 161) and with those of the gross enumeration (Eq. 7.32).
-

References

- [1] S. Fujita, “Symmetry and Combinatorial Enumeration in Chemistry”, Springer-Verlag, Berlin-Heidelberg (1991).
- [2] G. Pólya, *Compt. Rend.*, **201**, 1167–1169 (1935).
- [3] G. Pólya, *Helv. Chim. Acta*, **19**, 22–24 (1936).
- [4] G. Pólya, *Z. Kristal. (A)*, **93**, 415–443 (1936).
- [5] G. Pólya, *Acta Math.*, **68**, 145–254 (1937).
- [6] A. T. Balaban, ed., “Chemical Applications of Graph Theory”, Academic Press, London (1976).
- [7] G. Pólya, R. E. Tarjan, and D. R. Woods, “Notes on Introductory Combinatorics”, Birkhäuser, Boston (1983).
- [8] G. Pólya and R. C. Read, “Combinatorial Enumeration of Groups, Graphs, and Chemical Compounds”, Springer-Verlag, New York (1987).
- [9] D. H. Rouvray, *Chem. Soc. Rev.*, **3**, 355–372 (1974).
- [10] K. Balasubramanian, *Chem. Rev.*, **85**, 599–618 (1985).
- [11] D. Babic, D. J. Klein, J. V. Knop, and N. Trinajstić, in “Chemical Modelling: Applications and Theory”, The Royal Society of Chemistry, Cambridge (2004) Vol. 3 pp 127–170.
- [12] A. Milicevic and N. Trinajstić, in “Chemical Modelling: Applications and Theory”, The Royal Society of Chemistry, Cambridge (2006) Vol. 4 pp 405–469.
- [13] S. Fujita, *Croat. Chem. Acta*, **79**, 411–427 (2006).
- [14] S. Fujita, *Theor. Chem. Acc.*, **113**, 73–79 (2005).
- [15] S. Fujita, *Theor. Chem. Acc.*, **113**, 80–86 (2005).
- [16] S. Fujita, *Theor. Chem. Acc.*, **115**, 37–53 (2006).
- [17] S. Fujita, “Combinatorial Enumeration of Graphs, Three-Dimensional Structures, and Chemical Compounds”, University of Kragujevac, Faculty of Science, Kragujevac (2013).
- [18] S. Fujita, *Bull. Chem. Soc. Jpn.*, **83**, 1–18 (2010).

- [19] S. Fujita, *Theor. Chem. Acc.*, **117**, 353–370 (2007).
- [20] S. Fujita, *J. Comput. Chem. Jpn.*, **6**, 59–72 (2007).
- [21] S. Fujita, *Theor. Chem. Acc.*, **117**, 339–351 (2007).
- [22] S. Fujita, *MATCH Commun. Math. Comput. Chem.*, **57**, 265–298 (2007).
- [23] S. Fujita, *J. Comput. Chem. Jpn.*, **6**, 73–90 (2007).
- [24] S. Fujita, *MATCH Commun. Math. Comput. Chem.*, **57**, 299–340 (2007).
- [25] S. Fujita, *J. Math. Chem.*, **43**, 141–201 (2008).
- [26] S. Fujita, *Bull. Chem. Soc. Jpn.*, **81**, 193–219 (2008).
- [27] S. Fujita, *MATCH Commun. Math. Comput. Chem.*, **59**, 509–554 (2008).
- [28] S. Fujita, *Bull. Chem. Soc. Jpn.*, **81**, 1078–1093 (2008).
- [29] S. Fujita, *Bull. Chem. Soc. Jpn.*, **81**, 1423–1453 (2008).
- [30] S. Fujita, *MATCH Commun. Math. Comput. Chem.*, **67**, 5–24 (2012).
- [31] S. Fujita, *J. Math. Chem.*, **32**, 1–17 (2002).

8 Enumeration of Alkanes as 3D Structures¹

8.1 Surveys With Historical Comments

Enumeration of alkanes and monosubstituted alkanes with given carbon contents is a challenging target, which has been investigated by chemists and mathematicians over 130 years. In this chapter, the recent achievement provided by Fujita is discussed how it is in agreement with stereochemical and mathematical requirements.

There have been three epochs in the history of enumeration of *trees* (mathematically) or *alkanes* (chemically), as pointed out by Fujita's account article [1],

1. (First epoch) On the 1870s, Cayley a mathematician investigated problems of enumerating rooted trees [2] and trees [3,4]. He already recognized that the mathematical term *trees* was essentially equivalent to the chemical term *isomers represented by a formula* C_kH_{2k+2} , which were later specified in terms of a more systematic term *alkanes*. Henze and Blair [5,6] enumerated aliphatic alcohols (rooted trees) and alkanes (trees) after the development of recursive formulas.²
2. (Second epoch) On the same 1930s as the work conducted by Henze and Blair [5, 6], Pólya developed a versatile theorem named after him (cf. Section 7.2) [8]. The importance of Pólya's theorem is obvious by the fact that an English translation [9] appeared after 50 years. Mention should be made of several extensions [10,11], which enhanced the versatility of Pólya's theorem.

Pólya's theorem was applied to the enumeration of trees (as mathematical objects) or alkanes (as chemical objects).³ Pólya's enumeration of trees (or alkanes) was based on permutation groups without considering reflection operations, where trees were treated as graphs, but not as 3D structures.

More recently, Robinson et al. [13] reported enumeration of alkanes on the basis of Otter's method [14], where reflection operations were partially taken into consideration. However, their formulation suffered from an insufficient differentiation between permutation groups and point groups, as they misleadingly described "Taking the mir-

¹ This chapter is based on S. Fujita, "Graphs to Chemical Structures 4. Combinatorial Enumeration of Planted Three-Dimensional Trees as Stereochemical Models of Monosubstituted Alkanes", *Theor. Chem. Acc.*, **117**, 353–370 (2007); S. Fujita, "Graphs to Chemical Structures 5. Combinatorial Enumeration of Centroidal and Bicentroidal Three-Dimensional Trees as Stereochemical Models of Alkanes", *Theor. Chem. Acc.*, **117**, 339–351 (2007); S. Fujita, "Numbers of Monosubstituted Alkanes as Stereoisomers", *J. Comput. Chem. Jpn.*, **6**, 59–72 (2007); S. Fujita, "Enumeration of Alkanes as Stereoisomers", *MATCH Commun. Math. Comput. Chem.*, **57**, 265–298 (2007); and S. Fujita, "Alkanes as Stereoisomers. Enumeration by the Combination of Two Dichotomies for Three-Dimensional Trees", *MATCH Commun. Math. Comput. Chem.*, **57**, 299–340 (2007).

² Accomplishments up to 1936 have been summarized in a book on the graph theory [7, Chapter 4].

³ An introduction by Pólya himself has appeared in a textbook by Pólya et al. [12, Chapter 6].

ror image is equivalent to reversing the configuration” [13]. In other words, the enumerations by Pólya [8,9] and by Robinson et al. [13] did not arrive at the concept of sphericities.⁴

3. (Third epoch) On the first decade of this century, Fujita proposed the proligand method for enumerating promolecules as 3D structures (cf. Section 7.3) [16–18]. Immediately, Fujita’s proligand method was applied to the enumeration of alkanes as 3D structures [19,20]. Thereby, the interdisciplinary problems of enumerating planted trees (or monosubstituted alkanes) and trees (or alkanes), which have been pending over 130 years, have been solved in agreement with both stereochemical and mathematical requirements.

As described in Section 7.3, Fujita’s proligand method is based on the concept of sphericities of cycles, which succeeds the concept of sphericities of orbits for Fujita’s USCI approach (cf. Chapter 4). As a result, a cycle index with chirality fittingness (CI-CF) is devised in place of Pólya’s cycle index (CI), which lacks chirality fittingness. After an extension with respect to wreath products (coronas), Fujita’s proligand method was applied to recursive enumeration of planted 3D-trees as stereochemical models of monosubstituted alkanes [19,21]. Monosubstituted alkanes were categorized into primary, secondary, and tertiary ones, which were respectively enumerated by Fujita’s proligand method [22]. Effects of asymmetric and pseudoasymmetric centers [23] as well as of internal branching [24,25] on the numbers of achiral and chiral monosubstituted alkanes were investigated.

By starting from the data of monosubstituted alkanes (alkyl ligands), 3D-trees were enumerated as stereochemical models of alkanes according to Fujita’s proligand method [20,26], where they were categorized into centroidal and bicentroidal 3D-trees. After the proposal of a new dichotomy between balanced 3D-trees and unbalanced ones, 3D-trees (alkanes) were enumerated by combining the dichotomy with the other dichotomy between centroidal 3D-trees and bicentroidal ones [27]. An alternative method for enumerating 3D-trees was developed on the basis of the fact that they can be regarded dually as uninuclear and as binuclear promolecules [15]. Symmetry-itemized numbers of alkanes as 3D-structural isomers were obtained by applying Fujita’s proligand method [28]. Effect of asymmetric and pseudoasymmetric centers on the numbers of achiral and chiral 3D-trees (alkanes) was investigated [29]. Achiral and chiral alkanes of given carbon contents were categorized and enumerated by considering internal branching [30].

⁴ This point has been discussed in detail [15], where Fujita’s proligand method was combined with dual recognition as uninuclear and binuclear promolecules.

8.2 Enumeration of Alkyl Ligands as 3D Planted Trees

8.2.1 Enumeration of Methyl Proligands as Planted Promolecules

Let us first count proligands based on a trigonal pyramidal skeleton **8-1** of C_{3v} (**8-1** = **8-1a** in Fig. 8.1) by using a set of (inner) proligands listed in the following ligand inventory:

$$L_{\mathbf{8-1}} = \{H, X, Y; p, \bar{p}; q, \bar{q}; r, \bar{r}\}, \quad (8.1)$$

where the symbols H, X, and Y represent achiral proligands, while the pairs, p/\bar{p} , q/\bar{q} , and r/\bar{r} , denote enantiomeric pairs of chiral proligands. The proligands to be counted are referred to under the name *planted promolecules* [18,19]. Note that this enumeration presumes that such proligands as based on **8-1** are regarded as a hypothetical kind of promolecules (named *planted promolecules*), where the vacant bond of **8-1** is preliminarily substituted by a dummy substituent (\bullet). Or more concretely, this enumeration may be regarded as the enumeration of monosubstituted alkanes (e.g., alkanols, $\bullet = \text{OH}$).

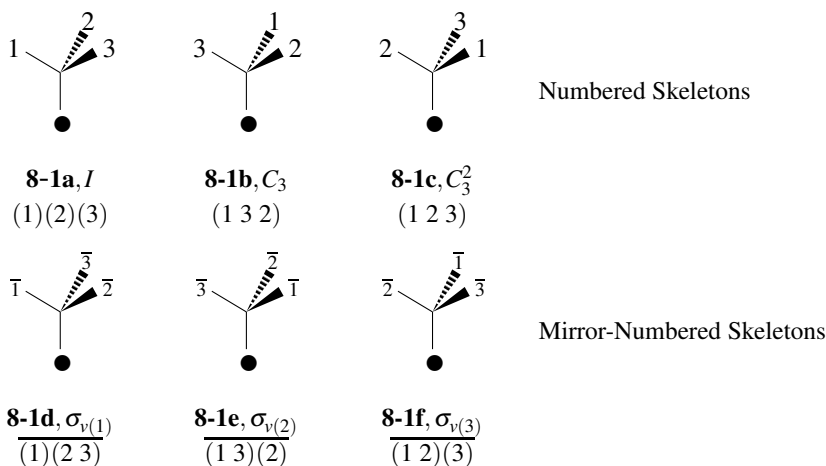


Fig. 8.1. Symmetry operations for a C_{3v} -skeleton (**8-1**). The identity operation (I) converts **8-1** into itself, where the resulting skeleton is denoted as **8-1a** [19]. The top row lists homomeric numbered skeletons, while the bottom row lists homomeric mirror-numbered skeletons.

According to Step 4 of Rule 7.1 described on page 183, the permutation representation $\mathbf{P}_{C_{3v}}$ is selected to be equal to the coset representation $C_{3v}/(C_s)$, as shown in Table 8.1 [18, 19]. The permutation representation $\mathbf{P}_{C_{3v}} (= C_{3v}/(C_s))$ is consistent to the behavior of the three positions of the trigonal pyramid skeleton **8-1** under the action of the point group C_{3v} , as depicted in Fig. 8.1. The top row of Fig. 8.1 lists homomeric numbered skeletons, while the bottom row lists homomeric mirror-numbered skeletons. For example, the reflection $\sigma_{v(1)}$, which is concerned with the mirror plane contained in the plane of 1—C— \bullet , fixes

Table 8.1. Operations of C_{3v} and Coset Representation $C_{3v}/(C_s)$ [19]

operation $g \in C_{3v}$	$C_{3v}/(C_s)$ (product of cycles)	PSI (product of sphericity indices)	cycle term
I	(1)(2)(3)	b_1^3	s_1^3
C_3	(1 3 2)	b_3	s_3
C_3^2	(1 2 3)	b_3	s_3
$\sigma_{v(1)}$	$\overline{(1)(2\ 3)}$	$a_1 c_2$	$s_1 s_2$
$\sigma_{v(2)}$	$\overline{(1\ 3)(2)}$	$a_1 c_2$	$s_1 s_2$
$\sigma_{v(3)}$	$\overline{(1\ 2)(3)}$	$a_1 c_2$	$s_1 s_2$

the 1-position and exchanges the 2- and 3-positions as found in **8-1d** (with accompanied by ligand reflections). Thereby it generates a permutation (a product of cycles):

$$\sigma_{v(1)} \sim \left(\begin{array}{ccc} 1 & 2 & 3 \\ \overline{1} & \overline{3} & \overline{2} \end{array} \right) = \overline{(1)(2\ 3)}, \quad (8.2)$$

where an overbar represents a ligand reflection.

Steps 5 and 6 of Rule 7.1 (page 183) generate the PSIs collected in the PSI-column of Table 8.1. Then, according to Eq. 7.23 of Def. 7.5 (Step 7 of Rule 7.1), the corresponding CI-CF is obtained as follows:

$$\text{CI-CF}_{\mathbf{8-1}}(C_{3v}, \$d) = \frac{1}{6}(b_1^3 + 2b_3 + 3a_1 c_2), \quad (8.3)$$

which counts achiral planted promolecules or enantiomeric pairs of chiral planted promolecules.

Because a set of (inner) proligands is selected from the ligand inventory $\mathbf{L}_{\mathbf{8-1}}$ (Eq. 8.1), the following ligand-inventory functions are calculated according to Theorem 7.6 (Step 8 of Rule 7.1):

$$a_d = H^d + X^d + Y^d \quad (8.4)$$

$$c_d = H^d + X^d + Y^d + 2p^{d/2}\overline{p}^{d/2} + 2q^{d/2}\overline{q}^{d/2} + 2r^{d/2}\overline{r}^{d/2} \quad (8.5)$$

$$b_d = H^d + X^d + Y^d + p^d + \overline{p}^d + q^d + \overline{q}^d + r^d + \overline{r}^d. \quad (8.6)$$

These ligand-inventory functions are introduced into Eq. 8.3 to give the following generating function:

$$\begin{aligned} f_{\mathbf{8-1}} = & \{H^3 + X^3 + Y^3\} + \{H^2Y + H^2X + \dots\} + \text{HXY} \\ & + \left\{ \frac{1}{2}(H^2p + H^2\overline{p}) + \dots \right\} + \left\{ \frac{2}{2}(\text{HXp} + \text{HX}\overline{p}) + \dots \right\} + \left\{ \frac{1}{2}(\text{Hp}^2 + \text{H}\overline{p}^2) + \dots \right\} \\ & + \{2\text{Hp}\overline{p} + \dots\} + \left\{ \frac{2}{2}(\text{Hpq} + \text{H}\overline{p}\overline{q}) + \dots \right\} + \left\{ \frac{2}{2}(\text{Hp}\overline{q} + \text{H}\overline{p}q) + \dots \right\} \end{aligned}$$

$$\begin{aligned}
& + \left\{ \frac{1}{2}(p^3 + \bar{p}^3) + \dots \right\} + \left\{ \frac{1}{2}(p^2\bar{p} + p\bar{p}^2) + \dots \right\} + \left\{ \frac{1}{2}(p^2q + \bar{p}^2\bar{q}) + \dots \right\} \\
& + \left\{ \frac{1}{2}(p^2\bar{q} + \bar{p}^2q) + \dots \right\} + \left\{ \frac{2}{2}(pqr + \bar{p}\bar{q}\bar{r}) \right\} + \left\{ \frac{2}{2}(pq\bar{r} + \bar{p}\bar{q}r) + \dots \right\} \\
& + \left\{ \frac{2}{2}(p\bar{p}\bar{q} + p\bar{p}q) + \dots \right\}. \tag{8.7}
\end{aligned}$$

This generating function derived from Eq. 8.3 is essentially equivalent to the one described in [18, Eq. 40 of Example 2].

For further discussions, the planted promolecules enumerated in Eq. 8.7 are shown in Fig. 8.2, where a representative of each pair of enantiomeric promolecules or that of an achiral promolecule is depicted with respect to the coefficient of each term of Eq. 8.7. For example, **8-2** (H^3) is a representative of achiral promolecules having H^3 , X^3 , Y^3 . The two promolecules **8-6** and **8-7** with the composition HXp corresponds to the term $\frac{2}{2}(HXp + HX\bar{p})$, which indicates the presence of two pairs of planted promolecules, because each enantiomeric pair is represented by the term $\frac{1}{2}(HXp + HX\bar{p})$. The two pairs are inequivalent under the action of C_{3v} , and diastereomeric to each other in accord with Def. 2.7 (page 40).

By starting from the PSI-column of Table 8.1, the CI-CF for counting steric isomers of planted promolecules is obtained according to Eq. 7.35 (Def. 7.6 on page 187) as follows:

$$\text{CI-CF}_{\mathbf{8-1}}^{(C)}(C_3, b_d) = \frac{1}{3}(b_1^3 + 2b_3). \tag{8.8}$$

Theorem 7.7 (page 187) shows that this CI-CF can be used to count achiral planted promolecules and chiral planted promolecules, where two enantiomers of each pair are counted separately.

The ligand-inventory functions (Eqs. 8.4–8.6) are introduced into Eq. 8.8 to give the following generating function for enumerating steric isomers:

$$\begin{aligned}
f_{\mathbf{8-1}}^{(C)} &= \{H^3 + X^3 + Y^3\} + \{H^2Y + H^2X + \dots\} + 2HXY \\
& + \left\{ \frac{2}{2}(H^2p + H^2\bar{p}) + \dots \right\} + \left\{ \frac{4}{2}(HXp + HX\bar{p}) + \dots \right\} + \left\{ \frac{2}{2}(Hp^2 + H\bar{p}^2) + \dots \right\} \\
& + \{2H\bar{p}\bar{p} + \dots\} + \left\{ \frac{4}{2}(Hpq + H\bar{p}\bar{q}) + \dots \right\} + \left\{ \frac{4}{2}(Hp\bar{q} + H\bar{p}q) + \dots \right\} \\
& + \left\{ \frac{2}{2}(p^3 + \bar{p}^3) + \dots \right\} + \left\{ \frac{2}{2}(p^2\bar{p} + p\bar{p}^2) + \dots \right\} + \left\{ \frac{2}{2}(p^2q + \bar{p}^2\bar{q}) + \dots \right\} \\
& + \left\{ \frac{2}{2}(p^2\bar{q} + \bar{p}^2q) + \dots \right\} + \left\{ \frac{4}{2}(pqr + \bar{p}\bar{q}\bar{r}) \right\} + \left\{ \frac{4}{2}(pq\bar{r} + \bar{p}\bar{q}r) + \dots \right\} \\
& + \left\{ \frac{4}{2}(p\bar{p}\bar{q} + p\bar{p}q) + \dots \right\} \tag{8.9}
\end{aligned}$$

This generating function derived from Eq. 8.8 is essentially equivalent to the one described in [18, Eq. 45 of Example 3].⁵

⁵ The term $\frac{1}{2}(H^2p + H^2\bar{p}) + \dots$ of [18, Eq. 45 of Example 3] should be read as $\frac{2}{2}(H^2p + H^2\bar{p}) + \dots$.

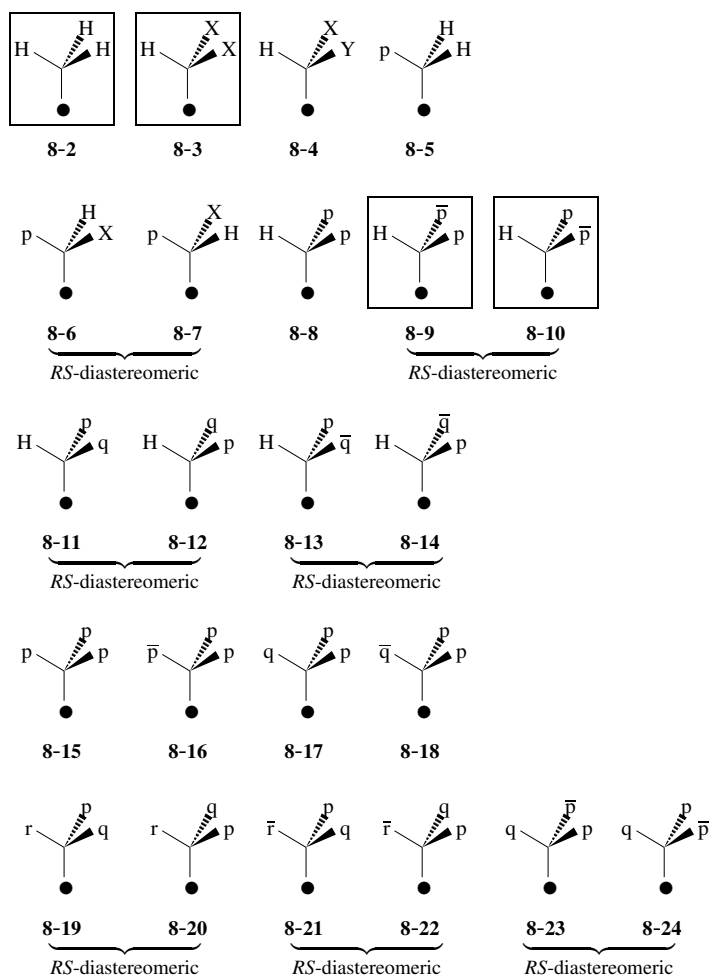


Fig. 8.2. Planted promolecules based on the trigonal pyramid skeleton of C_{3v} [19]. The symbols H, X, and Y represent achiral proligands, while the pairs, p/\bar{p} , q/\bar{q} , and r/\bar{r} , denote enantiomeric pairs of chiral proligands. The planted promolecules surrounded by a frame box are achiral. The other planted promolecules are chiral so that an appropriate enantiomer is depicted as a representative for each enantiomeric pair.

By combining Eq. 8.3 with Eq. 8.8 in accord with Eq. 7.43 (Def. 7.7 on page 188), the CI-CF for counting achiral planted promolecules is obtained as follows:

$$\begin{aligned} \text{CI-CF}_{8-1}^{(a)}(C_{3v}, \mathcal{S}_d) &= 2\text{CI-CF}_{8-1}(C_{3v}, \mathcal{S}_d) - \text{CI-CF}_{8-1}^{(C)}(C_3, b_d) \\ &= a_1 c_2, \end{aligned} \quad (8.10)$$

which counts achiral planted promolecules only according to Theorem 7.8 on page 189.

The ligand-inventory functions (Eqs. 8.4–8.6) are introduced into Eq. 8.10 to give the following generating function for enumerating achiral planted promolecules:

$$\begin{aligned} f_{\mathbf{8-1}}^{(a)} &= 2f_{\mathbf{8-1}} - f_{\mathbf{8-1}}^{(c)} \\ &= \{H^3 + X^3 + Y^3\} + \{H^2Y + H^2X + \dots\} + \{2H\bar{p}\bar{p} + \dots\}. \end{aligned} \quad (8.11)$$

This generating function derived from Eq. 8.10 is essentially equivalent to the one described in [18, Eq. 52 of Example 4].

By combining Eq. 8.3 with Eq. 8.8 in accord with Eq. 7.44 (Def. 7.7 on page 188), the CI-CF for counting pairs of enantiomeric planted promolecules is obtained as follows:

$$\begin{aligned} \text{CI-CF}_{\mathbf{8-1}}^{(e)}(C_{3v}, \$d) &= \text{CI-CF}_{\mathbf{8-1}}^{(c)}(C_3, b_d) - \text{CI-CF}_{\mathbf{8-1}}(C_{3v}, \$d) \\ &= \frac{1}{6}(b_1^3 + 2b_3 - 3a_1c_2), \end{aligned} \quad (8.12)$$

which counts pairs of chiral planted promolecules only according to Theorem 7.9 on page 189.

The ligand-inventory functions (Eqs. 8.4–8.6) are introduced into Eq. 8.12 to give the following generating function for enumerating pairs of enantiomeric planted promolecules:

$$\begin{aligned} f_{\mathbf{8-1}}^{(e)} &= f_{\mathbf{8-1}}^{(c)} - f_{\mathbf{8-1}} \\ &= \text{HXY} \\ &\quad + \left\{ \frac{1}{2}(H^2\bar{p} + H^2\bar{p}) + \dots \right\} + \left\{ \frac{2}{2}(HX\bar{p} + HX\bar{p}) + \dots \right\} + \left\{ \frac{1}{2}(H\bar{p}^2 + H\bar{p}^2) + \dots \right\} \\ &\quad + \left\{ \frac{2}{2}(H\bar{p}q + H\bar{p}q) + \dots \right\} + \left\{ \frac{2}{2}(H\bar{p}\bar{q} + H\bar{p}\bar{q}) + \dots \right\} \\ &\quad + \left\{ \frac{1}{2}(p^3 + \bar{p}^3) + \dots \right\} + \left\{ \frac{1}{2}(p^2\bar{p} + p\bar{p}^2) + \dots \right\} + \left\{ \frac{1}{2}(p^2q + \bar{p}^2\bar{q}) + \dots \right\} \\ &\quad + \left\{ \frac{1}{2}(p^2\bar{q} + \bar{p}^2q) + \dots \right\} + \left\{ \frac{2}{2}(pqr + \bar{p}\bar{q}\bar{r}) \right\} + \left\{ \frac{2}{2}(p\bar{q}\bar{r} + \bar{p}q\bar{r}) + \dots \right\} \\ &\quad + \left\{ \frac{2}{2}(p\bar{p}\bar{q} + p\bar{p}q) + \dots \right\}. \end{aligned} \quad (8.13)$$

This generating function derived from Eq. 8.12 is essentially equivalent to the one described in [18, Eq. 53 of Example 4].

The generating function $f_{\mathbf{8-1}}^{(a)}$ (Eq. 8.11) indicates the presence of three types of planted promolecules, each of which is surrounded by a frame in Fig. 8.2, i.e., **8-2** with the composition H^3 , **8-3** with the composition HX^2 (appearing as a representative H^2X in Eq. 8.11), as well as **8-9** and **8-10** with the composition $H\bar{p}\bar{p}$. They are all achiral.

The generating function $f_{\mathbf{8-1}}^{(e)}$ (Eq. 8.13) covers the remaining planted promolecules listed in Fig. 8.2 (without being surrounded by a frame). Each represents an appropriate representative selected from a pair of enantiomeric planted promolecules.

8.2.2 Recursive Enumeration of Alkyl ligands as Planted Promolecules

Preliminary Examination

Before we discuss recursive enumeration, let us evaluate the number of achiral alkyl ligands of carbon content 5 by starting from the data of carbon contents up to 4 ($k = 1-4$) listed in Fig. 8.3. Note that the symbol Z represents a root (e.g., the symbol ● in Fig. 8.2) or an achiral mono-valent ligand (e.g., -OH for alkanols). We use the CI-CF for counting achiral planted promolecules (Eq. 8.10).

The ligand-inventory functions (Eqs. 8.4–8.6) are rewritten to meet this evaluation. The data listed in Fig. 8.3 ($k = 1-4$) give the following ligand-inventory functions with respect of carbon contents up to 4:

$$a_d = 1 + x^d + x^{2d} + 2x^{3d} + 3x^{4d} \quad (8.14)$$

$$\begin{aligned} c_d &= (1 + x^d + x^{2d} + 2x^{3d} + 3x^{4d}) + (2x^{4d}) \\ &= 1 + x^d + x^{2d} + 2x^{3d} + 5x^{4d} \end{aligned} \quad (8.15)$$

$$\begin{aligned} b_d &= (1 + x^d + x^{2d} + 2x^{3d} + 3x^{4d}) + (2x^{4d}) \\ &= 1 + x^d + x^{2d} + 2x^{3d} + 5x^{4d}, \end{aligned} \quad (8.16)$$

where the coefficient of a dummy variable x^k represents the number of inner alkyl ligands with carbon content k . The value 1 corresponds to the substitution of a hydrogen atom. The term $2x^{3d}$, for example, represents the substitution of the number d of alkyl ligands with carbon content 3, where the coefficient 2 indicates that there are two alkyl ligands (**8-27** and **8-28**). The CI-CF represented by Eq. 8.10 is modified to take account of one central atom to be added by multiplying x . Then, the ligand-inventory functions (Eqs. 8.14 and 8.15) are introduced into the modified CI-CF. Thereby, the following generating function is obtained:

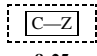
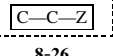
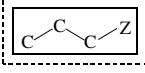
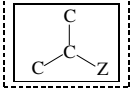
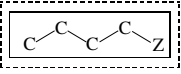
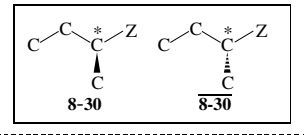
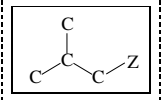
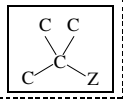
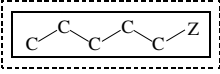
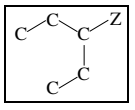
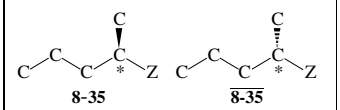
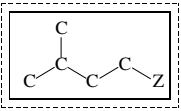
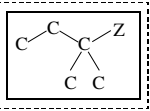
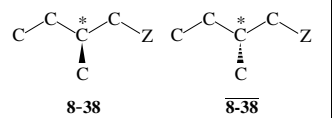
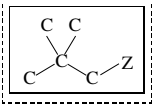
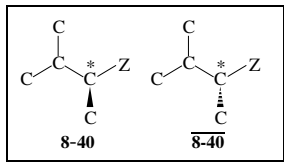
$$\begin{aligned} f_{k=5}^{(a)} &= xa_1c_2 \\ &= x(1 + x + x^2 + 2x^3 + 3x^4)(1 + x^2 + x^4 + 2x^6 + 5x^8) \\ &= x + x^2 + 2x^3 + 3x^4 + 5x^5 + \dots, \end{aligned} \quad (8.17)$$

where the terms up to $k = 5$ are effective. The coefficient 5 of the term $5x^5$ indicates the presence of five achiral alkyl ligands, which is confirmed to be **8-33**, **8-34**, **8-36**, **8-37**, and **8-39**, as depicted in Fig. 8.3.

Recursive Enumeration of Diploids

Although the terms up to x^5 appearing in Eq. 8.17 can be used as a ligand-inventory function a_1 for calculating $f_{k=6}^{(a)} = xa_1c_2$ recursively, the other ligand-inventory function c_2 should be evaluated in a rational fashion. To do this task, Fujita has proposed the concept of *diploids* [19]. Let us transform Eq. 8.15 into the following expression:

$$c_{2d} = (1 + x^{2d} + x^{4d} + 2x^{6d} + 3x^{8d}) + (2x^{8d})$$

CC ^{a)}	Achiral	Chiral	
$k = 1$	 8-25		
$k = 2$	 8-26		
$k = 3$	 8-27	 8-28	
$k = 4$	 8-29	 8-30	
	 8-31	 8-32	
$k = 5$	 8-33	 8-34	 8-35
	 8-36	 8-37	 8-38
	 8-39	 8-40	

^{a)}CC: carbon content.

Fig. 8.3. Monosubstituted alkanes of lower carbon contents ($k = 1-5$) [1]. Each constitutional isomer is surrounded by a broken-lined box; each 3D-structural isomers (each achiral molecule or each pair of enantiomeric molecules) is surrounded by a straight-lined box; and each molecule represents a steric isomer. The symbol Z denotes an atom (e.g., Cl), an achiral ligand (e.g., OH), or a root (the symbol ● in Fig. 8.2), which is regarded as a monovalent substituent. Hydrogen atoms are omitted for the sake of simplicity. Each asymmetric center is denoted by an asterisk.

$$= 1 + (x \cdot x)^d + (x^2 \cdot x^2)^d + 2(x^3 \cdot x^3)^d + 5(x^4 \cdot x^4)^d. \quad (8.18)$$

Thereby, each enantiospheric orbit concerned with c_{2d} accommodates an enantiomeric pair of inner proligands, as expressed by $(x \cdot x)$, $(x^2 \cdot x^2)$, etc., which correspond to ordered set (diploid), i.e., $\{\mathbf{8-25}, \mathbf{8-25}\}$, $\{\mathbf{8-26}, \mathbf{8-26}\}$, etc. for achiral inner proligands. As for chiral proligands, a pair of diploids, $\{\mathbf{8-30}, \mathbf{8-30}\}$ and $\{\overline{\mathbf{8-30}}, \mathbf{8-30}\}$, should be taken into consideration in the form of the term $2(x^4 \cdot x^4)^d$ (among $5(x^4 \cdot x^4)^d$). If we focus our attention on the first promolecule of each diploid, the enumeration of diploids corresponds to the enumeration of steric isomers. It follows that the CI-CF represented by Eq. 8.8 is modified by substituting c_2 and c_6 for b_1 and b_3 respectively to calculate a generating function for counting diploids:

$$\begin{aligned} f_{k=5}^{(D)} &= \frac{x^2}{3}(c_2^3 + 2c_6) \\ &= \frac{x^2}{3}\{(1 + x^2 + x^4 + 2x^6 + 5x^8)^3 + 2(1 + x^6 + x^{12} + 2x^{18} + 5x^{24})\} \\ &= x^2 + x^4 + 2x^6 + 5x^8 + 11x^{10} + \dots, \end{aligned} \quad (8.19)$$

The coefficient 11 of the term $11x^{10}$ represents the presence of eleven diploids which are generated on the basis of $\mathbf{8-37}$ – $\overline{\mathbf{8-40}}$. For example, a diploid $\{\mathbf{8-25}, \mathbf{8-25}\}$ ($(x \cdot x)$) and another diploid $\{\mathbf{8-27}, \mathbf{8-27}\}$ ($(x^3 \cdot x^3)$) produces two diploids represented by $\{\mathbf{8-35}, \overline{\mathbf{8-35}}\}$ ($(x^5 \cdot x^5)$) and $\{\overline{\mathbf{8-35}}, \mathbf{8-35}\}$ ($(x^5 \cdot x^5)$), where two carbons are added by multiplying x^2 in Eq. 8.18.

Recursive Enumeration of Steric Isomers for Alkyl Ligands

The parallelism between diploids and steric isomers permits us to enumerate steric isomers for alkyl ligands in a similar way. The CI-CF represented by Eq. 8.8 is modified to take account of one central atom to be added by multiplying x . Then, the ligand-inventory function (Eqs. 8.16) is introduced into the modified CI-CF. Thereby, the following generating function is obtained:

$$\begin{aligned} f_{k=5}^{(C)} &= \frac{x}{3}(b_1^3 + 2b_3) \\ &= \frac{x}{3}\{(1 + x + x^2 + 2x^3 + 5x^4)^3 + 2(1 + x^3 + x^6 + 2x^9 + 5x^{12})\} \\ &= x + x^2 + 2x^3 + 5x^4 + 11x^5 + \dots, \end{aligned} \quad (8.20)$$

The coefficient 11 of the term $11x^5$ represents the presence of eleven alkyl ligands depicted in Fig. 8.3.

8.2.3 Functional Equations for Recursive Enumeration of Alkyl ligands

Achiral-Structure Generator and Diploid Generator

The derivation of Eq. 8.17 ($k = 5$) from Eqs. 8.14 and 8.15 ($k = 1-4$), the derivation of Eq. 8.19 ($k = 5$) from Eq. 8.15 ($k = 1-4$), and the derivation of Eq. 8.20 ($k = 5$) from Eq. 8.16 ($k = 1-4$) can be systematized by devising *functional equations*.

Let us consider the following generating functions with infinite terms:

$$a(x) = \sum_{k=0}^{\infty} A_k x^k \quad (8.21)$$

$$c(x^2) = \sum_{k=0}^{\infty} \gamma_k x^{2k}, \quad (8.22)$$

where $A_0 (= 1)$ or $\gamma_0 (= 1)$ is an initial value for representing a hydrogen atom or a hydrogen diploid. These infinite polynomials are extensions of Eq. 8.17 and Eq. 8.19 respectively.

The derivation of Eq. 8.17 ($k = 5$) is extended into the following functional equation:

$$a(x) = 1 + xa(x)c(x^2). \quad (8.23)$$

This functional equation is an algebraic expression for implementing an achiral structure generator (Fig. 8.4) on the basis of Fujita's proligand method, where the left-hand side ($k = n + 1$) is evaluated from the right-hand side ($k \leq n$) recursively. The first term 1 is added to evaluate a hydrogen atom and the multiplication of x corresponds to a central carbon newly-formed. This equation has been once noted by Fujita [19].

The process of obtaining Eq. 8.17 is rewritten as follows. According to Eq. 8.23, Eqs. 8.14 and 8.15 are translated into a functional equation up to carbon content 4:

$$a(x) = 1 + x + x^2 + 2x^3 + 3x^4 \quad (8.24)$$

$$c(x^2) = 1 + x^2 + x^4 + 2x^6 + 5x^8. \quad (8.25)$$

Thereby, Eq. 8.17 is translated to represent the recursive process:

$$\begin{aligned} a(x) &= 1 + xa(x)c(x^2) \\ &= 1 + x(1 + x + x^2 + 2x^3 + 3x^4)(1 + x^2 + x^4 + 2x^6 + 5x^8) \\ &= 1 + x + x^2 + 2x^3 + 3x^4 + 5x^5 + \dots \end{aligned} \quad (8.26)$$

Hence, we are able to adopt six terms up to the term $5x^5$ for the purpose of the next recursion ($k = 5$ to $k = 6$). This adoption is illustrated in Fig. 8.4, where the increment of five 3D structures with carbon content 5 are shown in the upper-right frame.

The achiral-structure generator shown in Fig. 8.4 is applied repeatedly according to Eq. 8.23. After infinite recursion, we can obtain a set (\mathbf{A}_∞) of alkyl ligands (or monosubstituted alkanes) as 3D-structural isomers up to infinite carbon content, as shown in Eq. 8.21. Then the set \mathbf{A}_∞ is characterized by a generating function:

$$\begin{aligned} a(x) &= \sum_{k=0}^{\infty} A_k x^k \\ &= 1 (= A_0) + x + x^2 + 2x^3 + 3x^4 + 5x^5 + 8x^6 + 14x^7 + 23x^8 + 41x^9 + 69x^{10} \\ &\quad + 122x^{11} + 208x^{12} + 370x^{13} + 636x^{14} + 1134x^{15} \\ &\quad + 1963x^{16} + 3505x^{17} + 6099x^{18} + 10908x^{19} + 19059x^{20} \end{aligned}$$

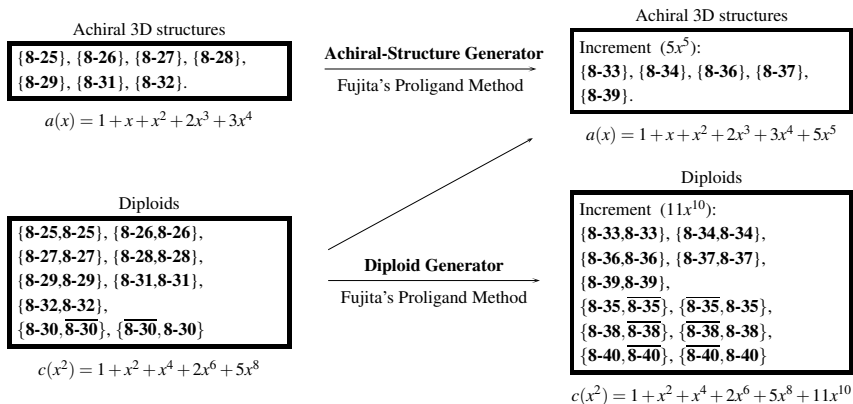


Fig. 8.4. Achiral-structure generator and diploid generator based on Fujita's proligand method. Monosubstituted alkanes are generated under the action of the C_{3v} point group (the coset representation $C_{3v}/(C_s)$). Each constitution which is derived by degeneration of component 3D structures involved in a pair of braces is counted just once. The number of substituted alkanes of carbon content k as constitutional isomers appears as the coefficient of the term x^k .

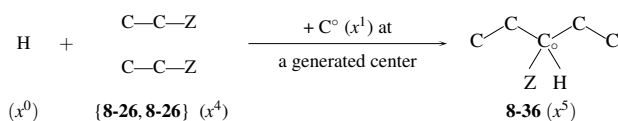


Fig. 8.5. Example of the effect of an achiral-structural generator. A central carbon (C°) is attached by a hydrogen (x^0) and the diploid {8-26, 8-26} (x^4).

$$+ 34129x^{21} + 59836x^{22} + 107256x^{23} + 188576x^{24} + 338322x^{25} + \dots, \quad (8.27)$$

where $A_0 (= 1)$ is an initial value for representing a hydrogen atom. A Maple programming code for a recursive calculation up to carbon content 100 and the resulting data in tabular form have been reported [21].

The effect of an achiral-structure generator (Fig. 8.4) is illustrated in Fig. 8.5, where a central carbon (C°) is attached by a hydrogen (x^0) and the diploid {8-26, 8-26} (x^4) to give an achiral alkyl ligand 8-36 of carbon content 5. Thereby, it contributes by 1 to the coefficient 5 of the term $5x^5$. Note that the symbol Z is a vacant bond (the symbol ● in Fig. 8.2) for an alkyl ligand or a monovalent ligand (e.g., OH and Cl) for a monosubstituted alkane.

On the other hand, the derivation of Eq. 8.19 ($k = 5$) is extended into the following functional equation:

$$c(x^2) = 1 + \frac{x^2}{3}(c(x^2)^3 + 2c(x^6)). \quad (8.28)$$

This functional equation is an algebraic expression for implementing a diploid generator (Fig. 8.4), where the left-hand side ($k = n + 1$) is evaluated from the right-hand side ($k \leq n$) recursively. The first term 1 is added to evaluate a hydrogen diploid and the multiplication

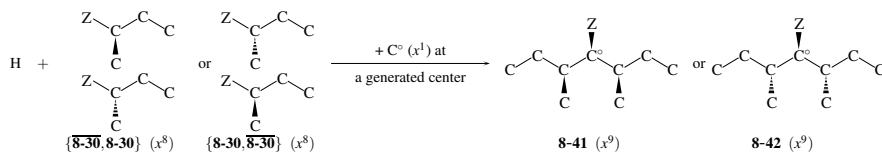


Fig. 8.6. Pseudoasymmetric alkyl ligands or monosubstituted alkanes (**8-41** and **8-42**) of carbon content 9, where an explicit effect of the diploid generator is realized.

of x^2 corresponds to two central carbons newly-formed. This equation has been once noted by Fujita [19].

The diploid generator shown in Fig. 8.4 is applied repeatedly according to Eq. 8.28. After infinite recursion, we can obtain a set (Γ_∞) of diploids for alkyl ligands (or diploids for monosubstituted alkanes) up to infinite carbon content, as shown in Eq. 8.22. Then the set Γ_∞ is characterized by a generating function:

$$\begin{aligned}
 c(x^2) &= \sum_{k=0}^{\infty} \gamma_{2k} x^{2k} \\
 &= 1 (= \gamma_0) + x^2 + x^4 + 2x^6 + 5x^8 + 11x^{10} \\
 &\quad + 28x^{12} + 74x^{14} + 199x^{16} + 551x^{18} + 1553x^{20} \\
 &\quad + 4436x^{22} + 12832x^{24} + 37496x^{26} + 110500x^{28} + 328092x^{30} \\
 &\quad + 980491x^{32} + 2946889x^{34} + 8901891x^{36} + 27012286x^{38} + 82300275x^{40} \\
 &\quad + 251670563x^{42} + 772160922x^{44} + 2376294040x^{46} + 7333282754x^{48} \\
 &\quad + 22688455980x^{50} + \dots, \tag{8.29}
 \end{aligned}$$

where $\gamma_0 (= 1)$ is an initial value for representing a hydrogen diploid.

As exemplified in Fig. 8.6, pseudoasymmetric cases can be explained by the explicit cooperation of the achiral-structure generator and the diploid generator according to Fujita's proligand method. Thus, two chiral butan-2-yl ligands (**8-30** and $\overline{8-30}$) of carbon content 4) construct two diploids $\{\overline{8-30}, 8-30\}$ and $\{8-30, \overline{8-30}\}$. The two diploids are regarded as ordered sets to be differentiated from each other. The former diploid $\{\overline{8-30}, 8-30\}$ along with a hydrogen atom generates **8-41** as a pseudoasymmetric alkyl ligand (or a monosubstituted alkane) of carbon content 9. The latter diploid $\{8-30, \overline{8-30}\}$ generates **8-42** in a parallel way. The products **8-41** and **8-42** are achiral because each of them coincides with itself under reflection. It should be emphasized that the concept of *diploids* is essential to characterize achiral ligands or achiral molecules without exceptions. This treatment is in sharp contrast to the conventional stereochemistry, which has treated such pseudoasymmetric cases as more or less exceptional cases.



Exercise 8.1.

- Confirm that the coefficient of the term x^5 is calculated to be $x \times \{1 \cdot x^4 + x^2 \cdot x^2 + 3x^4 \cdot 1\} = 5x^5$ by using the data appearing in the middle of Eq. 8.26.
- Calculate the coefficient of x^6 recursively by starting from the data up to carbon content 5 (cf. Fig. 8.4).
- Compare the results with the data listed in Fig. 8.9.

Steric-Isomer Generator

In a similar way to Eqs. 8.21 and 8.22, let us consider the following generating functions with infinite terms

$$b(x) = \sum_{k=0}^{\infty} \beta_k x^k, \quad (8.30)$$

where $\beta_0 (= 1)$ is an initial value for representing a hydrogen atom. This infinite polynomial is an extension of Eq. 8.20.

The derivation of Eq. 8.20 ($k = 5$) from Eq. 8.16 ($k = 1-4$) is extended into the following functional equation:

$$b(x) = 1 + \frac{x}{3}(b(x)^3 + 2b(x^3)), \quad (8.31)$$

where the left-hand side ($k = n + 1$) is evaluated from the right-hand side ($k \leq n$) recursively. The first term 1 is added to evaluate a hydrogen atom and the multiplication of x corresponds to a central carbon newly-formed. This equation has been once noted by Fujita [19].

The functional equation represented by Eq. 8.31 is an algebraic expression for implementing a steric-isomer generator (Fig. 8.7) on the basis of Fujita's proligand method, It should be noted that alkyl ligands or monosubstituted alkanes are generated under the action of the coset representation of the C_3 point group (Fujita), while they are generated under the alternating group of degree 3 ($A^{[3]}$) (Pólya), as discussed later.

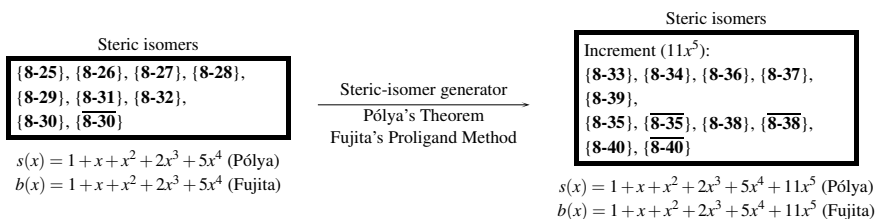


Fig. 8.7. Steric-isomer generator based on Pólya's theorem as well as on Fujita's proligand method. Alkyl ligands or monosubstituted alkanes are generated under the action of the alternating group of degree 3 ($A^{[3]}$) (Pólya) or under the action of the coset representation of the C_3 point group (Fujita). Each steric entity (3D structure) involved in a pair of braces is counted once. The number of substituted alkanes of carbon content k as steric isomers appears as the coefficient of the term x^k .

The steric-isomer generator shown in Fig. 8.7 is applied repeatedly according to Eq. 8.31. After infinite recursion, we can obtain a set (\mathbf{S}_∞) of alkyl ligands (monosubstituted alkanes) as steric isomers up to infinite carbon content, as shown in Eq. 8.30. Then the set \mathbf{S}_∞ is characterized by a generating function:

$$\begin{aligned}
 b(x) &= \sum_{k=0}^{\infty} \beta_k x^k \\
 &= 1 (= \beta_0) + x + x^2 + 2x^3 + 5x^4 + 11x^5 \\
 &\quad + 28x^6 + 74x^7 + 199x^8 + 551x^9 + 1553x^{10} \\
 &\quad + 4436x^{11} + 12832x^{12} + 37496x^{13} + 110500x^{14} + 328092x^{15} \\
 &\quad + 980491x^{16} + 2946889x^{17} + 8901891x^{18} + 27012286x^{19} + 82300275x^{20} \\
 &\quad + 251670563x^{21} + 772160922x^{22} + 2376294040x^{23} + 7333282754x^{24} \\
 &\quad + 22688455980x^{25} + \dots, \tag{8.32}
 \end{aligned}$$

where $\beta_0 (= 1)$ is an initial value for representing a hydrogen atom. By comparing Eq. 8.32 with Eq. 8.29, we obtain $\beta_k = \gamma_{2k}$, although these coefficients are conceptually different.

8.2.4 Achiral Alkyl Ligands and Pairs of Enantiomeric Alkyl Ligands

Let $C(x)$ and $B(x)$ denote generating functions for giving the number of enantiomeric pairs of chiral alkyl ligands (or monosubstituted alkanes) and the total number of 3D-structural isomers ($a(x) + C(x) = B(x)$):

$$C(x) = \sum_{k=0}^{\infty} C_k x^k \tag{8.33}$$

$$B(x) = \sum_{k=0}^{\infty} B_k x^k, \tag{8.34}$$

where $C_0 (= 0)$ or $B_0 (= 1)$ is an initial value. Because $b(x) = a(x) + 2C(x)$ and $B(x) = a(x) + C(x)$, we obtain the following equations [19]:

$$C(x) = \frac{1}{2}(b(x) - a(x)) \tag{8.35}$$

$$B(x) = \frac{1}{2}(b(x) + a(x)). \tag{8.36}$$

Because $a(x)$ and $b(x)$ are obtained recursively (Eqs. 8.27 and 8.32), the generating functions (Eqs. 8.33 and 8.34) are obtained by means of Eqs. 8.35 and 8.36. The calculated coefficients of the generating functions, i.e., A_k in Eq. 8.21 (or Eq. 8.27), C_k in Eq. 8.33, and B_k in Eq. 8.34, are collected in Table 8.2 up to carbon content 50. A Maple program code for a recursive calculation up to carbon content 100 and the resulting data in tabular form have been reported [21].

Table 8.2. Numbers of Alkyl Ligands or Monosubstituted Alkanes as 3D-Structural Isomers [21]

k	A_k (Achiral)	C_k (Enantiomeric Pairs)	B_k (Total $A_k + C_k$)
1	1	0	1
2	1	0	1
3	2	0	2
4	3	1	4
5	5	3	8
6	8	10	18
7	14	30	44
8	23	88	111
9	41	255	296
10	69	742	811
11	122	2157	2279
12	208	6312	6520
13	370	18563	18933
14	636	54932	55568
15	1134	163479	164613
16	1963	489264	491227
17	3505	1471692	1475197
18	6099	4447896	4453995
19	10908	13500689	13511597
20	19059	41140608	41159667
21	34129	125818217	125852346
22	59836	386050543	386110379
23	107256	1188093392	1188200648
24	188576	3666547089	3666735665
25	338322	11344058829	11344397151
26	596252	35180323336	35180919588
27	1070534	109339097119	109340167653
28	1890548	340508394528	340510285076
29	3396570	1062419370490	1062422767060
30	6008908	3320666310903	3320672319811
31	10801816	10395996250010	10396007051826
32	19139155	32596713516873	32596732656028
33	34422537	102354659356690	102354693779227
34	61074583	321832884381903	321832945456486
35	109894294	1013230630964436	1013230740858730
36	195217253	3193818534035050	3193818729252303
37	351404205	10078773177202180	10078773528606385
38	624913284	31840095204449021	31840095829362305
39	1125291874	100689937510048385	100689938635340259
40	2003090071	318728146981844679	318728148984934750
41	3608175239	1009849492883144730	1009849496491319969
42	6428430129	3202399570304430261	3202399576732860390
43	11582995444	10163870352469178059	10163870364052173503
44	20653101216	32284255140318002679	32284255160971103895
45	37223637886	102625414714074250195	102625414751297888081
46	66420162952	326465312628541253282	326465312694961416234
47	119740546576	1039258352830707100287	1039258352950447646863
48	213802390264	3310561173602401804486	3310561173816204194750
49	385525375648	10552597199971538944446	10552597200357064320094
50	688796847976	33657783567745352117595	33657783568434148965571

8.3 Enumeration of Alkyl Ligands as Planted Trees

8.3.1 Alkyl Ligands or Monosubstituted Alkanes as Graphs

Suppose that the C_{3v} -skeleton **8-1** degenerates to give a graph **8-1_g**, which is governed by the symmetric group of degree 3 (S^3). By placing $r_d = a_d = c_d = b_d$, the CI-CF shown in Eq. 8.3 is converted into the following CI (without chirality fittingness):

$$CI_{\mathbf{8-1}_g}(S^3, r_d) = \frac{1}{6}(r_1^3 + 2r_3 + 3r_1r_2). \quad (8.37)$$

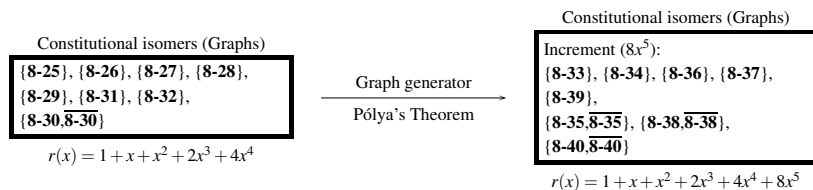


Fig. 8.8. Graph generator based on Pólya's theorem. Alkyl ligands or monosubstituted alkanes are generated under the action of the symmetric group of degree 3 ($S^{[3]}$). Each constitution which is derived by degeneration of component 3D structures involved in a pair of braces is counted just once. The number of alkyl ligands (or substituted alkanes) of carbon content k as constitutional isomers appears as the coefficient of the term x^k .

Let consider a set (R_∞) of alkyl ligands (or monosubstituted alkanes) as graphs up to infinite carbon content. Suppose that the number R_k of such alkyl ligands (or monosubstituted alkanes) of carbon content k appears as the coefficient of the term x^k in the following generating function:

$$r(x) = \sum_{k=0}^{\infty} R_k x^k, \quad (8.38)$$

where $R_0 (= 1)$ is an initial value for representing a hydrogen atom. To evaluate Eq. 8.38 on the basis of Eq. 8.37, we consider the following functional equation:

$$r(x) = 1 + \frac{x}{6}(r(x)^3 + 2r(x^3) + 3r(x)r(x^2)), \quad (8.39)$$

where the left-hand side ($k = n + 1$) is evaluated from the right-hand side ($k \leq n$) recursively. The first term 1 is added to evaluate a hydrogen atom and the multiplication of x corresponds to a central carbon newly-formed. This equation has been noted by Pólya [8,9].

The process of recursive calculations based on Eq. 8.39 is illustrated by the graph generator shown in Fig. 8.8, where the graphs of carbon contents $k = 5$ are derived from the graphs of lower contents $k = 1-4$ (corresponding to the 3D structures listed in Fig. 8.3). The recursive calculations provide the following results:

$$\begin{aligned}
r(x) &= \sum_{k=0}^{\infty} R_k x^k \\
&= 1 (= R_0) + x + x^2 + 2x^3 + 4x^4 + 8x^5 + 17x^6 + 39x^7 + 89x^8 + 211x^9 + 507x^{10} \\
&\quad + 1238x^{11} + 3057x^{12} + 7639x^{13} + 19241x^{14} + 48865x^{15} \\
&\quad + 124906x^{16} + 321198x^{17} + 830219x^{18} + 2156010x^{19} + 5622109x^{20} \\
&\quad + 14715813x^{21} + 38649152x^{22} + 101821927x^{23} + 269010485x^{24} \\
&\quad + 712566567x^{25} + \dots, \quad (8.40)
\end{aligned}$$

where $R_0 (= 1)$ is an initial value for representing a hydrogen atom.

If the graph **8-1_g** is governed by the alternating group of degree 3 ($A^{[3]}$), the CI-CF represented by Eq. 8.8 degenerates, so as to give a CI without chirality fittingness by placing

$s_d = b_d$:

$$\text{CI}_{8-1_g}(\mathbf{A}^{[3]}, s_d) = \frac{1}{3}(s_1^3 + 2s_3). \quad (8.41)$$

Note that $\mathbf{A}^{[3]}$ is isomorphic to the point group \mathbf{C}_3 . Let consider a set (\mathbf{S}_∞) of alkyl ligands (or monosubstituted alkanes) as steric isomers up to infinite carbon content. Suppose that the number S_k of such alkyl ligands (or monosubstituted alkanes) of carbon content k appears as the coefficient of the term x^k in the following generating function:

$$s(x) = \sum_{k=0}^{\infty} S_k x^k, \quad (8.42)$$

where $S_0 (= 1)$ is an initial value for representing a hydrogen atom. To evaluate Eq. 8.42 on the basis of Eq. 8.41, we consider the following functional equation:

$$s(x) = 1 + \frac{x}{3}(s(x)^3 + 2s(x^3)), \quad (8.43)$$

where the left-hand side ($k = n + 1$) is evaluated from the right-hand side ($k \leq n$) recursively. The first term 1 is added to evaluate a hydrogen atom and the multiplication of x corresponds to a central carbon newly-formed. This equation has been noted by Pólya [8,9].

By comparing Eq. 8.43 with Eq. 8.31, we find that the same steric-isomer generator as shown in Fig. 8.7 can be used. Thereby, we are able to obtain $S_k = \beta_k$, which have been listed in Eq. 8.32. The data of $S_k (= \beta_k)$ for steric isomers based on $\mathbf{A}^{[3]}$ have been reported in a tabular form up to carbon content 100 [21].

8.3.2 3D Structures vs. Graphs for Characterizing Alkyl Ligands or Monosubstituted Alkanes

It is worthwhile to compare the results of the above-mentioned enumerations by depicting alkyl ligands (or monosubstituted alkanes) of carbon content 6 (Fig. 8.9).

The term $28x^6$ in the generating function $b(x)$ (Eq. 8.32) indicates the presence of 28 alkyl ligands (or monosubstituted alkanes) as steric isomers, which are inequivalent under the recursive action of the point group \mathbf{C}_3 (Fujita's proligand method, $\beta_6 = 28$) or under the recursive action of the alternating group of degree 3 $\mathbf{A}^{[3]}$ (Pólya's theorem, $S_6 = 28$). These 28 alkyl ligands (or monosubstituted alkanes) are depicted in Fig. 8.9.

The term $17x^6$ in the generating function $r(x)$ (Eq. 8.40) indicates the presence of 17 alkyl ligands (or monosubstituted alkanes) as graphs (constitutional isomers), which are inequivalent under the recursive action of the symmetric group of degree 3 $\mathbf{S}^{[3]}$ (Pólya's theorem, $R_6 = 17$). These 17 alkyl ligands (or monosubstituted alkanes) as constitutional isomers are surrounded by a dashed frame in Fig. 8.9, where each set of stereoisomers surrounded by a dashed box (e.g., **8-59**, **8-59**, **8-60**, and **8-60**) is counted once.

The term $8x^6$ in the generating function $a(x)$ (Eq. 8.27) or the value 8 at the intersection between the ($k = 6$)-row and the A_k -column in Table 8.2 indicates the presence of 8 achiral alkyl ligands (or monosubstituted alkanes) as 3D-structural isomers (**8-43–8-50**), which are

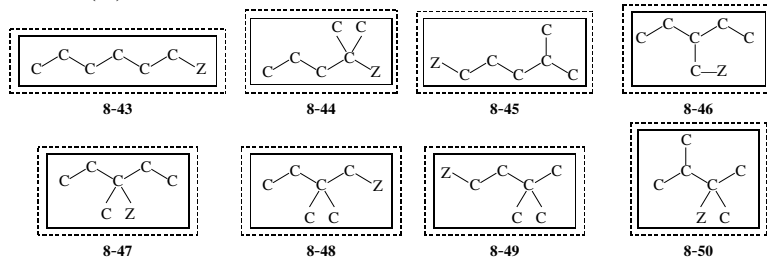
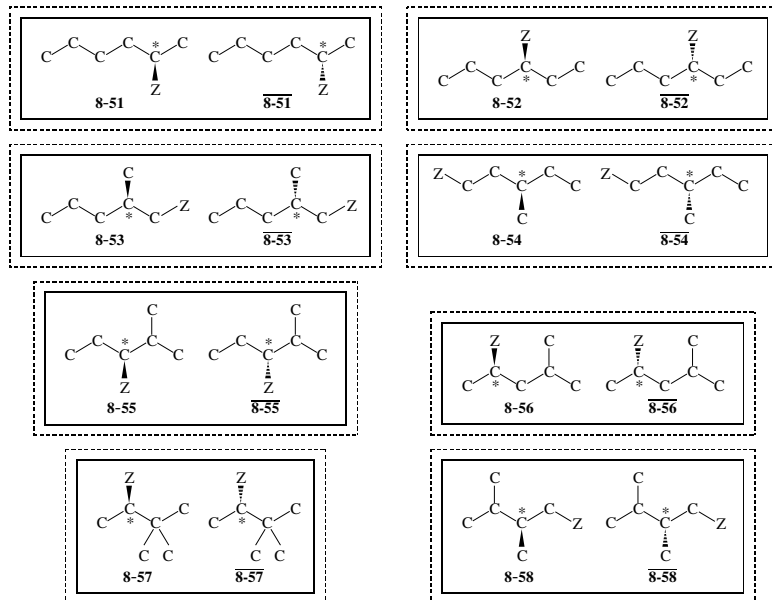
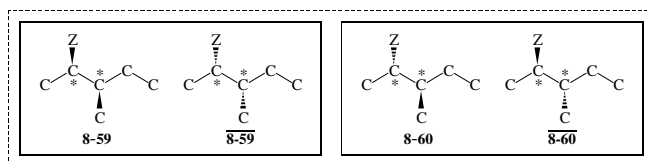
Achiral (x^6)Chiral with One Asymmetric Center (x^6y)Chiral with Two Asymmetric Centers (x^6y^2)

Fig. 8.9. Alkyl ligands or monosubstituted alkanes of carbon content 6 [1]. Each of 17 constitutional isomers is surrounded by a broken-lined box; each of 18 3D-structural isomers (each achiral molecule or each pair of enantiomeric molecules) is surrounded by a straight-lined box; and each molecule represents a steric entity of 28 steric isomers. The symbol Z denotes an atom (e.g., Cl) or an achiral ligand (e.g., OH) which is regarded as a monovalent substituent. Hydrogen atoms are omitted for the sake of simplicity. Each asymmetric center is denoted by an asterisk.

inequivalent under the recursive action of the point group C_{3v} (Fujita's proligand method, $A_6 = 8$). The 8 achiral alkyl ligands (or monosubstituted alkanes) are depicted in the top part of in Fig. 8.9, where each alkyl ligand is surrounded by a frame box and a dashed box to show its achirality.

The term $10x^6$ in the generating function $C(x)$ (Eq. 8.33 or Eq. 8.35) or the value 10 at the intersection between the ($k = 6$)-row and the C_k -column in Table 8.2 indicates the presence of 10 pairs of enantiomeric alkyl ligands (or monosubstituted alkanes) as 3D-structural isomers, which are inequivalent under the recursive action of the point group C_{3v} (Fujita's proligand method, $C_6 = 10$). Each of the 10 pairs is surrounded by a solid frame, as shown in the middle and bottom parts of Fig. 8.9.

The fate of asymmetry and pseudoasymmetry in the enumeration of monosubstituted alkanes has been discussed in detail [23,31]. Thereby, the 10 enantiomeric pairs are further divided into eight pairs with x^6y and two pairs with x^6y^2 , where the symbol y is a dummy variable to count asymmetric carbon centers, as shown in the middle and bottom parts of Fig. 8.9 [31].

The term $18x^6$ in the generating function $B(x)$ (Eq. 8.34 or Eq. 8.36) or the value 18 at the intersection between the ($k = 6$)-row and the B_k -column in Table 8.2 indicates the presence of 18 pairs of alkyl ligands (or monosubstituted alkanes) as 3D-structural isomers, which are inequivalent under the recursive action of the point group C_{3v} (Fujita's proligand method, $B_6 = 18$). Note that one achiral entity or one pair of enantiomeric entities is counted once in the value B_6 . We are able to confirm the relationship $B_6 = A_6 + C_6$ or generally $B_k = A_k + C_k$.

The value $R_6 = 17$ for graphs (Pólya's theorem) corresponds to the value $B_6 = 18$ for 3D-structural isomers (Fujita's proligand method), where their difference is clearly demonstrated by the modes of counting, which are illustrated by solid frames and dashed frames in Fig. 8.9.

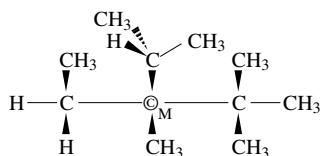
8.4 Enumeration of Alkanes (3D-Trees) as 3D-Structural Isomers

8.4.1 Alkanes as Centroidal and Bicentroidal 3D-Trees

The concept of centroidal and bicentroidal trees has been established by Jordan [32], as summarized in Biggs-Lloyd-Wilson's book [7, 3B for Jordan's paper] and Harary's book [33, Theorem 4.3].

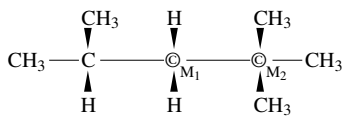
Suppose that a tree is given as a non-cyclic graph which has n vertices and e edges satisfying the relationship $n = e + 1$. Let m be the number of vertices contained in the largest branch among the branches attaching to the vertex. According to Jordan [32], trees are classified into two categories, i.e., trees having a centroid and trees having a bicentroid.

Examples:



8-61

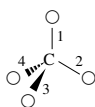
centroidal alkane



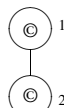
8-62

bicentroidal alkane

Skeletons for steric isomers or 3D-structural isomers (3D-trees):



8-63

centroidal 3D-skeleton ($T_d(/C_{3v})$)

8-64

bicentroidal 3D-skeleton ($K(/K')$)

Fig. 8.10. Alkanes and their skeletons as centroidal and bicentroidal 3D-trees, which are enumerated as steric isomers or 3D-structural isomers. The symbol © denotes a centroid, while the symbol ©—© denotes a bicentroid. The factor group K is represented by $K = D_{\infty h}/C_{\infty}$, which has a subgroup represented by $K' = D_{\infty h}/C_{\infty v}$.

Definition 8.1 (Centroidal and Bicentroidal Trees). There emerge two cases:

1. A given tree has an exceptional vertex (M) called a *centroid*, which satisfies the relationship $m < \frac{1}{2}n$. The tree is called a *centroidal tree*.
2. A given tree has two adjacent vertices (M_1 and M_2), each of which satisfies the relationship $m = \frac{1}{2}n$. The exceptional graph (M_1 — M_2) composed of the two adjacent vertices and the relevant edge is called a *bicentroid*. The tree is called a *bicentroidal tree*.

All of the vertices other than the centroid or the bicentroid in a tree satisfy the relationship $m > \frac{1}{2}n$. There are no cases in which a given tree has both a centroid and a bicentroid [32].

This concept should be extended to meet 3D-trees for the purpose of enumerating alkanes as 3D structures. Obviously, these properties of trees (Def. 8.1) maintain in 3D-trees, because 3D-trees are regarded as a kind of trees. Thereby, alkanes are categorized into centroidal 3D-trees and bicentroidal 3D-trees [20], as depicted in Fig. 8.10.

The difference between centroidal and bicentroidal 3D-trees can be grasped by a glance at a bicentroidal 3D-tree. That is to say, the two terminal nodes of a bicentroid carry residues of equal carbon contents which are halves of the carbon content of the tree or 3D-tree. For example, the two terminal nodes of a bicentroid (©—© attached by M_1 and M_2) in the 3D-tree 8-62 carry residues of carbon content 4, i.e., isobutyl and *tert*-butyl. Otherwise, a 3D-tree is determined to be centroidal, as exemplified by 8-61, where the centroid (© attached by M) accommodates four ligands, i.e., methyl, ethyl, isopropyl, and *tert*-butyl ligands.

8.4.2 Enumeration of Centroidal Alkanes (3D-Trees) as 3D-Structural Isomers

To enumerate centroidal alkanes as 3D-structural isomers, the centroidal 3D-skeleton **8-63** shown in Fig. 8.10 is used as a starting skeleton, where the four positions belong to an $T_d(/C_{3v})$ -orbit.

Let \widehat{A}_k be the number of achiral centroidal 3D-trees (promolecules or alkanes) of carbon content k . Let \widehat{C}_k be the number of chiral centroidal 3D-trees (promolecules or alkanes) of carbon content k , where a pair of enantiomeric 3D-trees is counted just once. Let \widehat{B}_k be the number of achiral and chiral centroidal 3D-trees (promolecules or alkanes) of carbon content k , where a pair of enantiomeric 3D-trees is counted just once. In agreement with the definition of centroidal 3D-trees (Def. 8.1), the terms up to x^v are collected to give the following generating functions:

$$\widehat{A}(x) = \sum_{k=0}^v \widehat{A}_k x^k \quad (8.44)$$

$$\widehat{C}(x) = \sum_{k=0}^v \widehat{C}_k x^k, \quad (8.45)$$

$$\widehat{B}(x) = \sum_{k=0}^v \widehat{B}_k x^k \quad (8.46)$$

where v runs stepwise from 0 to infinite. Note that $\text{CI-CF}^{(a)}(T_d; \$_d)$ (Eq. 7.54 on page 190) corresponds to Eq. 8.44, $\text{CI-CF}^{(e)}(T_d; \$_d)$ (Eq. 7.55 on page 190) to Eq. 8.45, and $\text{CI-CF}(T_d; \$_d)$ (Eq. 7.29 on page 183) to Eq. 8.46. Hence, Eqs. 7.54, 7.55, and 7.29 are transformed into the following functional equations [27,20]:

$$\widehat{A}(x) = \frac{x}{2}(a(x)^2 c(x^2) + c(x^4)) \quad (8.47)$$

$$\widehat{C}(x) = \frac{x}{24}(b(x)^4 + 3b(x^2)^2 + 8b(x)b(x^3) - 6a(x)^2 c(x^2) - 6c(x^4)) \quad (8.48)$$

$$\widehat{B}(x) = \frac{x}{24}(b(x)^4 + 3b(x^2)^2 + 8b(x)b(x^3) + 6a(x)^2 c(x^2) + 6c(x^4)) \quad (8.49)$$

according to Fujita's proligand method [16–18]. Note that the multiplication by x is necessary to evaluate the effect of a central carbon atom of the centroidal 3D-skeleton **8-63**.⁶

Because the functional equations under the criterion for centroidal 3D-trees, i.e., $a(x)$ (Eq. 8.27), $c(x^2)$ (Eq. 8.29), and $b(x)$ (Eq. 8.32), have been evaluated recursively, they are introduced into Eqs. 8.47–8.49 to evaluate $\widehat{A}(x)$ (Eq. 8.44), $\widehat{C}(x)$ (Eq. 8.45), and $\widehat{B}(x)$ (Eq. 8.46).

Suppose that $a(x)$ (Eq. 8.27), $c(x^2)$ (Eq. 8.29), and $b(x)$ (Eq. 8.32) have been evaluated up to the term x^m , i.e., $a(x)^{(m)} = \sum_{k=0}^m A_k x^k$, $c(x^2)^{(m)} = \sum_{k=0}^m \gamma_{2k} x^{2k}$, and $b(x)^{(m)} = \sum_{k=0}^m \beta_k x^k$.

⁶ As found in Eqs. 8.47–8.49 shown above, Eqs. 27–29 of [1] should be corrected by multiplying x to evaluate the effect of a central carbon atom.

This means that one of the branch in the resulting centroidal alkane has the maximum number (m) of carbon content. They are introduced into Eq. 8.47, Eq. 8.48, or Eq. 8.49. Let the symbol $\widehat{A}(x)^{(m)}$, $\widehat{C}(x)^{(m)}$, and $\widehat{B}(x)^{(m)}$ denote the generating functions generated from Eq. 8.47, Eq. 8.48, and Eq. 8.49, respectively. Our task is to select the effective terms for the criterion for centroidal 3D-trees (Def. 8.1) from the terms contained in the generating functions $\widehat{A}(x)^{(m)}$, $\widehat{C}(x)^{(m)}$, $\widehat{B}(x)^{(m)}$.

According to the criterion for centroidal 3D-trees (Def. 8.1), the power v of the term x^v appearing in the generating function $\widehat{A}(x)^{(m)}$, $\widehat{C}(x)^{(m)}$, or $\widehat{B}(x)^{(m)}$ should satisfy the following condition:

$$\frac{1}{2}v - 1 \leq m < \frac{1}{2}v \quad (8.50)$$

or equivalently

$$2m < v \leq 2m + 2. \quad (8.51)$$

Hence, centroidal alkanes of carbon contents $2m + 1$ and $2m + 2$ are permitted, so that the terms x^{2m+1} and x^{2m+2} are adopted as the next members of $\widehat{A}(x)$ (Eq. 8.44), $\widehat{C}(x)$ (Eq. 8.45), or $\widehat{B}(x)$ (Eq. 8.46).

Let the symbol $\text{coeff}(\widehat{A}(x)^{(m)}, x^{2m+1})$ etc. represent the coefficient of the term x^{2m+1} appearing in the equation $\widehat{A}(x)^{(m)}$ etc. after expansion. Then, we obtain the following coefficients:

$$\widehat{A}_{2m+1} = \text{coeff}(\widehat{A}(x)^{(m)}, x^{2m+1}) \quad (8.52)$$

$$\widehat{C}_{2m+1} = \text{coeff}(\widehat{C}(x)^{(m)}, x^{2m+1}) \quad (8.53)$$

$$\widehat{B}_{2m+1} = \text{coeff}(\widehat{B}(x)^{(m)}, x^{2m+1}) \quad (8.54)$$

for odd carbon contents as well as the following coefficients:

$$\widehat{A}_{2m+2} = \text{coeff}(\widehat{A}(x)^{(m)}, x^{2m+2}) \quad (8.55)$$

$$\widehat{C}_{2m+2} = \text{coeff}(\widehat{C}(x)^{(m)}, x^{2m+2}) \quad (8.56)$$

$$\widehat{B}_{2m+2} = \text{coeff}(\widehat{B}(x)^{(m)}, x^{2m+2}) \quad (8.57)$$

for even carbon contents. A Maple programming code for these calculations has been reported in addition to the resulting data up to carbon content 100 [27]. The resulting data up to carbon content 50 are cited in Table 8.3.

For example, the case of $m = 4$ for Eq. 8.47 can be calculated by the following Maple programming code:

```
restart;
Ax := (1/2)*x*(ax^2*cx2 + cx4);

ax := 1 + x + x^2 + 2*x^3 + 3*x^4;
cx2 := 1 + x^2 + x^4 + 2*x^6 + 5*x^8;
cx4 := 1 + x^4 + x^8 + 2*x^12 + 5*x^16;
```

Table 8.3. Numbers of Centroidal Alkanes (3D-Trees) as 3D-Structural Isomers [27]

k	\hat{A}_k (Achiral)	\hat{C}_k (Enantiomeric Pairs)	\hat{B}_k (Total)
1	1	0	1
2	0	0	0
3	1	0	1
4	1	0	1
5	3	0	3
6	2	0	2
7	7	2	9
8	7	1	8
9	21	17	38
10	22	24	46
11	61	142	203
12	72	211	283
13	186	1113	1299
14	220	1784	2004
15	567	8780	9347
16	717	15041	15758
17	1755	70750	72505
18	2209	127072	129281
19	5454	584158	589612
20	7149	1091507	1098656
21	17070	4937616	4954686
22	22476	9554169	9576645
23	53628	42617881	42671509
24	72656	84925546	84998202
25	169175	374580272	374749447
26	229676	765735799	765965475
27	535267	3344179169	3344714436
28	743026	6991686639	6992429665
29	1698322	30262422579	30264120901
30	2361476	64535740751	64538102227
31	5400908	277091404722	277096805630
32	7642893	601434086766	601441729659
33	17211368	2563401079994	2563418291362
34	24394779	5652876029848	5652900424627
35	54947147	23930997120150	23931052067297
36	79009726	53534824577018	53534903586744
37	175702378	225225850040744	225226025743122
38	252964410	510446275671249	510446528635659
39	562645937	2135108676616236	2135109239262173
40	819922295	4896888847857945	4896889667780240
41	1804088396	20372874776166747	20372876580255143
42	2631820744	47238611431657314	47238614063478058
43	5791497722	195544787602887105	195544793394384827
44	8536377160	457999551947828613	457999560484205773
45	18611821161	1886989260491307050	1886989279103128211
46	27458156708	4461040369492811082	4461040396950967790
47	59870273288	18298681682556106941	18298681742426380229
48	89120741244	43636081455029159803	43636081544149901047
49	192762694240	178246302421277075465	178246302614039769705
50	287167536146	428497964886295432421	428497965173462968567

```
f_Ax := sort(expand(Ax), [x], ascending);
```

```
m21 := coeff(f_Ax, x^9);
```

```
m22 := coeff(f_Ax, x^10);
```

where the data of $a(x)$ shown by Eq. 8.24 and $c(x^2)$ (and $c(x^4)$) shown by Eq. 8.25 are used. The result of f_Ax indicates the following generating function:

$$\hat{A}(x)^{(4)} = x + x^2 + 2x^3 + 4x^4 + 8x^5 + 9x^6 + 13x^7 + 16x^8 + 21x^9 + 22x^{10} + 28x^{11} + 31x^{12} + 43x^{13} + 37x^{14} + 34x^{15} + 30x^{16} + 25x^{17}, \quad (8.58)$$

where only the terms $21x^9$ (for $v = 2m + 1 = 9$) and $22x^{10}$ (for $v = 2m + 2 = 10$) are effective among the terms appearing in the right-hand side. As a result, the outputs of $m21$ and $m22$ indicate the following values according to Eq. 8.52 and Eq. 8.55:

$$\widehat{A}_9 = \text{coeff}(\widehat{A}(x)^{(4)}, x^9) = 21 \quad (8.59)$$

$$\widehat{A}_{10} = \text{coeff}(\widehat{A}(x)^{(4)}, x^{10}) = 22 \quad (8.60)$$

The values of $\widehat{C}_9 = 17$ and $\widehat{C}_{10} = 18$ (via Eq. 8.48) as well as those of $\widehat{B}_9 = 24$ and $\widehat{B}_{10} = 46$ (via Eq. 8.49) are obtained in a similar way. These values are collected in the ($k = 9$)- and ($k = 10$)-rows of Table 8.3.

Exercise 8.2.

- Calculate the values \widehat{A}_7 and \widehat{A}_8 manually by introducing $a(x) = 1 + x + x^2 + 2x^3$ and $c(x^2) = 1 + x^2 + x^4 + 2x^6$ into Eq. 8.47.
- If a Maple system (or another system for algebraic calculations) is available, write a code for the calculation of this case.

Seven achiral centroidal alkanes of carbon content 8 ($\widehat{A}_8 = 7$) and one enantiomeric pair of chiral centroidal alkanes of carbon content 8 ($\widehat{C}_8 = 1$) are shown in Fig. 8.11, where each centroid is represented by the symbol M.

The centroidal alkanes shown in Fig. 8.11 have the maximum number of carbon content $m = 3$ (for those other than **8-71**) or $m = 2$ (for **8-71**), which satisfies $m < \frac{1}{2}n$ because of $n = 8$ (cf. Def. 8.1).

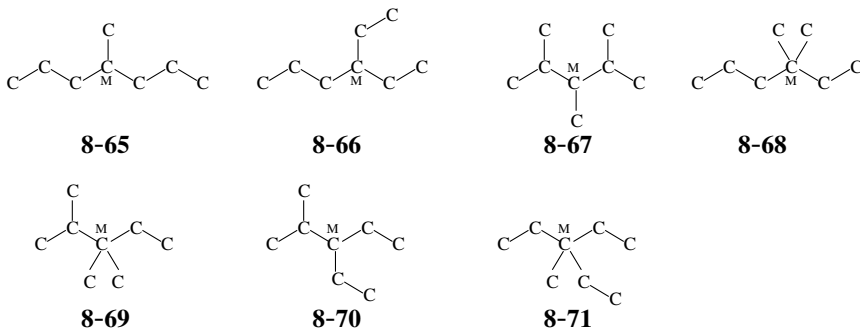
8.4.3 Enumeration of Bicentroidal Alkanes (3D-Trees) as 3D-Structural Isomers

The dumbbell skeleton **8-64** (Fig. 8.10) as a bicentroidal 3D-skeleton has been characterized by the coset representation of \mathbf{K}/\mathbf{K}' , where the factor group \mathbf{K} is represented by $\mathbf{K} = \mathbf{D}_{\infty h}/\mathbf{C}_{\infty}$ and its subgroup is represented by $\mathbf{K}' = \mathbf{D}_{\infty h}/\mathbf{C}_{\infty v}$ [27]. Although the factor group \mathbf{K} is suitable to treat the infinite character of the group $\mathbf{D}_{\infty h}$, a more intuitive treatment is adopted here for the simplicity's sake.

The two positions of **8-64** is alternatively characterized by the coset representation $\mathbf{D}_{\infty h}/\mathbf{C}_{\infty v}$ (cf. **4-26** in Fig. 4.13 on page 109). The coset decomposition of $\mathbf{D}_{\infty h}$ by $\mathbf{C}_{\infty v}$ is represented as follows:

$$\begin{array}{rcccl}
 \mathbf{D}_{\infty h} & = & \mathbf{C}_{\infty v} & + & \mathbf{C}_{\infty v}C_2 & \text{product of} \\
 & & 1 & & 2 & \text{cycles} & \text{PSI} \\
 \hline
 g \in \mathbf{C}_{\infty} & & 1 & & 2 & (1)(2) & b_1^2 \\
 g \in \mathbf{C}_{\infty}C_2 & & 2 & & 1 & (1\ 2) & b_2 \\
 g \in \mathbf{C}_{\infty h} - \mathbf{C}_{\infty} & & \bar{2} & & \bar{1} & (\bar{1}\ \bar{2}) & c_2 \\
 g \in \mathbf{C}_{\infty v} - \mathbf{C}_{\infty} & & \bar{1} & & \bar{2} & (\bar{1})(\bar{2}) & a_1^2
 \end{array} \quad (8.61)$$

Achiral centroidal alkanes of carbon content 8



Chiral centroidal alkanes of carbon content 8

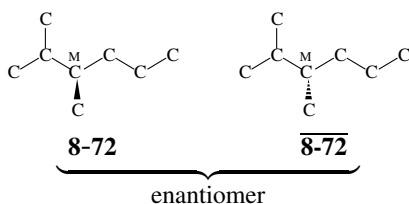


Fig. 8.11. Seven achiral centroidal alkanes of carbon content 8 and one enantiomeric pair of chiral centroidal alkanes of carbon content 8, where each carbon attached by the symbol M is a centroid.

Although the treatment of infinite number (∞) is not strict, the following expression is permitted:

$$\mathbf{D}_{\infty h}(/C_{\infty v}) = \left\{ \underbrace{(1)(2), \dots}_{C_{\infty}}, \underbrace{(1\ 2), \dots}_{C_{\infty}C_2}, \underbrace{\overline{(1\ 2)}, \dots}_{C_{\infty h} - C_{\infty}}, \underbrace{\overline{(1)(2)}, \dots}_{C_{\infty v} - C_{\infty}} \right\}, \quad (8.62)$$

where each permutation (each product of cycles) of the coset representation $\mathbf{D}_{\infty h}(/C_{\infty v})$ corresponds to a product of sphericity cycles (PSI). Thereby, the following CI-CFs are obtained according to Def. 7.5 (page 181) and Def. 7.7 (page 188):

$$\text{CI-CF}(\mathbf{D}_{\infty h}, \mathcal{S}_d) = \frac{1}{4}(b_1^2 + b_2 + a_1^2 + c_2) \quad (8.63)$$

$$\text{CI-CF}^{(a)}(\mathbf{D}_{\infty h}, \mathcal{S}_d) = \frac{1}{2}(a_1^2 + c_2) \quad (8.64)$$

$$\text{CI-CF}^{(e)}(\mathbf{D}_{\infty h}, \mathcal{S}_d) = \frac{1}{4}(b_1^2 + b_2 - a_1^2 - c_2). \quad (8.65)$$

Let \tilde{B}_k be the number of achiral bicentroidal promolecules (alkanes) plus enantiomeric pairs of chiral bicentroidal promolecules (alkanes) of carbon content k ; let \tilde{A}_k be the number of achiral bicentroidal promolecules (alkanes) of carbon content k ; and let \tilde{C}_k be the number of chiral bicentroidal promolecules (alkanes) of carbon content k , where each pair of enantiomers is counted just once. Then, they appear as the coefficients of the following

generating functions:

$$\tilde{A}(x) = \sum_{k=0}^{\nu} \tilde{A}_k x^k \quad (8.66)$$

$$\tilde{C}(x) = \sum_{k=0}^{\nu} \tilde{C}_k x^k \quad (8.67)$$

$$\tilde{B}(x) = \sum_{k=0}^{\nu} \tilde{B}_k x^k, \quad (8.68)$$

each of which contains the terms up to ν , where the ν runs stepwise from 0 to infinite.

To evaluate the generating functions represented by Eqs. 8.66–8.68, we derive functional equations by substituting $a(x^d)$, $c(x^d)$, and $b(x^d)$ for the SIs (a_d , c_d , and b_d) appearing in the CI-CFs (Eqs. 8.64, 8.65, and 8.63). Thereby, we obtain the following functional equations:

$$\tilde{A}(x) = \frac{1}{2} (a(x)^2 + c(x^2)) \quad (8.69)$$

$$\tilde{C}(x) = \frac{1}{4} (b(x)^2 + b(x^2) - a(x)^2 - c(x^2)) \quad (8.70)$$

$$\tilde{B}(x) = \frac{1}{4} (b(x)^2 + b(x^2) + a(x)^2 + c(x^2)). \quad (8.71)$$

The generating functions $a(x)$ (Eq. 8.27), $c(x^2)$ (Eq. 8.29), and $b(x)$ (Eq. 8.32), which have been evaluated up to the term x^m , are introduced into Eq. 8.69, Eq. 8.70, or Eq. 8.71. The resulting generating functions are denoted by the symbols $\tilde{A}(x)^{(m)}$, $\tilde{C}(x)^{(m)}$, and $\tilde{B}(x)^{(m)}$. According to the criterion for bicentroidal 3D-trees (Def. 8.1), the power ν of the term x^ν appearing in the generating function $\tilde{A}(x)^{(m)}$, $\tilde{C}(x)^{(m)}$, or $\tilde{B}(x)^{(m)}$ should satisfy the following condition:

$$m = \frac{1}{2}\nu \quad (8.72)$$

or

$$2m = \nu. \quad (8.73)$$

Let the symbol $\text{coeff}(\tilde{A}(x)^{(m)}, x^{2m})$ etc. represent the coefficient of the term x^{2m} appearing in the equation $\tilde{A}(x)^{(m)}$ etc. after expansion. Then, we obtain the following coefficients:

$$\tilde{A}_{2m} = \text{coeff}(\tilde{A}(x)^{(m)}, x^{2m}) \quad (8.74)$$

$$\tilde{C}_{2m} = \text{coeff}(\tilde{C}(x)^{(m)}, x^{2m}) \quad (8.75)$$

$$\tilde{B}_{2m} = \text{coeff}(\tilde{B}(x)^{(m)}, x^{2m}). \quad (8.76)$$

A Maple programming code for these calculations has been reported in addition to the resulting data up to carbon content 100 [27]. The resulting data up to carbon content 50 are cited in Table 8.4.

For example, the case of $m = 4$ for Eq. 8.69 can be calculated by the following Maple programming code:

Table 8.4. Numbers of Bicentroidal Alkanes (3D-Trees) as 3D-Structural Isomers [27]

k	\tilde{A}_k (Achiral)	\tilde{C}_k (Enantiomeric Pairs)	\tilde{B}_k (Total)
2	1	0	1
4	1	0	1
6	3	0	3
8	7	4	11
10	18	24	42
12	46	180	226
14	135	1320	1455
16	364	9768	10132
18	1116	75480	76596
20	3157	601762	604919
22	9660	4915803	4925463
24	28048	41154240	41182288
26	87198	351453279	351540477
28	257498	3052461376	3052718874
30	807024	26910768627	26911575651
32	2416930	240339686928	240342103858
34	7615957	2171035623324	2171043239281
36	23049846	19810906544520	19810929594366
38	72998375	182415868990333	182415941988708
40	222772878	1693333725457536	1693333948230414
42	708229602	1583451778987082	15834518487216684
44	2176253909	149058121470885797	149058123647139706
46	6940071788	1411693338258918016	1411693345198989804
48	21447095265	13444258978638229185	13444259000085324450
50	68575115832	128691508660483996179	128691508729059112011

```

restart;
AAx := (1/2)*(ax^2 + cx2);

ax := 1 + x + x^2 + 2*x^3 + 3*x^4;
cx2 := 1 + x^2 + x^4 + 2*x^6 + 5*x^8;

f_AAx := sort(expand(AAx), [x], ascending);

m2 := coeff(f_AAx, x^8);

```

where the data of $a(x)$ shown by Eq. 8.24 and $c(x^2)$ shown by Eq. 8.25 are introduced. The result of `f_AAx` indicates the following generating function:

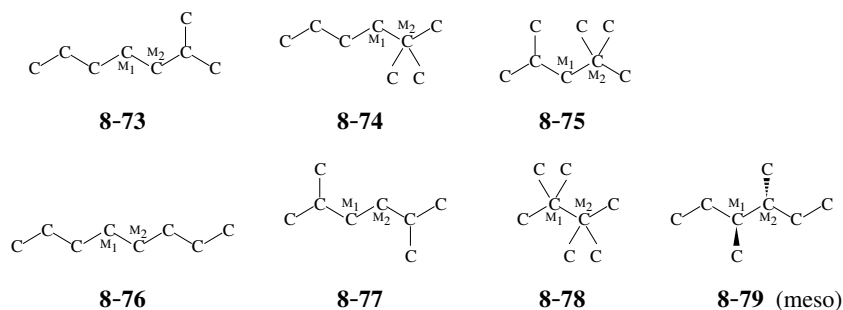
$$\tilde{A}(x)^{(4)} = 1 + x + 2x^2 + 3x^3 + 6x^4 + 5x^5 + 6x^6 + 6x^7 + 7x^8, \quad (8.77)$$

where only the term $7x^8$ (for $v = 2m = 8$) is effective among the terms appearing in the right-hand side. As a result, the output of `m2` indicates the following value according to Eq. 8.74:

$$\tilde{A}_8 = \text{coeff}(\tilde{A}(x)^{(4)}, x^8) = 7. \quad (8.78)$$

The value of $\tilde{C}_8 = 4$ (via Eq. 8.70) and the value of $\tilde{B}_8 = 11$ (via Eq. 8.71) are obtained in a similar way. These values are collected in the ($k = 8$)-row of Table 8.4

Achiral bicentroidal alkanes of carbon content 8



Chiral bicentroidal alkanes of carbon content 8

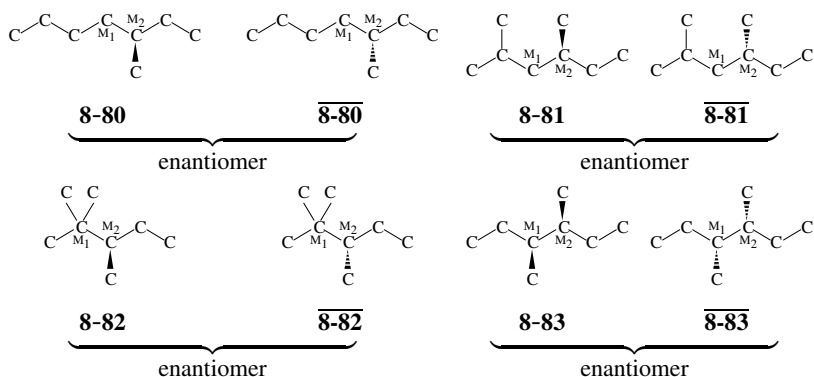


Fig. 8.12. Seven achiral bicentroidal alkanes of carbon content 8 and four enantiomeric pairs of chiral bicentroidal alkanes of carbon content 8, where each pair of carbons attached by the symbol M_1 and M_2 is a bicentroid.

Exercise 8.3.

- Calculate the value \tilde{A}_6 manually by introducing $a(x) = 1 + x + x^2 + 2x^3$ and $c(x^2) = 1 + x^2 + x^4 + 2x^6$ into Eq. 8.69.
- If a Maple system (or another system for algebraic calculations) is available, write a code for the calculation of this case.

Seven achiral bicentroidal alkanes of carbon content 8 ($\tilde{A}_8 = 7$) and four enantiomeric pairs of chiral bicentroidal alkanes of carbon content 8 ($\tilde{C}_8 = 4$) are shown in Fig. 8.12, where each bicentroid is represented by the symbol M_1 — M_2 .

The bicentroidal alkanes shown in Fig. 8.12 have the maximum number of carbon content $m = 4$, which satisfies $m = \frac{1}{2}n$ because of $n = 8$ (cf. Def. 8.1). Chemically speaking, the bond scission at the centroidal bond M_1 — M_2 leaves two fragments of the same carbon content $\frac{1}{2}n$, as exemplified by each alkane collected in Fig. 8.12.

**Exercise 8.4.**

- Discuss the *meso* character of **8-79** in comparison with *meso*-tartaric acid **4-28** in Fig. 4.13 (page 109).
- Compare a set of **8-79**, **8-83**, and $\overline{\mathbf{8-83}}$ with a set of stereoisomeric tartaric acids.

8.4.4 Total Enumeration of Alkanes as 3D-Trees

We have evaluated the values of \widehat{A}_k , \widehat{C}_k , and \widehat{B}_k for centroidal 3D-trees (Eqs. 8.44–8.46) as well as those of \widetilde{B}_k , \widetilde{A}_k , and \widetilde{C}_k for bicentroidal 3D-trees (Eqs. 8.66–8.68). Hence, total values can be calculated by summing up the respective data.

Let $B_k^{(T)}$ be the total number of achiral 3D-trees plus enantiomeric pairs of chiral 3D-trees of carbon content k ; let $A_k^{(T)}$ be the total number of achiral 3D-trees of carbon content k ; and let $C_k^{(T)}$ be the total number of chiral 3D-trees of carbon content k , where each pair of enantiomers is counted just once. Then, they appear as the coefficients of the following generating functions:

$$B(x)^{(T)} = \sum_{k=0}^{\infty} B_k^{(T)} x^k \quad (8.79)$$

$$A(x)^{(T)} = \sum_{k=0}^{\infty} A_k^{(T)} x^k \quad (8.80)$$

$$C(x)^{(T)} = \sum_{k=0}^{\infty} C_k^{(T)} x^k. \quad (8.81)$$

By means of Eqs. 8.44–8.46 and Eqs. 8.66–8.68, we obtain the following relationships:

$$B_k^{(T)} = \widehat{B}_k + \widetilde{B}_k \quad (8.82)$$

$$A_k^{(T)} = \widehat{A}_k + \widetilde{A}_k \quad (8.83)$$

$$C_k^{(T)} = \widehat{C}_k + \widetilde{C}_k. \quad (8.84)$$

According to Eqs. 8.82–8.84, the data of Table 8.3 and the data of Table 8.4 are summed up to give the total numbers of alkanes as 3D-trees, which are collected in Table 8.5. Note that \widetilde{B}_k , \widetilde{A}_k , and \widetilde{C}_k are equal to zero if k is odd.

The values in the ($k = 8$)-row of Table 8.5 can be confirmed by referring to Figs. 8.11 and 8.12.

**Exercise 8.5.**

- Depict alkanes with carbon contents $k = 4$ –7 by referring to the data of Table 8.5.
- Categorize them into centroidal and bicentroidal alkanes by referring to the data of Tables 8.3 and 8.4.

Table 8.5. Total Numbers of Alkanes (3D-Trees) as 3D-Structural Isomers [27]

k	$A_k^{(T)} = \widehat{A}_k + \widetilde{A}_k$ (Achiral)	$C_k^{(T)} = \widehat{C}_k + \widetilde{C}_k$ (Enantiomeric Pairs)	$B_k^{(T)} = \widehat{B}_k + \widetilde{B}_k$ (Total)
1	1	0	1
2	1	0	1
3	1	0	1
4	2	0	2
5	3	0	3
6	5	0	5
7	7	2	9
8	14	5	19
9	21	17	38
10	40	48	88
11	61	142	203
12	118	391	509
13	186	1113	1299
14	355	3104	3459
15	567	8780	9347
16	1081	24809	25890
17	1755	70750	72505
18	3325	202552	205877
19	5454	584158	589612
20	10306	1693269	1703575
21	17070	4937616	4954686
22	32136	14469972	14502108
23	53628	42617881	42671509
24	100704	126079786	126180490
25	169175	374580272	374749447
26	316874	1117189078	1117505952
27	535267	3344179169	3344714436
28	1000524	10044148015	10045148539
29	1698322	30262422579	30264120901
30	3168500	91446509378	91449677878
31	5400908	277091404722	277096805630
32	10059823	841773773694	841783833517
33	17211368	2563401079994	2563418291362
34	32010736	7823911653172	7823943663908
35	54947147	23930997120150	23931052067297
36	102059572	73345731121538	73345833181110
37	175702378	225225850040744	225226025743122
38	325962785	692862144661582	692862470624367
39	562645937	2135108676616236	2135109239262173
40	1042695173	6590222573315481	6590223616010654
41	1804088396	20372874776166747	20372876580255143
42	3340050346	63073129210644396	63073132550694742
43	5791497722	195544787602887105	195544793394384827
44	10712631069	607057673418714410	607057684131345479
45	18611821161	1886989260491307050	1886989279103128211
46	34398228496	5872733707751729098	5872733742149957594
47	59870273288	18298681682556106941	18298681742426380229
48	110567836509	57080340433667388988	57080340544235225497
49	192762694240	178246302421277075465	178246302614039769705
50	355742651978	557189473546779428600	557189473902522080578

Exercise 8.6.

- Depict 3,4,5-trimethylheptanes of carbon content 10.
- Discuss the resulting 3D structures in terms of so-called ‘pseudoasymmetry’. See 2,3,4-trihydroxyglutaric acids (Fig 2.1 on page 37).

It should be noted that the functional equations $\widehat{B}(x)$, $\widehat{A}(x)$, and $\widehat{C}(x)$ (Eqs. 8.47–8.49) for centroidal 3D-trees cannot be added to the functional equations $\widetilde{B}(x)$, $\widetilde{A}(x)$, and $\widetilde{C}(x)$ (eqs. 8.69–8.71) for bicentroidal 3D-trees. Simple summations of the two sets of functional

equations give erroneous results, because the integer m runs according to Eq. 8.51 for the former set and runs differently according to Eq. 8.73 for the latter set.

8.5 Enumeration of Alkanes (3D-Trees) as Steric Isomers

8.5.1 Centroidal Alkanes (3D-Trees) as Steric Isomers

In contrast to the enumeration of centroidal alkanes (3D-trees) as 3D-structural isomers under the action of T_d , the enumeration of centroidal alkanes (3D-trees) as steric isomers is based on the action of the maximum chiral subgroup T . It should be noted that the point group T is identical with the alternating group $A^{[4]}$ if they acts on the four positions of a centroidal 3D-skeleton **8-63**.

Let \widehat{S}_k be the number of centroidal alkanes (3D-trees) of carbon content k as steric isomers. In agreement with the definition of centroidal trees (Def. 8.1), the terms up to x^v are collected to give the following generating function:

$$\widehat{S}(x) = \sum_{k=0}^v \widehat{S}_k x^k \quad (8.85)$$

where v runs stepwise from 0 to infinite.

To evaluate the generating function represented by Eq. 8.85, the sphericity index b_d in the CI-CF for T (Eq. 7.53) is replaced by the term $b(x^d)$. Thereby we obtain the following functional equation:

$$\widehat{S}(x) = \frac{x}{12} (b(x)^4 + 3b(x^2)^2 + 8b(x)b(x^3)), \quad (8.86)$$

where the multiplying by x is required to take account of the centroid of the T -skeleton. This equation was first noted by Pólya [8,9], who directly used $A^{[4]}$.

Because we have obtained $b(x)$ of alkyl ligands (monosubstituted alkanes) as shown in Eq. 8.32, the data up to m , i.e., $b(x)^{(m)} = \sum_{k=0}^m \beta_k x^k$, is introduced into the functional equation (Eq. 8.86). The resulting function is expanded to give a generating function, where the terms of x^{2m+1} and x^{2m+2} are effective according to Jordan's criterion of centroidal trees (Def. 8.1). Their coefficients are adopted as the numbers for carbon content $k = 2m + 1$ and $2m + 2$. The evaluated values are listed in the \widehat{S}_k -column of Table 8.6.

The nine 3D structures collected in Fig. 8.11 are consistent with the value 9 at the intersection between the $k = 8$ -row and \widehat{S}_k -column of Table 8.6. Note that each 3D structure selected from a pair of enantiomers as well as each achiral 3D structure is counted once during the enumeration of steric isomers.

8.5.2 Bicentroidal Alkanes (3D-Trees) as Steric Isomers

To discuss bicentroidal alkanes (3D-trees) as steric isomers, the maximum chiral subgroup D_∞ of $D_{\infty h}$ (cf. Eq. 8.61) is taken into consideration. The two positions of the bicentroidal

Table 8.6. Numbers of Alkanes (3D-Trees) as Steric Isomers

k	\widehat{S}_k (Centroidal)	\widetilde{S}_k (Bicentroidal)	$S_k^{(T)} = \widehat{S}_k + \widetilde{S}_k$ (Total)
1	1	0	1
2	0	1	1
3	1	0	1
4	1	1	2
5	3	0	3
6	2	3	5
7	11	0	11
8	9	15	24
9	55	0	55
10	70	66	136
11	345	0	345
12	494	406	900
13	2412	0	2412
14	3788	2775	6563
15	18127	0	18127
16	30799	19900	50699
17	143255	0	143255
18	256353	152076	408429
19	1173770	0	1173770
20	2190163	1206681	3396844
21	9892302	0	9892302
22	19130814	9841266	28972080
23	85289390	0	85289390
24	169923748	82336528	252260276
25	749329719	0	749329719
26	1531701274	702993756	2234695030
27	6688893605	0	6688893605
28	13984116304	6105180250	20089296554
29	60526543480	0	60526543480
30	129073842978	53822344278	182896187256
31	554188210352	0	554188210352
32	1202875816425	480681790786	1683557607211
33	5126819371356	0	5126819371356
34	11305776454475	4342078862605	15647855317080
35	47862049187447	0	47862049187447
36	107069728163762	39621836138886	146691564302648
37	450451875783866	0	450451875783866
38	1020892804306908	364831810979041	1385724615285949
39	4270217915878409	0	4270217915878409
40	9793778515638185	3386667673687950	13180446189326135
41	40745751356421890	0	40745751356421890
42	94477225495135372	31669036266203766	126146261761339138
43	391089580997271932	0	391089580997271932
44	915999112432034386	298116245118025503	1214115357550059889
45	3773978539594435261	0	3773978539594435261
46	8922080766443778872	2823386683457907820	11745467449901686692
47	36597363424982487170	0	36597363424982487170
48	87272162999179060850	26888517978723553635	114160680977902614485
49	356492605035316845170	0	356492605035316845170
50	856995930059758400988	257383017389543108190	1114378947449301509178

3D-skeleton **8-64** are governed by the coset representation $D_\infty(/C_\infty)$. In a similar way to Eq. 8.61, the CI-CF of this case is obtained as follows:

$$\text{CI-CF}(D_\infty, \mathcal{S}_d) = \frac{1}{2}(b_1^2 + b_2). \quad (8.87)$$

Our target is to obtain the value \widetilde{S}_k for enumerating the number of bicentroidal alkanes (3D-trees) of carbon content k as steric isomers in the form of the following generating function:

$$\widetilde{S}(x) = \sum_{k=0}^{\nu} \widetilde{S}_k x^k. \quad (8.88)$$

To evaluate this equation, the CI-CF represented by Eq. 8.87 is converted into the following functional equation:

$$\tilde{S}(x) = \frac{1}{2}(b(x)^2 + b(x^2)). \quad (8.89)$$

Because we have obtained $b(x)$ of alkyl ligands (monosubstituted alkanes) as shown in Eq. 8.32, the data up to m , i.e., $b(x)^{(m)} = \sum_{k=0}^m \beta_k x^k$, is introduced into the functional equation (Eq. 8.89). The resulting function is expanded to give a generating function, where the term x^{2m} is effective according to Jordan's criterion of bicentroidal trees (Def. 8.1). The coefficient of the term x^{2m} is adopted as the number for carbon content $k = 2m$. The evaluated values are listed in the \tilde{S}_k -column of Table 8.6.

The fifteen 3D structures collected in Fig. 8.12 are consistent with the value 15 at the intersection between the $k = 8$ -row and \tilde{S}_k -column of Table 8.6. Note that each 3D structure selected from a pair of enantiomers as well as each achiral 3D structure is counted once during the enumeration of steric isomers.

8.5.3 Total Enumeration of Alkanes (3D-Trees) as Steric Isomers

Let $S_k^{(T)}$ be the total number of alkanes (3D-trees) as steric isomers:

$$S(x)^{(T)} = \sum_{k=0}^{\infty} S_k^{(T)} x^k. \quad (8.90)$$

By summing up Eq. 8.85 and Eq. 8.88, we obtain the following relationship:

$$S_k^{(T)} = \hat{S}_k + \tilde{S}_k. \quad (8.91)$$

The evaluated values are listed in the $S_k^{(T)}$ -column of Table 8.6.

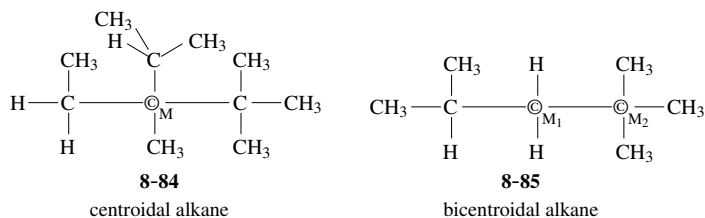
The nine 3D structures collected in Fig. 8.11 and the fifteen 3D structures collected in Fig. 8.12 are summed up to give twenty-four 3D structures of carbon content 8, which are consistent with the value 24 appearing at the intersection between the $k = 8$ -row and $S_k^{(T)}$ -column of Table 8.6.

8.6 Enumeration of Alkanes (Trees) as Graphs or Constitutional Isomers

8.6.1 Alkanes as Centroidal and Bicentroidal Trees

The definitions of centroidal and bicentroidal trees (Def. 8.1) originally aimed at characterizing trees (graphs), not 3D-trees, as proposed by Jordan [32]. In this section, trees are regarded as degenerate modes of 3D-trees described above. Accordingly, the scheme shown in Fig. 8.10 for characterizing centroidal and bicentroidal 3D-trees is converted into Fig. 8.13 for characterizing centroidal and bicentroidal trees.

Examples:



Skeletons for graphs or constitutional isomers (trees):



Fig. 8.13. Alkanes and their skeletons as centroidal and bicentroidal trees, which are enumerated as graphs (or constitutional isomers). The symbol \odot (attached by M) denotes a centroid, while the symbol $\odot-\odot$ (attached by M_1 and M_2) denotes a bicentroid.

8.6.2 Enumeration of Centroidal Alkanes (Trees) as Constitutional Isomers

To discuss centroidal alkanes (trees) as graphs, the centroidal 3D-skeleton **8-63** characterized by the coset representation T_d/C_{3v} (Fig. 8.10) is replaced by the centroidal skeleton **8-86** characterized by the symmetric group $S^{[4]}$ of degree 4 (Fig. 8.13), so that the concept of sphericities are disregarded.

According to this guideline, Eq. 7.29 degenerates to give the following CI:

$$CI(S^{[4]}; r_d) = \frac{1}{24}(r_1^4 + 3r_2^2 + 8r_1r_3 + 6r_1^2r_2 + 6r_4). \quad (8.92)$$

where we place $r_d = a_d = c_d = b_d$ to disregard sphericities. This equation has been noted by Pólya [8,9] by using $S^{[4]}$ directly according to Def. 7.1 (Eq. 7.11) and Theorem 7.2.

Our target is to obtain the value \widehat{R}_k for enumerating the number of alkanes of carbon content k as centroidal trees (graphs) in the form of the following generating function:

$$\widehat{R}(x) = \sum_{k=0}^v \widehat{R}_k x^k. \quad (8.93)$$

To evaluate this equation, the CI represented by Eq. 8.92 is converted into the following functional equation:

$$\widehat{R}(x) = \frac{x}{24}(r(x)^4 + 3r(x^2)^2 + 8r(x)r(x^3) + 6r(x)^2r(x^2) + 6r(x^4)). \quad (8.94)$$

Note that the multiplication by x is necessary to evaluate the effect of a central carbon atom of the centroidal skeleton **8-86**.⁷

Because we have obtained $r(x)$ of alkyl ligands (monosubstituted alkanes) as shown in Eq. 8.40, the data up to m , i.e., $r(x)^{(m)} = \sum_{k=0}^m R_k x^k$, is introduced into the functional equation (Eq. 8.94). The resulting function is expanded to give a generating function, where the terms of x^{2m+1} and x^{2m+2} are effective according to Jordan's criterion of centroidal trees (Def. 8.1). Their coefficients are adopted as the numbers for carbon content $k = 2m + 1$ and $2m + 2$. The evaluated values are listed in the \widehat{R}_k -column of Table 8.7.



Exercise 8.7. If an appropriate software for algebraic calculations (e.g., Maple and Mathematica) is available, conduct the calculation after the introduction of $r(x)^{(m)} = \sum_{k=0}^m R_k x^k$ (selected from Eq. 8.40) into the functional equation (Eq. 8.94). A code of Maple programming system for this purpose has been reported in [27, Section 6.2], which is available freely from the Web site of MATCH:

<http://match.pmf.kg.ac.rs/content57n2.htm>

Among the nine 3D structures collected in Fig. 8.11, a pair of enantiomers **8-72** and **8-72** is regarded as a set of stereoisomers, which coalesce to give a graph **8-72_g** and is counted once under the enumeration of constitutional isomers. As a result, the following partition is obtained:

$$\left(\langle \mathbf{8-65} \rangle \langle \mathbf{8-66} \rangle \langle \mathbf{8-67} \rangle \langle \mathbf{8-68} \rangle \langle \mathbf{8-69} \rangle \langle \mathbf{8-70} \rangle \langle \mathbf{8-71} \rangle \langle \mathbf{8-72} \overline{\mathbf{8-72}} \rangle \right), \quad (8.95)$$

where each equivalence class of stereoisomers is surrounded by a pair of angle brackets. Note that the graph **8-72_g** corresponds to an equivalence class of stereoisomers represented by $\langle \mathbf{8-72} \overline{\mathbf{8-72}} \rangle$. Hence, there are eight inequivalent entities, which are consistent with the value 8 appearing at the intersection between the $k = 8$ -row and \widehat{R} -column of Table 8.7.

8.6.3 Enumeration of Bicentroidal Alkanes (Trees) as Constitutional Isomers

To discuss bicentroidal alkanes (trees) as graphs, the bicentroidal 3D-skeleton **8-64** governed by \mathbf{K}/\mathbf{K}' or $\mathbf{D}_{\infty h}/\mathbf{C}_{\infty v}$ (Fig. 8.10) is replaced by the bicentroidal skeleton **8-87** governed by $\mathbf{S}^{[2]}$ (Fig. 8.13). Although these two skeletons have the same dumbbell shape, they are different in symmetry properties.

Because the two positions of **8-87** are governed by the symmetric group $\mathbf{S}^{[2]}$ of degree 2, they are characterized by the following CI:

$$\text{CI}(\mathbf{S}^{[2]}; r_d) = \frac{1}{2}(r_1^2 + r_2). \quad (8.96)$$

⁷ As found in Eq. 8.94 shown above, Eq. 23 of [1] should be corrected by multiplying x to evaluate the effect of a central carbon atom.

Table 8.7. Numbers of Alkanes (Trees) as Graphs or Constitutional Isomers

k	\widehat{R}_k (Centroidal)	\widetilde{R}_k (Bicentroidal)	$R_k^{(T)} = \widehat{R}_k + \widetilde{R}_k$ (Total)
1	1	0	1
2	0	1	1
3	1	0	1
4	1	1	2
5	3	0	3
6	2	3	5
7	9	0	9
8	8	10	18
9	35	0	35
10	39	36	75
11	159	0	159
12	202	153	355
13	802	0	802
14	1078	780	1858
15	4347	0	4347
16	6354	4005	10359
17	24894	0	24894
18	38157	22366	60523
19	148284	0	148284
20	237541	128778	366319
21	910726	0	910726
22	1511717	766941	2278658
23	5731580	0	5731580
24	9816092	4674153	14490245
25	36797588	0	36797588
26	64658432	29180980	93839412
27	240215803	0	240215803
28	431987953	185117661	617105614
29	1590507121	0	1590507121
30	2917928218	1193918545	4111846763
31	10660307791	0	10660307791
32	19910436898	7800816871	27711253769
33	72214088660	0	72214088660
34	137041997938	51584238201	188626236139
35	493782952902	0	493782952902
36	950665379038	344632209090	1295297588128
37	340490780161	0	340490780161
38	6640556836540	2324190638055	8964747474595
39	23647478933969	0	23647478933969
40	46677743532346	15804057614995	62481801147341
41	165351455535782	0	165351455535782
42	329965311285835	108277583483391	438242894769226
43	1163169707886427	0	1163169707886427
44	2344582517352728	746878494484128	3091461011836856
45	8227162372221203	0	8227162372221203
46	16737981626775790	5183852459907628	21921834086683418
47	58481806621987010	0	58481806621987010
48	120009045820117784	36183320654472855	156192366474590639
49	417612400765382272	0	417612400765382272
50	863868095187587242	253875556559366028	1117743651746953270

Our target is to obtain the value \widetilde{R}_k for enumerating the number of alkanes of carbon content k as bicentroidal trees (graphs) in the form of the following generating function:

$$\widetilde{R}(x) = \sum_{k=0}^{\infty} \widetilde{R}_k x^k. \quad (8.97)$$

To evaluate this equation, the CI represented by Eq. 8.96 is converted into the following functional equation:

$$\widetilde{R}(x) = \frac{1}{2}(r(x)^2 + r(x^2)). \quad (8.98)$$

Because we have obtained $r(x)$ of alkyl ligands (monosubstituted alkanes) as shown in Eq. 8.40, the data up to m , i.e., $r(x)^{(m)} = \sum_{k=0}^m R_k x^k$, is introduced into the functional equation (Eq. 8.98). The resulting function is expanded to give a generating function, where the term of x^{2m} is effective according to Jordan's criterion of bicentroidal trees (Def. 8.1). Their coefficients are adopted as the numbers for carbon content $k = 2m$. The evaluated values are listed in the \tilde{R}_k -column of Table 8.7.



Exercise 8.8. If an appropriate software for algebraic calculations (e.g., Maple and Mathematica) is available, conduct the calculation after the introduction of $r(x)^{(m)} = \sum_{k=0}^m R_k x^k$ (selected from Eq. 8.40) into the functional equation (Eq. 8.98). A code of Maple programming system for this purpose has been reported in [27, Section 6.2], which is available freely from the Web site of MATCH:

<http://match.pmf.kg.ac.rs/content57n2.htm>

Among the fifteen 3D structures collected in Fig. 8.12, a set of **8-79**, **8-83**, and $\overline{\mathbf{8-83}}$ is recognized as an equivalence class of stereoisomers, so that the set is counted once under the enumeration of constitutional isomers. Moreover, each pair of enantiomers linked with an underbrace as well as each achiral entity is counted once under the enumeration of constitutional isomers. When each equivalence class of stereoisomers is surrounded by a pair of angle brackets, the following partition is obtained:

$$\left(\langle \mathbf{8-73} \rangle \langle \mathbf{8-74} \rangle \langle \mathbf{8-75} \rangle \langle \mathbf{8-76} \rangle \langle \mathbf{8-77} \rangle \langle \mathbf{8-78} \rangle \langle \mathbf{8-79} \mathbf{8-83} \overline{\mathbf{8-83}} \rangle \right. \\ \left. \langle \mathbf{8-80} \overline{\mathbf{8-80}} \rangle \langle \mathbf{8-81} \overline{\mathbf{8-81}} \rangle \langle \mathbf{8-82} \overline{\mathbf{8-82}} \rangle \right). \quad (8.99)$$

Hence, there appear ten equivalence classes of stereoisomers, which are inequivalent under a stereoisomeric relationship during the enumeration of constitutional isomers. See the flowchart of Fig. 2.4 on page 47, where the judgement due to isoskeletomeric relationships is omitted to obtain the partition of Eq. 8.99. This value is consistent with the value 10 appearing at the intersection between the $k = 8$ -row and \tilde{R} -column of Table 8.7.



Exercise 8.9.

- Compare the set of **8-79**, **8-83**, and $\overline{\mathbf{8-83}}$ (Fig. 8.12) with the set of tartaric acids, where the enumeration results as constitutional isomers (Table 8.7) are taken into consideration.
- Discuss the prochirality of **8-79** as a *meso*-compound by referring to Fig. 4.13 (page 109).

8.6.4 Total Enumeration of Alkanes (Trees) as Graphs or Constitutional Isomers

Let $R_k^{(T)}$ be the total number of alkanes as trees (graphs):

$$R(x)^{(T)} = \sum_{k=0}^{\infty} R_k^{(T)} x^k. \quad (8.100)$$

By summing up Eq. 8.93 and Eq. 8.97, we obtain the following relationship:

$$R_k^{(T)} = \widehat{R}_k + \widetilde{R}_k. \quad (8.101)$$

The evaluated values are listed in the $R_k^{(T)}$ -column of Table 8.7.

The nine 3D structures collected in Fig. 8.11 and the fifteen 3D structures collected in Fig. 8.12 are respectively partitioned into Eq. 8.95 and Eq. 8.99. Hence, the total number is found to be 18 (= 8 + 10) by counting pairs of angle brackets. This value is consistent with the value 18 appearing at the intersection between the $k = 8$ -row and $R_k^{(T)}$ -column of Table 8.7.

References

- [1] S. Fujita, *Bull. Chem. Soc. Jpn.*, **83**, 1–18 (2010).
- [2] A. Cayley, *Philos. Mag.*, **47**, 444–446 (1874).
- [3] A. Cayley, *Rep. Brit. Assoc. Advance. Sci.*, **45**, 257–305 (1875).
- [4] A. Cayley, *Am. J. Math.*, **4**, 266–268 (1881).
- [5] H. R. Henze and C. M. Blair, *J. Am. Chem. Soc.*, **53**, 3042–3046 (1931).
- [6] H. R. Henze and C. M. Blair, *J. Am. Chem. Soc.*, **53**, 3077–3085 (1931).
- [7] N. L. Biggs, E. K. Lloyd, and R. J. Wilson, “Graph Theory 1736–1936”, Oxford Univ. Press, Oxford (1976).
- [8] G. Pólya, *Acta Math.*, **68**, 145–254 (1937).
- [9] G. Pólya and R. C. Read, “Combinatorial Enumeration of Groups, Graphs, and Chemical Compounds”, Springer-Verlag, New York (1987).
- [10] N. G. de Bruijn, *Indag. Math.*, **21**, 59–69 (1959).
- [11] L. Bytautas and D. J. Klein, *J. Chem. Inf. Comput. Sci.*, **38**, 1063–1078 (1998).
- [12] G. Pólya, R. E. Tarjan, and D. R. Woods, “Notes on Introductory Combinatorics”, Birkhäuser, Boston (1983).
- [13] R. W. Robinson, F. Harary, and A. T. Balaban, *Tetrahedron*, **32**, 355–361 (1976).
- [14] R. Otter, *Ann. Math.*, **49**, 583–599 (1948).
- [15] S. Fujita, *J. Math. Chem.*, **43**, 141–201 (2008).

- [16] S. Fujita, *Theor. Chem. Acc.*, **113**, 73–79 (2005).
- [17] S. Fujita, *Theor. Chem. Acc.*, **113**, 80–86 (2005).
- [18] S. Fujita, *Theor. Chem. Acc.*, **115**, 37–53 (2006).
- [19] S. Fujita, *Theor. Chem. Acc.*, **117**, 353–370 (2007).
- [20] S. Fujita, *Theor. Chem. Acc.*, **117**, 339–351 (2007).
- [21] S. Fujita, *J. Comput. Chem. Jpn.*, **6**, 59–72 (2007).
- [22] S. Fujita, *J. Comput. Chem. Jpn.*, **6**, 73–90 (2007).
- [23] S. Fujita, *Bull. Chem. Soc. Jpn.*, **81**, 193–219 (2008).
- [24] S. Fujita, *Bull. Chem. Soc. Jpn.*, **81**, 1078–1093 (2008).
- [25] S. Fujita, *MATCH Commun. Math. Comput. Chem.*, **61**, 273–312 (2009).
- [26] S. Fujita, *MATCH Commun. Math. Comput. Chem.*, **57**, 265–298 (2007).
- [27] S. Fujita, *MATCH Commun. Math. Comput. Chem.*, **57**, 299–340 (2007).
- [28] S. Fujita, *MATCH Commun. Math. Comput. Chem.*, **58**, 5–45 (2007).
- [29] S. Fujita, *MATCH Commun. Math. Comput. Chem.*, **59**, 509–554 (2008).
- [30] S. Fujita, *Bull. Chem. Soc. Jpn.*, **81**, 1423–1453 (2008).
- [31] S. Fujita, *MATCH Commun. Math. Comput. Chem.*, **62**, 23–64 (2009).
- [32] C. Jordan, *J. Reine Angew. Math.*, **70**, 185–190 (1869).
- [33] F. Harary, “Graph Theory”, Addison-Wesley, Reading (1969).

9 Permutation-Group Symmetry

9.1 Historical Comments

From a group-theoretical point of view, confusion in modern stereochemistry stems from the fact that permutation groups (e.g., the symmetric group $S^{[4]}$ of degree 4) are misleadingly used in place of point groups (e.g., T_d), as if permutation groups (not point groups) could describe geometric features (e.g., chirality/achirality) of stereochemistry. This chapter is devoted to demonstrate how permutation groups have been mixed up with point groups in modern stereochemistry. The concept of *RS*-permutation groups isomorphic to point groups will be introduced to settle the misleading situations of modern stereochemistry.

The application of permutation-group symmetry in chemical fields was first established by Pólya's theorem (Section 7.2), where the symmetric group $S^{[n]}$ (degree: $n = 3$ or 4) or the alternating group $A^{[n]}$ (degree: $n = 3$ or 4) was used for the purpose of counting monosubstituted alkanes (alkyl ligands) and alkanes, as described in Sections 8.3 and 8.6. There have appeared its generalization by de Bruijn [1] and its modification by Ruch et al. [2]. The term *permutational isomerism* has been defined by Ugi et al. [3,4]. The term *stereogenic* proposed by McCasland [5] has been revived by Mislow and Siegel [6], where models of stereoisomers are generated by permutation of ligands among the sites of a tetrahedral skeleton as a stereogenic center. Thereby, stereoisomers are recognized as prototypes of permutational isomers and the 'asymmetric carbon atom' as the prototype of a 'stereogenic atom' [5], as pointed out by Mislow and Siegel [6].

Even in Mislow-Siegel's discussion [6], the special effects of chiral ligands are not properly treated in the action of a permutation. For example, Mislow and Siegel [6, page 3321] stated that transposition of ligands in the *trans* sites of a chiral hexacoordinate complex with the skeleton **3-13** (page 73) leads to the enantiomorph (e.g., **3-13** \rightarrow **9-1**), while transposition of ligands in the *cis* sites does not afford the enantiomorph (e.g., **3-13** \rightarrow **9-2**). As found in Fig. 9.1, however, the first-half part of this statement presumes that all of the six ligands are achiral proligands (e.g., A, B, W, X, Y, and Z). In fact, if we take account of a set of proligands containing chiral proligands (e.g., A, B, X, Y, Z, and p, where p denotes a chiral proligand), the resulting complex **9-1** with A, B, X, Y, Z, and p is no longer the enantiomorph of the original complex **3-13** with A, B, X, Y, Z, and p.

This type of misleading presumptions, i.e., disregard of chiral (pro)ligands, have widely appeared, although a conventional attitude towards such disregard may be tentative according to the purpose of discussions. For example, Zelewsky's textbook [7, page 58] claimed that "An atomic center in a molecule is called stereogenic if an interchange of two ligands leads to a stereoisomer. If the stereoisomer obtained is the other enantiomer of a pair, the atom is a chiral center." This claim is somewhat misleading, because an interchange of two ligands is implicitly linked to stereogenicity as well as to chirality. The latter linkage to chirality is permitted only with respect to cases without chiral ligands. Remember that such an

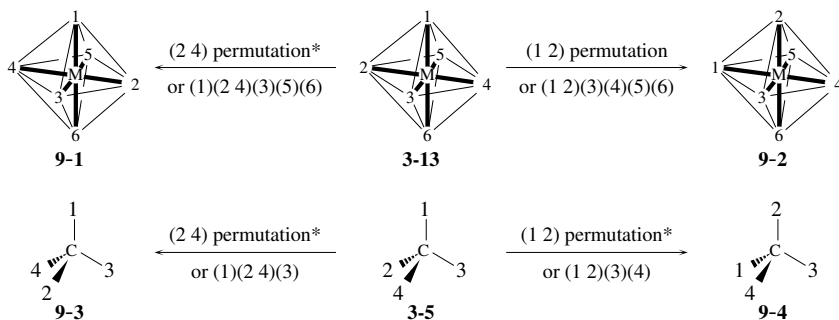


Fig. 9.1. Permutations of two positions in an octahedral skeleton and in a tetrahedral skeleton.

interchange of two ligands is conceptually distinct from a reflection, even though they may coalesce with each other in cases without chiral ligands.

Moreover, Mislow and Siegel [6, page 3321] stated that “It follows that among chiral assemblies constructed from achiral permutation frames and achiral ligands, *the regular tetrahedron is the only skeleton in which every transposition of ligands is equivalent to a reversal in the sense of chirality of ligand assembly.*” In fact, if all of the four ligands of **3-5** (page 55) are achiral proligands (e.g., A, B, X, and Y), every transposition of ligands results in the formation of the enantiomorph (e.g., **9-3** or **9-4**). See Fig. 9.1.

In contrast, if we take account of a set of proligands containing chiral proligands (e.g., A, B, X, and p, where p denotes a chiral proligand), the resulting entity with A, B, X, and p (e.g., **9-3** or **9-4**) is no longer the enantiomorph of the original entity **3-5** with A, B, X, and p. Strictly speaking, the word “equivalent” in the expression “every transposition of ligands is equivalent to a reversal in the sense of chirality of ligand assembly” [6] is misleading, because cases with chiral ligands are not referred to, so as to be treated as exceptions. Note that transposition of ligands is conceptually distinct from, and by no means equivalent to a reflection for a reversal in the sense of chirality of ligand assembly, even though they may coalesce with each other to provide the equivalent effects.

As found in the preceding historical comments, the distinction between stereogenicity and chirality in cases with chiral ligands is crucial to comprehend stereoisomerism and molecular geometry. In spite of this feature, the conventional ways described above have made light of such cases as having chiral ligands, so that main descriptions in the conventional ways have been concerned only with cases without chiral ligands, while cases with chiral ligands are entirely disregarded or treated at most as exceptions. It follows that a new theoretical framework for treating achiral and chiral ligands evenly is highly desirable, where stereogenicity and chirality should be integrated in a consistent fashion.

Fujita has developed the stereoisogram approach to such a new theoretical framework, where the concept of *RS-stereogenicity* is proposed as a substantial restriction of the concept of stereogenicity, so as to be integrated meaningfully with the concept of chirality to treat achiral and chiral ligands evenly [8–10]. Group-theoretically speaking, *RS*-permutation

groups are proposed as a substantial restriction of permutation groups [9,11]¹ and integrated meaningfully with point groups to give *RS*-stereoisomeric groups as a new class of groups. Thus, chirality is linked with point groups, *RS*-stereogenicity is linked with *RS*-permutation groups, and *RS*-stereoisomerism is linked with *RS*-stereoisomeric groups. Fujita has divided *stereoisograms* as diagrammatic expressions of *RS*-stereoisomeric groups (and *RS*-stereoisomerism).

Fujita's stereoisogram approach has revealed that, just as a pair of enantiomers (or an achiral molecular entity) belongs to a point group, a pair of *RS*-diastereomers (or an *RS*-astereogenic entity) belongs to an *RS*-permutation group. As a result, a point group is frequently confused with an *RS*-permutation group in the conventional ways described above.

In this chapter, the concept of *RS-stereogenicity* based *RS*-permutation groups will be discussed as a substantial restriction of the concept of stereogenicity based on permutation groups.

9.2 Permutation Groups

9.2.1 Permutation Groups as Subgroups of Symmetric Groups

The six positions of the octahedral skeleton **3-13** (the top row of Fig. 9.1), which are governed by the coset representation $O_h(/C_{4v})$ based on the point group O_h (order 48), are regarded as being alternatively governed by the symmetric group of degree 6 denoted by the symbol $S^{[6]}$. The symmetric group $S^{[6]}$ is composed of totally $6!$ ($= 720$) permutations. Among these permutations, the permutations stabilizing the skeleton **3-13** (and its homomeric skeletons) construct a permutation group of order 24, which can be equalized to the coset representation $O(/C_4)$.² Note the point group O_h has the maximum chiral subgroup O (order 24), which has 24 permutations common with the symmetric group $S^{[6]}$, if the coset representation $O_h(/C_{4v})$ is taken into consideration. For the simplicity's sake, the symbol O is tentatively used to denote a permutation group which is a subgroup of $S^{[6]}$. Thus, the group O is a subgroup of the point group O_h as well as a subgroup of the symmetric group $S^{[6]}$.

For example, a two-fold rotation along the axis 1—6 is represented by the permutation $(1)(2\ 4)(3\ 5)(6)$, which generates a homomer of the original skeleton **3-13**. This permutation is contained in the permutation group O .

¹ Integration of point groups and permutation groups has been first reported by Fujita [11], where the term *RS*-permutation group was not coined although the concept of *RS*-permutation groups was substantially described by characterizing the elements of the groups. The term *RS-permutation group* has been coined in a successive report by Fujita [9].

² For the coset representation for characterizing the octahedral skeleton **3-13**, see recent reports by Fujita [12–14].

On the other hand, the permutation (2 4) (or (1)(2 4)(3)(5)(6) $\in \mathbf{S}^{[6]}$) for the conversion **3-13** \rightarrow **9-1** is not contained in **O**. In addition, the permutation (1 2) (or (1 2)(3)(4)(5)(6) $\in \mathbf{S}^{[6]}$) for the conversion **3-13** \rightarrow **9-2** is not contained in **O**. The two permutations (2 4) and (1 2), however, are different in the effects on the skeleton **3-13** with achiral proligands (A, B, W, X, Y, and Z), as described above. It is desirable to differentiate the two permutations (2 4) and (1 2) by formulating an appropriate subgroup of $\mathbf{S}^{[6]}$.

The four positions of the octahedral skeleton **3-5** (the bottom row of Fig. 9.1), which are governed by the coset representation T_d/C_{3v} based on the point group T_d , are regarded as being alternatively governed by the symmetric group of degree 4 denoted by the symbol $\mathbf{S}^{[4]}$. The symmetric group $\mathbf{S}^{[4]}$ is composed of totally 4! (= 24) permutations. Among these permutations, the permutations stabilizing the skeleton **3-5** (and its homomeric skeletons) construct an alternating group $\mathbf{A}^{[4]}$ as a permutation group of order 12, which can be equalized to the coset representation T/C_3 .³

The permutation (2 4) (or (1)(2 4)(3) $\in \mathbf{S}^{[4]}$) for the conversion **3-5** \rightarrow **9-3** is not contained in $\mathbf{A}^{[4]}$. In addition, the permutation (1 2) (or (1 2)(3)(4) $\in \mathbf{S}^{[4]}$) for the conversion **3-5** \rightarrow **9-4** is not contained in $\mathbf{A}^{[4]}$. The two permutations (2 4) and (1 2) exhibit the same effect on the skeleton **3-5** with achiral proligands (A, B, X, and Y), as described above. It is desirable to rationalize the same effect in $\mathbf{S}^{[4]}$, where this rationalization should be consistent with the two permutations (2 4) and (1 2) which exhibit different effects in $\mathbf{S}^{[6]}$.

9.2.2 Permutations vs. Reflections

As found in the left part of Fig. 9.1, the conversion due to the permutation (2 4) from the numbered skeleton **3-13** to another numbered skeleton **9-1** does not represent a reflection (a mirror-image formation), because it takes account of achiral (pro)ligands only and disregards chiral (pro)ligands. These misleading features can be avoided by considering mirror-numbered skeletons defined by Def. 3.4 (page 57).

According to the proligand-promolecule model combined with Def. 3.4 (page 57), the reflection concerned with the mirror plane 1–3–6–5 in the numbered skeleton **3-13** is represented by a permutation $\overline{(1)(2\ 4)(3)(5)(6)}$, where an overbar represents the reverse of chirality sense at the position. The reflection $\overline{(1)(2\ 4)(3)(5)(6)}$ converts the numbered skeleton **3-13** into the mirror-numbered skeleton $\overline{\mathbf{3-13}}$, as shown in Fig. 9.2.⁴

³ For the coset representation for characterizing the tetrahedral skeleton **3-5**, see recent reports by Fujita [15–17].

⁴ According to Fujita's stereoisogram approach, the relationship between **9-1** and $\overline{\mathbf{3-13}}$ is holantimeric. The relationship between **3-13** and **9-1** is *RS*-diastereomeric. The relationship between **3-13** and $\overline{\mathbf{3-13}}$ is enantiomeric. In addition to the three skeletons, an additional skeleton $\overline{\mathbf{9-1}}$ holantimeric to the original skeleton **3-13** is taken into consideration. Then, the relationship between **9-1** and $\overline{\mathbf{9-1}}$ is enantiomeric, so that the totally four skeletons construct a stereoisogram.

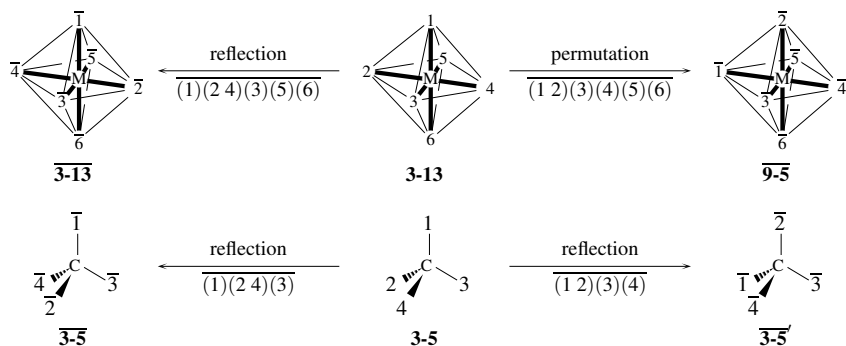


Fig. 9.2. Reflections vs. Permutations of two positions in an octahedral skeleton and in a tetrahedral skeleton.

The process due to the reflection $\overline{(1)(2\ 4)(3)(5)(6)}$, i.e., $\mathbf{3-13} \rightarrow \overline{\mathbf{3-13}}$ (Fig. 9.2), is strictly differentiated from the process due to the permutation $(2\ 4)$, i.e., $\mathbf{3-13} \rightarrow \mathbf{9-1}$ (Fig. 9.1). Note that $\overline{(1)(2\ 4)(3)(5)(6)}$ can be regarded as a combined operation of $(2\ 4)$ (or $(1)(2\ 4)(3)(5)(6)$) with an identity ligand reflection $\overline{(1)(2)(3)(4)(5)(6)}$. In the case that all of the six ligands attached are achiral proligands (e.g., A, B, W, X, Y, and Z), the resulting mirror-numbered skeleton $\overline{\mathbf{3-13}}$ (Fig. 9.2) generates a mirror-image complex, because $\overline{A} = A$, $\overline{B} = B$, $\overline{W} = W$, $\overline{X} = X$, $\overline{Y} = Y$, and $\overline{Z} = Z$, where the symbol \overline{A} etc. represent the mirror-image proligand of A etc. in isolation. At the same time, even if we take account of a set of proligands containing chiral proligands (e.g., A, B, X, Y, Z, and p, where p denotes a chiral proligand), the resulting complex $\overline{\mathbf{3-13}}$ with A, B, X, Y, Z, and \overline{p} is a mirror-image of the original complex $\mathbf{3-13}$ with A, B, X, Y, Z, and p, because $\overline{B} = B$, $\overline{X} = X$, $\overline{Y} = Y$, $\overline{Z} = Z$, and $\overline{p} = \overline{p}$. Hence, the permutation $(1)(2\ 4)(3)(5)(6)$ is paired with the reflection $\overline{(1)(2\ 4)(3)(5)(6)}$, where the pairing stems from the coalescence in cases without chiral ligands.

Remark 9.1 (Misleading Convention of Modern Stereochemistry). The convention of modern stereochemistry misleadingly equalizes the permutation $(1)(2\ 4)(3)(5)(6)$ and the reflection $\overline{(1)(2\ 4)(3)(5)(6)}$ in all cases without and with chiral (pro)ligands.⁵ This equalization could be justified only if the permutation $(1)(2\ 4)(3)(5)(6)$ and the reflection $\overline{(1)(2\ 4)(3)(5)(6)}$ bring about the same effect to a skeleton at issue, e.g., the case that all of the six ligands attached to the skeleton $\mathbf{3-13}$ are achiral proligands (e.g., A, B, W, X, Y, and Z). Such justification is impossible in general, as found in the above-mentioned discussions. In fact, by comparing the resulting numbered skeleton $\mathbf{9-1}$ (Fig. 9.1) with the corresponding mirror-numbered skeleton $\overline{\mathbf{3-13}}$ (Fig. 9.2), the misleading feature of the convention is clearly demonstrated in cases with chiral (pro)ligands (e.g., A, B, X, Y, Z, and p).

On the other hand, the permutation $\overline{(1\ 2)(3)(4)(5)(6)}$ converts **3-13** into $\overline{\mathbf{9-5}}$ (Fig. 9.2), which is not enantiomeric to **3-13**.⁶ In other words, the permutation $\overline{(1\ 2)(3)(4)(5)(6)}$ cannot be regarded as a reflection. Hence, the permutation $(1\ 2)(3)(4)(5)(6)$ is not paired with the permutation $\overline{(1\ 2)(3)(4)(5)(6)}$ from a viewpoint of enantiomeric relationships.

Let us next consider the application of a reflection to the numbered tetrahedral skeleton **3-5** (Fig. 9.2). According to the proligand-promolecule model combined with Def. 3.4 (page 57), the reflection concerned with the mirror plane 1—C—3 in the numbered skeleton **3-5** is represented by a permutation $\overline{(1)(2\ 4)(3)}$, where an overbar represents the reverse of chirality sense at the position. The reflection $\overline{(1)(2\ 4)(3)}$ converts the numbered skeleton **3-5** into the mirror-numbered skeleton $\overline{\mathbf{3-5}}$, as shown in Fig. 9.2.⁷

The process due to the reflection $\overline{(1)(2\ 4)(3)}$, i.e., **3-5** \rightarrow $\overline{\mathbf{3-5}}$ (Fig. 9.2), is strictly differentiated from the process due to the permutation $(2\ 4)$, i.e., **3-5** \rightarrow **9-3** (Fig. 9.1). In a similar way to the octahedral skeleton **3-13**, the tetrahedral skeleton **3-5** can be discussed, where a set of four achiral proligands A, B, X, and Y or a set of A, B, X, and p (p: chiral) is taken into consideration. Hence, the permutation $(1)(2\ 4)(3)$ is paired with the reflection $\overline{(1)(2\ 4)(3)}$. The pairing stems from coalescence in cases without chiral ligands.

The application of $\overline{(1\ 2)(3)(4)}$ to **3-5** generates $\overline{\mathbf{3-5'}}$, which is homomeric to $\overline{\mathbf{3-5}}$. This means that $\overline{(1\ 2)(3)(4)}$ paired with $(1\ 2)(3)(4)$ also represents a reflection.

Comparison between Fig. 9.1 and Fig. 9.2 reveals that there are two types of permutations: that is to say, the permutations with an asterisk in Fig. 9.1 are paired with the reflections shown in Fig. 9.2, while the permutation without an asterisk remains unpaired with a reflection.

9.3 *RS*-Permutation Groups

9.3.1 *RS*-Permutations and *RS*-Diastereomeric Relationships

The formulation of numbered skeletons and mirror-numbered skeletons (Def. 3.4 on page 57) has revealed the presence of two types of permutations, i.e., permutations which may be correlated to reflections and permutations with no correlation to reflections, as discussed in

⁵ Such a permutation (e.g., $(1)(2\ 4)(3)(5)(6)$) as paired with a reflection (e.g., $\overline{(1)(2\ 4)(3)(5)(6)}$) is called an *RS-permutation* (Def. 9.1) according to Fujita's stereoisogram approach.

⁶ According to Fujita's stereoisogram approach, the relationship between **9-2** (Fig. 9.1) and $\overline{\mathbf{9-5}}$ (Fig. 9.2) is holantimeric.

⁷ According to Fujita's stereoisogram approach, the relationship between **9-3** and $\overline{\mathbf{3-5}}$ is holantimeric. The relationship between **3-5** and **9-3** is *RS*-diastereomeric. The relationship between **3-5** and $\overline{\mathbf{3-5}}$ is enantiomeric. In addition to the three skeletons, an additional skeleton $\overline{\mathbf{9-3}}$ holantimeric to the original skeleton **3-5** is taken into consideration. Then, the relationship between **9-3** and $\overline{\mathbf{9-3}}$ is enantiomeric, so that the totally four skeletons construct a stereoisogram.

the preceding section. To differentiate these two types (cf. Remark 9.1), Fujita has coined the term *RS-permutation* [9]:

Definition 9.1 (*RS-Permutations*). Let us consider a permutation on the positions of a given skeleton. A permutation which corresponds to a reflection but exhibits no reverse of chirality sense at each position is called an *RS-permutation*.

The prefix *RS* stems from the fact that the concepts of *RS*-permutations and *RS*-permutation groups (not permutations nor permutation groups) have been proved by Fujita [10,18] to be a basis for the *RS*-stereodescriptors of the Cahn-Ingold-Prelog (CIP) system.

An *RS*-permutation (e.g., (1)(2 4)(3)(5)(6) or (1)(2 4)(3)) is concerned with the process converting a numbered-skeleton into another numbered skeleton (e.g., **3-13** → **9-1** or **3-5** → **9-3**), while a reflection (e.g., $\overline{(1)(2\ 4)(3)(5)(6)}$ or $\overline{(1)(2\ 4)(3)}$) is concerned with the process converting a numbered-skeleton into a mirror-numbered skeleton (e.g., **3-13** → $\overline{\mathbf{3-13}}$ or **3-5** → $\overline{\mathbf{3-5}}$).

A pair of two (pro)molecules which are convertible by a reflection is called a pair of *enantiomers*. To emphasize the difference between reflections and *RS*-permutations, the term *RS-diastereomeric* is coined by Fujita in the formulation of Fujita's stereoisogram approach [8–10]:

Definition 9.2 (*RS-Diastereomeric Relationships*). Suppose that a (pro)molecule based on a numbered skeleton is converted into a (pro)molecule on another numbered skeleton under the action of an *RS*-permutation (Def. 9.1). The relationship between the original (pro)molecule and the product (pro)molecule is defined as an *RS-diastereomeric* relationship. The two promolecules are referred to as a pair of *RS-diastereomers*.

9.3.2 *RS*-Permutation Groups vs. Point Groups

RS-Permutation Groups Based on *RS*-Permutations

To show a *RS*-permutation group based on *RS*-permutations, let us re-examine a trigonal pyramidal skeleton **8-1** shown in Fig. 8.1 (page 195). The trigonal pyramidal skeleton **8-1** can be regarded as a phosphine skeleton **9-6**, if the center is considered to be a phosphorus atom and the solid circle is considered to be a lone pair, as shown in Fig. 9.3.

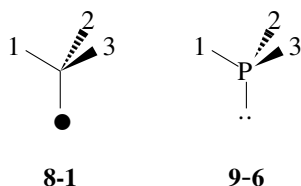


Fig. 9.3. Trigonal pyramidal skeleton and a phosphine skeleton

Table 9.1. *RS*-Permutation Group $C_{3\tilde{\sigma}}$, Coset Representation $C_{3\tilde{\sigma}}(/C_{\tilde{\sigma}})$, and the Symmetric Group $S^{[3]}$ of Degree 3

operation $g \in C_{3\tilde{\sigma}}$	$C_{3\tilde{\sigma}}(/C_{\tilde{\sigma}})$ (product of cycles)	$S^{[3]}$ (product of cycles)	cycle term
I	(1)(2)(3)	(1)(2)(3)	s_1^3
C_3	(1 3 2)	(1 3 2)	s_3
C_3^2	(1 2 3)	(1 2 3)	s_3
$\tilde{\sigma}_{v(1)}$	(1)(2 3)	(1)(2 3)	$s_1 s_2$
$\tilde{\sigma}_{v(2)}$	(1 3)(2)	(1 3)(2)	$s_1 s_2$
$\tilde{\sigma}_{v(3)}$	(1 2)(3)	(1 2)(3)	$s_1 s_2$

From a viewpoint of point-group symmetry, the three positions of **8-1** is governed by the coset representation $C_{3v}/(C_s)$, as summarized in Table 8.1 (page 196). As shown in Fig. 8.1 (page 195), each reflection, $\sigma_{v(1)}$ ($\sim \overline{(1)(2\ 3)}$), $\sigma_{v(2)}$ ($\sim \overline{(1\ 3)(2)}$), or $\sigma_{v(3)}$ ($\sim \overline{(1\ 2)(3)}$), brings about the conversion of the numbered skeleton **8-1a** into a mirror-numbered skeleton, i.e., **8-1a** \rightarrow **8-1d**, **8-1a** \rightarrow **8-1e**, or **8-1a** \rightarrow **8-1f**. It follows that the relationship between **8-1a** and **8-1d** (or **8-1e** or **8-1f**) is concluded to be an enantiomeric relationship.

By omitting a ligand reflection, each reflection, $\sigma_{v(1)}$ ($\sim \overline{(1)(2\ 3)}$), $\sigma_{v(2)}$ ($\sim \overline{(1\ 3)(2)}$), or $\sigma_{v(3)}$ ($\sim \overline{(1\ 2)(3)}$), generates an *RS*-permutation, $\tilde{\sigma}_{v(1)}$ ($\sim (1)(2\ 3)$), $\tilde{\sigma}_{v(2)}$ ($\sim (1\ 3)(2)$), or $\tilde{\sigma}_{v(3)}$ ($\sim (1\ 2)(3)$), as collected in Table 9.1. Thereby, the point group C_{3v} is converted into an *RS*-permutation group $C_{3\tilde{\sigma}}$ shown in Table 9.1. The three positions of the trigonal pyramidal skeleton **8-1** are governed by the coset representation $C_{3\tilde{\sigma}}(/C_{\tilde{\sigma}})$. The resulting *RS*-permutation group $C_{3\tilde{\sigma}}$ is isomorphic to the symmetric group $S^{[3]}$ of degree 3, so that the coset representation $C_{3\tilde{\sigma}}(/C_{\tilde{\sigma}})$ can be equalized to $S^{[3]}$, as collected in Table 9.1.

As shown in Fig. 9.4, each *RS*-permutation, $\tilde{\sigma}_{v(1)}$ ($\sim (1)(2\ 3)$), $\tilde{\sigma}_{v(2)}$ ($\sim (1\ 3)(2)$), or $\tilde{\sigma}_{v(3)}$ ($\sim (1\ 2)(3)$), brings about the conversion of the numbered skeleton **8-1a** into another numbered skeleton called an *RS-numbered skeleton*, i.e., **8-1a** \rightarrow **8-1d'**, **8-1a** \rightarrow **8-1e'**, or **8-1a** \rightarrow **8-1f'**. It follows that the relationship between **8-1a** and **8-1d'** (or **8-1e'** or **8-1f'**) is concluded to be an *RS*-diastereomeric relationship (Def. 9.2), but not to be an enantiomeric relationship. Compare Fig. 9.4 with Fig. 8.1 (page 195).

The point group C_{3v} has a non-redundant set of subgroups:

$$\text{SSG}_{C_{3v}} = \{C_1, C_s, C_3, C_{3v}\}, \quad (9.1)$$

where the respective subgroups are selected as follows:

$$C_1 = \{I\} \quad (9.2)$$

$$C_s = \{I, \sigma_{v(1)}\} \quad (9.3)$$

$$C_3 = \{I, C_{3(1)}, C_{3(1)}^2\} \quad (9.4)$$

$$C_{3v} = \{I, C_{3(1)}, C_{3(1)}^2, \sigma_{v(1)}, \sigma_{v(2)}, \sigma_{v(3)}\}. \quad (9.5)$$

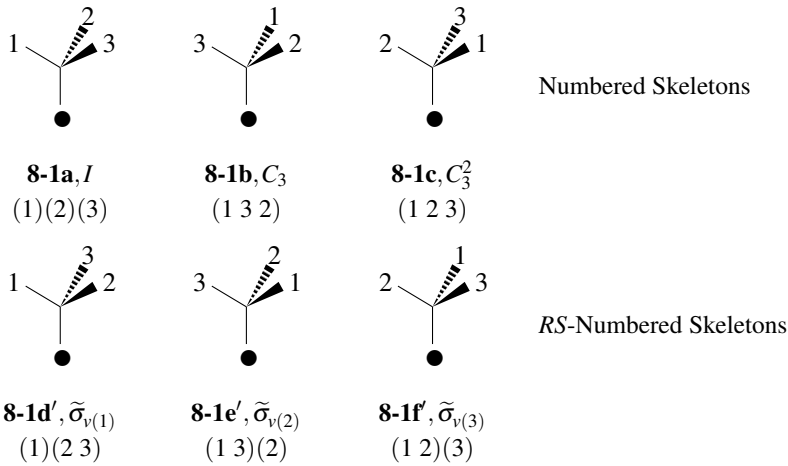


Fig. 9.4. Symmetry operations of the *RS*-permutation group $C_{3\tilde{\sigma}}$ for a trigonal pyramidal skeleton **8-1**. The identity operation (*I*) converts **8-1** into itself, where the resulting skeleton is denoted as **8-1a**. The top row lists homomeric numbered skeletons, while the bottom row lists homomeric *RS*-numbered skeletons.

Because the *RS*-permutation group $C_{3\tilde{\sigma}}$ is isomorphic to the point group C_{3v} , its non-redundant set of subgroups (SSG) is obtained as follows:

$$\text{SSG}_{C_{3\tilde{\sigma}}} = \{C_1, C_{\tilde{\sigma}}, C_3, C_{3\tilde{\sigma}}\}, \quad (9.6)$$

where the respective subgroups are selected as follows:

$$C_1 = \{I\} \quad (9.7)$$

$$C_{\tilde{\sigma}} = \{I, \tilde{\sigma}_{v(1)}\} \quad (9.8)$$

$$C_3 = \{I, C_{3(1)}, C_{3(1)}^2\} \quad (9.9)$$

$$C_{3\tilde{\sigma}} = \{I, C_{3(1)}, C_{3(1)}^2, \tilde{\sigma}_{v(1)}, \tilde{\sigma}_{v(2)}, \tilde{\sigma}_{v(3)}\}. \quad (9.10)$$

Enumeration Under *RS*-Permutation Groups

Let us examine the gross enumeration based on the trigonal pyramidal skeleton **8-1** under the *RS*-permutation group $C_{3\tilde{\sigma}}$ ($= \mathbf{S}^{[3]}$). The cycle terms appearing in Table 9.1 are summed up and divided by 6 ($= |C_{3\tilde{\sigma}}|$) so as to give a cycle index (CI) as follows:

$$\text{CI}_{\mathbf{8-1}}(C_{3\tilde{\sigma}}, s_d) = \frac{1}{6}(s_1^3 + 2s_3 + 3s_1s_2). \quad (9.11)$$

The same CI is alternatively obtained by substituting s_d for a_d , c_d , or b_d in the CI-CF shown in Eq. 8.3 (page 196).

Suppose that the three positions of **8-1** are substituted by a set of three proligands selected from the ligand inventory \mathbf{L}_{8-1} (Eq. 8.1 on page 195). Then, the following ligand-inventory function is obtained:

$$s_d = H^d + X^d + Y^d + p^d + \bar{p}^d + q^d + \bar{q}^d + r^d + \bar{r}^d. \quad (9.12)$$

After Eq. 9.12 is introduced into Eq. 9.11, the resulting equation is expanded to give the following generating function:

$$\begin{aligned} f'_{\mathbf{8-1}} = & \{H^3 + X^3 + Y^3\} + \{H^2Y + H^2X + \dots\} + HXY \\ & + \{(H^2p + H^2\bar{p}) + \dots\} + \{(HXp + HX\bar{p}) + \dots\} + \{(Hp^2 + H\bar{p}^2) + \dots\} \\ & + \{Hp\bar{p} + \dots\} + \{(Hpq + H\bar{p}\bar{q}) + \dots\} + \{(Hp\bar{q} + H\bar{p}q) + \dots\} \\ & + \{(p^3 + \bar{p}^3) + \dots\} + \{(p^2\bar{p} + p\bar{p}^2) + \dots\} + \{(p^2q + \bar{p}^2\bar{q}) + \dots\} \\ & + \{(p^2\bar{q} + \bar{p}^2q) + \dots\} + \{(pqr + \bar{p}\bar{q}\bar{r})\} + \{(p\bar{q}\bar{r} + \bar{p}q\bar{r}) + \dots\} \\ & + \{(p\bar{p}\bar{q} + p\bar{p}q) + \dots\}, \end{aligned} \quad (9.13)$$

where a pair of *RS*-diastereomers is counted once under the *RS*-permutation group $C_{3\bar{\sigma}}$.

Compare the generating function (Eq. 9.13) obtained under $C_{3\bar{\sigma}}$ with Eq. 8.7 (page 197) obtained under the point group C_{3v} . The promolecules listed in Fig. 8.2 (page 198), where they are counted originally under the point group C_{3v} , are reinterpreted on the basis of the generating function (Eq. 9.13) obtained under $C_{3\bar{\sigma}}$. Each pair of promolecules linked with an underbrace is determined to be *RS*-diastereomeric, so that it is counted once under the action of $C_{3\bar{\sigma}}$. For example, the pair of **8-6** and **8-7** in Fig. 8.2 is counted once because it is determined to be *RS*-diastereomeric. This mode of counting is confirmed by the coefficient 1 of the term HXp appearing in Eq. 9.13. Note that the counterpart pair of $\bar{\mathbf{8-6}}$ and $\bar{\mathbf{8-7}}$ is also determined to be *RS*-diastereomeric and counted once according to the term $HX\bar{p}$ in Eq. 9.13, although it is omitted from Fig. 8.2.

Each planted promolecule (alkyl ligand) listed in Fig. 8.2 belongs to a subgroup of the point group C_{3v} as well as to a subgroup of the *RS*-permutation group $C_{3\bar{\sigma}}$. Several promolecules are selected from Fig. 8.2 and their point groups and *RS*-permutation groups are listed in Fig. 9.5. Among them, **8-2** ($C_{3v}; C_{3\bar{\sigma}}$), **8-3** ($C_3; C_{\bar{\sigma}}$), **8-4** ($C_1; C_1$), or **8-5** ($C_3; C_3$) is characterized by a point group and a *RS*-permutation group of the same order.

Each of the remaining planted promolecules listed in Fig. 9.5 is characterized by a point group and an *RS*-permutation group of different orders. For example, the planted promolecule **8-5** is characterized by the symbol $C_1; C_{\bar{\sigma}}$, which is explained as follows:

- (Point group C_1) The action of the point group C_{3v} on **8-5** provides an equivalence class of $\mathbf{F}_{8-5} = \{\mathbf{8-5a}, \mathbf{8-5b}, \mathbf{8-5c}; \mathbf{8-5d}, \mathbf{8-5e}, \mathbf{8-5f}\}$ by starting from Fig. 8.1 (page 195), where we put p on 1-position, H on 2-position, and H on 3-position for the numbered skeletons **8-1a–8-1c** as well as \bar{p} on $\bar{1}$ -position, H on $\bar{2}$ -position, and H on $\bar{3}$ -position for the mirror-numbered skeletons **8-1d–8-1f** (see the discussions on Eq. 6.6). The planted promolecules $\{\mathbf{8-5a}, \mathbf{8-5b}, \mathbf{8-5c}\}$ are homomeric, that is to say, equivalent under the maximum point subgroup C_3 , so that the set of them represents the presence of **8-5** as a

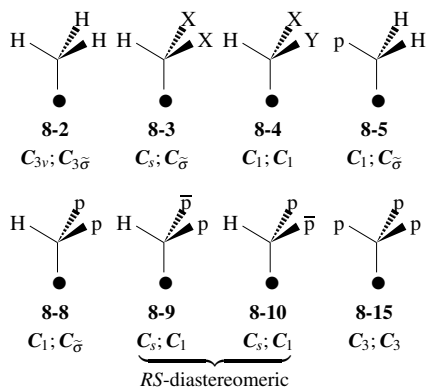


Fig. 9.5. Point groups and *RS*-permutation groups assigned to several planted promolecules listed in Fig. 8.2. A pair of symbols such as $C_{3v}; C_{3\bar{\sigma}}$ is assigned to each planted promolecule, where the former represents a subgroup of the point group C_{3v} , while the latter represents a subgroup of the *RS*-permutation group $C_{3\bar{\sigma}}$.

planted promolecule. At the same time, the planted promolecules {**8-5d**, **8-5e**, **8-5f**} are homomeric, that is to say, equivalent under the maximum point group C_3 , so that the set of them represents the presence of $\overline{\mathbf{8-5}}$ as a planted promolecule. Then, the pair of **8-5** and $\overline{\mathbf{8-5}}$ is recognized as a pair of enantiomers. Because the representative promolecule **8-5a** (= **8-5**) is fixed (stabilized) by the subgroup C_1 ($\subset C_{3v}$), the point group of **8-5** is determined to be C_1 .

- (*RS*-Permutation group $C_{\bar{\sigma}}$) The action of the *RS*-permutation group $C_{3\bar{\sigma}}$ on **8-5** provides an equivalence class of $\mathbf{F}'_{8.5} = \{\mathbf{8-5a}, \mathbf{8-5b}, \mathbf{8-5c}; \mathbf{8-5d}', \mathbf{8-5e}', \mathbf{8-5f}'\}$ by starting from Fig. 9.4, where we put p on 1-position, H on 2-position, and H on 3-position for a set of numbered skeletons **8-1a–8-1c** as well as for another set of numbered skeletons (*RS*-numbered skeletons) **8-1d'–8-1f'**. All of the planted promolecules contained in $\mathbf{F}'_{8.5}$ are equivalent under the *RS*-permutation group of **8-5**. The representative promolecules **8-5a** (= **8-5**) and **8-5d'** (= $\overline{\mathbf{8-5}}$) are identical with each other so as to be fixed (stabilized) by the subgroup $C_{\bar{\sigma}}$ ($\subset C_{3\bar{\sigma}}$). Hence, the *RS*-permutation group of **8-5** is determined to be $C_{\bar{\sigma}}$.

Exercise 9.1.

- Depict planted promolecules contained in $\mathbf{F}_{8.5} = \{\mathbf{8-5a}, \mathbf{8-5b}, \mathbf{8-5c}; \mathbf{8-5d}, \mathbf{8-5e}, \mathbf{8-5f}\}$ according to Fig. 8.1. Confirm that the point group of **8-5** is determined to be C_1 .
 - Depict planted promolecules contained in $\mathbf{F}'_{8.5} = \{\mathbf{8-5a}, \mathbf{8-5b}, \mathbf{8-5c}; \mathbf{8-5d}', \mathbf{8-5e}', \mathbf{8-5f}'\}$ according to Fig. 9.4. Confirm that the *RS*-permutation group of **8-5** is determined to be $C_{\bar{\sigma}}$.
 - Discuss the symbol $C_s; C_1$ assigned to **8-9** (or **8-10**) in Fig. 9.5.
-



Exercise 9.2. In a similar way to Fig. 9.5, assign a pair of a point group and an *RS*-permutation group to each of the remaining planted promolecules listed in Fig. 8.2 (page 198).

9.3.3 Formulation of *RS*-Permutation Groups

The above-mentioned transformation of the point group C_{3v} into the *RS*-permutation group $C_{3\tilde{\sigma}}$ is extended into a general case:

Definition 9.3 (*RS*-Permutation Groups). Suppose that all of the reflection operations of a given point group are modified by omitting ligand reflection to generate *RS*-permutations. Then, the resulting group is defined as an *RS-permutation group*.

If a point group is chiral, the corresponding *RS*-permutation group due to Def. 9.3 is presumed to be identical with the original chiral point group. Just as point groups are classified into achiral and chiral point groups, so *RS*-permutation groups are classified into *RS*-stereogenic and *RS*-astereogenic *RS*-permutation groups or simply *RS*-stereogenic and *RS*-astereogenic groups:

Definition 9.4 (*RS*-Stereogenic and *RS*-Astereogenic).

- For the sake of convenience, a chiral group (composed of rotations) is also regarded as an *RS-stereogenic group* within the scope of an *RS*-permutation group. An *RS*-permutation group having *RS*-permutations is referred to as an *RS-astereogenic group* or an *RS-non-stereogenic group*.
- If a given molecular entity belongs to an *RS*-stereogenic group, it is referred to as being *RS-stereogenic*.
- If a given molecular entity belongs to an *RS*-astereogenic group, it is referred to as being *RS-astereogenic* or *RS-non-stereogenic*.

Note that a pair of terms *RS-stereogenic/RS-astereogenic* for *RS*-permutation groups corresponds to a pair of terms *chiral/achiral* for point groups. According to Def. 9.4, the maximum chiral subgroup of a point group (Subsection 3.2.4) is, at the same time, the maximum *RS*-stereogenic subgroup of the corresponding *RS*-permutation group.

Suppose that an *RS*-permutation group G_X is constructed by starting from an achiral point group G_Y (Eq. 3.21 on page 62) according to Def. 9.3. The maximum chiral subgroup G_C of the point group G_Y is also the maximum *RS*-stereogenic subgroup of G_X , where $|G_C| = |G_X|/2$. Hence, the coset decomposition of G_Y by G_C (Eq. 3.21 on page 62) is converted into the coset decomposition of G_X by G_C :

$$G_X = G_C + G_C\tilde{\sigma}, \quad (9.14)$$

where the operation $\tilde{\sigma}$ is selected appropriately from the set of *RS*-permutations. Then, all of the *RS*-permutations are contained in the coset $G_C\tilde{\sigma}$.

Let us select an element g from G_C ($g \in G_C$). Then, we obtain $G_Cg = G_C$. This means that the coset $G_C (= G_CI)$ is fixed under the action of $g \in G_C$. On the other hand, $\tilde{\sigma}g$ is an

RS-permutation, i.e., $\tilde{\sigma}g \in G_C\tilde{\sigma}$. This means that $G_C\tilde{\sigma}g = G_C\tilde{\sigma}$. The coset $G_C\tilde{\sigma}$ is fixed under the action of $g \in G_C$.

The fixation of the cosets under the action of $g \in G_C$ is interpreted chemically. A given molecular entity **A** as a reference corresponds to the coset G_C ($= G_C I$), while its *RS*-diastereomeric entity $\tilde{\mathbf{A}}$ corresponds to the other coset $G_C\tilde{\sigma}$. The number $|G_C|$ of entities corresponding to the coset G_C are homomeric to the reference molecule **A** under the action of G_C . The number $|G_C\tilde{\sigma}|$ of entities corresponding to the coset $G_C\tilde{\sigma}$ are homomeric to the reference molecule $\tilde{\mathbf{A}}$ under the action of G_C .

Theorem 3.3 (page 62) for point groups is rewritten to meet *RS*-permutation groups.

Theorem 9.1 (Homomeric Relationship under *RS*-permutation groups). Suppose that a given numbered skeleton belongs to an *RS*-permutation group (which is *RS*-astereogenic). Then the numbered skeleton is fixed (or converted into a homomer) under the action of the maximum *RS*-stereogenic subgroup. The corresponding *RS*-numbered skeleton (cf. Fig. 9.4) is also fixed (or converted into a homomer) under the action of the maximum *RS*-stereogenic group.

This theorem gives an extended foundation of the term *homomeric* (cf. Theorem 3.3 on page 62). For example, the numbered skeletons **8-1a–8-1c** listed in the top row of Fig. 9.4 are homomeric under the action of C_3 , which is the maximum *RS*-stereogenic subgroup of the *RS*-permutation group $C_{3\tilde{\sigma}}$. At the same time, the *RS*-numbered skeletons **8-1d'–8-1f'** listed in the bottom row of Fig. 9.4 are homomeric under the action of C_3 .

A numbered skeleton (e.g., **8-1a**) and the corresponding *RS*-numbered skeleton (e.g., **8-1d'**) are equivalent under the action of an *RS*-permutation group (e.g., $C_{3\tilde{\sigma}}$ which is *RS*-astereogenic). They are *RS*-diastereomeric to each other according to Def. 9.2.

9.3.4 Action of *RS*-Permutation Groups

The formulation of *RS*-permutation groups by starting from point groups is suggestive to demonstrate the action of an *RS*-permutation group, because a given skeleton is characterized by a coset representation of a point group as well as by a coset representation of the corresponding *RS*-permutation group. Just as a single point group can act various skeletons in the form of coset representations, a single *RS*-permutation group can act various skeletons in the form of coset representations.

As a skeleton other than the trigonal pyramidal skeleton **8-5** described above, let us examine a 1-azabicyclo[1.1.1]pentane skeleton **9-7** belonging to the point group C_{3v} . The six positions of **9-7** construct an orbit governed by the coset representation $C_{3v}/(C_1)$. As shown in Fig. 9.6, the numbered skeleton **9-7a** ($= \mathbf{9-7}$) is converted into another numbered skeleton (**9-7a**, **9-7b**, or **9-7c**) under the action of a rotation ($\in C_3$) as well as into a mirror-numbered skeleton (**9-7d**, **9-7e**, or **9-7f**) under the action of a reflection ($\in C_{3v} - C_3$).

The 1-azabicyclo[1.1.1]pentane skeleton **9-7** is alternatively considered to belong to the *RS*-permutation group $C_{3\tilde{\sigma}}$, as shown in Fig. 9.7. The six positions of **9-7** construct an orbit governed by the coset representation $C_{3\tilde{\sigma}}/(C_1)$. As shown in Fig. 9.7, the numbered skeleton **9-7a** ($= \mathbf{9-7}$) is converted into another numbered skeleton (**9-7a**, **9-7b**, or **9-7c**)

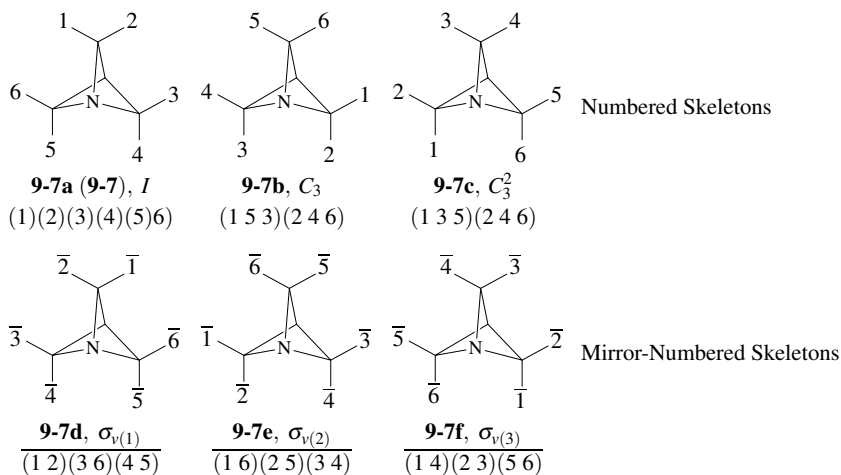


Fig. 9.6. Symmetry operations of the point group C_{3v} for a 1-azabicyclo[1.1.1]pentane skeleton **9-7**. The identity operation (I) converts **9-7** into itself, where the resulting skeleton is denoted as **9-7a**.

under the action of a rotation ($\in C_3$) as well as into an RS -numbered skeleton (**9-7d'**, **9-7e'**, or **9-7f'**) under the action of an RS -permutation ($\in C_{3\bar{\sigma}} - C_3$).

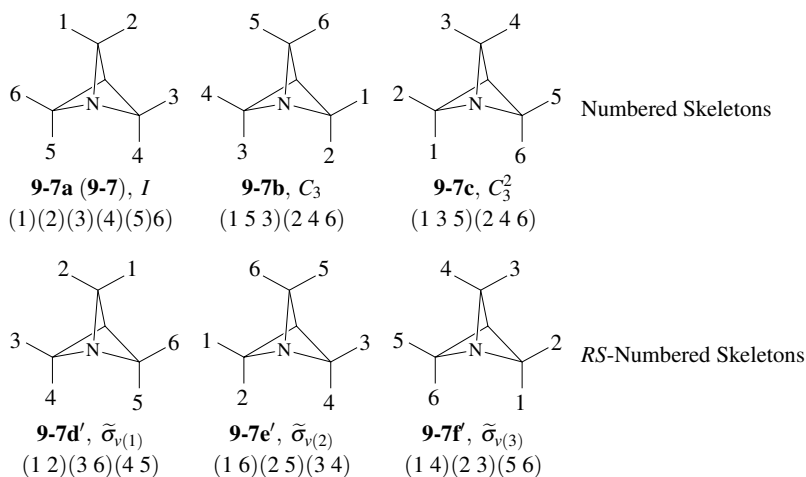


Fig. 9.7. Symmetry operations of the RS -permutation group $C_{3\bar{\sigma}}$ for a 1-azabicyclo[1.1.1]pentane skeleton **9-7**. The identity operation (I) converts **9-7** into itself, where the resulting skeleton is denoted as **9-7a**.

Table 9.2. Point Group C_{3v} and *RS*-Permutation Group $C_{3\hat{\sigma}}$ as Well as Coset Representations C_{3v}/C_1 and $C_{3\hat{\sigma}}/C_1$.

point group C_{3v}			<i>RS</i> -permutation group $C_{3\hat{\sigma}}$		
operation $g \in C_{3v}$	C_{3v}/C_1 (product of cycles)	PSI	operation $g \in C_{3\hat{\sigma}}$	$C_{3\hat{\sigma}}/C_1$ (product of cycles)	cycle term
I	$(1)(2)(3)(4)(5)(6)$	b_1^6	I	$(1)(2)(3)(4)(5)(6)$	s_1^6
C_3	$(1\ 5\ 3)(2\ 6\ 4)$	b_3^2	C_3	$(1\ 5\ 3)(2\ 6\ 4)$	s_3^2
C_3^2	$(1\ 3\ 5)(2\ 4\ 6)$	b_3^2	C_3^2	$(1\ 3\ 5)(2\ 4\ 6)$	s_3^2
$\sigma_{v(1)}$	$(1\ 2)(3\ 6)(4\ 5)$	c_2^3	$\tilde{\sigma}_{v(1)}$	$(1\ 2)(3\ 6)(4\ 5)$	s_2^3
$\sigma_{v(2)}$	$(1\ 6)(2\ 5)(3\ 4)$	c_2^3	$\tilde{\sigma}_{v(2)}$	$(1\ 6)(2\ 5)(3\ 4)$	s_2^3
$\sigma_{v(3)}$	$(1\ 4)(2\ 3)(5\ 6)$	c_2^3	$\tilde{\sigma}_{v(3)}$	$(1\ 4)(2\ 3)(5\ 6)$	s_2^3

Table 9.3. Terminology for Point Groups vs. for *RS*-Permutation Groups

point group	\iff	<i>RS</i> -permutation group
(Operations)		
— rotation	\iff	— rotation
— reflection	\iff	— <i>RS</i> -permutation
(Pairwise Attributes)		
chirality	\iff	<i>RS</i> -stereogenicity
— chiral/achiral	\iff	— <i>RS</i> -stereogenic/ <i>RS</i> -astereogenic
(Pairwise Relationships)		
— enantiomeric	\iff	— <i>RS</i> -diastereomeric

The coset representation C_{3v}/C_1 for the point group C_{3v} and the coset representation $C_{3\hat{\sigma}}/C_1$ for the *RS*-permutation group $C_{3\hat{\sigma}}$ are summarized in Table 9.2. The latter coset representation $C_{3\hat{\sigma}}/C_1$ is regarded as a subgroup of the symmetric group $S^{[6]}$ of degree 6. Note that the coset representation $C_{3\hat{\sigma}}/C_{\hat{\sigma}}$ is regarded as the symmetric group $S^{[3]}$, as shown in Table 9.1.

Table 9.3 summarizes the correspondence between the concepts of point groups and those of *RS*-permutation groups. Modern stereochemistry lays stress on a pair of chirality/achirality even under the action of permutations. As a result, a pair of *RS*-stereogenicity/*RS*-astereogenicity is beyond the scope of modern stereochemistry, so that an enantiomeric relationship is misleadingly used even when an *RS*-diastereomeric relationship should be used.

9.3.5 Misleading Features of the Conventional Terminology

The conceptual distinction between reflections and *RS*-permutations is crucial to comprehend stereochemistry and stereoisomerism. Hence, more examples would be desirable to clarify misleading features of the conventional terminology of modern stereochemistry, where they stem from the lack of the concepts of *RS*-permutations and *RS*-permutation groups.

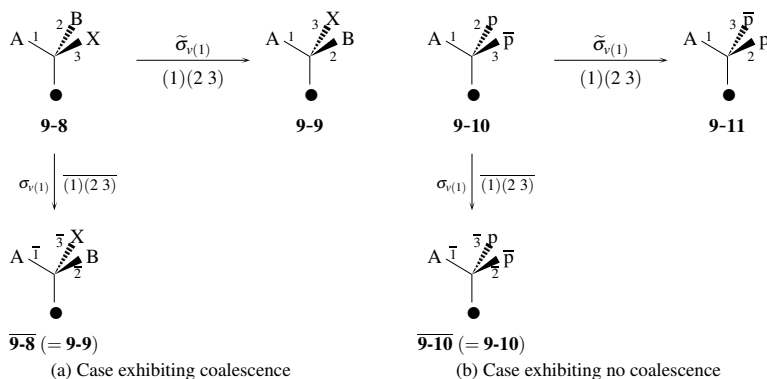


Fig. 9.8. Distinction between an *RS*-permutation and a reflection in trigonal pyramidal derivatives. (a) A case exhibiting coalescence between an *RS*-permutation and a reflection and (b) a case with no coalescence. The symbol A, B, or X represents an achiral proligand in isolation, while a pair of p and \bar{p} represents a pair of enantiomeric proligands in isolation.

As illustrated in Fig. 9.8(a), the action of an *RS*-permutation $\tilde{\sigma}_{v(1)}$ ($\sim (1)(2\ 3)$) on **9-8** with the composition ABX (cf. **8-4** of Fig. 9.5) results in the formation of its *RS*-diastereomer **9-9**. This mode of conversion is represented by the following partition:

$$[\mathbf{9-8\ 9-9}], \quad (9.15)$$

where a pair of floor brackets represents an equivalence class governed by $C_{\tilde{\sigma}}(/C_1)$ under the action of $C_{3\tilde{\sigma}}$. The *RS*-diastereomer **9-9** is identical with its enantiomer $\overline{\mathbf{9-8}}$ produced by the action of a reflection $\sigma_{v(1)}$ ($\sim \overline{(1)(2\ 3)}$) on the original entity **9-8**. This mode of conversion is represented by the following partition:

$$[\mathbf{9-8\ 9-9} (= \overline{\mathbf{9-8}})] \quad (9.16)$$

where a pair of square brackets represents an equivalence class governed by $C_s(/C_1)$ under the action of C_{3v} .

Hence, the effect of the *RS*-permutation $\tilde{\sigma}_{v(1)}$ ($\sim (1)(2\ 3)$) coalesces with the effect of the reflection $\sigma_{v(1)}$ ($\sim \overline{(1)(2\ 3)}$) although the *RS*-permutation is conceptually different from the reflection. In other words, the *RS*-diastereomeric relationship between **9-8** and

9-9 coalesces with the enantiomeric relationship between **9-8** and $\overline{\mathbf{9-8}}$. A seemingly parallel partition of Eq. 9.15 to that of Eq. 9.16 stems from the coalescence between the *RS*-diastereomeric relationship (due to $C_{3\bar{\sigma}}$) and the enantiomeric relationship (due to C_{3v}).

Note that **9-8** belongs to the point group C_1 as well as to the *RS*-permutation group C_1 . This exhibits the same feature as **8-4**, which is characterized by the symbol $C_1; C_1$ in Fig. 9.5.

On the other hand, Fig. 9.8(b) shows that the action of an *RS*-permutation $\tilde{\sigma}_{v(1)}$ ($\sim (1)(2\ 3)$) on **9-10** with the composition $A\bar{p}\bar{p}$ (the symbol *A* represents an achiral proligand in isolation, while a pair of *p* and \bar{p} represents a pair of enantiomeric proligands in isolation) results in the formation of its *RS*-diastereomer **9-11**. This mode of conversion is represented by the following partition:



where a pair of floor brackets represents an equivalence class governed by $C_{\bar{\sigma}}(/C_1)$ under the action of $C_{3\bar{\sigma}}$.

Because **9-10** is achiral as found under the action of a reflection $\sigma_{v(1)}$ ($\sim \overline{(1)(2\ 3)}$), the effect of the *RS*-permutation $\tilde{\sigma}_{v(1)}$ ($\sim (1)(2\ 3)$) by no means coalesces with the effect of the reflection $\sigma_{v(1)}$ ($\sim \overline{(1)(2\ 3)}$). The latter mode of conversion is represented by the following partition:



where a pair of square brackets represents an equivalence class governed by $C_s(/C_s)$ under the action of C_{3v} .

The difference of partitions in Eq. 9.17 and Eq. 9.18 is faithful to our finding that the *RS*-permutation is conceptually different from the reflection. Note that **9-10** (or **9-11**) belongs to the point group C_s as well as to the *RS*-permutation group C_1 (cf. **8-9** and **8-10** of Fig. 9.5).

From a group-theoretical point of view, modern stereochemistry lacks the concept of *RS*-permutation groups, where worse followed, so that the *RS*-permutation groups defined here are confused with point groups. As a result, the action of the *RS*-permutation $\tilde{\sigma}_{v(1)}$ ($\sim (1)(2\ 3)$) illustrated in Fig. 9.8(a) is misleadingly regarded as a permutation for giving an enantiomer in modern stereochemistry. At the same time, the action of the *RS*-permutation $\tilde{\sigma}_{v(1)}$ ($\sim (1)(2\ 3)$) illustrated in Fig. 9.8(b) is regarded as a permutation for giving a diastereomer in modern stereochemistry. Thus, the same permutation $\tilde{\sigma}_{v(1)}$ ($\sim (1)(2\ 3)$) is related to enantiomers as well as to diastereomers, because of the dichotomy between enantiomers and diastereomers in modern stereochemistry (see Section 1.3). Note that the dichotomy between enantiomers and diastereomers in the modern stereochemistry do not permit the coalescence between enantiomeric relationships and diastereomeric relationships. This exhibits sharp contrast to the present approach which permits the coalescence between enantiomeric relationships and *RS*-diastereomeric relationships, as shown in Fig. 9.8(a). It should be emphasized again that the action of the *RS*-permutation $\tilde{\sigma}_{v(1)}$ ($\sim (1)(2\ 3)$) illustrated in Fig. 9.8(a) give an *RS*-diastereomer **9-9**, which eventually coalesces with an enantiomer $\overline{\mathbf{9-8}}$ (= **9-9**) in the present approach.

A similar example is obtained from the 1-azabicyclo[1.1.1]pentane skeleton **9-7**, as shown in Fig. 9.9. The promolecule **9-12** with the composition ABX^4 , which is generated by putting ABX^4 on the six positions of **9-7** (Fig. 9.6 or Fig. 9.7), is an example exhibiting coalescence between an RS -permutation (the horizontal direction) and a reflection (the vertical direction in Fig. 9.9(a)), while the promolecule **9-14** with the composition $X^4p\bar{p}$ is an example with no coalescence (Fig. 9.9(b)).

In the present approach, the RS -permutation $(1\ 2)(3\ 6)(4\ 5)$ is used to refer to an RS -diastereomeric relationship between **9-12** and **9-13** (the horizontal direction in Fig. 9.9(a)) as well as to an RS -diastereomeric relationship between **9-14** and **9-15** (the horizontal direction in Fig. 9.9(b)). It should be emphasized that the RS -permutation $(1\ 2)(3\ 6)(4\ 5)$ is assigned to an RS -diastereomeric relationship in a one-to-one fashion. And then, the RS -diastereomeric relationship between **9-12** and **9-13** coalesces with the enantiomeric relationship between them (the vertical direction in Fig. 9.9(a)).

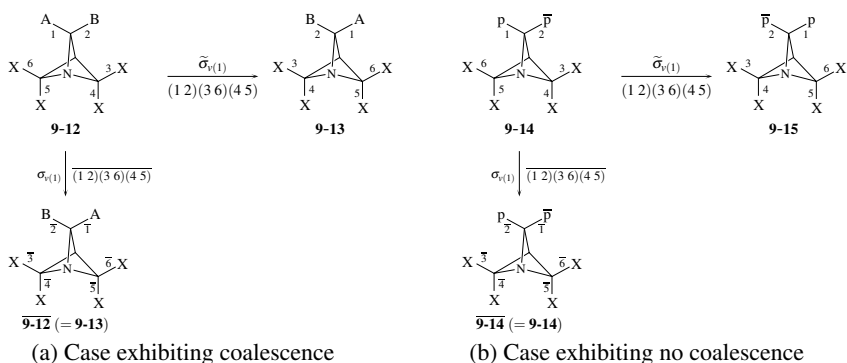


Fig. 9.9. Distinction between an RS -permutation and a reflection in 1-azabicyclo[1.1.1]pentane derivatives. (a) A case exhibiting coalescence between an RS -permutation and a reflection and (b) a case with no coalescence. The symbol A, B, or X represents an achiral proligand in isolation, while a pair of p and \bar{p} represents a pair of enantiomeric proligands in isolation.

In modern stereochemistry, in contrast, the same permutation $(1\ 2)(3\ 6)(4\ 5)$ is used to refer to an enantiomeric relationship between **9-12** and **9-13** as well as to a diastereomeric relationship between **9-14** and **9-15**. Note that these two relationships are not permitted to coalesce with each other by the misleading rule that “diastereoisomerism is stereoisomerism other than enantiomerism” or “diastereoisomers (or diastereomers) are stereoisomers not related as mirror images” [19]. As a result, modern stereochemistry depends on the dual assignment of the permutation $(1\ 2)(3\ 6)(4\ 5)$ to an enantiomeric relationship (enantiomerism) and to a diastereomeric relationship (diastereoisomerism). This dual assignment is misleading because these two relationships are conceptually distinct.

Remark 9.2 (*RS*-Permutations vs. Permutations). If the modes of numbering are ignored, the permutation (1 2)(3)(4)(5)(6) provides the same effect provided by the *RS*-permutation $\tilde{\sigma} \sim (1\ 2)(3\ 6)(4\ 5)$ for the process of **9-12** \rightarrow **9-13**. However, the permutation (1 2)(3)(4)(5)(6) is not contained in the *RS*-permutation group $C_{3\tilde{\sigma}}$ (Table 9.2). The permutations (1 2)(3)(4)(5)(6), (1)(2)(3 4)(5)(6), and (1)(2)(3)(4)(5 6) correspond to epimerizations at three methylene carbons, respectively. Totally, there appear 48 ($= |C_{3\tilde{\sigma}}| \times 2^3 = 6 \times 8$) permutations, which construct a permutation group. The permutation group (without considering reflections) has a half size of a stereoisomeric group (with considering reflections).

Exercise 9.3.

- Assign a point group and an *RS*-permutation group to **9-12**. Examine their orders. Compare them as subgroups of C_{3v} and $C_{3\tilde{\sigma}}$.
- Assign a point group and an *RS*-permutation group to **9-14** (or **9-15**). Examine their orders. Compare them as subgroups of C_{3v} and $C_{3\tilde{\sigma}}$.

A further example to be mentioned is the formulation of permutational isomerism by Ugi et al. [3,4], which suffers from influences brought about by the lack of *RS*-permutation groups, as found in the following Remark.

Remark 9.3 (Misleading Concepts and Terminology on Permutational Isomerism).

Although the concept of ‘the racemate group’ is a key for the formulation of permutational isomerism by Ugi et al. [4, 4.1 Definition], it is misleading because the words ‘racemate’ and ‘enantiomer’ have been used improperly in combination with permutations. Thus, the relationship between **8-1a** and **8-1f’** (Fig. 9.4) has been misleadingly concluded to be ‘enantiomeric’ according to the formulation of permutational isomerism by Ugi et al. [4, page 28, lines 2–3]. The term ‘the racemate group’ is claimed to specify a ‘racemic’ mixture of the ‘enantiomeric’ tertiary phosphines **8-1a** and **8-1f’** [4, 4.2 Example]. However, the terms ‘the racemate group’, ‘racemic’, and ‘enantiomeric’ are misleading because the relationship between **8-1a** and **8-1f’** is concluded to be *RS*-diastereomeric, not to be enantiomeric according to the present method. Although stereoisomerism has once been recognized as prototypes of permutational isomerism by Mislow and Siegel [6], the permutational isomerism by Ugi et al. [4] and by Mislow and Siegel [6] is unable to cover the exact connotation of stereoisomerism, conceptually speaking, because it lacks the concept of *RS*-permutation groups as well as the proper consideration of reflections.

9.4 *RS*-Permutation Groups for Skeletons of Ligancy 4

9.4.1 *RS*-Permutation Group for a Tetrahedral Skeleton

RS-Permutation Group, Point Group, and Symmetric Group of Degree 4

As a representative skeleton of ligancy 4 (cf. Fig. 3.7 on page 68), the point-group symmetry of a tetrahedral skeleton **3-5** (belonging to the point group T_d) has been detailedly discussed in Section 3.2. The four positions of the tetrahedral skeleton **3-5** construct an orbit governed by the the coset representation $T_d(/C_{3v})$. According to Def. 9.3, the corresponding *RS*-permutation group $T_{\bar{\sigma}}$ can be constructed, where Table 3.1 (page 61) for the point group T_d is transformed into Table 9.4 for the *RS*-permutation group $T_{\bar{\sigma}}$.

Just as the point group T_d has subgroups represented by Eqs. 3.4–3.14 (page 60) up to conjugacy, the *RS*-permutation group $T_{\bar{\sigma}}$ has the following subgroups up to conjugacy:

$$C_1 \stackrel{1}{=} \{I\} \quad (9.19)$$

$$C_2 \stackrel{2}{=} \{I, C_{2(1)}\} \quad (9.20)$$

$$C_{\bar{\sigma}} \stackrel{3}{=} \{I, \tilde{\sigma}_{d(1)}\} \quad (9.21)$$

$$C_3 \stackrel{4}{=} \{I, C_{3(1)}, C_{3(1)}^2\} \quad (9.22)$$

$$S_4 \stackrel{5}{=} \{I, \tilde{S}_{4(1)}, C_{2(1)}, \tilde{S}_{4(1)}^3\} \quad (9.23)$$

$$D_2 \stackrel{6}{=} \{I, C_{2(1)}, C_{2(2)}, C_{2(3)}\} \quad (9.24)$$

$$C_{2\bar{\sigma}} \stackrel{7}{=} \{I, C_{2(3)}, \tilde{\sigma}_{d(1)}, \tilde{\sigma}_{d(6)}\} \quad (9.25)$$

$$C_{3\bar{\sigma}} \stackrel{8}{=} \{I, C_{3(1)}, C_{3(1)}^2, \tilde{\sigma}_{d(1)}, \tilde{\sigma}_{d(2)}, \tilde{\sigma}_{d(3)}\} \quad (9.26)$$

$$D_{2\bar{\sigma}} \stackrel{9}{=} \{I, C_{2(1)}, C_{2(2)}, C_{2(3)}, \tilde{\sigma}_{d(1)}, \tilde{\sigma}_{d(2)}, \tilde{S}_{4(3)}, \tilde{S}_{4(3)}^3\} \quad (9.27)$$

$$T \stackrel{10}{=} \{I, C_{2(1)}, C_{2(2)}, C_{2(3)}, \\ C_{3(1)}, C_{3(1)}^2, C_{3(2)}, C_{3(2)}^2, C_{3(3)}, C_{3(3)}^2, C_{3(4)}, C_{3(4)}^2\} \quad (9.28)$$

$$T_{\bar{\sigma}} \stackrel{11}{=} \{A, C\}, \quad (\text{cf. Table 9.4}) \quad (9.29)$$

where a representative subgroup is selected from a set of conjugate subgroups. In a similar way to Eq. 3.19 on page 62 (cf. Eqs. 3.4–3.14), such non-redundant set of subgroups as Eqs. 9.19–9.29 is aligned in an ascending order of the orders, so as to give the following set:

$$\text{SSG}_{T_{\bar{\sigma}}} = \{C_1, C_2, C_{\bar{\sigma}}, C_3, S_4, D_2, C_{2\bar{\sigma}}, C_{3\bar{\sigma}}, D_{2\bar{\sigma}}, T, T_{\bar{\sigma}}\}, \quad (9.30)$$

which is called a *non-redundant set of subgroups* (SSG) for the *RS*-permutation group $T_{\bar{\sigma}}$. For the sake of convenience, a reference number is sequentially attached to each subgroup in $\text{SSG}_{T_{\bar{\sigma}}}$. See the reference numbers attached over the equality symbols in Eqs. 9.19–9.29.

Among the subgroups of $T_{\bar{\sigma}}$ listed in Eq. 9.30, the *RS*-permutation subgroups C_1 , C_2 , C_3 , D_2 , and T are *RS*-stereogenic, while the *RS*-permutation subgroups $C_{\bar{\sigma}}$, S_4 , $C_{2\bar{\sigma}}$,

Table 9.4. RS-Permutation group $T_{\bar{\sigma}}$, Coset Representation $T_{\bar{\sigma}}(/C_{3\bar{\sigma}})$, and the Symmetric Group $S^{[4]}$ of Degree 4

reference number*	operation $g \in T_{\bar{\sigma}}$	$T_{\bar{\sigma}}(/C_{3\bar{\sigma}})$ (product of cycles)	$S^{[4]}$ (product of cycles)	cycle term
1	I	(1)(2)(3)(4)	(1)(2)(3)(4)	s_1^4
2	$C_{2(1)}$	(1 2)(3 4)	(1 2)(3 4)	s_2^2
3	$C_{2(2)}$	(1 4)(2 3)	(1 4)(2 3)	s_2^2
4	$C_{2(3)}$	(1 3)(2 4)	(1 3)(2 4)	s_2^2
5	$C_{3(1)}$	(1)(2 3 4)	(1)(2 3 4)	$s_1 s_3$
6	$C_{3(3)}$	(1 2 4)(3)	(1 2 4)(3)	$s_1 s_3$
7	$C_{3(2)}$	(1 4 3)(2)	(1 4 3)(2)	$s_1 s_3$
8	$C_{3(4)}$	(1 3 2)(4)	(1 3 2)(4)	$s_1 s_3$
9	$C_{3(1)}^2$	(1)(2 4 3)	(1)(2 4 3)	$s_1 s_3$
10	$C_{3(4)}^2$	(1 2 3)(4)	(1 2 3)(4)	$s_1 s_3$
11	$C_{3(3)}^2$	(1 4 2)(3)	(1 4 2)(3)	$s_1 s_3$
12	$C_{3(2)}^2$	(1 3 4)(2)	(1 3 4)(2)	$s_1 s_3$
13	$\tilde{\sigma}_{d(1)}$	(1)(2 4)(3)	(1)(2 4)(3)	$s_1^2 s_2$
16	$\tilde{\sigma}_{d(6)}$	(1 3)(2)(4)	(1 3)(2)(4)	$s_1^2 s_2$
17	$\tilde{\sigma}_{d(2)}$	(1)(2)(3 4)	(1)(2)(3 4)	$s_1^2 s_2$
18	$\tilde{\sigma}_{d(4)}$	(1 2)(3)(4)	(1 2)(3)(4)	$s_1^2 s_2$
21	$\tilde{\sigma}_{d(3)}$	(1)(2 3)(4)	(1)(2 3)(4)	$s_1^2 s_2$
23	$\tilde{\sigma}_{d(5)}$	(1 4)(2)(3)	(1 4)(2)(3)	$s_1^2 s_2$
14	$\tilde{S}_{4(3)}$	(1 2 3 4)	(1 2 3 4)	s_4
15	$\tilde{S}_{4(3)}^3$	(1 4 3 2)	(1 4 3 2)	s_4
19	$\tilde{S}_{4(1)}$	(1 4 2 3)	(1 4 2 3)	s_4
20	$\tilde{S}_{4(1)}^3$	(1 3 2 4)	(1 3 2 4)	s_4
22	$\tilde{S}_{4(2)}$	(1 2 4 3)	(1 2 4 3)	s_4
24	$\tilde{S}_{4(2)}^3$	(1 3 4 2)	(1 3 4 2)	s_4

* The reference number corresponds to that of the multiplication table of T_d reported in [20, Table 2.2].

$C_{3\bar{\sigma}}$, $D_{2\bar{\sigma}}$, and $T_{\bar{\sigma}}$ are RS-astereogenic. Note that the RS-stereogenic subgroups of the RS-permutation group $T_{\bar{\sigma}}$, i.e., C_1 , C_2 , C_3 , D_2 , and T , are common to the chiral subgroups of the point group T_d .

As a result, the four positions of **3-5** alternatively construct an orbit governed by the coset representation $T_{\bar{\sigma}}(/C_{3\bar{\sigma}})$, which is regarded as identical with the symmetric group $S^{[4]}$ of degree 4. The SSG $_{T_{\bar{\sigma}}}$ has once been reported as SSG $_{S^{[4]}}$ [21, Tables 4 and 5]:

$$\text{SSG}_{S^{[4]}} = \{S_1^{[4]} (= C_1), S_2^{[4]}, S_3^{[4]}, S_4^{[4]}, S_5^{[4]}, S_6^{[4]}, S_7^{[4]}, S_8^{[4]}, S_9^{[4]}, S_{10}^{[4]}, S_{11}^{[4]} (= S^{[4]})\}, \quad (9.31)$$

where the subgroups of SSG_{S^4} appear in the same order of the subgroups of $SSG_{T_{\bar{\sigma}}}$ (Eq. 9.30). The subscript of each subgroup in Eq. 9.31 corresponds to the reference number attached over the equality symbol in each of Eqs. 9.19–9.29.

The tetrahedral promolecules listed in Fig. 6.9 (page 157) are characterized by the subgroups of the point group T_d (Eqs. 3.4–3.14). These promolecules are alternatively considered to be characterized by the subgroups of the *RS*-permutation group $T_{\bar{\sigma}}$ (Eqs. 9.19–9.29), as shown in Fig. 9.10. The combinatorial enumerations of tetrahedral promolecules (Fig. 6.9) have been conducted under the point group T_d as well as under the *RS*-permutation group $T_{\bar{\sigma}}$, where the subgroups of $T_{\bar{\sigma}}$ are regarded as the subgroups of the symmetric group $S^{[4]}$ of degree 4 [21, Tables 4 and 5].

Comparison between Fig. 6.9 (page 157) and Fig. 9.10 provides us with useful pieces of information on the difference between T_d and $T_{\bar{\sigma}}$.

- Among them, the *RS*-permutation group of each promolecule listed in type I, III, or IV has the same order as the point group. For example, the symbol $C_1; C_1$ assigned to **6-65** (type I) indicates that the point group C_1 and the *RS*-permutation group C_1 have the same order $|C_1| = 1$. The symbol $C_1; C_1$ assigned to **6-82** (type III) indicates that the point group C_1 and the *RS*-permutation group C_1 have the same order $|C_1| = 1$. The symbol $T_d; T_{\bar{\sigma}}$ assigned to **6-94** (type IV) indicates that the point group T_d and the *RS*-permutation group $T_{\bar{\sigma}}$ have the same order $|T_d| = |T_{\bar{\sigma}}| = 24$.
- On the other hand, the *RS*-permutation group of each promolecule listed in type II has a larger order than the point group. For example, the symbol $T; T_{\bar{\sigma}}$ assigned to **6-67** (type II) indicates that the order of the *RS*-permutation group $T_{\bar{\sigma}}$ ($|T_{\bar{\sigma}}| = 24$) is larger than that of the point group T ($|T| = 12$).
- On the contrary, the *RS*-permutation group of each promolecule listed in type V has a smaller order than the point group. For example, the symbol $C_s; C_1$ assigned to **6-100** (type V) indicates that the order of the *RS*-permutation group C_1 ($|C_1| = 1$) is smaller than that of the point group C_s ($|C_s| = 2$).

The classification of types I–V will be discussed later according to the stereoisogram approach.

Symmetry-Itemized Enumeration of Tetrahedral Derivatives Under the *RS*-Permutation Group

Suppose that the tetrahedral skeleton **3-5** (page 55) belongs to $T_{\bar{\sigma}}$, which has the non-redundant set of subgroups (SSG) represented by Eq. 9.30. The symmetry-itemized enumeration of tetrahedral promolecules under the *RS*-permutation group $T_{\bar{\sigma}}$ has been reported in comparison with the enumeration under the point group T_d [9,21,22].

Because an *RS*-permutation exchanges proligands without taking chirality/achirality into consideration, chirality fittingness is unnecessary to be considered. As a result, a dummy variable s_d is used in place of the sphericity indices a_d , b_d , and c_d . The following

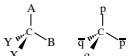
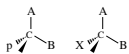
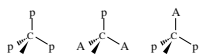
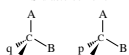

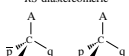
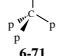
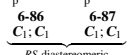
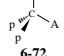
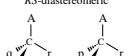
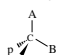
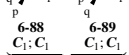

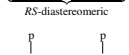

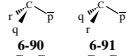
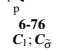
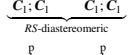
	<i>RS</i> -astereogenic	<i>RS</i> -stereogenic
chiral		Type I  6-65 6-66 $C_1; C_1$ $C_1; C_1$
		Type III  6-82 6-83 $C_1; C_1$ $C_1; C_1$
	Type II  6-67 6-68 6-69 $T; T_{\bar{\sigma}}$ $C_3; C_3\bar{\sigma}$ $C_3; C_3\bar{\sigma}$	<i>RS</i> -diastereomeric  6-84 6-85 $C_1; C_1$ $C_1; C_1$
	 6-70 $C_3; C_3\bar{\sigma}$	<i>RS</i> -diastereomeric  6-86 6-87 $C_1; C_1$ $C_1; C_1$
	 6-71 $C_3; C_3\bar{\sigma}$	<i>RS</i> -diastereomeric  6-88 6-89 $C_1; C_1$ $C_1; C_1$
	 6-72 $C_2; C_2\bar{\sigma}$	<i>RS</i> -diastereomeric  6-90 6-91 $C_1; C_1$ $C_1; C_1$
	 6-73 $C_2; C_2\bar{\sigma}$	<i>RS</i> -diastereomeric  6-88 6-89 $C_1; C_1$ $C_1; C_1$
	 6-74 $C_1; C_{\bar{\sigma}}$	<i>RS</i> -diastereomeric  6-92 6-93 $C_1; C_1$ $C_1; C_1$
	 6-75 $C_1; C_{\bar{\sigma}}$	<i>RS</i> -diastereomeric  6-90 6-91 $C_1; C_1$ $C_1; C_1$
	 6-76 $C_1; C_{\bar{\sigma}}$	<i>RS</i> -diastereomeric  6-92 6-93 $C_1; C_1$ $C_1; C_1$

Fig. 9.10. Tetrahedral promolecules enumerated under the point group T_d and $T_{\bar{\sigma}}$. The symbols A, B, X, and Y represent atoms or achiral ligands. The symbols p, q, r, and s represents chiral ligands, while each symbol with an overbar represents the corresponding chiral ligand with the opposite chirality. An arbitrary promolecule is depicted as a representative of each pair of enantiomers. Types I–V will be discussed later.

PCIs are obtained according to Fujita's USCI approach [23]:

$$\text{PCI}_{3.5}(\mathbf{C}_1) = \frac{1}{24}s_1^4 + \frac{1}{8}s_2^2 - \frac{1}{4}s_1^2s_2 + \frac{1}{3}s_1s_3 - \frac{1}{4}s_4 \quad (9.32)$$

$$\text{PCI}_{3.5}(\mathbf{C}_2) = 0 \quad (9.33)$$

$$\text{PCI}_{3.5}(\mathbf{C}_{\bar{\sigma}}) = \frac{1}{2}s_1^2s_2 - \frac{1}{2}s_2^2 - s_1s_3 + s_4 \quad (9.34)$$

$$\text{PCI}_{3.5}(\mathbf{C}_3) = 0 \quad (9.35)$$

$$\text{PCI}_{3.5}(\mathbf{S}_4) = 0 \quad (9.36)$$

$$\text{PCI}_{3.5}(\mathbf{D}_2) = 0 \quad (9.37)$$

$$\text{PCI}_{3.5}(\mathbf{C}_{2\bar{\sigma}}) = \frac{1}{2}s_2^2 - \frac{1}{2}s_4 \quad (9.38)$$

$$\text{PCI}_{3.5}(\mathbf{C}_{3\bar{\sigma}}) = s_1s_3 - s_4 \quad (9.39)$$

$$\text{PCI}_{3.5}(\mathbf{D}_{2\bar{\sigma}}) = 0 \quad (9.40)$$

$$\text{PCI}_{3.5}(\mathbf{T}) = 0 \quad (9.41)$$

$$\text{PCI}_{3.5}(\mathbf{T}_{\bar{\sigma}}) = s_4. \quad (9.42)$$

These PCIs have been once noted in the author's articles [9,21,22]. Compare these PCIs for enumeration under the *RS*-permutation group $\mathbf{T}_{\bar{\sigma}}$ with the PCI-CFs (Eqs. 6.83–6.93 on page 155) for enumeration under the point group \mathbf{T}_d .

The four positions of the tetrahedral skeleton **3-5** are substituted by proligands selected from the proligand inventory \mathbf{L} (Eq. 6.73 on page 153). According to the degenerate features of the PCIs (Eqs. 9.32–9.42), we use the following single ligand-inventory function s_d , which is derived from the ligand-inventory function for b_d (cf. Eqs. 6.74–6.76 on page 153):

$$s_d = A^d + B^d + X^d + Y^d + p^d + q^d + r^d + s^d + \bar{p}^d + \bar{q}^d + \bar{r}^d + \bar{s}^d. \quad (9.43)$$

The ligand-inventory function (Eq. 9.43) is introduced into the PCIs (Eqs. 9.32–9.42). The resulting equations are expanded to give the following generating functions:

$$\begin{aligned} f'_{3.5}(\mathbf{C}_1) = & \{(\text{ABXp} + \text{ABX}\bar{p}) + \dots\} + \{(\text{ABpq} + \text{AB}\bar{p}\bar{q}) + \dots\} \\ & + \{(\text{Ap}\bar{p}\bar{q} + \text{Ap}\bar{p}\bar{q}) + \dots\} + \{(\text{Apqr} + \text{Ap}\bar{q}\bar{r}) + \dots\} \\ & + \{(\text{pqrs} + \text{p}\bar{q}\bar{r}\bar{s}) + \dots\} + \{(\text{p}\bar{p}\bar{q}\bar{r} + \text{p}\bar{p}\bar{q}\bar{r}) + \dots\} \\ & + \{(\text{p}\bar{p}\bar{q}\bar{q} + \text{p}\bar{p}\bar{r}\bar{r}) + \dots\} + \{(\text{ABp}\bar{p} + \text{ABq}\bar{q}) + \dots\} \\ & + \{\text{ABXY}\} \end{aligned} \quad (9.44)$$

$$\begin{aligned} f'_{3.5}(\mathbf{C}_{\bar{\sigma}}) = & \{(\text{A}^2\text{Bp} + \text{A}^2\text{B}\bar{p}) + \dots\} + \{(\text{ABp}^2 + \text{AB}\bar{p}^2) + \dots\} \\ & + \{(\text{A}^2\text{pq} + \text{A}^2\bar{p}\bar{q}) + \dots\} + \{(\text{Ap}^2\bar{p} + \text{Ap}\bar{p}^2) + \dots\} \\ & + \{(\text{Ap}^2\bar{q} + \text{A}\bar{p}^2\bar{q}) + \dots\} + \{(\text{p}^2\bar{p}\bar{q} + \text{p}\bar{p}^2\bar{q}) + \dots\} \end{aligned}$$

$$\begin{aligned}
& + \{ (p^2 q \bar{q} + \bar{p}^2 q \bar{q}) + \dots \} + \{ (p^2 q r + \bar{p}^2 q \bar{r}) + \dots \} \\
& + \{ A^2 p \bar{p} + \dots \} + \{ A^2 B X + A^2 B Y + \dots \} \quad (9.45)
\end{aligned}$$

$$\begin{aligned}
f'_{3.5}(C_{2\bar{\sigma}}) & = \{ (A^2 p^2 + A^2 \bar{p}^2) + \dots \} + \{ (p^2 q^2 + \bar{p}^2 \bar{q}^2) + \dots \} \\
& + \{ p^2 \bar{p}^2 + q^2 \bar{q}^2 + r^2 \bar{r}^2 + s^2 \bar{s}^2 \} + \{ A^2 B^2 + A^2 X^2 + A^2 Y^2 + \dots \} \quad (9.46)
\end{aligned}$$

$$\begin{aligned}
f'_{3.5}(C_{3\bar{\sigma}}) & = \{ (A^3 p + A^3 \bar{p}) + \dots \} + \{ (A p^3 + A \bar{p}^3) + \dots \} \\
& + \{ (p^3 q + \bar{p}^3 \bar{q}) + \dots \} + \{ (p^3 \bar{p} + p \bar{p}^3) + \dots \} \\
& + \{ A^3 B + A^3 X + A^3 Y + \dots \} \quad (9.47)
\end{aligned}$$

$$f'_{3.5}(T_{\bar{\sigma}}) = \{ (p^4 + \bar{p}^4) + \dots \} + \{ A^4 + B^4 + X^4 + Y^4 \}. \quad (9.48)$$

In these generating functions, the coefficient of the term $A^a B^b X^x Y^y p^p \bar{p}^{\bar{p}} q^q \bar{q}^{\bar{q}} r^r \bar{r}^{\bar{r}} s^s \bar{s}^{\bar{s}}$ indicates the number of inequivalent (self-)*RS*-diastereomeric pairs to be counted. The enumeration results represented by the generating functions (Eqs. 9.44–9.48) are consistent with the data listed in Tables 4 and 5 of Ref. [21], in which the notation for the subgroups of the symmetric group $S^{[4]}$ has been used in place of the present notation of the subgroups of the *RS*-permutation group $T_{\bar{\sigma}}$.

Gross Enumeration of Tetrahedral Derivatives Under the *RS*-Permutation Group

Let us examine gross enumeration under the *RS*-permutation group $T_{\bar{\sigma}}$. Because $T_{\bar{\sigma}}$ is isomorphic to $S^{[4]}$, the CI shown in Eq. 9.92 (page 227) is rewritten by substituting s_d for r_d to give the following CI for the gross enumeration:

$$CI(T_{\bar{\sigma}}; s_d) = \frac{1}{24} (s_1^4 + 3s_2^2 + 8s_1 s_3 + 6s_1^2 s_2 + 6s_4). \quad (9.49)$$

The ligand-inventory function (Eq. 9.43) is introduced into Eq. 9.49. After expansion, we obtain the following generating function for gross enumeration:

$$\begin{aligned}
f''_{3.5} & = \{ A^4 + \dots \} + \{ A^3 B + \dots \} + \{ (A^3 p + A^3 \bar{p}) + \dots \} \\
& + \{ A^2 B^2 + \dots \} + \{ (A^2 p^2 + A^2 \bar{p}^2) + \dots \} + \{ A^2 B X + \dots \} \\
& + \{ (A^2 B p + A^2 B \bar{p}) + \dots \} + \{ A^2 p \bar{p} + \dots \} + \{ (A^2 p q + A^2 p \bar{q}) + \dots \} \\
& + \{ A B X Y + \dots \} + \{ (A B X p + A B X \bar{p}) + \dots \} + \{ (A B p^2 + A B \bar{p}^2) + \dots \} \\
& + \{ A B p \bar{p} + \dots \} + \{ (A B p q + A B p \bar{q}) + \dots \} + \{ (A p^3 + A \bar{p}^3) + \dots \} \\
& + \{ (A p^2 \bar{p} + A p \bar{p}^2) + \dots \} + \{ (A p^2 q + A p^2 \bar{q}) + \dots \} \\
& + \{ (A p \bar{p} q + A p \bar{p} \bar{q}) + \dots \} + \{ (A p q r + A p \bar{q} \bar{r}) + \dots \}
\end{aligned}$$

$$\begin{aligned}
& + \{(p^4 + \bar{p}^4) + \dots\} + \{(p^3\bar{p} + p\bar{p}^3) + \dots\} + \{(p^3q + \bar{p}^3\bar{q}) + \dots\} \\
& + \{p^2\bar{p}^2 + \dots\} + \{(p^2\bar{p}q + p\bar{p}^2\bar{q}) + \dots\} + \{(p^2q^2 + \bar{p}^2\bar{q}^2) + \dots\} \\
& + \{(p^2q\bar{q} + \bar{p}^2q\bar{q}) + \dots\} + \{(p^2qr + \bar{p}^2q\bar{r}) + \dots\} + \{p\bar{p}q\bar{q} + \dots\} \\
& + \{(p\bar{p}qr + p\bar{p}q\bar{r}) + \dots\} + \{(pqrs + \overline{pqr\bar{s}}) + \dots\}.
\end{aligned} \tag{9.50}$$

Compare Eq. 9.50 for the *RS*-permutation group $T_{\bar{\sigma}}$ with Eq. 7.30 (page 184) for the point group T_d . Each pair of *RS*-diastereomeric promolecules is counted once under the action of $T_{\bar{\sigma}}$ (Eq. 9.50), while each pair of enantiomers is counted once under the action of T_d (Eq. 7.30).

A pair of *RS*-diastereomeric promolecules listed in the type-III and type-V frames of Fig. 9.10 is counted once under the action of $T_{\bar{\sigma}}$. This means that a pair of *RS*-diastereomers linked by an underbrace (Fig. 9.10) is regarded as a single entity to be counted once under $T_{\bar{\sigma}}$. For example, a pair of **6-82** and **6-83** with the composition ABXp (type III) is counted once as the term ABXp has the coefficient 1 in Eq. 9.50 (also Eq. 9.44). A pair of $\overline{\mathbf{6-82}}$ and $\overline{\mathbf{6-83}}$ with the composition ABX \bar{p} is separately counted once as the term ABX \bar{p} has the coefficient 1 in Eq. 9.50 (also Eq. 9.44). On the other hand, a pair of achiral *RS*-diastereomers **6-100** and **6-101** with the composition ABp \bar{p} is counted once as the term ABp \bar{p} has the coefficient 1 in Eq. 9.50 (also Eq. 9.44). Note that **6-100** (or **6-101**) belongs to C_s (achiral) under the point group T_d , while it belongs to C_1 (*RS*-stereogenic) under the *RS*-permutation group $T_{\bar{\sigma}}$ (cf. so-called ‘pseudoasymmetry’).

Each promolecule listed in the type-I frame of Fig. 9.10 is counted once under the action of $T_{\bar{\sigma}}$. For example, the term ABXY in Eq. 9.50 (also Eq. 9.44) indicates the presence of one pair of *RS*-diastereomeric promolecules **6-65** and $\overline{\mathbf{6-65}}$ with the composition ABXY, which is counted once under the action of $T_{\bar{\sigma}}$ and coalesces with a pair of enantiomers. Note that the pair of **6-65** and $\overline{\mathbf{6-65}}$ belongs to C_1 (as an enantiomeric pair) under the point group T_d (Eq. 6.94 on page 156), while it belongs to C_1 (as an *RS*-diastereomeric pair) under the *RS*-permutation group $T_{\bar{\sigma}}$ (Eq. 9.44).

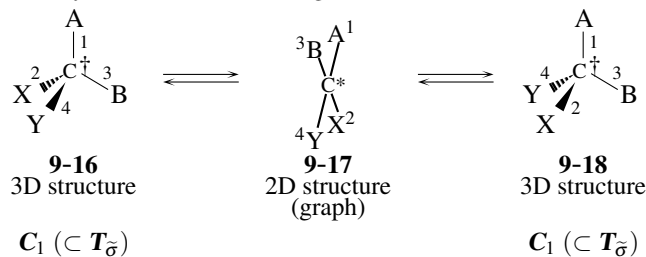
Each promolecule listed in the type-II frame of Fig. 9.10 is counted once under the action of $T_{\bar{\sigma}}$. The term A³p in Eq. 9.50 (also Eq. 9.47) indicates the presence of one *RS*-astereogenic promolecule **6-68** with the composition A³p (as a self-*RS*-diastereomeric pair), while the term A³ \bar{p} indicates the presence of one *RS*-astereogenic promolecule $\overline{\mathbf{6-68}}$ with the composition A³ \bar{p} (as a self-*RS*-diastereomeric pair), which is not depicted in Fig. 9.10. Note that **6-68** and $\overline{\mathbf{6-68}}$ are counted separately under the $T_{\bar{\sigma}}$ as found in Eq. 9.50 (also Eq. 9.47).

So-Called Asymmetric Carbon Centers

The concept of ‘asymmetric carbon’ is a key of stereochemistry developed by van’t Hoff [24,25]. However, the term ‘asymmetric carbon’ is now encountered less frequently and replaced by the more justified term ‘stereogenic center’ or the less justified term ‘chiral center’ [26]. In spite of such seeming justification, the replacement of the term ‘asymmetry

carbon' by the term 'stereogenic center' has provided a broader and ambiguous connotation, because *cis/trans*-stereoisomerism is also characterized by the term 'stereogenic'.

(a) Asymmetric vs. *RS*-Stereogenic



(b) Pseudoasymmetric vs. *RS*-Stereogenic

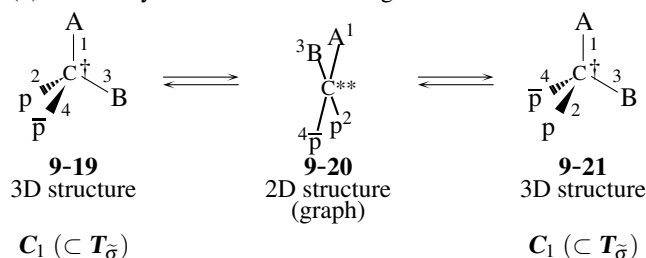


Fig. 9.11. Asymmetric carbon (*) or pseudoasymmetric carbon (**) of a 2D structure and *RS*-stereogenic carbons (†) of the resulting 3D structures. (a) Asymmetric vs. *RS*-stereogenic and (b) pseudoasymmetric vs. *RS*-stereogenic.

For the purpose of comprehending stereochemistry and stereoisomerism, it is worthwhile to compare the attitudes of several approaches towards the term 'asymmetric atom'.

1. (Traditional Approach) The concept of 'asymmetric carbon' by van't Hoff [24,25] is originally concerned with a 2D structure **9-17** with four different achiral proligands A, B, X, and Y, as shown in Fig. 9.11(a). A rise from 2D to 3D generates chiral promolecules **9-16** (= **6-65** in Fig. 6.9 on page 157 or in Fig. 9.10) and **9-18**, which are regarded as enantiomers in the traditional terminology initiated by van't Hoff [24,25]. Then such an asymmetric center (*) is correlated to a pair of enantiomers.

On the other hand, a 2D structure **9-20** with four different ligands A, B, p, and \bar{p} (A and B: achiral; p/ \bar{p} : a pair of enantiomeric proligands) generates achiral 3D structures **9-19** (= **6-100**) and **9-21** (= **6-101**), which are regarded as diastereomeric in the traditional terminology. Because the asymmetric center (**) of **9-20** provides such achiral promolecules as **9-19** and **9-21**, it is called 'pseudoasymmetric center' as an exceptional case of 'asymmetric center'. In fact, the prefix 'pseudo' of the term 'pseudoasymmetric' aims at concealing the inconsistency of the term 'asymmetric', which is originally ascribed to a chiral point group C_1 assigned to **9-16** and **9-18** but is later required to be

related to an achiral point group C_s assigned to the promolecule **9-19** (or **9-21**) under the action of the point group T_d . This attitude of recognizing exceptions stems from the implicit but misleading presumption that ‘asymmetry’ should be directly linked with chirality (or enantiomeric relationships).

2. (Modern Stereochemical Approach) In the terminology of modern stereochemistry, the concept of ‘asymmetric carbon atom’ is regarded as the prototype of a ‘stereogenic atom’ [5], as pointed out by Mislow and Siegel [6]. The term ‘stereogenic’ is related with the term ‘stereoisomeric’, so that it mixes up ‘asymmetric carbon’ (‘chiral center’ related to an enantiomeric relationship, e.g., between **9-16** and **9-18**) with ‘pseudoasymmetric carbon’ (‘pseudoasymmetric center’ related to a diastereomeric relationship, e.g., between **9-19** and **9-21**) as well as with ‘*cis/trans*-stereoisomeric double bond’ under the coinage of the term ‘stereogenic units’ [26]. As a result, the differentiation between chirality and stereogenicity is not fully demonstrated under the framework of the terminology of modern stereochemistry (e.g., the term ‘chiral center’ vs. the term ‘stereogenic center’ [26]). Moreover, the concept of ‘stereogenicity’ is misleadingly regarded as a common basis for both *R/S*-stereodescriptors and *Z/E*-descriptors, which should be conceptually differentiated from each other.
3. (The Present Stereoisogram Approach) The concept of *RS-stereogenicity* derived from *RS*-permutation groups by Fujita [10,18] integrates (by no means mixes up) ‘asymmetric carbon’ with ‘pseudoasymmetric carbon’ in a rational fashion. The term ‘*cis/trans*-stereoisomeric double bond’ is automatically excluded by the definition of *RS*-permutation groups (Def. 9.3). Moreover, the concept of *RS-stereogenicity* is distinct from the concept of chirality.

The promolecule **9-16** (or **9-18**) belongs to the *RS*-permutation group C_1 ($\subset T_{\bar{\sigma}}$), while it belongs to the point group C_1 ($\subset T_d$). The promolecule **9-19** (or **9-21**) belongs to the *RS*-permutation group C_1 ($\subset T_{\bar{\sigma}}$), while it belongs to the point group C_s ($\subset T_d$). The elucidation of the common *RS*-permutation group C_1 ($\subset T_{\bar{\sigma}}$) is important to indicate that the *RS*-stereogenic promolecules of C_1 ($\subset T_{\bar{\sigma}}$) as 3D structures (**9-16/9-18** and **9-19/9-21**) correspond to the term ‘asymmetric’ as 2D structures. As a result, the term ‘pseudoasymmetric’ is unnecessary to be considered under the action of the *RS*-permutation group $T_{\bar{\sigma}}$. If the term ‘pseudoasymmetric’ is maintained for the sake of historical convenience, the prefix ‘pseudo’ of the term ‘pseudoasymmetric’ should be related solely to an achiral point group such as C_s assigned to the promolecule **9-19** (or **9-21**) under the action of the point group T_d . See the *RS*-stereogenicity-column of Fig. 9.10, which lists promolecules ascribed to type-I, -III, and -V cases according to Fujita’s stereoisogram approach [8,9,10].

In the present approach, the term ‘asymmetric carbon’ is restricted to the 2D structures (e.g., the carbon attached by the symbol * in **9-17** or the carbon attached by the symbol ** in **9-20**). This attitude succeeds the implicit connotation of the original definition by van’t Hoff [24,25], in which an ‘asymmetric carbon’ and a ‘pseudoasymmetric carbon’ are not explicitly differentiated within the scope of 2D structures. The term ‘asymmetric carbon’ should not be used to specify the 3D structures (e.g., the carbon attached by

the symbol † in **9-16**, **9-18**, **9-19**, or **9-21**), which should be specified by the term *RS-stereogenic carbon*.

It should be emphasized that the term *RS-stereogenic carbon* of the present approach is more specific than the broader term ‘stereogenic carbon’ of the approach of modern stereochemistry. The concept of *RS-stereogenicity* is a single basis for *R/S*-stereodescriptors, because *Z/E*-descriptors for ‘*cis/trans*-stereoisomeric double bond’ are automatically excluded from the scope of *RS-stereogenicity*.

Both the relationship between **9-16** and **9-18** and the relationship between **9-19** and **9-21** are determined to be *RS*-diastereomeric because both the relationships are concerned with *RS-stereogenicity*. This mode of classification under the action of the *RS*-permutation group $T_{\tilde{\sigma}}$ is schematically represented as follows:

$$T_{\tilde{\sigma}} : [\mathbf{9-16} \ \mathbf{9-18}] \quad (9.51)$$

$$T_{\tilde{\sigma}} : [\mathbf{9-19} \ \mathbf{9-21}], \quad (9.52)$$

where a pair of floor brackets represents an equivalence class under the action of $T_{\tilde{\sigma}}$. In contrast, the mode of classification under the action of the point group T_d is schematically represented as follows:

$$T_d : [\mathbf{9-16} \ \mathbf{9-18}] \quad (9.53)$$

$$T_d : [\mathbf{9-19}] \ [\mathbf{9-21}], \quad (9.54)$$

where a pair of square brackets represents an equivalence class under the action of T_d . In Eq. 9.54, both the symbols $[\mathbf{9-19}]$ and $[\mathbf{9-21}]$ denote achiral entities, each of which is contained in a one-membered orbit under T_d .

Compare the set of Eqs. 9.51 and 9.52 with the set of Eqs. 9.53 and 9.54. The *RS*-diastereomeric relationship between **9-16** and **9-18** (Eq. 9.51) coalesces with the enantiomeric relationship between **9-16** and $\overline{\mathbf{9-16}}$ (= **9-18**) (Eq. 9.53). In contrast, Eqs. 9.52 and 9.54 exhibit no coalescence.

9.4.2 *RS*-Permutation Group for an Allene Skeleton

RS-Permutation Group $D_{2\tilde{\sigma}}$

As another representative skeleton of ligancy 4 (Fig. 3.7 on page 68), the allene skeleton **3-9** belonging to the point group D_{2d} has been detailedly discussed in Section 3.3. The four positions of the allene skeleton **3-9** construct an orbit governed by the the coset representation $D_{2d}/(C_s)$. According to Def. 9.3, the corresponding *RS*-permutation group $D_{2\tilde{\sigma}}$ can be constructed, where Table 3.2 (page 68) for the point group D_{2d} is transformed into Table 9.5 for the *RS*-permutation group $D_{2\tilde{\sigma}}$.

Table 9.5. Operations of $D_{2\tilde{\sigma}}$ and Coset Representation $D_{2\tilde{\sigma}}(/C_{\tilde{\sigma}})$

operation $g \in D_{2\tilde{\sigma}}$	$D_{2\tilde{\sigma}}(/C_{\tilde{\sigma}})$ (product of cycles)	cycle term
I	(1)(2)(3)(4)	s_1^4
$C_{2(1)}$	(1 2)(3 4)	s_2^2
$C_{2(2)}$	(1 4)(2 3)	s_2^2
$C_{2(3)}$	(1 3)(2 4)	s_2^2
$\tilde{\sigma}_{d(1)}$	(1)(2 4)(3)	$s_1^2 s_2$
$\tilde{\sigma}_{d(2)}$	(1 3)(2)(4)	$s_1^2 s_2$
\tilde{S}_4	(1 2 3 4)	s_4
\tilde{S}_4^3	(1 4 3 2)	s_4

By referring to the non-redundant set of subgroups (SSG) of D_{2d} (Eq. 6.103 on page 159), the SSG of $D_{2\tilde{\sigma}}$ is obtained as follows:

$$\text{SSG}_{D_{2\tilde{\sigma}}} = \{C_1, C_2, C_2', C_{\tilde{\sigma}}, S_4, C_{2\tilde{\sigma}}, D_2, D_{2\tilde{\sigma}}\}, \quad (9.55)$$

where the reference number is attached to each subgroup in accord with Eq. 9.30, because $D_{2\tilde{\sigma}}$ is a subgroup of $T_{\tilde{\sigma}}$. See the reference numbers attached over the equality symbols in Eqs. 9.19–9.29. Note that C_2 and C_2' are conjugate within $T_{\tilde{\sigma}}$, but not conjugate within $D_{2\tilde{\sigma}}$.

Gross Enumeration of Allene Derivatives Under the *RS*-Permutation Group

$D_{2\tilde{\sigma}}$

The combinatorial enumerations of promolecules derived from the allene skeleton **3-9** have been conducted under the point group D_{2d} as well as under the *RS*-permutation group $D_{2\tilde{\sigma}}$ [27, Tables 3 and 4], where the subgroups of $D_{2\tilde{\sigma}}$ are regarded as the subgroups of $S_9^{[4]}$ ($\subset S^{[4]}$):

$$\text{SSG}_{S_9^{[4]}} = \{S_1^{[4]} (= C_1), S_2^{[4]}, S_{2'}^{[4]}, S_3^{[4]}, S_5^{[4]}, S_7^{[4]}, S_6^{[4]}, S_9^{[4]}\} \quad (9.56)$$

where the subgroups of $\text{SSG}_{S_9^{[4]}}$ appear in the same order of the subgroups of $\text{SSG}_{D_{2\tilde{\sigma}}}$ (Eq. 9.55). The subscript of each subgroup in Eq. 9.56 corresponds to the reference number attached over the equality symbol in each of Eqs. 9.19–9.29.

To confirm the data obtained under the *RS*-permutation group $D_{2\tilde{\sigma}}$ ($\cong S_9^{[4]}$) [27, Table 3], let us examine the gross enumeration of allene derivatives under $D_{2\tilde{\sigma}}$. The CI-CF shown in Eq. 7.31 (page 185) is rewritten by substituting s_d for a_d , c_d , or b_d . Thereby, we obtain

the CI for gross enumeration:

$$\text{CI}(\mathbf{D}_{2\bar{\sigma}}; s_d) = \frac{1}{8}(s_1^4 + 3s_2^2 + 2s_1^2s_2 + 2s_4). \quad (9.57)$$

Suppose that the four positions are substituted by proligands selected from the proligand inventory \mathbf{L} (Eq. 6.73 on page 153). Then, the ligand-inventory function shown in Eq. 9.43 is introduced into the CI (Eq. 9.57). After expansion, we obtain the following generating function for gross enumeration:

$$\begin{aligned} f'_{3,9} = & \{A^4 + \dots\} + \{A^3B + \dots\} + \{(A^3p + A^3\bar{p}) + \dots\} \\ & + \{2A^2B^2 + \dots\} + \{2(A^2p^2 + A^2\bar{p}^2) + \dots\} + \{2A^2BX + \dots\} \\ & + \{2(A^2Bp + A^2B\bar{p}) + \dots\} + \{2A^2p\bar{p} + \dots\} \\ & + \{2(A^2pq + A^2\bar{p}\bar{q}) + \dots\} + \{3ABXY + \dots\} \\ & + \{3(ABXp + ABX\bar{p}) + \dots\} + \{2(ABp^2 + AB\bar{p}^2) + \dots\} \\ & + \{3ABp\bar{p} + \dots\} + \{3(ABp\bar{q} + AB\bar{p}\bar{q}) + \dots\} + \{(Ap^3 + A\bar{p}^3) + \dots\} \\ & + \{2(Ap^2\bar{p} + A\bar{p}\bar{p}^2) + \dots\} + \{2(Ap^2q + A\bar{p}^2\bar{q}) + \dots\} \\ & + \{3(A\bar{p}\bar{p}q + A\bar{p}\bar{p}\bar{q}) + \dots\} + \{3(Apqr + A\bar{p}\bar{q}\bar{r}) + \dots\} \\ & + \{(p^4 + \bar{p}^4) + \dots\} + \{(p^3\bar{p} + p\bar{p}^3) + \dots\} + \{(p^3q + \bar{p}^3\bar{q}) + \dots\} \\ & + \{2p^2\bar{p}^2 + \dots\} + \{2(p^2\bar{p}q + p\bar{p}^2\bar{q}) + \dots\} + \{2(p^2q^2 + \bar{p}^2\bar{q}^2) + \dots\} \\ & + \{2(p^2q\bar{q} + \bar{p}^2q\bar{q}) + \dots\} + \{2(p^2qr + \bar{p}^2q\bar{r}) + \dots\} + \{3p\bar{p}q\bar{q} + \dots\} \\ & + \{3(p\bar{p}qr + p\bar{p}\bar{q}\bar{r}) + \dots\} + \{3(pqrs + \bar{p}\bar{q}\bar{r}\bar{s}) + \dots\}. \end{aligned} \quad (9.58)$$

Compare this generating function with Eq. 7.32 (page 185). The coefficient of each term in Eq. 9.58 is consistent with the sum of the corresponding row of the tables obtained by the symmetry-itemized enumeration under the *RS*-permutation group $\mathbf{D}_{2\bar{\sigma}}$ ($\cong \mathbf{S}_9^{[4]}$) [27, Tables 3 and 4].

***RS*-Diastereomeric and Enantiomeric Relationships**

According to the coefficient 3 of the term 3ABXY in Eq. 9.58, there appear three inequivalent promolecules with the composition ABXY, which belong to \mathbf{C}_1 under the action of the *RS*-permutation group $\mathbf{D}_{2\bar{\sigma}}$ [27, Table 3]. They are depicted in Fig. 9.12(a).⁸ Compare this figure with Fig. 6.13 (page 162) obtained under the point group \mathbf{D}_{2d} .

⁸ The numbering of positions in Fig. 9.12 obeys the action of $\mathbf{S}^{[4]}$. This means that the reference promolecule **6-103** (or **6-106**) is permuted under the action of $\mathbf{S}^{[4]}$. If the action is restricted to that of $\mathbf{D}_{2\bar{\sigma}}$ ($\cong \mathbf{S}_9^{[4]}$), the respective pairs {**6-103**, **9-22**}, {**6-104**, **9-23**}, and {**6-105**, **9-24**} should be permuted separately under the action of $\mathbf{D}_{2\bar{\sigma}}$ ($\cong \mathbf{S}_9^{[4]}$). In this permutation, the mode of position numbering for {**6-103**, **9-22**} should be used. For example, **6-104** is generated by placing { $f(1) = A$, $f(2) = B$, $f(3) = X$, $f(4) = Y$ } on the positions numbered for {**6-103**, **9-22**}. This is the way adopted in the combinatorial enumeration under the action of $\mathbf{D}_{2\bar{\sigma}}$ ($\cong \mathbf{S}_9^{[4]}$) [27].

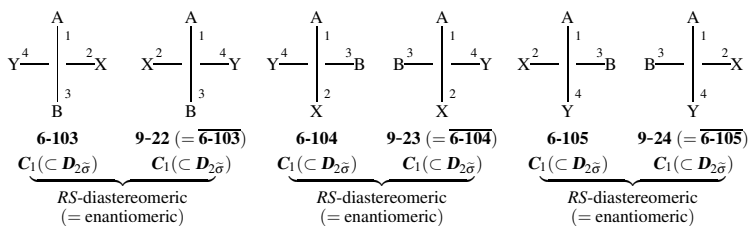
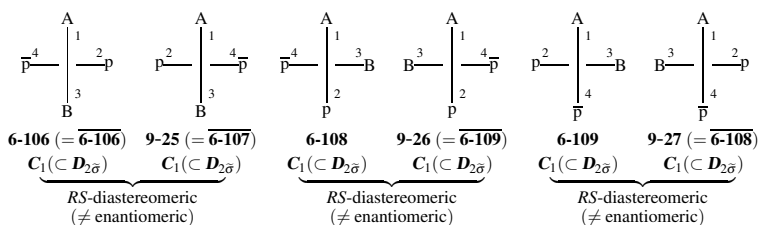
(a) Coalescence Between *RS*-Diastereomeric and Enantiomeric Relationships(b) No Coalescence Between *RS*-Diastereomeric and Enantiomeric Relationships

Fig. 9.12. Allene derivatives (a) with the composition ABXY exhibiting coalescence between *RS*-diastereomeric and enantiomeric relationships as well as (b) with the composition ABp̄p̄ exhibiting no coalescence between *RS*-diastereomeric and enantiomeric relationships.

Each pair {6-103, 9-22}, {6-104, 9-23}, or {6-105, 9-24} constructs an equivalence class (orbit) under the action of $\mathbf{D}_{2\tilde{\sigma}}$, so that two molecules of each pair are *RS*-diastereomeric to each other. The result of the action of $\mathbf{D}_{2\tilde{\sigma}}$ is summarized as follows:

$$\{ [6-103 \ 9-22] \ [6-104 \ 9-23] \ [6-105 \ 9-24] \}, \quad (9.59)$$

where a pair of floor brackets represents an equivalence class under the action of $\mathbf{D}_{2\tilde{\sigma}}$. The *RS*-diastereomeric relationship shown in Fig. 9.12(a) is concluded to coalesce with an enantiomeric relationship shown in Fig. 6.13(a) (page 162), which has been obtained under the point group \mathbf{D}_{2d} . The result of the action of \mathbf{D}_{2d} is summarized as follows:

$$\{ [6-103 \ 9-22] \ [6-104 \ 9-23] \ [6-105 \ 9-24] \}, \quad (9.60)$$

where a pair of square brackets represents an equivalence class under the action of \mathbf{D}_{2d} . A seemingly parallel partition of Eq. 9.59 to that of Eq. 9.60 stems from the coalescence between the *RS*-diastereomeric relationship (due to $\mathbf{D}_{2\tilde{\sigma}}$) and the enantiomeric relationship (due to \mathbf{D}_{2d}).

According to the coefficient 3 of the term $3\text{ABp}\bar{\text{p}}$ in Eq. 9.58, there appear three inequivalent promolecules with the composition ABp̄p̄, which belong to \mathbf{C}_1 under the action of the *RS*-permutation group $\mathbf{D}_{2\tilde{\sigma}}$ [27, Table 3]. They are depicted in Fig. 9.12(b). Each pair {6-106, 9-25}, {6-108, 9-26}, or {6-109, 9-27} constructs an equivalence class (orbit) under the action of $\mathbf{D}_{2\tilde{\sigma}}$, so that two molecules of each pair are *RS*-diastereomeric to each other.

From the viewpoint of the *RS*-permutation group $D_{2\bar{\sigma}}$ (not from the viewpoint of the point group D_{2d}), the comparison between Fig. 9.12(a) and Fig. 9.12(b) indicates the parallelism of the two cases, each of which consists of three pairs of *RS*-diastereomers (not three pairs of enantiomers).

The data depicted in Fig. 9.12(b) exhibit sharp contrast to the data of enumeration under the point group D_{2d} [27, Table 3], which indicate the presence of two achiral promolecules of C_s ($\subset D_{2d}$) and two enantiomeric pairs of promolecules of C_1 ($\subset D_{2d}$), as shown in Fig. 6.13(b) on page 162.

It should be emphasized that **6-106** (or **9-25**) belongs to C_1 under the action of the *RS*-permutation group $D_{2\bar{\sigma}}$, so that a pair of *RS*-diastereomers **6-106** and **9-25** is counted once under $D_{2\bar{\sigma}}$. This mode of counting is schematically represented as follows:

$$\{[\mathbf{6-106} \ \mathbf{9-25}] \ [\mathbf{6-108} \ \mathbf{9-26}] \ [\mathbf{6-109} \ \mathbf{9-27}]\}, \quad (9.61)$$

where a pair of floor brackets represents an equivalence class under the action of $D_{2\bar{\sigma}}$. In contrast, the same **6-106** (or **9-25**) belongs to C_s under the action of the point group D_{2d} , so that the respective promolecules **6-106** and **9-25** separately counted as two achiral entities under D_{2d} . This mode of counting is schematically represented in a different fashion from Eq. 9.61:

$$\{[\mathbf{6-106}] \ [\mathbf{9-25}] \ [\mathbf{6-108} \ \mathbf{9-27}] \ [\mathbf{6-109} \ \mathbf{9-26}]\}, \quad (9.62)$$

where a pair of square brackets represents an equivalence class under the action of D_{2d} . Thus, the action of the *RS*-permutation group $D_{2\bar{\sigma}}$ (Eq. 9.61) is clearly differentiated from the action of the point group D_{2d} (Eq. 9.62). See Remark 9.3 for the confusion between *RS*-permutation groups (e.g., $C_{3\bar{\sigma}}$) and point groups (e.g., C_{3v}), which has been widely spread in modern stereochemistry. The confusion stems from the misleading extension of the seemingly parallel partition between Eq. 9.59 and Eq. 9.60 into a general case.

9.4.3 *RS*-Permutation Group for an Ethylene Skeleton

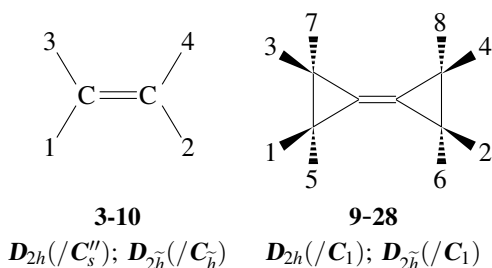
Degeneration of the Coset Representation of an *RS*-Permutation Group

As a further representative skeleton of ligancy 4 (Fig. 3.7 on page 68), the ethylene skeleton **3-10** belonging to the point group D_{2h} has been detailedly discussed in Section 3.3. The four positions of the ethylene skeleton **3-10** construct an orbit governed by the the coset representation $D_{2h}/(C_s'')$. According to Def. 9.3, the corresponding *RS*-permutation group $D_{2\tilde{h}}$ can be constructed, so that Table 3.3 (page 69) for the point group D_{2h} is transformed into Table 9.6 for the *RS*-permutation group $D_{2\tilde{h}}$.

The four position of **3-10** constructs an orbit governed by the coset representation $D_{2h}/(C_s'')$ derived from the point group D_{2h} . The corresponding coset representation $D_{2\tilde{h}}/(C_{\tilde{h}}')$ based on the *RS*-permutation group $D_{2\tilde{h}}$ degenerates to give $D_2/(C_1)$, because the operations corresponding to rotations are identical with those corresponding to *RS*-permutations.

Table 9.6. Operations of D_{2h}^- as Well as a Degenerate Coset Representation $D_{2h}^-(/C_h^-)$ and a Non-Degenerate Coset representation $D_{2h}^-(/C_1)$

operation $g \in D_{2h}^-$	$D_{2h}^-(/C_h^-)$ (product of cycles)	cycle term	$D_{2h}^-(/C_1)$ (product of cycles)	cycle term
I	(1)(2)(3)(4)	s_1^4	(1)(2)(3)(4)(5)(6)(7)(8)	s_1^8
$C_{2(1)}$	(1 2)(3 4)	s_2^2	(1 2)(3 4)(5 6)(7 8)	s_2^4
$C_{2(2)}$	(1 4)(2 3)	s_2^2	(1 4)(2 3)(5 8)(6 7)	s_2^4
$C_{2(3)}$	(1 3)(2 4)	s_2^2	(1 3)(2 4)(5 7)(6 8)	s_2^4
$\tilde{\sigma}_h$	(1)(2)(3)(4)	s_1^4	(1 5)(2 6)(3 7)(4 8)	s_2^4
$\tilde{\tau}$	(1 4)(2 3)	s_2^2	(1 8)(2 7)(3 6)(4 5)	s_2^4
$\tilde{\sigma}_{d(1)}$	(1 2)(3 4)	s_2^2	(1 2)(3 4)(5 6)(7 8)	s_2^4
$\tilde{\sigma}_{d(2)}$	(1 3)(2 4)	s_2^2	(1 3)(2 4)(5 7)(6 8)	s_2^4

**Fig. 9.13.** Skeletons belonging to the point group D_{2h} as well as to the RS -permutation group D_{2h}^- .

It is worthwhile to refer to a cyclopropylidenecyclopropane skeleton **9-28** (Fig. 9.13) as a non-degenerate case of a coset representation of the RS -permutation group D_{2h}^- . The eight positions of **9-28** construct an orbit governed by the coset representation $D_{2h}^-(/C_1)$ of the RS -permutation group D_{2h}^- , which is non-degenerate as shown in the right part of Table 9.6. The coset representation $D_{2h}^-(/C_1)$ is derived from the coset representation $D_{2h}^-(/C_h^-)$ of the point group D_{2h} according to Def. 9.3.

Enumeration of Ethylene Derivatives Under the RS -Permutation Group

Because the RS -permutation group D_{2h}^- for characterizing the ethylene skeleton **3-10** turns out to degenerate to D_2 , the four positions of **3-10** (Fig. 9.13) is regarded as being governed by the coset representation $D_2(/C_1)$. Hence, the cycle terms appearing in the **A** part of Table

9.6 are selected to give a cycle index (CI) without chirality fittingness as follows:

$$\text{CI}(\mathbf{D}_2; s_d) = \frac{1}{4}(s_1^4 + 3s_2^2), \quad (9.63)$$

which is a simple application of the Pólya's theorem (cf. Section 7.2). In other words, the chirality fittingness based on the concept of sphericities, which has been introduced in Fujita's proligand method (cf. Section 7.3), is not taken into consideration. Suppose that the four positions are substituted by proligands selected from the proligand inventory \mathbf{L} (Eq. 6.73 on page 153). The ligand-inventory function (Eq. 9.43) is introduced into the CI (Eq. 9.63) and the resulting equation is expanded to give the following generating function:

$$\begin{aligned} f'_{3-10} = & \{A^4 + \dots\} + \{A^3B + \dots\} + \{(A^3p + A^3\bar{p}) + \dots\} \\ & + \{3A^2B^2 + \dots\} + \{3(A^2p^2 + A^2\bar{p}^2) + \dots\} + \{3A^2BX + \dots\} \\ & + \{3(A^2Bp + A^2B\bar{p}) + \dots\} + \{3A^2p\bar{p} + \dots\} + \{3(A^2pq + A^2\bar{p}\bar{q}) + \dots\} \\ & + \{6ABXY + \dots\} + \{6(ABXp + ABX\bar{p}) + \dots\} + \{3(ABp^2 + AB\bar{p}^2) + \dots\} \\ & + \{6ABp\bar{p} + \dots\} + \{6(ABpq + AB\bar{p}\bar{q}) + \dots\} + \{(Ap^3 + A\bar{p}^3) + \dots\} \\ & + \{3(Ap^2\bar{p} + Ap\bar{p}^2) + \dots\} + \{3(Ap^2q + A\bar{p}^2\bar{q}) + \dots\} \\ & + \{6(Ap\bar{p}q + Ap\bar{p}\bar{q}) + \dots\} + \{6(Apqr + A\bar{p}\bar{q}\bar{r}) + \dots\} \\ & + \{(p^4 + \bar{p}^4) + \dots\} + \{(p^3\bar{p} + p\bar{p}^3) + \dots\} + \{(p^3q + \bar{p}^3\bar{q}) + \dots\} \\ & + \{3p^2\bar{p}^2 + \dots\} + \{3(p^2\bar{p}q + p\bar{p}^2\bar{q}) + \dots\} + \{3(p^2q^2 + \bar{p}^2\bar{q}^2) + \dots\} \\ & + \{3(p^2q\bar{q} + \bar{p}^2q\bar{q}) + \dots\} + \{3(p^2qr + \bar{p}^2q\bar{r}) + \dots\} + \{6p\bar{p}q\bar{q} + \dots\} \\ & + \{6(p\bar{p}qr + p\bar{p}\bar{q}\bar{r}) + \dots\} + \{6(pqrs + \bar{p}\bar{q}\bar{r}\bar{s}) + \dots\}. \end{aligned} \quad (9.64)$$

The term $6ABXY$ appearing in Eq. 9.64 indicates the presence of six promolecules with the composition $ABXY$, which are inequivalent under the action of the *RS*-permutation group \mathbf{D}_2 (or \mathbf{D}_{2h}). Each of them (9-29–9-34) belongs to the *RS*-permutation group \mathbf{C}_1 ($\subset \mathbf{D}_2$), as depicted in Fig. 9.14(a). For the sake of convenience, the four positions of each promolecule numbered according to the action of $\mathbf{S}^{[4]}$, where the same function $\{f(1) = A, f(2) = B, f(3) = X, f(4) = Y\}$ is applied to give each of the promolecules (9-29–9-34). If the action of \mathbf{D}_2 (or \mathbf{D}_{2h}) is focused on, the mode of numbering in 9-29 should be selected, so that a distinct function (e.g., $\{f(1) = A, f(2) = Y, f(3) = B, f(4) = X\}$ for 9-29) should be applied to give each of them (9-29–9-34).

This mode of counting is schematically represented as follows:

$$\{[\mathbf{9-29}] [\mathbf{9-30}] [\mathbf{9-31}] [\mathbf{9-32}] [\mathbf{9-33}] [\mathbf{9-34}]\}, \quad (9.65)$$

where a pair of floor brackets represents an equivalence class under the action of \mathbf{D}_2 (or \mathbf{D}_{2h}).

From the viewpoint of the point group \mathbf{D}_{2h} , each of 9-29–9-34 belongs to the point group \mathbf{C}_s'' ($= \{I, \sigma_h\}$) [27, Table 3]. The term $6ABXY$ in the generating function for \mathbf{D}_{2h} (Eq. 7.34 on page 186) indicates that there are six achiral promolecules with the composition

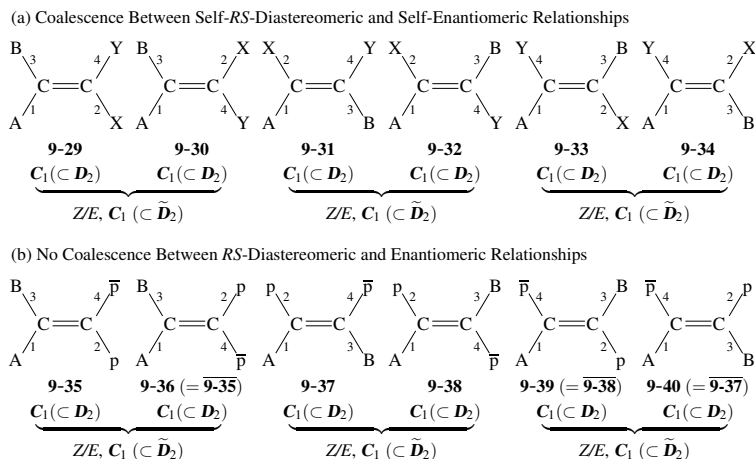


Fig. 9.14. Ethylene derivatives (a) with the composition $ABXY$ exhibiting coalescence between self-*RS*-diastereomeric and self-enantiomeric relationships as well as (b) with the composition $AB\bar{p}\bar{p}$ exhibiting no coalescence between *RS*-diastereomeric and enantiomeric relationships.

$ABXY$. This mode of counting is schematically represented in a different fashion from Eq. 9.65:

$$\{[9-29] [9-30] [9-31] [9-32] [9-33] [9-34]\}, \quad (9.66)$$

where a pair of square brackets represents an equivalence class under the action of D_{2h} . Although there appears a seeming parallelism between Eq. 9.65 and Eq. 9.66, such a seeming parallelism should not be extended into a general case.

The term $6AB\bar{p}\bar{p}$ appearing in Eq. 9.64 indicates the presence of six promolecules with the composition $AB\bar{p}\bar{p}$, which are inequivalent under the action of the *RS*-permutation group D_2 (or D_{2h}). Each of them (9-35–9-40) belongs to the *RS*-permutation group $C_1(\subset D_2)$, as depicted in Fig. 9.14(b). This mode of counting is schematically represented as follows:

$$\{[9-35] [9-36] [9-37] [9-38] [9-39] [9-40]\}, \quad (9.67)$$

where a pair of floor brackets represents an equivalence class under the action of D_2 (or D_{2h}).

The symmetry-itemized enumeration under the point group D_{2h} indicates the presence of three pairs of enantiomers [27, Table 3]. This enumeration is confirmed by the gross enumeration shown in the generating function of Eq. 7.34 (page 186). Thus the term $3AB\bar{p}\bar{p}$ in Eq. 7.34 indicates the presence of three pairs of enantiomers, each pair of which is counted once as an equivalence class under the action of the point group D_{2h} . These are found to be a pair of 9-35/9-36 ($=\overline{9-35}$), a pair of 9-37/9-40 ($=\overline{9-37}$), and a pair of 9-38/9-39 ($=\overline{9-38}$), if Fig. 9.14(b) is carefully examined. This mode of counting is schematically represented in a different fashion from Eq. 9.67:

$$\{[9-35 \ 9-36 (= \overline{9-35})] [9-37 \ 9-40 (= \overline{9-37})] [9-38 \ 9-39 (= \overline{9-38})]\}, \quad (9.68)$$

where a pair of square brackets represents an equivalence class under the action of D_{2h} .

Thus, the action of the *RS*-permutation group D_2 (or D_{2h}^-) (Eq. 9.67) is clearly differentiated from the action of the point group D_{2h} (Eq. 9.68). See Remark 9.3. The confusion concerning D_2 (or D_{2h}^-) and D_{2h} stems from the misleading extension of the seemingly parallel partition between Eq. 9.65 and Eq. 9.66 into a general case.

Enumeration of Ethylene Derivatives Under the Permutation Group With Respect to *Z/E*-Isomerism

To characterize *Z/E*-isomerism of an ethylene skeleton **3-10**, let us define a new permutation group called a *ZE*-permutation group:

$$\tilde{D}_2 = D_2 + D_2\tilde{e}, \quad (9.69)$$

where the symbol \tilde{e} represents the twist of the double bond, e.g., $\tilde{e} \sim (1)(2\ 4)(3)$. Note that the operation $\tilde{e} (\sim (1)(2\ 4)(3))$ can be equalized to the operation $\tilde{\sigma}_{d(1)} (\sim (1)(2\ 4)(3))$ listed in Table 9.5. Then, the *ZE*-permutation group \tilde{D}_2 is isomorphic to the group $S_9^{[4]} (\cong D_{2\tilde{\sigma}})$ described above.⁹ The data of $D_{2\tilde{\sigma}}$ (the cycle terms collected in Table 9.5) are used for the enumeration under the *ZE*-permutation group \tilde{D}_2 . Thereby, the following CI without chirality fittingness is obtained:

$$CI(\tilde{D}_2; s_d) = \frac{1}{8}(s_1^4 + 3s_2^2 + 2s_1^2s_2 + 2s_4). \quad (9.70)$$

The ligand-inventory function (Eq. 9.43) is introduced into the CI (Eq. 9.70). The resulting equation is expanded to give the following generating function:

$$\begin{aligned} \tilde{f}_{3.5} = & \{A^4 + \dots\} + \{A^3B + \dots\} + \{(A^3p + A^3\bar{p}) + \dots\} \\ & + \{2A^2B^2 + \dots\} + \{2(A^2p^2 + A^2\bar{p}^2) + \dots\} + \{2A^2BX + \dots\} \\ & + \{2(A^2Bp + A^2B\bar{p}) + \dots\} + \{2A^2p\bar{p} + \dots\} + \{2(A^2pq + A^2\bar{p}q) + \dots\} \\ & + \{3ABXY + \dots\} + \{3(ABXp + ABX\bar{p}) + \dots\} + \{2(ABp^2 + AB\bar{p}^2) + \dots\} \\ & + \{3ABp\bar{p} + \dots\} + \{3(ABpq + AB\bar{p}q) + \dots\} + \{(Ap^3 + A\bar{p}^3) + \dots\} \\ & + \{2(Ap^2\bar{p} + Ap\bar{p}^2) + \dots\} + \{2(Ap^2q + A\bar{p}^2q) + \dots\} \\ & + \{3(Ap\bar{p}q + Ap\bar{p}q) + \dots\} + \{3(Apqr + A\bar{p}q\bar{r}) + \dots\} \\ & + \{(p^4 + \bar{p}^4) + \dots\} + \{(p^3\bar{p} + p\bar{p}^3) + \dots\} + \{(p^3q + \bar{p}^3q) + \dots\} \\ & + \{2p^2\bar{p}^2 + \dots\} + \{2(p^2\bar{p}q + p\bar{p}^2q) + \dots\} + \{2(p^2q^2 + \bar{p}^2q^2) + \dots\} \\ & + \{2(p^2q\bar{q} + \bar{p}^2q\bar{q}) + \dots\} + \{2(p^2qr + \bar{p}^2q\bar{r}) + \dots\} + \{3p\bar{p}q\bar{q} + \dots\} \\ & + \{3(p\bar{p}qr + p\bar{p}q\bar{r}) + \dots\} + \{3(pqrs + \bar{p}q\bar{r}s) + \dots\}. \end{aligned} \quad (9.71)$$

⁹ The symmetry-itemized enumeration under the group $S_9^{[4]} (\cong D_{2\tilde{\sigma}})$ has been reported in comparison with the enumeration under the point group D_{2h} [27].

The term 3ABXY in Eq. 9.71 indicates the presence of three pairs of *Z/E*-isomers with the composition ABXY. As a result, the six promolecules listed in Fig 9.14(a) are categorized into a pair of **9-29/9-30**, a pair of **9-31/9-32**, and a pair of **9-33/9-34**. Note that each pair constructs an equivalence class, which is counted once under the action of the *ZE*-permutation group \tilde{D}_2 . This mode of counting is schematically represented by Eq. 9.72, which is derived from Eq. 9.65 by applying the *ZE*-permutation group \tilde{D}_2 :

$$\{\langle [9-29] [9-30] \rangle \langle [9-31] [9-32] \rangle \langle [9-33] [9-34] \rangle\}, \quad (9.72)$$

where a pair of angle brackets represents an equivalence class under the action of \tilde{D}_2 .

A seeming parallel partition is obtained by applying \tilde{D}_2 to Eq. 9.66 as follows:

$$\{\langle [9-29] [9-30] \rangle \langle [9-31] [9-32] \rangle \langle [9-33] [9-34] \rangle\}, \quad (9.73)$$

where a pair of angle brackets represents an equivalence class under the action of \tilde{D}_2 . Note that each promolecule in Eq. 9.73 is achiral so that the effect of a reflection does not appear explicitly.

The term 3ABp \bar{p} in Eq. 9.71 indicates the presence of three pairs of *Z/E*-isomers with the composition ABp \bar{p} . As a result, the six promolecules listed in Fig 9.14(b) are categorized into a pair of **9-35/9-36**, a pair of **9-37/9-38**, and a pair of **9-39/9-40**, where each pair constructs an equivalence class, which is counted once under the action of the *ZE*-permutation group \tilde{D}_2 . This mode of counting is schematically represented by Eq. 9.74, which is derived from Eq. 9.65 by applying the *ZE*-permutation group \tilde{D}_2 :

$$\{\langle [9-35] [9-36] \rangle \langle [9-37] [9-38] \rangle \langle [9-39] [9-40] \rangle\}, \quad (9.74)$$

where a pair of angle brackets represents an equivalence class under the action of \tilde{D}_2 . Because **9-37** and **9-40** ($=\overline{9-37}$) (or **9-38** and **9-39** ($=\overline{9-38}$)) should be paired as a pair of enantiomers, Eq. 9.74 does not properly support such a mode of pairing.

It is worthwhile to discuss the partition $\langle [9-35] [9-36] \rangle$ in Eq. 9.74 from the viewpoint of ‘geometric enantiomerism’ which has been discussed for Fig. 1.8 (page 13). The symbols $[9-35]$ and $[9-36]$ indicate that they are separately counted once under the action of D_2 (or D_{2h}^-), so that they are inequivalent to each other under D_2 (or D_{2h}^-). Even though D_2 (or D_{2h}^-) is confused with D_{2h} in modern stereochemistry, the enantiomeric relationship between **9-35** and **9-36** cannot be elucidated by the action of D_2 (or D_{2h}^-). The partition $\langle [9-35] [9-36] \rangle$ in Eq. 9.74 indicates that $[9-35]$ and $[9-36]$ are equivalent to each other under the action of \tilde{D}_2 . It follows that **9-35** and **9-36** are ‘geometric isomers’ which are characterized by a pair of *Z/E*-descriptors. However, Eq. 9.74 cannot indicate an enantiomeric relationship, so that it is insufficient to derive the term ‘geometric enantiomers’. To derive the term ‘geometric enantiomers’, strictly speaking, modern stereochemistry mixes up the action of D_2 (or D_{2h}^-) with the action of D_{2h} .

By applying the *ZE*-permutation group \tilde{D}_2 to Eq. 9.68, we obtain the following partition:

$$\{\langle [9-35] [9-36] (= \overline{9-35}) \rangle \langle [9-37] [9-40] (= \overline{9-37}) \rangle \langle [9-38] [9-39] (= \overline{9-38}) \rangle\}, \quad (9.75)$$

where a pair of angle brackets represents an equivalence class under the action of \tilde{D}_2 . To bundle the four promolecules (i.e., [9-37 9-40 (= 9-37)] [9-38 9-39 (= 9-38)]) in a pair of angle brackets, each pair of enantiomers should be considered in a bundle. This treatment is rather artificial but can be rationalized later by developing Fujita's stereoisogram approach.

Exercise 9.4.

- Review a pair of enantiomers and a pair of *Z/E*-descriptors by examining 9-35–9-40 shown in Fig. 9.14(b).
 - Review the difference between the term ‘stereogenicity’ of modern stereochemistry and the term *RS-stereogenicity* defined in this chapter.
-

References

- [1] N. G. de Bruijn, *Indag. Math.*, **21**, 59–69 (1959).
- [2] E. Ruch, W. Hässelbarth, and B. Richter, *Theor. Chim. Acta*, **19**, 288–300 (1970).
- [3] I. Ugi, D. Marquarding, H. Klusacek, G. Gokel, and P. Gillespie, *Angew. Chem. Int. Ed. Engl.*, **9**, 703–730 (1970).
- [4] I. Ugi, J. Dugundji, R. Kopp, and D. Marquarding, “Perspectives in Theoretical Stereochemistry”, Vol. 36 of *Lecture Notes in Chemistry*, Springer-Verlag, Heidelberg (1984).
- [5] G. E. McCasland, “A New General System for the Naming of Stereoisomers”, *Chemical Abstracts*, Columbus (1953).
- [6] K. Mislow and J. Siegel, *J. Am. Chem. Soc.*, **106**, 3319–3328 (1984).
- [7] A. von Zelewsky, “Stereochemistry of Coordination Compounds”, John Wiley & Sons, Chichester (1996).
- [8] S. Fujita, *J. Org. Chem.*, **69**, 3158–3165 (2004).
- [9] S. Fujita, *J. Math. Chem.*, **35**, 265–287 (2004).
- [10] S. Fujita, *Tetrahedron*, **60**, 11629–11638 (2004).
- [11] S. Fujita, *J. Math. Chem.*, **33**, 113–143 (2003).
- [12] S. Fujita, *MATCH Commun. Math. Comput. Chem.*, **71**, 511–536 (2014).
- [13] S. Fujita, *MATCH Commun. Math. Comput. Chem.*, **71**, 537–574 (2014).
- [14] S. Fujita, *MATCH Commun. Math. Comput. Chem.*, **71**, 575–608 (2014).
- [15] S. Fujita, *J. Math. Chem.*, **52**, 508–542 (2014).
- [16] S. Fujita, *J. Math. Chem.*, **52**, 543–574 (2014).
- [17] S. Fujita, *J. Math. Chem.*, **52**, 1514–1534 (2014).
- [18] S. Fujita, *Tetrahedron: Asymmetry*, **25**, 1169–1189 (2014).

- [19] IUPAC Organic Chemistry Division, *Pure Appl. Chem.*, **68**, 2193–2222 (1996).
- [20] S. Fujita, “Diagrammatical Approach to Molecular Symmetry and Enumeration of Stereoisomers”, University of Kragujevac, Faculty of Science, Kragujevac (2007).
- [21] S. Fujita, *Bull. Chem. Soc. Jpn.*, **74**, 1585–1603 (2001).
- [22] S. Fujita, *Chem. Rec.*, **2**, 164–176 (2002).
- [23] S. Fujita, “Symmetry and Combinatorial Enumeration in Chemistry”, Springer-Verlag, Berlin-Heidelberg (1991).
- [24] J. H. van’t Hoff, *Archives Néerlandaises des Sciences exactes et naturelles*, **9**, 445–454 (1874).
- [25] J. H. van’t Hoff, A Suggestion Looking to the Extension into Space of the Structural Formulas at Present Used in Chemistry. And a Note Upon the Relation Between the Optical Activity and the Chemical Constitution of Organic Compounds, in “Foundations of Stereochemistry, Memoirs of Pasteur, van’t Hoff, Le Bel and Wislicenus”, ed. by G. M. Richardson, American Book Co., New York (1901) pp 35–46.
- [26] G. Helmchen, A. General Aspects. 1. Nomenclature and Vocabulary of Organic Stereochemistry, in “Stereochemical Synthesis. Methods of Organic Chemistry (Houben-Weyl). Workbench Edition E21”, 4th ed., ed. by G. Helmchen, R. W. Hoffmann, J. Mulzer, and E. Schaumann, Georg Thieme, Stuttgart New York (1996) Vol. 1 pp 1–74.
- [27] S. Fujita, *Bull. Chem. Soc. Jpn.*, **75**, 1949–1962 (2002).

10 Stereoisograms and *RS*-Stereoisomers¹

10.1 Stereoisograms as Integrated Diagrammatic Expressions

As discussed in Section 9.4, point groups are different from *RS*-permutation groups in the actions on skeletons of ligancy 4 and so on. Although point groups and *RS*-permutation groups exhibit seemingly parallel behaviors towards derivatives of the composition ABXY, they exhibit different behaviors towards derivatives of the composition ABp \bar{p} . Modern stereochemistry has selected the seemingly parallel behaviors towards the composition ABXY as standards for discussions and has regarded the different behaviors towards the composition ABp \bar{p} as exceptions. This means that modern stereochemistry has suffered from the duality of standard cases and exceptional cases without arriving at a single criterion. Thus, the lack of the concept of *RS*-permutation groups inhibits proper recognitions of state-of-the-art situations so as to cause continuous confusion. In this chapter, stereoisograms are introduced as diagrammatic expressions for integrating point groups and *RS*-permutation groups.

10.1.1 Elementary Stereoisograms of Skeletons with Position Numbering

Integration of Point Groups and *RS*-Permutation Groups

To integrate point groups (Chapter 3) and *RS*-permutation groups (Chapter 9), the stereoisogram approach has been developed by Fujita [1–3]. It should be emphasized that permutation groups are substantially restricted to *RS*-permutation groups in order to accomplish the integration of geometric features and stereoisomeric features in stereochemistry.

Let us first select the numbered skeleton **8-1a** as a reference skeleton from the homomeric numbered skeletons listed in the top row of Fig. 8.1 (page 195) or in the top row of Fig. 9.4 (page 241). This skeleton is renumbered to be **10-1**, which is placed at the upper-left corner of Fig. 10.1. The mirror-numbered skeleton **8-1d** is selected from the homomeric mirror-numbered skeletons listed in the bottom row of Fig. 8.1. This skeleton is renumbered to be $\overline{10-1}$, which is placed at the lower-left corner of Fig. 10.1. Thereby, the vertical direction of Fig. 10.1 (linked with a double-headed arrow attached by an encircled solid circle) represents the conversions shown in Fig. 8.1, which are based on the action of the point group C_{3v} . In other words, the trigonal pyramidal skeleton **10-1** and the mirror-numbered skeleton $\overline{10-1}$ in the vertical direction are in an enantiomeric relationship.

¹ This chapter is based on S. Fujita, "Stereogenicity Revisited. Proposal of Holantimers for Comprehending the Relationship between Stereogenicity and Chirality", *J. Org. Chem.*, **69**, 3158–3165 (2004); S. Fujita, "Integrated Discussion on Stereogenicity and Chirality for Restructuring Stereochemistry", *J. Math. Chem.*, **35**, 265–287 (2004); and S. Fujita, Pseudoasymmetry, Stereogenicity, and the *RS*-Nomenclature Comprehended by the Concepts of Holantimers and Stereoisograms", *Tetrahedron*, **60**, 11629–11638 (2004).

The point group C_{3v} (cf. Table 8.1 on page 196) is divided into two parts (**A** and **B**) by the coset decomposition:

$$C_{3v} = \underset{\text{A}}{C_3} + \underset{\text{B}}{C_3\sigma_{v(1)}}, \quad (10.1)$$

where the homomeric numbered skeletons listed in the top row of Fig. 8.1 (page 195) corresponds to the coset $C_3 (= C_3I)$, while the homomeric mirror-numbered skeletons listed in the bottom row of Fig. 8.1 corresponds to the coset $C_3\sigma_{v(1)}$. Hence, the coset $C_3 (= C_3I)$ is represented by the reference numbered skeleton **10-1**, while the coset $C_3\sigma_{v(1)}$ is represented by the mirror-numbered skeleton $\overline{\mathbf{10-1}}$.

Next, the *RS*-numbered skeleton **8-1d'** is selected from the homomeric *RS*-numbered skeletons listed in the bottom row of Fig. 9.4 (page 241). This skeleton is renumbered to be **10-2**, which is placed at the upper-right corner of Fig. 10.1. Thereby, the horizontal direction of Fig. 10.1 (linked with a double-headed arrow attached by an open circle) represents the conversions shown in Fig. 9.4, which are based on the action of the *RS*-permutation group $C_{3\tilde{\sigma}}$. In other words, the skeleton **10-1** and the *RS*-numbered skeleton **10-2** in the horizontal direction are in an *RS*-diastereomeric relationship.

The *RS*-permutation group $C_{3\tilde{\sigma}}$ (cf. Table 9.1 on page 240) is divided into two parts (**A** and **C**) by the coset decomposition:

$$C_{3\tilde{\sigma}} = \underset{\text{A}}{C_3} + \underset{\text{C}}{C_3\tilde{\sigma}_{v(1)}}, \quad (10.2)$$

where the homomeric numbered skeletons listed in the top row of Fig. 9.4 corresponds to the coset $C_3 (= C_3I)$, while the homomeric *RS*-numbered skeletons listed in the bottom row of Fig. 9.4 corresponds to the coset $C_3\tilde{\sigma}_{v(1)}$. Hence, the coset $C_3 (= C_3I)$ corresponds to the reference numbered skeleton **10-1**, while the coset $C_3\tilde{\sigma}_{v(1)}$ corresponds to the *RS*-numbered skeleton **10-2**.

Ligand-Reflection Groups

Now, let us examine the relationship between the mirror-numbered skeleton $\overline{\mathbf{10-1}}$ and the *RS*-numbered skeleton **10-2** in the diagonal direction of Fig. 10.1. The interconversion of $\overline{\mathbf{10-1}}$ into **10-2** represented by the following equation:

$$\widehat{I}\sigma_{v(1)} = \tilde{\sigma}_{v(1)} \quad \text{or} \quad \sigma_{v(1)} = \widehat{I}\tilde{\sigma}_{v(1)} \quad (10.3)$$

where the operation \widehat{I} is represented by $\widehat{I} \sim \overline{(1)(2)(3)}$, because of $\sigma_{v(1)} \sim \overline{(1)(23)}$ and $\tilde{\sigma}_{v(1)} \sim (1)(23)$. Thus, we obtain:

$$\widehat{I} = \tilde{\sigma}_{v(1)}\sigma_{v(1)}^{-1} = \sigma_{v(1)}\tilde{\sigma}_{v(1)}^{-1} \sim \overline{(1)(2)(3)}. \quad (10.4)$$

By using $\widehat{I} \sim \overline{(1)(2)(3)}$, we introduce the following operations named *ligand reflections*:

$$\widehat{I} = \widehat{I}I = I\widehat{I} \quad (10.5)$$

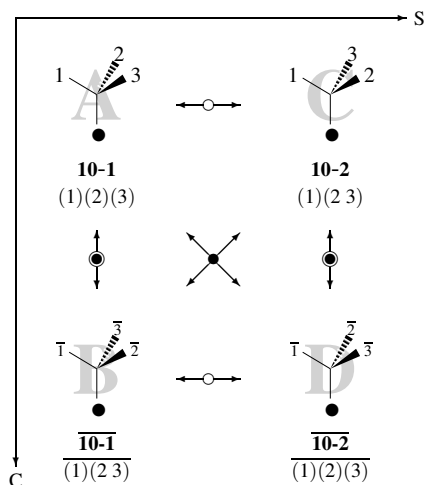


Fig. 10.1. Elementary stereoisogram of numbered trigonal pyramidal skeletons. The other modes of sequential numbering are permitted without losing generality.

$$\widehat{C}_3 = \widehat{I}C_3 = C_3\widehat{I} \quad (10.6)$$

$$\widehat{C}_3^2 = \widehat{I}C_3^2 = C_3^2\widehat{I}, \quad (10.7)$$

where the skeleton **10-1** is not changed, while the chirality sense of each proligand is converted into the opposite chirality sense. Thereby, we are able to construct the following group $C_{3\widehat{I}}$ named a *ligand-reflection group*:

$$C_{3\widehat{I}} = \{I, C_3, C_3^2, \widehat{I}, \widehat{C}_3, \widehat{C}_3^2\} \quad (10.8)$$

$$\sim \{(1)(2)(3), (1\ 3\ 2), (1\ 2\ 3), \overline{(1)(2)(3)}, \overline{(1\ 3\ 2)}, \overline{(1\ 2\ 3)}\}, \quad (10.9)$$

the elements of which are listed in Table 10.1. Because each position is fixed (stabilized) by the action of $C_{\widehat{I}} = \{I, \widehat{I}\}$, Eq. 10.9 is found to be the coset representation $C_{3\widehat{I}}(/C_{\widehat{I}})$.

In a parallel way to Fig. 8.1 (page 195) showing symmetry operations of the point group C_{3v} as well as to Fig. 9.4 (page 241) showing symmetry operations of the *RS*-permutation group $C_{3\widehat{\sigma}}$, the action of the ligand-reflection group $C_{3\widehat{I}}$ on **8-1** is illustrated in Fig. 10.2, where the bottom row lists homomeric ligand-mirror-numbered (*LM*-numbered) skeletons.

The coset decomposition of the ligand-reflection group $C_{3\widehat{I}}$ is obtained as follows:

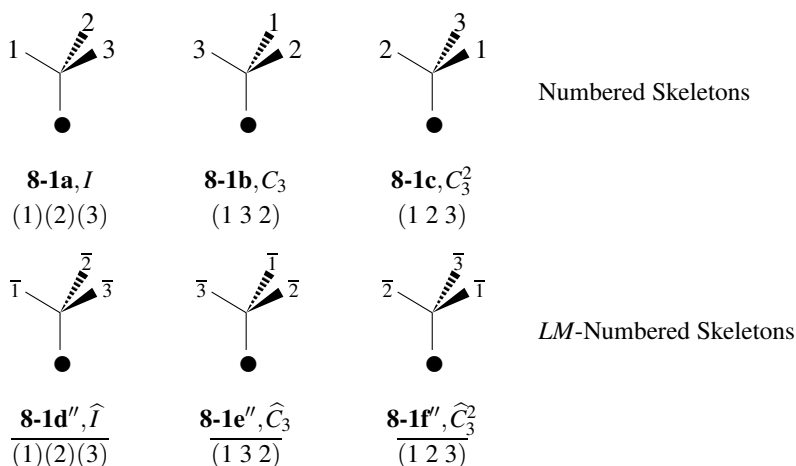
$$C_{3\widehat{I}} = \underset{\mathbf{A}}{C_3} + \underset{\mathbf{D}}{C_3\widehat{I}}, \quad (10.10)$$

which divides the ligand-reflection group $C_{3\widehat{I}}$ into two parts (**A** and **D**). The coset $C_3 (= C_3I)$ corresponds to the top row of Fig. 10.2, while the coset $C_3\widehat{I}$ corresponds to the bottom row which lists homomeric *LM*-numbered skeletons.

In a similar way to Theorem 3.3 (page 62) for point groups as well as to Theorem 9.1 (page 245) for *RS*-permutation groups, the term *homomeric* is used under the action of ligand-reflection groups in accord with the following theorem:

Table 10.1. Operations of $C_{3\hat{I}}$ and Coset Representation $C_{3\hat{I}}(/C_3)$

operation $g \in C_{3\hat{I}}$	$C_{3\hat{I}}(/C_3)$ (product of cycles)	PSI (product of sphericity indices)	cycle term
I	(1)(2)(3)	b_1^3	s_1^3
C_3	(1 3 2)	b_3	s_3
C_3^2	(1 2 3)	b_3	s_3
\hat{I}	$\overline{(1)(2)(3)}$	a_1^3	s_1^3
\hat{C}_3	$\overline{(1 3 2)}$	a_3	s_3
\hat{C}_3^2	$\overline{(1 2 3)}$	a_3	s_3

**Fig. 10.2.** Symmetry operations for a trigonal pyramidal skeleton (**8-1**) under the ligand-reflection group $C_{3\hat{I}}$. The identity operation (I) converts **8-1** into itself, where the resulting skeleton is denoted as **8-1a** [4]. The top row lists homomeric numbered skeletons, while the bottom row lists homomeric *LM*-numbered skeletons.

Theorem 10.1 (Homomeric Relationship under Ligand-Reflection Groups). Suppose that a given numbered skeleton belongs to a ligand-reflection group (which is ascleral). Then the numbered skeleton is fixed (or converted into a homomer) under the action of the maximum scleral subgroup. The corresponding *LM*-numbered skeleton (cf. Fig. 10.2) is also fixed (or converted into a homomer) under the action of the maximum scleral group.

This theorem gives an extended foundation of the term *homomeric*. Note that the maximum chiral subgroup, the maximum *RS*-stereogenic subgroup, and the maximum scleral subgroup designates the same group (e.g., C_3 for Fig. 10.2).

To grasp the behavior of $\overline{(1)(2)(3)}$, let us now consider the point group C_{3h} :

$$C_{3h} = \{I, C_3, C_3^2, \sigma_h, S_3, S_3^5\} \quad (10.11)$$

$$\sim \{(1)(2)(3), (1\ 3\ 2), (1\ 2\ 3), \overline{(1)(2)(3)}, \overline{(1\ 3\ 2)}, \overline{(1\ 2\ 3)}\}, \quad (10.12)$$

where the horizontal mirror plane σ_h of the point group C_{3h} is represented by $\sigma_h \sim \overline{(1)(2)(3)}$, because three positions to be considered are governed by the coset representation C_{3h}/C_3 . The coset decomposition of the point group C_{3h} by C_3 is represented as follows:

$$C_{3h} = C_3 + C_3\sigma_h. \quad (10.13)$$

Compare Eq. 10.9 with Eq. 10.12. In the parallel way to Eq. 10.12 showing the coset representation C_{3h}/C_3 , Eq. 10.9 is found to be the coset representation $C_{3\hat{r}}/C_{\hat{r}}$.

Exercise 10.1.

- Place a set of three pairs of proligands p/\bar{p} on the six positions of the cyclopropane skeleton **3-16** of D_{3h} (Fig. 3.9 on page 73), where the function denoted by f : $f(1) = p$, $f(2) = p$, $f(3) = p$, $f(4) = \bar{p}$, $f(5) = \bar{p}$, and $f(6) = \bar{p}$ is applied.
 - Confirm that the resulting promolecule with the composition $p^3\bar{p}^3$ belongs to the point group C_{3h} .
 - Confirm that the three ring carbons construct an orbit governed by the coset representation C_{3h}/C_3 .
-

RS-Stereoisomeric Groups

The *LM*-numbered skeleton **8-1d''** is selected from the homomeric *LM*-numbered skeletons listed in the bottom row of Fig. 10.2. This skeleton is renumbered to be **10-2**, which is placed at the lower-right corner of Fig. 10.1. Thereby, the diagonal direction of Fig. 10.1 (linked with a double-headed arrow attached by a solid circle) represents the conversions shown in Fig. 10.2, which are based on the action of the ligand-reflection group $C_{3\hat{r}}$. The relationship between the skeleton **10-1** and the *LM*-numbered skeleton **10-2** in the diagonal direction is called a *holantimeric relationship*.

The completed diagram shown in Fig. 10.1 is called an *elementary stereoisogram*, where the vertical directions are concerned with enantiomeric relationships due to the point group C_{3v} , the horizontal directions are concerned with *RS*-diastereomeric relationships due to the *RS*-permutation group $C_{3\bar{\sigma}}$, and the diagonal directions are concerned with holantimeric relationships due to the ligand-reflection group $C_{3\hat{r}}$. See Fig. 8.1 (page 195) for the vertical directions, Fig. 9.4 (page 241) for the horizontal directions, and Fig. 10.2 for the diagonal directions.

Because the point group C_{3v} (Eq. 10.1), the *RS*-permutation group $C_{3\bar{\sigma}}$ (Eq. 10.2), and the ligand-reflection group $C_{3\hat{r}}$ (Eq. 10.10) contain a maximum subgroup C_3 in common, they are integrated to give a new group called an *RS-stereoisomeric group* denoted by the

Table 10.2. *RS*-Stereoisomeric Group $C_{3v\tilde{\sigma}\hat{I}}$ as Well as Coset Representations $C_{3v\tilde{\sigma}\hat{I}}/C_{3\tilde{\sigma}\hat{I}}$

operation $g \in C_{3v\tilde{\sigma}\hat{I}}$	$C_{3v\tilde{\sigma}\hat{I}}/C_{3\tilde{\sigma}\hat{I}}$ (product of cycles)	PSI	operation $g \in C_{3v\tilde{\sigma}\hat{I}}$	$C_{3v\tilde{\sigma}\hat{I}}/C_{3\tilde{\sigma}\hat{I}}$ (product of cycles)	PSI
I	(1)(2)(3)	b_1^3	$\tilde{\sigma}_{v(1)}$	(1)(2 3)	$b_1 b_2$
C_3	(1 3 2)	b_3	$\tilde{\sigma}_{v(2)}$	(1 3)(2)	$b_1 b_2$
C_3^2	(1 2 3)	b_3	$\tilde{\sigma}_{v(3)}$	(1 2)(3)	$b_1 b_2$
$\sigma_{v(1)}$	$\overline{(1)(2 3)}$	$a_1 c_2$	\hat{I}	$\overline{(1)(2)(3)}$	a_1^3
$\sigma_{v(2)}$	$\overline{(1 3)(2)}$	$a_1 c_2$	\hat{C}_3	$\overline{(1 3 2)}$	a_3
$\sigma_{v(3)}$	$\overline{(1 2)(3)}$	$a_1 c_2$	\hat{C}_3^2	$\overline{(1 2 3)}$	a_3

symbol $C_{3v\tilde{\sigma}\hat{I}}$ as follows:

$$C_{3v\tilde{\sigma}\hat{I}} = \underset{\mathbf{A}}{C_3} + \underset{\mathbf{B}}{C_3\sigma_{v(1)}} + \underset{\mathbf{C}}{C_3\tilde{\sigma}_{v(1)}} + \underset{\mathbf{D}}{C_3\hat{I}}, \quad (10.14)$$

which represents the coset decomposition of $C_{3v\tilde{\sigma}\hat{I}}$ by C_3 . The operations of $C_{3v\tilde{\sigma}\hat{I}}$ are listed in Table 10.2, in which the **A**-part consists of the proper rotations commonly contained in the three component groups, the **B**-part consists of the reflections listed in Table 8.1 (the point group C_{3v} on page 196), the **C**-part consists of the *RS*-permutations listed in Table 9.1 (the *RS*-permutation group $C_{3\tilde{\sigma}}$ on page 240), and the **D**-part consists of the ligand reflections listed in Table 10.1 (the ligand-reflection group $C_{3\hat{I}}$). These four parts (**A**, **B**, **C**, and **D**) correspond to the four cosets appearing in Eq. 10.14.

The above discussions on the *RS*-stereoisomeric group $C_{3v\tilde{\sigma}\hat{I}}$ hold true in general. To support further discussions, let us define an *RS*-stereoisomeric group \hat{G} in general by starting from a point group G .

Definition 10.1 (*RS*-Stereoisomeric Groups). Suppose that an achiral point group G exhibits a coset decomposition by the maximum chiral subgroup G_C , as found in Eq. 10.15. The corresponding *RS*-permutation group $G_{\tilde{\sigma}}$ is defined by Eq. 10.16, while the corresponding ligand-reflection group $G_{\hat{I}}$ is defined by Eq. 10.17:

$$G = \underset{\mathbf{A}}{G_C} + \underset{\mathbf{B}}{G_C\sigma} \quad (10.15)$$

$$G_{\tilde{\sigma}} = \underset{\mathbf{A}}{G_C} + \underset{\mathbf{C}}{G_C\tilde{\sigma}} \quad (10.16)$$

$$G_{\hat{I}} = \underset{\mathbf{A}}{G_C} + \underset{\mathbf{D}}{G_C\hat{I}}, \quad (10.17)$$

where the symbol σ represents a reflection, the symbol $\tilde{\sigma}$ represents an *RS*-permutation, and the symbol \hat{I} represents a ligand-reflection. Then, the corresponding *RS*-stereoisomeric group is defined as follows:

$$\hat{G} = \underset{\mathbf{A}}{G_C} + \underset{\mathbf{B}}{G_C\sigma} + \underset{\mathbf{C}}{G_C\tilde{\sigma}} + \underset{\mathbf{D}}{G_C\hat{I}}. \quad (10.18)$$

The subgroup G_C under the *RS*-stereoisomeric group \hat{G} (Eq. 10.18) is called *the maximum normal subgroup*. The maximum normal subgroup G_C is identical with the maximum chiral

subgroup G_C under the point group G (Eq. 10.15), where G_C is a stabilizer of the coset $G_C\sigma$ (**B**) as follows:

$$G_C\sigma = \sigma G_C \quad \text{i.e.,} \quad \sigma^{-1}G_C\sigma = G_C. \quad (10.19)$$


The maximum normal subgroup G_C is identical with the maximum *RS*-stereogenic subgroup G_C under the *RS*-permutation group $G_{\tilde{\sigma}}$ (Eq. 10.16), where G_C is a stabilizer of the coset $G_C\tilde{\sigma}$ (**C**) as follows:

$$G_C\tilde{\sigma} = \tilde{\sigma}G_C \quad \text{i.e.,} \quad \tilde{\sigma}^{-1}G_C\tilde{\sigma} = G_C. \quad (10.20)$$

The maximum normal subgroup G_C is identical with the maximum scleral subgroup G_C under the ligand-reflection group $G_{\hat{I}}$ (Eq. 10.17), where G_C is a stabilizer of the coset $G_C\hat{I}$ (**D**) as follows:

$$G_C\hat{I} = \hat{I}G_C \quad \text{i.e.,} \quad \hat{I}^{-1}G_C\hat{I} = G_C. \quad (10.21)$$

Because of Eqs. 10.19–10.21, the maximum normal subgroup G_C is a stabilizer of each coset (**A**, **B**, **C**, and **D**) appearing in the right-hand side of the coset decomposition of \hat{G} by G_C (Eq. 10.18). It follows that each coset represented by the letter **A**, **B**, **C**, or **D** in Eq. 10.18 corresponds to a set of homomers produced under the action of the maximum normal subgroup G_C represented by **A**.


Exercise 10.2. Confirm that the maximum chiral subgroup C_3 of the point group C_{3v} is identical with the maximum normal subgroup of the corresponding *RS*-stereoisomeric group $C_{3v}\tilde{\sigma}\hat{I}$ (Eq. 10.14). 

Theorem 3.3 (page 62) for point groups, Theorem 9.1 (page 245) for *RS*-permutation groups, and Theorem 10.1 for ligand-reflection groups are integrated to support the term *homomeric* under the action of *RS*-stereoisomeric groups.

Theorem 10.2 (Homomeric Relationship under *RS*-Stereoisomeric Groups). Suppose that a given numbered skeleton belongs to an *RS*-stereoisomeric group. Then, each of the numbered skeleton, the mirror-numbered skeleton, the *RS*-numbered skeleton, and the *LM*-numbered skeleton is fixed (or converted into a homomer) under the action of the maximum normal subgroup.

This theorem gives an extended foundation of the term *homomeric*. Note that the letters **A**, **B**, **C**, and **D** in Eq. 10.18 correspond to the respective parts of such an elementary stereoisogram as Fig. 10.1.

Remark 10.1 (A Misleading Standpoint of Modern Stereochemistry). Modern stereochemistry confuses Theorem 9.1 (page 245) for *RS*-permutation groups with Theorem 3.3 (page 62) for point groups. In addition, modern stereochemistry is in entire ignorance of Theorem 10.1 for ligand-reflection groups. On the other hand, the judgment concerning ‘homomeric’ in the flowchart of Fig. 1.13 (page 18) ignores Theo-



rem 9.1 (page 245) for *RS*-permutation groups as well as Theorem 10.1 for ligand-reflection groups, even though the left branch of the flowchart of Fig. 1.13 can be regarded to give equivalent effects to Theorem 3.3 (page 62) for point groups.

In contrast, Fujita's stereoisogram approach has reached an integrated standpoint based on Theorem 10.2. See Remark 10.2.

10.1.2 Stereoisograms Based on Elementary Stereoisograms

Stereoisograms as Diagrammatic Expressions of *RS*-Stereoisomeric Groups

Suppose that the three positions of variously numbered skeletons in the elementary stereoisogram (Fig. 10.1) accommodate a set of proligands selected from a ligand inventory:

$$\mathbf{L}' = \{A, B, X, p, \bar{p}, q, \bar{q}, r, \bar{r}\} \quad (10.22)$$

so as to give a stereoisogram of a derived promolecule. To survey derivatives based on the trigonal pyramidal skeleton, Fig. 10.3 collects reference promolecules for constructing stereoisograms [5, Fig. 1].

Let us first consider a set of achiral proligands of the same kind:

$$f : \{f(1) = A, f(2) = A, f(3) = A\}, \quad (10.23)$$

which are placed on the three positions. Thereby, the four skeletons of the elementary stereoisogram (Fig. 10.1) generate a quadruplet of identical promolecules, as found in Fig. 10.4. Hence, there appear equality symbols in all of the directions of the stereoisogram. The reference promolecule **10-17** with the composition A^3 belongs to the *RS*-stereoisomeric group $C_{3v\bar{\sigma}\bar{f}}$, so that the action of $C_{3v\bar{\sigma}\bar{f}}$ generates a set of identical promolecules. Such stereoisograms as characterized by all equality symbols (Fig. 10.4) are referred to as type IV.

Second, let us consider a set of achiral proligands in isolation:

$$f : \{f(1) = A, f(2) = B, f(3) = X\}, \quad (10.24)$$

which indicates a proligand A on the 1-position, a proligand B on the 2-position, and a proligand X on the 3-position. Thereby, the reference skeleton **10-1** in the elementary stereoisogram (Fig. 10.1) generates a reference promolecule **9-8** with the composition ABX (cf. Fig. 9.8(a) on page 248; the same as **10-3** in Fig. 10.3), as depicted in the upper-left corner of Fig. 10.5. The other skeletons in Fig. 10.1 generate the respective promolecules. Thus, the mirror-numbered skeleton $\overline{\mathbf{10-1}}$ generates its enantiomer $\overline{\mathbf{9-8}}$; the *RS*-numbered skeleton **10-2** generates its *RS*-diastereomer **9-9**; and the *LM*-numbered skeleton $\overline{\mathbf{10-2}}$ generates its holantimer $\overline{\mathbf{9-9}}$. As shown by the equality symbols in the diagonal directions, the reference promolecule **9-8** is identical with the holantimer $\overline{\mathbf{9-9}}$; and the enantiomer $\overline{\mathbf{9-8}}$ is identical

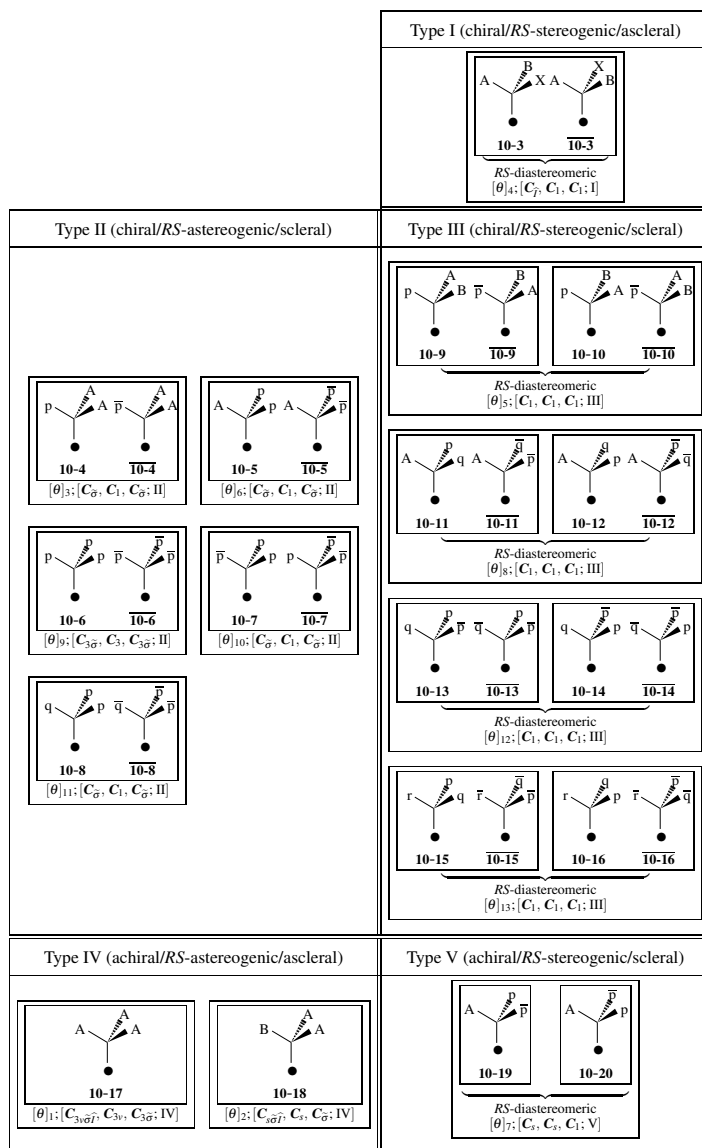


Fig. 10.3. Symmetry-itemized enumeration based on a trigonal pyramidal skeleton under the *RS*-stereoisomeric group $C_{3v}\widehat{\sigma}_h$. The symbols A, B, and X represent achiral proligands, while the pairs, p/\bar{p} , q/\bar{q} , and r/\bar{r} , denote enantiomeric pairs of chiral proligands. Two derivative or one derivative surrounded by each inner box are enantiomeric or an achiral promolecule. Each outer box shows a quadruplet of a stereoisogram (or a degenerate format) to be counted once under $C_{3v}\widehat{\sigma}_h$, where the corresponding partition $[\theta]_i$ and the symbol [*RS*-stereoisomeric group, point group, *RS*-permutation group; type] are attached for specifying symmetry properties.

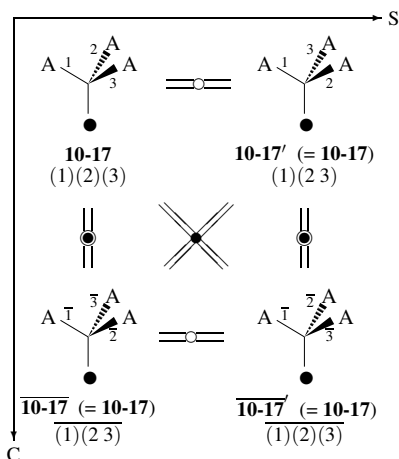


Fig. 10.4. Type-IV stereoisogram that consists of a quadruplet of promolecules derived from a trigonal pyramidal skeleton with composition A^3 .

with the *RS*-diastereomer **9-9**. In other words, the enantiomeric relationships are congruent with the *RS*-diastereomeric relationships. Such stereoisograms as Fig. 10.5 are referred to as type I.

The reference promolecule **9-8** (the same as **10-3** in Fig. 10.3) belongs to the *RS*-stereoisomeric group $C_{\hat{I}} (= \{I, \hat{I}\})$. Thus, the *RS*-stereoisomeric group $C_{\hat{I}}$ fixes (stabilizes) the promolecule **9-8** under the action of $C_{3v\sigma\hat{I}}$, so as to be consistent with the diagonal equality symbols.

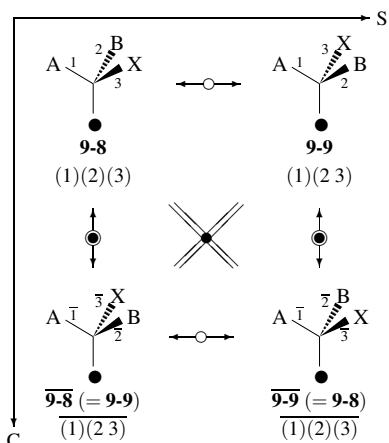


Fig. 10.5. Type-I stereoisogram that consists of a quadruplet of promolecules derived from a trigonal pyramidal skeleton with composition ABX .

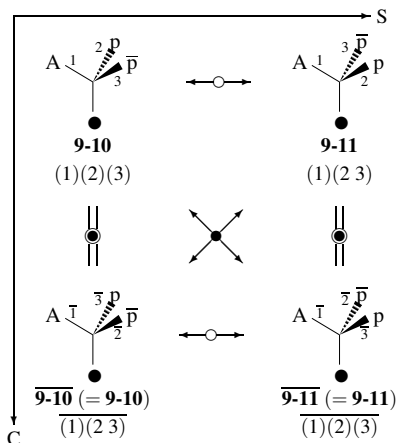


Fig. 10.6. Type-V stereoisogram that consists of a quadruplet of promolecules derived from a trigonal pyramidal skeleton with composition $A p \bar{p}$.

Let us next consider the following set of proligands:

$$f: \{f(1) = A, f(2) = p, f(3) = \bar{p}\}, \quad (10.25)$$

where the symbols p and \bar{p} represent a pair of enantiomeric proligands in isolation. Thereby, the reference skeleton **10-1** in the elementary stereoisogram (Fig. 10.1) generates a reference promolecule **9-10** with the composition $A p \bar{p}$ (cf. Fig. 9.8(b) on page 248; the same as **10-19** in Fig. 10.3), as depicted in the upper-left corner of Fig. 10.6. The other skeletons in Fig. 10.1 generate the respective promolecules. Thus, the mirror-numbered skeleton $\overline{10-1}$ generates its enantiomer $\overline{9-10}$; the RS -numbered skeleton **10-2** generates its RS -diastereomer **9-11**; and the LM -numbered skeleton $\overline{10-2}$ generates its holantimer $\overline{9-11}$. As shown by the equality symbols in the vertical directions, the reference promolecule **9-10** and the RS -diastereomer **9-11** are achiral. Such stereoisograms as Fig. 10.6 are referred to as type V.

The reference promolecule **9-10** or **9-11** in Fig. 10.6 (**10-19** or **10-20** in Fig. 10.3) is achiral and belongs to the RS -stereoisomeric group $C_s (= \{I, \sigma_{v(1)}\})$, which is also regarded as a point group. Thus, the RS -stereoisomeric group C_s fixes (stabilizes) the promolecule **9-10** or **9-11** under the action of $C_{3v\bar{\sigma}\hat{I}}$, so as to be consistent with the vertical equality symbols.

Let us further consider the following set of proligands:

$$f: \{f(1) = A, f(2) = p, f(3) = p\}. \quad (10.26)$$

Thereby, the reference skeleton **10-1** in the elementary stereoisogram (Fig. 10.1) generates a reference promolecule **10-4** with the composition $A p^2$, which is depicted in the upper-left corner of Fig. 10.7. The other skeletons in Fig. 10.1 generate the respective promolecules. Thus, the mirror-numbered skeleton $\overline{10-1}$ generates its enantiomer $\overline{10-4}$; the RS -numbered skeleton **10-2** generates its RS -diastereomer **10-21**; and the LM -numbered skeleton $\overline{10-4}$

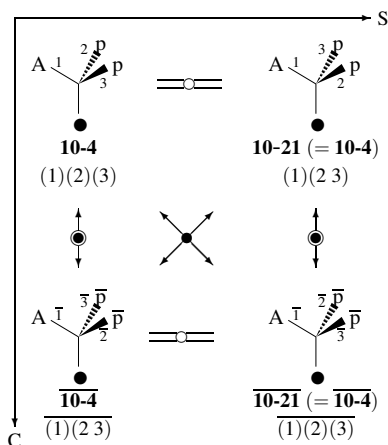


Fig. 10.7. Type-II stereoisogram that consists of a quadruplet of promolecules derived from a trigonal pyramidal skeleton with composition Ap^2 or $A\bar{p}^2$.

generates its holantimer $\overline{10-21}$. Note that there appear equality symbols in the horizontal directions of Fig. 10.7, because **10-21** is identical with **10-4** as well as $\overline{10-21}$ is identical with $\overline{10-4}$. Such stereoisograms as Fig. 10.7 are referred to as type II.

The reference promolecule **10-4** belongs to the *RS*-stereoisomeric group $C_{\tilde{\sigma}} (= \{I, \tilde{\sigma}_{v(1)}\})$, which is also regarded as an *RS*-permutation group. Thus, the *RS*-stereoisomeric group $C_{\tilde{\sigma}}$ fixes (stabilizes) the promolecule **10-4** under the action of $C_{3v\tilde{\sigma}\hat{I}}$, so as to be consistent with the horizontal equality symbols.

Finally, let us consider the following set of proligands:

$$f : \{f(1) = p, f(2) = A, f(3) = B\}. \quad (10.27)$$

Thereby, the reference skeleton **10-1** in the elementary stereoisogram (Fig. 10.1) generates a reference promolecule **10-9** with the composition ABp , as depicted in the upper-left corner of Fig. 10.8. The other skeletons in Fig. 10.1 generate the respective promolecules shown in Fig. 10.8. Thus, the mirror-numbered skeleton $\overline{10-1}$ generates its enantiomer $\overline{10-9}$; the *RS*-numbered skeleton **10-2** generates its *RS*-diastereomer **10-10**; and the *LM*-numbered skeleton $\overline{10-4}$ generates its holantimer $\overline{10-10}$. Note that there appear no equality symbols in Fig. 10.8. Such stereoisograms as Fig. 10.8 are referred to as type III.

The reference promolecule **10-9** belongs to the *RS*-stereoisomeric group $C_1 (= \{I\})$. Thus, the *RS*-stereoisomeric group C_1 fixes (stabilizes) the promolecule **10-9** under the action of $C_{3v\tilde{\sigma}\hat{I}}$, so as to be consistent with the absence of equality symbols.

Three Relationships and Three Attributes in a Stereoisogram

As found in Figs. 10.4–10.8, there appear three relationships in a stereoisogram. They correspond to three pairwise attributes, as summarized in Table 10.3. The vertical directions

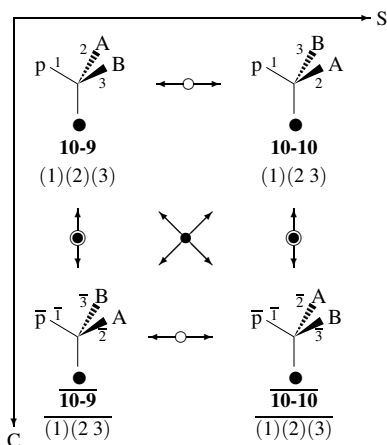


Fig. 10.8. Type-III stereoisogram that consists of a quadruplet of promolecules derived from a trigonal pyramidal skeleton with composition AB_p or $AB_{\bar{p}}$.

Table 10.3. Relationships and Attributes Appearing in Stereoisograms.

symbol	relationship	attribute
[Point-group symmetry] (Concerned with reflections ●)		
$\leftarrow \bullet \rightarrow$	enantiomeric	chiral
$\equiv \bullet \equiv$	(self-enantiomeric)	achiral
[RS-permutation-group symmetry] (Concerned with RS-permutations ○)		
$\leftarrow \circ \rightarrow$	RS-diastereomeric	RS-stereogenic
$\equiv \circ \equiv$	(self-RS-diastereomeric)	RS-astereogenic
[Ligand-reflection-group symmetry] (Concerned with ligand reflections ●)		
$\leftarrow \bullet \rightarrow$	holantimeric	scleral
$\equiv \bullet \equiv$	(self-holantimeric)	ascleral

of each stereoisogram (cf. Figs. 10.4–10.8) are concerned with enantiomeric relationships, which stem from a pair of attributes related to point-group symmetry, i.e., chirality/achirality; the horizontal directions are concerned with *RS*-diastereomeric relationships, which stem from another pair of attributes related to *RS*-permutation-group symmetry, i.e., *RS*-stereogenicity/*RS*-astereogenicity; and the diagonal directions are concerned with holantimeric relationships, which stem from a further pair of attributes related to ligand-reflection-group symmetry, i.e., sclerality/asclerality.

Remark 10.2 (A Single Pair in Modern Stereochemistry). Modern stereochemistry is based on a pair of chirality/achirality as a single pair. In other words, mod-



ern stereochemistry has not pay attention to the other two pairs of attributes, i.e., a pair of *RS*-stereogenicity/*RS*-astereogenicity and a pair of sclerality/asclerality. As a result, conventional discussions in modern stereochemistry (in particular, on *RS*-stereodescriptors [6,7] and on *pro-R/pro-S*-descriptors [8]) have misleadingly mixed up the pair of chirality/achirality with the pair of *RS*-stereogenicity/*RS*-astereogenicity. For Fujita's stereoisogram approach for reorganizing theoretical foundations of such stereochemical nomenclature, see his recent articles [9–12].

For the sake of simplicity, three pairs of attributes in a stereoisogram are represented by a type index $[-/a, -/a, -/a]$, where the symbol ‘-’ represents chirality, *RS*-stereogenicity, or sclerality, while the symbol ‘a’ represents achirality, *RS*-astereogenicity, or asclerality. Thereby, a stereoisogram is characterized by a type index: $[-, -, a]$ for type I, $[-, a, -]$ for type II, $[-, -, -]$ for type III, $[a, a, a]$ for type IV, and $[a, -, -]$ for type V.

Stereoisograms of Five Types

Three pairs of $-/a$ in each type index permit eight ($= 2^3$) possibilities of type indices, among which a type index with two *a*'s results in the type index $[a, a, a]$. Because the type indices $[a, a, -]$, $[a, -, a]$, and $[-, a, a]$ are impossible to characterize stereoisograms, there remain 5 ($= 8 - 3$) possibilities, which show the existence of five types of stereoisograms (types I–V).

A more mathematical proof is based on Eq. 10.14 (or Eq. 10.18 in general). Because C_3 is a normal subgroup of $C_{3v\tilde{\sigma}\hat{I}}$, we obtain the following factor group:

$$C_{3v\tilde{\sigma}\hat{I}}/C_3 = \{ \underset{\text{A}}{C_3}, \underset{\text{B}}{C_3\sigma_{v(1)}}, \underset{\text{C}}{C_3\tilde{\sigma}_{v(1)}}, \underset{\text{D}}{C_3\hat{I}} \}, \quad (10.28)$$

which is isomorphic to the Klein four-group of order 4 or to the point group C_{2v} . Hence, the factor group $C_{3v\tilde{\sigma}\hat{I}}/C_3$ has five subgroups, just as the Klein four-group has five subgroups and as the point group C_{2v} has five subgroups.

Because the four cosets contained in the factor group $C_{3v\tilde{\sigma}\hat{I}}/C_3$ correspond to the four skeletons contained in the elementary stereoisogram (Fig. 10.1), the existence of five types of stereoisograms is proven. The above proof holds in general, because the point group C_{3v} can be changed to any achiral point groups.

The five subgroups of the factor group $C_{3v\tilde{\sigma}\hat{I}}/C_3$ are listed as follows:

$$\text{Type I: } C_{3\hat{I}}/C_3 = \{ \underset{\text{A}}{C_3}, \underset{\text{D}}{C_3\hat{I}} \} \quad (10.29)$$

$$\text{Type II: } C_{3\tilde{\sigma}}/C_3 = \{ \underset{\text{A}}{C_3}, \underset{\text{C}}{C_3\tilde{\sigma}_{v(1)}} \} \quad (10.30)$$

$$\text{Type III: } C_3/C_3 = \{ \underset{\text{A}}{C_3} \} \quad (10.31)$$

$$\text{Type IV : } C_{3v\tilde{\sigma}\hat{I}}/C_3 = \{ \underset{\text{A}}{C_3}, \underset{\text{B}}{C_3\sigma_{v(1)}}, \underset{\text{C}}{C_3\tilde{\sigma}_{v(1)}}, \underset{\text{D}}{C_3\hat{I}} \} \quad (10.32)$$

$$\text{Type V : } C_{3v}/C_3 = \{ \underset{\text{A}}{C_3}, \underset{\text{B}}{C_3\sigma_{v(1)}} \}, \quad (10.33)$$

where these subgroups are correlated to five types of stereoisograms. The factor group C_3/C_3 for type III serves as an identity element of the factor group $C_{3v\tilde{\sigma}\hat{I}}/C_3$, which is assigned to type IV. The factor group $C_{3\hat{I}}/C_3$ for type I is correlated to the ligand-reflection group $C_{3\hat{I}}$ (Eq. 10.10); the factor group $C_{3\tilde{\sigma}}/C_3$ for type II is correlated to the *RS*-permutation group $C_{3\tilde{\sigma}}$ (Eq. 10.2); and the factor group C_{3v}/C_3 for type V is correlated to the point group C_{3v} (Eq. 10.1).

The cosets attached by **A** and **D** in Eq. 10.29 are coupled with the diagonal data of Fig. 10.1, so that the diagonal equality symbols of a type-I stereoisogram can be deduced. The cosets attached by **A** and **C** in Eq. 10.30 are coupled with the horizontal data of Fig. 10.1, so that the horizontal equality symbols of a type-II stereoisogram can be deduced. The cosets attached by **A** and **B** in Eq. 10.33 are coupled with the vertical data of Fig. 10.1, so that the vertical equality symbols of a type-V stereoisogram can be deduced. As one extreme case, Eq. 10.31 of type III results in the absence of equality symbols. As the other extreme case, Eq. 10.32 of type IV results in the full appearance of equality symbols.

In summary, Fig. 10.9 schematically illustrates such stereoisograms of five types, where the symbols **A** and $\bar{\text{A}}$ (or **B** and $\bar{\text{B}}$) represent a pair of enantiomers based on a given skeleton (e.g., a trigonal pyramidal skeleton). For example, the **A** at the upper-left position of each stereoisogram is selected from the promolecules listed in Fig. 10.3. For concrete examples of stereoisograms, see Figs. 10.4–10.8.

10.2 Enumeration Under *RS*-Stereoisomeric Groups

A quadruplet of *RS*-stereoisomers contained in a stereoisogram is an equivalence class under the action of an *RS*-stereoisomeric group. Both the FPM method (cf. Subsection 6.2) and the PCI method (cf. Subsection 6.3), which have been originally developed for enumeration under point groups in Fujita's USCI approach [14], can be extended to support enumeration under *RS*-stereoisomeric groups [15,16]. In this section, we focus our attention to the extension and application of the PCI method.

10.2.1 Subgroups of the *RS*-Stereoisomeric Group $C_{3v\tilde{\sigma}\hat{I}}$

Non-Redundant Set of Subgroups

The *RS*-stereoisomeric group $C_{3v\tilde{\sigma}\hat{I}}$ is isomorphic to the point group D_{3d} , which has once been referred to as a subgroup of a pseudo-point group [17–19]. The point group D_{3d} is also isomorphic to the point group D_{3h} , which has been applied to symmetry-itemized enumeration of various compounds according to Fujita's USCI approach [20,21]. Hence, the data of

	<i>RS</i> -astereogenic	<i>RS</i> -stereogenic
chiral		<p>Type I: $[-, -, a]$ chiral <i>RS</i>-stereogenic ascleral</p>
		<p>Type II: $[-, a, -]$ chiral <i>RS</i>-astereogenic scleral</p>
achiral		<p>Type III: $[-, -, -]$ chiral <i>RS</i>-stereogenic scleral</p>
		<p>Type IV: $[a, a, a]$ achiral <i>RS</i>-astereogenic ascleral</p>
		<p>Type V: $[a, -, -]$ achiral <i>RS</i>-stereogenic scleral</p>

Fig. 10.9. Stereoisograms for representing *RS*-stereoisomers of five types. This figure is a modification of Fig. 6 of [3] and of Fig. 2 of [13]. The symbols **A** and **A** (or **B** and **B**) represent a pair of enantiomers based on a given skeleton (e.g., a trigonal pyramidal skeleton).

the point group D_{3d} or D_{3h} can be applied to discuss the properties of the *RS*-stereoisomeric group $C_{3v\tilde{\sigma}\hat{I}}$.

The point group D_{3d} has the following non-redundant set of subgroups (SSG):

$$\text{SSG}_{D_{3d}} = \{C_1^1, C_2^2, C_s^3, C_i^4, C_3^5, C_{2h}^6, D_3^7, C_{3v}^8, C_{3i}^9, D_{3d}^{10}\}. \quad (10.34)$$

In a similar way, the point group D_{3h} has the following non-redundant set of subgroups (SSG):

$$\text{SSG}_{D_{3h}} = \{C_1^1, C_2^2, C_s^3, C_s'^4, C_3^5, C_{2v}^6, C_{3v}^8, C_{3h}^9, D_3^7, D_{3h}^{10}\}, \quad (10.35)$$

where the sequence of subgroups obeys the sequence described in previous references [14, 20,21]. The sequence of subgroups in Eq. 10.34 is adopted in the present book, because the sequence 2, 3, and 4 and the sequence 7, 8, and 9 give parallel effects.

The *RS*-stereoisomeric group $C_{3v\tilde{\sigma}\hat{I}}$ isomorphic to D_{3d} or D_{3h} has the corresponding non-redundant set of subgroups:

$$\text{SSG}_{C_{3v\tilde{\sigma}\hat{I}}} = \{C_1^1, C_{\tilde{\sigma}}^2, C_s^3, C_{\hat{I}}^4, C_3^5, C_{s\tilde{\sigma}\hat{I}}^6, C_{3\tilde{\sigma}}^7, C_{3v}^8, C_{3\hat{I}}^9, C_{3v\tilde{\sigma}\hat{I}}^{10}\}, \quad (10.36)$$

where each subgroup corresponds to the counterpart subgroup collected in Eq. 10.34, as indicated by an attached sequential number. Each subgroup of the SSG (Eq. 10.36) is selected as a representative of conjugate subgroups:

$$C_1 \stackrel{1}{\text{III}} \{I\} \quad (10.37)$$

$$C_{\tilde{\sigma}} \stackrel{2}{\text{II}} \{I, \tilde{\sigma}_{v(1)}\} \quad (10.38)$$

$$C_s \stackrel{3}{\text{V}} \{I, \sigma_{v(1)}\} \quad (10.39)$$

$$C_{\hat{I}} \stackrel{4}{\text{I}} \{I, \hat{I}\} \quad (10.40)$$

$$C_3 \stackrel{5}{\text{III}} \{I, C_3, C_3^2\} \quad (10.41)$$

$$C_{s\tilde{\sigma}\hat{I}} \stackrel{6}{\text{IV}} \{I, \tilde{\sigma}_{v(1)}, \sigma_{v(1)}, \hat{I}\} \quad (10.42)$$

$$C_{3\tilde{\sigma}} \stackrel{7}{\text{II}} \underbrace{\{I, C_3, C_3^2\}}_A, \underbrace{\{\tilde{\sigma}_{v(1)}, \tilde{\sigma}_{v(2)}, \tilde{\sigma}_{v(3)}\}}_C \quad (10.43)$$

$$C_{3v} \stackrel{8}{\text{V}} \underbrace{\{I, C_3, C_3^2\}}_A, \underbrace{\{\sigma_{v(1)}, \sigma_{v(2)}, \sigma_{v(3)}\}}_B \quad (10.44)$$

$$C_{3\hat{I}} \stackrel{9}{\text{I}} \underbrace{\{I, C_3, C_3^2\}}_A, \underbrace{\{\hat{I}, \hat{C}_3, \hat{C}_3^2\}}_D \quad (10.45)$$

$$C_{3v\tilde{\sigma}\hat{I}} \stackrel{10}{\text{IV}} \underbrace{\{I, C_3, C_3^2\}}_A, \underbrace{\{\sigma_{v(1)}, \sigma_{v(2)}, \sigma_{v(3)}\}}_B, \underbrace{\{\tilde{\sigma}_{v(1)}, \tilde{\sigma}_{v(2)}, \tilde{\sigma}_{v(3)}\}}_C, \underbrace{\{\hat{I}, \hat{C}_3, \hat{C}_3^2\}}_D, \quad (10.46)$$

where the sequential number over each equality symbol represents the reference to the corresponding point group and the Roman number under each equality symbol represents the type of the subgroup, as discussed below.

Five Types of Subgroups

The subgroups of the SSG (Eq. 10.36) are categorized into five types according to the factor groups shown by Eqs. 10.29–10.33:

$$\text{Type I: } \text{SG}^{\text{I}} = \{ \overset{4}{\mathbf{C}}_{\hat{I}}, \overset{9}{\mathbf{C}}_{3\hat{I}} \} \quad (10.47)$$

$$\text{Type II: } \text{SG}^{\text{II}} = \{ \overset{2}{\mathbf{C}}_{\tilde{\sigma}}, \overset{7}{\mathbf{C}}_{3\tilde{\sigma}} \} \quad (10.48)$$

$$\text{Type III: } \text{SG}^{\text{III}} = \{ \overset{1}{\mathbf{C}}_1, \overset{5}{\mathbf{C}}_3 \} \quad (10.49)$$

$$\text{Type IV: } \text{SG}^{\text{IV}} = \{ \overset{6}{\mathbf{C}}_{s\tilde{\sigma}\hat{I}}, \overset{10}{\mathbf{C}}_{3v\tilde{\sigma}\hat{I}} \} \quad (10.50)$$

$$\text{Type V: } \text{SG}^{\text{V}} = \{ \overset{3}{\mathbf{C}}_s, \overset{8}{\mathbf{C}}_{3v} \}, \quad (10.51)$$

where the reference number above each symbol of an *RS*-stereoisomeric group corresponds to the reference number attached on the equality symbol of each equation listed in Eqs. 10.37–10.46. Note that a reflection is represented by a σ -symbol with no accent; an *RS*-permutation is represented by a symbol with a tilde accent; and a ligand reflection is represented by a symbol with a hat accent. The largest subgroup contained in each type of Eqs. 10.47–10.51 gives the factor group listed in each of Eqs. 10.29–10.33 (e.g., $\mathbf{C}_{3\hat{I}}$ of Eq. 10.47 gives $\mathbf{C}_{3\hat{I}}/\mathbf{C}_3$ of Eq. 10.29).

10.2.2 Coset Representations

The discussions on coset representations of point groups in Subsection 5.1.1 can be applied to *RS*-stereoisomeric groups. Each subgroup $\hat{\mathbf{G}}_i$ contained in $\text{SSG}_{\mathbf{C}_{3v\tilde{\sigma}\hat{I}}}$ (Eq. 10.36) corresponds to a coset representation $\mathbf{C}_{3v\tilde{\sigma}\hat{I}}(\hat{\mathbf{G}}_i)$, as shown in the following list:

$$\begin{aligned} \text{SCR}_{\mathbf{C}_{3v\tilde{\sigma}\hat{I}}} = \{ & \overset{1}{\mathbf{C}}_{3v\tilde{\sigma}\hat{I}}(\mathbf{C}_1), \overset{2}{\mathbf{C}}_{3v\tilde{\sigma}\hat{I}}(\mathbf{C}_{\tilde{\sigma}}), \overset{3}{\mathbf{C}}_{3v\tilde{\sigma}\hat{I}}(\mathbf{C}_s), \overset{4}{\mathbf{C}}_{3v\tilde{\sigma}\hat{I}}(\mathbf{C}_{\hat{I}}), \overset{5}{\mathbf{C}}_{3v\tilde{\sigma}\hat{I}}(\mathbf{C}_3), \\ & \overset{6}{\mathbf{C}}_{3v\tilde{\sigma}\hat{I}}(\mathbf{C}_{s\tilde{\sigma}\hat{I}}), \overset{7}{\mathbf{C}}_{3v\tilde{\sigma}\hat{I}}(\mathbf{C}_{3\tilde{\sigma}}), \overset{8}{\mathbf{C}}_{3v\tilde{\sigma}\hat{I}}(\mathbf{C}_{3v}), \\ & \overset{9}{\mathbf{C}}_{3v\tilde{\sigma}\hat{I}}(\mathbf{C}_{3\hat{I}}), \overset{10}{\mathbf{C}}_{3v\tilde{\sigma}\hat{I}}(\mathbf{C}_{3v\tilde{\sigma}\hat{I}}) \}. \end{aligned} \quad (10.52)$$

For example, the coset representation $\mathbf{C}_{3v\tilde{\sigma}\hat{I}}(\mathbf{C}_{s\tilde{\sigma}\hat{I}})$ is obtained through a coset decomposition of $\mathbf{C}_{3v\tilde{\sigma}\hat{I}}$ by $\mathbf{C}_{s\tilde{\sigma}\hat{I}}$, as collected in Table 10.2.

**Exercise 10.3.**

- A staggered conformation of an ethane skeleton belongs to the point group D_{3d} . Consider an orbit of three planes corresponding to the reflection operations ($\sigma_{d(1)}$, $\sigma_{d(2)}$, and $\sigma_{d(3)}$). Confirm that a coset representation for characterizing the orbit is D_{3d}/C_{2h} .
- An eclipsed conformation of an ethane molecule belongs to the point group D_{3h} . Consider an orbit of three planes corresponding to the reflection operations ($\sigma_{v(1)}$, $\sigma_{v(2)}$, and $\sigma_{v(3)}$). Confirm that a coset representation for characterizing the orbit is D_{3h}/C_{2v} (cf. [20, Table 4]).
- Compare these coset representations with the coset representation $C_{3v\tilde{\sigma}\tilde{\tau}}/C_{s\tilde{\sigma}\tilde{\tau}}$ listed in Table 10.2.

**Exercise 10.4.**

- The three carbon atoms of a cyclopropane skeleton **3-16** of D_{3h} (Fig. 3.9 on page 73) construct an orbit. Confirm that a coset representation for characterizing the orbit is D_{3h}/C_{2v} (cf. [20, Table 4]).
- Compare this coset representation with the coset representation $C_{3v\tilde{\sigma}\tilde{\tau}}/C_{s\tilde{\sigma}\tilde{\tau}}$ listed in Table 10.2.

The concrete forms of coset representations of the point group D_{3h} , which is isomorphic to the *RS*-stereoisomeric group $C_{3v\tilde{\sigma}\tilde{\tau}}$, have been reported [20, Table 4].

10.2.3 Mark Table and its Inverse

Mark tables or tables of marks, which have been developed by Burnside [22], are one of the key data necessary to Fujita's USCI approach [14]. The discussions on mark tables of point groups in Subsection 5.1.2 can be extended to be applied to *RS*-stereoisomeric groups. For example, the coset representation $C_{3v\tilde{\sigma}\tilde{\tau}}/C_{s\tilde{\sigma}\tilde{\tau}}$ shown in Table 10.2 gives the following fixed-point vector (FPV):

$$\text{FPV}_{C_{3v\tilde{\sigma}\tilde{\tau}}/C_{s\tilde{\sigma}\tilde{\tau}}} = (3, 1, 1, 3, 0, 1, 0, 0, 0, 0), \quad (10.53)$$

which is obtained by counting the numbers of fixed points (1-cycles) under the action of the respective subgroups (Eqs. 10.37–10.46). This procedure is repeated to cover all of the coset representations shown in Eq. 10.52. The resulting FPVs are collected to give a table of marks or a mark table. The resulting mark table for $C_{3v\tilde{\sigma}\tilde{\tau}}$ (Table 10.4) can be regarded as a 10×10 square matrix, which is denoted by the symbol $M_{C_{3v\tilde{\sigma}\tilde{\tau}}}$. Because the *RS*-stereoisomeric group $C_{3v\tilde{\sigma}\tilde{\tau}}$ and the point group D_{3d} are isomorphic to each other, they have a common mark table shown in Table 10.4. The mark table of the point group D_{3h} , which is isomorphic to $C_{3v\tilde{\sigma}\tilde{\tau}}$ or D_{3d} , has been reported in [20, Table 5] and [14, Table A.13].

Table 10.4. Mark Table of the *RS*-Stereoisomeric Group $C_{3v\bar{\sigma}\hat{I}}$ and of the Point Group D_{3d}

$M_{D_{3d}}$	$M_{C_{3v\bar{\sigma}\hat{I}}}$	C_1	C_2	C_s	C_i	C_3	C_{2h}	D_3	C_{3v}	C_{3i}	D_{3d}
		C_1	$C_{\bar{\sigma}}$	C_s	$C_{\hat{I}}$	C_3	$C_{s\bar{\sigma}\hat{I}}$	$C_{3\bar{\sigma}}$	C_{3v}	$C_{3\hat{I}}$	$C_{3v\bar{\sigma}\hat{I}}$
$D_{3d}/(C_1)$	$C_{3v\bar{\sigma}\hat{I}}/(C_1)$	12	0	0	0	0	0	0	0	0	0
$D_{3d}/(C_2)$	$C_{3v\bar{\sigma}\hat{I}}/(C_{\bar{\sigma}})$	6	2	0	0	0	0	0	0	0	0
$D_{3d}/(C_s)$	$C_{3v\bar{\sigma}\hat{I}}/(C_s)$	6	0	2	0	0	0	0	0	0	0
$D_{3d}/(C_i)$	$C_{3v\bar{\sigma}\hat{I}}/(C_{\hat{I}})$	6	0	0	6	0	0	0	0	0	0
$D_{3d}/(C_3)$	$C_{3v\bar{\sigma}\hat{I}}/(C_3)$	4	0	0	0	4	0	0	0	0	0
$D_{3d}/(C_{2h})$	$C_{3v\bar{\sigma}\hat{I}}/(C_{s\bar{\sigma}\hat{I}})$	3	1	1	3	0	1	0	0	0	0
$D_{3d}/(D_3)$	$C_{3v\bar{\sigma}\hat{I}}/(C_{3\bar{\sigma}})$	2	2	0	0	2	0	2	0	0	0
$D_{3d}/(C_{3v})$	$C_{3v\bar{\sigma}\hat{I}}/(C_{3v})$	2	0	2	0	2	0	0	2	0	0
$D_{3d}/(C_{3i})$	$C_{3v\bar{\sigma}\hat{I}}/(C_{3\hat{I}})$	2	0	0	2	2	0	0	0	2	0
$D_{3d}/(D_{3d})$	$C_{3v\bar{\sigma}\hat{I}}/(C_{3v\bar{\sigma}\hat{I}})$	1	1	1	1	1	1	1	1	1	1

In general, a mark table exhibits a lower-triangular format, as exemplified by Table 10.4. Mark tables are used to calculate subductions of coset representations, which have been developed by Fujita [14].

The inverse of the mark table or the inverse mark table is also important to Fujita's USCI approach [14]. The discussions on inverse mark tables of point groups in Subsection 5.1.2 can be extended to be applied to *RS*-stereoisomeric groups. As shown in Table 10.5, the resulting inverse mark table denoted by the symbol $M_{C_{3v\bar{\sigma}\hat{I}}}^{-1}$ or $M_{D_{3d}}^{-1}$ (Table 10.5) is also regarded as a 10×10 square matrix, which exhibits a lower-triangular format.

The inverse mark table of the point group D_{3h} , which is isomorphic to $C_{3v\bar{\sigma}\hat{I}}$ or D_{3d} , has been reported in [20, Table 6], [21, Table 1], and [14, Table B.13].

The properties of such inverse mark tables have been discussed in Appendix B of Fujita's monograph [23] in general. One of the remarkable properties is shown in the row-sum column of Table 10.5, where the sum of row elements is positive for each cyclic subgroup, while it is equal to zero for each non-cyclic subgroup. The total value of the row sums over the SSG is equal to 1. Note that the point group C_{3i} (the $C_{3i}, C_{3\hat{I}}$ -row of Table 10.5, cf. Eq. 10.45) has a positive sum, because it is alternatively denoted by the symbol S_6 , which is a cyclic subgroup of order 6 generated from a rotoreflection S_6 as a generator. Such an inverse mark table as Table 10.5 is used to calculate isomer-counting matrices (ICMs) in the fixed-point-matrix (FPM) method or to derive partial cycle indices (PCIs) in the partial-cycle-index (PCI) method, where both of the methods are devised as powerful methods for symmetry-itemized enumeration under Fujita's USCI approach [14].

10.2.4 Subduction for *RS*-Stereoisomeric Groups

The discussions on subduction of point groups in Subsection 5.2.1 are also effective to *RS*-stereoisomeric groups. The subduction for a point group G (Eq. 5.37 on page 123) can be easily extended to an *RS*-stereoisomeric group \hat{G} . Thus, Eq. 5.37 is extended to cover \hat{G} , so

Table 10.5. Inverse Mark Table of the *RS*-Stereoisomeric Group $C_{3v\widehat{\sigma I}}$ and of the Point Group D_{3d}

$M_{D_{3d}}^{-1}$		$/C_1$	$/C_2$	$/C_s$	$/C_i$	$/C_3$	$/C_{2h}$	$/D_3$	$/C_{3v}$	$/C_{3i}$	$/D_{3d}$	row
$M_{C_{3v\widehat{\sigma I}}}^{-1}$		$/C_1$	$/C_{\widehat{\sigma}}$	$/C_s$	$/C_{\widehat{I}}$	$/C_3$	$/C_{s\widehat{\sigma I}}$	$/C_{3\widehat{\sigma}}$	$/C_{3v}$	$/C_{3\widehat{I}}$	$/C_{3v\widehat{\sigma I}}$	sum
C_1	C_1	$\frac{1}{12}$	0	0	0	0	0	0	0	0	0	$\frac{1}{12}$
C_2	$C_{\widehat{\sigma}}$	$-\frac{1}{4}$	$\frac{1}{2}$	0	0	0	0	0	0	0	0	$\frac{1}{4}$
C_s	C_s	$-\frac{1}{4}$	0	$\frac{1}{2}$	0	0	0	0	0	0	0	$\frac{1}{4}$
C_i	$C_{\widehat{I}}$	$-\frac{1}{12}$	0	0	$\frac{1}{6}$	0	0	0	0	0	0	$\frac{1}{12}$
C_3	C_3	$-\frac{1}{12}$	0	0	0	$\frac{1}{4}$	0	0	0	0	0	$\frac{1}{6}$
C_{2h}	$C_{s\widehat{\sigma I}}$	$\frac{1}{2}$	$-\frac{1}{2}$	$-\frac{1}{2}$	$-\frac{1}{2}$	0	1	0	0	0	0	0
D_3	$C_{3\widehat{\sigma}}$	$\frac{1}{4}$	$-\frac{1}{2}$	0	0	$-\frac{1}{4}$	0	$\frac{1}{2}$	0	0	0	0
C_{3v}	C_{3v}	$\frac{1}{4}$	0	$-\frac{1}{2}$	0	$-\frac{1}{4}$	0	0	$\frac{1}{2}$	0	0	0
C_{3i}	$C_{3\widehat{I}}$	$\frac{1}{12}$	0	0	$-\frac{1}{6}$	$-\frac{1}{4}$	0	0	0	$\frac{1}{2}$	0	$\frac{1}{6}$
D_{3d}	$C_{3v\widehat{\sigma I}}$	$-\frac{1}{2}$	$\frac{1}{2}$	$\frac{1}{2}$	$\frac{1}{2}$	$\frac{1}{2}$	-1	$-\frac{1}{2}$	$-\frac{1}{2}$	$-\frac{1}{2}$	1	0

that the subduced representation $\widehat{G}(/ \widehat{G}_i) \downarrow \widehat{G}_j$ is divided into a sum of coset representations of a subgroup \widehat{G}_j as follows:

$$\widehat{G}(/ \widehat{G}_i) \downarrow \widehat{G}_j = \sum_{k=1}^{v_j} \widehat{\beta}_k^{(ij)} \widehat{G}_j(/ \widehat{H}_k^{(j)}) \quad (10.54)$$

for $i = 1, 2, \dots, s$ and $j = 1, 2, \dots, s$, where the subgroup $\widehat{H}_k^{(j)}$ covers the following SSG of \widehat{G}_j with the multiplicity $\widehat{\beta}_k^{(ij)}$ (cf. Eq. 5.36 on page 123):

$$\text{SSG}_{\widehat{G}_j} = \{ \widehat{H}_1^{(ij)}, \widehat{H}_2^{(ij)}, \dots, \widehat{H}_k^{(ij)}, \dots, \widehat{H}_{v_j}^{(ij)} \}. \quad (10.55)$$

Each $\widehat{H}_k^{(ij)}$ is equal to a subgroup contained in the SSG $_{\widehat{G}}$ (e.g., Eq. 10.36) or to its conjugate subgroup. The results of the subduction $C_{3v\widehat{\sigma I}}(/ C_{s\widehat{\sigma I}}) \downarrow \widehat{G}_j$ (for $\widehat{G}_j \in \text{SSG}_{C_{3v\widehat{\sigma I}}}$) are summarized in Table 10.6.

Table 10.6. Subduction of $C_{3v\widehat{\sigma I}}(/ C_{s\widehat{\sigma I}})$ into Subgroups of $C_{3v\widehat{\sigma I}}$

Subgroup ($\downarrow \widehat{G}_j$)	Subduction ($C_{3v\widehat{\sigma I}}(/ C_{s\widehat{\sigma I}}) \downarrow \widehat{G}_j$)	USCI-CF	USCI	TEM						
				\widehat{N}_j	$\widehat{N}_j^{(I)}$	$\widehat{N}_j^{(II)}$	$\widehat{N}_j^{(III)}$	$\widehat{N}_j^{(IV)}$	$\widehat{N}_j^{(V)}$	
1	C_1	$3C_1(/ C_1)$	b_1^3	s_1^3	$\frac{1}{12}$	0	0	$\frac{1}{12}$	0	0
2	$C_{\widehat{\sigma}}$	$C_{\widehat{\sigma}}(/ C_1) + C_{\widehat{\sigma}}(/ C_{\widehat{\sigma}})$	$b_1 b_2$	$s_1 s_2$	$\frac{1}{4}$	0	$\frac{1}{2}$	$-\frac{1}{4}$	0	0
3	C_s	$C_s(/ C_1) + C_s(/ C_s)$	$a_1 c_2$	$s_1 s_2$	$\frac{1}{4}$	0	0	$-\frac{1}{4}$	0	$\frac{1}{2}$
4	$C_{\widehat{I}}$	$3C_{\widehat{I}}(/ C_{\widehat{I}})$	a_1^3	s_1^3	$\frac{1}{12}$	$\frac{1}{6}$	0	$-\frac{1}{12}$	0	0
5	C_3	$C_3(/ C_1)$	b_3	s_3	$\frac{1}{6}$	0	0	$\frac{1}{6}$	0	0
6	$C_{s\widehat{\sigma I}}$	$C_{s\widehat{\sigma I}}(/ C_{\widehat{I}}) + C_{s\widehat{\sigma I}}(/ C_{s\widehat{\sigma I}})$	$a_1 a_2$	$s_1 s_2$	0	$-\frac{1}{2}$	$-\frac{1}{2}$	$\frac{1}{2}$	1	$-\frac{1}{2}$
7	$C_{3\widehat{\sigma}}$	$C_{3\widehat{\sigma}}(/ C_{\widehat{\sigma}})$	b_3	s_3	0	0	0	0	0	0
8	C_{3v}	$C_{3v}(/ C_s)$	a_3	s_3	0	0	0	0	0	0
9	$C_{3\widehat{I}}$	$C_{3\widehat{I}}(/ C_{\widehat{I}})$	a_3	s_3	$\frac{1}{6}$	$\frac{1}{3}$	0	$-\frac{1}{6}$	0	0
10	$C_{3v\widehat{\sigma I}}$	$C_{3v\widehat{\sigma I}}(/ C_{s\widehat{\sigma I}})$	a_3	s_3	0	0	0	0	0	0

Table 10.7. Subduction Table of the *RS*-Stereoisomeric Group $C_{3v}\widehat{\sigma I}$

	1	2	3	4	5	6	7	8	9	10
	C_1	$C_{\bar{\sigma}}$	C_s	C_7	C_3	$C_{s\widehat{\sigma I}}$	$C_{3\bar{\sigma}}$	C_{3v}	$C_{3\bar{I}}$	$C_{3v\widehat{\sigma I}}$
1 $C_{3v\widehat{\sigma I}}(/C_1)$	12 $C_1(/C_1)$	6 $C_{\bar{\sigma}}(/C_1)$	6 $C_s(/C_1)$	6 $C_7(/C_1)$	4 $C_3(/C_1)$	3 $C_{s\widehat{\sigma I}}(/C_1)$	2 $C_{3\bar{\sigma}}(/C_1)$	2 $C_{3v}(/C_1)$	2 $C_{3\bar{I}}(/C_1)$	$C_{3v\widehat{\sigma I}}(/C_1)$
2 $C_{3v\widehat{\sigma I}}(/C_{\bar{\sigma}})$	6 $C_1(/C_1)$	2 $C_{\bar{\sigma}}(/C_1)$	3 $C_s(/C_1)$	3 $C_7(/C_1)$	2 $C_3(/C_1)$	$C_{s\widehat{\sigma I}}(/C_1)$	2 $C_{3\bar{\sigma}}(/C_{\bar{\sigma}})$	$C_{3v}(/C_1)$	$C_{3\bar{I}}(/C_1)$	$C_{3v\widehat{\sigma I}}(/C_{\bar{\sigma}})$
3 $C_{3v\widehat{\sigma I}}(/C_s)$	6 $C_1(/C_1)$	$+2C_{\bar{\sigma}}(/C_{\bar{\sigma}})$ 3 $C_{\bar{\sigma}}(/C_1)$	2 $C_s(/C_1)$	3 $C_7(/C_1)$	2 $C_3(/C_1)$	$C_{s\widehat{\sigma I}}(/C_1)$	$C_{3\bar{\sigma}}(/C_1)$	2 $C_{3v}(/C_1)$	$C_{3\bar{I}}(/C_1)$	$C_{3v\widehat{\sigma I}}(/C_s)$
4 $C_{3v\widehat{\sigma I}}(/C_7)$	6 $C_1(/C_1)$	3 $C_{\bar{\sigma}}(/C_1)$	3 $C_s(/C_1)$	6 $C_7(/C_7)$	2 $C_3(/C_1)$	3 $C_{s\widehat{\sigma I}}(/C_7)$	$C_{3\bar{\sigma}}(/C_1)$	$C_{3v}(/C_1)$	2 $C_{3\bar{I}}(/C_7)$	$C_{3v\widehat{\sigma I}}(/C_7)$
5 $C_{3v\widehat{\sigma I}}(/C_3)$	4 $C_1(/C_1)$	2 $C_{\bar{\sigma}}(/C_1)$	2 $C_s(/C_1)$	2 $C_7(/C_1)$	4 $C_3(/C_3)$	$C_{s\widehat{\sigma I}}(/C_1)$	2 $C_{3\bar{\sigma}}(/C_3)$	2 $C_{3v}(/C_3)$	2 $C_{3\bar{I}}(/C_3)$	$C_{3v\widehat{\sigma I}}(/C_3)$
6 $C_{3v\widehat{\sigma I}}(/C_{s\widehat{\sigma I}})$	3 $C_1(/C_1)$	$C_{\bar{\sigma}}(/C_1)$	$C_s(/C_1)$	3 $C_7(/C_7)$	$C_3(/C_1)$	$C_{s\widehat{\sigma I}}(/C_7)$	$C_{3\bar{\sigma}}(/C_{\bar{\sigma}})$	$C_{3v}(/C_3)$	$C_{3\bar{I}}(/C_7)$	$C_{3v\widehat{\sigma I}}(/C_{s\widehat{\sigma I}})$
7 $C_{3v\widehat{\sigma I}}(/C_{3\bar{\sigma}})$	2 $C_1(/C_1)$	2 $C_{\bar{\sigma}}(/C_{\bar{\sigma}})$	$C_s(/C_1)$	$C_7(/C_1)$	2 $C_3(/C_3)$	$C_{s\widehat{\sigma I}}(/C_{\bar{\sigma}})$	2 $C_{3\bar{\sigma}}(/C_{3\bar{\sigma}})$	$C_{3v}(/C_3)$	$C_{3\bar{I}}(/C_3)$	$C_{3v\widehat{\sigma I}}(/C_{3\bar{\sigma}})$
8 $C_{3v\widehat{\sigma I}}(/C_{3v})$	2 $C_1(/C_1)$	$C_{\bar{\sigma}}(/C_1)$	2 $C_s(/C_s)$	$C_7(/C_1)$	2 $C_3(/C_3)$	$C_{s\widehat{\sigma I}}(/C_s)$	$C_{3\bar{\sigma}}(/C_3)$	2 $C_{3v}(/C_{3v})$	$C_{3\bar{I}}(/C_3)$	$C_{3v\widehat{\sigma I}}(/C_{3v})$
9 $C_{3v\widehat{\sigma I}}(/C_{3\bar{I}})$	2 $C_1(/C_1)$	$C_{\bar{\sigma}}(/C_1)$	$C_s(/C_1)$	2 $C_7(/C_7)$	2 $C_3(/C_3)$	$C_{s\widehat{\sigma I}}(/C_7)$	$C_{3\bar{\sigma}}(/C_3)$	$C_{3v}(/C_3)$	2 $C_{3\bar{I}}(/C_{3\bar{I}})$	$C_{3v\widehat{\sigma I}}(/C_{3\bar{I}})$
10 $C_{3v\widehat{\sigma I}}(/C_{3v\widehat{\sigma I}})$	$C_1(/C_1)$	$C_{\bar{\sigma}}(/C_{\bar{\sigma}})$	$C_s(/C_s)$	$C_7(/C_7)$	$C_3(/C_3)$	$C_{s\widehat{\sigma I}}(/C_{s\widehat{\sigma I}})$	$C_{3\bar{\sigma}}(/C_{3\bar{\sigma}})$	$C_{3v}(/C_{3v})$	$C_{3\bar{I}}(/C_{3\bar{I}})$	$C_{3v\widehat{\sigma I}}(/C_{3v\widehat{\sigma I}})$

The procedure of calculating Table 10.6 is repeated to cover all of the subgroups \widehat{G}_i appearing in $C_{3v\widehat{\sigma I}}(/ \widehat{G}_i)$. Thereby, the subduction $C_{3v\widehat{\sigma I}}(/ \widehat{G}_i) \downarrow \widehat{G}_j$ (for $\widehat{G}_i, \widehat{G}_j \in \text{SSG}_{C_{3v\widehat{\sigma I}}}$) is obtained in a parallel way to the subduction $D_{3d}(/C_{2h}) \downarrow G_j$ ($G_j \in \text{SSG}_{D_{3d}}$) or $D_{3h}(/C_{2v}) \downarrow G_j$ ($G_j \in \text{SSG}_{D_{3h}}$). The results of the subduction are collected to form a subduction table such as Table 10.7. Note that the data listed in the subduction-column of Table 10.6 appear in the $C_{3v\widehat{\sigma I}}(/C_{s\widehat{\sigma I}})$ -row (the 6th row) of Table 10.7.

The subduction table of the point group D_{3h} , which is isomorphic to the *RS*-stereoisomeric group $C_{3v}\widehat{\sigma I}$, has been reported in [20, Table 12] and [14, Table C.13].²

10.2.5 USCI-CFs for *RS*-Stereoisomeric Groups

Properties of Orbits Under the Action of *RS*-Stereoisomeric Groups

Fujita's USCI approach, which has originally been developed on the basis of point groups [14,24], is extended so as to be applied to *RS*-stereoisomeric groups derived from point groups [9,15]. For example, the trigonal pyramidal skeleton **8-1** belonging to the point group C_{3v} is alternatively regarded as belonging to the *RS*-stereoisomeric group $C_{3v}\widehat{\sigma I}$, so that the orbit of the three positions is governed by the coset representation $C_{3v\widehat{\sigma I}}(/C_{s\widehat{\sigma I}})$ of degree 3, which is calculated to be $|C_{3v\widehat{\sigma I}}|/|C_{s\widehat{\sigma I}}| = 12/4 = 3$. The elements of $C_{3v\widehat{\sigma I}}(/C_{s\widehat{\sigma I}})$ are listed in Table 10.2. The coset representation $C_{3v\widehat{\sigma I}}(/C_{s\widehat{\sigma I}})$ is derived by the extension of the coset representation $C_{3v}(/C_s)$ of the point group C_{3v} , where the global *RS*-stereoisomeric group $C_{3v}\widehat{\sigma I}$ is an extension of the point group C_{3v} , while the local *RS*-stereoisomeric group $C_{s\widehat{\sigma I}}$ is an extension of the point group C_s .

For the purpose of extending the concept of sphericities to be applicable to *RS*-stereoisomeric groups, the chirality/achirality of point groups is extended to meet *RS*-stereoisomeric groups as follows:

² The subduction of $D_{3h}(/C_s) \downarrow C_{2v}$ should be corrected to be read as $C_{2v}(/C_1) + C_{2v}(/C_s)$ in Table C.13.

Definition 10.2 (Ex-Chiral and Ex-Achiral). An *RS*-stereoisomeric group \hat{G} is *ex-achiral* if it contains a reflection (**B**) and/or a ligand reflection (**D**); and it is *ex-chiral* if it is composed of rotations (**A**) and/or *RS*-permutations (**C**). See Table 10.2 for $C_{3v\hat{\sigma}\hat{\tau}}$. The prefix *ex* of the term *ex-achiral* or *ex-chiral* denotes *extended*.

Then, the concept of sphericities is extended to cover *RS*-stereoisomeric groups as follows [15]:

Definition 10.3 (Extended Sphericities of *RS*-Stereoisomeric Groups). A coset representation $\hat{G}/(\hat{G}_i)$ defined under an *RS*-stereoisomeric group \hat{G} is characterized by either one of three kinds of sphericities in an extended fashion:

1. The coset representation $\hat{G}/(\hat{G}_i)$ is determined to be *homospheric* if both \hat{G} and \hat{G}_i are ex-achiral *RS*-stereoisomeric groups. It is characterized by a sphericity index a_d .
2. The coset representation $\hat{G}/(\hat{G}_i)$ is determined to be *enantiospheric* if \hat{G} is an ex-achiral *RS*-stereoisomeric group and \hat{G}_i is an ex-chiral *RS*-stereoisomeric group. It is characterized by a sphericity index c_d .
3. The coset representation $\hat{G}/(\hat{G}_i)$ is determined to be *hemispheric* if both \hat{G} and \hat{G}_i are ex-chiral *RS*-stereoisomeric groups. It is characterized by a sphericity index b_d .

The subscript d of each sphericity index is the degree of $\hat{G}/(\hat{G}_i)$, which is calculated to be $d = |\hat{G}|/|\hat{G}_i|$.

According to its extended sphericity, an orbit governed by the coset representation $\hat{G}/(\hat{G}_i)$ is called a $\hat{G}/(\hat{G}_i)$ -orbit, which is characterized by the sphericity index, a_d , c_d , or b_d . For example, the coset representation $C_{3v\hat{\sigma}\hat{\tau}}/(C_{s\hat{\sigma}\hat{\tau}})$ is determined to be homospheric, because the global symmetry $C_{3v\hat{\sigma}\hat{\tau}}$ is ex-achiral and the local symmetry $C_{s\hat{\sigma}\hat{\tau}}$ is also ex-achiral. Hence, a $C_{3v\hat{\sigma}\hat{\tau}}/(C_{s\hat{\sigma}\hat{\tau}})$ -orbit of the three positions in the trigonal pyramidal skeleton **8-1** is characterized by the sphericity index a_3 , where $|C_{3v\hat{\sigma}\hat{\tau}}|/|C_{s\hat{\sigma}\hat{\tau}}| = 12/4 = 3$.

Just as a $G/(G_i)$ -orbit exhibits chirality fittingness according to its sphericity [14,24], a $\hat{G}/(\hat{G}_i)$ -orbit exhibits *chirality fittingness* according to its extended sphericity [15]:

Theorem 10.3 (Chirality Fittingness due to Extended Sphericities). A d -membered homospheric orbit accommodates d achiral proligands of the same kind in isolation; a d -membered enantiospheric orbit accommodates d achiral proligands of the same kind or pairwise $d/2$ chiral proligands and $d/2$ enantiomeric proligands in isolation; and a d -membered hemispheric orbit accommodates d achiral or chiral proligands of the same kind in isolation.

USCI-CF Tables Under the Action of *RS*-Stereoisomeric Groups

By applying discussions on point groups (Subsection 5.2.2) to *RS*-stereoisomeric groups, a unit subduced cycle index with chirality faithfulness (USCI-CF) is defined on the basis of Eq. 10.54:

Definition 10.4 (USCI-CFs for an *RS*-Stereoisomeric Group). The coset representation $\hat{G}_j/(\hat{H}_k^{(j)})$ contained in the right-hand side of Eq. 10.54 is characterized by a sphericity index $\$_{d_{jk}}$ ($\$ = a, c, \text{ or } b$) defined in Def. 10.3. Then, a unit subduced cycle index with chirality faithfulness (USCI-CF) is defined on the basis of Eq. 10.54 as follows:

$$\text{USCI-CF}(\hat{G}/(\hat{G}_i) \downarrow \hat{G}_j; \$_d) = \prod_{k=1}^{\hat{v}_j} \$_{d_{jk}}^{\hat{\beta}_k^{(ij)}}, \quad (10.56)$$

where $s_{d_{jk}}$ is equal to $a_{d_{jk}}$, $c_{d_{jk}}$, or $b_{d_{jk}}$ according to the sphericity of $\hat{G}_j(/ \hat{H}_k^{(j)})$ and the subscript is calculated to be

$$d_{jk} = \frac{|\hat{G}_j|}{|\hat{H}_k^{(j)}|}. \tag{10.57}$$

This definition shows that Eq. 10.56 for an *RS*-stereoisomeric group \hat{G} corresponds to Eq. 5.46 (page 127) for a point group G (Subsection 5.2.2). Mathematically speaking, Def. 10.4 for *RS*-stereoisomeric groups is equivalent to Def. 5.2 (page 127) for point groups. Note that the maximum ex-chiral subgroup (i.e., the maximum *RS*-permutation group) of an ex-achiral *RS*-stereoisomeric group \hat{G} has an order of $|\hat{G}|/2$, just as the maximum chiral subgroup of an achiral point group G has an order of $|G|/2$. By applying Def. 10.4 to the data collected in the subduction-column of Table 10.6, we obtain USCI-CFs collected in the USCI-CF-column of the same table.

By starting from the data collected in the subduction table of \hat{G} (e.g., Table 10.7), the whole set of USCI-CFs for \hat{G} is obtained easily. Thus, the data collected in Table 10.7 for the *RS*-stereoisomeric group $C_{3v\bar{\sigma}\bar{I}}$ give the USCI-CF table of $C_{3v\bar{\sigma}\bar{I}}$, as shown in Table 10.8. Note that the USCI-CFs collected in the USCI-CF-column of Table 10.6 appear in the the $C_{3v\bar{\sigma}\bar{I}}(/C_{s\bar{\sigma}\bar{I}})$ -row (the 6th row) of Table 10.8.

The USCI-CF table of the point group D_{3h} , which is isomorphic to the point group D_{3d} and to the *RS*-stereoisomeric group $C_{3v\bar{\sigma}\bar{I}}$, has been reported in Ref. [24, Table 15]³, Ref. [21, Table 2]⁴, and Ref. [14, Table E.13].⁵

Table 10.8. USCI-CF Table of the *RS*-Stereoisomeric Group $C_{3v\bar{\sigma}\bar{I}}$

			1	2	3	4	5	6	7	8	9	10
D_{3d}	$C_{3v\bar{\sigma}\bar{I}}$	$C_{3v\bar{\sigma}\bar{I}}(/C_1)$	C_1	C_2	C_s	C_i	C_3	C_{2h}	D_3	C_{3v}	C_{3i}	D_{3d}
		$C_{3v\bar{\sigma}\bar{I}}(/C_{\bar{\sigma}})$	C_1	$C_{\bar{\sigma}}$	C_s	$C_{\bar{I}}$	C_3	$C_{s\bar{\sigma}\bar{I}}$	$C_{3\bar{\sigma}}$	C_{3v}	$C_{3\bar{I}}$	$C_{3v\bar{\sigma}\bar{I}}$
1	$D_{3d}(/C_1)$	$C_{3v\bar{\sigma}\bar{I}}(/C_1)$	b_1^2	b_2^6	c_2^6	c_2^6	b_3^4	c_4^3	b_6^2	c_6^2	c_6^2	c_{12}
2	$D_{3d}(/C_2)$	$C_{3v\bar{\sigma}\bar{I}}(/C_{\bar{\sigma}})$	b_1^6	$b_1^2 b_2^2$	c_2^3	c_2^3	b_3^2	$c_2 c_4$	b_3^2	c_6	c_6	c_6
3	$D_{3d}(/C_s)$	$C_{3v\bar{\sigma}\bar{I}}(/C_s)$	b_1^6	b_2^3	$a_1^2 c_2^2$	c_2^3	b_3^2	$a_2 c_4$	b_6	a_3^2	c_6	a_6
4	$D_{3d}(/C_i)$	$C_{3v\bar{\sigma}\bar{I}}(/C_{\bar{I}})$	b_1^6	b_2^3	c_2^3	a_1^6	b_3^2	a_2^3	b_6	c_6	a_3^2	a_6
5	$D_{3d}(/C_3)$	$C_{3v\bar{\sigma}\bar{I}}(/C_3)$	b_1^4	b_2^2	c_2^2	c_2^2	b_4^1	c_4	b_2^2	c_2^2	c_2^2	c_4
6	$D_{3d}(/C_{2h})$	$C_{3v\bar{\sigma}\bar{I}}(/C_{s\bar{\sigma}\bar{I}})$	b_1^3	$b_1 b_2$	$a_1 c_2$	a_1^3	b_3	$a_1 a_2$	b_3	a_3	a_3	a_3
7	$D_{3d}(/D_3)$	$C_{3v\bar{\sigma}\bar{I}}(/C_{3\bar{\sigma}})$	b_1^2	b_1^2	c_2	c_2	b_1^2	c_2	b_1^2	c_2	c_2	c_2
8	$D_{3d}(/C_{3v})$	$C_{3v\bar{\sigma}\bar{I}}(/C_{3v})$	b_1^2	b_2	a_1^2	c_2	b_1^2	a_2	b_2	a_1^2	c_2	a_2
9	$D_{3d}(/C_{3i})$	$C_{3v\bar{\sigma}\bar{I}}(/C_{3\bar{I}})$	b_1^2	b_2	c_2	a_1^2	b_1^2	a_2	b_2	c_2	a_1^2	a_2
10	$D_{3d}(/D_{3d})$	$C_{3v\bar{\sigma}\bar{I}}(/C_{3\bar{\sigma}\bar{I}})$	b_1	b_1	a_1	a_1	b_1	a_1	b_1	a_1	a_1	a_1

3 The USCI-CF (and USCI) for the subduction of $D_{3h}(/C'_s) \downarrow D_3$ should be corrected to be read as b_6 (s_6) in Table 15.

4 The USCI-CF for the subduction of $D_{3h}(/C_s) \downarrow C_s$ should be corrected to be read as $a_1^2 c_2^2$ in Table 2. The USCI-CF (and USCI) for the subduction of $D_{3h}(/C'_s) \downarrow D_3$ should be read as b_6 (s_6) in Table 2.

5 The USCI-CF for the subduction of $D_{3h}(/C'_s) \downarrow D_3$ should be corrected to be read as b_6 in Table E.13. The corresponding USCI should be read as s_6 in Table D.13.

10.2.6 SCI-CFs for *RS*-Stereoisomeric Groups

The substitution positions of a stereoskeleton, which are controlled by a permutation representation \mathbf{P}_G for a point group G (Subsection 6.1.3), are alternatively regarded as being controlled by a permutation representation $\mathbf{P}_{\hat{G}}$ under the action of the corresponding *RS*-stereoisomeric group \hat{G} . Thereby, Eq. 6.21 (page 139) for a point group G is converted to support the present case of an *RS*-stereoisomeric group \hat{G} according to Def. 10.4:

$$\begin{aligned} \mathbf{P}_{\hat{G}} \downarrow \hat{G}_j &= \sum_{i=1}^s \hat{\alpha}_i \hat{G}(/ \hat{G}_i) \downarrow \hat{G}_j \\ &= \sum_{i=1}^s \hat{\alpha}_i \sum_{k=1}^{\hat{\nu}_j} \hat{\beta}_k^{(ij)} \hat{G}_j(/ \hat{H}_k^{(j)}). \end{aligned} \quad (10.58)$$

By referring to Eq. 10.58, Def. 6.1 (page 139) for point groups is extended to support the present case of *RS*-stereoisomeric groups:

Definition 10.5 (SCI-CFs for *RS*-Stereoisomeric Groups). When a permutation representation $\mathbf{P}_{\hat{G}}$ for controlling the substitution positions of a stereoskeleton is represented by Eq. 10.58, the corresponding subduced cycle index with chirality fittingness (SCI-CF) is defined as follows:

$$\begin{aligned} \text{SCI-CF}_{\mathbf{P}_{\hat{G}}}(\hat{G}_j; \$_{d_{jk}}) &= \prod_{i=1}^s \left(\text{USCI-CF}(\hat{G}(/ \hat{G}_i) \downarrow \hat{G}_j; \$_d) \right)^{\hat{\alpha}_i} \\ &= \prod_{i=1}^s \left(\prod_{k=1}^{\hat{\nu}_j} \$_{d_{jk}}^{\hat{\beta}_k^{(ij)}} \right)^{\hat{\alpha}_i} \end{aligned} \quad (10.59)$$

where $\$_{d_{jk}}$ is equal to $a_{d_{jk}}$, $c_{d_{jk}}$, or $b_{d_{jk}}$ according to the sphericity of $\hat{G}_j(/ \hat{H}_k^{(j)})$ and the subscript is calculated to be

$$d_{jk} = \frac{|\hat{G}_j|}{|\hat{H}_k^{(j)}|}. \quad (10.60)$$

10.2.7 The PCI Method for *RS*-Stereoisomeric Groups

The FPM method (Subsection 6.2) and the PCI method (Subsection 6.3), which have been originally developed as powerful tools of enumeration under the action of point groups in Fujita's USCI approach, can be easily extended to support enumeration under the action of *RS*-stereoisomeric groups. Thus, USCI-CFs for an *RS*-stereoisomeric group (Def. 10.4) is adopted in place of USCI-CFs for a point group (Def. 5.2 on page 127); and SCI-CFs for an *RS*-stereoisomeric group (Def. 10.5) is adopted in place of SCI-CFs for a point group (Def. 6.1 on page 139). The following discussions are based on the PCI method (cf. Subsection 6.3).

The definition of PCI-CFs for point groups (Def. 6.5 on page 150) is extended to support the corresponding *RS*-stereoisomeric groups:

Definition 10.6 (PCI-CFs for *RS*-Stereoisomeric Groups). A partial cycle index with chirality fittingness (PCI-CF) is defined by the following equation:

$$\begin{aligned} \text{PCI-CF}_{\mathbf{P}_{\hat{\mathbf{G}}}}(\hat{\mathbf{G}}_i; \mathcal{S}_d) &= \sum_{j=1}^{\xi} \hat{m}_{ji} \text{SCI-CF}_{\mathbf{P}_{\hat{\mathbf{G}}}}(\hat{\mathbf{G}}_j; \mathcal{S}_{d_{jk}}) = \sum_{j=1}^{\xi} \hat{m}_{ji} \prod_{i=1}^{\xi} \left(\text{USCI-CF}(\hat{\mathbf{G}} / \hat{\mathbf{G}}_i \downarrow \hat{\mathbf{G}}_j; \mathcal{S}_{d_{jk}}) \right)^{\hat{\alpha}_i} \\ &= \sum_{j=1}^{\xi} \hat{m}_{ji} \left(\prod_{i=1}^{\xi} \left(\prod_{k=1}^{\nu_j} \mathcal{S}_{d_{jk}}^{\beta_k^{(ij)}} \right)^{\hat{\alpha}_i} \right) \end{aligned} \quad (10.61)$$

for $i = 1, 2, \dots, \xi$, where $\text{SCI-CF}_{\mathbf{P}_{\hat{\mathbf{G}}}}$ comes from Eq. 10.59 of Def. 10.5. The symbol \hat{m}_{ji} denotes an element of the inverse mark table $M_{\hat{\mathbf{G}}}^{-1}$ (e.g., Table 10.5 for $\hat{\mathbf{G}} = \mathbf{C}_{3v\tilde{\sigma}\tilde{\tau}}$).

Theorem 6.3 (page 150) for point groups can be extended to the present case of *RS*-stereoisomeric groups, where the ligand inventory \mathbf{L} (Eq. 6.26 on page 140) for point groups can be used to select proligands to be accommodated. The PCI-CFs defined in Def. 10.6 give generating functions for giving the numbers of quadruplets \hat{A}_{θ_i} with $\hat{\mathbf{G}}_i$ and $[\theta]$:

Theorem 10.4. Suppose that the substitution positions of a stereoskeleton belonging to an *RS*-stereoisomeric group $\hat{\mathbf{G}}$ accommodate proligands selected from a ligand inventory \mathbf{L} (Eq. 6.26) to give promolecules with the composition W_{θ} . A generating function for evaluating the number of quadruplets of promolecules \hat{A}_{θ_i} with $\hat{\mathbf{G}}_i$ and $[\theta]$ is obtained to be:

$$\sum_{[\theta]} \hat{A}_{\theta_i} W_{\theta} = \text{PCI-CF}_{\mathbf{P}_{\hat{\mathbf{G}}}}(\hat{\mathbf{G}}_i; \mathcal{S}_d) \Big|_{\mathcal{S}_d = \Sigma_{\mathbf{L}}} \quad (10.62)$$

for $j = 1, 2, \dots, \xi$, where the symbol W_{θ} denotes the composition represented by Eq. 6.27 and the symbol $\mathcal{S}_d = \Sigma_{\mathbf{L}}$ denotes the introduction of a ligand-inventory function to the sphericity index \mathcal{S}_d as follows:

$$a_d = \sum_{\ell=1}^n X_{\ell}^d \quad (10.63)$$

$$c_d = \sum_{\ell=1}^n X_{\ell}^d + 2 \sum_{\ell=1}^{n'} \mathbf{P}_{\ell}^{d/2} \bar{\mathbf{P}}_{\ell}^{d/2} \quad (10.64)$$

$$b_d = \sum_{\ell=1}^n X_{\ell}^d + \sum_{\ell=1}^{n'} \mathbf{p}_{\ell}^d + \sum_{\ell=1}^{n'} \bar{\mathbf{p}}_{\ell}^d \quad (10.65)$$

Note that the ligand inventory \mathbf{L} (Eq. 6.26), the composition W_{θ} (Eq. 6.27), and the partition $[\theta]$ (Eq. 6.28) for Theorem 10.4 are common with those of Theorem 6.3, because the substitution positions of the same stereoskeleton are considered to belong to a point group \mathbf{G} or alternatively to an *RS*-stereoisomeric group $\hat{\mathbf{G}}$.

According to Theorem 10.4, let us now examine enumeration of trigonal pyramidal derivatives under the action of the *RS*-stereoisomeric group $\mathbf{C}_{3v\tilde{\sigma}\tilde{\tau}}$. A manual derivation of trigonal pyramidal derivatives is summarized in Fig. 10.3, where a quadruplet of each stereoisogram is counted once, as surrounded by an outer box.

The data of the USCI-CF-column of Table 10.6 (or the $\mathbf{C}_{3v\tilde{\sigma}\tilde{\tau}} / \mathbf{C}_{s\tilde{\sigma}\tilde{\tau}}$ -row of Table 10.8) are regarded as a formal row vector of SCI-CFs, which is multiplied by the inverse mark table $M_{\mathbf{C}_{3v\tilde{\sigma}\tilde{\tau}}}^{-1}$ (Table 10.5). Thereby, PCI-CFs for the *RS*-stereoisomeric group $\mathbf{C}_{3v\tilde{\sigma}\tilde{\tau}}$

are obtained according to Def. 10.6.

$$\text{PCI-CF}(C_1) = \frac{1}{12}b_1^3 - \frac{1}{4}b_1b_2 - \frac{1}{4}a_1c_2 - \frac{1}{12}a_1^3 + \frac{1}{6}b_3 + \frac{1}{2}a_1a_2 - \frac{1}{6}a_3 \quad (10.66)$$

$$\text{PCI-CF}(C_{\bar{\sigma}}) = \frac{1}{2}b_1b_2 - \frac{1}{2}a_1a_2 - \frac{1}{2}b_3 + \frac{1}{2}a_3 \quad (10.67)$$

$$\text{PCI-CF}(C_s) = \frac{1}{2}a_1c_2 - \frac{1}{2}a_1a_2 \quad (10.68)$$

$$\text{PCI-CF}(C_{\hat{\gamma}}) = \frac{1}{6}a_1^3 - \frac{1}{2}a_1a_2 + \frac{1}{3}a_3 \quad (10.69)$$

$$\text{PCI-CF}(C_3) = 0 \quad (10.70)$$

$$\text{PCI-CF}(C_{s\hat{\sigma}\hat{\gamma}}) = a_1a_2 - a_3 \quad (10.71)$$

$$\text{PCI-CF}(C_{3\bar{\sigma}}) = \frac{1}{2}b_3 - \frac{1}{2}a_3 \quad (10.72)$$

$$\text{PCI-CF}(C_{3v}) = 0 \quad (10.73)$$

$$\text{PCI-CF}(C_{3\hat{\gamma}}) = 0 \quad (10.74)$$

$$\text{PCI-CF}(C_{3v\hat{\sigma}\hat{\gamma}}) = a_3 \quad (10.75)$$

Suppose that a trigonal pyramidal skeleton **8-1** accommodates a set of three proligands which is selected from the ligand inventory \mathbf{L}' (Eq. 10.22). According to Theorem 10.4, we use the following ligand-inventory functions:

$$a_d = A^d + B^d + X^d \quad (10.76)$$

$$c_d = A^d + B^d + X^d + 2p^{d/2}\bar{p}^{d/2} + 2q^{d/2}\bar{q}^{d/2} + 2r^{d/2}\bar{r}^{d/2} \quad (10.77)$$

$$b_d = A^d + B^d + X^d + p^d + q^d + r^d + \bar{p}^d + \bar{q}^d + \bar{r}^d. \quad (10.78)$$

These ligand-inventory functions are introduced into each PCI-CF (Eqs. 10.66–10.75) to give a generating function, in which the coefficient of the term $A^a B^b X^x p^p \bar{p}^{\bar{p}} q^q \bar{q}^{\bar{q}} r^r \bar{r}^{\bar{r}}$ indicates the number of fixed promolecules to be counted.

Because A, B, etc. appear symmetrically, the term can be represented by the following partition:

$$[\theta] = [a, b, x; p, \bar{p}, q, \bar{q}, r, \bar{r}], \quad (10.79)$$

where we put $a \geq b \geq x$; $p \geq \bar{p}$, $q \geq \bar{q}$, $r \geq \bar{r}$; and $p \geq q \geq r$ without losing generality. For example, the ligand inventory \mathbf{L}' (Eq. 10.22) gives terms corresponding to the following partitions:

$$[\theta]_1 = [3, 0, 0; 0, 0, 0, 0, 0, 0] \quad (\text{for } A^3 \text{ etc.}) \quad (10.80)$$

$$[\theta]_2 = [2, 1, 0; 0, 0, 0, 0, 0, 0] \quad (\text{for } A^2B \text{ etc.}) \quad (10.81)$$

$$[\theta]_3 = [2, 0, 0; 1, 0, 0, 0, 0, 0] \quad (\text{for } A^2p \text{ etc.}) \quad (10.82)$$

$$[\theta]_4 = [1, 1, 1; 0, 0, 0, 0, 0, 0] \quad (\text{for } ABX) \quad (10.83)$$

$$[\theta]_5 = [1, 1, 0; 1, 0, 0, 0, 0, 0] \quad (\text{for } ABp \text{ etc.}) \quad (10.84)$$

$$[\theta]_6 = [1, 0, 0; 2, 0, 0, 0, 0, 0] \quad (\text{for } Ap^2 \text{ etc.}) \quad (10.85)$$

$$[\theta]_7 = [1, 0, 0; 1, 1, 0, 0, 0, 0] \quad (\text{for } \text{Ap}\bar{\text{p}} \text{ etc.}) \quad (10.86)$$

$$[\theta]_8 = [1, 0, 0; 1, 0, 1, 0, 0, 0] \quad (\text{for } \text{Apq} \text{ etc.}) \quad (10.87)$$

$$[\theta]_9 = [0, 0, 0; 3, 0, 0, 0, 0, 0] \quad (\text{for } \text{p}^3 \text{ etc.}) \quad (10.88)$$

$$[\theta]_{10} = [0, 0, 0; 2, 1, 0, 0, 0, 0] \quad (\text{for } \text{p}^2\bar{\text{p}} \text{ etc.}) \quad (10.89)$$

$$[\theta]_{11} = [0, 0, 0; 2, 0, 1, 0, 0, 0] \quad (\text{for } \text{p}^2\text{q} \text{ etc.}) \quad (10.90)$$

$$[\theta]_{12} = [0, 0, 0; 1, 1, 1, 0, 0, 0] \quad (\text{for } \text{p}\bar{\text{p}}\text{q} \text{ etc.}) \quad (10.91)$$

$$[\theta]_{13} = [0, 0, 0; 1, 0, 1, 0, 1, 0] \quad (\text{for } \text{pqr} \text{ etc.}) \quad (10.92)$$

The ligand-inventory functions (Eqs. 10.76–10.78) are introduced into the PCI-CFs (Eqs. 10.66–10.75) so as to give the following generating functions:

$$f_{C_1} = \left\{ \frac{1}{2} (\text{ABp} + \text{AB}\bar{\text{p}}) + \dots \right\} + \left\{ \frac{1}{2} (\text{Apq} + \text{A}\bar{\text{p}}\bar{\text{q}}) + \dots \right\} \\ + \left\{ \frac{1}{2} (\text{p}\bar{\text{p}}\text{q} + \text{p}\bar{\text{p}}\bar{\text{q}}) + \dots \right\} + \left\{ \frac{1}{2} (\text{pqr} + \bar{\text{p}}\bar{\text{q}}\bar{\text{q}}) + \dots \right\} \quad (10.93)$$

$$f_{C_{\bar{\sigma}}} = \left\{ \frac{1}{2} (\text{A}^2\text{p} + \text{A}^2\bar{\text{p}}) + \dots \right\} + \left\{ \frac{1}{2} (\text{Ap}^2 + \text{A}\bar{\text{p}}^2) + \dots \right\} \\ + \left\{ \frac{1}{2} (\text{p}^2\bar{\text{p}} + \text{p}\bar{\text{p}}^2) + \dots \right\} + \left\{ \frac{1}{2} (\text{p}^2\text{q} + \bar{\text{p}}^2\bar{\text{q}}) + \dots \right\} \quad (10.94)$$

$$f_{C_s} = \left\{ \text{A}\bar{\text{p}}\bar{\text{p}} + \dots \right\} \quad (10.95)$$

$$f_{C_{\hat{I}}} = \text{ABX} \quad (10.96)$$

$$f_{C_3} = 0 \quad (10.97)$$

$$f_{C_{s\bar{\sigma}\hat{I}}} = \left\{ \text{A}^2\text{B} + \dots \right\} \quad (10.98)$$

$$f_{C_{3\bar{\sigma}}} = \left\{ \frac{1}{2} (\text{p}^3 + \bar{\text{p}}^3) + \dots \right\} \quad (10.99)$$

$$f_{C_{3v}} = 0 \quad (10.100)$$

$$f_{C_{3\hat{I}}} = 0 \quad (10.101)$$

$$f_{C_{3v\bar{\sigma}\hat{I}}} = \left\{ \text{A}^3 + \dots \right\}, \quad (10.102)$$

where the partitions $[\theta]_i$ ($i = 1 - 13$) are attached to the corresponding compositions.

Each term corresponds to one quadruplet of a stereoisogram, the reference promolecule of which is shown in Fig. 10.3. For example, the term $\frac{1}{2}(\text{ABp} + \text{AB}\bar{\text{p}})$ appearing in Eq. 10.93 indicates the presence of one quadruplet **10-9** of a stereoisogram, which is denoted by the symbol $[\theta]_5; [C_1, C_1, C_1; \text{III}]$. The outer box containing a quadruplet of **10-9/10-9/10-10/10-10** indicates that the quadruplet is counted once under the action of the *RS*-stereoisomeric group $C_{3v\bar{\sigma}\hat{I}}$, although the quadruplet is divided into two pairs of enan-

tiomers $10\text{-}9/\overline{10\text{-}9}$ and $10\text{-}10/\overline{10\text{-}10}$ under the action of the point group C_{3v} , as surrounded by an inner box. The corresponding stereoisogram of type III has been shown in Fig. 10.8.

Exercise 10.5. Confirm that each term of Eqs. 10.93–10.102 corresponds to a quadruplet surrounding by an outer box in Fig. 10.3. Note that a quadruplet may degenerate into one pair of enantiomers (type I or type II), one achiral promolecule (type IV), or a set of two achiral promolecules (type V).

10.2.8 Type-Itemized Enumeration by the PCI Method

Let \hat{m}_{ji} be the ji -element of the inverse mark table $M_{\hat{G}}^{-1}$ (e.g., Table 10.5 for $M_{C_{3v\hat{\sigma}\hat{T}}}^{-1}$). The \hat{G}_j -row is tentatively fixed and the row is summed up according to the categorization of type I–V (e.g. Eqs. 10.47–10.51 for $C_{3v\hat{\sigma}\hat{T}}$) as follows:

$$\hat{N}_j^{(I)} = \sum_{\hat{G}_i \in \text{SG}^{[I]}} \hat{m}_{ji} \quad (10.103)$$

$$\hat{N}_j^{(II)} = \sum_{\hat{G}_i \in \text{SG}^{[II]}} \hat{m}_{ji} \quad (10.104)$$

$$\hat{N}_j^{(III)} = \sum_{\hat{G}_i \in \text{SG}^{[III]}} \hat{m}_{ji} \quad (10.105)$$

$$\hat{N}_j^{(IV)} = \sum_{\hat{G}_i \in \text{SG}^{[IV]}} \hat{m}_{ji} \quad (10.106)$$

$$\hat{N}_j^{(V)} = \sum_{\hat{G}_i \in \text{SG}^{[V]}} \hat{m}_{ji} \quad (10.107)$$

$$\hat{N}_j = \hat{N}_j^{(I)} + \hat{N}_j^{(II)} + \hat{N}_j^{(III)} + \hat{N}_j^{(IV)} + \hat{N}_j^{(V)}, \quad (10.108)$$

where $\text{SG}^{[I]}\text{--}\text{SG}^{[V]}$ are concerned with five types of the RS -stereoisomeric group \hat{G} . When \hat{G}_j runs over $\text{SSG}_{\hat{G}}$, a type-enumeration matrix (TEM) for type-itemized enumerations is generated as an $|\text{SSG}_{\hat{G}}| \times 6$ matrix, where the j -th row (TEM_j) as a row vector is represented as follows:

$$\text{TEM}_j = (\hat{N}_j, \hat{N}_j^{(I)}, \hat{N}_j^{(II)}, \hat{N}_j^{(III)}, \hat{N}_j^{(IV)}, \hat{N}_j^{(V)}). \quad (10.109)$$

The respective elements of TEM_j for $\text{SSG}_{C_{3v\hat{\sigma}\hat{T}}}$ are collected in Table 10.6.

The definition of PCI-CFs (Def. 10.6) is modified to generate CI-CFs for characterizing five types are calculated by starting from $\hat{N}_j^{(K)}$ ($K = I - V$).

Definition 10.7 (CI-CFs for Five Types). A *cycle index with chirality fittingness* (CI-CF) is defined by the following equation:

$$\text{CI-CF}^{[K]}(\hat{G}; \mathcal{S}_d) = \sum_{j=1}^{\mathcal{S}} \hat{N}_j^{(K)} \text{SCI-CF}_{\hat{G}}(\hat{G}_j; \mathcal{S}_{d_{jk}}) = \sum_{j=1}^{\mathcal{S}} \hat{N}_j^{(K)} \prod_{i=1}^{\mathcal{S}} \left(\text{USCI-CF}(\hat{G}(/ \hat{G}_i) \downarrow \hat{G}_j; \mathcal{S}_{d_{jk}}) \right)^{\hat{\alpha}_i}$$

$$= \sum_{j=1}^{\xi} \widehat{N}_j^{(K)} \left(\prod_{i=1}^{\xi} \left(\prod_{k=1}^{\nu_j} \mathbb{S}_{d_{jk}}^{\beta^{(ij)}} \right)^{\alpha_i} \right) \quad (10.110)$$

for $K = I - V$, where $\text{SCI-CF}_{\mathbf{P}\hat{\mathbf{G}}}$ comes from Eq. 10.59 of Def. 10.5. The symbol $\widehat{N}_j^{(K)}$ denotes an element of the TEM (Eq. 10.109).

The CI-CFs due to Def. 10.7 are alternatively obtained by adding PCI-CFs categorized by each of $\text{SG}^{\text{[I]}}\text{-SG}^{\text{[V]}}$ of $\hat{\mathbf{G}}$ (e.g., Eqs. 10.47–10.51 for $\mathbf{C}_{3\nu\tilde{\sigma}\tilde{\tau}}$).

In a similar way to Theorem 10.4 concerning PCI-CFs, the CI-CFs defined in Def. 10.7 give generating functions for giving the numbers of quadruplets $\hat{T}_{\theta K}$ with type K (I to V) and $[\theta]$:

Theorem 10.5. Suppose that the substitution positions of a stereoskeleton belonging to an *RS*-stereoisomeric group $\hat{\mathbf{G}}$ accommodate proligands selected from a ligand inventory \mathbf{L} (Eq. 6.26 on page 140) to give promolecules with the composition W_{θ} . A generating function for evaluating the number of quadruplets of promolecules $\hat{T}_{\theta K}$ with type K (I to V) and $[\theta]$: is obtained to be:

$$\sum_{[\theta]} \hat{T}_{\theta K} W_{\theta} = \text{CI-CF}^{[K]}(\hat{\mathbf{G}}; \mathbb{S}_d) \Big|_{\mathbb{S}_d = \Sigma_{\mathbf{L}}} \quad (10.111)$$

for $K = I - V$, where the symbol W_{θ} denotes the composition represented by Eq. 6.27 (page 140) and the symbol $\mathbb{S}_d = \Sigma_{\mathbf{L}}$ denotes the introduction of a ligand-inventory function to the sphericity index \mathbb{S}_d represented by Eqs. 10.63–10.65.

The data of the USCI-CF-column of Table 10.6 (or the $\mathbf{C}_{3\nu\tilde{\sigma}\tilde{\tau}} / (\mathbf{C}_{s\tilde{\sigma}\tilde{\tau}})$ -row of Table 10.8) are regarded as a formal row vector of SCI-CFs, which is multiplied by the TEM listed also in Table 10.8. Thereby, CI-CFs for characterizing five types are calculated according to Def. 10.7. Alternatively, the CI-CFs for characterizing five types are calculated by starting from Eqs. 10.66–10.75 according to Eqs. 10.47–10.51:

$$\begin{aligned} \text{CI-CF}^{\text{[I]}}(\mathbf{C}_{3\nu\tilde{\sigma}\tilde{\tau}}) &= \text{PCI-CF}(\mathbf{C}_{\tilde{\tau}}) + \text{PCI-CF}(\mathbf{C}_{3\tilde{\tau}}) \\ &= \frac{1}{6}a_1^3 - \frac{1}{2}a_1a_2 + \frac{1}{3}a_3 \end{aligned} \quad (10.112)$$

$$\begin{aligned} \text{CI-CF}^{\text{[II]}}(\mathbf{C}_{3\nu\tilde{\sigma}\tilde{\tau}}) &= \text{PCI-CF}(\mathbf{C}_{\tilde{\sigma}}) + \text{PCI-CF}(\mathbf{C}_{3\tilde{\sigma}}) \\ &= \frac{1}{2}b_1b_2 - \frac{1}{2}a_1a_2 \end{aligned} \quad (10.113)$$

$$\begin{aligned} \text{CI-CF}^{\text{[III]}}(\mathbf{C}_{3\nu\tilde{\sigma}\tilde{\tau}}) &= \text{PCI-CF}(\mathbf{C}_1) + \text{PCI-CF}(\mathbf{C}_3) \\ &= \frac{1}{12}b_1^3 - \frac{1}{4}b_1b_2 - \frac{1}{4}a_1c_2 - \frac{1}{12}a_1^3 \\ &\quad + \frac{1}{6}b_3 + \frac{1}{2}a_1a_2 - \frac{1}{6}a_3 \end{aligned} \quad (10.114)$$

$$\begin{aligned} \text{CI-CF}^{\text{[IV]}}(\mathbf{C}_{3\nu\tilde{\sigma}\tilde{\tau}}) &= \text{PCI-CF}(\mathbf{C}_{s\tilde{\sigma}\tilde{\tau}}) + \text{PCI-CF}(\mathbf{C}_{3\nu\tilde{\sigma}\tilde{\tau}}) \\ &= a_1a_2 \end{aligned} \quad (10.115)$$

$$\begin{aligned} \text{CI-CF}^{\text{[V]}}(\mathbf{C}_{3\nu\tilde{\sigma}\tilde{\tau}}) &= \text{PCI-CF}(\mathbf{C}_s) + \text{PCI-CF}(\mathbf{C}_{3\nu}) \\ &= \frac{1}{2}a_1c_2 - \frac{1}{2}a_1a_2 \end{aligned} \quad (10.116)$$

These CI-CFs corresponds to the CI-CFs reported in [5].⁶

According to Theorem 10.5, the ligand-inventory functions (Eqs. 10.76–10.78) are introduced into the CI-CFs (Eqs. 10.112–10.116) so as to give the following generating functions:

$$f^{[I]} = \text{ABX}^{\theta_4} \quad (10.117)$$

$$f^{[II]} = \left\{ \frac{1}{2} (A^2 \text{p} + A^2 \overline{\text{p}}) + \dots \right\} + \left\{ \frac{1}{2} (A \text{p}^2 + A \overline{\text{p}}^2) + \dots \right\} + \left\{ \frac{1}{2} (\text{p}^3 + \overline{\text{p}}^3) + \dots \right\} \\ + \left\{ \frac{1}{2} (\text{p}^2 \overline{\text{p}} + \overline{\text{p}} \text{p}^2) + \dots \right\} + \left\{ \frac{1}{2} (\text{p}^2 \text{q} + \overline{\text{p}}^2 \overline{\text{q}}) + \dots \right\} \quad (10.118)$$

$$f^{[III]} = \left\{ \frac{1}{2} (A \text{Bp} + A \text{B} \overline{\text{p}}) + \dots \right\} + \left\{ \frac{1}{2} (A \text{p} \text{q} + A \overline{\text{p}} \overline{\text{q}}) + \dots \right\} \\ + \left\{ \frac{1}{2} (\text{p} \overline{\text{p}} \text{q} + \overline{\text{p}} \text{p} \overline{\text{q}}) + \dots \right\} + \left\{ \frac{1}{2} (\text{p} \text{q} \text{r} + \overline{\text{p}} \overline{\text{q}} \overline{\text{r}}) + \dots \right\} \quad (10.119)$$

$$f^{[IV]} = \left\{ A^3 + \dots \right\} + \left\{ A^2 B + \dots \right\} \quad (10.120)$$

$$f^{[V]} = \left\{ A \text{p} \overline{\text{p}} + \dots \right\} \quad (10.121)$$

Each term corresponds to one quadruplet of a stereoisogram, the reference promolecule of which is shown in Fig. 10.3.

10.2.9 Gross Enumeration Under *RS*-Stereoisomeric Groups

Cycle Indices with Chirality Fittingness

The first column of the TEM (Eq. 10.109) is the collection of the row sums of an inverse mark table (e.g., the row-sum-column of Table 10.5 for the *RS*-stereoisomeric group $C_{3v} \widetilde{\sigma} \widehat{I}$).

According to a general discussion on inverse mark tables in Appendix B of Fujita's monograph [23], the definition of CI-CFs for point groups (e.g., [14,25]) can be extended to support *RS*-stereoisomeric groups:

Definition 10.8 (CI-CF for Gross Enumeration). A cycle index with chirality fittingness (CI-CF) is defined by the following equation:

$$\text{CI-CF}(\hat{G}; \$d) = \sum_{j=1}^{\hat{s}} \widehat{N}_j \widehat{\text{SCI-CF}}_{\hat{G}}(\hat{G}_j; \$d_{jk}) = \sum_{j=1}^{\hat{s}} \widehat{N}_j \prod_{i=1}^{\hat{s}} \left(\text{USCI-CF}(\hat{G} / \hat{G}_i \downarrow \hat{G}_j; \$d_{jk}) \right)^{\hat{a}_i}$$

⁶ Eq. 10.112 is a half of Eq. 28 of Ref.[5] (CI-CF^[I](C_3)); Eq. 10.113 is a half of Eq. 24 of Ref.[5] (CI-CF^[II](C_3)); Eq. 10.114 is a quarter of Eq. 30 of Ref.[5] (CI-CF^[III](C_3)); Eq. 10.115 is identical with Eq. 18 of Ref.[5] (CI-CF^[IV](C_3)); Eq. 10.116 is a half of Eq. 20 of Ref.[5] (CI-CF^[V](C_3)). Note that the calculations of Ref.[5] have been conducted under the action of the point group C_3 , while the present calculations (Eqs. 10.112–10.116) are conducted under the action of the *RS*-stereoisomeric group $C_{3v} \widetilde{\sigma} \widehat{I}$.

$$= \sum_{j=1}^s \widehat{N}_j \left(\prod_{i=1}^s \left(\prod_{k=1}^{v_j} \$_{d_{jk}}^{\beta_{(ij)}} \right)^{\alpha_i} \right) \quad (10.122)$$

where SCI-CF $_{\mathbf{P}_{\widehat{\mathbf{G}}}}$ comes from Eq. 10.59 of Def. 10.5. The symbol \widehat{N}_j denotes an element appearing in the first column the TEM (Eq. 10.109).

Def. 10.8 means that a CI-CF is obtained by summing up PCI-CFs over the subgroups of SSG $_{\widehat{\mathbf{G}}}$. As for the *RS*-stereoisomeric group $\mathbf{C}_{3v\widetilde{\sigma}\widehat{\Gamma}}$, a CI-CF for gross enumeration is obtained by summing up the PCI-CFs listed in Eqs. 10.66–10.75 or equivalently by summing up the CI-CFs listed in Eqs. 10.112–10.116:

$$\text{CI-CF}(\mathbf{C}_{3v\widetilde{\sigma}\widehat{\Gamma}}) = \frac{1}{12}b_1^3 + \frac{1}{4}b_1b_2 + \frac{1}{4}a_1c_2 + \frac{1}{12}a_1^3 + \frac{1}{6}b_3 + \frac{1}{6}a_3. \quad (10.123)$$

The ligand-inventory functions (Eqs. 10.76–10.78) are introduced into the CI-CF (Eq. 10.123) so as to give the following generating function:

$$\begin{aligned} f^{[T]} = & \{A^3 + \dots\} + \{A^2B + \dots\} \\ & + \frac{1}{2}\{(A^2p + A^2\bar{p}) + \dots\} + ABX + \left\{\frac{1}{2}(ABp + AB\bar{p}) + \dots\right\} \\ & + \left\{\frac{1}{2}(Ap^2 + A\bar{p}^2) + \dots\right\} + \{A\bar{p}\bar{p} + \dots\} + \left\{\frac{1}{2}(Apq + A\bar{p}\bar{q}) + \dots\right\} \\ & + \left\{\frac{1}{2}(p^3 + \bar{p}^3) + \dots\right\} + \left\{\frac{1}{2}(p^2\bar{p} + p\bar{p}^2) + \dots\right\} + \left\{\frac{1}{2}(p^2q + \bar{p}^2\bar{q}) + \dots\right\} \\ & + \left\{\frac{1}{2}(p\bar{p}q + p\bar{p}\bar{q}) + \dots\right\} + \left\{\frac{1}{2}(pqr + \bar{p}\bar{q}\bar{r}) + \dots\right\}. \end{aligned} \quad (10.124)$$

The Proligand Method for Gross Enumeration

The proligand method developed by Fujita [23,26–28] does not require the data of subgroups such as mark tables and inverse mark tables during gross enumeration under point groups. Fujita's proligand method can be extended to be applied to gross enumeration under an *RS*-stereoisomeric group. Thus, Def. 7.5 (page 181) is extended as follows:

Definition 10.9 (Cycle Index With Chirality Fittingness (CI-CF) for *RS*-Stereoisomeric Groups). Suppose that a permutation p_g ($\in \mathbf{P}_{\widehat{\mathbf{G}}}$) has a cycle structure $(1^{v_1}2^{v_2}\dots d^{v_d}\dots n^{v_n})^{(p_g)}$ ($\sum_{i=1}^n i v_i = n$), as shown in Def. 7.2 (page 178) and that the corresponding product of sphericity indices (PSIs) shown in Def. 7.4 (page 180) is extended to meet the requirement of *RS*-stereoisomeric groups. Then, a *cycle index with chirality fittingness* (CI-CF) is defined as follows:

$$\begin{aligned} \text{CI-CF}(\mathbf{P}_{\widehat{\mathbf{G}}}; \$_d) &= \frac{1}{|\mathbf{P}_{\widehat{\mathbf{G}}}|} \sum_{p_g \in \mathbf{P}_{\widehat{\mathbf{G}}}} \text{PSI}(p_g; \$_d) \\ &= \frac{1}{|\mathbf{P}_{\widehat{\mathbf{G}}}|} \sum_{p_g \in \mathbf{P}_{\widehat{\mathbf{G}}}} (\$_1^{v_1} \$_2^{v_2} \dots \$_d^{v_d} \dots \$_n^{v_n})^{(p_g)}, \end{aligned} \quad (10.125)$$

where $\$_d$ denotes a_d , c_d , or b_d after Def. 10.3 is extended to meet sphericities of cycles.

According to Def. 10.9, the products of sphericity indices listed in the PSI-column of Table 10.1 are summed up and divided by 12 ($= |\mathbf{C}_{3v\bar{\sigma}\bar{\Gamma}}|$) so as to give the following CI-CF:

$$\text{CI-CF}'(\mathbf{C}_{3v\bar{\sigma}\bar{\Gamma}}) = \frac{1}{12} (b_1^3 + 3b_1b_2 + 2b_3 + 3a_1c_2 + a_1^3 + 2a_3), \quad (10.126)$$

which is identical with Eq. 10.123. Hence, a generating function identical with Eq. 10.124 is obtained by introducing the ligand-inventory functions (Eqs. 10.76–10.78) into Eq. 10.126.

10.3 Comparison with Enumeration Under Subgroups

10.3.1 Comparison with Enumeration Under Point Groups

The reference promolecule of a stereoisogram, which belongs to an *RS*-stereoisomeric group, can be alternatively regarded as belonging to a point group. Let us now examine a trigonal pyramidal skeleton **8-1** (page 195) under the action of the point group \mathbf{C}_{3v} .

Because the USCI-CFs of the coset representation $\mathbf{C}_{3v}/(\mathbf{C}_s)$ [14, Table E.7] and the inverse mark table of \mathbf{C}_{3v} [14, Table B.7] have been reported, Fujita's USCI approach is applied to the three positions of **8-1**. Thereby, the PCI-CFs are obtained according to Def. 6.5 (page 150) in a formal matrix calculation:

$$\begin{aligned} & (\text{PCI-CF}'(\mathbf{C}_1), \text{PCI-CF}'(\mathbf{C}_s), \text{PCI-CF}'(\mathbf{C}_3), \text{PCI-CF}'(\mathbf{C}_{3v})) \\ &= (b_1^3, a_1c_2, b_3, a_3) \begin{pmatrix} \frac{1}{6} & 0 & 0 & 0 \\ -\frac{1}{2} & 1 & 0 & 0 \\ -\frac{1}{6} & 0 & \frac{1}{2} & 0 \\ \frac{1}{2} & -1 & -\frac{1}{2} & 1 \end{pmatrix}. \end{aligned} \quad (10.127)$$

This equation gives the following PCI-CFs under the action of the point group \mathbf{C}_{3v} :

$$\text{PCI-CF}'(\mathbf{C}_1) = \frac{1}{6}b_1^3 - \frac{1}{2}a_1c_2 - \frac{1}{6}b_3 + \frac{1}{2}a_3 \quad (10.128)$$

$$\text{PCI-CF}'(\mathbf{C}_s) = a_1c_2 - a_3 \quad (10.129)$$

$$\text{PCI-CF}'(\mathbf{C}_3) = \frac{1}{2}b_3 - \frac{1}{2}a_3 \quad (10.130)$$

$$\text{PCI-CF}'(\mathbf{C}_{3v}) = a_3. \quad (10.131)$$

The ligand-inventory functions (Eqs. 10.76–10.78) are introduced into the PCI-CFs (Eqs. 10.128–10.131). The expansion of the resulting equations give the following generating functions:

$$\begin{aligned} f'_{\mathbf{C}_1} &= \{2 \times \frac{1}{2} (\text{ABp} + \text{AB}\bar{\text{p}}) + \dots\} + \{2 \times \frac{1}{2} (\text{Apq} + \text{A}\bar{\text{p}}\bar{\text{q}}) + \dots\} \\ &+ \{2 \times \frac{1}{2} (\text{p}\bar{\text{p}}\text{q} + \text{p}\bar{\text{p}}\bar{\text{q}}) + \dots\} + \{2 \times \frac{1}{2} (\text{pqr} + \text{p}\bar{\text{q}}\bar{\text{q}}) + \dots\} \end{aligned}$$

$$\begin{aligned}
& + \left\{ \frac{1}{2} (A^2p + A^2\bar{p}) + \dots \right\} + \left\{ \frac{1}{2} (Ap^2 + A\bar{p}^2) + \dots \right\} \\
& + \left\{ \frac{1}{2} (p^2\bar{p} + p\bar{p}^2) + \dots \right\} + \left\{ \frac{1}{2} (p^2q + \bar{p}^2\bar{q}) + \dots \right\} \\
& + ABX \quad (10.132)
\end{aligned}$$

$$f'_{C_s} = \{2A\bar{p}\bar{p} + \dots\} + \{A^2B + \dots\} \quad (10.133)$$

$$f'_{C_3} = \left\{ \frac{1}{2} (p^3 + \bar{p}^3) + \dots \right\} \quad (10.134)$$

$$f'_{C_{3v}} = \{A^3 + \dots\}. \quad (10.135)$$

The terms of these generating functions are consistent to the data depicted in Fig. 10.3. Note that a set of one or two promolecules surrounded in an inner box is counted once as a (self-)enantiomeric pair under the action of the point group C_{3v} . For example, the term $2 \times \frac{1}{2} (ABp + AB\bar{p})$ ($[\theta]_5$) in the generating function f'_{C_1} (Eq. 10.132) indicates the presence of two enantiomeric pairs, i.e., one pair of **10-9/10-9** surrounded by an inner box and the other pair of **10-10/10-10** surrounded by another inner box, as found in Fig. 10.3. In contrast, a quadruplet of **10-9/10-9/10-10/10-10** surrounded by an outer box constructs a type-III stereoisogram, which is counted once under the *RS*-stereoisomeric group $C_{3v\hat{\sigma}\hat{\tau}}$.

The generating functions for the *RS*-stereoisomeric group $C_{3v\hat{\sigma}\hat{\tau}}$ (Eqs. 10.93–10.102) are concerned with numbers of inequivalent quadruplets (or stereoisograms), while the generating functions of the point group C_{3v} (Eqs. 10.132–10.135) are concerned with numbers of inequivalent pairs of enantiomers. These two types of generating functions are correlated by referring to Fig. 10.9. The following theorem holds true in general according to Fig. 10.9.

Theorem 10.6 (Quadruplets and Pairs of Enantiomers).

- A quadruplet of a type-I stereoisogram consists of one pair of enantiomers.
- A quadruplet of a type-II stereoisogram consists of one pair of enantiomers.
- A quadruplet of a type-III stereoisogram consists of two pairs of enantiomers.
- A quadruplet of a type-IV stereoisogram consists of one achiral promolecule.
- A quadruplet of a type-V stereoisogram consists of two achiral promolecules.

The PCI-CFs for the point group C_{3v} (Eqs. 10.128–10.128) can be calculated from the PCI-CFs for the *RS*-stereoisomeric group $C_{3v\hat{\sigma}\hat{\tau}}$ (Eqs. 10.66–10.75), where Theorem 10.6 requires the multiplication by 2 if a subgroup of $C_{3v\hat{\sigma}\hat{\tau}}$ is classified to type III or type V.

$$\begin{aligned}
\text{PCI-CF}'(C_1) &= 2\text{PCI-CF}(C_1) + \text{PCI-CF}(C_{\hat{\sigma}}) + \text{PCI-CF}(C_{\hat{\tau}}) \\
&= \frac{1}{6}b_1^3 - \frac{1}{2}a_1c_2 - \frac{1}{6}b_3 + \frac{1}{2}a_3 \quad (10.136)
\end{aligned}$$

$$\begin{aligned}
\text{PCI-CF}'(C_s) &= 2\text{PCI-CF}(C_s) + \text{PCI-CF}(C_{s\hat{\sigma}\hat{\tau}}) \\
&= a_1c_2 - a_3 \quad (10.137)
\end{aligned}$$

$$\text{PCI-CF}'(C_3) = 2\text{PCI-CF}(C_3) + \text{PCI-CF}(C_{3\hat{\sigma}}) + \text{PCI-CF}(C_{3\hat{\tau}})$$

$$= \frac{1}{2}b_3 - \frac{1}{2}a_3 \quad (10.138)$$

$$\begin{aligned} \text{PCI-CF}'(\mathbf{C}_{3v}) &= 2\text{PCI-CF}(\mathbf{C}_{3v}) + \text{PCI-CF}(\mathbf{C}_{3v\tilde{\sigma}\tilde{I}}) \\ &= a_3. \end{aligned} \quad (10.139)$$

The resulting PCI-CFs (Eqs. 10.136–10.139) are identical with the PCI-CFs (Eqs. 10.128–10.131) obtained directly by Fujita's USCI approach. Note that the *RS*-stereoisomeric groups selected for Eq. 10.136 satisfy $\mathbf{C}_1 \cap \mathbf{C}_{3v} = \mathbf{C}_1$, $\mathbf{C}_{\tilde{\sigma}} \cap \mathbf{C}_{3v} = \mathbf{C}_1$, and $\mathbf{C}_{\tilde{I}} \cap \mathbf{C}_{3v} = \mathbf{C}_1$; the *RS*-stereoisomeric groups selected for Eq. 10.137 satisfy $\mathbf{C}_s \cap \mathbf{C}_{3v} = \mathbf{C}_s$ and $\mathbf{C}_{s\tilde{\sigma}\tilde{I}} \cap \mathbf{C}_{3v} = \mathbf{C}_s$; \dots ; as well as the *RS*-stereoisomeric groups selected for Eq. 10.139 satisfy $\mathbf{C}_{3v} \cap \mathbf{C}_{3v} = \mathbf{C}_{3v}$ and $\mathbf{C}_{3v\tilde{\sigma}\tilde{I}} \cap \mathbf{C}_{3v} = \mathbf{C}_{3v}$.

Exercise 10.6.

- Enumerate trigonal pyramidal promolecules under the action of the chiral point group \mathbf{C}_3 , where each promolecule is counted once.
- Derive the relationship between the enumeration under \mathbf{C}_3 and the enumeration under $\mathbf{C}_{3v\tilde{\sigma}\tilde{I}}$ in a similar way to Theorem 10.6. See Footnote 6.

10.3.2 Comparison with Enumeration Under *RS*-Permutation Groups

The reference promolecule of a stereoisogram, which belongs to an *RS*-stereoisomeric group, can be alternatively regarded as belonging to an *RS*-permutation group. Let us now examine a trigonal pyramidal skeleton **8-1** under the action of the *RS*-permutation group $\mathbf{C}_{3\tilde{\sigma}}$.

Because the *RS*-permutation group $\mathbf{C}_{3\tilde{\sigma}}$ is isomorphic to the point group \mathbf{C}_{3v} , the three positions of the trigonal pyramidal skeleton **8-1** construct an orbit governed by $\mathbf{C}_{3\tilde{\sigma}}(\mathbf{C}_{\tilde{\sigma}})$. In a similar way to Eq. 10.127, the PCIs are obtained in a formal matrix calculation:

$$\begin{aligned} &(\text{PCI}'(\mathbf{C}_1), \text{PCI}'(\mathbf{C}_{\tilde{\sigma}}), \text{PCI}'(\mathbf{C}_3), \text{PCI}'(\mathbf{C}_{3\tilde{\sigma}})) \\ &= (s_1^3, s_1s_2, s_3, s_3) \begin{pmatrix} \frac{1}{6} & 0 & 0 & 0 \\ -\frac{1}{2} & 1 & 0 & 0 \\ -\frac{1}{6} & 0 & \frac{1}{2} & 0 \\ \frac{1}{2} & -1 & -\frac{1}{2} & 1 \end{pmatrix}. \end{aligned} \quad (10.140)$$

This equation gives the following PCIs under the action of the *RS*-permutation group $\mathbf{C}_{3\tilde{\sigma}}$:

$$\text{PCI}'(\mathbf{C}_1) = \frac{1}{6}s_1^3 - \frac{1}{2}s_1s_2 + \frac{1}{3}s_3 \quad (10.141)$$

$$\text{PCI}'(\mathbf{C}_{\tilde{\sigma}}) = s_1s_2 - s_3 \quad (10.142)$$

$$\text{PCI}'(\mathbf{C}_3) = 0 \quad (10.143)$$

$$\text{PCI}'(\mathbf{C}_{3\tilde{\sigma}}) = s_3. \quad (10.144)$$

The ligand-inventory functions (Eqs. 10.76–10.78) degenerate into a single function:

$$s_d = A^d + B^d + X^d + p^d + q^d + r^d + \bar{p}^d + \bar{q}^d + \bar{r}^d, \quad (10.145)$$

which is introduced into the SCIs (Eqs. 10.141–10.144). The expansion of the resulting equations give the following generating functions:

$$\begin{aligned} f''_{C_1} = & \{ (ABp + AB\bar{p}) + \dots \} + \{ (Apq + A\bar{p}\bar{q}) + \dots \} \\ & + \{ (p\bar{p}q + p\bar{p}\bar{q}) + \dots \} + \{ (pqr + \bar{p}\bar{q}\bar{q}) + \dots \} \\ & + \{ A\bar{p}\bar{p} + \dots \} + ABX \end{aligned} \quad (10.146)$$

$$\begin{aligned} f''_{C_{3\bar{\sigma}}} = & \{ (A^2p + A^2\bar{p}) + \dots \} + \{ (Ap^2 + A\bar{p}^2) + \dots \} \\ & + \{ (p^2\bar{p} + p\bar{p}^2) + \dots \} + \{ (p^2q + \bar{p}^2\bar{q}) + \dots \} \\ & + \{ A^2B + \dots \} \end{aligned} \quad (10.147)$$

$$f''_{C_3} = 0 \quad (10.148)$$

$$f''_{C_{3\bar{\sigma}}} = \{ (p^3 + \bar{p}^3) + \dots \} + \{ A^3 + \dots \}. \quad (10.149)$$

Note that a pair of *RS*-diastereomers is counted once under the action of an *RS*-permutation group. For example, the term ABp ($[\theta]_5$) in the generating function f''_{C_1} (Eq. 10.146) indicates the presence of one pair of *RS*-diastereomers **10-9/10-10**, while the counterpart term $AB\bar{p}$ indicates the presence of one pair of *RS*-diastereomers $\overline{\mathbf{10-9/10-10}}$, as depicted in Fig. 10.3. Thus, a quadruplet of a type-III stereoisogram is divided into two pairs of *RS*-diastereomers under the *RS*-permutation group $C_{3\bar{\sigma}}$.

The generating functions for the *RS*-stereoisomeric group $C_{3v\bar{\sigma}\bar{f}}$ (Eqs. 10.93–10.102) are concerned with numbers of inequivalent quadruplets (or stereoisograms), while the generating functions of the *RS*-permutation group $C_{3\bar{\sigma}}$ (Eqs. 10.146–10.149) are concerned with numbers of inequivalent pairs of *RS*-diastereomers. These two types of generating functions are correlated by referring to Fig. 10.9. The following theorem holds true in general according to Fig. 10.9.

Theorem 10.7 (Quadruplets and Pairs of *RS*-Diastereomers).

- A quadruplet of a type-I stereoisogram consists of one pair of *RS*-diastereomers.
- A quadruplet of a type-II stereoisogram consists of two *RS*-astereogenic promolecules.
- A quadruplet of a type-III stereoisogram consists of two pairs of *RS*-diastereomers.
- A quadruplet of a type-IV stereoisogram consists of one *RS*-astereogenic promolecule.
- A quadruplet of a type-V stereoisogram consists of one pair of *RS*-diastereomers.



Exercise 10.7. Compare Theorem 10.7 with Theorem 10.6.

The PCIs for the RS -permutation group $C_{3\tilde{\sigma}}$ (Eqs. 10.141–10.144) can be calculated from the PCI-CFs for the RS -stereoisomeric group $C_{3v\tilde{\sigma}\hat{\tau}}$ (Eqs. 10.66–10.75) by putting $s_d = a_d = c_d = b_d$, where Theorem 10.7 requires the multiplication by 2 if a subgroup of $C_{3v\tilde{\sigma}\hat{\tau}}$ is classified to type II or type III.

$$\begin{aligned} \text{PCI}'(C_1) &= 2\text{PCI-CF}(C_1) + \text{PCI-CF}(C_s) + \text{PCI-CF}(C_{\hat{\tau}}) \\ &= \frac{1}{6}s_1^3 - \frac{1}{2}s_1s_2 + \frac{1}{3}s_3 \end{aligned} \quad (10.150)$$

$$\begin{aligned} \text{PCI}'(C_{\tilde{\sigma}}) &= 2\text{PCI-CF}(C_{\tilde{\sigma}}) + \text{PCI-CF}(C_{s\tilde{\sigma}\hat{\tau}}) \\ &= s_1s_2 - s_3 \end{aligned} \quad (10.151)$$

$$\begin{aligned} \text{PCI}'(C_3) &= 2\text{PCI-CF}(C_3) + \text{PCI-CF}(C_{3v}) + \text{PCI-CF}(C_{3\hat{\tau}}) \\ &= 0 \end{aligned} \quad (10.152)$$

$$\begin{aligned} \text{PCI}'(C_{3\tilde{\sigma}}) &= 2\text{PCI-CF}(C_{3\tilde{\sigma}}) + \text{PCI-CF}(C_{3v\tilde{\sigma}\hat{\tau}}) \\ &= s_3. \end{aligned} \quad (10.153)$$

The resulting PCIs (Eqs. 10.150–10.153) are identical with the PCIs (Eqs. 10.141–10.144) obtained directly by Fujita's USCI approach. Note that the RS -stereoisomeric groups selected for Eq. 10.150 satisfy $C_1 \cap C_{3\tilde{\sigma}} = C_1$, $C_s \cap C_{3\tilde{\sigma}} = C_1$, and $C_{\hat{\tau}} \cap C_{3\tilde{\sigma}} = C_1$; the RS -stereoisomeric groups selected for Eq. 10.151 satisfy $C_{\tilde{\sigma}} \cap C_{3\tilde{\sigma}} = C_{\tilde{\sigma}}$ and $C_{s\tilde{\sigma}\hat{\tau}} \cap C_{3\tilde{\sigma}} = C_{\tilde{\sigma}}$; the RS -stereoisomeric groups selected for Eq. 10.152 satisfy $C_3 \cap C_{3\tilde{\sigma}} = C_3$, $C_{3v} \cap C_{3\tilde{\sigma}} = C_3$, and $C_{3\hat{\tau}} \cap C_{3\tilde{\sigma}} = C_3$; as well as the RS -stereoisomeric groups selected for Eq. 10.153 satisfy $C_{3\tilde{\sigma}} \cap C_{3\tilde{\sigma}} = C_{3\tilde{\sigma}}$ and $C_{3v\tilde{\sigma}\hat{\tau}} \cap C_{3\tilde{\sigma}} = C_{3\tilde{\sigma}}$.

Exercise 10.8. During the derivation of Eqs. 10.150–10.153, omit the procedure of putting $s_d = a_d = c_d = b_d$. Then, confirm that Eqs. 10.150–10.153 are converted into polynomials with the variable b_d , where the terms with a_d and/or c_d vanish.

10.3.3 Comparison with Enumeration Under Maximum-Chiral Point Subgroups

The reference promolecule of a stereoisogram, which belongs to an RS -stereoisomeric group, can be alternatively regarded as belonging to a maximum-chiral point group (cf. Subsection 7.3.5). Note that the maximum-chiral point group is the maximum subgroup of a point group, and at the same time, the maximum subgroup of the corresponding RS -permutation groups (cf. Def. 10.1).

Let us now examine a trigonal pyramidal skeleton **8-1** under the action of the maximum-chiral point group C_3 . Suppose that the three positions of the trigonal pyramidal skeleton **8-1** construct an orbit governed by C_3 ($/C_1$). For the inverse mark table of the point group

C_3 , see Table B.3 of [14]. For the USCI-CF table of C_3 , see Table E.3 of [14]. Thereby, the PCI-CFs are obtained in a formal matrix calculation:

$$(\text{PCI-CF}''(C_1), \text{PCI-CF}''(C_3)) = (b_1^3, b_3) \begin{pmatrix} \frac{1}{3} & 0 \\ -\frac{1}{3} & 1 \end{pmatrix}. \quad (10.154)$$

This equation gives the following PCI-CFs under the action of the the maximum-chiral subgroup C_3 :

$$\text{PCI-CF}''(C_1) = \frac{1}{3}b_1^3 - \frac{1}{3}b_3 \quad (10.155)$$

$$\text{PCI-CF}''(C_3) = b_3. \quad (10.156)$$

The ligand-inventory function b_d (Eq. 10.78) is introduced into the PCI-CFs (Eqs. 10.155 and 10.156). The expansion of the resulting equations give the following generating functions:

$$\begin{aligned} f_{C_1}''' &= \{2(\overline{ABp} + \overline{AB\bar{p}}) + \dots\} + \{2(\overline{Apq} + \overline{A\bar{p}\bar{q}}) + \dots\} \\ &+ \{2(\overline{p\bar{p}q} + \overline{p\bar{p}\bar{q}}) + \dots\} + \{2(\overline{pqr} + \overline{p\bar{q}\bar{q}}) + \dots\} \\ &+ \{(A^2\bar{p} + A^2\bar{\bar{p}}) + \dots\} + \{(A\bar{p}^2 + A\bar{\bar{p}}^2) + \dots\} \\ &+ \{(p^2\bar{p} + p\bar{\bar{p}}^2) + \dots\} + \{(p^2q + p\bar{\bar{q}}^2) + \dots\} \\ &+ 2\overline{ABX} + \{2\overline{A\bar{p}\bar{p}} + \dots\} + \{A^2\bar{B} + \dots\} \end{aligned} \quad (10.157)$$

$$f_{C_3}''' = \{(p^3 + \bar{p}^3) + \dots\} \{A^3 + \dots\}. \quad (10.158)$$

Note that each promolecule is counted once under the action of a maximum-chiral point subgroup. For example, the term $2\overline{ABp}$ ($[\theta]_5$) in the generating function f_{C_1}''' (Eq. 10.157) indicates the presence of two promolecules **10-9** and **10-10**, while the counterpart term $2\overline{AB\bar{p}}$ indicates the presence of two promolecules $\overline{10-9}$ and $\overline{10-10}$. Thus, a quadruplet of a type-III stereoisogram is divided into four promolecules.

The generating functions for the *RS*-stereoisomeric group $C_{3v\bar{\sigma}\bar{\tau}}$ (Eqs. 10.93–10.102) are concerned with numbers of inequivalent quadruplets (or stereoisograms), while the generating functions of the maximum-chiral group C_3 (Eqs. 10.157 and 10.158) are concerned with numbers of inequivalent promolecules. These two types of generating functions are correlated by referring to Fig. 10.9. The following theorem holds true in general according to Fig. 10.9.

Theorem 10.8 (Quadruplets and Respective Promolecules).

- A quadruplet of a type-I stereoisogram consists of two promolecules.
- A quadruplet of a type-II stereoisogram consists of two promolecules.
- A quadruplet of a type-III stereoisogram consists of four promolecules.
- A quadruplet of a type-IV stereoisogram consists of one promolecule.

– A quadruplet of a type-V stereoisogram consists of two promolecules.

The PCI-CFs for the maximum-chiral point group C_3 (Eqs. 10.155 and 10.156) can be calculated from the PCI-CFs for the *RS*-stereoisomeric group $C_{3v\tilde{\sigma}I}$ (Eqs. 10.66–10.75), where Theorem 10.8 requires the multiplication by 4 or by 2 according to type I to V.

$$\begin{aligned} \text{PCI-CF}''(C_1) &= 4\text{PCI-CF}(C_1) + 2\text{PCI-CF}(C_{\tilde{\sigma}}) + 2\text{PCI-CF}(C_{\tilde{I}}) \\ &\quad + 2\text{PCI-CF}(C_s) + \text{PCI-CF}(C_{s\tilde{\sigma}\tilde{I}}) \\ &= \frac{1}{3}b_1^3 - \frac{1}{3}b_3 \end{aligned} \quad (10.159)$$

$$\begin{aligned} \text{PCI-CF}''(C_3) &= 4\text{PCI-CF}(C_3) + 2\text{PCI-CF}(C_{3\tilde{\sigma}}) + 2\text{PCI-CF}(C_{3\tilde{I}}) \\ &\quad + 2\text{PCI-CF}(C_{3v}) + \text{PCI-CF}(C_{3v\tilde{\sigma}\tilde{I}}) \\ &= b_3 \end{aligned} \quad (10.160)$$

The resulting PCI-CFs (Eqs. 10.159 and 10.160) are identical with the PCI-CFs (Eqs. 10.155 and 10.156) obtained directly by Fujita's USCI approach. As for Eq. 10.159, the selected *RS*-stereoisomeric groups satisfy $C_1 \cap C_3 = C_1$, $C_{\tilde{\sigma}} \cap C_3 = C_1$, a $C_{\tilde{I}} \cap C_3 = C_1$, $C_s \cap C_3 = C_1$ and $C_{s\tilde{\sigma}\tilde{I}} \cap C_3 = C_1$. The *RS*-stereoisomeric groups selected for Eq. 10.160 satisfy $C_3 \cap C_3 = C_3$, $C_{3\tilde{\sigma}} \cap C_3 = C_3$, $C_{3\tilde{I}} \cap C_3 = C_3$, $C_{3v} \cap C_3 = C_3$ and $C_{3v\tilde{\sigma}\tilde{I}} \cap C_3 = C_3$.

10.4 *RS*-Stereoisomers as Intermediate Concepts

Before closing this chapter, it is worthwhile to point out the importance of the concept of *stereoisograms* in the theoretical framework of stereoisomerism. A stereoisogram generates a quadruplet of *RS*-stereoisomers, which is an equivalence class under the action of an *RS*-stereoisomeric group. This means that such a quadruplet of *RS*-stereoisomers can be regarded as a new hierarchical item.

In contrast to modern stereochemistry which has adopted the hierarchy of molecular entities — enantiomers — stereoisomers, Fujita's stereoisogram approach has demonstrated the hierarchy of (pro)molecular entities — enantiomers — *RS*-stereoisomers — stereoisomers. Thus, Fujita's stereoisogram approach creates the intermediate concept of *RS*-stereoisomers, which mediates between enantiomers and stereoisomers.

Such an intermediate concept brings about a paradigm shift, so that modern stereochemistry has been restructured substantially on the basis of mathematical formulations. Thus, the hierarchy of modern stereochemistry emphasizes pairs of enantiomers (or achiral molecules), which are based on a single pair of attributes (chirality/achirality). In contrast, the hierarchy of Fujita's stereoisogram approach emphasizes five types of quadruplets of *RS*-stereoisomers, which are based on three pairs of attributes (chirality/achirality, *RS*-stereogenicity/*RS*-astereogenicity, and sclerality/asclerality).

References

- [1] S. Fujita, *J. Org. Chem.*, **69**, 3158–3165 (2004).
- [2] S. Fujita, *J. Math. Chem.*, **35**, 265–287 (2004).
- [3] S. Fujita, *Tetrahedron*, **60**, 11629–11638 (2004).
- [4] S. Fujita, *Theor. Chem. Acc.*, **117**, 353–370 (2007).
- [5] S. Fujita, *Bull. Chem. Soc. Jpn.*, **81**, 193–219 (2008).
- [6] R. S. Cahn, C. K. Ingold, and V. Prelog, *Angew. Chem. Int. Ed. Eng.*, **5**, 385–415 (1966).
- [7] V. Prelog and G. Helmchen, *Angew. Chem. Int. Ed. Eng.*, **21**, 567–583 (1982).
- [8] K. R. Hanson, *J. Am. Chem. Soc.*, **88**, 2731–2742 (1966).
- [9] S. Fujita, *Tetrahedron: Asymmetry*, **25**, 1153–1168 (2014).
- [10] S. Fujita, *Tetrahedron: Asymmetry*, **25**, 1169–1189 (2014).
- [11] S. Fujita, *Tetrahedron: Asymmetry*, **25**, 1190–1204 (2014).
- [12] S. Fujita, *Tetrahedron: Asymmetry*, **25**, 1612–1623 (2014).
- [13] S. Fujita, *MATCH Commun. Math. Comput. Chem.*, **61**, 71–115 (2009).
- [14] S. Fujita, “Symmetry and Combinatorial Enumeration in Chemistry”, Springer-Verlag, Berlin-Heidelberg (1991).
- [15] S. Fujita, *J. Math. Chem.*, **52**, 508–542 (2014).
- [16] S. Fujita, *J. Math. Chem.*, **52**, 543–574 (2014).
- [17] S. Fujita, *Bull. Chem. Soc. Jpn.*, **67**, 2935–2948 (1994).
- [18] S. Fujita, *Theor. Chim. Acta*, **94**, 105–124 (1996).
- [19] S. Fujita, *Proc. Japan Acad. Ser. B*, **77**, 197–202 (2001).
- [20] S. Fujita, *Bull. Chem. Soc. Jpn.*, **63**, 315–327 (1990).
- [21] S. Fujita, *Bull. Chem. Soc. Jpn.*, **63**, 1876–1883 (1990).
- [22] W. Burnside, “Theory of Groups of Finite Order”, 2nd ed., Cambridge University Press, Cambridge (1911).
- [23] S. Fujita, “Combinatorial Enumeration of Graphs, Three-Dimensional Structures, and Chemical Compounds”, University of Kragujevac, Faculty of Science, Kragujevac (2013).
- [24] S. Fujita, *J. Am. Chem. Soc.*, **112**, 3390–3397 (1990).
- [25] S. Fujita, *J. Math. Chem.*, **5**, 99–120 (1990).
- [26] S. Fujita, *Theor. Chem. Acc.*, **113**, 73–79 (2005).
- [27] S. Fujita, *Theor. Chem. Acc.*, **113**, 80–86 (2005).
- [28] S. Fujita, *Theor. Chem. Acc.*, **115**, 37–53 (2006).

11 Stereoisograms for Tetrahedral Derivatives¹

11.1 *RS*-Stereoisomeric Group $T_{d\widehat{\sigma\hat{I}}}$ and Elementary Stereoisogram

Tetrahedral promolecules enumerated under the point group T_d are listed in Fig. 6.9 (page 157), where a pair of (self-)enantiomers is counted once as an equivalence class under T_d . On the other hand, tetrahedral promolecules enumerated under the *RS*-permutation group $T_{\widehat{\sigma}}$ are listed in Fig. 9.10 (page 255), where a pair of (self-)*RS*-diastereomers is counted once as an equivalence class under $T_{\widehat{\sigma}}$. In this chapter, the point group T_d and the *RS*-permutation group $T_{\widehat{\sigma}}$ are integrated into an *RS*-stereoisomeric group $T_{d\widehat{\sigma\hat{I}}}$ according to the discussions of Chapter 10 on Fujita's stereoisogram approach.

The point group T_d (cf. Table 3.1 on page 61), the *RS*-permutation group $T_{\widehat{\sigma}}$ (cf. Table 9.4 on page 253), and the ligand-reflection group $T_{\widehat{\Gamma}}$ have a common subgroup T , as summarized in the following coset decompositions:

$$T_d = \underset{\mathbf{A}}{T} + \underset{\mathbf{B}}{T\sigma} \quad (11.1)$$

$$T_{\widehat{\sigma}} = \underset{\mathbf{A}}{T} + \underset{\mathbf{C}}{T\widehat{\sigma}} \quad (11.2)$$

$$T_{\widehat{\Gamma}} = \underset{\mathbf{A}}{T} + \underset{\mathbf{D}}{T\widehat{\Gamma}}. \quad (11.3)$$

These three groups are integrated into an *RS*-stereoisomeric group $T_{d\widehat{\sigma\hat{I}}}$ as follows:

$$T_{d\widehat{\sigma\hat{I}}} = \underset{\mathbf{A}}{T} + \underset{\mathbf{B}}{T\sigma} + \underset{\mathbf{C}}{T\widehat{\sigma}} + \underset{\mathbf{D}}{T\widehat{\Gamma}}, \quad (11.4)$$

which represents the coset decomposition of $T_{d\widehat{\sigma\hat{I}}}$ by T .

The operations of $T_{d\widehat{\sigma\hat{I}}}$ and the coset representation $T_{d\widehat{\sigma\hat{I}}}/(C_{3v\widehat{\sigma\hat{I}}})$ are listed in Table 11.1, where the symbols \mathbf{A} , \mathbf{B} , \mathbf{C} , and \mathbf{D} correspond to the respective cosets appearing in Eq. 11.4. For the \mathbf{A} - and \mathbf{B} -parts, see Table 3.1 of the point group T_d . For the \mathbf{A} - and \mathbf{C} -parts, see Table 9.4 of the *RS*-permutation group $T_{\widehat{\sigma}}$. Detailed discussions in [1] have indicated that the *RS*-stereoisomeric group $T_{d\widehat{\sigma\hat{I}}}$ is isomorphic to the point group O_h , so that the coset representations $T_{d\widehat{\sigma\hat{I}}}/(C_{3v\widehat{\sigma\hat{I}}})$ and $O_h/(D_{3d})$ consist of an identical set of permutations.

Suppose that the four positions of the tetrahedral skeleton **3-5** (page 55) are controlled by the *RS*-stereoisomeric group $T_{d\widehat{\sigma\hat{I}}}$ through the coset representation $T_{d\widehat{\sigma\hat{I}}}/(C_{3v\widehat{\sigma\hat{I}}})$. The

¹ This chapter is based on S. Fujita, "Symmetry-Itemized Enumeration of Quadruplets of *RS*-Stereoisomers: I — The Fixed-Point Matrix Method of the USCI Approach Combined with the Stereoisogram Approach", *J. Math. Chem.*, **52**, 508–542 (2014); S. Fujita, "Symmetry-Itemized Enumeration of Quadruplets of *RS*-Stereoisomers: II — The Partial-Cycle-Index Method of the USCI Approach Combined with the Stereoisogram Approach", *J. Math. Chem.*, **52**, 543–574 (2014); and S. Fujita, "Stereoisograms for Reorganizing the Theoretical Foundations of Stereochemistry and Stereoisomerism: I. Diagrammatic Representations of *RS*-Stereoisomeric Groups for Integrating Point Groups and *RS*-Permutation Groups", *Tetrahedron: Asymmetry*, **25**, 1153–1168 (2014).

Table 11.1. Operations of $T_{d\tilde{\sigma}\tilde{\tau}}$ and Coset Representation of $T_{d\tilde{\sigma}\tilde{\tau}}(/C_{3v\tilde{\sigma}\tilde{\tau}})$ vs. Operations of O_h and Coset Representation of $O_h(/D_{3d})$

operation		$O_h(/D_{3d})$ or $T_{d\tilde{\sigma}\tilde{\tau}}(/C_{3v\tilde{\sigma}\tilde{\tau}})$	PSI	operation		$O_h(/D_{3d})$ or $T_{d\tilde{\sigma}\tilde{\tau}}(/C_{3v\tilde{\sigma}\tilde{\tau}})$	PSI
$g \in O_h$	$g \in T_{d\tilde{\sigma}\tilde{\tau}}$	(product of cycles)		$g \in O_h$	$g \in T_{d\tilde{\sigma}\tilde{\tau}}$	(product of cycles)	
I	I	(1)(2)(3)(4)	b_1^4	$C'_{2(6)}$	$\tilde{\sigma}_{d(1)}$	(1)(2 4)(3)	$b_1^2 b_2$
$C_{2(1)}$	$C_{2(1)}$	(1 2)(3 4)	b_2^2	$C'_{2(1)}$	$\tilde{\sigma}_{d(6)}$	(1 3)(2)(4)	$b_1^2 b_2$
$C_{2(2)}$	$C_{2(2)}$	(1 4)(2 3)	b_2^2	$C'_{2(4)}$	$\tilde{\sigma}_{d(5)}$	(1 4)(2)(3)	$b_1^2 b_2$
$C_{2(3)}$	$C_{2(3)}$	(1 3)(2 4)	b_2^2	$C'_{2(2)}$	$\tilde{\sigma}_{d(2)}$	(1)(2)(3 4)	$b_1^2 b_2$
$C_{3(1)}$	$C_{3(1)}$	(1)(2 3 4)	$b_1 b_3$	$C'_{2(5)}$	$\tilde{\sigma}_{d(3)}$	(1)(2 3)(4)	$b_1^2 b_2$
$C_{3(3)}$	$C_{3(3)}$	(1 3 4)(3)	$b_1 b_3$	$C'_{2(3)}$	$\tilde{\sigma}_{d(4)}$	(1 2)(3)(4)	$b_1^2 b_2$
$C_{3(2)}$	$C_{3(2)}$	(1 4 3)(2)	$b_1 b_3$	$C_{4(3)}$	$\tilde{S}_{4(3)}$	(1 2 3 4)	b_4
$C_{3(4)}$	$C_{3(4)}$	(1 3 2)(4)	$b_1 b_3$	$C_{4(3)}$	$\tilde{S}_{4(3)}$	(1 4 3 2)	b_4
$C_{3(1)}^2$	$C_{3(1)}^2$	(1)(2 4 3)	$b_1 b_3$	$C_{4(1)}$	$\tilde{S}_{4(1)}$	(1 4 2 3)	b_4
$C_{3(4)}^2$	$C_{3(4)}^2$	(1 2 3)(4)	$b_1 b_3$	$C_{4(1)}$	$\tilde{S}_{4(1)}$	(1 3 2 4)	b_4
$C_{3(3)}^2$	$C_{3(3)}^2$	(1 4 2)(3)	$b_1 b_3$	$C_{4(2)}$	$\tilde{S}_{4(2)}$	(1 2 4 3)	b_4
$C_{3(2)}^2$	$C_{3(2)}^2$	(1 3 4)(2)	$b_1 b_3$	$C_{4(2)}$	$\tilde{S}_{4(2)}$	(1 3 4 2)	b_4
$\sigma_{d(1)}$	$\sigma_{d(1)}$	$\overline{(1)(2 4)(3)}$	$a_1^2 c_2$	i	\hat{I}	$\overline{(1)(2)(3)(4)}$	a_1^4
$\sigma_{d(6)}$	$\sigma_{d(6)}$	$\overline{(1 3)(2)(4)}$	$a_1^2 c_2$	$\sigma_{h(3)}$	$\hat{C}_{2(1)}$	$\overline{(1 2)(3 4)}$	c_2^2
$\sigma_{d(2)}$	$\sigma_{d(2)}$	$\overline{(1)(2)(3 4)}$	$a_1^2 c_2$	$\sigma_{h(2)}$	$\hat{C}_{2(2)}$	$\overline{(1 4)(2 3)}$	c_2^2
$\sigma_{d(4)}$	$\sigma_{d(4)}$	$\overline{(1 2)(3)(4)}$	$a_1^2 c_2$	$\sigma_{h(1)}$	$\hat{C}_{2(3)}$	$\overline{(1 3)(2 4)}$	c_2^2
$\sigma_{d(3)}$	$\sigma_{d(3)}$	$\overline{(1)(2 3)(4)}$	$a_1^2 c_2$	$S_{6(1)}^5$	$\hat{C}_{3(1)}$	$\overline{(1)(2 3 4)}$	$a_1 a_3$
$\sigma_{d(5)}$	$\sigma_{d(5)}$	$\overline{(1 4)(2)(3)}$	$a_1^2 c_2$	$S_{6(3)}^5$	$\hat{C}_{3(3)}$	$\overline{(1 4 2)(3)}$	$a_1 a_3$
$S_{4(3)}$	$S_{4(3)}$	$\overline{(1 2 3 4)}$	c_4	$S_{6(2)}^5$	$\hat{C}_{3(2)}$	$\overline{(1 4 3)(2)}$	$a_1 a_3$
$S_{4(3)}^3$	$S_{4(3)}^3$	$\overline{(1 4 3 2)}$	c_4	$S_{6(4)}^5$	$\hat{C}_{3(4)}$	$\overline{(1 2 3)(4)}$	$a_1 a_3$
$S_{4(1)}$	$S_{4(1)}$	$\overline{(1 4 2 3)}$	c_4	$S_{6(1)}$	$\hat{C}_{3(1)}$	$\overline{(1)(2 4 3)}$	$a_1 a_3$
$S_{4(1)}^3$	$S_{4(1)}^3$	$\overline{(1 3 2 4)}$	c_4	$S_{6(4)}$	$\hat{C}_{3(4)}^2$	$\overline{(1 3 2)(4)}$	$a_1 a_3$
$S_{4(2)}$	$S_{4(2)}$	$\overline{(1 2 4 3)}$	c_4	$S_{6(3)}$	$\hat{C}_{3(3)}$	$\overline{(1 2 4)(3)}$	$a_1 a_3$
$S_{4(2)}^3$	$S_{4(2)}^3$	$\overline{(1 3 4 2)}$	c_4	$S_{6(2)}$	$\hat{C}_{3(2)}$	$\overline{(1 3 4)(2)}$	$a_1 a_3$

twelve operations listed in the **A**-part of Table 11.1 (or the coset \mathbf{TI} ($= \mathbf{T}$) of Eq. 11.4) generate a reference-numbered skeleton **11-1** and its homomeric skeletons, where they are equivalent under the subgroup \mathbf{T} (cf. Theorem 10.2 on page 279). The reference-numbered skeleton **11-1** is placed in the upper-left corner of Fig. 11.1, which is an elementary stereoisogram for **11-1** ($= \mathbf{3-5}$). The twelve operations listed in the **B**-part of Table 11.1 (or the coset $\mathbf{T}\sigma$ of Eq. 11.4) generate a mirror-numbered skeleton **11-1** and its homomeric skeletons, where they are equivalent under the subgroup \mathbf{T} . The twelve operations listed in the **C**-part of Table 11.1 (or the coset $\mathbf{T}\tilde{\sigma}$ of Eq. 11.4) generate an *RS*-numbered skeleton **11-2** and its homomeric skeletons, where they are equivalent under the subgroup \mathbf{T} . The twelve operations listed in the **D**-part of Table 11.1 (or the coset $\mathbf{T}\hat{I}$ of Eq. 11.4) generate an *LM*-numbered

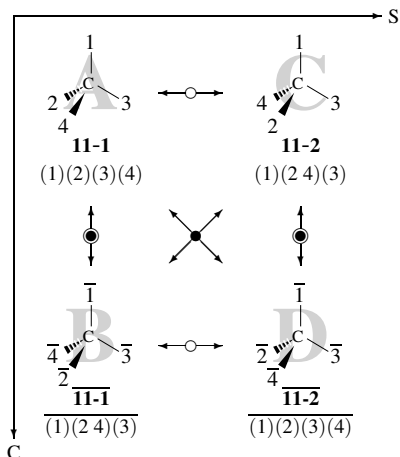


Fig. 11.1. Elementary stereoisogram of numbered tetrahedral skeletons. The other modes of sequential numbering are permitted without losing generality.

skeleton $\overline{11-2}$ and its homomeric skeletons, where they are equivalent under the subgroup T . The quadruplet of $11-1/\overline{11-1}/11-2/\overline{11-2}$ is arranged to give an elementary stereoisogram shown in Fig. 11.1.

Suppose that the four positions of the tetrahedral skeleton $3-5$ ($= 11-1$) are substituted by a set of proligands selected from a ligand inventory L (Eq. 6.73 on page 153). To survey stereoisograms generated from the tetrahedral skeleton, Fig. 11.2 collects reference promolecules for constructing stereoisograms [2, Fig. 1]. When each promolecule listed in Fig. 11.2 is placed to fill the four positions of the reference skeleton $11-1$, there appears a quadruplet of promolecules according to the elementary stereoisogram of Fig. 11.1.

11.2 Stereoisograms of Five Types for Tetrahedral Derivatives

The list of stereoisograms of five types (Fig. 10.9 on page 288) is effective to tetrahedral derivatives.

11.2.1 Type-I Stereoisograms of Tetrahedral Derivatives

When a promolecule $11-3$ with the composition $ABXY$ is selected as a reference from Fig. 11.2, the elementary stereoisogram (Fig. 11.1) generates a type-I stereoisogram shown in Fig. 11.3, which is characterized by the presence of diagonal equality symbols.

The promolecule $11-3$ shown in Fig. 11.2 is attached by a pair of square brackets [C_7 , C_1 , C_1 ;], which indicates the RS -stereoisomeric group C_7 , the point group C_1 , and the RS -

	<i>RS</i> -astereogenic	<i>RS</i> -stereogenic
chiral	<p style="text-align: center;">Type II</p>	<p style="text-align: center;">Type I</p>
	<p style="text-align: center;">Type III</p>	<p style="text-align: center;">Type III</p>
achiral	<p style="text-align: center;">Type IV</p>	<p style="text-align: center;">Type V</p>

Fig. 11.2. Reference promolecules of quadruplets of *RS*-stereoisomers (Types I to V) for tetrahedral promolecules. The symbols A, B, X, and Y represent atoms or achiral ligands. The symbols p, q, r, and s represents chiral ligands, while each symbol with an overbar represents the corresponding chiral ligand with the opposite chirality. An arbitrary promolecule is depicted as a representative of each quadruplet of *RS*-stereoisomers. The compound number and its partition is attached to each promolecule. The *RS*-stereoisomeric group, the point group, the *RS*-permutation group, and the stereoisogram type are placed in a bracket attached to each promolecule. A gray box is drawn to show a chirality-unfaithful case [3].

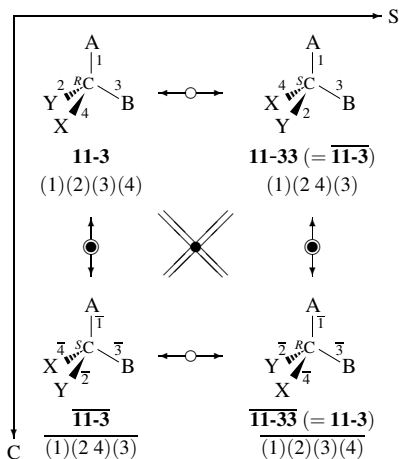


Fig. 11.3. Stereoisogram of type I on the basis of a tetrahedral skeleton. The promolecule **11-3** belongs to the RS -stereoisomeric group C_7 and to the point group C_1 . A pair of R/S -stereodescriptors, 'R' and 'S', is assigned to a pair of RS -diastereomers **11-3/11-33** (or $\overline{\mathbf{11-3}}/\mathbf{11-33}$) where the priority sequence $A > B > X > Y$ is presumed.

permutation group C_1 , and a stereoisogram type (type I). Note that the RS -stereoisomeric group $C_7 (= \{I, \hat{I}\})$ corresponds to the equality symbols located in the diagonal directions of the type-I stereoisogram shown in Fig. 11.3.

The other promolecule **11-4** with the composition $p\bar{p}q\bar{q}$ in the type-I frame of Fig. 11.2 generates a type-I stereoisogram in a similar way to Fig. 11.3.

Exercise 11.1. Draw a stereoisogram of **11-4** with the composition $p\bar{p}q\bar{q}$. Confirm that the resulting stereoisogram belongs to type I.

11.2.2 Type-II Stereoisograms of Tetrahedral Derivatives

An enantiomeric pair of chiral 2,3,4-trihydroxyglutaric acids **11-34** and $\overline{\mathbf{11-34}}$ can be regarded as an enantiomeric pair of promolecules **11-14** and $\overline{\mathbf{11-14}}$, which have the compositions ABp^2 and $AB\bar{p}^2$ respectively, if we focus our attention to the central 3-carbon atom. When the promolecule **11-14** with the composition ABp^2 is selected as a reference, the elementary stereoisogram (Fig. 11.1) generates a type-II stereoisogram shown in Fig. 11.4, which is characterized by the presence of horizontal equality symbols.

The promolecule **11-14** shown in Fig. 11.2 is attached by a pair of square brackets $[C_{\tilde{\sigma}}, C_1, C_{\tilde{\sigma}}; II]$. The RS -stereoisomeric group $C_{\tilde{\sigma}} (= \{I, \tilde{\sigma}_{d(1)}\})$ corresponds to the equality symbols located in the horizontal directions of the type-II stereoisogram shown in Fig. 11.4.

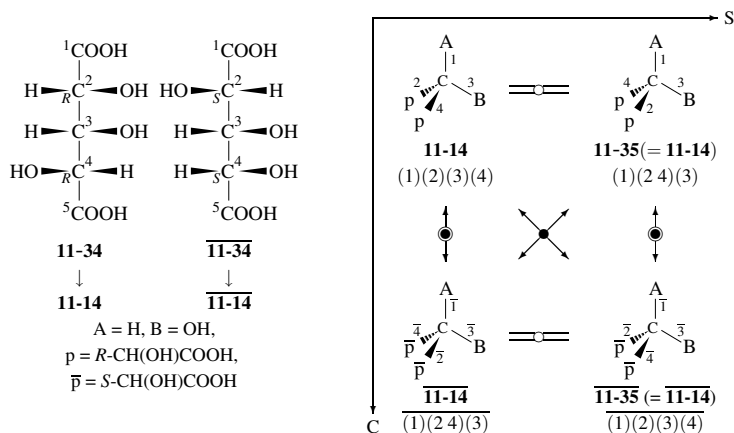


Fig. 11.4. Stereoisogram of type II on the basis of a tetrahedral skeleton. The promolecule **11-14** belongs to the RS -stereoisomeric group $C_{\bar{S}}$ and to the point group C_1 .

The promolecules **11-5–11-19** in the type-II frame of Fig. 11.2 generate type-II stereoisograms in a similar way to Fig. 11.4.



Exercise 11.2. Draw a stereoisogram for an appropriate promolecule selected from **11-5–11-19**. Confirm that the resulting stereoisogram belongs to type II.

11.2.3 Type-III Stereoisograms of Tetrahedral Derivatives

When a promolecule **11-20** with the composition $ABXp$ is selected as a reference from Fig. 11.2, the elementary stereoisogram (Fig. 11.1) generates a type-III stereoisogram shown in Fig. 11.5, which is characterized by the absence of equality symbols in any directions. The promolecule $\overline{\mathbf{11-20}}$ has the composition $ABX\overline{p}$, because it is enantiomeric to the reference promolecule **11-20**. The promolecule **11-36** has the composition $ABXp$, because it is RS -diastereomeric to the reference promolecule **11-20**. The promolecule $\overline{\mathbf{11-36}}$ has the composition $ABX\overline{p}$, because it is holantimeric to the reference promolecule **11-20**. The four promolecules are different molecular entities from each other.

The promolecule **11-20** shown in Fig. 11.2 is attached by a pair of square brackets [C_1 , C_1 , C_1 ; III]. The RS -stereoisomeric group $C_1 (= \{I\})$ corresponds to the absence of equality symbols in any directions, as found in the type-III stereoisogram of Fig. 11.5.

The promolecules **11-20–11-25** in the type-III frame of Fig. 11.2 generate type-III stereoisograms in a similar way to Fig. 11.5.

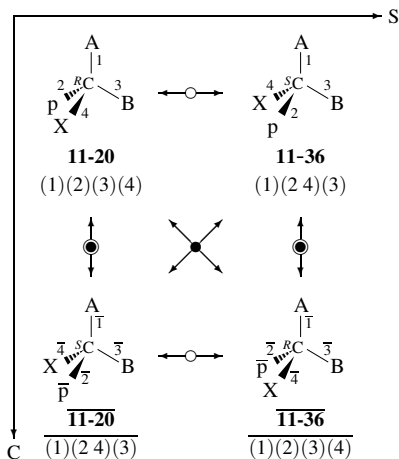



Fig. 11.5. Chirality-faithful stereoisogram of type III on the basis of a tetrahedral skeleton. The promolecule **11-20** belongs to the RS -stereoisomeric group C_1 and to the point group C_1 . A pair of R/S -stereodescriptors, ' R ' and ' S ', is assigned to a pair of RS -diastereomers **11-20/11-36** (or $\overline{11-20}/\overline{11-36}$), where the priority sequence $A > B > X > p$ (or $A > B > X > \bar{p}$) is presumed. Thus, this stereoisogram exhibits chirality faithfulness. The same pair of R/S -stereodescriptors is obtained by presuming the priority sequence $A > p > B > X$ (or $A > \bar{p} > B > X$).

Exercise 11.3. Draw a stereoisogram for an appropriate promolecule selected from **11-20–11-25**. Confirm that the resulting stereoisogram belongs to type III. 

11.2.4 Type-IV Stereoisograms of Tetrahedral Derivatives

When a promolecule **11-30** with the composition A^2BX is selected as a reference from Fig. 11.2, the elementary stereoisogram (Fig. 11.1) generates a type-IV stereoisogram shown in Fig. 11.6, which is characterized by the presence of equality symbols in all directions. Hence, the resulting quadruplet of promolecules degenerates into a single achiral promolecule.

The promolecule **11-30** shown in Fig. 11.2 is attached by a pair of square brackets [$C_{s\hat{\sigma}I}$, C_s , $C_{\hat{\sigma}}$; IV]. The RS -stereoisomeric group $C_{s\hat{\sigma}I}$ ($= \{I, \tilde{\sigma}_{d(1)}, \hat{I}, \sigma_{d(1)}\}$) corresponds to the presence of equality symbols in all directions, as found in the type-IV stereoisogram of Fig. 11.6.

The promolecules **11-26–11-31** in the type-IV frame of Fig. 11.2 generate type-IV stereoisograms in a similar way to Fig. 11.6.

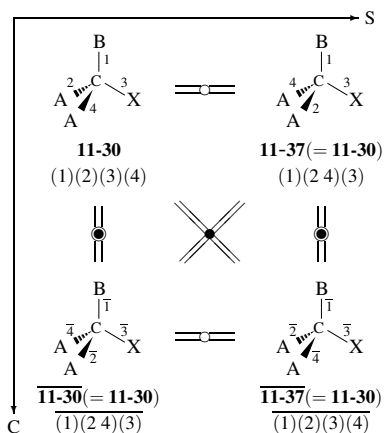


Fig. 11.6. Stereoisogram of type IV on the basis of a tetrahedral skeleton. The promolecule **11-30** belongs to the RS -stereoisomeric group $C_{s\hat{\sigma}_I}$ and to the point group C_s .



Exercise 11.4. Draw a stereoisogram for an appropriate promolecule selected from **11-26–11-31**. Confirm that the resulting stereoisogram belongs to type IV.

11.2.5 Type-V Stereoisograms of Tetrahedral Derivatives

Two achiral 2,3,4-trihydroxyglutaric acids **11-38** and **11-39** can be regarded as an RS -diastereomeric pair of promolecules **11-32** and **11-40** which have the same composition $AB\bar{p}\bar{p}$, if we focus our attention to the central 3-carbon atom. When the promolecule **11-32** is selected as a reference, the elementary stereoisogram (Fig. 11.1) generates a type-V stereoisogram shown in Fig. 11.7, which is characterized by the presence of vertical equality symbols.

The promolecule **11-32** shown in Fig. 11.2 is attached by a pair of square brackets [C_s , C_s , C_1 ; V]. The RS -stereoisomeric group C_s ($= \{I, \sigma_{d(1)}\}$) is a subgroup of T_d and of $T_{d\hat{\sigma}_I}$, so that it corresponds to the presence of vertical equality symbols, as found in the type-V stereoisogram of Fig. 11.7.

It should be noted that the type-V frame of Fig. 6.9 (page 157) indicates that there appear two promolecules **6-100** and **6-101** under the action of point group T_d , whereas they degenerate to give a single representative **11-32**, as found in the type-V frame of Fig. 11.2. Thus, the single representative **11-32** produces a quadruplet of Fig. 11.7 under the action of the RS -stereoisomeric group $T_{d\hat{\sigma}_I}$, where the quadruplet consists of a pair of RS -diastereomers **11-32/11-40** ($=$ **6-100/6-101**).

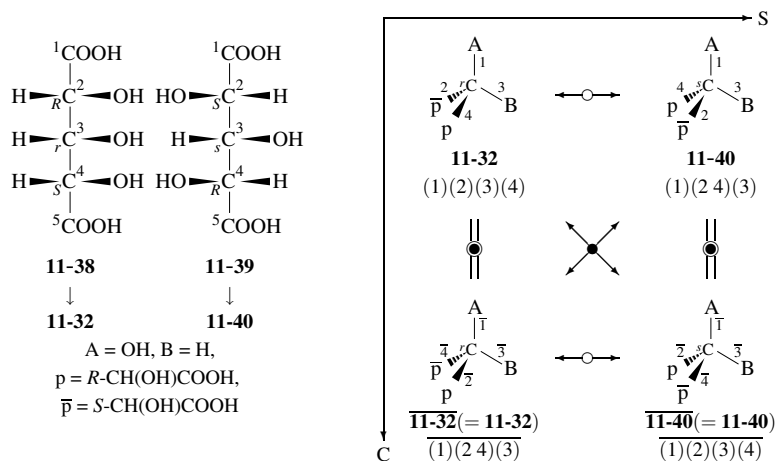


Fig. 11.7. Stereoisogram of type V on the basis of a tetrahedral skeleton. The promolecule **11-32** belongs to the RS -stereoisomeric group C_s and the point group C_s . A pair of R/S -stereodescriptors, 'r' and 's', is assigned to a pair of RS -diastereomers **11-32/11-40**, where the priority sequence $A > B > p > \bar{p}$ (or $A > p > \bar{p} > B$) is presumed. The lowercase letters are used because of chirality unfaithfulness.

Exercise 11.5. Compare the group C_s under the action of the point group T_d with the group C_s under the action of the RS -stereoisomeric group $T_{d\hat{\sigma}I}$. Note that **6-100** and **6-101** are inequivalent under the point group T_d . In contrast, they (= **11-32** and **11-40**) are bundled into a single quadruplet, which is regarded as an equivalence class under the RS -stereoisomeric group $T_{d\hat{\sigma}I}$ (cf. Fig. 11.7).

Remark 11.1. When we consider an RS -stereoisomeric group such as $T_{d\hat{\sigma}I}$, a quadruplet of promolecules such as Fig. 11.7 is regarded as a single entity to be discussed, i.e., an equivalence class under the RS -stereoisomeric group. The action of the RS -stereoisomeric group $T_{d\hat{\sigma}I}$ on the quadruplet (e.g., Fig. 11.7 of type V) results in the stabilization (fixation) of the quadruplet by a subgroup of $T_{d\hat{\sigma}I}$. In the case of Fig. 11.7, the subgroup C_s ($\subset T_{d\hat{\sigma}I}$) stabilizes the quadruplet.

On the other hand, when we consider a point group such as T_d , each pair of (self-)enantiomeric promolecules in a stereoisogram (e.g., each of the two achiral promolecules in Fig. 11.7) is regarded as an entity to be discussed, i.e., an equivalence class under the point group. The action of the point group T_d on each pair of (self-)enantiomeric promolecules in the stereoisogram (Fig. 11.7) results in the stabilization (fixation) of the pair of (self-)enantiomers by a subgroup of T_d . In the case of Fig. 11.7, the subgroup C_s ($\subset T_d$) stabilizes the pair of (self-)enantiomers.

It should be noted that C_s as a subgroup of the RS -stereoisomeric group $T_{d\widehat{\sigma}\widehat{\tau}}$ is distinct from C_s as a subgroup of the point group T_d in target entities, i.e., a quadruplet vs. pairs of (self-)enantiomers in a stereoisogram.

11.3 Enumeration Under the RS -Stereoisomeric Group $T_{d\widehat{\sigma}\widehat{\tau}}$

The FPM method of the USCI approach has been extended to support RS -stereoisomeric groups and applied to enumeration under the RS -stereoisomeric group $T_{d\widehat{\sigma}\widehat{\tau}}$ [1]. As discussed in Section 10.2, the PCI method has been extended to accomplish the same purpose [4]. As a continuation of Section 10.2, we adopt the extended PCI method in enumeration under $T_{d\widehat{\sigma}\widehat{\tau}}$ in this section,

11.3.1 Non-Redundant Set of Subgroups and Five Types of Subgroups

The RS -stereoisomeric group $T_{d\widehat{\sigma}\widehat{\tau}}$ is isomorphic to the point group O_h [1]. The point group O_h has the following non-redundant set of subgroups (SSG) [5]:

$$\text{SSG}_{O_h} = \left\{ \begin{array}{l} 1, 2, 3, 4, 5, 6, 7, 8, 9, 10, 11, 12, 13, 14, 15, 16 \\ C_1, C_2, C_2', C_s, C_s', C_i, C_3, C_4, S_4, D_2, D_2', C_{2v}, C_{2v}', C_{2v}'', C_{2h}, C_{2h}', \\ 17, 18, 19, 20, 21, 22, 23, 24, 25, 26, 27, 28, 29 \\ D_3, C_{3v}, C_{3i}, D_4, C_{4v}, C_{4h}, D_{2d}, D_{2d}', D_{2h}, D_{2h}', T, D_{3d}, D_{4h}, \\ 30, 31, 32, 33 \\ O, T_h, T_d, O_h \end{array} \right\}, \quad (11.5)$$

where the subgroups are aligned in the ascending order of their orders. In a parallel way, a non-redundant set of subgroups (SSG) for $T_{d\widehat{\sigma}\widehat{\tau}}$ is obtained as follows [1]:

$$\text{SSG}_{T_{d\widehat{\sigma}\widehat{\tau}}} = \left\{ \begin{array}{l} 1, 2, 3, 4, 5, 6, 7, 8, 9, 10, 11, 12, 13, 14, 15, 16 \\ C_1, C_2, C_{\widehat{\sigma}}, C_{\widehat{\sigma}}, C_s, C_{\widehat{\tau}}, C_3, S_4, S_4, D_2, C_{2\widehat{\sigma}}, C_{2\widehat{\sigma}}, C_{2v}, C_{s\widehat{\sigma}\widehat{\sigma}}, C_{2\widehat{\tau}}, C_{s\widehat{\sigma}\widehat{\tau}}, \\ 17, 18, 19, 20, 21, 22, 23, 24, 25, 26, 27, 28, 29 \\ C_{3\widehat{\sigma}}, C_{3v}, C_{3\widehat{\tau}}, D_{2\widehat{\sigma}}, S_{4\widehat{\sigma}}, S_{4\widehat{\tau}}, D_{2d}, S_{4\widehat{\sigma}\widehat{\sigma}}, D_{2\widehat{\tau}}, C_{2v\widehat{\sigma}\widehat{\tau}}, T, C_{3v\widehat{\sigma}\widehat{\tau}}, D_{2d\widehat{\sigma}\widehat{\tau}}, \\ 30, 31, 32, 33 \\ T_{\widehat{\sigma}}, T_{\widehat{\tau}}, T_d, T_{d\widehat{\sigma}\widehat{\tau}} \end{array} \right\}, \quad (11.6)$$

where the subgroups are aligned in the ascending order of their orders. For the convenience of cross reference, sequential numbers from 1 to 33 are attached to the respective subgroups. According to the discussion of [1], the 33 subgroups of $\text{SSG}_{T_{d\widehat{\sigma}\widehat{\tau}}}$ are categorized into five types:

$$\text{Type I: SG}^{[1]} = \{ C_{\widehat{\sigma}}, C_{\widehat{\tau}}, C_{2\widehat{\sigma}}, C_{2\widehat{\tau}}, C_{3\widehat{\tau}}, D_{2\widehat{\tau}}, T_{\widehat{\tau}} \} \quad (11.7)$$

$$\text{Type II: } SG^{[II]} = \{C_{\tilde{\sigma}}^3, S_{\tilde{\sigma}}^8, C_{2\tilde{\sigma}}^{11}, C_{3\tilde{\sigma}}^{17}, D_{2\tilde{\sigma}}^{20}, T_{\tilde{\sigma}}^{30}\} \quad (11.8)$$

$$\text{Type III: } SG^{[III]} = \{C_1, C_2, C_3, D_2, T\} \quad (11.9)$$

$$\text{Type IV: } SG^{[IV]} = \{C_{s\tilde{\sigma}\hat{\tau}}^{14}, C_{s\tilde{\sigma}\hat{\tau}}^{16}, C_{s\tilde{\sigma}\hat{\tau}}^{21}, C_{s\tilde{\sigma}\hat{\tau}}^{22}, C_{s\tilde{\sigma}\hat{\tau}}^{24}, C_{2v\tilde{\sigma}\hat{\tau}}^{26}, C_{3v\tilde{\sigma}\hat{\tau}}^{28}, D_{2d\tilde{\sigma}\hat{\tau}}^{29}, T_{d\tilde{\sigma}\hat{\tau}}^{33}\} \quad (11.10)$$

$$\text{Type V: } SG^{[V]} = \{C_s, S_4, C_{2v}, C_{3v}, D_{2d}, T_d\}, \quad (11.11)$$

which correspond to stereoisograms of five types shown in Fig. 11.2. Note that each subgroup of type I (Eq. 11.7) is characterized by a subscript containing a hat accent; each subgroup of type II (Eq. 11.8) is characterized by a subscript containing a tilde accent; each subgroup of type III (Eq. 11.8) is contained in T and characterized by a subscript containing no accents; each subgroup of type IV (Eq. 11.10) is characterized by a subscript containing both hat and tilde accents; and each subgroup of type V (Eq. 11.11) is contained in T_d and characterized by a subscript containing no accents.

Because we find that T_d is a common subgroup of O_h and $T_{d\tilde{\sigma}\hat{\tau}}$ and because we find the correspondence between $T_d (\subset O_h)$ and $T_{\tilde{\sigma}} (\subset T_{d\tilde{\sigma}\hat{\tau}})$ as well as between $T_h (\subset O_h)$ and $T_{\hat{\tau}} (\subset T_{d\tilde{\sigma}\hat{\tau}})$, we are able to construct each subgroup by referring to the five types shown in Eqs. 11.7–11.11:

- (Type-III Subgroups) The subgroups categorized to type III (Eq. 11.9) are identical with the five subgroups of the point group T :

$$C_1 \stackrel{1}{=} \{I\} \quad (11.12)$$

$$C_2 \stackrel{2}{=} \{I, C_{2(1)}\} \quad (11.13)$$

$$C_3 \stackrel{7}{=} \{I, C_{3(1)}, C_{3(1)}^2\} \quad (11.14)$$

$$D_2 \stackrel{10}{=} \{I, C_{2(1)}, C_{2(2)}, C_{2(3)}\} \quad (11.15)$$

$$T \stackrel{27}{=} \{A\} \quad (11.16)$$

- (Type-V Subgroups) The subgroups categorized to type V (Eq. 11.11) are identical with the six subgroups of T_d (except those of T):

$$C_s \stackrel{5}{=} \{I, \sigma_{d(1)}\} \quad (11.17)$$

$$S_4 \stackrel{9}{=} \{I, S_{4(3)}, C_{2(3)}, S_{4(3)}^3\} \quad (11.18)$$

$$C_{2v} \stackrel{13}{=} \{I, C_{2(3)}, \sigma_{d(1)}, \sigma_{d(6)}\} \quad (11.19)$$

$$C_{3v} \stackrel{18}{=} \{I, C_{3(1)}, C_{3(1)}^2, \sigma_{d(1)}, \sigma_{d(2)}, \sigma_{d(3)}\} \quad (11.20)$$

$$D_{2d} \stackrel{23}{=} \{I, C_{2(1)}, C_{2(2)}, C_{2(3)}, \sigma_{d(1)}, \sigma_{d(6)}, S_{4(3)}, S_{4(3)}^3\} \quad (11.21)$$

$$T_d \stackrel{32}{=} \{A, B\} \quad (11.22)$$

- (Type-II Subgroups) The subgroups categorized to type II (Eq. 11.8) are the subgroups of $T_{\tilde{\sigma}}$ ($-T$):

$$C_{\tilde{\sigma}} \stackrel{3}{=} \{I, \tilde{\sigma}_{d(1)}\} \quad (\supset C_1) \quad (11.23)$$

$$\mathbf{S}_4^8 \equiv \{I, \tilde{S}_{4(3)}, C_{2(3)}, \tilde{S}_{4(3)}^3\} \quad (\supset C_2) \quad (11.24)$$

$$\mathbf{C}_{2\tilde{\sigma}}^{11} \equiv \{I, C_{2(3)}, \tilde{\sigma}_{d(1)}, \tilde{\sigma}_{d(6)}\} \quad (\supset C_2) \quad (11.25)$$

$$\mathbf{C}_{3\tilde{\sigma}}^{17} \equiv \{I, C_{3(1)}, C_{3(1)}^2, \tilde{\sigma}_{d(1)}, \tilde{\sigma}_{d(2)}, \tilde{\sigma}_{d(3)}\} \quad (\supset C_3) \quad (11.26)$$

$$\mathbf{D}_{2\tilde{\sigma}}^{20} \equiv \{I, C_{2(1)}, C_{2(2)}, C_{2(3)}, \tilde{\sigma}_{d(1)}, \tilde{\sigma}_{d(6)}, \tilde{S}_{4(3)}, \tilde{S}_{4(3)}^3\} \quad (\supset D_2) \quad (11.27)$$

$$\mathbf{T}_{\tilde{\sigma}}^{30} \equiv \{A, C\} \quad (\supset T) \quad (11.28)$$

which correspond to the six subgroups of \mathbf{O} (except those of \mathbf{T}). Each of the symbols contains a tilde accent in its suffix. For example, the symbol $\mathbf{C}_{2\tilde{\sigma}}$ stems from the largest subgroup \mathbf{C}_2 (as a common subgroup to \mathbf{T}_d) and from an uncommon operation $\tilde{\sigma}_{d(1)}$. The symbol \mathbf{S}_4^8 is adopted for the purpose of avoiding the confusion with $\mathbf{C}_{2\tilde{\sigma}}$.

4. (Type-I Subgroups) The subgroups categorized to type I (Eq. 11.7) are the subgroups of $\mathbf{T}_{\hat{\gamma}}(-\mathbf{T})$:

$$\mathbf{C}_{\hat{\sigma}}^4 \equiv \{I, \hat{C}_{2(3)}\} \quad (\supset C_1) \quad (11.29)$$

$$\mathbf{C}_{\hat{\gamma}}^6 \equiv \{I, \hat{I}\} \quad (\supset C_1) \quad (11.30)$$

$$\mathbf{C}_{2\hat{\sigma}}^{12} \equiv \{I, C_{2(3)}, \hat{C}_{2(1)}, \hat{C}_{2(2)}\} \quad (\supset C_2) \quad (11.31)$$

$$\mathbf{C}_{2\hat{I}}^{15} \equiv \{I, C_{2(3)}, \hat{C}_{2(3)}, \hat{I}\} \quad (\supset C_2) \quad (11.32)$$

$$\mathbf{C}_{3\hat{I}}^{19} \equiv \{I, C_{3(1)}, C_{3(1)}^2, \hat{I}, \hat{C}_{3(1)}, \hat{C}_{3(1)}^2\} \quad (\supset C_3) \quad (11.33)$$

$$\mathbf{D}_{2\hat{I}}^{25} \equiv \{I, C_{2(1)}, C_{2(2)}, C_{2(3)}, \hat{I}, \hat{C}_{2(1)}, \hat{C}_{2(2)}, \hat{C}_{2(3)}\} \quad (\supset D_2) \quad (11.34)$$

$$\mathbf{T}_{\hat{\gamma}}^{31} \equiv \{A, D\} \quad (\supset T) \quad (11.35)$$

which correspond to the seven subgroups of \mathbf{T}_h (except those of \mathbf{T}). The names of the subgroups are characterized by the symbols with a hat accent.

5. (Type-IV Subgroups) The nine subgroups of \mathbf{O}_h (except those of \mathbf{T} , \mathbf{T}_d , \mathbf{O} , and \mathbf{T}_h) correspond to the following subgroups of $\mathbf{T}_{d\tilde{\sigma}\hat{\gamma}}$:

$$\mathbf{C}_{s\tilde{\sigma}\hat{\sigma}}^{14} \equiv \{I, \tilde{\sigma}_{d(1)}, \hat{C}_{2(3)}, \sigma_{d(6)}\} \quad (\supset C_s) \quad (11.36)$$

$$\mathbf{C}_{s\tilde{\sigma}\hat{I}}^{16} \equiv \{I, \tilde{\sigma}_{d(1)}, \hat{I}, \sigma_{d(1)}\} \quad (\supset C_s) \quad (11.37)$$

$$\mathbf{S}_{4\hat{\sigma}}^{21} \equiv \{I, \tilde{S}_{4(3)}, C_{2(3)}, \tilde{S}_{4(3)}^3, \hat{C}_{2(1)}, \hat{C}_{2(2)}, \sigma_{d(1)}, \sigma_{d(6)}\} \quad (\supset \mathbf{S}_4, \mathbf{C}_{2v}) \quad (11.38)$$

$$\mathbf{S}_{4\hat{I}}^{22} \equiv \{I, \tilde{S}_{4(3)}, C_{2(3)}, \tilde{S}_{4(3)}^3, \hat{I}, \hat{C}_{2(3)}, S_{4(3)}, S_{4(3)}^3\} \quad (\supset \mathbf{S}_4, \mathbf{S}_4) \quad (11.39)$$

$$\mathbf{S}_{4\tilde{\sigma}\hat{\sigma}}^{24} \equiv \{I, C_{2(3)}, \tilde{\sigma}_{d(1)}, \tilde{\sigma}_{d(6)}, \hat{C}_{2(1)}, \hat{C}_{2(2)}, S_{4(3)}, S_{4(3)}^3\} \quad (\supset \mathbf{S}_4) \quad (11.40)$$

$$\mathbf{C}_{2v\tilde{\sigma}\hat{I}}^{26} \equiv \{I, C_{2(3)}, \tilde{\sigma}_{d(1)}, \tilde{\sigma}_{d(6)}, \hat{I}, \hat{C}_{2(3)}, \sigma_{d(1)}, \sigma_{d(6)}\} \quad (\supset \mathbf{C}_{2v}) \quad (11.41)$$

$$\mathbf{C}_{3v\tilde{\sigma}\hat{I}}^{28} \equiv \{I, C_{3(1)}, C_{3(1)}^2, \tilde{\sigma}_{d(1)}, \tilde{\sigma}_{d(2)}, \tilde{\sigma}_{d(3)}, \\ \hat{I}, \hat{C}_{3(1)}, \hat{C}_{3(1)}^2, \sigma_{d(1)}, \sigma_{d(2)}, \sigma_{d(3)}\} \quad (\supset \mathbf{C}_{3v}) \quad (11.42)$$

$$\mathbf{D}_{2d\tilde{\sigma}\hat{I}}^{29} \equiv \{I, C_{2(1)}, C_{2(2)}, C_{2(3)}, \tilde{\sigma}_{d(1)}, \tilde{\sigma}_{d(6)}, \tilde{S}_{4(3)}, \tilde{S}_{4(3)}^3\},$$

Table 11.2. Subduction of $T_{d\bar{\sigma}\bar{I}}(/C_{3v\bar{\sigma}\bar{I}})$

	Subgroup ($\downarrow \hat{G}_j$)	Subduction ($T_{d\bar{\sigma}\bar{I}}(/C_{3v\bar{\sigma}\bar{I}}) \downarrow \hat{G}_j$)	USCI-CF		USCI						TEM						
			USCI-CF	USCI	\hat{N}_j	$\hat{N}_j^{(I)}$	$\hat{N}_j^{(II)}$	$\hat{N}_j^{(III)}$	$\hat{N}_j^{(IV)}$	$\hat{N}_j^{(V)}$	$\hat{N}_j^{(VI)}$	$\hat{N}_j^{(VII)}$	$\hat{N}_j^{(VIII)}$	$\hat{N}_j^{(IX)}$	$\hat{N}_j^{(X)}$		
1	C_1	$4C_1(/C_1)$	b_1^4	s_1^4	$\frac{1}{48}$	0	0	$\frac{1}{48}$	0	0	0	0	0	0	0	0	0
2	C_2	$2C_2(/C_1)$	b_2^2	s_2^2	$\frac{1}{16}$	0	0	$\frac{1}{16}$	0	0	0	0	0	0	0	0	0
3	$C_{\bar{\sigma}}$	$C_{\bar{\sigma}}(/C_1) + 2C_{\bar{\sigma}}(/C_{\bar{\sigma}})$	$b_1^2 b_2$	$s_1^2 s_2$	$\frac{1}{8}$	0	$\frac{1}{4}$	$-\frac{1}{8}$	0	0	0	0	0	0	0	0	0
4	$C_{\bar{\sigma}}$	$2C_{\bar{\sigma}}(/C_1)$	c_2^2	s_2^2	$\frac{1}{16}$	$\frac{1}{8}$	0	$-\frac{1}{16}$	0	0	0	0	0	0	0	0	0
5	C_s	$C_s(/C_1) + 2C_s(/C_s)$	$a_1^2 c_2$	$s_1^2 s_2$	$\frac{1}{8}$	0	0	$-\frac{1}{8}$	0	$\frac{1}{4}$	0	0	0	0	0	0	0
6	$C_{\hat{I}}$	$4C_{\hat{I}}(/C_{\hat{I}})$	a_1^4	a_1^4	$\frac{1}{48}$	$\frac{1}{24}$	0	$-\frac{1}{48}$	0	0	0	0	0	0	0	0	0
7	C_3	$C_3(/C_1) + C_3(/C_3)$	$b_1 b_3$	$s_1 s_3$	$\frac{1}{6}$	0	0	$\frac{1}{6}$	0	0	0	0	0	0	0	0	0
8	S_4	$S_4(/C_1)$	b_4	s_4	$\frac{1}{8}$	0	$\frac{1}{4}$	$-\frac{1}{8}$	0	0	0	0	0	0	0	0	0
9	S_4	$S_4(/C_1)$	c_4	s_4	$\frac{1}{8}$	0	0	$-\frac{1}{8}$	0	0	0	0	0	0	0	0	0
10	D_2	$D_2(/C_1)$	b_4	s_4	0	0	0	0	0	0	0	0	0	0	0	0	0
11	$C_{2\bar{\sigma}}$	$C_{2\bar{\sigma}}(/C_{\bar{\sigma}}) + C_{2\bar{\sigma}}(/C_{\bar{\sigma}}')$	b_2^2	s_2^2	0	0	0	0	0	0	0	0	0	0	0	0	0
12	$C_{2\bar{\sigma}}$	$C_{2\bar{\sigma}}(/C_1)$	c_4	s_4	0	0	0	0	0	0	0	0	0	0	0	0	0
13	C_{2v}	$C_{2v}(/C_s) + C_{2v}(/C_s')$	a_2^2	s_2^2	0	0	0	0	0	0	0	0	0	0	0	0	0
14	$C_{s\bar{\sigma}\bar{\sigma}}$	$C_{s\bar{\sigma}\bar{\sigma}}(/C_{\bar{\sigma}}) + C_{s\bar{\sigma}\bar{\sigma}}(/C_s)$	$a_2 c_2$	s_2^2	0	$-\frac{1}{4}$	$-\frac{1}{4}$	$\frac{1}{4}$	$\frac{1}{2}$	$-\frac{1}{4}$	0	0	0	0	0	0	0
15	$C_{2\hat{I}}$	$2C_{2\hat{I}}(/C_{\hat{I}})$	a_2^2	s_2^2	0	0	0	0	0	0	0	0	0	0	0	0	0
16	$C_{s\bar{\sigma}\hat{I}}$	$C_{s\bar{\sigma}\hat{I}}(/C_{\hat{I}}) + 2C_{s\bar{\sigma}\hat{I}}(/C_{s\bar{\sigma}\hat{I}})$	$a_1^2 a_2$	$s_1^2 s_2$	0	$-\frac{1}{4}$	$-\frac{1}{4}$	$\frac{1}{4}$	$\frac{1}{2}$	$-\frac{1}{4}$	0	0	0	0	0	0	0
17	$C_{3\bar{\sigma}}$	$C_{3\bar{\sigma}}(/C_{\bar{\sigma}}) + C_{3\bar{\sigma}}(/C_{3\bar{\sigma}})$	$b_1 b_3$	$s_1 s_3$	0	0	0	0	0	0	0	0	0	0	0	0	0
18	C_{3v}	$C_{3v}(/C_s) + C_{3v}(/C_{3v})$	$a_1 a_3$	$s_1 s_3$	0	0	0	0	0	0	0	0	0	0	0	0	0
19	$C_{3\hat{I}}$	$C_{3\hat{I}}(/C_{\hat{I}}) + C_{3\hat{I}}(/C_{3\hat{I}})$	$a_1 a_3$	$s_1 s_3$	$\frac{1}{6}$	$\frac{1}{3}$	0	$-\frac{1}{6}$	0	0	0	0	0	0	0	0	0
20	$D_{2\bar{\sigma}}$	$D_{2\bar{\sigma}}(/C_{\bar{\sigma}})$	b_4	s_4	0	0	0	0	0	0	0	0	0	0	0	0	0
21	$S_{4\bar{\sigma}}$	$S_{4\bar{\sigma}}(/C_s)$	a_4	s_4	0	$-\frac{1}{4}$	$-\frac{1}{4}$	$\frac{1}{4}$	$\frac{1}{2}$	$-\frac{1}{4}$	0	0	0	0	0	0	0
22	$S_{4\hat{I}}$	$S_{4\hat{I}}(/C_{\hat{I}})$	a_4	s_4	0	$-\frac{1}{4}$	$-\frac{1}{4}$	$\frac{1}{4}$	$\frac{1}{2}$	$-\frac{1}{4}$	0	0	0	0	0	0	0
23	D_{2d}	$D_{2d}(/C_s)$	a_4	s_4	0	0	0	0	0	0	0	0	0	0	0	0	0
24	$S_{4\bar{\sigma}\bar{\sigma}}$	$S_{4\bar{\sigma}\bar{\sigma}}(/C_{\bar{\sigma}})$	c_4	s_4	0	$-\frac{1}{4}$	$-\frac{1}{4}$	$\frac{1}{4}$	$\frac{1}{2}$	$-\frac{1}{4}$	0	0	0	0	0	0	0
25	$D_{2\hat{I}}$	$D_{2\hat{I}}(/C_{\hat{I}})$	a_4	s_4	0	0	0	0	0	0	0	0	0	0	0	0	0
26	$C_{2v\bar{\sigma}\hat{I}}$	$C_{2v\bar{\sigma}\hat{I}}(/C_{s\bar{\sigma}\hat{I}}) + C_{2v\bar{\sigma}\hat{I}}(/C_{s\bar{\sigma}\hat{I}}')$	a_2^2	s_2^2	0	$\frac{1}{4}$	$\frac{1}{4}$	$-\frac{1}{4}$	$-\frac{1}{2}$	$\frac{1}{4}$	0	0	0	0	0	0	0
27	T	$T(/C_3)$	b_4	s_4	0	0	0	0	0	0	0	0	0	0	0	0	0
28	$C_{3v\bar{\sigma}\hat{I}}$	$C_{3v\bar{\sigma}\hat{I}}(/C_{s\bar{\sigma}\hat{I}}) + C_{3v\bar{\sigma}\hat{I}}(/C_{3v\bar{\sigma}\hat{I}})$	$a_1 a_3$	$s_1 s_3$	0	0	0	0	0	0	0	0	0	0	0	0	0
29	$D_{2d\bar{\sigma}\hat{I}}$	$D_{2d\bar{\sigma}\hat{I}}(/C_{s\bar{\sigma}\hat{I}})$	a_4	s_4	0	$\frac{1}{2}$	$\frac{1}{2}$	$-\frac{1}{2}$	-1	$\frac{1}{2}$	0	0	0	0	0	0	0
30	$T_{\bar{\sigma}}$	$T_{\bar{\sigma}}(/C_{3\bar{\sigma}})$	b_4	s_4	0	0	0	0	0	0	0	0	0	0	0	0	0
31	$T_{\hat{I}}$	$T_{\hat{I}}(/C_{3\hat{I}})$	a_4	s_4	0	0	0	0	0	0	0	0	0	0	0	0	0
32	T_d	$T_d(/C_{3v})$	a_4	s_4	0	0	0	0	0	0	0	0	0	0	0	0	0
33	$T_{d\bar{\sigma}\hat{I}}$	$T_{d\bar{\sigma}\hat{I}}(/C_{3v\bar{\sigma}\hat{I}})$	a_4	s_4	0	0	0	0	0	0	0	0	0	0	0	0	0

The four positions of the tetrahedral skeleton **3-5** (page 55) construct an orbit governed by a coset representation $T_{d\bar{\sigma}\bar{I}}(/C_{3v\bar{\sigma}\bar{I}})$, the degree of which is calculated to be $|T_{d\bar{\sigma}\bar{I}}|/|C_{3v\bar{\sigma}\bar{I}}| = 48/12 = 4$. The subduction of the coset representation $T_{d\bar{\sigma}\bar{I}}(/C_{3v\bar{\sigma}\bar{I}})$ by a subgroup \hat{G}_j is shown in Table 11.2, which is cited from [1, Table 2].

According to Eq. 10.56 (Def. 10.4 on page 295), the data of the subduction-column of Table 11.2 give the corresponding USCI-CFs, as collected in the USCI-CF-column of Table 11.2. The USCI-CFs collected in the USCI-CF-column of Table 11.2 are identical with the USCI-CFs collected in the $O_h(/D_{3d})$ -row of the USCI table of O_h [6, Table 4 and 5].

11.3.3 The PCI Method for the *RS*-Stereoisomeric Group $T_{d\hat{\sigma}\hat{\tau}}$

PCI-CFs for Characterizing Subgroups

The PCI-CFs for *RS*-stereoisomeric group $T_{d\hat{\sigma}\hat{\tau}}$ are calculated according to Def. 10.6 (page 298). To accomplish this calculation, the data of the USCI-CF-column of Table 11.2 are regarded as a formal row vector of SCI-CFs, which is multiplied by the inverse mark table $M_{T_{d\hat{\sigma}\hat{\tau}}}^{-1}$ (Eq. 11.45), as represented schematically to be:

$$\begin{aligned} & \left(\text{PCI-CF}(C_1), \text{PCI-CF}(C_2), \dots, \text{PCI-CF}(\hat{G}_j), \dots, \text{PCI-CF}(T_{d\hat{\sigma}\hat{\tau}}) \right) \\ &= (b_1^4, b_2^2, b_1^2 b_2, c_2^2, a_1^2 c_2, a_1^4, b_1 b_3, b_4, c_4, b_4, b_2^2, c_4, a_2^2, a_2 c_2, a_2^2, a_1^2 a_2, \\ & \quad b_1 b_3, a_1 a_3, a_1 a_3, b_4, a_4, a_4, a_4, c_4, a_4, a_2^2, b_4, a_1 a_3, a_4, b_4, a_4, a_4, a_4) \times M_{T_{d\hat{\sigma}\hat{\tau}}}^{-1} \quad (11.46) \end{aligned}$$

Thereby, PCI-CFs for every subgroups of $\text{SSG}_{T_{d\hat{\sigma}\hat{\tau}}}$ (Eq. 11.6) are obtained as follows, where the sequential numbers are shown over the respective equality symbols for the convenience of cross reference:

$$\begin{aligned} \text{PCI-CF}(C_1) & \frac{1}{\text{III}} \frac{1}{48} b_1^4 - \frac{1}{48} a_1^4 - \frac{1}{8} b_1^2 b_2 + \frac{1}{4} a_1^2 a_2 - \frac{1}{8} a_1^2 c_2 + \frac{1}{6} b_1 b_3 - \frac{1}{6} a_1 a_3 \\ & \quad + \frac{1}{16} b_2^2 - \frac{1}{4} a_2^2 + \frac{1}{4} a_2 c_2 - \frac{1}{16} c_2^2 + \frac{1}{8} c_4 - \frac{1}{8} b_4 \quad (11.47) \end{aligned}$$

$$\text{PCI-CF}(C_2) \frac{2}{\text{III}} 0 \quad (11.48)$$

$$\begin{aligned} \text{PCI-CF}(C_{\hat{\sigma}}) & \frac{3}{\text{II}} \frac{1}{4} b_1^2 b_2 - \frac{1}{4} a_1^2 a_2 - \frac{1}{2} b_1 b_3 + \frac{1}{2} a_1 a_3 - \frac{1}{4} b_2^2 + \frac{1}{2} a_2^2 \\ & \quad - \frac{1}{4} a_2 c_2 + \frac{1}{2} b_4 - \frac{1}{2} a_4 \quad (11.49) \end{aligned}$$

$$\text{PCI-CF}(C_{\hat{\sigma}}) \frac{4}{\text{I}} \frac{1}{8} a_2^2 - \frac{1}{4} a_2 c_2 + \frac{1}{8} c_2^2 - \frac{1}{4} c_4 + \frac{1}{4} a_4 \quad (11.50)$$

$$\text{PCI-CF}(C_s) \frac{5}{\text{V}} \frac{1}{4} a_1^2 c_2 - \frac{1}{4} a_1^2 a_2 + \frac{1}{4} a_2^2 - \frac{1}{4} a_2 c_2 \quad (11.51)$$

$$\text{PCI-CF}(C_{\hat{\tau}}) \frac{6}{\text{I}} \frac{1}{24} a_1^4 - \frac{1}{4} a_1^2 a_2 + \frac{1}{3} a_1 a_3 + \frac{1}{8} a_2^2 - \frac{1}{4} a_4 \quad (11.52)$$

$$\text{PCI-CF}(C_3) \frac{7}{\text{III}} 0 \quad (11.53)$$

$$\text{PCI-CF}(S_4) \frac{8}{\text{II}} 0 \quad (11.54)$$

$$\text{PCI-CF}(S_4) \frac{9}{\text{V}} 0 \quad (11.55)$$

$$\text{PCI-CF}(D_2) \frac{10}{\text{III}} 0 \quad (11.56)$$

$$\text{PCI-CF}(\mathbf{C}_{2\bar{\sigma}}) \stackrel{11}{\equiv} \frac{1}{4}b_2^2 - \frac{1}{4}a_2^2 - \frac{1}{4}b_4 - \frac{1}{4}c_4 + \frac{1}{2}a_4 \quad (11.57)$$

$$\text{PCI-CF}(\mathbf{C}_{2\hat{\sigma}}) \stackrel{12}{\equiv} 0 \quad (11.58)$$

$$\text{PCI-CF}(\mathbf{C}_{2\nu}) \stackrel{13}{\equiv} 0 \quad (11.59)$$

$$\text{PCI-CF}(\mathbf{C}_{s\bar{\sigma}\hat{\sigma}}) \stackrel{14}{\equiv} \frac{1}{2}a_2c_2 - \frac{1}{2}a_2^2 \quad (11.60)$$

$$\text{PCI-CF}(\mathbf{C}_{2\hat{\tau}}) \stackrel{15}{\equiv} 0 \quad (11.61)$$

$$\text{PCI-CF}(\mathbf{C}_{s\bar{\sigma}\hat{\tau}}) \stackrel{16}{\equiv} \frac{1}{2}a_1^2a_2 - a_1a_3 - \frac{1}{2}a_2^2 + a_4 \quad (11.62)$$

$$\text{PCI-CF}(\mathbf{C}_{3\bar{\sigma}}) \stackrel{17}{\equiv} \frac{1}{2}b_1b_3 - \frac{1}{2}a_1a_3 - \frac{1}{2}b_4 + \frac{1}{2}a_4 \quad (11.63)$$

$$\text{PCI-CF}(\mathbf{C}_{3\nu}) \stackrel{18}{\equiv} 0 \quad (11.64)$$

$$\text{PCI-CF}(\mathbf{C}_{3\hat{\tau}}) \stackrel{19}{\equiv} 0 \quad (11.65)$$

$$\text{PCI-CF}(\mathbf{D}_{2\bar{\sigma}}) \stackrel{20}{\equiv} 0 \quad (11.66)$$

$$\text{PCI-CF}(\mathbf{S}_{4\bar{\sigma}}) \stackrel{21}{\equiv} 0 \quad (11.67)$$

$$\text{PCI-CF}(\mathbf{S}_{4\hat{\tau}}) \stackrel{22}{\equiv} 0 \quad (11.68)$$

$$\text{PCI-CF}(\mathbf{D}_{2d}) \stackrel{23}{\equiv} 0 \quad (11.69)$$

$$\text{PCI-CF}(\mathbf{S}_{4\bar{\sigma}\hat{\sigma}}) \stackrel{24}{\equiv} \frac{1}{2}c_4 - \frac{1}{2}a_4 \quad (11.70)$$

$$\text{PCI-CF}(\mathbf{D}_{2\hat{\tau}}) \stackrel{25}{\equiv} 0 \quad (11.71)$$

$$\text{PCI-CF}(\mathbf{C}_{2\nu\bar{\sigma}\hat{\tau}}) \stackrel{26}{\equiv} \frac{1}{2}a_2^2 - \frac{1}{2}a_4 \quad (11.72)$$

$$\text{PCI-CF}(\mathbf{T}) \stackrel{27}{\equiv} 0 \quad (11.73)$$

$$\text{PCI-CF}(\mathbf{C}_{3\nu\bar{\sigma}\hat{\tau}}) \stackrel{28}{\equiv} a_1a_3 - a_4 \quad (11.74)$$

$$\text{PCI-CF}(\mathbf{D}_{2d\bar{\sigma}\hat{\tau}}) \stackrel{29}{\equiv} 0 \quad (11.75)$$

$$\text{PCI-CF}(\mathbf{T}_{\bar{\sigma}}) \stackrel{30}{\equiv} \frac{1}{2}b_4 - \frac{1}{2}a_4 \quad (11.76)$$

$$\text{PCI-CF}(\mathbf{T}_{\hat{\tau}}) \stackrel{31}{\equiv} 0 \quad (11.77)$$

$$\text{PCI-CF}(\mathbf{T}_d) \stackrel{32}{\equiv} 0 \quad (11.78)$$

$$\text{PCI-CF}(\mathbf{T}_{d\bar{\sigma}\hat{\tau}}) \stackrel{33}{\equiv} a_4 \quad (11.79)$$

Note that a Roman numeral below each equality symbol represents the stereoisogram type at issue (types I–V). These PCI-CFs have once been noted in [4].

Generating Functions for Symmetry-Itemized Enumeration

Suppose that the four positions of the tetrahedral skeleton **3-5** (page 55) are substituted by a set of proligands selected from a ligand inventory \mathbf{L} (Eq. 6.73 on page 153). According to Theorem 10.4 (page 298), which is an extended version of Theorem 19.6 (or Theorem 9.7) of [7], we use the following ligand-inventory functions:

$$a_d = A^d + B^d + X^d + Y^d \quad (11.80)$$

$$c_d = A^d + B^d + X^d + Y^d + 2p^{d/2}\bar{p}^{d/2} + 2q^{d/2}\bar{q}^{d/2} + 2r^{d/2}\bar{r}^{d/2} + 2s^{d/2}\bar{s}^{d/2} \quad (11.81)$$

$$b_d = A^d + B^d + X^d + Y^d + p^d + q^d + r^d + s^d + \bar{p}^d + \bar{q}^d + \bar{r}^d + \bar{s}^d, \quad (11.82)$$

where the power $d/2$ appearing in Eq. 11.81 is an integer because the subscript d of c_d is always even in the light of the enantiosphericity of the corresponding orbit.

The ligand-inventory functions (Eqs. 11.80–11.82) are introduced into the PCI-CFs (Eqs. 11.47–11.79). After expansion of the resulting equations, the following generating functions for symmetry-itemized enumeration under $T_{d\bar{\sigma}\bar{\tau}}$ are obtained:

$$\begin{aligned} f_{C_1} \frac{1}{\text{III}} & \left\{ \frac{1}{2} (\text{ABXp} + \text{ABX}\bar{p}) + \dots \right\} + \left\{ \frac{1}{2} (\text{ABpq} + \text{AB}\bar{p}\bar{q}) + \dots \right\} \\ & + \left\{ \frac{1}{2} (\text{App}\bar{q} + \text{Ap}\bar{p}\bar{q}) + \dots \right\} + \left\{ \frac{1}{2} (\text{Apqr} + \text{Ap}\bar{q}\bar{r}) + \dots \right\} \\ & + \left\{ \frac{1}{2} (\text{pqrs} + \text{p}\bar{q}\bar{r}\bar{s}) + \dots \right\} + \left\{ \frac{1}{2} (\text{p}\bar{p}\bar{q}\bar{r} + \text{p}\bar{p}\bar{q}\bar{r}) + \dots \right\} \end{aligned} \quad (11.83)$$

$$\begin{aligned} f_{C_{\bar{\sigma}}} \frac{3}{\text{II}} & \left\{ \frac{1}{2} (\text{A}^2\text{Bp} + \text{A}^2\text{B}\bar{p}) + \dots \right\} + \left\{ \frac{1}{2} (\text{ABp}^2 + \text{AB}\bar{p}^2) + \dots \right\} \\ & + \left\{ \frac{1}{2} (\text{A}^2\text{pq} + \text{A}^2\text{p}\bar{q}) + \dots \right\} + \left\{ \frac{1}{2} (\text{Ap}^2\bar{p} + \text{Ap}\bar{p}^2) + \dots \right\} \\ & + \left\{ \frac{1}{2} (\text{Ap}^2\text{q} + \text{Ap}^2\bar{q}) + \dots \right\} + \left\{ \frac{1}{2} (\text{p}^2\bar{p}\text{q} + \text{p}\bar{p}^2\bar{q}) + \dots \right\} \\ & + \left\{ \frac{1}{2} (\text{p}^2\text{q}\bar{q} + \text{p}^2\bar{q}\bar{q}) + \dots \right\} + \left\{ \frac{1}{2} (\text{p}^2\text{qr} + \text{p}^2\bar{q}\bar{r}) + \dots \right\} \end{aligned} \quad (11.84)$$

$$f_{C_{\bar{\sigma}}} \frac{4}{\text{I}} \left\{ \text{p}\bar{p}\text{q}\bar{q} + \text{p}\bar{p}\bar{r}\bar{r} + \dots \right\} \quad (11.85)$$

$$f_{C_s} \frac{5}{\text{V}} \left\{ \text{ABp}\bar{p} + \text{ABq}\bar{q} + \dots \right\} \quad (11.86)$$

$$f_{C_7} \frac{6}{\text{I}} \text{ABXY} \quad (11.87)$$

$$f_{C_{2\bar{\sigma}}} \frac{11}{\text{II}} \left\{ \frac{1}{2} (\text{A}^2\text{p}^2 + \text{A}^2\bar{p}^2) + \dots \right\} + \left\{ \frac{1}{2} (\text{p}^2\text{q}^2 + \text{p}^2\bar{q}^2) + \dots \right\} \quad (11.88)$$

$$f_{C_{3\bar{\sigma}\hat{\sigma}}} \stackrel{14}{\equiv} \frac{[\theta]_8}{IV} \{A^2 p \bar{p} + \dots\} \quad (11.89)$$

$$f_{C_{3\bar{\sigma}\hat{\tau}}} \stackrel{16}{\equiv} \frac{[\theta]_6}{IV} \{A^2 B X + A^2 B Y + \dots\} \quad (11.90)$$

$$f_{C_{3\bar{\sigma}}} \stackrel{17}{\equiv} \frac{1}{II} \left\{ \frac{1}{2} (A^3 p + A^3 \bar{p}) + \dots \right\} + \left\{ \frac{1}{2} (A p^3 + A \bar{p}^3) + \dots \right\} \\ + \left\{ \frac{1}{2} (p^3 q + \bar{p}^3 \bar{q}) + \dots \right\} + \left\{ \frac{1}{2} (p^3 \bar{p} + p \bar{p}^3) + \dots \right\} \quad (11.91)$$

$$f_{S_{4\bar{\sigma}\hat{\sigma}}} \stackrel{24}{\equiv} \frac{[\theta]_{23}}{IV} \{p^2 \bar{p}^2 + q^2 \bar{q}^2 + r^2 \bar{r}^2 + s^2 \bar{s}^2\} \quad (11.92)$$

$$f_{C_{2\bar{\nu}\hat{\tau}}} \stackrel{26}{\equiv} \frac{[\theta]_{14}}{IV} \{A^2 B^2 + A^2 X^2 + A^2 Y^2 + \dots\} \quad (11.93)$$

$$f_{C_{3\bar{\nu}\hat{\tau}}} \stackrel{28}{\equiv} \frac{[\theta]_2}{IV} \{A^3 B + A^3 X + A^3 Y + \dots\} \quad (11.94)$$

$$f_{T_{\bar{\sigma}}} \stackrel{30}{\equiv} \frac{1}{II} \left\{ \frac{1}{2} (p^4 + \bar{p}^4) + \dots \right\} \quad (11.95)$$

$$f_{T_{d\bar{\sigma}\hat{\tau}}} \stackrel{33}{\equiv} \frac{[\theta]_1}{IV} \{A^4 + B^4 + X^4 + Y^4\} \quad (11.96)$$

where generating functions of zero value are omitted (cf. the sequential numbers above the equality symbols). The coefficient of the term $A^a B^b X^x Y^y p^p \bar{p}^{\bar{p}} q^q \bar{q}^{\bar{q}} r^r \bar{r}^{\bar{r}} s^s \bar{s}^{\bar{s}}$ in each generating function indicates the number of fixed promolecules (quadruplets) to be counted. These generating functions have been once noted in [4].

Because A, B, etc. appear symmetrically in the generating functions (Eqs. 11.83–11.96), each pair of braces contains at least one representative of such symmetrically appearing terms, which can be represented by the following partition:

$$[\theta] = [a, b, x, y; p, \bar{p}, q, \bar{q}, r, \bar{r}, s, \bar{s}], \quad (11.97)$$

where we put $a \geq b \geq x \geq y$, $p \geq \bar{p}$, $q \geq \bar{q}$, $r \geq \bar{r}$, $s \geq \bar{s}$, and $p \geq q \geq r \geq s$ without losing generality:

$$[\theta]_1 = [4, 0, 0, 0; 0, 0, 0, 0, 0, 0, 0, 0] \quad (\text{for } A^4 \text{ etc.}) \quad (11.98)$$

$$[\theta]_2 = [3, 1, 0, 0; 0, 0, 0, 0, 0, 0, 0, 0] \quad (\text{for } A^3 B \text{ etc.}) \quad (11.99)$$

$$[\theta]_3 = [3, 0, 0, 0; 1, 0, 0, 0, 0, 0, 0, 0] \quad (\text{for } A^3 p \text{ etc.}) \quad (11.100)$$

$$[\theta]_4 = [2, 2, 0, 0; 0, 0, 0, 0, 0, 0, 0, 0] \quad (\text{for } A^2 B^2 \text{ etc.}) \quad (11.101)$$

$$[\theta]_5 = [2, 0, 0, 0; 2, 0, 0, 0, 0, 0, 0, 0] \quad (\text{for } A^2 p^2 \text{ etc.}) \quad (11.102)$$

$$[\theta]_6 = [2, 1, 1, 0; 0, 0, 0, 0, 0, 0, 0, 0] \quad (\text{for } A^2 B X \text{ etc.}) \quad (11.103)$$

$$[\theta]_7 = [2, 1, 0, 0; 1, 0, 0, 0, 0, 0, 0, 0] \quad (\text{for } A^2 B p \text{ etc.}) \quad (11.104)$$

$$[\theta]_8 = [2, 0, 0, 0; 1, 1, 0, 0, 0, 0, 0, 0] \quad (\text{for } A^2 p \bar{p} \text{ etc.}) \quad (11.105)$$

$[\theta]_9 = [2, 0, 0, 0; 1, 0, 1, 0, 0, 0, 0, 0]$	(for A^2pq etc.)	(11.106)
$[\theta]_{10} = [1, 1, 1, 1; 0, 0, 0, 0, 0, 0, 0, 0]$	(for $ABXY$)	(11.107)
$[\theta]_{11} = [1, 1, 1, 0; 1, 0, 0, 0, 0, 0, 0, 0]$	(for $ABXp$ etc.)	(11.108)
$[\theta]_{12} = [1, 1, 0, 0; 2, 0, 0, 0, 0, 0, 0, 0]$	(for ABp^2 etc.)	(11.109)
$[\theta]_{13} = [1, 1, 0, 0; 1, 1, 0, 0, 0, 0, 0, 0]$	(for $ABp\bar{p}$ etc.)	(11.110)
$[\theta]_{14} = [1, 1, 0, 0; 1, 0, 1, 0, 0, 0, 0, 0]$	(for $ABpq$ etc.)	(11.111)
$[\theta]_{15} = [1, 0, 0, 0; 3, 0, 0, 0, 0, 0, 0, 0]$	(for Ap^3 etc.)	(11.112)
$[\theta]_{16} = [1, 0, 0, 0; 2, 1, 0, 0, 0, 0, 0, 0]$	(for $Ap^2\bar{p}$ etc.)	(11.113)
$[\theta]_{17} = [1, 0, 0, 0; 2, 0, 1, 0, 0, 0, 0, 0]$	(for Ap^2q etc.)	(11.114)
$[\theta]_{18} = [1, 0, 0, 0; 1, 1, 1, 0, 0, 0, 0, 0]$	(for $Ap\bar{p}q$ etc.)	(11.115)
$[\theta]_{19} = [1, 0, 0, 0; 1, 0, 1, 0, 1, 0, 0, 0]$	(for $Apqr$ etc.)	(11.116)
$[\theta]_{20} = [0, 0, 0, 0; 4, 0, 0, 0, 0, 0, 0, 0]$	(for p^4 etc.)	(11.117)
$[\theta]_{21} = [0, 0, 0, 0; 3, 1, 0, 0, 0, 0, 0, 0]$	(for $p^3\bar{p}$ etc.)	(11.118)
$[\theta]_{22} = [0, 0, 0, 0; 3, 0, 1, 0, 0, 0, 0, 0]$	(for p^3q etc.)	(11.119)
$[\theta]_{23} = [0, 0, 0, 0; 2, 2, 0, 0, 0, 0, 0, 0]$	(for $p^2\bar{p}^2$ etc.)	(11.120)
$[\theta]_{24} = [0, 0, 0, 0; 2, 1, 1, 0, 0, 0, 0, 0]$	(for $p^2\bar{p}q$ etc.)	(11.121)
$[\theta]_{25} = [0, 0, 0, 0; 2, 0, 2, 0, 0, 0, 0, 0]$	(for p^2q^2 etc.)	(11.122)
$[\theta]_{26} = [0, 0, 0, 0; 2, 0, 1, 1, 0, 0, 0, 0]$	(for $p^2q\bar{q}$ etc.)	(11.123)
$[\theta]_{27} = [0, 0, 0, 0; 2, 0, 1, 0, 1, 0, 0, 0]$	(for p^2qr etc.)	(11.124)
$[\theta]_{28} = [0, 0, 0, 0; 1, 1, 1, 1, 0, 0, 0, 0]$	(for $p\bar{p}q\bar{q}$ etc.)	(11.125)
$[\theta]_{29} = [0, 0, 0, 0; 1, 1, 1, 0, 1, 0, 0, 0]$	(for $p\bar{p}qr$ etc.)	(11.126)
$[\theta]_{30} = [0, 0, 0, 0; 1, 0, 1, 0, 1, 0, 1, 0]$	(for $pqrs$ etc.)	(11.127)

Each term appearing in Eqs. 11.83–11.96) is attached by a partition $[\theta]_i$ for the sake of cross reference. Thereby, the data of the generating functions (Eqs. 11.83–11.96) are found to be consistent with the isomer-counting matrices (ICMs) obtained by the FPM method reported previously [1].

Exercise 11.6. Check each term appearing in Eqs. 11.83–11.96 by referring to Fig. 11.2. Note that each representative promolecule with its composition (e.g., $ABXY$ for **11-3**) is attached by a partition (e.g., $[\theta]_{10}$ for **11-3**) and a symbol for characterizing symmetry itemization (e.g., $[C_{\bar{I}}, C_1, C_1; I]$ for **11-3**).

11.3.4 Type-Itemized Enumeration by the PCI Method

CI-CFs for Characterizing Five Types of Stereoisograms

Cycle indices with chirality fittingness (CI-CFs) for characterizing five types are calculated according to the categorization of Eqs. 11.7–11.11, where we start from the data of PCI-CFs (Eqs. 11.47–11.79).

$$\begin{aligned} \text{CI-CF}^{\text{[I]}}(\mathbf{T}_{d\tilde{\sigma}\tilde{\tau}}) &= \text{PCI-CF}(\mathbf{C}_{\tilde{\sigma}}) + \text{PCI-CF}(\mathbf{C}_{\tilde{\tau}}) + \text{PCI-CF}(\mathbf{C}_{2\tilde{\sigma}}) \\ &\quad + \text{PCI-CF}(\mathbf{C}_{2\tilde{\tau}}) + \text{PCI-CF}(\mathbf{C}_{3\tilde{\tau}}) + \text{PCI-CF}(\mathbf{D}_{2\tilde{\tau}}) + \text{PCI-CF}(\mathbf{T}_{\tilde{\tau}}) \\ &= \frac{1}{24}a_1^4 - \frac{1}{4}a_1^2a_2 + \frac{1}{3}a_1a_3 + \frac{1}{4}a_2^2 - \frac{1}{4}a_2c_2 + \frac{1}{8}c_2^2 - \frac{1}{4}c_4 \end{aligned} \quad (11.128)$$

$$\begin{aligned} \text{CI-CF}^{\text{[II]}}(\mathbf{T}_{d\tilde{\sigma}\tilde{\tau}}) &= \text{PCI-CF}(\mathbf{C}_{\tilde{\sigma}}) + \text{PCI-CF}(\mathbf{S}_4) + \text{PCI-CF}(\mathbf{C}_{2\tilde{\sigma}}) \\ &\quad + \text{PCI-CF}(\mathbf{C}_{3\tilde{\sigma}}) + \text{PCI-CF}(\mathbf{D}_{2\tilde{\sigma}}) + \text{PCI-CF}(\mathbf{T}_{\tilde{\sigma}}) \\ &= \frac{1}{4}b_1^2b_2 - \frac{1}{4}a_1^2a_2 + \frac{1}{4}a_2^2 - \frac{1}{4}a_2c_2 + \frac{1}{4}b_4 - \frac{1}{4}c_4 \end{aligned} \quad (11.129)$$

$$\begin{aligned} \text{CI-CF}^{\text{[III]}}(\mathbf{T}_{d\tilde{\sigma}\tilde{\tau}}) &= \text{PCI-CF}(\mathbf{C}_1) + \text{PCI-CF}(\mathbf{C}_2) + \text{PCI-CF}(\mathbf{C}_3) \\ &\quad + \text{PCI-CF}(\mathbf{D}_2) + \text{PCI-CF}(\mathbf{T}) \\ &= \frac{1}{48}b_1^4 - \frac{1}{48}a_1^4 - \frac{1}{8}b_1^2b_2 + \frac{1}{4}a_1^2a_2 - \frac{1}{8}a_1^2c_2 + \frac{1}{6}b_1b_3 - \frac{1}{6}a_1a_3 \\ &\quad + \frac{1}{16}b_2^2 - \frac{1}{4}a_2^2 + \frac{1}{4}a_2c_2 - \frac{1}{16}c_2^2 + \frac{1}{8}c_4 - \frac{1}{8}b_4 \end{aligned} \quad (11.130)$$

$$\begin{aligned} \text{CI-CF}^{\text{[IV]}}(\mathbf{T}_{d\tilde{\sigma}\tilde{\tau}}) &= \text{PCI-CF}(\mathbf{C}_{s\tilde{\sigma}\tilde{\sigma}}) + \text{PCI-CF}(\mathbf{C}_{s\tilde{\sigma}\tilde{\tau}}) + \text{PCI-CF}(\mathbf{S}_{4\tilde{\sigma}}) \\ &\quad + \text{PCI-CF}(\mathbf{S}_{4\tilde{\tau}}) + \text{PCI-CF}(\mathbf{S}_{4\tilde{\sigma}\tilde{\sigma}}) + \text{PCI-CF}(\mathbf{C}_{2v\tilde{\sigma}\tilde{\tau}}) \\ &\quad + \text{PCI-CF}(\mathbf{C}_{3v\tilde{\sigma}\tilde{\tau}}) + \text{PCI-CF}(\mathbf{D}_{2d\tilde{\sigma}\tilde{\tau}}) + \text{PCI-CF}(\mathbf{T}_{d\tilde{\sigma}\tilde{\tau}}) \\ &= \frac{1}{2}a_1^2a_2 - \frac{1}{2}a_2^2 + \frac{1}{2}a_2c_2 + \frac{1}{2}c_4 \end{aligned} \quad (11.131)$$

$$\begin{aligned} \text{CI-CF}^{\text{[V]}}(\mathbf{T}_{d\tilde{\sigma}\tilde{\tau}}) &= \text{PCI-CF}(\mathbf{C}_s) + \text{PCI-CF}(\mathbf{S}_4) + \text{PCI-CF}(\mathbf{C}_{2v}) \\ &\quad + \text{PCI-CF}(\mathbf{C}_{3v}) + \text{PCI-CF}(\mathbf{D}_{2d}) + \text{PCI-CF}(\mathbf{T}_d) \\ &= \frac{1}{4}a_1^2c_2 - \frac{1}{4}a_1^2a_2 + \frac{1}{4}a_2^2 - \frac{1}{4}a_2c_2. \end{aligned} \quad (11.132)$$

These CI-CFs for type-itemized enumeration can be alternatively obtained by starting from the data of the USCI-CF-column and of the TEM-column of Table 11.2 according to Def. 10.7 (page 301). These CI-CFs have been once noted in [4].

The CI-CFs (Eq. 11.128–11.132) are verified by comparison with those of [8], which have been calculated by means of an alternative method of type itemization without subdivision through the 33 subgroups of $\text{SSG}\mathbf{T}_{d\tilde{\sigma}\tilde{\tau}}$. That is to say, CI-CF^[I] (Eq. 11.128) is identical with Eq. 83 of [8]; CI-CF^[II] (Eq. 11.129) with Eq. 84 of [8]; CI-CF^[III] (Eq. 11.130) with Eq. 85 of [8]; CI-CF^[IV] (Eq. 11.131) with Eq. 81 of [8]; and CI-CF^[V] (Eq. 11.132) is identical with Eq. 82 of [8].

Generating Functions for Type-Itemized Enumeration

The ligand-inventory functions (Eqs. 11.80–11.82) are introduced into the CI-CFs (Eqs. 11.128–11.132) so as to give the following generating functions:

$$f^{[I]} = \{p\bar{p}q\bar{q} + p\bar{p}r\bar{r} + \dots\} + ABXY \quad (11.133)$$

$$\begin{aligned} f^{[II]} = & \left\{ \frac{1}{2} (A^2 B p + A^2 B \bar{p}) + \dots \right\} + \left\{ \frac{1}{2} (A B p^2 + A B \bar{p}^2) + \dots \right\} \\ & + \left\{ \frac{1}{2} (A^2 p q + A^2 \bar{p} \bar{q}) + \dots \right\} + \left\{ \frac{1}{2} (A p^2 \bar{p} + A p \bar{p}^2) + \dots \right\} \\ & + \left\{ \frac{1}{2} (A p^2 q + A \bar{p}^2 \bar{q}) + \dots \right\} + \left\{ \frac{1}{2} (p^2 \bar{p} q + p \bar{p}^2 \bar{q}) + \dots \right\} \\ & + \left\{ \frac{1}{2} (p^2 q \bar{q} + \bar{p}^2 q \bar{q}) + \dots \right\} + \left\{ \frac{1}{2} (p^2 q r + \bar{p}^2 \bar{q} r) + \dots \right\} \\ & + \left\{ \frac{1}{2} (A^2 p^2 + A^2 \bar{p}^2) + \dots \right\} + \left\{ \frac{1}{2} (p^2 q^2 + \bar{p}^2 \bar{q}^2) + \dots \right\} \\ & + \left\{ \frac{1}{2} (A^3 p + A^3 \bar{p}) + \dots \right\} + \left\{ \frac{1}{2} (A p^3 + A \bar{p}^3) + \dots \right\} \\ & + \left\{ \frac{1}{2} (p^3 q + \bar{p}^3 \bar{q}) + \dots \right\} + \left\{ \frac{1}{2} (p^3 \bar{p} + p \bar{p}^3) + \dots \right\} \\ & + \left\{ \frac{1}{2} (p^4 + \bar{p}^4) + \dots \right\} \end{aligned} \quad (11.134)$$

$$\begin{aligned} f^{[III]} = & \left\{ \frac{1}{2} (A B X p + A B X \bar{p}) + \dots \right\} + \left\{ \frac{1}{2} (A B p q + A B \bar{p} \bar{q}) + \dots \right\} \\ & + \left\{ \frac{1}{2} (A p \bar{p} q + A p \bar{p} \bar{q}) + \dots \right\} + \left\{ \frac{1}{2} (A p q r + A p \bar{q} r) + \dots \right\} \\ & + \left\{ \frac{1}{2} (p q r s + \bar{p} \bar{q} r \bar{s}) + \dots \right\} + \left\{ \frac{1}{2} (p \bar{p} q r + p \bar{p} \bar{q} r) + \dots \right\} \end{aligned} \quad (11.135)$$

$$\begin{aligned} f^{[IV]} = & \{A^2 p \bar{p} + \dots\} + \{A^2 B X + A^2 B Y + \dots\} \\ & + \{p^2 \bar{p}^2 + q^2 \bar{q}^2 + r^2 \bar{r}^2 + s^2 \bar{s}^2\} + \{A^2 B^2 + A^2 X^2 + A^2 Y^2 + \dots\} \\ & + \{A^3 B + A^3 X + A^3 Y + \dots\} + \{A^4 + B^4 + X^4 + Y^4\} \end{aligned} \quad (11.136)$$

$$f^{[V]} = \{A B p \bar{p} + A B q \bar{q} + \dots\}. \quad (11.137)$$

These generating functions have been once noted in [4].



Exercise 11.7. Check each term appearing in the generating functions (Eqs. 11.133–11.137) by referring to Fig. 11.2, where representative promolecules are categorized into five types.

The generating functions (Eqs. 11.133–11.137) are also obtained by starting from the generating functions for the respective subgroups (Eq. 11.83–11.96), where these are added according to the categories shown in Eqs. 11.7–11.11. The generating functions (Eqs. 11.133–11.137) are identical with Eqs. 86–90 of [8], which have been calculated by an alternative method.



Exercise 11.8.

- Calculate a CI-CF for gross enumeration under the *RS*-stereoisomeric group $T_{d\widehat{\sigma}\widehat{\tau}}$ according to Def. 10.8 (page 303). For the USCI-CFs and the TEM of $T_{d\widehat{\sigma}\widehat{\tau}}$, see Table 11.2.
- Apply Def. 10.9 (page 304) to another calculation of the CI-CF for $T_{d\widehat{\sigma}\widehat{\tau}}$. For PSIs necessary to this calculation, see the PSI-column Table 11.1.
- Confirm that the two modes of calculations generate identical CI-CFs.

11.4 Comparison with Enumeration Under Subsymmetries

11.4.1 Enumeration of Tetrahedral Promolecules Under the Point-Group Symmetry

The enumeration of tetrahedral promolecules under the point-group symmetry has been already discussed in Chapter 5. According to Theorem 10.6 (page 306), the symmetry-itemized generating functions under the action of the point group T_d (Eqs. 6.94–6.102) are correlated to those under the action of $T_{d\widehat{\sigma}\widehat{\tau}}$ (Eqs. 11.83–11.96).

$$f_{3-5}(C_1) = 2f_{C_1} + f_{C_{\bar{\sigma}}} + f_{C_{\bar{\sigma}}} + f_{C_{\bar{\tau}}} \quad (11.138)$$

$$f_{3-5}(C_2) = f_{C_{2\bar{\sigma}}} \quad (11.139)$$

$$f_{3-5}(C_s) = 2f_{C_s} + f_{C_{s\bar{\sigma}\bar{\sigma}}} + f_{C_{s\bar{\sigma}\bar{\tau}}} \quad (11.140)$$

$$f_{3-5}(C_3) = f_{C_{3\bar{\sigma}}} \quad (11.141)$$

$$f_{3-5}(S_4) = f_{S_{4\bar{\sigma}\bar{\sigma}}} \quad (11.142)$$

$$f_{3-5}(C_{2v}) = f_{C_{2v\bar{\sigma}\bar{\tau}}} \quad (11.143)$$

$$f_{3-5}(C_{3v}) = f_{C_{3v\bar{\sigma}\bar{\tau}}} \quad (11.144)$$

$$f_{3-5}(T) = f_{T_{\bar{\sigma}}} \quad (11.145)$$

$$f_{3-5}(T_d) = f_{T_{d\bar{\sigma}\bar{\tau}}}, \quad (11.146)$$

where the generating functions other than Eqs. 11.83–11.96 are omitted in the right-hand sides for the simplicity's sake, because they vanish to zero.

The terms appearing in the right-hand sides of the generating functions represented by Eqs. 6.94 ($f_{3.5}(C_1)$), 6.95 ($f_{3.5}(C_2)$), 6.97 ($f_{3.5}(C_3)$), 6.101 ($f_{3.5}(T)$) cover all of the promolecules collected in the type-I, type-II, and type-III frames of Fig. 6.9 (page 157). All of these promolecules are concluded to be chiral. This conclusion is confirmed by the *RS*-stereoisomeric groups appearing in the right-hand sides of Eqs. 11.138, 11.139, 11.141, and 11.145. As shown in Eqs. 11.7–11.11, these *RS*-stereoisomeric groups belong to type I, II, or III, which exhibits chirality.

On the other hand, the terms appearing in the right-hand sides of the generating functions represented by Eqs. 11.140 ($f_{3.5}(C_s)$), 11.142 ($f_{3.5}(S_4)$), 11.143 ($f_{3.5}(C_{2v})$), 11.144 ($f_{3.5}(C_{3v})$), and 11.146 ($f_{3.5}(T_d)$) cover all of the promolecules collected in the type-IV and type-V frames of Fig. 6.9 (page 157). All of these promolecules are concluded to be achiral. This conclusion is confirmed by the *RS*-stereoisomeric groups appearing in the right-hand sides of Eqs. 11.140–11.144, and 11.146. As shown in Eqs. 11.7–11.11, these *RS*-stereoisomeric groups belong to type IV or V, which exhibits achirality.

The validity of the alternative calculation by Eqs. 11.138–11.146 is confirmed by the derivation of the PCI-CFs (Eqs. 6.83–6.93) from the PCI-CFs (Eqs. 11.47–11.79). According to Theorem 10.6 (page 306), the PCI-CFs of type-III and type-V among Eqs. 11.47–11.79 are multiplied by 2:

$$\begin{aligned} \text{PCI-CF}_{3.5}(C_1) &= 2\text{PCI-CF}(C_1) + \text{PCI-CF}(C_{\bar{\sigma}}) + \text{PCI-CF}(C_{\bar{\sigma}}) + \text{PCI-CF}(C_{\bar{\tau}}) \\ &= \frac{1}{24}b_1^4 - \frac{1}{8}b_2^2 - \frac{1}{4}a_1^2c_2 - \frac{1}{6}b_1b_3 + \frac{1}{4}b_4 \\ &\quad + \frac{1}{4}a_2^2 + \frac{1}{2}a_1a_3 - \frac{1}{2}a_4 \end{aligned} \quad (11.147)$$

$$\begin{aligned} \text{PCI-CF}_{3.5}(C_2) &= 2\text{PCI-CF}(C_2) + \text{PCI-CF}(S_4) + \text{PCI-CF}(C_{2\bar{\sigma}}) \\ &\quad + \text{PCI-CF}(C_{2\bar{\sigma}}) + \text{PCI-CF}(C_{2\bar{\tau}}) \\ &= \frac{1}{4}b_2^2 - \frac{1}{4}c_4 - \frac{1}{4}b_4 - \frac{1}{4}a_2^2 + \frac{1}{2}a_4 \end{aligned} \quad (11.148)$$

$$\begin{aligned} \text{PCI-CF}_{3.5}(C_s) &= 2\text{PCI-CF}(C_s) + \text{PCI-CF}(C_{s\bar{\sigma}\bar{\sigma}}) + \text{PCI-CF}(C_{s\bar{\sigma}\bar{\tau}}) \\ &= \frac{1}{2}a_1^2c_2 - \frac{1}{2}a_2^2 - a_1a_3 + a_4; \end{aligned} \quad (11.149)$$

$$\begin{aligned} \text{PCI-CF}_{3.5}(C_3) &= 2\text{PCI-CF}(C_3) + \text{PCI-CF}(C_{3\bar{\sigma}}) + \text{PCI-CF}(C_{3\bar{\tau}}) \\ &= \frac{1}{2}b_1b_3 - \frac{1}{2}a_1a_3 - \frac{1}{2}b_4 + \frac{1}{2}a_4 \end{aligned} \quad (11.150)$$

$$\begin{aligned} \text{PCI-CF}_{3.5}(S_4) &= 2\text{PCI-CF}(S_4) + \text{PCI-CF}(S_{4\bar{\sigma}}) + \text{PCI-CF}(S_{4\bar{\tau}}) + \text{PCI-CF}(S_{4\bar{\sigma}\bar{\sigma}}) \\ &= \frac{1}{2}c_4 - \frac{1}{2}a_4 \end{aligned} \quad (11.151)$$

$$\begin{aligned} \text{PCI-CF}_{3.5}(D_2) &= 2\text{PCI-CF}(D_2) + \text{PCI-CF}(D_{2\bar{\sigma}}) + \text{PCI-CF}(D_{2\bar{\tau}}) \\ &= 0 \end{aligned} \quad (11.152)$$

$$\text{PCI-CF}_{3.5}(C_{2v}) = 2\text{PCI-CF}(C_{2v}) + \text{PCI-CF}(C_{2v\bar{\sigma}\bar{\tau}})$$

$$= \frac{1}{2}a_2^2 - \frac{1}{2}a_4 \quad (11.153)$$

$$\begin{aligned} \text{PCI-CF}_{3.5}(\mathbf{C}_{3v}) &= 2\text{PCI-CF}(\mathbf{C}_{3v}) + \text{PCI-CF}(\mathbf{C}_{3v\widehat{\sigma I}}) \\ &= a_1a_3 - a_4 \end{aligned} \quad (11.154)$$

$$\begin{aligned} \text{PCI-CF}_{3.5}(\mathbf{D}_{2d}) &= 2\text{PCI-CF}(\mathbf{D}_{2d}) + \text{PCI-CF}(\mathbf{D}_{2d\widehat{\sigma I}}) \\ &= 0 \end{aligned} \quad (11.155)$$

$$\begin{aligned} \text{PCI-CF}_{3.5}(\mathbf{T}) &= 2\text{PCI-CF}(\mathbf{T}) + \text{PCI-CF}(\mathbf{T}_{\widehat{\sigma}}) + \text{PCI-CF}(\mathbf{T}_{\widehat{\tau}}) \\ &= \frac{1}{2}b_4 - \frac{1}{2}a_4 \end{aligned} \quad (11.156)$$

$$\begin{aligned} \text{PCI-CF}_{3.5}(\mathbf{T}_d) &= 2\text{PCI-CF}(\mathbf{T}_d) + \text{PCI-CF}(\mathbf{T}_{d\widehat{\sigma I}}) \\ &= a_4. \end{aligned} \quad (11.157)$$

Note that, as for $\text{PCI-CF}_{3.5}(\mathbf{G}_i)$ ($\mathbf{G}_i \in \text{SSG}_{\mathbf{T}_d}$), the PCI-CF of $\widehat{\mathbf{G}}_j$ ($\widehat{\mathbf{G}}_j \in \text{SSG}_{\mathbf{T}_{d\widehat{\sigma I}}}$) is adopted if $\widehat{\mathbf{G}}_j \cap \mathbf{T}_d = \mathbf{G}_i$. The resulting PCI-CFs (Eqs. 11.147–11.157) are identical with the PCI-CFs calculated by Fujita's USCI approach (Eqs. 6.83–6.93 on page 155).

11.4.2 Enumeration of Tetrahedral Promolecules Under the *RS*-Permutation-Group Symmetry

The enumeration of tetrahedral promolecules under the *RS*-permutation group has been already discussed in Chapter 9. The generating functions (Eqs. 9.44–9.48 on page 256) calculated under the action of the *RS*-permutation group $\mathbf{T}_{\widehat{\sigma}}$ can be correlated to those listed in Eqs. 11.83–11.96, which are calculated under the action of the *RS*-stereoisomeric group $\mathbf{T}_{d\widehat{\sigma I}}$.

They are concerned with the numbers of inequivalent (self-)*RS*-diastereomeric pairs, so that the quadruplet of each type-II (or type-III) stereoisogram consists of two inequivalent (self-)*RS*-diastereomeric pairs, while the quadruplet of each type-I (or type-IV, or type-V) stereoisogram consists of one (self-)*RS*-diastereomeric pairs (Theorem 10.7 on page 308). Thereby, the generating functions represented by Eqs. 9.44–9.48 can be alternatively obtained by starting from Eqs. 11.83–11.96. For example, the four groups \mathbf{C}_1 , $\mathbf{C}_{\widehat{\sigma}}$, \mathbf{C}_s , and $\mathbf{C}_{\widehat{\tau}}$ as subgroups of $\mathbf{T}_{d\widehat{\sigma I}}$ degenerate into the subgroup \mathbf{C}_1 of $\mathbf{T}_{\widehat{\sigma}}$, because of $\mathbf{C}_1 \cap \mathbf{T}_{\widehat{\sigma}} = \mathbf{C}_1$, $\mathbf{C}_{\widehat{\sigma}} \cap \mathbf{T}_{\widehat{\sigma}} = \mathbf{C}_1$, $\mathbf{C}_s \cap \mathbf{T}_{\widehat{\sigma}} = \mathbf{C}_1$, and $\mathbf{C}_{\widehat{\tau}} \cap \mathbf{T}_{\widehat{\sigma}} = \mathbf{C}_1$. It follows that the generating function $f'_{3.5}(\mathbf{C}_1)$ (Eq. 9.44) can be calculated by the sum represented by $2f_{\mathbf{C}_1} + f_{\mathbf{C}_{\widehat{\sigma}}} + f_{\mathbf{C}_s} + f_{\mathbf{C}_{\widehat{\tau}}}$, in which the coefficient 2 of the term $2f_{\mathbf{C}_1}$ stems from the type-III feature of the subgroup \mathbf{C}_1 ($\subset \mathbf{T}_{\widehat{\sigma}}$). In a similar way, the generating functions represented by Eqs. 9.44–9.48 are alternatively calculated as follows:

$$f'_{3.5}(\mathbf{C}_1) = 2f_{\mathbf{C}_1} + f_{\mathbf{C}_{\widehat{\sigma}}} + f_{\mathbf{C}_s} + f_{\mathbf{C}_{\widehat{\tau}}} \quad (11.158)$$

$$f'_{3.5}(\mathbf{C}_{\widehat{\sigma}}) = 2f_{\mathbf{C}_{\widehat{\sigma}}} + f_{\mathbf{C}_{s\widehat{\sigma\sigma}}} + f_{\mathbf{C}_{s\widehat{\sigma I}}} \quad (11.159)$$

$$f'_{3.5}(\mathbf{C}_{2\widehat{\sigma}}) = 2f_{\mathbf{C}_{2\widehat{\sigma}}} + f_{\mathbf{S}_{4\widehat{\sigma\sigma}}} + f_{\mathbf{C}_{2v\widehat{\sigma I}}} \quad (11.160)$$

$$f'_{3.5}(\mathbf{C}_{3\widehat{\sigma}}) = 2f_{\mathbf{C}_{3\widehat{\sigma}}} + f_{\mathbf{C}_{3v\widehat{\sigma I}}} \quad (11.161)$$

$$f'_{3.5}(\mathbf{T}_{\bar{\sigma}}) = 2f_{T_{\bar{\sigma}}} + f_{T_{d\bar{\sigma}\bar{\Gamma}}}, \quad (11.162)$$

where the generating functions other than Eqs. 11.83–11.96 are omitted in the right-hand sides for the simplicity's sake, because they vanish to zero.

Exercise 11.9. Derive the PCI (Eqs. 9.32–9.42 on page 256) from the PCI-CFs (Eqs. 11.47–11.79). See the derivation of Eqs. 10.150–10.153 (page 309).

The terms appearing in the right-hand side of the generating function $f'_{3.5}(\mathbf{C}_1)$ (Eq. 9.44 on page 256) cover all of the promolecules collected in the type-I, type-III, and type-V frames of Fig. 9.10 (page 255). All of these promolecules are concluded to be *RS*-stereogenic, so as to be specified by *RS*-stereodescriptors, which will be discussed later. This conclusion is confirmed by the *RS*-stereoisomeric groups appearing in the right-hand side of Eq. 11.158. As shown in Eqs. 11.7–11.11, the *RS*-stereoisomeric groups $\mathbf{C}_{\bar{\Gamma}}$ and $\mathbf{C}_{\bar{\sigma}}$ are categorized to type I; \mathbf{C}_1 is categorized to type III; and \mathbf{C}_s is categorized to type V.

The terms appearing in the right-hand side of the generating function $f'_{3.5}(\mathbf{C}_{\bar{\sigma}})$ (Eq. 9.45 on page 257) cover all of the promolecules (type II or type IV) specified by *pro-R/pro-S*-descriptors. This point will be discussed later.

The validity of the alternative calculation by Eqs. 11.158–11.162 is confirmed by the derivation of the PCI (Eqs. 9.32–9.42 on page 256) from the PCI-CFs (Eqs. 11.47–11.79). According to Theorem 10.7 (page 308), the PCI-CFs of type-II and type-III among Eqs. 11.47–11.79 are multiplied by 2:

$$\begin{aligned} \text{PCI-CF}'_{3.5}(\mathbf{C}_1) &= 2\text{PCI-CF}(\mathbf{C}_1) + \text{PCI-CF}(\mathbf{C}_s) + \text{PCI-CF}(\mathbf{C}_{\bar{\sigma}}) + \text{PCI-CF}(\mathbf{C}_{\bar{\Gamma}}) \\ &= \frac{1}{24}b_1^4 + \frac{1}{8}b_2^2 - \frac{1}{4}b_1^2b_2 + \frac{1}{3}b_1b_3 - \frac{1}{4}b_4 \end{aligned} \quad (11.163)$$

$$\begin{aligned} \text{PCI-CF}'_{3.5}(\mathbf{C}_2) &= 2\text{PCI-CF}(\mathbf{C}_2) + \text{PCI-CF}(\mathbf{S}_4) + \text{PCI-CF}(\mathbf{C}_{2v}) \\ &\quad + \text{PCI-CF}(\mathbf{C}_{2\bar{\sigma}}) + \text{PCI-CF}(\mathbf{C}_{2\bar{\Gamma}}) \\ &= 0 \end{aligned} \quad (11.164)$$

$$\begin{aligned} \text{PCI-CF}'_{3.5}(\mathbf{C}_{\bar{\sigma}}) &= 2\text{PCI-CF}(\mathbf{C}_{\bar{\sigma}}) + \text{PCI-CF}(\mathbf{C}_{s\bar{\sigma}\bar{\sigma}}) + \text{PCI-CF}(\mathbf{C}_{s\bar{\sigma}\bar{\Gamma}}) \\ &= \frac{1}{2}b_1^2b_2 - \frac{1}{2}b_2^2 - b_1b_3 + b_4 \end{aligned} \quad (11.165)$$

$$\begin{aligned} \text{PCI-CF}'_{3.5}(\mathbf{C}_3) &= 2\text{PCI-CF}(\mathbf{C}_3) + \text{PCI-CF}(\mathbf{C}_{3v}) + \text{PCI-CF}(\mathbf{C}_{3\bar{\Gamma}}) \\ &= 0 \end{aligned} \quad (11.166)$$

$$\begin{aligned} \text{PCI-CF}'_{3.5}(\mathbf{S}_4) &= 2\text{PCI-CF}(\mathbf{S}_4) + \text{PCI-CF}(\mathbf{S}_{4\bar{\sigma}}) + \text{PCI-CF}(\mathbf{S}_{4\bar{\Gamma}}) \\ &= 0 \end{aligned} \quad (11.167)$$

$$\begin{aligned} \text{PCI-CF}'_{3.5}(\mathbf{D}_2) &= 2\text{PCI-CF}(\mathbf{D}_2) + \text{PCI-CF}(\mathbf{D}_{2d}) + \text{PCI-CF}(\mathbf{D}_{2\bar{\Gamma}}) \\ &= 0 \end{aligned} \quad (11.168)$$

$$\begin{aligned} \text{PCI-CF}'_{3.5}(\mathbf{C}_{2\bar{\sigma}}) &= 2\text{PCI-CF}(\mathbf{C}_{2\bar{\sigma}}) + \text{PCI-CF}(\mathbf{S}_{4\bar{\sigma}\bar{\sigma}}) + \text{PCI-CF}(\mathbf{C}_{2v\bar{\sigma}\bar{\Gamma}}) \\ &= \frac{1}{2}b_2^2 - \frac{1}{2}b_4 \end{aligned} \quad (11.169)$$

$$\begin{aligned} \text{PCI-CF}'_{3.5}(\mathbf{C}_{3\bar{\sigma}}) &= 2\text{PCI-CF}(\mathbf{C}_{3\bar{\sigma}}) + \text{PCI-CF}(\mathbf{C}_{3v\bar{\sigma}\hat{\Gamma}}) \\ &= b_1 b_3 - b_4 \end{aligned} \quad (11.170)$$

$$\begin{aligned} \text{PCI-CF}'_{3.5}(\mathbf{D}_{2\bar{\sigma}}) &= 2\text{PCI-CF}(\mathbf{D}_{2\bar{\sigma}}) + \text{PCI-CF}(\mathbf{D}_{2d\bar{\sigma}\hat{\Gamma}}) \\ &= 0 \end{aligned} \quad (11.171)$$

$$\begin{aligned} \text{PCI-CF}'_{3.5}(\mathbf{T}) &= 2\text{PCI-CF}(\mathbf{T}) + \text{PCI-CF}(\mathbf{T}_d) + \text{PCI-CF}(\mathbf{T}_{\hat{\Gamma}}) \\ &= 0 \end{aligned} \quad (11.172)$$

$$\begin{aligned} \text{PCI-CF}'_{3.5}(\mathbf{T}_{\bar{\sigma}}) &= 2\text{PCI-CF}(\mathbf{T}_{\bar{\sigma}}) + \text{PCI-CF}(\mathbf{T}_{d\bar{\sigma}\hat{\Gamma}}) \\ &= b_4, \end{aligned} \quad (11.173)$$

where the terms containing a_d and/or c_d vanish to give zero values. Note that, as for $\text{PCI-CF}_{3.5}(\mathbf{G}_i)$ ($\mathbf{G}_i \in \text{SSG}_{\mathbf{T}_{\bar{\sigma}}}$), the PCI-CF of $\hat{\mathbf{G}}_j$ ($\hat{\mathbf{G}}_j \in \text{SSG}_{\mathbf{T}_{d\bar{\sigma}\hat{\Gamma}}}$) is adopted if $\hat{\mathbf{G}}_j \cap \mathbf{T}_{d\bar{\sigma}\hat{\Gamma}} = \mathbf{G}_i$.

The resulting PCI-CFs (Eqs. 11.163–11.173) are identical with the PCIs (Eqs. 9.32–9.42 on page 256) if we put $s_d = b_d$.

11.4.3 Comparison with Enumeration Under Maximum-Chiral Point Subgroups

As discussed in Subsection 10.3.3, the reference promolecule of a stereoisogram, which belongs to an *RS*-stereoisomeric group, can be alternatively regarded as belonging to a maximum-chiral point group (cf. Subsection 7.3.5). The practices of enumeration under the action of \mathbf{T} are open to readers as an exercise:



Exercise 11.10. The data of the point group \mathbf{T} have been reported in Fujita's monograph [7], e.g., the inverse mark table [7, Table B.9] and the USCI-CF table [7, Table E.9].

- Calculate PCI-CFs for characterizing the tetrahedral skeleton **3-5** (page 55) under the action of \mathbf{T} .
- Calculate generating functions, where each promolecule is counted once under the action of \mathbf{T} .

The validity of the calculation for Exercise 11.10 is confirmed by the derivation of PCI-CFs from the PCIs (Eqs. 11.47–11.79). According to Theorem 10.8 (page 310), the PCI-CFs of type-III among Eqs. 11.47–11.79 are multiplied by 4; and the PCI-CFs of type-I, II, and V among Eqs. 11.47–11.79 are multiplied by 2.

$$\begin{aligned} \text{PCI-CF}''_{3.5}(\mathbf{C}_1) &= 4\text{PCI-CF}(\mathbf{C}_1) + 2\text{PCI-CF}(\mathbf{C}_s) + 2\text{PCI-CF}(\mathbf{C}_{\bar{\sigma}}) + 2\text{PCI-CF}(\mathbf{C}_{\hat{\Gamma}}) \\ &\quad + 2\text{PCI-CF}(\mathbf{C}_{\bar{\sigma}}) + \text{PCI-CF}(\mathbf{C}_{s\bar{\sigma}\hat{\Gamma}}) + \text{PCI-CF}(\mathbf{C}_{s\bar{\sigma}\hat{\Gamma}}) \\ &= \frac{1}{12}b_1^4 - \frac{1}{4}b_2^2 - \frac{1}{3}b_1b_3 + \frac{1}{2}b_4 \end{aligned} \quad (11.174)$$

$$\text{PCI-CF}''_{3.5}(\mathbf{C}_2) = 4\text{PCI-CF}(\mathbf{C}_2) + 2\text{PCI-CF}(\mathbf{S}_4) + 2\text{PCI-CF}(\mathbf{C}_{2v})$$

$$\begin{aligned}
& + 2\text{PCI-CF}(\mathbf{C}_{2\tilde{\sigma}}) + 2\text{PCI-CF}(\mathbf{C}_{2\tilde{\tau}}) \\
& + 2\text{PCI-CF}(\mathbf{S}_{\tilde{4}}) + \text{PCI-CF}(\mathbf{S}_{4\tilde{\sigma}}) + \text{PCI-CF}(\mathbf{S}_{4\tilde{\tau}}) \\
& + 2\text{PCI-CF}(\mathbf{C}_{2\tilde{\sigma}}) + \text{PCI-CF}(\mathbf{S}_{4\tilde{\sigma}\tilde{\sigma}}) + \text{PCI-CF}(\mathbf{C}_{2\nu\tilde{\sigma}\tilde{\tau}}) \\
& = \frac{1}{2}b_2^2 - \frac{1}{2}b_4
\end{aligned} \tag{11.175}$$

$$\begin{aligned}
\text{PCI-CF}_{3.5}''(\mathbf{C}_3) & = 4\text{PCI-CF}(\mathbf{C}_3) + 2\text{PCI-CF}(\mathbf{C}_{3\nu}) + 2\text{PCI-CF}(\mathbf{C}_{3\tilde{\tau}}) \\
& + 2\text{PCI-CF}(\mathbf{C}_{3\tilde{\sigma}}) + \text{PCI-CF}(\mathbf{C}_{3\nu\tilde{\sigma}\tilde{\tau}}) \\
& = b_1b_3 - b_4
\end{aligned} \tag{11.176}$$

$$\begin{aligned}
\text{PCI-CF}_{3.5}''(\mathbf{D}_2) & = 4\text{PCI-CF}(\mathbf{D}_2) + 2\text{PCI-CF}(\mathbf{D}_{2d}) + 2\text{PCI-CF}(\mathbf{D}_{2\tilde{\tau}}) \\
& + 2\text{PCI-CF}(\mathbf{D}_{2\tilde{\sigma}}) + \text{PCI-CF}(\mathbf{D}_{2d\tilde{\sigma}\tilde{\tau}}) \\
& = 0
\end{aligned} \tag{11.177}$$

$$\begin{aligned}
\text{PCI-CF}_{3.5}''(\mathbf{T}) & = 4\text{PCI-CF}(\mathbf{T}) + 2\text{PCI-CF}(\mathbf{T}_d) + 2\text{PCI-CF}(\mathbf{T}_{\tilde{\tau}}) \\
& + 2\text{PCI-CF}(\mathbf{T}_{\tilde{\sigma}}) + \text{PCI-CF}(\mathbf{T}_{d\tilde{\sigma}\tilde{\tau}}) \\
& = b_4,
\end{aligned} \tag{11.178}$$

where the terms containing a_d and/or c_d vanish during summation. Note that, as for $\text{PCI-CF}_{3.5}(\mathbf{G}_i)$ ($\mathbf{G}_i \in \text{SSG}_{\mathbf{T}}$), the PCI-CF of $\hat{\mathbf{G}}_j$ ($\hat{\mathbf{G}}_j \in \text{SSG}_{\mathbf{T}_{d\tilde{\sigma}\tilde{\tau}}}$) is adopted if $\hat{\mathbf{G}}_j \cap \mathbf{T} = \mathbf{G}_i$.

11.4.4 Confusion Between the Point-Group Symmetry and the *RS*-Permutation-Group Symmetry

Each promolecule shown in Fig. 11.2 is a representative of a set of terms contained in each pair of braces in the generating functions, i.e., Eqs. 11.83–11.96 (page 329) under the action of *RS*-stereoisomeric group $\mathbf{T}_{d\tilde{\sigma}\tilde{\tau}}$, Eqs. 6.94–6.102 (page 156) under the action of the point group \mathbf{T}_d , or Eqs. 9.44–9.48 (page 256) under the action of the *RS*-permutation group $\mathbf{T}_{\tilde{\sigma}}$. For the convenience of cross reference, each pair of braces in these generating functions is characterized by the partition ($[\theta]_i$, $i = 1-30$) attached above.

Each promolecule shown in Fig. 11.2 is attached by a pair of brackets which contains a list of its *RS*-stereoisomeric group (cf. Eqs. 11.83–11.96), its point group (cf. Eqs. 6.94–6.102), its *RS*-permutation group (cf. Eqs. 9.44–9.48), and the stereoisogram type. For example, the bracket symbol [$\mathbf{C}_{\tilde{\tau}}$, \mathbf{C}_1 , \mathbf{C}_1 ; I] attached to **11-3** (Fig. 11.2) indicates that the promolecule **11-3** belongs to the *RS*-stereoisomeric group $\mathbf{C}_{\tilde{\tau}}$ (cf. Eq. 11.83), to the point group \mathbf{C}_1 (cf. Eq. 6.94), and to the *RS*-permutation group \mathbf{C}_1 (cf. Eq. 9.44); as well as **11-3** is characterized by a type-I stereoisogram.

Point-group symmetry is effective to discuss geometrical features of stereochemistry, while *RS*-permutation-group symmetry is concerned with the assignment of *R/S*-stereodescriptors to type-I, type-III, and type-V promolecules. They are conceptually distinct, although they have been closely linked in the practice of organic chemistry.

The two modes of enumerations under subsymmetries, i.e., the generating functions (Eqs. 6.94–6.102 on page 156) under the point-group symmetry and the generating functions (Eqs. 9.44–9.48 on page 256) under the *RS*-permutation-group symmetry, clearly demonstrate that modern stereochemistry has confused the point-group symmetry with the *RS*-permutation-group symmetry. As found by this quantitative comparison based on combinatorial enumeration, the confusion stems from the fact that modern stereochemistry is restricted to qualitative discussions without mathematical formulations.

The enumerations under subsymmetries have been integrated to accomplish the enumeration under *RS*-stereoisomeric-group symmetry, i.e., the generating functions represented by Eqs. 11.83–11.96. Thereby, we are able to obtain reliable mathematical formulations on the basis of stereoisograms.

References

- [1] S. Fujita, *J. Math. Chem.*, **52**, 508–542 (2014).
- [2] S. Fujita, *Tetrahedron: Asymmetry*, **25**, 1169–1189 (2014).
- [3] S. Fujita, *Tetrahedron: Asymmetry*, **25**, 1153–1168 (2014).
- [4] S. Fujita, *J. Math. Chem.*, **52**, 543–574 (2014).
- [5] S. Fujita, *Polyhedron*, **12**, 95–110 (1993).
- [6] S. Fujita, *Bull. Chem. Soc. Jpn.*, **84**, 1192–1207 (2011).
- [7] S. Fujita, “Symmetry and Combinatorial Enumeration in Chemistry”, Springer-Verlag, Berlin-Heidelberg (1991).
- [8] S. Fujita, *MATCH Commun. Math. Comput. Chem.*, **61**, 71–115 (2009).

12 Stereoisograms for Allene Derivatives¹

12.1 *RS*-Stereoisomeric Group $D_{2d\tilde{\sigma}\hat{I}}$ and Elementary Stereoisogram

Allene derivatives have been enumerated under the point group D_{2d} by the PCI method of Fujita's USCI approach, where the generating functions are shown in Eqs. 6.114–6.121 (page 161) in a symmetry-itemized fashion. The allene skeleton **3-9** (or a top view **6-102**) is depicted in Fig. 6.12 on page 159. Three pairs of enantiomeric allene derivatives with the composition ABXY are depicted in Fig. 6.13(a) on page 162. Two achiral allene derivatives and two pairs of enantiomeric allene derivatives as promolecules with the composition ABp̄p̄ are depicted in Fig. 6.13(b). Gross enumeration of allene derivative under the point group D_{2d} has been conducted to give a generating function Eq. 7.32 (page 185), while gross enumeration under the *RS*-permutation group $D_{2\tilde{\sigma}}$ has been conducted to give a generating function shown in Eq. 9.58 (page 263). The next task is to integrate these results on the basis of Fujita's stereoisogram approach.

In this chapter, the point group D_{2d} and the *RS*-permutation group $D_{2\tilde{\sigma}}$ are integrated into an *RS*-stereoisomeric group $D_{2d\tilde{\sigma}\hat{I}}$ according to the discussions of Chapter 10. As for recent reports on this topic, see [1–4].

The coset representation $D_{2d}/(C_s)$ of the point group D_{2d} is shown in Table 3.2 (page 68). The coset representation $D_{2\tilde{\sigma}}/(C_{\tilde{\sigma}})$ of the *RS*-permutation group $D_{2\tilde{\sigma}}$ is shown in Table 9.5 (page 262). The corresponding ligand-reflection group $D_{2\hat{I}}$ can be easily constructed according to the discussions of Chapter 10. These three groups have a common subgroup D_2 , as summarized in the following coset decompositions:

$$D_{2d} = \underset{A}{D_2} + \underset{B}{D_2\sigma} \quad (12.1)$$

$$D_{2\tilde{\sigma}} = \underset{A}{D_2} + \underset{C}{D_2\tilde{\sigma}} \quad (12.2)$$

$$D_{2\hat{I}} = \underset{A}{D_2} + \underset{D}{D_2\hat{I}}, \quad (12.3)$$

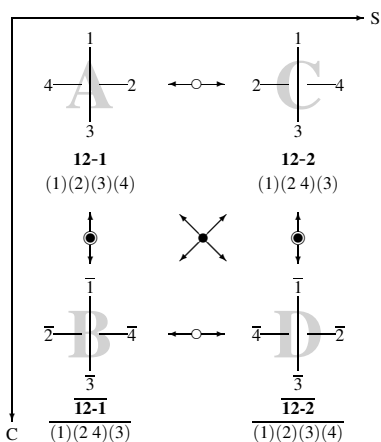
where the symbol σ represents a reflection, the symbol $\tilde{\sigma}$ represents an *RS*-permutation, and the symbol \hat{I} represents a ligand reflection. These three groups are integrated into an *RS*-stereoisomeric group $D_{2d\tilde{\sigma}\hat{I}}$ as follows:

$$D_{2d\tilde{\sigma}\hat{I}} = \underset{A}{D_2} + \underset{B}{D_2\sigma} + \underset{C}{D_2\tilde{\sigma}} + \underset{D}{D_2\hat{I}}, \quad (12.4)$$

¹ This chapter is based on S. Fujita, "Symmetry-Itemized Enumeration of *RS*-Stereoisomers of Allenes. I. The Fixed-Point Matrix Method of the USCI Approach Combined with the Stereoisogram Approach", *J. Math. Chem.*, **52**, 1717–1750 (2014); and S. Fujita, "Symmetry-Itemized Enumeration of *RS*-Stereoisomers of Allenes. II. The Partial-Cycle-Index Method of the USCI Approach Combined with the Stereoisogram Approach", *J. Math. Chem.*, **52**, 1751–1793 (2014).

Table 12.1. Operations of $D_{2d\bar{\sigma}\bar{\tau}}$ and Coset Representation of $D_{2d\bar{\sigma}\bar{\tau}}(/C_{s\bar{\sigma}\bar{\tau}})$ vs. Operations of D_{4h} and Coset Representation of $D_{4h}(/C_{2v}''')$

operation		$D_{4h}(/C_{2v}''')$ or $D_{2d\bar{\sigma}\bar{\tau}}(/C_{s\bar{\sigma}\bar{\tau}})$	PSI	operation		$D_{4h}(/C_{2v}''')$ or $D_{2d\bar{\sigma}\bar{\tau}}(/C_{s\bar{\sigma}\bar{\tau}})$	PSI
$g \in D_{4h}$	$g \in D_{2d\bar{\sigma}\bar{\tau}}$	(product of cycles)		$g \in D_{4h}$	$g \in D_{2d\bar{\sigma}\bar{\tau}}$	(product of cycles)	
I	I	(1)(2)(3)(4)	b_1^4	$C_{2(1)}'$	$\bar{\sigma}_{d(1)}$	(1)(2 4)(3)	$b_1^2 b_2$
$C_{2(3)}$	$C_{2(3)}$	(1 3)(2 4)	b_2^2	$C_{2(2)}'$	$\bar{\sigma}_{d(2)}$	(1 3)(2)(4)	$b_1^2 b_2$
$C_{2(1)}$	$C_{2(1)}$	(1 2)(3 4)	b_2^2	C_4	\bar{S}_4	(1 2 3 4)	b_4
$C_{2(2)}$	$C_{2(2)}$	(1 4)(2 3)	b_2^2	C_4^3	\bar{S}_4^3	(1 4 3 2)	b_4
$\sigma_{d(1)}$	$\sigma_{d(1)}$	(1)(2 4)(3)	$a_1^2 c_2$	σ_h	\bar{I}	(1)(2)(3)(4)	a_1^4
$\sigma_{d(2)}$	$\sigma_{d(2)}$	(1 3)(2)(4)	$a_1^2 c_2$	i	$\bar{C}_{2(3)}$	(1 3)(2 4)	c_2^2
S_4	S_4	(1 2 3 4)	c_4	$\sigma_{v(1)}$	$\bar{C}_{2(1)}$	(1 2)(3 4)	c_2^2
S_4^3	S_4^3	(1 4 3 2)	c_4	$\sigma_{v(2)}$	$\bar{C}_{2(2)}$	(1 4)(2 3)	c_2^2

**Fig. 12.1.** Elementary stereoisogram of numbered allene skeletons. The other modes of sequential numbering are permitted without losing generality.

which represents the coset decomposition of $D_{2d\bar{\sigma}\bar{\tau}}$ by D_2 .

The operations of $D_{2d\bar{\sigma}\bar{\tau}}$ and coset representation of $D_{2d\bar{\sigma}\bar{\tau}}(/C_{s\bar{\sigma}\bar{\tau}})$ are listed in Table 12.1, where the symbols A, B, C, and D correspond to the respective cosets appearing in Eq. 12.4. The A- and B-parts of Table 12.1 stem from Table 3.2 (page 68) of the point group D_{2d} . The A- and C-parts stem from Table 9.5 (page 262) of the *RS*-permutation group $D_{2\bar{\sigma}}$. Recent detailed discussions in [3] have indicated that the *RS*-stereoisomeric group $D_{2d\bar{\sigma}\bar{\tau}}$ is isomorphic to the point group D_{4h} , so that the coset representations $D_{2d\bar{\sigma}\bar{\tau}}(/C_{s\bar{\sigma}\bar{\tau}})$ and $D_{4h}(/D_{2v}''')$ consist of an identical set of permutations. For the point group D_{4h} , see the discussions on square-planar complexes [5].

Suppose that the four positions of the allene skeleton **3-9** (top view: **6-102** on page 159) are controlled by the *RS*-stereoisomeric group $D_{2d\bar{\sigma}\bar{\tau}}$ through the coset representation $D_{2d\bar{\sigma}\bar{\tau}}(/C_{s\bar{\sigma}\bar{\tau}})$. Let us adopt the top view **6-102** (page 159) in the following discussions.

The four operations listed in the **A**-part of Table 12.1 (or the coset $D_2I (= D_2)$ of Eq. 12.4) are operated onto the allene skeleton **6-102** ($=$ **3-9**). As a result, there appear a reference-numbered skeleton **12-1** and its homomeric skeletons, where the term *homomeric* means that they are equivalent with each other under the subgroup D_2 (cf. Theorem 10.2 on page 279). The reference-numbered skeleton **12-1** is placed at the upper-left corner of Fig. 12.1 to construct an elementary stereoisogram. In a similar way, the four operations listed in the **B**-part (or the coset $D_2\sigma$ of Eq. 12.4) generate a mirror-numbered skeleton $\overline{12-1}$ and its homomeric skeletons; the four operations listed in the **C**-part (or the coset $D_2\tilde{\sigma}$ of Eq. 12.4) generate a *RS*-numbered skeleton **12-2** and its homomeric skeletons; and the four operations listed in the **D**-part (or the coset $D_2\hat{I}$ of Eq. 12.4) generate a ligand-mirror (LM)-numbered skeleton $\overline{12-2}$ and its homomeric skeletons. The quadruplet of **12-1**/ $\overline{12-1}$ /**12-2**/ $\overline{12-2}$ is arranged to give an elementary stereoisogram shown in Fig. 12.1.

12.2 Stereoisograms of Five Types for Allene Derivatives

The list of stereoisograms of five types shown in Fig. 10.9 (on page 288) is effective to allene derivatives.

12.2.1 Type-I Stereoisograms of Allene Derivatives

Let us examine the allene derivatives with the composition ABXY collected in Fig. 6.13 (page 162), i.e., three enantiomeric pairs of allene derivatives (**6-103**/ $\overline{6-103}$, **6-104**/ $\overline{6-104}$, and **6-105**/ $\overline{6-105}$).

When the promolecule **6-103** ($=$ **12-3**) with the composition ABXY is selected as a reference, the elementary stereoisogram (Fig. 12.1) generates a type-I stereoisogram shown in the left of Fig. 12.2, which is characterized by the presence of diagonal equality symbols. The diagonal equality symbols are concerned with asclerality, so that each promolecule contained in such a type-I stereoisogram is chiral, *RS*-stereogenic, and ascleral. The quadruplet of **12-3**/ $\overline{12-3}$ /**12-4**/ $\overline{12-4}$ (the left diagram of Fig. 12.2) is counted once on the action of the *RS*-stereoisomeric group $D_{2d}\hat{\sigma}\hat{I}$.

In a parallel way, the middle stereoisogram of type I is concerned with **6-104** ($=$ **12-5**), and the right stereoisogram of type I is concerned with **6-105** ($=$ **12-7**).

As found in Fig. 12.2, each quadruplet degenerates into a single pair of enantiomers, **12-3**/ $\overline{12-3}$ ($=$ **6-103**/ $\overline{6-103}$), **12-5**/ $\overline{12-5}$ ($=$ **6-104**/ $\overline{6-104}$), or **12-7**/ $\overline{12-7}$ ($=$ **6-105**/ $\overline{6-105}$), which is counted once under the point group D_{2d} (cf. the term 3ABXY of Eq. 6.114 on page 161). On the other hand, each quadruplet can be regarded to degenerate into a single pair of *RS*-diastereomers, **12-3**/**12-4** ($=$ $\overline{12-3}$), **12-5**/**12-6** ($=$ $\overline{12-5}$), or **12-7**/**12-8** ($=$ $\overline{12-7}$), which is counted once under the *RS*-permutation group $D_{2\sigma}$. See the term 3ABXY in Eq. 9.58 on page 263.

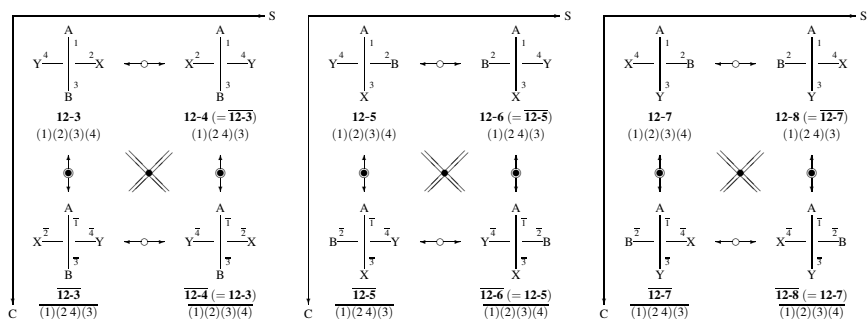


Fig. 12.2. Three quadruplets of allene promolecules with the composition ABXY, which are inequivalent under the RS -stereoisomeric group $D_{2d\hat{\sigma}\hat{\tau}}$. Each quadruplet is contained in a type-I stereoisogram under $D_{2d\hat{\sigma}\hat{\tau}}$. Each reference promolecule belongs to the RS -stereoisomeric group C_1 and to the point group C_1 .

As characterized by a type-I stereoisogram (Fig. 12.2), each pair of enantiomers (e.g., $\mathbf{12-3}/\overline{\mathbf{12-3}}$) is, at the same time, regarded as a pair of RS -diastereomers in a degenerate fashion. The three quadruplets, which are recognized to be the three pairs of enantiomers (as well as the three pairs of RS -diastereomers), are inequivalent to each other under the RS -stereoisomeric group $D_{2d\hat{\sigma}\hat{\tau}}$, although they have the same composition ABXY on the basis of the same allene skeleton. Hence, they are isoskeletal to each other but not RS -diastereomeric to each other.

The promolecules listed in Fig. 12.3 are representatives for constructing type-I stereoisograms in a similar way to Fig. 12.2. Three promolecules linked with an underbrace (*) have the same composition but produce three different stereoisograms of type I. Note that two or more promolecules with the symbol $\mathbb{Q}1$ (or $\mathbb{Q}2, \mathbb{Q}3, \mathbb{Q}4$) have the same partition but belong to different types of stereoisograms. For example, $\mathbf{12-9}$ attached by $\mathbb{Q}1$ (type I) has the same composition A^2B^2 ($[\theta]_4$) as $\mathbf{12-64}$ attached by $\mathbb{Q}1$ (type IV) shown in Fig. 12.9, where these two promolecules belong to different types of stereoisograms. Note that $\mathbf{12-9}$ and $\mathbf{12-64}$ are inequivalent under the RS -stereoisomeric group $D_{2d\hat{\sigma}\hat{\tau}}$. Hence, they are isoskeletal to each other but not RS -diastereomeric to each other.



Exercise 12.1. Draw a stereoisogram for an appropriate promolecule selected from Fig. 12.3. Confirm that the resulting stereoisogram belongs to type I.



Exercise 12.2. Compare Fig. 12.2 for allene derivatives with the composition ABXY with Fig. 11.3 (page 317) for tetrahedral derivatives with the same composition.

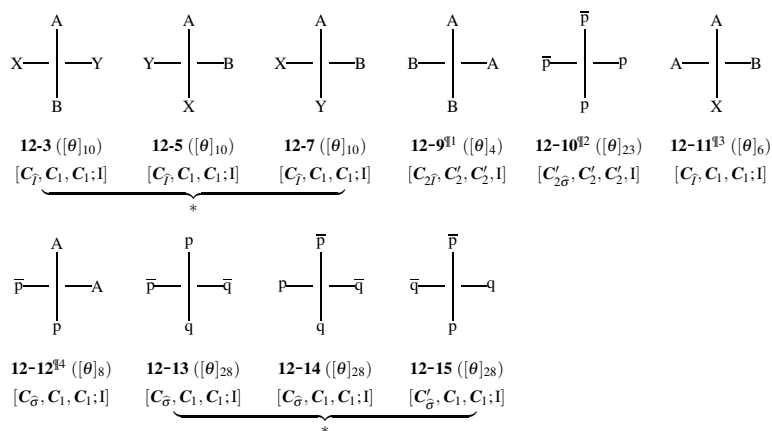


Fig. 12.3. Representatives of type-I quadruplets for allene derivatives [3]. The partitions $[\theta]_i$ ($i = 1-30$) are shown in Eqs. 11.98–11.127. The *RS*-stereoisomeric groups are accompanied with the corresponding point groups, *RS*-permutation groups, and stereoisogram types.

12.2.2 Type-II Stereoisograms of Allene Derivatives

When a promolecule with the composition ABp^2 , i.e., **12-16**, is selected as a reference, the elementary stereoisogram (Fig. 12.1) generates a type-II stereoisogram shown in Fig. 12.4, which is characterized by the presence of horizontal equality symbols. The horizontal equality symbols are concerned with *RS*-astereogenicity, so that each promolecule contained in such a type-II stereoisogram is chiral, *RS*-astereogenic, and scleral.

The promolecules listed in Fig. 12.5 are representatives for constructing type-II stereoisograms in a similar way to Fig. 12.4. Each promolecule attached by a dagger with a number ($\dagger 1$ etc.) has counterparts with the same composition but belong to different types of stereoisograms. For example, **12-19** attached by $\dagger 1$ (type II) has the same composition A^2p^2 ($[\theta]_5$) as **12-34** attached by $\dagger 1$ (type III) shown in Fig. 12.7. They are inequivalent to each other under the *RS*-stereoisomeric group $\mathbf{D}_{2d\bar{\sigma}\bar{\tau}}$, although they have the same composition A^2p^2 on the basis of the same allene skeleton. As another example, the promolecule **12-16** ^{$\dagger 5$} collected in Fig. 12.5 is isoskeletomeric to the promolecule **12-32** ^{$\dagger 5$} collected in Fig. 12.7, where the former is characterized by the type-II stereoisogram (Fig. 12.4), while the latter is characterized by the type-III stereoisogram (Fig. 12.6).

Exercise 12.3. Draw a stereoisogram for an appropriate promolecule selected from Fig. 12.5. Confirm that the resulting stereoisogram belongs to type II.



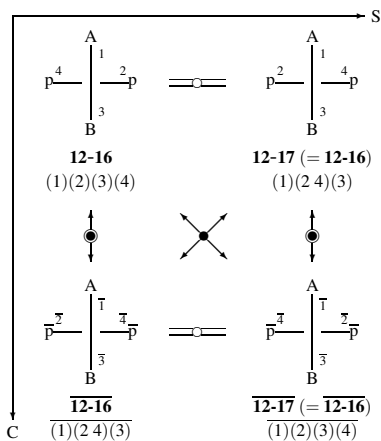


Fig. 12.4. Type-II stereoisogram of allene derivatives. One quadruplet of allene promolecules with the composition ABp^2 or $AB\bar{p}^2$, which is counted once under the RS -stereoisomeric group $D_{2d\bar{\sigma}\hat{I}}$. The quadruplet is contained in a type-II stereoisogram under $D_{2d\bar{\sigma}\hat{I}}$. The reference promolecule belongs to the RS -stereoisomeric group $C_{\bar{\sigma}}$ and to the point group C_1 .

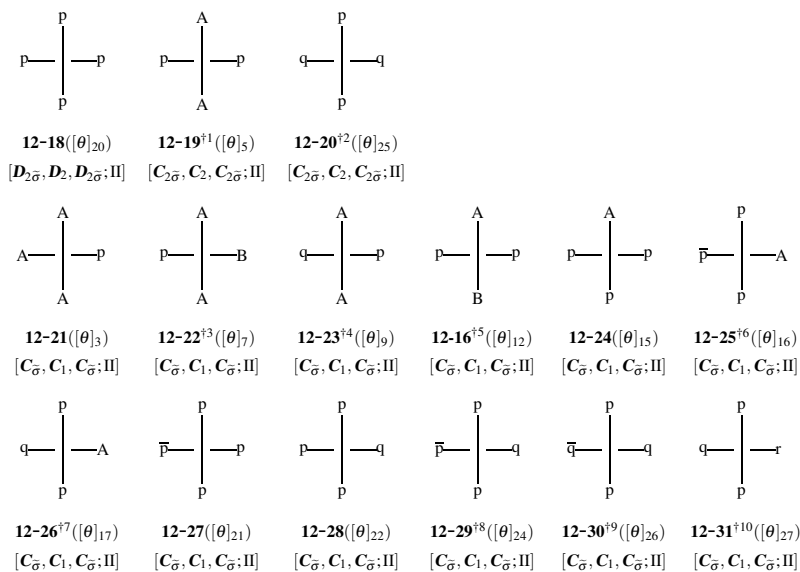


Fig. 12.5. Representatives of type-II quadruplets for allene derivatives [3]. The partitions $[\theta]_i$ ($i = 1-30$) are shown in Eqs. 11.98–11.127. The RS -stereoisomeric groups are accompanied with the corresponding point groups, RS -permutation groups, and stereoisogram types.

Exercise 12.4. Compare Fig. 12.4 for allene derivatives with the composition ABp^2 with Fig. 11.4 (page 318) for tetrahedral derivatives with the same composition.

12.2.3 Type-III Stereoisograms of Allene Derivatives

When another promolecule with the composition ABp^2 , i.e., **12-32** attached by †5, is selected as a reference from Fig. 12.7, the elementary stereoisogram (Fig. 12.1) generates a type-III stereoisogram shown in Fig. 12.6, which is characterized by no equality symbols. The absence of equality symbols indicates that each promolecule contained in such a type-III stereoisogram is chiral, *RS*-stereogenic, and scleral.

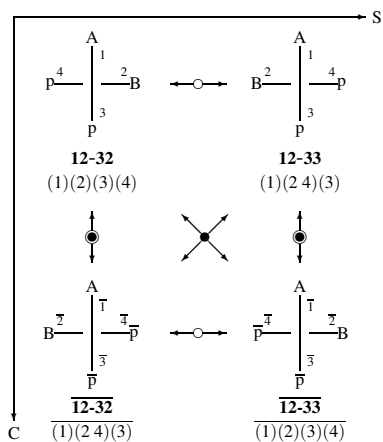


Fig. 12.6. Type-III stereoisogram of allene derivatives. One quadruplet of allene promolecules with the composition ABp^2 or $AB\bar{p}^2$, which is counted once under the *RS*-stereoisomeric group $D_{2d}\hat{\sigma}\hat{\tau}$. The quadruplet is contained in a type-III stereoisogram under $D_{2d}\hat{\sigma}\hat{\tau}$. The reference promolecule belongs to the *RS*-stereoisomeric group $C_{\bar{\sigma}}$ and to the point group C_1 .

The four promolecules contained in the type-III stereoisogram (Fig. 12.6) are different to each other under the action of the chiral point group D_2 , so that they are counted separately to give value 4 (cf. Theorem 10.8 on page 310). Each pair of enantiomers **12-32/12-32** (or **12-33/12-33**) is an equivalence class under the action of the achiral point group D_{2d} , so that it is counted once under D_{2d} . There appear two pairs of enantiomers inequivalent under D_{2d} (cf. Theorem 10.6 on page 306). Each pair of *RS*-diastereomers **12-32/12-33** (or **12-32/12-33**) is an equivalence class under the action of the *RS*-permutation group $D_{2\bar{\sigma}}$, so that it is counted once under $D_{2\bar{\sigma}}$. There appear two pairs of *RS*-diastereomers inequivalent under $D_{2\bar{\sigma}}$ (cf. Theorem 10.7 on page 308). The quadruplet of the type-III stereoisogram

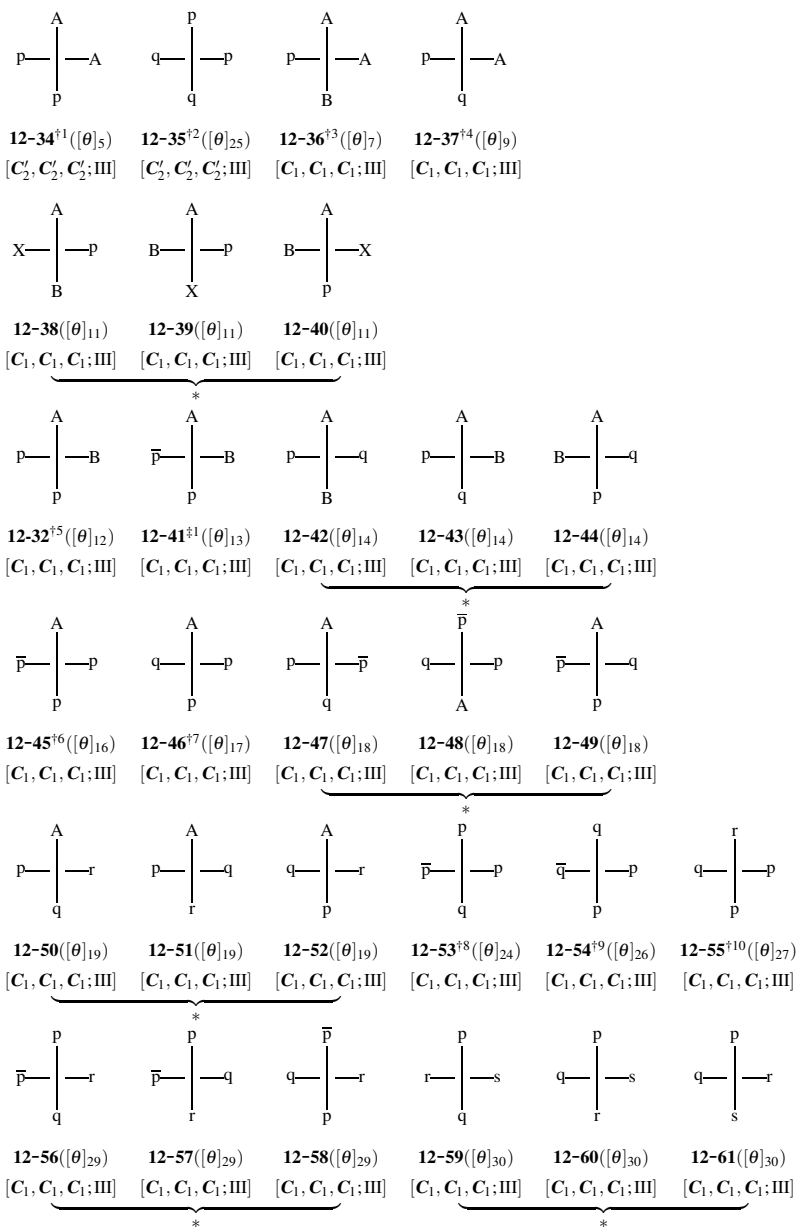


Fig. 12.7. Representatives of type-III quadruplets for allene derivatives [3]. The partitions [θ]_{*i*} (*i* = 1–30) are shown in Eqs. 11.98–11.127. The *RS*-stereoisomeric groups are accompanied with the corresponding point groups, *RS*-permutation groups, and stereoisogram types.

(Fig. 12.6) is an equivalence class under the action of the *RS*-stereoisomeric group $D_{2d\bar{\sigma}\hat{\tau}}$ so that it is counted once under $D_{2d\bar{\sigma}\hat{\tau}}$.

The promolecules listed in Fig. 12.7 are representatives for constructing type-III stereoisograms in a similar way to Fig. 12.6.

The promolecule **12-41**^{‡1} (type III) has the same composition $AB\bar{p}\bar{p}$ ($[\theta]_{13}$) as **12-69**^{‡1} (type V) shown in Fig. 12.9. They are inequivalent to each other under the *RS*-stereoisomeric group $D_{2d\bar{\sigma}\hat{\tau}}$, although they have the same composition $AB\bar{p}\bar{p}$ on the basis of the same allene skeleton.

Exercise 12.5.

- Draw a stereoisogram for an appropriate promolecule selected from Fig. 12.7. Confirm that the resulting stereoisogram belongs to type III.
- In particular, draw stereoisograms for **12-38–12-40** having the composition $ABXp$ ($[\theta]_{11}$). The resulting type-III stereoisograms should be compared with the type-III stereoisogram shown in Fig. 11.5 (page 319) for tetrahedral derivatives having the same composition.

Exercise 12.6. Compare the type-III stereoisogram shown in Fig. 12.6 for allene derivatives having the composition ABp^2 with the type-II stereoisogram shown in Fig. 11.4 (page 318) for tetrahedral derivatives having the same composition. See also Exercise 12.4.

12.2.4 Type-IV Stereoisograms of Allene Derivatives

When a promolecule with the composition A^4 , i.e., **12-62**, is selected as a reference, the elementary stereoisogram (Fig. 12.1) generates a type-IV stereoisogram shown in Fig. 12.8, which is characterized by the presence of equality symbols in all the directions. Thus, there appears a single promolecule which is characterized to be achiral, *RS*-astereogenic, and ascleral.

The promolecules listed in the top row of Fig. 12.9 are representatives for constructing type-IV stereoisograms in a similar way to Fig. 12.8.

Exercise 12.7.

- Draw a stereoisogram for an appropriate promolecule selected from the top row of Fig. 12.9. Confirm that the resulting stereoisogram belongs to type IV.
- In particular, draw a type-IV stereoisogram for **12-67** having the composition A^2BX ($[\theta]_6$). The resulting stereoisogram should be compared with the type-IV stereoisogram shown in Fig. 11.6 (page 320) for tetrahedral derivatives having the same composition.

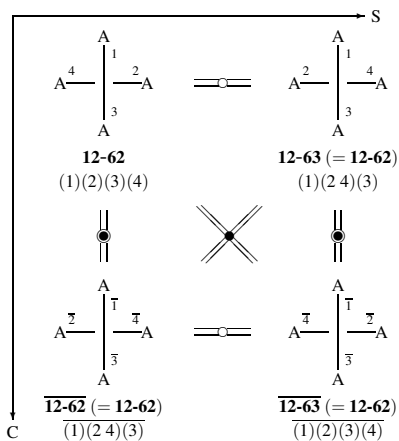


Fig. 12.8. Type-IV stereoisogram of an allene derivative. One quadruplet of allene promolecules with the composition A^4 , which is counted once under the RS -stereoisomeric group $D_{2d}\widehat{\sigma}\widehat{\tau}$. The quadruplet is contained in a type-IV stereoisogram under $D_{2d}\widehat{\sigma}\widehat{\tau}$. The reference promolecule belongs to the RS -stereoisomeric group $D_{2d}\widehat{\sigma}\widehat{\tau}$ and to the point group D_{2d} .

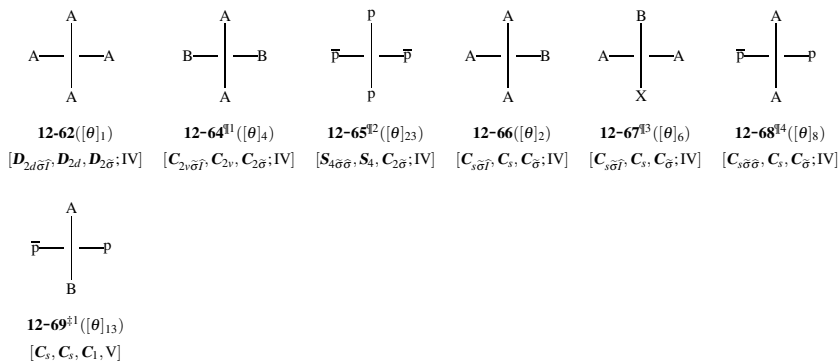


Fig. 12.9. Representatives of type-IV and type-V quadruplets for allene derivatives. The partitions $[\theta]_i$ ($i = 1-30$) are shown in Eqs. 11.98–11.127. The RS -stereoisomeric group of each representative is accompanied with the corresponding point group, RS -permutation group, and stereoisogram type, as shown in a pair of square brackets.

12.2.5 Type-V Stereoisograms of Allene Derivatives

There appears one promolecule **12-69** as a reference of a type-V stereoisogram, as shown in the left of Fig. 12.10. The type-V stereoisogram is characterized by the presence of vertical equality symbols, so that **12-69** is characterized to be achiral, RS -stereogenic, and scleral. The RS -stereogenicity means the presence of a pair of RS -diastereomers **12-69/12-70**, which are achiral as listed in the upper row of Fig. 6.13(b) on page 162 (6-106/6-107).

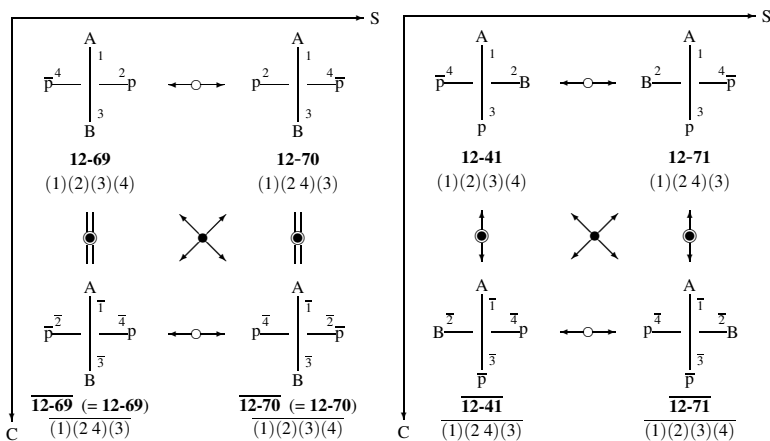


Fig. 12.10. Type-V stereoisogram of allene derivatives (left) and the related type-III stereoisogram (right). Each promolecule is characterized by the composition $ABp\bar{p}$.

The right diagram of Fig. 12.10 shows the related type-III stereoisogram, which contains a quadruplet of promolecules having the same composition $ABp\bar{p}$, as designated by the attached symbol $\ddagger 1$ in Fig. 12.7 (**12-41** $\ddagger 1$ ($[\theta]_{13}$)) and Fig. 12.9 (**12-69** $\ddagger 1$ ($[\theta]_{13}$)). The quadruplet of **12-41/12-41/12-71/12-71** is counted once under the action of the RS -stereoisomeric group $D_{2d\sigma\bar{I}}$. For symmetry-itemized enumeration of allene derivatives with $ABp\bar{p}$ under the point group D_{2d} , see the bottom row of Fig. 6.13(b) on page 162, where a pair of enantiomers is counted once. Note that the enantiomeric pair of **6-108/6-108** is identical with the pair of **12-41/12-41** and that the enantiomeric pair of **6-109/6-109** is identical with the pair of **12-71/12-71**.

Exercise 12.8. Compare the type-V stereoisogram shown in Fig. 12.10 (left) for allene derivatives having the composition $ABp\bar{p}$ with the type-V stereoisogram shown in Fig. 11.7 (page 321) for tetrahedral derivatives having the same composition.

Exercise 12.9. Rule P-92.1.6 of IUPAC Provisional Recommendations 2004 [6] specifies ‘pseudoasymmetric axes’ by stereodescriptors ‘ r_a ’ and ‘ s_a ’. For example, **12-72** is named ($3R,4r_a,5S$)-4-(2-Bromoethenylidene)heptane-3,5-dithiol, as shown in Fig. 12.11. Draw a stereoisogram for **12-72** by using the corresponding top view **12-73**. Confirm that the resulting stereoisogram belongs to type V. Note that the label ‘ r_a ’ or ‘ s_a ’ assigned to a ‘pseudoasymmetric axis’ is rationalized to be assigned to a *type-V promolecule* in Fujita’s stereoisogram approach (see Chapter 13).

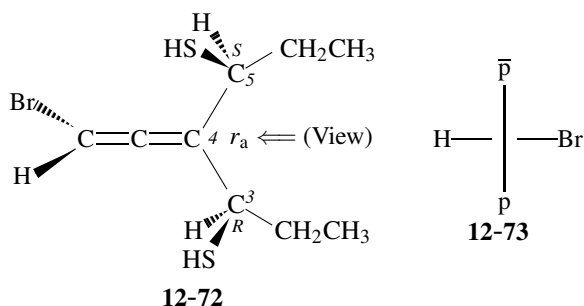


Fig. 12.11. (3*R*,4*r_a*,5*S*)-4-(2-Bromoethenylidene)heptane-3,5-dithiol.

12.3 Enumeration Under the *RS*-Stereoisomeric Group $D_{2d\tilde{\sigma}\hat{I}}$

The FPM method of the USCI approach has been extended to support *RS*-stereoisomeric groups and applied to enumeration under the *RS*-stereoisomeric group $D_{2d\tilde{\sigma}\hat{I}}$ [3]. On the other hand, the PCI method has been extended to accomplish the same purpose [4]. In this section, we apply the extended PCI method to enumeration under $D_{2d\tilde{\sigma}\hat{I}}$.

12.3.1 Non-Redundant Set of Subgroups and Five Types of Subgroups

The *RS*-stereoisomeric group $D_{2d\tilde{\sigma}\hat{I}}$ is isomorphic to the point group D_{4h} [3]. The point group D_{4h} has the following non-redundant set of subgroups (SSG) [5]:

$$\text{SSG}_{D_{4h}} = \left\{ \begin{array}{l} 1, 2, 3, 4, 5, 6, 7, 8, 9, 10, 11, 12, 13, 14 \\ C_1, C_2, C_2', C_2'', C_s, C_s', C_s'', C_i, C_4, S_4, C_{2v}, C_{2v}', C_{2v}'', C_{2v}''', \\ 15, 16, 17, 18, 19, 20, 21, 22, 23, 24, 25, 26, 27 \\ C_{2h}, C_{2h}', C_{2h}'', D_2, D_2', C_{4v}, C_{4h}, D_{2d}, D_{2d}', D_{2d}'', D_{2d}''', D_4, D_{4h} \end{array} \right\}, \quad (12.5)$$

where the subgroups are aligned in the ascending order of their orders. For the convenience of cross reference, sequential numbers from 1 to 27 are attached to the respective subgroups. In a parallel way, a non-redundant set of subgroups (SSG) for the *RS*-stereoisomeric group $D_{2d\tilde{\sigma}\hat{I}}$ is obtained as follows [3]:

$$\text{SSG}_{D_{2d\tilde{\sigma}\hat{I}}} = \left\{ \begin{array}{l} 1, 2, 3, 4, 5, 6, 7, 8, 9, 10, 11, 12, 13, 14 \\ C_1, C_2, C_2', C_{\tilde{\sigma}}, C_{\tilde{\sigma}}', C_s, C_{\hat{I}}, C_{\hat{I}}', S_4, S_4', C_{2\tilde{\sigma}}, C_{2\tilde{\sigma}}', C_{2\hat{I}}, C_{s\tilde{\sigma}\hat{I}}, \\ 15, 16, 17, 18, 19, 20, 21, 22, 23, 24, 25, 26, 27 \\ C_{2\hat{I}}', C_{2\tilde{\sigma}\hat{I}}', C_{s\tilde{\sigma}\hat{I}}, D_2, C_{2\tilde{\sigma}}, S_{4\tilde{\sigma}\hat{I}}, D_{2d}, S_{4\tilde{\sigma}\hat{I}}', D_{2\hat{I}}, C_{2v\tilde{\sigma}\hat{I}}, D_{2\tilde{\sigma}}, D_{2d\tilde{\sigma}\hat{I}} \end{array} \right\}, \quad (12.6)$$

where the subgroups are aligned in the ascending order of their orders. For the convenience of cross reference, sequential numbers from 1 to 27 are attached to the respective subgroups.

According to the discussion of [3], the 27 subgroups of $SSG_{D_{2d\tilde{\sigma}\hat{\Gamma}}}$ are categorized into five types:

$$\text{Type I: } SG^{[I]} = \{C_{\tilde{\sigma}}^5, C_{\hat{\Gamma}}^7, C_{\tilde{\sigma}}^8, C_{2\tilde{\sigma}}^{11}, C_{2\hat{\Gamma}}^{13}, C_{2\tilde{\sigma}}^{15}, C_{2\hat{\Gamma}}^{16}, D_{2\tilde{\sigma}}^{24}\} \quad (12.7)$$

$$\text{Type II: } SG^{[II]} = \{C_{\tilde{\sigma}}^4, S_4^9, C_{2\tilde{\sigma}}^{19}, D_{2\tilde{\sigma}}^{26}\} \quad (12.8)$$

$$\text{Type III: } SG^{[III]} = \{C_1^1, C_2^2, C_2^3, D_2^{18}\} \quad (12.9)$$

$$\text{Type IV: } SG^{[IV]} = \{C_{s\tilde{\sigma}\hat{\Gamma}}^{14}, C_{s\tilde{\sigma}\hat{\sigma}}^{17}, S_{4\tilde{\sigma}}^{20}, S_{4\hat{\Gamma}}^{21}, S_{4\tilde{\sigma}\hat{\sigma}}^{23}, C_{2v\tilde{\sigma}\hat{\Gamma}}^{25}, D_{2d\tilde{\sigma}\hat{\Gamma}}^{27}\} \quad (12.10)$$

$$\text{Type V: } SG^{[V]} = \{C_s^6, S_4^{10}, C_{2v}^{12}, D_{2d}^{22}\}. \quad (12.11)$$

Because we find that D_{2d} is a common subgroup of D_{4h} and $D_{2d\tilde{\sigma}\hat{\Gamma}}$ and because we find the correspondence between D_4 ($\subset D_{4h}$) and $D_{2\tilde{\sigma}}$ ($\subset D_{2d\tilde{\sigma}\hat{\Gamma}}$) as well as between D_{2h} ($\subset D_{4h}$) and $D_{2\hat{\Gamma}}$ ($\subset D_{2d\tilde{\sigma}\hat{\Gamma}}$), we are able to construct each subgroup by referring to the five types shown in Eqs. 12.7–12.11:

- (Type-III Subgroups) The four subgroups of the point group D_2 are also the subgroups of the RS -stereoisomeric group $D_{2d\tilde{\sigma}\hat{\Gamma}}$.

$$C_1 \stackrel{1}{=} \{I\} \quad (12.12)$$

$$C_2 \stackrel{2}{=} \{I, C_{2(3)}\} \quad (12.13)$$

$$C_2' \stackrel{3}{=} \{I, C_{2(1)}\} \quad (12.14)$$

$$D_2 \stackrel{18}{=} \{I, C_{2(3)}, C_{2(1)}, C_{2(2)}\} \quad (12.15)$$

These RS -stereoisomeric groups are categorized to type III.

- (Type-V Subgroups) The four subgroups of D_{2d} (except those of D_2) are, at the same time, recognized as the subgroups of the RS -stereoisomeric group $D_{2d\tilde{\sigma}\hat{\Gamma}}$:

$$C_s \stackrel{6}{=} \{I, \sigma_{d(1)}\} \quad (12.16)$$

$$S_4 \stackrel{10}{=} \{I, S_4, C_{2(3)}, S_4^3\} \quad (12.17)$$

$$C_{2v} \stackrel{12}{=} \{I, C_{2(3)}, \sigma_{d(1)}, \sigma_{d(2)}\} \quad (12.18)$$

$$D_{2d} \stackrel{22}{=} \{I, C_{2(3)}, C_{2(1)}, C_{2(2)}, \sigma_{d(1)}, \sigma_{d(2)}, S_4, S_4^3\} \quad (12.19)$$

These RS -stereoisomeric groups are categorized to type V.

- (Type-II Subgroups) The four subgroups of D_4 (except those of D_2) correspond to the following subgroups of $D_{2\tilde{\sigma}}$ ($-D_2$).

$$C_{\tilde{\sigma}} \stackrel{4}{=} \{I, \tilde{\sigma}_{d(1)}\} \quad (\supset C_1) \quad (12.20)$$

$$S_4 \stackrel{9}{=} \{I, \tilde{S}_{4(3)}, C_{2(3)}, \tilde{S}_{4(3)}^3\} \quad (\supset C_2) \quad (12.21)$$

$$C_{2\tilde{\sigma}} \stackrel{19}{=} \{I, C_{2(3)}, \tilde{\sigma}_{d(1)}, \tilde{\sigma}_{d(2)}\} \quad (\supset C_2) \quad (12.22)$$

$$\mathbf{D}_{2\tilde{\sigma}} \stackrel{26}{=} \{I, C_{2(1)}, C_{2(2)}, C_{2(3)}, \tilde{\sigma}_{d(1)}, \tilde{\sigma}_{d(2)}, \tilde{S}_{4(3)}, \tilde{S}_{4(3)}^3\} \quad (\supset \mathbf{D}_2) \quad (12.23)$$

The symbols of the subgroups are selected by designating a common subgroup to \mathbf{D}_{2d} (denoted in a pair of parentheses) which is attached by a suffix to refer to an uncommon operation. Each of the symbols contains a tilde accent in its suffix. For example, the symbol $\mathbf{C}_{2\tilde{\sigma}}$ stems from the largest subgroup \mathbf{C}_2 (as a common subgroup to \mathbf{D}_{2d}) and from an uncommon operation $\tilde{\sigma}_{d(1)}$. The symbol \mathbf{S}_4 is adopted for the purpose of avoiding the confusion with $\mathbf{C}_{2\tilde{\sigma}}$. These *RS*-stereoisomeric groups are categorized to type II.

4. (Type-I Subgroups) The eight subgroups of \mathbf{D}_{2h} (except those of \mathbf{D}_2) correspond to the following subgroups of $\mathbf{D}_{2\hat{I}} (-\mathbf{D}_2)$.

$$\mathbf{C}_{\hat{\sigma}} \stackrel{5}{=} \{I, \hat{C}_{2(1)}\} \quad (\supset \mathbf{C}_1) \quad (12.24)$$

$$\mathbf{C}_{\hat{I}} \stackrel{7}{=} \{I, \hat{I}\} \quad (\supset \mathbf{C}_1) \quad (12.25)$$

$$\mathbf{C}'_{\hat{\sigma}} \stackrel{8}{=} \{I, \hat{C}_{2(3)}\} \quad (\supset \mathbf{C}_1) \quad (12.26)$$

$$\mathbf{C}_{2\hat{\sigma}} \stackrel{11}{=} \{I, C_{2(3)}, \hat{C}_{2(1)}, \hat{C}_{2(2)}\} \quad (\supset \mathbf{C}_2) \quad (12.27)$$

$$\mathbf{C}_{2\hat{I}} \stackrel{13}{=} \{I, C_{2(1)}, \hat{C}_{2(1)}, \hat{I}\} \quad (\supset \mathbf{C}_2) \quad (12.28)$$

$$\mathbf{C}'_{2\hat{I}} \stackrel{15}{=} \{I, C_{2(3)}, \hat{C}_{2(3)}, \hat{I}\} \quad (\supset \mathbf{C}_2) \quad (12.29)$$

$$\mathbf{C}'_{2\hat{\sigma}} \stackrel{16}{=} \{I, C_{2(1)}, \hat{C}_{2(3)}, \hat{C}_{2(2)}\} \quad (\supset \mathbf{C}_2) \quad (12.30)$$

$$\mathbf{D}_{2\hat{I}} \stackrel{24}{=} \{I, C_{2(1)}, C_{2(2)}, C_{2(3)}, \hat{I}, \hat{C}_{2(1)}, \hat{C}_{2(2)}, \hat{C}_{2(3)}\} \quad (\supset \mathbf{D}_2) \quad (12.31)$$

The names of the subgroups are characterized by the symbols with a hat accent. These *RS*-stereoisomeric groups are categorized to type I.

5. (Type-IV Subgroups) The seven subgroups of \mathbf{D}_{4h} (except those of \mathbf{D}_2 , \mathbf{D}_{2d} , \mathbf{D}_4 , and \mathbf{D}_{2h}) correspond to the following subgroups of $\mathbf{D}_{2d\tilde{\sigma}\hat{I}}$.

$$\mathbf{C}_{s\tilde{\sigma}\hat{I}} \stackrel{14}{=} \{I, \tilde{\sigma}_{d(1)}, \hat{I}, \sigma_{d(1)}\} \quad (\supset \mathbf{C}_s) \quad (12.32)$$

$$\mathbf{C}_{s\tilde{\sigma}\hat{\sigma}} \stackrel{17}{=} \{I, \tilde{\sigma}_{d(1)}, \hat{C}_{2(3)}, \sigma_{d(2)}\} \quad (\supset \mathbf{C}_s) \quad (12.33)$$

$$\mathbf{S}_{4\hat{\sigma}} \stackrel{20}{=} \{I, \tilde{S}_{4(3)}, C_{2(3)}, \tilde{S}_{4(3)}^3, \hat{C}_{2(1)}, \hat{C}_{2(2)}, \sigma_{d(1)}, \sigma_{d(2)}\} \quad (\supset \mathbf{S}_4, \mathbf{C}_{2v}) \quad (12.34)$$

$$\mathbf{S}_{4\hat{I}} \stackrel{21}{=} \{I, \tilde{S}_{4(3)}, C_{2(3)}, \tilde{S}_{4(3)}^3, \hat{I}, \hat{C}_{2(3)}, S_{4(3)}, S_{4(3)}^3\} \quad (\supset \mathbf{S}_4, \mathbf{S}_4) \quad (12.35)$$

$$\mathbf{S}_{4\tilde{\sigma}\hat{\sigma}} \stackrel{23}{=} \{I, C_{2(3)}, \tilde{\sigma}_{d(1)}, \tilde{\sigma}_{d(2)}, \hat{C}_{2(1)}, \hat{C}_{2(2)}, S_{4(3)}, S_{4(3)}^3\} \quad (\supset \mathbf{S}_4) \quad (12.36)$$

$$\mathbf{C}_{2v\tilde{\sigma}\hat{I}} \stackrel{25}{=} \{I, C_{2(3)}, \tilde{\sigma}_{d(1)}, \tilde{\sigma}_{d(2)}, \hat{I}, \hat{C}_{2(3)}, \sigma_{d(1)}, \sigma_{d(2)}\} \quad (\supset \mathbf{C}_{2v}) \quad (12.37)$$

$$\mathbf{D}_{2d\tilde{\sigma}\hat{I}} \stackrel{27}{=} \{I, C_{2(1)}, C_{2(2)}, C_{2(3)}, \tilde{\sigma}_{d(1)}, \tilde{\sigma}_{d(2)}, \tilde{S}_{4(3)}, \tilde{S}_{4(3)}^3, \hat{I}, \hat{C}_{2(1)}, \hat{C}_{2(2)}, \hat{C}_{2(3)}, \sigma_{d(1)}, \sigma_{d(2)}, S_{4(3)}, S_{4(3)}^3\} \quad (\supset \mathbf{D}_{2d}) \quad (12.38)$$

The names of the subgroups are characterized by the symbols with both a hat accent and a tilde accent. These *RS*-stereoisomeric groups are categorized to type IV.

Table 12.2. Subduction of $D_{2d\tilde{\sigma}\tilde{\Gamma}}(/C_{s\tilde{\sigma}\tilde{\Gamma}})$ [3]

Subgroup (↓ \hat{G}_j type)	Subduction ($D_{2d\tilde{\sigma}\tilde{\Gamma}}(/C_{s\tilde{\sigma}\tilde{\Gamma}}) \downarrow \hat{G}_j$)	USCI-CF	USCI	TEM						
				\widehat{N}_j	$\widehat{N}_j^{(I)}$	$\widehat{N}_j^{(II)}$	$\widehat{N}_j^{(III)}$	$\widehat{N}_j^{(IV)}$	$\widehat{N}_j^{(V)}$	
1	C_1 III	$4C_1(/C_1)$	b_1^4	s_1^4	$\frac{1}{16}$	0	0	$\frac{1}{16}$	0	0
2	C_2 III	$2C_2(/C_1)$	b_2^2	s_2^2	$\frac{1}{16}$	0	0	$\frac{1}{16}$	0	0
3	C_2' III	$2C_2'(/C_1)$	b_2^2	s_2^2	$\frac{1}{8}$	0	0	$\frac{1}{8}$	0	0
4	$C_{\tilde{\sigma}}$ II	$C_{\tilde{\sigma}}(/C_1) + 2C_{\tilde{\sigma}}(/C_{\tilde{\sigma}})$	$b_1^2 b_2$	$s_1^2 s_2$	$\frac{1}{8}$	0	$\frac{1}{4}$	$-\frac{1}{8}$	0	0
5	$C_{\tilde{\sigma}}$ I	$2C_{\tilde{\sigma}}(/C_1)$	c_2^2	s_2^2	$\frac{1}{8}$	$\frac{1}{4}$	0	$-\frac{1}{8}$	0	0
6	C_s V	$C_s(/C_1) + 2C_s(/C_s)$	$a_1^2 c_2$	$s_1^2 s_2$	$\frac{1}{8}$	0	0	$-\frac{1}{8}$	0	$\frac{1}{4}$
7	$C_{\tilde{\Gamma}}$ I	$4C_{\tilde{\Gamma}}(/C_{\tilde{\Gamma}})$	a_1^4	a_1^4	$\frac{1}{16}$	$\frac{1}{8}$	0	$-\frac{1}{16}$	0	0
8	$C_{\tilde{\sigma}}$ I	$2C_{\tilde{\sigma}}'(/C_1)$	c_2^2	s_2^2	$\frac{1}{16}$	$\frac{1}{8}$	0	$-\frac{1}{16}$	0	0
9	S_4 II	$S_4(/C_1)$	b_4	s_4	$\frac{1}{8}$	0	$\frac{1}{4}$	$-\frac{1}{8}$	0	0
10	S_4 V	$S_4(/C_1)$	c_4	s_4	$\frac{1}{8}$	0	0	$-\frac{1}{8}$	0	$\frac{1}{4}$
11	$C_{2\tilde{\sigma}}$ I	$C_{2\tilde{\sigma}}(/C_1)$	c_4	s_4	0	0	0	0	0	0
12	C_{2v} V	$C_{2v}(/C_s) + C_{2v}(/C_s)$	a_2^2	s_2^2	0	0	0	0	0	0
13	$C_{2\tilde{\Gamma}}$ I	$2C_{2\tilde{\Gamma}}(/C_{\tilde{\Gamma}})$	a_2^2	s_2^2	0	0	0	0	0	0
14	$C_{s\tilde{\sigma}\tilde{\Gamma}}$ IV	$C_{s\tilde{\sigma}\tilde{\Gamma}}(/C_{\tilde{\Gamma}}) + 2C_{s\tilde{\sigma}\tilde{\Gamma}}(/C_{s\tilde{\sigma}\tilde{\Gamma}})$	$a_1^2 a_2$	$s_1^2 s_2$	0	$-\frac{1}{4}$	$-\frac{1}{4}$	$\frac{1}{4}$	$\frac{1}{2}$	$-\frac{1}{4}$
15	$C_{2\tilde{\Gamma}}$ I	$2C_{2\tilde{\Gamma}}'(/C_{\tilde{\Gamma}})$	a_2^2	s_2^2	0	0	0	0	0	0
16	$C_{2\tilde{\sigma}}$ I	$C_{2\tilde{\sigma}}(/C_1)$	c_4	s_4	0	0	0	0	0	0
17	$C_{s\tilde{\sigma}\tilde{\sigma}}$ IV	$C_{s\tilde{\sigma}\tilde{\sigma}}(/C_{\tilde{\sigma}}) + C_{s\tilde{\sigma}\tilde{\sigma}}(/C_s)$	$a_2 c_2$	s_2^2	0	$-\frac{1}{4}$	$-\frac{1}{4}$	$\frac{1}{4}$	$\frac{1}{2}$	$-\frac{1}{4}$
18	D_2 III	$D_2(/C_1)$	b_4	s_4	0	0	0	0	0	0
19	$C_{2\tilde{\sigma}}$ II	$C_{2\tilde{\sigma}}(/C_{\tilde{\sigma}}) + C_{2\tilde{\sigma}}(/C_{\tilde{\sigma}}')$	b_2^2	s_2^2	0	0	0	0	0	0
20	$S_{4\tilde{\sigma}}$ IV	$S_{4\tilde{\sigma}}(/C_s)$	a_4	s_4	0	$-\frac{1}{4}$	$-\frac{1}{4}$	$\frac{1}{4}$	$\frac{1}{2}$	$-\frac{1}{4}$
21	$S_{4\tilde{\Gamma}}$ IV	$S_{4\tilde{\Gamma}}(/C_{\tilde{\Gamma}})$	a_4	s_4	0	$-\frac{1}{4}$	$-\frac{1}{4}$	$\frac{1}{4}$	$\frac{1}{2}$	$-\frac{1}{4}$
22	D_{2d} V	$D_{2d}(/C_s)$	a_4	s_4	0	0	0	0	0	0
23	$S_{4\tilde{\sigma}\tilde{\sigma}}$ IV	$S_{4\tilde{\sigma}\tilde{\sigma}}(/C_{\tilde{\sigma}})$	c_4	s_4	0	$-\frac{1}{4}$	$-\frac{1}{4}$	$\frac{1}{4}$	$\frac{1}{2}$	$-\frac{1}{4}$
24	$D_{2\tilde{\Gamma}}$ I	$D_{2\tilde{\Gamma}}(/C_{\tilde{\Gamma}})$	a_4	s_4	0	0	0	0	0	0
25	$C_{2v\tilde{\sigma}\tilde{\Gamma}}$ IV	$C_{2v\tilde{\sigma}\tilde{\Gamma}}(/C_{s\tilde{\sigma}\tilde{\Gamma}}) + C_{2v\tilde{\sigma}\tilde{\Gamma}}(/C_{s\tilde{\sigma}\tilde{\Gamma}}')$	a_2^2	s_2^2	0	$\frac{1}{4}$	$\frac{1}{4}$	$-\frac{1}{4}$	$-\frac{1}{2}$	$\frac{1}{4}$
26	$D_{2\tilde{\sigma}}$ II	$D_{2\tilde{\sigma}}(/C_{\tilde{\sigma}})$	b_4	s_4	0	0	0	0	0	0
27	$D_{2d\tilde{\sigma}\tilde{\Gamma}}$ IV	$D_{2d\tilde{\sigma}\tilde{\Gamma}}(/C_{s\tilde{\sigma}\tilde{\Gamma}})$	a_4	s_4	0	$\frac{1}{2}$	$\frac{1}{2}$	$-\frac{1}{2}$	-1	$\frac{1}{2}$

regarded as a formal row vector of SCI-CFs, which is multiplied by the inverse mark table $M_{D_{2d\tilde{\sigma}\tilde{\Gamma}}}^{-1}$ (Eq. 12.39), as represented schematically as follows:

$$\begin{aligned}
 & \left(\text{PCI-CF}(C_1), \text{PCI-CF}(C_2), \dots, \text{PCI-CF}(\hat{G}_j), \dots, \text{PCI-CF}(D_{2d\tilde{\sigma}\tilde{\Gamma}}) \right) \\
 &= (b_1^4, b_2^2, b_2^2, b_1^2 b_2, c_2^2, a_1^2 c_2, a_1^4, c_2^2, b_4, c_4, c_4, a_2^2, a_2^2, a_1^2 a_2, a_2^2, \\
 & \quad c_4, a_2 c_2, b_4, b_2^2, a_4, a_4, a_4, c_4, a_4, a_2^2, b_4, a_4) \times M_{D_{2d\tilde{\sigma}\tilde{\Gamma}}}^{-1}. \quad (12.40)
 \end{aligned}$$

Thereby, PCI-CFs for every subgroups of $\text{SSG}_{D_{2d\tilde{\sigma}\tilde{\Gamma}}}$ (Eq. 12.6) are obtained as follows:

$$\text{PCI-CF}(C_1) \frac{1}{\text{III}} \frac{1}{16} b_1^4 - \frac{1}{16} a_1^4 - \frac{1}{8} b_1^2 b_2 + \frac{1}{4} a_1^2 a_2 - \frac{1}{8} a_1^2 c_2 - \frac{1}{16} b_2^2$$

$$+\frac{1}{4}a_2c_2 - \frac{3}{16}c_2^2 + \frac{1}{8}b_4 + \frac{3}{8}c_4 - \frac{1}{2}a_4 \quad (12.41)$$

$$\text{PCI-CF}(\mathbf{C}_2) \stackrel{2}{\text{III}} 0 \quad (12.42)$$

$$\text{PCI-CF}(\mathbf{C}'_2) \stackrel{3}{\text{III}} \frac{1}{4}b_2^2 - \frac{1}{4}a_2^2 - \frac{1}{4}b_4 - \frac{1}{4}c_4 + \frac{1}{2}a_4 \quad (12.43)$$

$$\text{PCI-CF}(\mathbf{C}_{\bar{\sigma}}) \stackrel{4}{\text{II}} \frac{1}{4}b_1^2b_2 - \frac{1}{4}a_1^2a_2 - \frac{1}{4}b_2^2 + \frac{1}{2}a_2^2 - \frac{1}{4}a_2c_2 \quad (12.44)$$

$$\text{PCI-CF}(\mathbf{C}_{\hat{\sigma}}) \stackrel{5}{\text{I}} \frac{1}{4}c_2^2 - \frac{1}{4}a_2^2 - \frac{1}{2}c_4 + \frac{1}{2}a_4 \quad (12.45)$$

$$\text{PCI-CF}(\mathbf{C}_s) \stackrel{6}{\text{V}} \frac{1}{4}a_1^2c_2 - \frac{1}{4}a_1^2a_2 + \frac{1}{4}a_2^2 - \frac{1}{4}a_2c_2 \quad (12.46)$$

$$\text{PCI-CF}(\mathbf{C}_{\bar{\tau}}) \stackrel{7}{\text{I}} \frac{1}{8}a_1^4 - \frac{1}{4}a_1^2a_2 - \frac{1}{8}a_2^2 + \frac{1}{4}a_4 \quad (12.47)$$

$$\text{PCI-CF}(\mathbf{C}'_{\hat{\sigma}}) \stackrel{8}{\text{I}} \frac{1}{8}a_2^2 - \frac{1}{4}a_2c_2 + \frac{1}{8}c_2^2 - \frac{1}{4}c_4 + \frac{1}{4}a_4 \quad (12.48)$$

$$\text{PCI-CF}(\mathbf{S}_4) \stackrel{9}{\text{II}} 0 \quad (12.49)$$

$$\text{PCI-CF}(\mathbf{S}_4) \stackrel{10}{\text{V}} 0 \quad (12.50)$$

$$\text{PCI-CF}(\mathbf{C}_{2\hat{\sigma}}) \stackrel{11}{\text{I}} 0 \quad (12.51)$$

$$\text{PCI-CF}(\mathbf{C}_{2v}) \stackrel{12}{\text{V}} 0 \quad (12.52)$$

$$\text{PCI-CF}(\mathbf{C}_{2\bar{\tau}}) \stackrel{13}{\text{I}} \frac{1}{2}a_2^2 - \frac{1}{2}a_4 \quad (12.53)$$

$$\text{PCI-CF}(\mathbf{C}_{s\hat{\sigma}\bar{\tau}}) \stackrel{14}{\text{IV}} \frac{1}{2}a_1^2a_2 - \frac{1}{2}a_2^2 \quad (12.54)$$

$$\text{PCI-CF}(\mathbf{C}'_{2\bar{\tau}}) \stackrel{15}{\text{I}} 0 \quad (12.55)$$

$$\text{PCI-CF}(\mathbf{C}'_{2\hat{\sigma}}) \stackrel{16}{\text{I}} \frac{1}{2}c_4 - \frac{1}{2}a_4 \quad (12.56)$$

$$\text{PCI-CF}(\mathbf{C}_{s\bar{\sigma}\hat{\sigma}}) \stackrel{17}{\text{IV}} \frac{1}{2}a_2c_2 - \frac{1}{2}a_2^2 \quad (12.57)$$

$$\text{PCI-CF}(\mathbf{D}_2) \stackrel{18}{\text{III}} 0 \quad (12.58)$$

$$\text{PCI-CF}(\mathbf{C}_{2\bar{\sigma}}) \stackrel{19}{\text{II}} \frac{1}{4}b_2^2 - \frac{1}{4}a_2^2 - \frac{1}{4}b_4 - \frac{1}{4}c_4 + \frac{1}{2}a_4 \quad (12.59)$$

$$\text{PCI-CF}(\mathbf{S}_{4\hat{\sigma}}) \stackrel{20}{\text{IV}} 0 \quad (12.60)$$

$$\text{PCI-CF}(\mathbf{S}_{4\bar{\tau}}) \stackrel{21}{\text{IV}} 0 \quad (12.61)$$

$$\text{PCI-CF}(\mathbf{D}_{2d}) \stackrel{22}{\text{V}} 0 \quad (12.62)$$

$$\text{PCI-CF}(\mathbf{S}_{4\bar{\sigma}\hat{\sigma}}) \stackrel{23}{\text{IV}} \frac{1}{2}c_4 - \frac{1}{2}a_4 \quad (12.63)$$

$$\text{PCI-CF}(\mathbf{D}_{2\hat{\tau}}) \stackrel{24}{\equiv} 0 \quad (12.64)$$

$$\text{PCI-CF}(\mathbf{C}_{2\nu\tilde{\sigma}\hat{\tau}}) \stackrel{25}{\equiv} \frac{1}{2}a_2^2 - \frac{1}{2}a_4 \quad (12.65)$$

$$\text{PCI-CF}(\mathbf{D}_{2\tilde{\sigma}}) \stackrel{26}{\equiv} \frac{1}{2}b_4 - \frac{1}{2}a_4 \quad (12.66)$$

$$\text{PCI-CF}(\mathbf{D}_{2d\tilde{\sigma}\hat{\tau}}) \stackrel{27}{\equiv} a_4, \quad (12.67)$$

where the sequential numbers are shown over the respective equality symbols for the convenience of cross reference.

Generating Functions for Symmetry-Itemized Enumeration

Suppose that the four positions of the allene skeleton **3-9** (page 68) are substituted by a set of proligands selected from a ligand inventory **L** (Eq. 6.73 on page 153). According to Theorem 10.4 (page 298), we use the ligand-inventory functions shown in Eqs. 11.80–11.82 (page 329), which are common to the tetrahedral skeleton **3-5** (page 55).

The ligand-inventory functions (Eqs. 11.80–11.82) are introduced into the PCI-CFs (Eqs. 12.41–12.67). After expansion of the resulting equations, the following generating functions are obtained:

$$\begin{aligned} f_{C_1} &\stackrel{1}{\equiv} \frac{1}{\text{III}} \left\{ \frac{1}{2}(A^2B\bar{p} + A^2B\bar{p}) + \dots \right\} + \left\{ \frac{1}{2}(A^2p\bar{q} + A^2p\bar{q}) + \dots \right\} \\ &+ \left\{ \frac{3}{2}(ABX\bar{p} + ABX\bar{p}) + \dots \right\} + \left\{ \frac{1}{2}(ABp^2 + ABp^2) + \dots \right\} \\ &+ \left\{ AB\bar{p}\bar{p} + \dots \right\} + \left\{ \frac{3}{2}(ABp\bar{q} + ABp\bar{q}) + \dots \right\} \\ &+ \left\{ \frac{1}{2}(Ap^2\bar{p} + Ap^2\bar{p}) + \dots \right\} + \left\{ \frac{1}{2}(Ap^2q + Ap^2q) + \dots \right\} \\ &+ \left\{ \frac{3}{2}(Ap\bar{p}\bar{q} + Ap\bar{p}\bar{q}) + \dots \right\} + \left\{ \frac{3}{2}(Apq\bar{r} + Apq\bar{r}) + \dots \right\} \\ &+ \left\{ \frac{1}{2}(p^2\bar{p}q + p^2\bar{p}q) + \dots \right\} + \left\{ \frac{1}{2}(p^2q\bar{q} + p^2q\bar{q}) + \dots \right\} \\ &+ \left\{ \frac{1}{2}(p^2qr + p^2qr) + \dots \right\} + \left\{ \frac{3}{2}(p\bar{p}qr + p\bar{p}qr) + \dots \right\} \\ &+ \left\{ \frac{3}{2}(pqrs + pqrs) + \dots \right\} \end{aligned} \quad (12.68)$$

$$f_{C_2} \stackrel{3}{\equiv} \frac{1}{\text{III}} \left\{ \frac{1}{2}(A^2p^2 + A^2p^2) + \dots \right\} + \left\{ \frac{1}{2}(p^2q^2 + p^2q^2) + \dots \right\} \quad (12.69)$$

$$f_{C_{\tilde{\sigma}}} \stackrel{4}{\equiv} \frac{1}{\text{II}} \left\{ \frac{1}{2}(A^3p + A^3p) + \dots \right\} + \left\{ \frac{1}{2}(A^2B\bar{p} + A^2B\bar{p}) + \dots \right\}$$

$$\begin{aligned}
& + \left\{ \frac{1}{2} (A^2 p q + A^2 \bar{p} \bar{q}) + \dots \right\} + \left\{ \frac{1}{2} (A B p^2 + A B \bar{p}^2) + \dots \right\} \\
& + \left\{ \frac{1}{2} (A p^3 + A \bar{p}^3) + \dots \right\} + \left\{ \frac{1}{2} (A p^2 \bar{p} + A p \bar{p}^2) + \dots \right\} \\
& + \left\{ \frac{1}{2} (A p^2 q + A \bar{p}^2 \bar{q}) + \dots \right\} + \left\{ \frac{1}{2} (p^3 \bar{p} + p \bar{p}^3) + \dots \right\} \\
& + \left\{ \frac{1}{2} (p^3 q + \bar{p}^3 \bar{q}) + \dots \right\} + \left\{ \frac{1}{2} (p^2 \bar{p} q + p \bar{p}^2 \bar{q}) + \dots \right\} \\
& + \left\{ \frac{1}{2} (p^2 q \bar{q} + \bar{p}^2 q \bar{q}) + \dots \right\} + \left\{ \frac{1}{2} (p^2 q r + \bar{p}^2 q \bar{r}) + \dots \right\}
\end{aligned} \tag{12.70}$$

$$f_{C_{\bar{\sigma}}} \stackrel{5}{=} \frac{1}{I} \left\{ A^2 p \bar{p} + A^2 q \bar{q} + \dots \right\} + \left\{ 2 p \bar{p} q \bar{q} + 2 p \bar{p} r \bar{r} + \dots \right\} \tag{12.71}$$

$$f_{C_s} \stackrel{6}{=} \frac{1}{V} \left\{ A B p \bar{p} + A B q \bar{q} + \dots \right\} \tag{12.72}$$

$$f_{C_i} \stackrel{7}{=} \frac{1}{I} \left\{ A^2 B X + A^2 B Y \dots \right\} + \left\{ 3 A B X Y \right\} \tag{12.73}$$

$$f_{C'_{\bar{\sigma}}} \stackrel{8}{=} \frac{1}{I} \left\{ p \bar{p} q \bar{q} + \dots \right\} \tag{12.74}$$

$$f_{C_{2i}} \stackrel{13}{=} \frac{1}{I} \left\{ A^2 B^2 + \dots \right\} \tag{12.75}$$

$$f_{C_{s\bar{\sigma}i}} \stackrel{14}{=} \frac{1}{IV} \left\{ A^3 B + \dots \right\} + \left\{ A^2 B X + \dots \right\} \tag{12.76}$$

$$f_{C_{2\bar{\sigma}'}} \stackrel{16}{=} \frac{1}{I} \left\{ p^2 \bar{p}^2 + \dots \right\} \tag{12.77}$$

$$f_{C_{s\bar{\sigma}\bar{\sigma}}} \stackrel{17}{=} \frac{1}{IV} \left\{ A^2 p \bar{p} + \dots \right\} \tag{12.78}$$

$$f_{C_{2\bar{\sigma}}} \stackrel{19}{=} \frac{1}{II} \left\{ \frac{1}{2} (A^2 p^2 + A^2 \bar{p}^2) + \dots \right\} + \left\{ \frac{1}{2} (p^2 q^2 + \bar{p}^2 \bar{q}^2) + \dots \right\} \tag{12.79}$$

$$f_{S_{4\bar{\sigma}\bar{\sigma}}} \stackrel{23}{=} \frac{1}{IV} \left\{ p^2 \bar{p}^2 + \dots \right\} \tag{12.80}$$

$$f_{C_{2v\bar{\sigma}i}} \stackrel{25}{=} \frac{1}{IV} \left\{ A^2 B^2 + \dots \right\} \tag{12.81}$$

$$f_{D_{2\bar{\sigma}}} \stackrel{26}{=} \frac{1}{II} \left\{ \frac{1}{2} (p^4 + \bar{p}^4) + \dots \right\} \tag{12.82}$$

$$f_{D_{2d\bar{\sigma}i}} \stackrel{27}{=} \frac{1}{IV} \left\{ A^4 + B^4 + X^4 + Y^4 \right\} \tag{12.83}$$

where generating functions of zero value are omitted (cf. the sequential numbers above the equality symbols). The coefficient of the term $A^a B^b X^c Y^d p^r \bar{p}^s q^t \bar{q}^u r^v \bar{r}^w s^x \bar{s}^y q^z \bar{q}^w$ or the partition

$[\theta]_i$ (Eqs. 11.98–11.127 on page 330) indicates the number of inequivalent quadruplets of promolecules to be counted.

The terms appearing in $f_{C_{\hat{\sigma}}}$ (Eq. 12.71), $f_{C_{\hat{\tau}}}$ (Eq. 12.73), $f_{C'_{\hat{\sigma}}}$ (Eq. 12.74), $f_{C_{2\hat{\tau}}}$ (Eq. 12.75), and $f_{C_{2\hat{\sigma}'}}$ (Eq. 12.77) correspond to type-I stereoisograms, so that they are confirmed by the reference promolecules listed in Fig. 12.3. It should be noted that the molecules with the composition $p\bar{p}q\bar{q}$ ($[\theta]_{28}$) are separately counted by the term $2p\bar{p}q\bar{q}$ ($[\theta]_{28}$) in Eq. 12.71 (**12-13** and **12-14** of $C_{\hat{\sigma}}$) and by the term $p\bar{p}q\bar{q}$ ($[\theta]_{28}$) in Eq. 12.74 (**12-15** of $C'_{\hat{\sigma}}$).

In a similar way, the terms appearing in $f_{C_{\tilde{\sigma}}}$ (Eq. 12.70), $f_{C_{2\tilde{\sigma}}}$ (Eq. 12.79), and $f_{D_{2\tilde{\sigma}}}$ (Eq. 12.82) correspond to type-II stereoisograms, so that they are confirmed by the reference promolecules listed in Fig. 12.5. The terms appearing in f_{C_1} (Eq. 12.68) and f_{C_2} (Eq. 12.69) correspond to type-III stereoisograms, so that they are confirmed by the reference promolecules listed in Fig. 12.7. The terms appearing in $f_{C_{s\hat{\sigma}\hat{\tau}}}$ (Eq. 12.77), $f_{C_{s\tilde{\sigma}\tilde{\sigma}}}$ (Eq. 12.78), $f_{S_{4\tilde{\sigma}\tilde{\sigma}}}$ (Eq. 12.80), $f_{C_{2v\hat{\sigma}\hat{\tau}}}$ (Eq. 12.81), and $f_{D_{2d\hat{\sigma}\hat{\tau}}}$ (Eq. 12.83) correspond to type-IV stereoisograms. Hence, they are confirmed by referring to the top row of Fig. 12.9. The term $ABp\bar{p}$ ($[\theta]_{13}$) appearing in f_{C_s} (Eq. 12.72) corresponds to a type-V stereoisogram, which can be confirmed by referring to the bottom row of Fig. 12.9.

12.3.4 Type-Itemized Enumeration by the PCI Method

CI-CFs for Characterizing Five Types of Stereoisograms

To obtain CI-CFs for characterizing five types of stereoisograms, the PCI-CFs listed in Eqs. 12.41–12.67 are added according to the definitions shown by Eqs. 12.7–12.11. Note that the symbols I–V below the equality symbols in the PCI-CFs (Eqs. 12.41–12.67) represent the categories of the five types. Thereby, we obtain the following type-itemized CI-CFs [4]:

$$\begin{aligned} \text{CI-CF}^{\text{I}} &= \text{PCI-CF}(C_{\hat{\sigma}}) + \text{PCI-CF}(C_{\hat{\tau}}) + \text{PCI-CF}(C'_{\hat{\sigma}'}) + \text{PCI-CF}(C_{2\hat{\sigma}}) \\ &\quad + \text{PCI-CF}(C_{2\hat{\tau}}) + \text{PCI-CF}(C'_{2\hat{\tau}}) + \text{PCI-CF}(C'_{2\hat{\sigma}}) + \text{PCI-CF}(D_{2\hat{\tau}}) \\ &= \frac{1}{8}a_1^4 - \frac{1}{4}a_1^2a_2 + \frac{1}{4}a_2^2 - \frac{1}{4}a_2c_2 + \frac{3}{8}c_2^2 - \frac{1}{4}c_4 \end{aligned} \quad (12.84)$$

$$\begin{aligned} \text{CI-CF}^{\text{II}} &= \text{PCF-CF}(C_{\tilde{\sigma}}) + \text{PCF-CF}(S_4) + \text{PCF-CF}(C_{2\tilde{\sigma}}) + \text{PCF-CF}(D_{2\tilde{\sigma}}) \\ &= \frac{1}{4}b_1^2b_2 - \frac{1}{4}a_1^2a_2 + \frac{1}{4}a_2^2 - \frac{1}{4}a_2c_2 + \frac{1}{4}b_4 - \frac{1}{4}c_4 \end{aligned} \quad (12.85)$$

$$\begin{aligned} \text{CI-CF}^{\text{III}} &= \text{PCF-CF}(C_1) + \text{PCF-CF}(C_2) + \text{PCF-CF}(C'_2) + \text{PCF-CF}(D_2) \\ &= \frac{1}{16}b_1^4 - \frac{1}{16}a_1^4 - \frac{1}{8}b_1^2b_2 + \frac{1}{4}a_1^2a_2 - \frac{1}{8}a_1^2c_2 \\ &\quad + \frac{3}{16}b_2^2 - \frac{1}{4}a_2^2 + \frac{1}{4}a_2c_2 - \frac{3}{16}c_2^2 - \frac{1}{8}b_4 + \frac{1}{8}c_4 \end{aligned} \quad (12.86)$$

$$\begin{aligned} \text{PCI-CF}^{\text{IV}} &= \text{PCF-CF}(C_{s\hat{\sigma}\hat{\tau}}) + \text{PCF-CF}(C_{s\tilde{\sigma}\tilde{\sigma}}) + \text{PCF-CF}(S_{4\tilde{\sigma}}) + \text{PCF-CF}(S_{4\hat{\tau}}) \\ &\quad + \text{PCF-CF}(S_{4\tilde{\sigma}\tilde{\sigma}}) + \text{PCF-CF}(C_{2v\hat{\sigma}\hat{\tau}}) + \text{PCF-CF}(D_{2d\hat{\sigma}\hat{\tau}}) \\ &= \frac{1}{2}a_1^2a_2 - \frac{1}{2}a_2^2 + \frac{1}{2}a_2c_2 + \frac{1}{2}c_4 \end{aligned} \quad (12.87)$$

$$\begin{aligned} \text{PCI-CF}^{[V]} &= \text{PCF-CF}(C_s) + \text{PCF-CF}(S_4) + \text{PCF-CF}(C_{2v}) + \text{PCF-CF}(D_{2d}) \\ &= \frac{1}{4}a_1^2c_2 - \frac{1}{4}a_1^2a_2 + \frac{1}{4}a_2^2 - \frac{1}{4}a_2c_2 \end{aligned} \quad (12.88)$$

These CI-CFs for type-itemized enumeration can be alternatively obtained by a formal matrix calculation in a similar way to Eq. 12.40, where the inverse mark table ($M_{D_{2d\bar{\sigma}i}}^{-1}$) is replaced by the type-enumeration matrix (TEM) shown in the right part of Table 12.2.

Generating Functions for Type-Itemized Enumeration

The ligand-inventory functions (Eqs. 11.80–11.82 on page 329) are introduced into the CI-CFs (Eqs. 12.84–12.88), so as to give the following generating functions:

$$\begin{aligned} f^{[I]} &= \{A^2p\bar{p} + A^2q\bar{q} + \dots\} + \{3p\bar{p}q\bar{q} + 3p\bar{p}r\bar{r} + \dots\} \\ &\quad + \{A^2BX + A^2BY \dots\} + \{3ABXY\} + \\ &\quad + \{A^2B^2 + \dots\} + \{p^2\bar{p}^2 + \dots\} \end{aligned} \quad (12.89)$$

$$\begin{aligned} f^{[II]} &= \left\{ \frac{1}{2}(A^3p + A^3\bar{p}) + \dots \right\} + \left\{ \frac{1}{2}(A^2Bp + A^2B\bar{p}) + \dots \right\} \\ &\quad + \left\{ \frac{1}{2}(A^2pq + A^2\bar{p}q) + \dots \right\} + \left\{ \frac{1}{2}(ABp^2 + AB\bar{p}^2) + \dots \right\} \\ &\quad + \left\{ \frac{1}{2}(Ap^3 + A\bar{p}^3) + \dots \right\} + \left\{ \frac{1}{2}(Ap^2\bar{p} + A\bar{p}p^2) + \dots \right\} \\ &\quad + \left\{ \frac{1}{2}(Ap^2q + A\bar{p}^2\bar{q}) + \dots \right\} + \left\{ \frac{1}{2}(p^3\bar{p} + p\bar{p}^3) + \dots \right\} \\ &\quad + \left\{ \frac{1}{2}(p^3q + \bar{p}^3\bar{q}) + \dots \right\} + \left\{ \frac{1}{2}(p^2\bar{p}q + p\bar{p}^2\bar{q}) + \dots \right\} \\ &\quad + \left\{ \frac{1}{2}(p^2q\bar{q} + \bar{p}^2q\bar{q}) + \dots \right\} + \left\{ \frac{1}{2}(p^2qr + \bar{p}^2q\bar{r}) + \dots \right\} \\ &\quad + \left\{ \frac{1}{2}(A^2p^2 + A^2\bar{p}^2) + \dots \right\} + \left\{ \frac{1}{2}(p^2q^2 + \bar{p}^2\bar{q}^2) + \dots \right\} \\ &\quad + \left\{ \frac{1}{2}(p^4 + \bar{p}^4) + \dots \right\} \end{aligned} \quad (12.90)$$

$$\begin{aligned} f^{[III]} &= \left\{ \frac{1}{2}(A^2Bp + A^2B\bar{p}) + \dots \right\} + \left\{ \frac{1}{2}(A^2pq + A^2\bar{p}q) + \dots \right\} \\ &\quad + \left\{ \frac{3}{2}(ABXp + ABX\bar{p}) + \dots \right\} + \left\{ \frac{1}{2}(ABp^2 + AB\bar{p}^2) + \dots \right\} \\ &\quad + \left\{ ABp\bar{p} + \dots \right\} + \left\{ \frac{3}{2}(ABpq + AB\bar{p}q) + \dots \right\} \end{aligned}$$

$$\begin{aligned}
& + \left\{ \frac{1}{2} (A p^2 \bar{p} + A p \bar{p}^2) + \dots \right\} + \left\{ \frac{1}{2} (A p^2 q + A p \bar{q}^2) + \dots \right\} \\
& + \left\{ \frac{3}{2} (A p \bar{p} q + A p \bar{p} \bar{q}) + \dots \right\} + \left\{ \frac{3}{2} (A p q r + A p \bar{q} \bar{r}) + \dots \right\} \\
& + \left\{ \frac{1}{2} (p^2 \bar{p} q + p \bar{p}^2 \bar{q}) + \dots \right\} + \left\{ \frac{1}{2} (p^2 q \bar{q} + \bar{p}^2 q \bar{q}) + \dots \right\} \\
& + \left\{ \frac{1}{2} (p^2 q r + \bar{p}^2 \bar{q} r) + \dots \right\} + \left\{ \frac{3}{2} (p \bar{p} q r + p \bar{p} \bar{q} \bar{r}) + \dots \right\} \\
& + \left\{ \frac{3}{2} (p q r s + \bar{p} \bar{q} \bar{r} s) + \dots \right\} \\
& + \left\{ \frac{1}{2} (A^2 p^2 + A^2 \bar{p}^2) + \dots \right\} + \left\{ \frac{1}{2} (p^2 q^2 + \bar{p}^2 \bar{q}^2) + \dots \right\} \quad (12.91)
\end{aligned}$$

$$\begin{aligned}
f^{[IV]} &= \{ A^3 B + \dots \} + \{ A^2 B X + \dots \} + \{ A^2 p \bar{p} + \dots \} \\
&+ \{ p^2 \bar{p}^2 + \dots \} + \{ A^2 B^2 + \dots \} + \{ A^4 + B^4 + X^4 + Y^4 \} \quad (12.92)
\end{aligned}$$

$$f^{[V]} = \{ A B p \bar{p} + A B q \bar{q} + \dots \}. \quad (12.93)$$

The generating function $f^{[I]}$ (Eq. 12.89) is the sum of the generating functions of the subgroups contained in $SG^{[I]}$ (Eq. 12.7). They are confirmed by the reference promolecules listed in Fig. 12.3. In particular, the term $3p\bar{p}q\bar{q}$ ($[\theta]_{28}$) is the sum of the term $2p\bar{p}q\bar{q}$ in Eq. 12.71 and the term $p\bar{p}q\bar{q}$ in Eq. 12.74. The total value 3 is consistent with the presence of **12-13**, **12-14**, and **12-15**, as shown in Fig. 12.3.

In a similar way, the generating function $f^{[II]}$ (Eq. 12.90) is the sum of the generating functions of the subgroups contained in $SG^{[II]}$ (Eq. 12.8). They are confirmed by the reference promolecules listed in Fig. 12.5. The generating function $f^{[III]}$ (Eq. 12.91) is the sum of the generating functions of the subgroups contained in $SG^{[III]}$ (Eq. 12.9). They are confirmed by the reference promolecules listed in Fig. 12.7. The generating function $f^{[IV]}$ (Eq. 12.92) is the sum of the generating functions of the subgroups contained in $SG^{[IV]}$ (Eq. 12.10). They are confirmed by the reference promolecules listed in the top row of Fig. 12.9. The generating function $f^{[V]}$ (Eq. 12.93) is the sum of the generating functions of the subgroups contained in $SG^{[V]}$ (Eq. 12.11). They are confirmed by the reference promolecules listed in the bottom row of Fig. 12.9.

12.4 Comparison with Enumeration Under Subsymmetries

12.4.1 Enumeration of Allene Promolecules Under the Point-Group Symmetry

The enumeration of allene promolecules under the point-group symmetry D_{2d} has been already discussed in Chapter 5. The PCI-CFs for symmetry-itemized enumeration of allene

derivatives have been calculated to give Eqs. 6.106–6.113 (page 160). The corresponding generating functions are shown in Eqs. 6.114–6.121 (page 161).

According to Theorem 10.6 (page 306), the symmetry-itemized generating functions under the action of the point group D_{2d} (Eqs. 6.114–6.121 on page 161) can be correlated to those under the action of $D_{2d\bar{\sigma}\bar{\Gamma}}$ (Eqs. 12.68–12.83).

The relationship between the enumeration under D_{2d} and the enumeration under $D_{2d\bar{\sigma}\bar{\Gamma}}$ can be confirmed by the derivation of the PCI-CFs of D_{2d} (Eqs. 6.106–6.113 on page 160) from the PCI-CFs of $D_{2d\bar{\sigma}\bar{\Gamma}}$ (Eqs. 12.41–12.67), where Theorem 10.6 (page 306) is taken into consideration.

These tasks are open to readers as an exercise:

Exercise 12.10.

- In a similar way to the procedure described for T_d in Section 11.4, correlate the generation functions for D_{2d} (Eqs. 6.114–6.121 on page 161) to those for $D_{2d\bar{\sigma}\bar{\Gamma}}$ (Eqs. 12.68–12.83).
 - In a similar way to the procedure described for T_d in Section 11.4, derive the PCI-CFs of D_{2d} (Eqs. 6.106–6.113 on page 160) from the PCI-CFs of $D_{2d\bar{\sigma}\bar{\Gamma}}$ (Eqs. 12.41–12.67).
-

12.4.2 Enumeration of Allene Promolecules Under the *RS*-Permutation-Group Symmetry

Gross enumeration of allene derivatives under the *RS*-permutation group $D_{2\bar{\sigma}}$ has been discussed in Chapter 9. Symmetry-itemized enumeration of allene derivatives under $D_{2\bar{\sigma}}$ ($\simeq S_9^{[4]}$, cf. Eq. 9.56 on page 262) has been reported, where the coefficients of the generating functions calculated from PCIs the subgroups of $S_9^{[4]}$ in a tabular form [7, Tables 3 and 4] and the required PCIs for the subgroups of $S_9^{[4]}$ are given in the form of functions concerning s_d [7, Eqs. 16–23]. These PCIs for $S_9^{[4]}$ are permitted to be adopted as the PCIs for $D_{2\bar{\sigma}}$, which can be derived from the PCI-CFs of D_{2d} (Eqs. 6.106–6.113 on page 160) by putting $s_d = a_d = c_d = b_d$, where the correspondence among the SSGs of D_{2d} (Eq. 6.103 on page 159), $D_{2\bar{\sigma}}$ (Eq. 9.55 on page 262), and $S_9^{[4]}$ (Eq. 9.56 on page 262) is taken into consideration.

The PCIs for $D_{2\bar{\sigma}}$ (containing s_d) obtained from Eqs. 6.106–6.113 correspond to PCI-CFs for $D_{2\bar{\sigma}}$ (containing b_d), which are, in turn, derived by starting from the PCI-CFs of $D_{2d\bar{\sigma}\bar{\Gamma}}$ (Eqs. 12.41–12.67) according to Theorem 10.7 (page 308).

This task is open to readers as an exercise:

**Exercise 12.11.**

- In a similar way to the procedure described for $T_{\bar{\sigma}}$ in Section 11.4, derive the PCI-CFs of $D_{2\bar{\sigma}}$ from the PCI-CFs of $D_{2d\bar{\sigma}\hat{I}}$ (Eqs. 12.41–12.67).
- Confirm that the resulting PCI-CFs of $D_{2\bar{\sigma}}$ consists of only terms of b_d 's with disappearance of terms of a_d and/or c_d .
- Prove the disappearance of terms of a_d and/or c_d in general.
- By putting $s_d = b_d$, calculate the PCIs for $D_{2\bar{\sigma}}$.

References

- [1] S. Fujita, *MATCH Commun. Math. Comput. Chem.*, **52**, 3–18 (2004).
- [2] S. Fujita, *Memoirs of the Faculty of Engineering and Design, Kyoto Institute of Technology*, **53**, 19–38 (2005).
- [3] S. Fujita, *J. Math. Chem.*, **52**, 1717–1750 (2014).
- [4] S. Fujita, *J. Math. Chem.*, **52**, 1751–1793 (2014).
- [5] S. Fujita, *Helv. Chim. Acta*, **85**, 2440–2457 (2002).
- [6] IUPAC Chemical Nomenclature and Structure Representation Division, *Provisional Recommendations. Nomenclature of Organic Chemistry* (2004), http://old.iupac.org/reports/provisional/abstract04/favre_310305.html.
cf. H. A. Favre, W. H. Powell, “Nomenclature of Organic Chemistry. IUPAC Recommendations and Preferred Names 2013”, The Royal Society of Chemistry, Cambridge (2013).
- [7] S. Fujita, *Bull. Chem. Soc. Jpn.*, **75**, 1949–1962 (2002).

13 Stereochemical Nomenclature¹

13.1 Absolute Configuration

13.1.1 Single Pair of Attributes ‘Chirality/Achirality’ in Modern Stereochemistry

In the glossary of the IUPAC Recommendations 1996 [1], the term *configuration* is defined as “In the context of stereochemistry, the term is restricted to the arrangement of atoms of a molecular entity in space that distinguishes *stereoisomers*, the *isomerism* between which is not due to conformation differences. See also *absolute configuration* and *relative configuration*”. And then, the term *absolute configuration* is defined as “The spatial arrangement of the atoms of a chiral molecular entity (or group) and its stereochemical description, e.g., *R* or *S*.”

The term ‘stereogenic’ has later been proposed to rationalize the foundations of *R/S*-stereodescriptors [2]. Helmchen [3, Section 1.3] has pointed out that the term *chirality element* is one of problematic terms: “This previously common term should be used with care. More appropriate is the term *stereogenic unit*”. However, Helmchen [3, Table 1] maintains the usage of the terms ‘chirality center’ (⊂ ‘chirality units’) and ‘pseudoasymmetric center’ (⊂ ‘pseudoasymmetric units’). Moreover, Rule 91.1.1.1 of Provisional Recommendations 2004 [4] refers to the term ‘stereogenic unit’ and points out the presence of three kinds of stereogenic units (a central atom such as a chirality center, a central bond such as a chirality axis, and a double bond). Then, it states “... A chirality center, formerly known as an ‘asymmetric atom’, is the classical example of a stereogenic unit.” and shows an example of assigning an *R*-descriptor to a ‘chirality center’ of Xabcd.

The term ‘stereogenic centers’ is used to designate a pair of Cl-substituted carbons in *cis*- and *trans*-1,3-dichlorocyclobutanes, where interchange of two ligands (Cl and H) at a ‘stereogenic’ center leads to a stereoisomer [5, Fig. 3.8]. It is to be noted that the dichlorocyclobutanes are achiral. This means that ‘stereogenic’ centers may be chiral or achiral.

The discussions in the preceding paragraphs demonstrate that the terminology concerning ‘chirality center’, ‘stereogenic unit’, and *absolute configuration* is suffering from serious confusion because of the lack of an appropriate mathematical framework. In particular, the relationship between ‘chirality center’ and ‘stereogenic unit’ has been discussed in a qual-

¹ This chapter is based on S. Fujita, “Three Aspects of an Absolute Configuration on the Basis of the Stereoisogram Approach and Revised Terminology on Related Stereochemical Concepts”, *J. Math. Chem.*, **52**, 1514–1534 (2014); and S. Fujita, “Stereoisograms for Reorganizing the Theoretical Foundations of Stereochemistry and Stereoisomerism: II. Rational Avoidance of Misleading Standpoints for *R/S*-Stereodescriptors of the Cahn-Ingold-Prelog System”, *Tetrahedron: Asymmetry*, **25**, 1169–1189 (2014).

itative fashion, because these terms have not been defined definitely from a mathematical point of view.

If we obey the above-mentioned terminology of modern stereochemistry, a plausible (but misleading) interpretation may be summarized as follows:



Remark 13.1 (Misleading Interpretation due to Modern Stereochemistry). A ‘chirality center’ is a kind of a stereogenic unit and the absolute configuration of such a ‘chirality center’ is characterized by a label *R* or *S*.

Although this interpretation is seemingly plausible, it suffers from serious confusion: the concept of *absolute configuration* is linked solely with the concept of chirality. Because the concept of *absolute configuration* is linked with the label *R* or *S* due to the Cahn-Ingold-Prelog (CIP) system, the label *R* or *S* is misleadingly linked with chirality after considering the connotation of ‘chirality \subset stereogenicity’. The confusion stems from the following over-simplified foundation of modern stereochemistry:



Remark 13.2 (Over-Simplified Theoretical Foundation of Modern Stereochemistry). Modern stereochemistry is based on a single pair of attributes *chirality/achirality* in the discussions on absolute configuration and on *R/S*-stereodescriptors.

13.1.2 Three Pairs of Attributes in Fujita’s Stereoisogram Approach

To avoid such confusion, Fujita has proposed the concepts of *RS-diastereomers* and *holantimers* in addition to *enantiomers*, which are integrated to give a quadruplet of *RS-stereoisomers* contained in a *stereoisogram* [6,7]. Such quadruplets of *RS-stereoisomers* are characterized by a new concept of *RS-stereoisomeric groups* [8–11]. As summarized in Chapters 10–12, the crux of Fujita’s stereoisogram approach is to clarify three pairs of attributes:



Rule 13.1. There are three pairs of attributes on the basis of Fujita’s stereoisogram approach, i.e., a pair of *chirality/achirality*, a pair of *RS-stereogenicity/RS-astereogenicity*, and a pair of *sclerality/asclerality*, as summarized in Table 10.3 (page 285).

This exhibits a sharp contrast to modern stereochemistry, which presumes only one pair of chirality/achirality and disregards the other pairs of attributes. Note that the term ‘stere-

ogenicity' of modern stereochemistry is not restricted to permit such a consistent treatment as provided by the term *RS-stereogenicity* of Fujita's stereoisogram approach.

An attribute *chirality* is linked with an enantiomeric relationship as a pairwise relationship, which is concerned with a (pro)molecular entity and its enantiomeric entity (mirror-image entity). Note that a self-enantiomeric relationship means achirality. Another attribute *RS-stereogenicity* is linked with an *RS*-diastereomeric relationship as a pairwise relationship, which is concerned with a (pro)molecular entity and its *RS*-diastereomeric entity. Note that a self-*RS*-diastereomeric relationship means *RS*-astereogenicity. An additional attribute *sclerality* is linked with a holantimeric relationship as a pairwise relationship, which is concerned with a (pro)molecular entity and its holantimeric entity. Note that a self-holantimeric relationship means asclerality.



Rule 13.2. There are three types of pairwise relationships on the basis of Fujita's stereoisogram approach, i.e., an *enantiomeric* relationship concerning a pair of enantiomers; an *RS-diastereomeric* relationship concerning a pair of *RS*-diastereomers; and a holantimeric relationship concerning a pair of holantimers, as summarized in Table 10.3 (page 285).

This exhibits a sharp contrast to modern stereochemistry, which presumes only an enantiomeric relationship and disregards the other *pairwise* relationships. Note that the term 'diastereomeric' of modern stereochemistry is not restricted to permit such a consistent treatment as provided by the term *RS-diastereomeric* of Fujita's stereoisogram approach.



Exercise 13.1. Review the distinction between the term 'diastereomeric' of modern stereochemistry and the term *RS-diastereomeric* of Fujita's stereoisogram approach. Review the distinction between the term 'stereogenic' of modern stereochemistry and the term *RS-stereogenic* of Fujita's stereoisogram approach.

13.1.3 Three Aspects of Absolute Configuration

In accord with the three pairs of attributes and with the three types of pairwise relationships, the term *absolute configuration* is concluded to exhibit three aspects [12]:

1. **Chiral aspect:** The chiral aspect of the term *absolute configuration* is generated by reflection operations and corresponds to enantiomeric relationships, each of which is concerned with the appearance of a pair of enantiomers.
2. ***RS*-Stereogenic aspect:** The *RS*-stereogenic aspect of the term *absolute configuration* is generated by *RS*-permutation operations and corresponds to *RS*-diastereomeric relationships, each of which is concerned with the appearance of a pair of *RS*-

diastereomers. The *RS*-diastereomers of each pair are differentiated by the *R/S*-stereodescriptors due to the CIP system.

3. **Scleral aspect:** The scleral aspect of the term *absolute configuration* is generated by ligand-reflection operations and corresponds to holantimeric relationships, each of which is concerned with the appearance of a pair of holantimers.

It follows that the term *absolute configuration* is determined by examining properties of a quadruplet of *RS*-stereoisomers, which belongs to one of the five types of stereoisograms. The definition of the term *absolute configuration* appearing in the IUPAC Recommendations 1996 [1] should be revised to connote the three aspects described above.

13.2 Quadruplets of *RS*-Stereoisomers as Equivalence Classes

13.2.1 Three Types of Pairwise Relationships in a Quadruplet of *RS*-Stereoisomers

As discussed in Section 1.3, the dichotomy between enantiomers and diastereomers, which is widely adopted in modern stereochemistry, suffers from the confusion of the chiral aspect with the *RS*-stereogenic aspect during discussions on absolute configuration. From a mathematical point of view [13], enantiomeric relationships (Def. 2.3 on page 36) and stereoisomeric relationships (Def. 2.5 on page 38) serve as respective criteria for categorizing molecules into equivalence classes, while diastereomeric relationships (Def. 2.7 on page 40) are unable to generate equivalence classes.²

As discussed in Chapters 5 and 7, Fujita's USCI approach [14] is based on enantiomeric relationships as equivalence relationships, so that it counts each pair of enantiomers (or each achiral entity) once during combinatorial enumeration of tetrahedral entities under the point group T_d . As discussed in Chapters 10–12, on the other hand, a quadruplet of *RS*-stereoisomers contained in a stereoisogram is an equivalence class, which is characterized by enantiomeric relationships, *RS*-diastereomeric relationships, and holantimeric relationships. As for tetrahedral derivatives, a quadruplet of *RS*-stereoisomers is counted once under the *RS*-stereoisomeric group $T_{d\overline{\sigma}\hat{I}}$ (cf. Chapter 11).

The data summarized in Table 10.3 (page 285) are illustrated in Fig. 13.1 by using a tetrahedral skeleton **13-1**, where four substituents are represented by solid circles or half-

² Suppose that a molecule (e.g., **13-2**) is diastereomeric to a reference molecule (e.g., **13-1**). Then, another molecule (e.g., **13-2**) enantiomeric to the former molecule is also diastereomeric to the reference molecule (e.g., **13-1**). This means that a set of diastereomeric molecules (e.g., **13-2** and **13-2**) contains a pair of enantiomeric molecules. In other words, a holantimeric relationship devised by Fujita's stereoisogram approach is regarded as a diastereomeric relationship in modern stereochemistry.

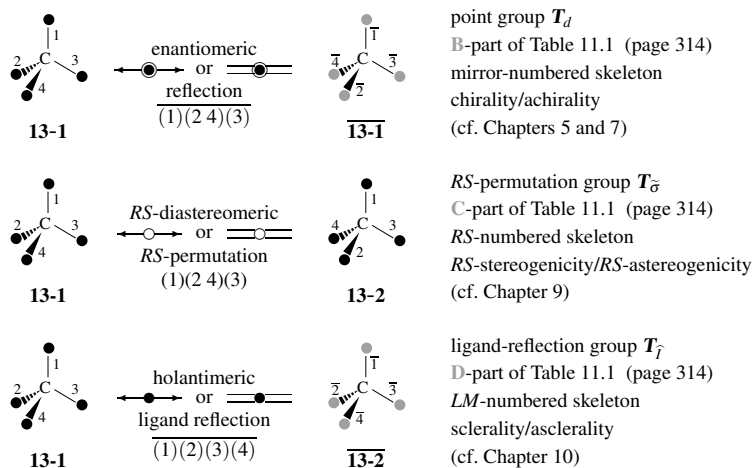


Fig. 13.1. Enantiomeric, *RS*-diastereomeric, and holantimeric relationships in a tetrahedral skeleton. A solid circle and a half-tone solid circle at a vertex represent a pair of enantiomeric ligands in isolation. They may coalesce to give an achiral ligand in isolation.

tone solid circles in order to illustrate the interconversion of chirality senses during the action of operations listed in Table 11.1 (page 314). Note that the **A**-part of Table 11.1 generates homomers, which are regarded as being equivalent to the original skeleton **13-1**. The four vertices are numbered sequentially according to an elementary stereoisogram shown in Fig. 11.1 (page 315):

1. The reference promolecule **13-1** is converted into $\overline{13-1}$ by means of a reflection operation, where the four substituents (proligands) represented by solid circles are converted into their counterparts with an opposite chirality sense (a half-tone solid circle). The pair of proligands may coalesce to give an achiral proligand in isolation. The resulting pair, **13-1**/ $\overline{13-1}$, is in an enantiomeric relationship (if chiral) or in a self-enantiomeric relationship (if achiral).
2. The reference promolecule **13-1** is converted into **13-2** by means of an *RS*-permutation operation, where the four substituents (proligands) represented by solid circles maintain chirality sense in isolation. The resulting pair, **13-1**/**13-2**, is in an *RS*-diastereomeric relationship (if *RS*-stereogenic) or in a self-*RS*-diastereomeric relationship (if *RS*-astereogenic).
3. The reference promolecule **13-1** is converted into $\overline{13-2}$ by means of a ligand-reflection operation, where the four substituents (proligands) represented by solid circles are converted into their counterparts with an opposite chirality sense (a half-tone solid circle). The pair of proligands may coalesce to give an achiral proligand in isolation. The resulting pair, **13-1**/ $\overline{13-2}$, is in a holantimeric relationship (if scleral) or in a self-holantimeric relationship (if ascleral).

13.2.2 Formulation of Stereoisograms as Quadruplets of *RS*-Stereoisomers

By starting from Fig. 13.1, the elementary stereoisogram shown in Fig. 11.1 generates a stereoisogram shown in Fig. 13.2, in which the four positions of each entity are substituted by solid circles or half-tone solid circles. By using such solid circles or half-tone solid circles, enantiomeric relationships along the vertical directions are clearly differentiated from *RS*-diastereomeric relationships along the horizontal directions in Fig. 13.2.

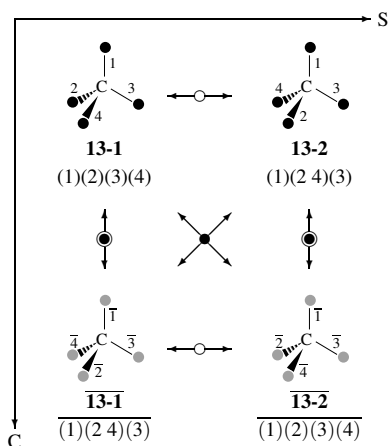


Fig. 13.2. Stereoisogram concerning a quadruplet of **13-1**, **13-1**, **13-2**, and **13-2**. The double-headed arrows may be changed into equality symbols according to the five types of stereoisograms.

The quadruplet of *RS*-stereoisomers (**13-1**, **13-1**, **13-2**, and **13-2**) and the corresponding stereoisogram are governed by an *RS*-stereoisomeric group $T_{d\hat{\sigma}\hat{\tau}}$, which is an extension of the point group T_d (cf. Chapter 11). Fujita's USCI (unit-subduced-cycle-index) approach has been extended to enumerate tetrahedral entities under the *RS*-stereoisomeric group $T_{d\hat{\sigma}\hat{\tau}}$, where each quadruplet of *RS*-stereoisomers (Type I–V) is counted once as discussed in Chapter 11 [15,16]. The reference promolecule for such a quadruplet of *RS*-stereoisomers is fixed (stabilized) by a subgroup of the *RS*-stereoisomeric group $T_{d\hat{\sigma}\hat{\tau}}$, just as the reference promolecule for a pair of enantiomers is fixed (stabilized) by a subgroup of the point group T_d .

13.3 Inner Structures of Promolecules

The four vertices of a tetrahedral skeleton construct an orbit governed by the coset representation $T_{d\hat{\sigma}\hat{\tau}}(/C_{3v\hat{\sigma}\hat{\tau}})$, where the global symmetry $T_{d\hat{\sigma}\hat{\tau}}$ and the local symmetry $C_{3v\hat{\sigma}\hat{\tau}}$ characterize the behavior of the four vertices. To characterize the global and local symme-

tries of a derivative, subduction of $T_{d\bar{\sigma}\hat{\tau}}(/C_{3v\bar{\sigma}\hat{\tau}})$ to each subgroup $\hat{G}_j (\subset T_{d\bar{\sigma}\hat{\tau}})$ is listed in Table 11.2 (page 326). Such subduction provides us with useful pieces of information on inner structures of promolecules to be specified by *R/S*-stereodescriptors.

13.3.1 Inner Structures of *RS*-Stereogenic Promolecules

According to Fujita's stereoisogram approach, *RS*-stereogenic promolecules (type I, III, and type V) are concluded to be specified by *R/S*-stereodescriptors because of the *RS*-stereogenicity common to type I, III, and type V (not because of chirality). This conclusion is clearly demonstrated by examining their inner structures.

Inner Structures of Type-I Promolecules

To derive a promolecule having a type-I stereoisogram, the subgroup \hat{G}_j is selected from Eq. 11.7 (page 322). The symmetry-itemized enumeration under $T_{d\bar{\sigma}\hat{\tau}}$ indicates the presence of the promolecule **11-3** of $C_{\hat{\tau}}$ with the composition ABXY. The type-I stereoisogram of **11-3** is shown in Fig. 11.3 (page 317).

The inner structure of **11-3** is characterized by the following subduction of the *RS*-stereoisomeric group $T_{d\bar{\sigma}\hat{\tau}}$:

$$T_{d\bar{\sigma}\hat{\tau}}(/C_{3v\bar{\sigma}\hat{\tau}}) \downarrow C_{\hat{\tau}} = 4C_{\hat{\tau}}(/C_{\hat{\tau}}), \quad (13.1)$$

which is taken from the 6th row of Table 11.2 (page 326). Hence, each proligand A, B, X, or Y constructs a one-membered $C_{\hat{\tau}}(/C_{\hat{\tau}})$ -orbit. This behavior is illustrated by Young's tableau shown in the intersection of the type-I row and the *RS*-stereoisomerism column of Fig. 13.3.

Under the point group T_d , the following subduction is obtained [14, Table C.10]:

$$T_d(/C_{3v}) \downarrow C_1 = 4C_1(/C_1). \quad (13.2)$$

Hence, each proligand A, B, X, or Y constructs a one-membered $C_1(/C_1)$ -orbit under the point group T_d . This behavior is illustrated by Young's tableau shown in the intersection of the type-I row and the chirality column of Fig. 13.3.

Under the *RS*-permutation group $T_{\bar{\sigma}}$, the following subduction is obtained:

$$T_{\bar{\sigma}}(/C_{3\bar{\sigma}}) \downarrow C_1 = 4C_1(/C_1) \quad (13.3)$$

Hence, each proligand A, B, X, or Y constructs a one-membered $C_1(/C_1)$ -orbit under the *RS*-permutation group $T_{\bar{\sigma}}$. This behavior is illustrated by Young's tableau shown in the intersection of the type-I row and the *RS*-stereogenicity column of Fig. 13.3.

The inequivalence of all the proligands (A, B, X, or Y) is illustrated by a gray-coloring of Young's tableau, so that **11-3** of type I is specified by *R/S*-stereodescriptors.

	<i>RS</i> -stereoisomerism	chirality	<i>RS</i> -stereogenicity	sclerality
	<i>RS</i> -stereoisomeric-group symmetry (under $T_{d\bar{\sigma}f}$)	point-group symmetry (under T_d)	<i>RS</i> -permutation-group symmetry (under $T_{\bar{\sigma}}$)	ligand-reflection-group symmetry (under $T_{\bar{\gamma}}$)
type I (e.g., 11-3)	$4C_7(/C_7)$ 	$4C_1(/C_1)$ 	$4C_1(/C_1)$ 	$4C_7(/C_7)$
type III (e.g., 11-20)	$4C_1(/C_1)$ 	$4C_1(/C_1)$ 	$4C_1(/C_1)$ 	$4C_1(/C_1)$
type V (e.g., 11-32)	$C_s(/C_1) + 2C_s(/C_s)$ 	$C_s(/C_1) + 2C_s(/C_s)$ 	$4C_1(/C_1)$ 	$4C_1(/C_1)$
type II (e.g., 11-14)	$C_{\bar{\sigma}}(/C_1) + 2C_{\bar{\sigma}}(/C_{\bar{\sigma}})$ 	$4C_1(/C_1)$ 	$C_{\bar{\sigma}}(/C_1) + 2C_{\bar{\sigma}}(/C_{\bar{\sigma}})$ 	$4C_1(/C_1)$
type IV (e.g., 11-31)	$C_{s\bar{\sigma}\bar{\sigma}}(/C_{\bar{\sigma}}) + C_{s\bar{\sigma}\bar{\sigma}}(/C_s)$ 	$C_s(/C_1) + 2C_s(/C_s)$ 	$C_{\bar{\sigma}}(/C_1) + 2C_{\bar{\sigma}}(/C_{\bar{\sigma}})$ 	$2C_{\bar{\sigma}}(/C_1)$
(e.g., 11-30)	$C_{s\bar{\sigma}f}(/C_7) + 2C_{s\bar{\sigma}f}(/C_{s\bar{\sigma}f})$ 	$C_s(/C_1) + 2C_s(/C_s)$ 	$C_{\bar{\sigma}}(/C_1) + 2C_{\bar{\sigma}}(/C_{\bar{\sigma}})$ 	$4C_7(/C_7)$

Fig. 13.3. Chiral aspects due to the point-group symmetry, *RS*-stereogenic aspects due to the *RS*-permutation-group symmetry, and scleral aspects due to the ligand-reflection-group symmetry [17]. These three aspects are conceptually distinct to one another. They are integrated to characterize the total features of five types, which are represented by the *RS*-stereoisomeric-group symmetry.

Inner Structures of Type-III Promolecules

To derive a promolecule having a type-III stereoisogram, the subgroup \hat{G}_j is selected from Eq. 11.9 (page 323). The symmetry-itemized enumeration under $T_{d\hat{\sigma}\hat{\tau}}$ indicates the presence of the promolecule **11-20** with the composition ABXp. The type-III stereoisogram of **11-20** is shown in Fig. 11.5 (page 319).

The inner structure of **11-20** is characterized by the following subduction of the *RS*-stereoisomeric group $T_{d\hat{\sigma}\hat{\tau}}$:

$$T_{d\hat{\sigma}\hat{\tau}}(/C_{3v\hat{\sigma}\hat{\tau}}) \downarrow C_1 = 4C_1(/C_1), \quad (13.4)$$

which is taken from the first row of Table 11.2 (page 326). Hence, each proligand A, B, X, or p constructs a one-membered $C_1(/C_1)$ -orbit. This behavior is illustrated by Young's tableau shown in the intersection of the type-III row and the *RS*-stereoisomerism column of Fig. 13.3.

The promolecule **11-20** behaves under the point group T_d in a similar way to Eq. 13.2. Hence, each proligand A, B, X, or p constructs a one-membered $C_1(/C_1)$ -orbit under the point group T_d . This behavior is illustrated by Young's tableau shown in the intersection of the type-III row and the chirality column of Fig. 13.3.

The promolecule **11-20** behaves under the *RS*-permutation group $T_{\hat{\sigma}}$ in a similar way to Eq. 13.3. Hence, each proligand A, B, X, or p constructs a one-membered $C_1(/C_1)$ -orbit under the *RS*-permutation group $T_{\hat{\sigma}}$. This behavior is illustrated by Young's tableau shown in the intersection of the type-III row and the *RS*-stereogenicity column of Fig. 13.3.

The inequivalence of all the proligands (A, B, X, or p) is illustrated by a gray-coloring of Young's tableau, so that **11-20** of type III is specified by *R/S*-stereodescriptors.

Inner Structures of Type-V Promolecules

To derive a promolecule having a type-V stereoisogram, the subgroup \hat{G}_j is selected from Eq. 11.11 (page 323). The symmetry-itemized enumeration under $T_{d\hat{\sigma}\hat{\tau}}$ indicates the presence of the promolecule **11-32** (or **11-40**) of C_s with the composition ABp \bar{p} . The type-V stereoisogram of **11-32** (or **11-40**) is shown in Fig. 11.7 (page 321).

The inner structure of **11-32** (or **11-40**) is characterized by the following subduction of the *RS*-stereoisomeric group $T_{d\hat{\sigma}\hat{\tau}}$:

$$T_{d\hat{\sigma}\hat{\tau}}(/C_{3v\hat{\sigma}\hat{\tau}}) \downarrow C_s = C_s(/C_1) + 2C_s(/C_s), \quad (13.5)$$

which is taken from the 5th row of Table 11.2 (page 326). Hence, a pair of proligands p \bar{p} constructs a two-membered enantiospheric orbit, while each of achiral proligands A and B constructs a one-membered homospheric orbit under the action of the *RS*-stereoisomeric group $T_{d\hat{\sigma}\hat{\tau}}$. This behavior is illustrated by Young's tableau shown in the intersection of the type-V row and the *RS*-stereoisomerism column of Fig. 13.3.

Under the point group T_d , the following subduction is obtained [14, Table C.10]:

$$T_d(/C_{3v}) \downarrow C_s = C_s(/C_1) + 2C_s(/C_s). \quad (13.6)$$

Hence, a pair of proligands p/\bar{p} constructs a two-membered enantiospheric orbit, while each of achiral proligands A and B constructs a one-membered homospheric orbit under the point group T_d . This behavior is illustrated by Young's tableau shown in the intersection of the type-V row and the chirality column of Fig. 13.3.

Under the RS -permutation group $T_{\bar{\sigma}}$, the following subduction is obtained:

$$T_{\bar{\sigma}}(/C_{3\bar{\sigma}}) \downarrow C_1 = 4C_1(/C_1). \quad (13.7)$$

Hence, each proligand A, B, p, or \bar{p} constructs a one-membered $C_1(/C_1)$ -orbit under the RS -permutation group $T_{\bar{\sigma}}$. This behavior is illustrated by Young's tableau shown in the intersection of the type-V row and the RS -stereogenicity column of Fig. 13.3.

The inequivalence of all the proligands (A, B, p, or \bar{p}) under the RS -permutation group $T_{\bar{\sigma}}$ is illustrated by a gray-coloring of Young's tableau, so that **11-32** (or **11-40**) of type V is specified by R/S -stereodescriptors.

13.3.2 Inner Structures of RS -Astereogenic Promolecules

According to Fujita's stereoisogram approach, RS -astereogenic promolecules (type II and type IV) are concluded not to be specified by R/S -stereodescriptors. This conclusion is clearly demonstrated by examining their inner structures.

Inner Structures of Type-II Promolecules

As a representative of type-II promolecules, the inner structure of **11-14** with the composition ABp^2 is characterized by the following subduction of the RS -stereoisomeric group $T_{d\bar{\sigma}\bar{t}}$:

$$T_{d\bar{\sigma}\bar{t}}(/C_{3v\bar{\sigma}\bar{t}}) \downarrow C_{\bar{\sigma}} = C_{\bar{\sigma}}(/C_1) + 2C_{\bar{\sigma}}(/C_{\bar{\sigma}}), \quad (13.8)$$

which is taken from the third row of Table 11.2 (page 326). Hence, a pair of proligands p 's constructs a two-membered hemispheric $C_{\bar{\sigma}}(/C_1)$ -orbit, while each of achiral proligands A and B constructs a one-membered hemispheric $C_{\bar{\sigma}}(/C_{\bar{\sigma}})$ -orbit under the action of the RS -stereoisomeric group $T_{d\bar{\sigma}\bar{t}}$. This behavior is illustrated by Young's tableau shown in the intersection of the type-II row and the RS -stereoisomerism column of Fig. 13.3. Note that the type-II stereoisogram of **11-14** is shown in Fig. 11.4 (page 318).

Under the point group T_d , the following subduction is obtained [14, Table C.10]:

$$T_d(/C_{3v}) \downarrow C_1 = 4C_1(/C_1). \quad (13.9)$$

Hence, each of achiral or chiral proligands (A, B, p, or \bar{p}) constructs a one-membered hemispheric orbit under the point group T_d . This behavior is illustrated by Young's tableau shown in the intersection of the type-II row and the chirality column of Fig. 13.3.

Under the RS -permutation group $T_{\bar{\sigma}}$, the following subduction is obtained:

$$T_{\bar{\sigma}}(/C_{3\bar{\sigma}}) \downarrow C_{\bar{\sigma}} = C_{\bar{\sigma}}(/C_1) + 2C_{\bar{\sigma}}(/C_{\bar{\sigma}}). \quad (13.10)$$

Hence, a pair of chiral proligands p 's in isolation constructs a two-membered RS -hemitropic $C_{\tilde{\sigma}}(/C_1)$ -orbit, while each of achiral proligands A and B in isolation constructs a one-membered RS -hemitropic $C_{\tilde{\sigma}}(/C_{\tilde{\sigma}})$ -orbit under the action of the RS -permutation group $T_{\tilde{\sigma}}$.³ This behavior is illustrated by Young's tableau shown in the intersection of the type-II row and the RS -stereogenicity column of Fig. 13.3.

The presence of a two-membered $C_{\tilde{\sigma}}(/C_1)$ -orbit indicates the equivalence between two p 's as illustrated by the top row of the Young's tableau, so that **11-14** of type-II is not characterized by RS -stereodescriptors.

Exercise 13.2.

- Show that the central atom of **11-14** of type II (Fig. 11.4 on page 318) belongs to a one-membered $C_1(/C_1)$ -orbit under the action of the point group T_d . Discuss that the local chirality of the central atom of **11-14** is not characterized by RS -stereodescriptors.
 - Show that the central atom of **11-14** of type II (Fig. 11.4 on page 318) belongs to a one-membered $C_{\tilde{\sigma}}(/C_{\tilde{\sigma}})$ -orbit under the action of the RS -permutation group $T_{\tilde{\sigma}}$. Discuss that the local RS -astereogenicity of the central atom of **11-14** is not characterized by RS -stereodescriptors.
 - Discuss the local chirality and the local RS -astereogenicity in combination with the global chirality and the global RS -astereogenicity.
-

Inner Structures of Type-IV Promolecules

For the purpose of comparing the inner structure of **11-32** (or **11-40**) of type V (the composition $ABp\bar{p}$), let us examine the promolecule **11-31** of type IV (the composition $A^2p\bar{p}$), which is listed in Fig. 11.2 (page 316).

Exercise 13.3. Draw the stereoisogram of **11-31** by referring to the type-IV stereoisogram of Fig. 11.6 (page 320).

The promolecule **11-31** is characterized by the following subduction of the RS -stereoisomeric group $T_{d\tilde{\sigma}\hat{t}}$:

$$T_{d\tilde{\sigma}\hat{t}}(/C_{3v\tilde{\sigma}\hat{t}}) \downarrow C_{s\tilde{\sigma}\hat{t}} = C_{s\tilde{\sigma}\hat{t}}(/C_{\tilde{\sigma}}) + C_{s\tilde{\sigma}\hat{t}}(/C_s), \quad (13.11)$$

which is taken from the 14th row of Table 11.2 (page 326). Hence, a pair of proligands $p\bar{p}$ constructs a two-membered enantiospheric $C_{s\tilde{\sigma}\hat{t}}(/C_{\tilde{\sigma}})$ -orbit, while a pair of proligands A 's of the same kind constructs a two-membered homospheric $C_{s\tilde{\sigma}\hat{t}}(/C_s)$ -orbit under the action of the RS -stereoisomeric group $T_{d\tilde{\sigma}\hat{t}}$. This behavior is illustrated by Young's tableau

³ The term RS -hemitropic will be introduced later.

shown in the intersection of the upper type-IV row and the *RS*-stereoisomerism column of Fig. 13.3.

Under the point group T_d , the following subduction is obtained [14, Table C.10]:

$$T_d(/C_{3v}) \downarrow C_s = C_s(/C_1) + 2C_s(/C_s). \quad (13.12)$$

Hence, a pair of p/\bar{p} constructs a two-membered enantiospheric $C_s(/C_1)$ -orbit, while each achiral promolecule selected from two *A*'s constructs a one-membered homospheric $C_s(/C_s)$ -orbit under the point group T_d . This behavior is illustrated by Young's tableau shown in the intersection of the upper type-IV row and the chirality column of Fig. 13.3.



Exercise 13.4. Under the point group T_d , the subduction (Eq. 13.6) for **11-32** of type V (with the composition $ABp\bar{p}$) is the same as the subduction (Eq. 13.12) for **11-31** of type IV (with the composition $A^2p\bar{p}$).

- Compare **11-32** with **11-31** from the viewpoint of chirality fittingness.
- Confirm the validity of Young's tableaux collected in the chirality-column of Fig. 13.3.
- Discuss that the assignability of *RS*-stereodescriptors of the CIP system is not based on chirality.

Under the *RS*-permutation group $T_{\bar{\sigma}}$, the following subduction is obtained:

$$T_{\bar{\sigma}}(/C_{3\bar{\sigma}}) \downarrow C_{\bar{\sigma}} = C_{\bar{\sigma}}(/C_1) + 2C_{\bar{\sigma}}(/C_{\bar{\sigma}}). \quad (13.13)$$

Hence, a pair of proligands *A*'s constructs a two-membered *RS*-hemitropic $C_{\bar{\sigma}}(/C_1)$ -orbit, while each of chiral proligands *p* and \bar{p} constructs a one-membered *RS*-hemitropic $C_{\bar{\sigma}}(/C_{\bar{\sigma}})$ -orbit under the action of the *RS*-stereoisomeric group $T_{d\bar{\sigma}\hat{r}}$. This behavior is illustrated by Young's tableau shown in the intersection of the upper type-IV row and the *RS*-stereogenicity column of Fig. 13.3.

The presence of a two-membered $C_{\bar{\sigma}}(/C_1)$ -orbit indicates the equivalence between two *A*'s as illustrated by the top row of Young's tableau, so that **11-31** of type-IV is not characterized by *RS*-stereodescriptors.



Exercise 13.5.

- Examine the inner structure of **11-30** of type IV (the composition A^2BX) according to the lower Type-IV row of Fig. 13.3.
- Compare **11-30** of type IV with **11-3** of type I (the composition $ABXY$).

13.4 Assignment of Stereochemical Nomenclature

From a viewpoint of Fujita's stereoisogram approach, the CIP system for assigning *RS*-stereodescriptors [2,18] is concerned with the *RS*-stereogenic aspect of absolute configura-

tion, not with the chiral aspect of absolute configuration. In other words, the CIP priority system characterizes a pair of *RS*-diastereomers, but not a pair of enantiomers.

13.4.1 Single Criterion for Giving *RS*-Stereodescriptors

As illustrated by the gray-colored Young tableaux in Fig. 13.3, the four proligands in a tetrahedral promolecule of type I, III, or V are inequivalent to one another under the *RS*-permutation group T_{σ}^2 . As a result, such a promolecule of type I, III, or V is *RS*-stereogenic, so that there appears a pair of *RS*-diastereomers, which is characterized by a pair of *R/S*-stereodescriptors:

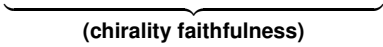
Rule 13.3. (*R/S*-Stereodescriptors Assigned by *RS*-Stereogenicity) [17]. A stereoisogram of type I, III, or V is characterized to be *RS*-stereogenic, so that the corresponding promolecules are called *RS-stereogenic promolecules*. Among them, a pair of *RS*-diastereomers is differentiated by a pair of *R/S*-stereodescriptors of the CIP system. In other words, the *R/S*-stereodescriptors are concerned with the *RS*-stereogenic aspect of absolute configuration, not with the chiral aspect of absolute configuration.

As illustrated by Young's tableaux in the chirality column of Fig. 13.3, promolecules of type I $[-, -, a]$ and III $[-, -, -]$ are chiral under the point group T_d (cf. Fig. 11.3 on page 317 and Fig. 11.5 on page 319), while promolecules of type V $[a, -, -]$ are achiral (Fig. 11.7 on page 321). Hence, the chirality and achirality of such promolecules have nothing to do with the assignment of *R/S*-stereodescriptors of the CIP system. By adopting a single criterion based on the *RS*-stereogenicity, the assignment of *R/S*-stereodescriptors of the CIP system is concluded to decide a pairwise *RS*-diastereomeric relationship, not a pairwise enantiomeric relationship, as surrounded by a solid-line frame in Table 13.1 [19]. The inequivalence between four proligands in a type-I, III, or V promolecule is clearly demonstrated by each Young's tableau shadowed in the *RS*-stereogenicity column of Fig. 13.3.

On the other hand, promolecules of type II $[-, a, -]$ or IV $[a, a, a]$ are characterized to be *RS*-astereogenic, as illustrated by Young's tableaux in the *RS*-stereogenicity column of Fig. 13.3. They are not targets of *R/S*-stereodescriptors of the CIP system. Note that the promolecule **11-14** of type II (page 316) is not specified by *R/S*-stereodescriptors of the CIP system, even though all of its proligands A, B, p, and p are inequivalent to one another as shown in Young's tableau at the chirality column. This fact demonstrates that the chiral aspect of absolute configuration is not concerned with the assignability of *R/S*-stereodescriptors.

Table 13.1. Single Criterion for Giving *RS*-Stereodescriptors of the CIP system in Fujita's Stereoisogram Approach [19]

	type index	chirality	<i>RS</i> -stereogenicity
Type I	$[-, -, a]$	chiral (enantiomeric)	<i>RS</i> -stereogenic (<i>RS</i> -diastereomeric)
Type III	$[-, -, -]$	chiral (enantiomeric)	<i>RS</i> -stereogenic (<i>RS</i> -diastereomeric)
Type V	$[a, -, -]$	achiral (self-enantiomeric)	<i>RS</i> -stereogenic (<i>RS</i> -diastereomeric)



 (chirality faithfulness)

13.4.2 *RS*-Diastereomers: the CIP Priority System

Let us apply the procedure of the sequence rules of the CIP system [2,18,20] to a given promolecule with proligands.⁴ Then, the proligands in the promolecule can be arranged according to a *priority sequence*. Suppose that achiral or chiral proligands {a, b, c, d} are placed on the four positions of a tetrahedral promolecule, where such a priority sequence is represented as $a > b > c > d$ tentatively, where the symbol $>$ denotes 'has priority over'. We here adopt the following *RS-stereogenicity rule* expressed by Fujita [17] and abandon the 'chirality rule' expressed by Prelog and Helmchen [2].

i

Rule 13.4. (The *RS*-Stereogenicity Rule) [17]. Among proligands in an *RS*-stereogenic promolecule (a type-I, type-III, or type-V promolecule) to be considered, the proligand of lowest precedence is placed in the back side and the remaining proligands of higher precedence are placed on the front side of viewing. The path of the sequence of the higher proligands is examined whether it turns to right (clockwise) or left (anti-clockwise). According to this examination, the *RS*-stereogenic promolecule is assigned the *RS*-stereogenic label *R* (Rectus, right) or *S* (Sinister, left), or if chirality-unfaithful, *r* or *s*.

The assignment of *RS*-stereodescriptors according to the *RS*-stereogenicity rule is illustrated in Fig. 13.4, where a pair of numbered and *RS*-numbered skeletons shown in the middle row of Fig. 13.1 is adopted to accommodate a set of four proligands with a priority sequence $a > b > c > d$. It follows that **13-3** and **13-4** are *RS*-diastereomeric, but not enantiomeric. In other words, the interconversion between **13-3** and **13-4** is not a mirror-image

⁴ The practices for determining the order of precedence in the CIP system [2,4,18] are maintained to be unchanged in Fujita's stereoisogram approach, except that a digraph of a molecule is divided into digraphs of proligands according to the proligand-promolecule model. See [17].

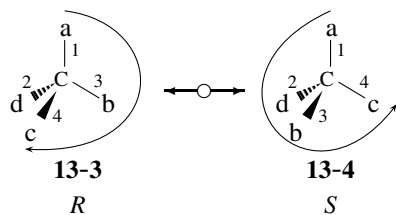


Fig. 13.4. *R/S*-Stereodescriptors assigned to a pair of *RS*-diastereomers according to the *RS*-stereogenicity rule, where the priority sequence is presumed to be $a > b > c > d$. The path of the sequence of the higher proligands is determined to be $a \rightarrow b \rightarrow c$, after the proligand of lowest precedence (d) is located in the background.

formation, so that it stems from the *RS*-permutation between the proligands b and c after these proligands are presumed to be detached.

Remark 13.3. (Comments on the abandoned ‘chirality rule’) [17]. The ‘chirality rule’ is expressed by Prelog and Helmchen [2]: “Among ligands of highest precedence the path of their sequence is followed from the preferred side of the model, that is, the side remote from the group of lowest precedence, and, depending on whether the path turns to right or left, the chirality unit will be assigned the chiral label *R* or *S*, or if pseudoasymmetric, *r* or *s*.” The ‘chirality rule’ is replaced by the *RS-stereogenicity rule* in Fujita’s stereoisogram approach. Thus, the term ‘chirality rule’ is replaced by the term *RS-stereogenicity rule*; the term ‘chirality unit’ is replaced by the term *RS-stereogenic promolecule*; the term ‘chiral label’ is replaced by the term *RS-stereogenic label*; as well as the expression ‘if pseudoasymmetric’ is replaced by the expression *if chirality-unfaithful*. The concept of *chirality faithfulness* will be discussed later.

The scheme shown in Fig. 13.4 is integrated to give a stereoisogram of type III (Fig. 13.5), where **13-3** and **13-4** are placed in the top horizontal direction. The mirror-image promolecules with proligands \bar{a} , \bar{b} , \bar{c} , and \bar{d} , i.e., **13-5** and **13-6**, are generated as depicted in the bottom horizontal direction. They are *RS*-diastereomeric to each other. If the priority sequence $a > b > c > d$ produces another priority sequence $\bar{a} > \bar{b} > \bar{c} > \bar{d}$,⁵ the resulting pair of **13-5** and **13-6** is specified by an alternative pair of labels ‘*S*’ and ‘*R*’. It should be emphasized that a priority sequence $a > b > c > d$ is conceptually different from a priority sequence $\bar{a} > \bar{b} > \bar{c} > \bar{d}$, even if the former provides the latter in most cases.⁶

⁵ This is not always true, as found in chirality-unfaithful cases.

⁶ These cases are referred to by the term *chirality-faithful* in Fujita’s stereoisogram approach.

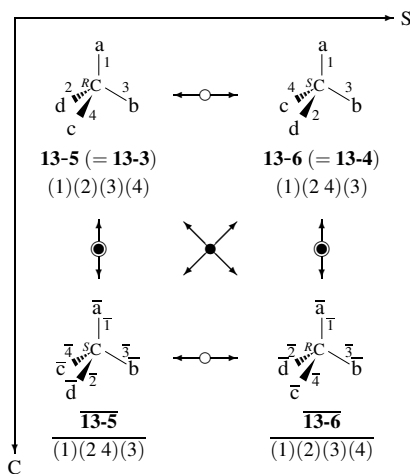


Fig. 13.5. Assignment of *R/S*-stereodescriptors to each pair of *RS*-diastereomers in terms of a priority sequence $a > b > c > d$ (for **13-5/13-6**) or another priority sequence $\bar{a} > \bar{b} > \bar{c} > \bar{d}$ (for **13-5/13-6**).

The stereoisogram shown in Fig. 13.5 clearly demonstrates that a pair of enantiomers **13-5/13-5** (or **13-6/13-6**) is not examined in the above-mentioned process of assigning *R/S*-stereodescriptors (Rule 13.4), so long as the different priority sequences $a > b > c > d$ and $\bar{a} > \bar{b} > \bar{c} > \bar{d}$ are applied. In other words, *R/S*-stereodescriptors specify the *RS*-stereogenic aspect, but not the chiral aspect of absolute configuration.

13.4.3 *R/S*-Stereodescriptors and Stereoisograms

R/S-Stereodescriptors Assigned to *RS*-Stereogenic Promolecules of Type I

The promolecule **11-3** with the composition ABXY is characterized by the stereoisogram of type I (Fig. 11.3 on page 317). The *RS*-stereogenicity rule (Rule 13.4) is applied to the promolecule **11-3** by adopting the priority sequence $A > B > X > Y$. Thereby, **11-3** is determined to have *R*. The *RS*-stereogenic label '*S*' is assigned to its *RS*-diastereomer **11-33** (Fig. 11.3).

Because achiral proligands A, B, X, Y satisfy $\bar{A} = A$, $\bar{B} = B$, $\bar{X} = X$, and $\bar{Y} = Y$ under reflections, the priority sequence $A > B > X > Y$ applied originally to **11-3** can be applied to its enantiomer $\bar{\mathbf{11-3}}$. As indicated by diagonal equality symbols in Fig. 11.3, the pair of *RS*-diastereomers **11-3/11-33** coincides with a pair of enantiomers **11-3/11-3** in the case of a stereoisogram of type I. This means that the assignment based on the *RS*-diastereomeric relationship for a type I case can be safely regarded as the assignment to the enantiomeric relationship. This is an example of chirality-faithful case, which will be later discussed in general.

Exercise 13.6. By referring to Fig. 9.11(a) on page 259, discuss the term ‘asymmetric’ vs. the term *RS-stereogenic* from the viewpoint of Fujita’s stereoisogram approach. Note that the term ‘asymmetric’ has nothing to do with the chiral aspect of absolute configuration (cf. Fig. 13.3).

***R/S*-Stereodescriptors Assigned to *RS*-Stereogenic Promolecules of Type III**

The promolecule **11-20** with the composition ABXp gives a stereoisogram shown in Fig. 11.5 (page 319). A pair of *RS*-diastereomers **11-20** and **11-36** is characterized by a pair of *R/S*-stereodescriptors, ‘*R*’ and ‘*S*’, by using the priority sequence $A > p > B > X$, which is obtained by placing $A = \text{OH}$, $p = \text{CH}_2\text{CH}(\text{ClF})$, $B = \text{CH}_2\text{CH}_3$, and $X = \text{H}$ for 1-chloro-1-fluoropentan-3-ol. On the other hand, another pair of *RS*-diastereomers, **11-20** and **11-36** is characterized by a pair of opposite *R/S*-stereodescriptors, ‘*S*’ and ‘*R*’, by using the priority sequence $A > \bar{p} > B > X$.

This case is categorized into a chirality-faithful type-III case according to Fujita’s stereoisogram approach. A pair of enantiomers **11-20**/**11-20** is permitted to be designated by a pair of *R/S*-stereodescriptors, ‘*R*’ and ‘*S*’, although the priority sequences $A > p > B > X$ presumed for **11-20** is different from the priority sequence $A > \bar{p} > B > X$ presumed for **11-20**. Among the type-III promolecules listed in Fig. 11.2 (page 316), the promolecules which are not surrounded by a gray box are designated by *R/S*-stereodescriptors in a similar way.

***R/S*-Stereodescriptors Assigned to *RS*-Stereogenic Promolecules of Type V**

Let us examine a pair of *RS*-diastereomers **11-32/11-40**, which is derived from a pair of achiral 2,3,4-trihydroxyglutaric acids **11-38/11-39**, as shown in Fig. 11.7 (page 321). Because the priority sequence $A > p > \bar{p} > B$ is obtained for the achiral 2,3,4-trihydroxyglutaric acids, the pair of *RS*-diastereomers **11-32/11-40** are characterized by a pair of labels ‘*r*’ and ‘*s*’. The lowercase labels are used to emphasize that the case of type V is chirality-unfaithful, as discussed in the next subsection.

Exercise 13.7. By referring to Fig. 9.11(b) on page 259, discuss the term ‘pseudoasymmetric’ vs. the term *RS-stereogenic* from the viewpoint of Fujita’s stereoisogram approach. Confirm that the term ‘pseudoasymmetric’ mixes up the chirality aspect and the *RS*-stereogenic aspect of absolute configuration (cf. Fig. 13.3).

13.4.4 Chirality Faithfulness

Chirality Faithfulness vs. Reflection Invariance

The lowercase labels *r* and *s* are used for specifying ‘pseudoasymmetric units’ by the coinage of the term ‘reflection-invariant’ in the CIP system [2]. The determination of the lowercase labels based on the term ‘reflection-invariant’ emphasizes enantiomeric relationships and implicitly nullifies the participation of *RS*-diastereomeric relationships.

In contrast, Fujita’s stereoisogram approach has adopted the concept of *chirality faithfulness* [12,21,22] to rationalize the assignment of lowercase labels. In Fujita’s stereoisogram approach, a pair of *R/S*-stereodescriptors assigned originally to a pair of *RS*-diastereomers is interpreted to be assigned to a pair of enantiomers. And then, the interpretation is examined to be faithful or unfaithful.

Chirality-Faithful and Chirality-Unfaithful Cases

The term *chirality-faithful* is defined to comprehend type-I and most type-III stereoisograms [22]:

Definition 13.1. (Chirality-faithful absolute configurations) If the stereodescriptor of a reference promolecule, *R* (or *S*), is identical with that of its holantimer, *R* (or *S*), this case is referred to as being *chirality-faithful* and characterized by uppercase labels.

If chirality-faithful, a pair of *R/S*-stereodescriptors originally based on the *RS*-diastereomeric relationship is allowed to be interpreted to be given to the enantiomeric relationship. This allowed interpretation is also referred to as being chirality-faithful, so that the *R/S*-stereodescriptors are designated in uppercase labels.

On the other hand, the term *chirality-unfaithful* is defined to comprehend type-V and some type-III stereoisograms [22]:

Definition 13.2. (Chirality-unfaithful absolute configurations) If the stereodescriptor of a reference promolecule, *R* (or *S*), is opposite to that of its holantimer, *S* (or *R*), this case is referred to as being *chirality-unfaithful* and characterized by lowercase labels.

If chirality-unfaithful, a pair of *R/S*-stereodescriptors originally based on the proper *RS*-diastereomeric relationship is not allowed to be interpreted to be given to the enantiomeric relationship. This forbidden interpretation is also referred to as being chirality-unfaithful, so that the *R/S*-stereodescriptors are designated in lowercase labels.



Remark 13.4. The term *chirality-unfaithful* is capable of deriving the conventional term ‘reflection-invariant’, while the term ‘reflection-invariant’ is incapable of deriving the present term *chirality-unfaithful*. This is because the conventional term ‘reflection-invariant’ lacks the concepts of *RS*-diastereomeric relationships and *RS*-stereogenicity.

13.4.5 Stereochemical Notations for Other Skeletons

Allene Derivatives

Stereochemical notation for allene derivatives has been discussed on the basis of three aspects of absolute configuration [23]. To judge whether or not the *R/S*-stereodescriptors (assigned originally on the basis of the *RS*-stereogenic aspect of an absolute configuration) are permitted to be applied to the chiral aspect, the concept of chirality faithfulness [21] is used after redefined.

Oxirane Derivatives

The scope and limitations of *R/S*-stereodescriptors for oxirane derivatives have been discussed on the basis of three aspects of absolute configuration [24]. Thereby, *R/S*-stereodescriptors of the CIP system are found to specify local symmetries at each ring positions of an oxirane derivative. The specification of global symmetry of oxirane derivatives requires other types of descriptors, which have been proposed in [22], i.e., *R_a/S_a*-descriptors and *Z/E*-descriptors.

Trigonal Bipyramidal Compounds

Stereoisograms of trigonal bipyramidal compounds have been categorized into five types (Types I–V). Among them, stereoisograms of Types I, III, and V are shown to be capable of giving *C/A*-descriptors because of their *RS*-stereogenicity (or *RS*-diastereomeric relationships) [25]. A revised interpretation of Berry's pseudorotation has been discussed [26].

Prismane Derivatives

After combinatorial enumeration of prismane derivatives, the stereoisograms of prismane derivatives have been discussed [27]. A *C/A*-convention for characterizing absolute configurations has been proposed on the basis of Fujita's stereoisogram approach [28]. Chirality, *RS*-stereogenicity, and sclerality of prismane derivatives have been discussed by putting emphasis on the independence between chirality and *RS*-stereogenicity, on extended features of pseudoasymmetry, and on the assignability of *C/A*-descriptors [28].

Octahedral Complexes

The relationship between *RS*-stereoisomeric groups and stereoisomeric groups has been discussed by using octahedral complexes as examples, where the difference between *RS*-stereogenicity and stereogenicity has been determined decisively after group-theoretical consideration [29,30]. Thereby, stereogenicity has nothing to do with the capability of giving *C/A*-descriptors. The assignability of *C/A*-descriptors has been ascribed to *RS*-stereogenicity (or *RS*-diastereomeric relationships), but not to chirality [30]. Thereby,

Fujita's stereoisogram approach, which has originally been developed to rationalize organic stereochemistry [6,13,31], is clarified to be effective to inorganic stereochemistry [29,30,32].

References

- [1] IUPAC Organic Chemistry Division, *Pure Appl. Chem.*, **68**, 2193–2222 (1996).
- [2] V. Prelog and G. Helmchen, *Angew. Chem. Int. Ed. Eng.*, **21**, 567–583 (1982).
- [3] G. Helmchen, A. General Aspects. 1. Nomenclature and Vocabulary of Organic Stereochemistry, in “Stereoselective Synthesis. Methods of Organic Chemistry (Houben-Weyl). Workbench Edition E21”, 4 ed., ed. by G. Helmchen, R. W. Hoffmann, J. Mulzer, and E. Schaumann, Georg Thieme, Stuttgart New York (1996) Vol. 1 pp 1–74.
- [4] IUPAC Chemical Nomenclature and Structure Representation Division, *Provisional Recommendations. Nomenclature of Organic Chemistry* (2004), http://old.iupac.org/reports/provisional/abstract04/favre_310305.html.
cf. H. A. Favre, W. H. Powell, “Nomenclature of Organic Chemistry. IUPAC Recommendations and Preferred Names 2013”, The Royal Society of Chemistry, Cambridge (2013).
- [5] E. L. Eliel, S. H. Wilen, and M. P. Doyle, “Basic Organic Stereochemistry”, Wiley-Interscience, New York (2001).
- [6] S. Fujita, *J. Org. Chem.*, **69**, 3158–3165 (2004).
- [7] S. Fujita, *Tetrahedron*, **60**, 11629–11638 (2004).
- [8] S. Fujita, *J. Math. Chem.*, **35**, 265–287 (2004).
- [9] S. Fujita, *MATCH Commun. Math. Comput. Chem.*, **52**, 3–18 (2004).
- [10] S. Fujita, *J. Chem. Inf. Comput. Sci.*, **44**, 1719–1726 (2004).
- [11] S. Fujita, *MATCH Commun. Math. Comput. Chem.*, **53**, 147–159 (2005).
- [12] S. Fujita, *J. Math. Chem.*, **52**, 1514–1534 (2014).
- [13] S. Fujita, *Tetrahedron*, **65**, 1581–1592 (2009).
- [14] S. Fujita, “Symmetry and Combinatorial Enumeration in Chemistry”, Springer-Verlag, Berlin-Heidelberg (1991).
- [15] S. Fujita, *MATCH Commun. Math. Comput. Chem.*, **61**, 71–115 (2009).
- [16] S. Fujita, *J. Math. Chem.*, **52**, 508–542 (2014).
- [17] S. Fujita, *Tetrahedron: Asymmetry*, **25**, 1169–1189 (2014).
- [18] R. S. Cahn, C. K. Ingold, and V. Prelog, *Angew. Chem. Int. Ed. Eng.*, **5**, 385–415 (1966).

- [19] S. Fujita, Prochirality and Pro-*RS*-Stereogenicity. Stereoisogram Approach Free from the Conventional “Prochirality” and “Prostereogenicity”, in “Carbon Bonding and Structures. Advances in Physics and Chemistry”, ed. by M. V. Putz, Springer-Verlag, Dordrecht Heidelberg London (2011) Vol. 5 of Carbon Materials: Chemistry and Physics Chapter 10, pp 227–271.
- [20] R. S. Cahn, C. K. Ingold, and V. Prelog, *Experientia*, **XII**, 81–124 (1956).
- [21] S. Fujita, *J. Comput. Aided Chem.*, **10**, 16–29 (2009).
- [22] S. Fujita, *J. Math. Chem.*, **53**, 305–352 (2015).
- [23] S. Fujita, *J. Math. Chem.*, **52**, 1751–1793 (2014).
- [24] S. Fujita, *J. Math. Chem.*, **53**, 353–373 (2015).
- [25] S. Fujita, *J. Math. Chem.*, **50**, 1791–1814 (2012).
- [26] S. Fujita, *J. Math. Chem.*, **50**, 1815–1860 (2012).
- [27] S. Fujita, *J. Math. Chem.*, **50**, 2202–2222 (2012).
- [28] S. Fujita, *J. Math. Chem.*, **50**, 2168–2201 (2012).
- [29] S. Fujita, *MATCH Commun. Math. Comput. Chem.*, **71**, 511–536 (2014).
- [30] S. Fujita, *MATCH Commun. Math. Comput. Chem.*, **71**, 537–574 (2014).
- [31] S. Fujita, *Tetrahedron*, **62**, 691–705 (2006).
- [32] S. Fujita, *MATCH Commun. Math. Comput. Chem.*, **71**, 575–608 (2014).

14 Pro-*RS*-Stereogenicity Based on Orbits¹

14.1 Prochirality vs. Pro-*RS*-Stereogenicity

A pair of *pro-R/pro-S*-descriptors is clarified to be assigned to a pair of *RS*-diastereotopic proligands, which is characterized under pro-*RS*-stereogenicity. In general, the pro-*RS*-stereogenicity is ascribed to the presence of an *RS*-enantiotropic orbit of proligands, which are divided into *RS*-diastereotopic halves. The term ‘prochirality’ for assigning a pair of *pro-R/pro-S*-descriptors in modern stereochemistry should be abandoned and replaced by the term *pro-*RS*-stereogenicity*. The term *prochirality* should be used in a purely geometric meaning (cf. Section 4.2).

14.1.1 Prochirality as a Geometric Concept

Modern stereochemistry uses the term ‘prochirality’ in different, sometimes contradictory ways, as pointed out in IUPAC Recommendations 1996 [1]. In contrast, the present book is based on the standpoint that the term *prochirality* should be used as a geometric concept for discussing point-group symmetries of molecular entities, as discussed detailedly in Section 4.2. The prochirality of a promolecule (as an abstract molecular entity) is ascribed to the presence of at least one *enantiospheric* orbit of proligands. Such an enantiospheric orbit of proligands is divided into two halves, which are interconvertible by a reflection. The mode of packing two halves with proligands is controlled by *chirality fittingness* (cf. Fig. 4.2(b) on page 90). The two halves are separated energetically under an appropriate chiral condition, so that the attack of a chiral reagent to either one half produces the corresponding chiral compound selectively. The two halves are *enantiotopic*, if we obey the terminology of modern stereochemistry. The attributive term *enantiospheric* for characterizing an orbit of proligands corresponds to the relational term *enantiotopic* for characterizing the relationship between two positions (cf. Remark 4.1 on page 106).

It should be emphasized that the concept of *prochirality* as a geometric concept should not be used to assign *pro-R/pro-S*-descriptors, just as the concept of *chirality* as a geometric concept should not be used to assign *R/S*-stereodescriptors (cf. Chapter 13).

¹ This chapter is based on S. Fujita, “Stereogenicity/Astereogenicity as Global/Local Permutation-Group Symmetry and Relevant Concepts for Restructuring Stereochemistry”, *J. Math. Chem.*, **33**, 113–143 (2003); S. Fujita, “Complete Settlement of Long-Standing Confusion on the Term ‘Prochirality’ in Stereochemistry. Proposal of Pro-*RS*-Stereogenicity and Integrated Treatment with Prochirality”, *Tetrahedron*, **62**, 691–705 (2006); and S. Fujita, “Stereoisograms for Reorganizing the Theoretical Foundations of Stereochemistry and Stereoisomerism: III. Rational Avoidance of Misleading Standpoints for *Pro-R/Pro-S*-Descriptors”, *Tetrahedron: Asymmetry*, **25**, 1190–1204 (2014).

14.1.2 Pro-*RS*-Stereogenicity as a Stereoisomeric Concept

Just as the term *RS-stereogenicity* has been coined to rationalize the assignment of *R/S*-stereodescriptors in Fujita's stereoisogram approach (cf. Chapter 13), the term *pro-R/S-stereogenicity* should be coined to rationalize the assignment of *pro-R/pro-S*-descriptors. Thereby, the term 'prochirality' used in the misleading rationalization of *pro-R/pro-S*-descriptors by Hanson [2] (cf. Section 4.2) is abandoned thoroughly and should be replaced by the term *pro-R/S-stereogenicity*.

To rationalize the assignment of *pro-R/pro-S*-descriptors, the term *pro-R/S-stereogenicity* should be used as a stereoisomeric concept for discussing *RS*-permutation-group symmetries of molecular entities (cf. Chapter 9). This means that equivalence classes (orbits) under the action of an *RS*-permutation group are examined in a parallel way to equivalence classes (orbits) under the action of a point group.

14.1.3 Prochirality and Pro-*RS*-Stereogenicity for Tetrahedral Derivatives

Necessary data for surveying the difference between prochirality and pro-*RS*-stereogenicity are added to the list shown in Fig. 11.2 (page 316). Thereby, we are able to obtain Fig. 14.1 [3], where a frame box is drawn to show pro-*RS*-stereogenicity, a dashed frame box is drawn to show prochirality [4], and a gray box is drawn to show a chirality-unfaithful case [5].

In the remaining parts of this chapter, we focus our attention on pro-*RS*-stereogenicity, which aims at rational avoidance of misleading standpoints for *pro-R/pro-S*-descriptors. The discussions to be developed for pro-*RS*-stereogenicity are parallel to those of prochirality developed in Section 4.2, where the importance of orbits (equivalence classes) will be emphasized.

14.2 Orbits under *RS*-Permutation Groups

14.2.1 *RS*-Tropicity

An *RS*-permutation group $\mathbf{G}_{\tilde{\sigma}}$ as a subgroup of an *RS*-stereoisomeric group $\hat{\mathbf{G}}$ is represented by the coset decomposition of Eq. 10.16 (Def. 10.1 on page 278). Hence, each subgroup of the *RS*-permutation group $\mathbf{G}_{\tilde{\sigma}}$ is categorized either one of two types, i.e., an *RS*-stereogenic group and an *RS*-astereogenic group, where an *RS*-stereogenic group consists of elements selected from $\mathbf{G}^{(C)}$, while an *RS*-astereogenic group consists of elements selected from $\mathbf{G}^{(C)}$ and $\mathbf{G}^{(C)}\tilde{\sigma}$.

When the *RS*-permutation group $\mathbf{G}_{\tilde{\sigma}}$ acts on a set of equivalent proligands, this set is regarded as an equivalence class (orbit) governed by a coset representation $\mathbf{G}_{\tilde{\sigma}}(/ \mathbf{G}_{\tilde{\sigma}(i)})$, where $\mathbf{G}_{\tilde{\sigma}}$ is a global symmetry, while $\mathbf{G}_{\tilde{\sigma}(i)} (\subset \mathbf{G}_{\tilde{\sigma}})$ is a local symmetry. The definition

	<i>RS</i> -astereogenic	<i>RS</i> -stereogenic
chiral		<p style="text-align: center;">Type I</p> <div style="display: flex; justify-content: space-around;"> <div style="text-align: center;"> <p>11-3 ($[\theta]_{10}$) [C₇, C₁, C₁; I]</p> </div> <div style="text-align: center;"> <p>11-4 ($[\theta]_{28}$) [C_σ, C₁, C₁; I]</p> </div> </div>
		<p style="text-align: center;">Type II</p> <div style="display: grid; grid-template-columns: repeat(3, 1fr); gap: 10px;"> <div style="text-align: center;"> <p>11-5 ($[\theta]_{20}$) [T_σ, T, T_σ; II]</p> </div> <div style="text-align: center;"> <p>11-6 ($[\theta]_3$) [C_{3σ}, C₃, C_{3σ}; II]</p> </div> <div style="text-align: center;"> <p>11-7 ($[\theta]_{15}$) [C_{3σ}, C₃, C_{3σ}; II]</p> </div> <div style="text-align: center;"> <p>11-8 ($[\theta]_{22}$) [C_{3σ}, C₃, C_{3σ}; II]</p> </div> <div style="text-align: center;"> <p>11-9 ($[\theta]_{21}$) [C_{3σ}, C₃, C_{3σ}; II]</p> </div> <div style="text-align: center;"> <p>11-10 ($[\theta]_5$) [C_{2σ}, C₂, C_{2σ}; II]</p> </div> <div style="text-align: center;"> <p>11-11 ($[\theta]_{25}$) [C_{2σ}, C₂, C_{2σ}; II]</p> </div> <div style="text-align: center;"> <p>11-12 ($[\theta]_7$) [C_σ, C₁, C_σ; II]</p> </div> <div style="text-align: center;"> <p>11-13 ($[\theta]_9$) [C_σ, C₁, C_σ; II]</p> </div> <div style="text-align: center;"> <p>11-14 ($[\theta]_{12}$) [C_σ, C₁, C_σ; II]</p> </div> <div style="text-align: center;"> <p>11-15 ($[\theta]_{16}$) [C_σ, C₁, C_σ; II]</p> </div> <div style="text-align: center;"> <p>11-16 ($[\theta]_{17}$) [C_σ, C₁, C_σ; II]</p> </div> <div style="text-align: center;"> <p>11-17 ($[\theta]_{24}$) [C_σ, C₁, C_σ; II]</p> </div> <div style="text-align: center;"> <p>11-18 ($[\theta]_{26}$) [C_σ, C₁, C_σ; II]</p> </div> <div style="text-align: center;"> <p>11-19 ($[\theta]_{27}$) [C_σ, C₁, C_σ; II]</p> </div> </div>
		<p style="text-align: center;">Type III</p> <div style="display: grid; grid-template-columns: repeat(2, 1fr); gap: 10px;"> <div style="text-align: center;"> <p>11-20 ($[\theta]_{11}$) [C₁, C₁, C₁; III]</p> </div> <div style="text-align: center;"> <p>11-21 ($[\theta]_{14}$) [C₁, C₁, C₁; III]</p> </div> <div style="text-align: center;"> <p>11-22 ($[\theta]_{18}$) [C₁, C₁, C₁; III]</p> </div> <div style="text-align: center;"> <p>11-23 ($[\theta]_{19}$) [C₁, C₁, C₁; III]</p> </div> <div style="text-align: center;"> <p>11-24 ($[\theta]_{29}$) [C₁, C₁, C₁; III]</p> </div> <div style="text-align: center;"> <p>11-25 ($[\theta]_{30}$) [C₁, C₁, C₁; III]</p> </div> </div>
achiral	<p style="text-align: center;">Type IV</p> <div style="display: grid; grid-template-columns: repeat(3, 1fr); gap: 10px;"> <div style="text-align: center;"> <p>11-26 ($[\theta]_{11}$) [T_d$\bar{\sigma}$$\bar{r}$, T_d, T_σ; IV]</p> </div> <div style="text-align: center;"> <p>11-27 ($[\theta]_{12}$) [C_{3$\bar{\sigma}$$\bar{r}$}, C_{3$\bar{\sigma}$}, C_{3$\bar{\sigma}$}; IV]</p> </div> <div style="text-align: center;"> <p>11-28 ($[\theta]_4$) [C_{2$\bar{\sigma}$$\bar{r}$}, C_{2$\bar{\sigma}$}, C_{2$\bar{\sigma}$}; IV]</p> </div> <div style="text-align: center;"> <p>11-29 ($[\theta]_{23}$) [S_{4$\bar{\sigma}$$\bar{r}$}, S₄, C_{2$\bar{\sigma}$}; IV]</p> </div> <div style="text-align: center;"> <p>11-30 ($[\theta]_6$) [C_{3$\bar{\sigma}$$\bar{r}$}, C₃, C_σ; IV]</p> </div> <div style="text-align: center;"> <p>11-31 ($[\theta]_8$) [C_{3$\bar{\sigma}$$\bar{r}$}, C₃, C_σ; IV]</p> </div> </div>	<p style="text-align: center;">Type V</p> <div style="text-align: center;"> <p>11-32 ($[\theta]_{13}$) [C₃, C₃, C₁; V]</p> </div>

Fig. 14.1. Reference promolecules of quadruplets of *RS*-stereoisomers (Types I to V) for tetrahedral promolecules, which are attached by the data of prochirality and pro-*RS*-stereogenicity [3]. As for the symbols, see the caption of Fig. 11.2. An arbitrary promolecule is depicted as a representative of each quadruplet of *RS*-stereoisomers. A gray box is drawn to show a chirality-unfaithful case [5]. A frame box is drawn to show pro-*RS*-stereogenicity, while a dashed frame box is drawn to show prochirality [4].

of *RS-tropicitities* for *RS*-permutation groups is given in a parallel way to the definition of *sphericities* for point groups (Def. 4.1 on page 89).

The term *RS-tropicity* has been coined by Fujita to refer to three cases generated by the coset representation $G_{\bar{\sigma}}(/G_{\bar{\sigma}(i)})$ [6]:²

Definition 14.1 (*RS-Tropicitities for Characterizing Coset Representations and Orbits*).

- **(*RS-Homotropicity*)** If both the global *RS*-permutation-group symmetry $G_{\bar{\sigma}}$ and the local *RS*-permutation-group symmetry $G_{\bar{\sigma}(i)}$ are *RS*-astereogenic, the coset representation $G_{\bar{\sigma}}(/G_{\bar{\sigma}(i)})$ is defined as being *RS-homotropic*. The corresponding orbit of size $|G_{\bar{\sigma}}|/|G_{\bar{\sigma}(i)}|$ is referred to as an *RS-homotropic orbit*.
- **(*RS-Enantiotropicity*)** If the global *RS*-permutation-group symmetry $G_{\bar{\sigma}}$ is *RS*-astereogenic, but the local *RS*-permutation-group symmetry $G_{\bar{\sigma}(i)}$ is *RS*-stereogenic, the coset representation $G_{\bar{\sigma}}(/G_{\bar{\sigma}(i)})$ is defined as being *RS-enantiotropic*. The corresponding orbit of size $|G_{\bar{\sigma}}|/|G_{\bar{\sigma}(i)}|$ is referred to as an *RS-enantiotropic orbit*, which is divided into two halves of size $|G_{\bar{\sigma}}|/2|G_{\bar{\sigma}(i)}|$ under the maximum *RS*-stereogenic subgroup of $G_{\bar{\sigma}}$.
- **(*RS-Hemitropicity*)** If both the global *RS*-permutation-group symmetry $G_{\bar{\sigma}}$ and the local *RS*-permutation-group symmetry $G_{\bar{\sigma}(i)}$ are *RS*-stereogenic, the coset representation $G_{\bar{\sigma}}(/G_{\bar{\sigma}(i)})$ is defined as being *RS-hemitropic*. The corresponding orbit of size $|G_{\bar{\sigma}}|/|G_{\bar{\sigma}(i)}|$ is referred to as an *RS-hemitropic orbit*.

For example, the subgroups contained in the SSG of the *RS*-permutation group $T_{\bar{\sigma}}$ (Eq. 9.30 on page 252) are categorized into the following types:

$$\text{RS-stereogenic group } \{C_1, C_2, C_3, D_2, T\} \quad \text{and} \quad (14.1)$$

$$\text{RS-astereogenic group } \{C_{\bar{\sigma}}, S_4, C_{2\bar{\sigma}}, C_{3\bar{\sigma}}, D_{2\bar{\sigma}}, T_{\bar{\sigma}}\}. \quad (14.2)$$

The four positions of a tetrahedral skeleton construct an orbit governed by the coset representation $T_{\bar{\sigma}}(/C_{3\bar{\sigma}})$, the degree of which is calculated to be $|T_{\bar{\sigma}}|/|C_{3\bar{\sigma}}| = 24/6 = 4$. Because both $T_{\bar{\sigma}}$ and $C_{3\bar{\sigma}}$ are *RS*-astereogenic, the coset representation $T_{\bar{\sigma}}(/C_{3\bar{\sigma}})$ is determined to be *RS-homotropic*.




Exercise 14.1. Discuss conceptual parallelism between sphericities (Def. 4.1 on page 89) and *RS-tropicitities* (Def. 14.1).

14.2.2 Pro-*RS*-Stereogenicity as a Stereoisomeric Concept

A recent article by Fujita [3] has discussed rational avoidance of misleading standpoints of the conventional term ‘prochirality’ for supporting *pro-R/pro-S*-descriptors. Instead, the term *pro-*RS*-stereogenicity* [6] is defined by starting from the term *RS-enantiotropicity* (Def. 14.1):

² The original terms with suffix *tropicity* [7] are restricted to the terms with *RS-tropicity* [6] in order to avoid confusion due to the similar term *tropicity*.


Definition 14.2 (*Pro-*RS*-Stereogenicity*). A *pro-*RS*-stereogenic* molecule or promolecule is defined as an *RS*-astereogenic molecule or promolecule that has at least one *RS*-enantiotropic orbit (cf. Def. 14.1)

Exercise 14.2. Discuss conceptual parallelism between prochirality (Def. 4.2 on page 95) and *pro-*RS*-stereogenicity* (Def. 14.2). 

According to Def. 14.2, the following theorem is obvious:

Theorem 14.1 (*Single-Step Conversion*). A *pro-*RS*-stereogenic* (pro)molecule defined by Def. 14.2 can be converted into an *RS*-stereogenic (pro)molecule or its *RS*-diastereomeric counterpart by a single-step conversion (*RS*-permutation).

The expression “by a single-step conversion” in Theorem 14.1 is essential to develop further discussions.

Exercise 14.3. Discuss conceptual parallelism between Theorem 4.5 (page 95) and Theorem 14.1. 

Let us examine the tetrahedral promolecules surrounded by a solid-line frame in Fig. 14.1. Def. 14.2 indicates that *pro-*RS*-stereogenicity* appears among type-II promolecules (the type index: $[-, a, -]$) or among type IV-promolecules (the type index $[a, a, a]$).

As the first example, we take account of the type-II promolecule **11-12** surrounded by a solid frame in Fig. 14.1. This promolecule with the composition A^2Bp corresponds to D-(+)-glyceraldehyde **4-9** (page 94).

As shown in Section 4.2, the four positions of the type-II promolecule **11-12** are separated into four one-membered $C_1(/C_1)$ -orbits under the action of the point group T_d . The mode of separation has been illustrated by the diagram **4-8**, as shown in Fig. 4.4 (page 94). At the same time, the mode of separation is schematically represented by Young’s tableau shown in the rightmost part of Fig. 4.4.

Under the action of the *RS*-permutation group $T_{\bar{\sigma}}$, the four positions of the type-II promolecule **11-12** are separated in accord with the following subduction:

$$T_{d\bar{\sigma}\bar{l}}(/C_{3v\bar{\sigma}\bar{l}}) \downarrow C_{\bar{\sigma}} = C_{\bar{\sigma}}(/C_1) + 2C_{\bar{\sigma}}(/C_{\bar{\sigma}}), \quad (14.3)$$

which has once been noted as Eq. 13.8 (page 374). Hence, the mode of separation is illustrated by the diagram **14-1** or by the diagram **14-2** shown in Fig. 14.2. The two A’s in **14-1** (or the two H’s in **14-2**) construct a two-membered $C_{\bar{\sigma}}(/C_1)$ -orbit, which is *RS*-enantiotropic according to Def. 14.1, because the global symmetry $C_{\bar{\sigma}}$ is *RS*-astereogenic, while the local symmetry C_1 is *RS*-stereogenic. The proligand B (or p) belongs to a one-membered $C_{\bar{\sigma}}(/C_{\bar{\sigma}})$ -orbit, which exhibits *RS*-homotropicity according to Def. 14.1. The diagram **14-1** indicates that the type-II promolecule **11-12** (= **14-1**) is *pro-*RS*-stereogenic* according to Def. 14.2, because of the presence of the *RS*-enantiotropic $C_{\bar{\sigma}}(/C_1)$ -orbit. The

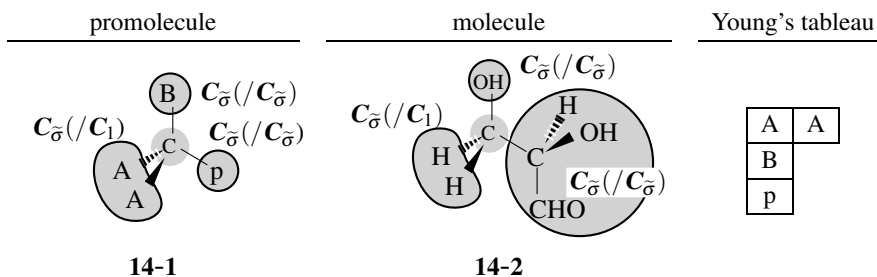


Fig. 14.2. Orbits in glyceraldehyde under the *RS*-permutation group $C_{\bar{\sigma}}$

mode of separation is schematically represented by Young's tableau shown in the rightmost part of Fig. 14.2.



Exercise 14.4. Compare Fig. 14.2 with Fig. 4.4 (page 94). Discuss the difference between the orbits under the point group and the orbits under the *RS*-permutation group.

In a similar way, each promolecule of $C_{\bar{\sigma}}$, which is surrounded by a solid-line frame in Fig. 14.1, exhibits pro-*RS*-stereogenicity because of the presence of an *RS*-enantiotropic $C_{\bar{\sigma}}(/C_1)$ -orbit.



Exercise 14.5. Discuss the pro-*RS*-stereogenicity of **11-14** (Fig. 14.1) by referring to the type-II row of Fig. 13.3 (page 372).

14.3 pro-*R*/pro-*S*-Descriptors

14.3.1 *RS*-Diastereotopic Relationships

Modern stereochemistry relies on relational terms rather than attributive terms. Just as the attributive term *enantiospheric* is related to the relational term *enantiotopic* under the point-group symmetry (Def. 4.3 on page 98), the relational term *RS-diastereotopic* is coined by Fujita, starting from the attributive term *RS-enantiotropic*. Because an *RS*-enantiotropic $G_{\bar{\sigma}}(/G_{\bar{\sigma}(i)})$ -orbit is divided into two halves as shown in Def. 14.1, the relationship between the two halves is characterized by the term *RS-diastereotopic* defined as follows [8]:

Definition 14.3 (*RS*-Diastereotopic Relationship). An *RS-diastereotopic* relationship is defined as a relationship between one half and the other half of an *RS*-enantiotropic orbit (Def. 14.1).

The two halves are differentiated to derive *RS*-stereogenic promolecules, so that they are specified by pro-*R*/pro-*S*-descriptors. For the sake of simplicity, each half is considered to consist of a single member, when pro-*R*/pro-*S*-descriptors are given.

Exercise 14.6. Discuss the parallelism between the term *enantiotopic* (Def. 4.3 on page 98) and the term *RS-diastereotopic* (Def. 14.3).

14.3.2 Single Criterion for Giving *pro-R/pro-S*-descriptors

In a parallel way to the assignment of *R/S*-stereodescriptors by a single criterion due to *RS*-stereogenicity (Rule 13.3 on page 377 and Table 13.1 on 378), the assignment of *pro-R/pro-S*-descriptors is conducted by a single criterion due to *pro-RS*-stereogenicity (Def. 14.2 and Theorem 14.1). Thus, a pair of *RS*-diastereotopic proligands (Def. 14.3) is determined to have a pair of *pro-R/pro-S*-descriptors of the *pro-R/pro-S* system [9].

Rule 14.1. (*pro-R/pro-S*-Descriptors Assigned by *Pro-RS*-Stereogenicity) [3]. A proligand selected from a pair of *RS*-diastereotopic proligands in a *pro-RS*-stereogenic promolecule (cf. Def. 14.2, Theorem 14.1, and Def. 14.3) is described as *pro-R* (or *pro-r*) if, when it is arbitrarily assigned CIP priority over the other proligand of the pair, then the configuration of the thus generated *RS*-stereogenic promolecule is assigned the *R*-stereodescriptor (or *r*-stereodescriptor). Along the same procedure, the other proligand is described as *pro-S* (or *pro-s*).

As shown in Table 14.1 [4], the concept of *pro-RS*-stereogenicity is concluded to be a single criterion for giving *pro-R/pro-S*-descriptors in accord with Fujita's stereoisogram approach. This is parallel to the concept of *RS*-stereogenicity as a single criterion for giving *R/S*-stereodescriptors (Table 13.1 on page 378).

Table 14.1. Single Criterion for Giving *pro-R/pro-S*-Descriptors in Fujita's Stereoisogram Approach [4].

stereoisogram change		prochirality	pro- <i>RS</i> -stereogenicity
(achiral → chiral & <i>RS</i>-astereogenic → <i>RS</i>-stereogenic)			
Type IV → I	$[a, a, a] \rightarrow [-, -, a]$ (Fig. 14.6)	prochiral (enantiotopic)	pro- <i>RS</i> -stereogenic (<i>RS</i> -diastereotopic)
(<i>RS</i>-astereogenic → <i>RS</i>-stereogenic)			
Type IV → V	$[a, a, a] \rightarrow [a, -, -]$ (Fig. 14.5(c))	–	pro- <i>RS</i> -stereogenic (<i>RS</i> -diastereotopic)
Type II → III	$[-, a, -] \rightarrow [-, -, -]$ (Fig. 14.3)	–	pro- <i>RS</i> -stereogenic (<i>RS</i> -diastereotopic)
		–	pro- <i>RS</i> -stereogenic (<i>RS</i> -diastereotopic)
		(chirality-faithfulness)	



Remark 14.1. (Comments on the terminology of modern stereochemistry) [3]. Rule 14.1 is a conceptual revision of the *pro-R/pro-S*-descriptors described in the IUPAC Recommendations 1996 [1], where the term ‘stereoheterotopic’ is replaced by the term *RS-diastereotopic* and the term ‘prochiral’ is replaced by the term *pro-RS-stereogenic*.³ Rule 14.1 indicates that *pro-R/pro-S*-descriptors are concerned with *RS*-diastereotopic relationships, but not with stereoheterotopic relationships (nor with enantiotopic relationships). Thereby, they are controlled by a single criterion summarized in Table 14.1 (as surrounded by a solid-line frame).

14.3.3 Probe Stereoisograms for Assigning *pro-R/pro-S*-Descriptors

As examined in Exercise 14.5, the type-II promolecule **11-14** (Fig. 14.1) is determined to be *pro-RS*-stereogenic. The inner structure has been discussed by using Young’s tableaux shown in the type-II-row of Fig. 13.3 (page 372), where the two proligands p’s construct a two-membered *RS*-enantiotopic $C_{\tilde{\sigma}}(/C_1)$ -orbit. Hence, the promolecule **11-14** is concluded to be *pro-RS*-stereogenic, so that the two proligands p’s are differentiated by *pro-R/pro-S*-descriptors.

The assignment of *pro-R/pro-S*-descriptors can be conducted by using a *probe stereoisogram*, which is derived a stereoisogram of a *pro-RS*-stereogenic promolecule. For example, the type-II stereoisogram of **11-14** (Fig. 11.4 on page 318), which has been determined to be *pro-RS*-stereogenic as described in the preceding paragraph, is converted into a probe stereoisogram (Fig. 14.3) to assign *pro-R/pro-S*-descriptors as follows:

1. By labelling the two proligands p’s with α and β , the promolecule **11-14** (Fig. 11.4) is converted into a promolecule **11-14 $^{\alpha}$** , which constructs a stereoisogram of type III tentatively. Such a tentative type-III stereoisogram is called a *probe stereoisogram*, as shown in Fig. 14.3.
2. The pair of *RS*-diastereomeric promolecules **11-14 $^{\alpha}$** and **11-14 $^{\beta}$** in the type-III probe stereoisogram (Fig. 14.3) indicates that the proligands p $^{\alpha}$ and p $^{\beta}$ are differentiated under the *RS*-permutation group $T_{\tilde{\sigma}}$. The proligands p $^{\alpha}$ and p $^{\beta}$ are *RS*-diastereotopic

³ It should be noted that the term ‘stereoheterotopic’ is defined as “Either enantiotopic or diastereotopic” in the IUPAC Recommendations 1996 [1]. Thus, the conventional term ‘stereoheterotopic’ misleadingly mixes up ‘enantiotopic’ and ‘diastereotopic’, just as the terms ‘enantiomeric’ and ‘diastereomeric’ are mixed up to generate the term ‘stereoheteromeric’ (= ‘stereoisomeric’). This mixing-up is unreasonable because ‘enantiotopic’ (or ‘enantiomeric’) is correlated to chirality, while ‘diastereotopic’ (or ‘diastereomeric’) is correlated to stereogenicity. Remember the oversimplified dichotomy between enantiomers and diastereomers (cf. Remark 1.1 on page 11). In Fujita’s stereoisogram approach, the term *RS-diastereotopic* (Def. 14.3) is coined after the concept of *pro-RS*-stereogenicity is developed.

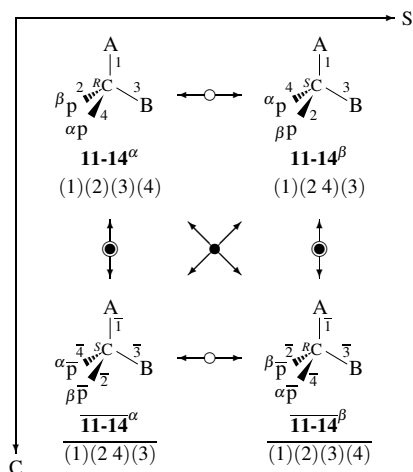


Fig. 14.3. Probe stereoisogram generated by stereoisogram change from type II to type III for testifying *pro-RS*-stereogenicity [3].

to each other. It follows that the original type-II promolecule **11-14** is concluded to be *pro-RS*-stereogenic with respect of the two p's. This conclusion is consistent with the conclusion derived from the presence of an *RS*-enantiotropic orbit (cf. Exercise 14.5).

- The proligand p^α in **11-14^α** is determined to have *pro-R*, because **11-14^α** is determined to have an *R*-stereodescriptor under a tentative priority sequence $A > B > p^\alpha > p^\beta$ or $A > p^\alpha > p^\beta > B$. Note that proligand p^α to be labelled has precedence over the other p^β . On the other hand, the proligand p^α in **11-14^β** is determined to have *pro-S* because **11-14^β** is specified to have an *S*-stereodescriptor.

It should be emphasized that the *RS*-diastereotopic relationship between the proligands p^α and p^β corresponds to the *RS*-diastereomeric relationship between the tentative promolecules **11-14^α** and **11-14^β** in the probe stereoisogram of Fig. 14.3.

The *pro-RS*-stereogenicity of **11-14** corresponds to the conversion of **11-14** (type II) into **11-20** (type III) or to the conversion of **11-14** (type II) into **11-21** (type III), where an *RS*-astereogenic (and chiral) promolecule is converted into an *RS*-stereogenic (and chiral) promolecule in a single desymmetrization step.

Exercise 14.7.

- Draw a probe stereoisogram for differentiated two A's of the type-II promolecule **11-12** (= **14-1** in Fig. 14.2).
- Discuss the *pro-RS*-stereogenicity of **11-12** and assign *pro-R/pro-S*-descriptors to the two A's.

Probe stereoisograms devised by Fujita [3,8] provide us with information on the difference between prochirality and pro-*RS*-stereogenicity. Compare the type-II stereoisogram of Fig. 11.4 (page 318) for the promolecule **11-14** with the corresponding type-III probe stereoisogram of Fig. 14.3 for the tentative promolecule **11-14 α** . The *RS*-astereogenicity of Fig. 11.4 (the self-*RS*-diastereomeric relationship represented by an equality symbol in a horizontal direction) is converted into the *RS*-stereogenicity of Fig. 14.3 (the *RS*-diastereomeric relationship represented by a double-headed arrow in a horizontal direction). The process from *RS*-astereogenicity to *RS*-stereogenicity (Fig. 11.4 \rightarrow Fig. 14.3) indicates pro-*RS*-stereogenicity.

On the other hand, the chirality of Fig. 11.4 (the enantiomeric relationship represented by a double-headed arrow in a vertical direction) is converted into the chirality of Fig. 14.3 (the enantiomeric relationship represented by a double-headed arrow in a vertical direction). This conversion is accompanied with no change of chirality, so that it is not concerned with prochirality.

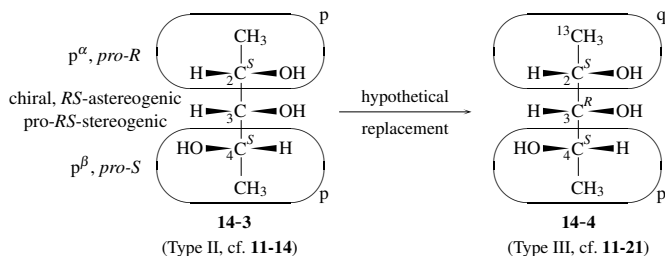
14.3.4 Misleading Interpretation of ‘Prochirality’ in Modern Stereochemistry

According to Fujita’s stereoisogram approach, 2,3,4-trihydroxypentane **14-3** shown in Fig. 14.4(a) is chiral and *RS*-astereogenic, as characterized by a stereoisogram of type II (cf. Fig. 11.4 on page 318). The pro-*RS*-stereogenicity of **14-3** is determined by placing A = OH, X = H, and p = *R*-CH(OH)CH₃, where each proligand p is indicated by an oval box in Fig. 14.4(a). Thereby, **14-3** corresponds to a promolecule with the composition ABp², so that it gives a probe stereoisogram shown in Fig. 14.3.

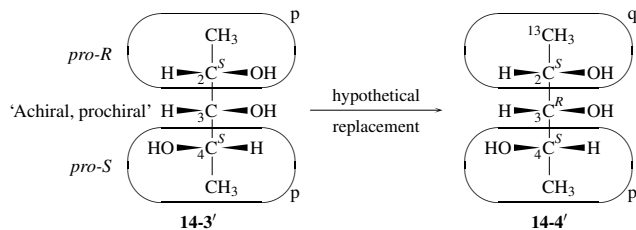
The probe stereoisogram shown in Fig. 14.3 indicates that the proligand p ^{α} (assigned to be *pro-R*) and the proligand p ^{β} (assigned to be *pro-S*) are in an *RS*-diastereotopic relationship, not in an enantiotopic relationship. It follows that the 2,3,4-trihydroxypentane **14-3** with p ^{α} and p ^{β} is pro-*RS*-stereogenic, not prochiral at the C-3 in terms of Fujita’s stereoisogram approach.

A hypothetical replacement of CH₃ by ¹³CH₃ in the proligand p ^{α} generates a proligand q (= *S*-CH(OH)¹³CH₃). The resulting promolecule **14-4** belongs to type III (cf. **11-21**). The *R*-configuration at the C-3 of **14-4** enable us to assign the *pro-R*-descriptor to the proligand p ^{α} of **14-3**. Note that the priority sequence is considered to be A > q > p > B. This assignment due to a tentative replacement is consistent with the assignment due to the probe stereoisogram of Fig. 14.3.

It is worthwhile to cite Fig. 23 of [10] (and Fig. 8.18 of [11]) as an example of misleading interpretation of ‘prochirality’ in modern stereochemistry (Fig. 14.4(b)), where the C-3 atom of **14-3'** is determined to be ‘Achiral, prochiral’. This terminology of ‘prochirality’ claims that the ‘achiral’ central C-3 atom of **14-3'** changes into the ‘chiral’ C-3 atom of **14-4'** during the hypothetical replacement from **14-3'** to **14-4'**. This claim is erroneous, geometrically speaking, because the C-3 atom of **14-3** (also **14-3'**) is locally chiral as well as the global symmetry of **14-3** (also **14-3'**) is determined to be chiral. This reasoning is con-



(a) Consistent interpretation in Fujita's stereoisogram approach



(b) Misleading interpretation in modern stereochemistry [10,11]

Fig. 14.4. Consistent concept of *pro-RS*-stereogenicity vs. misleading concept of 'prochirality' [3]. (a) Consistent interpretation in the stereoisogram approach of the present book, where the C-3 atom is chiral and *RS*-astereogenic so as to exhibit *pro-RS*-stereogenicity. (b) Misleading interpretation in modern stereochemistry [10,11], where the C-3 atom is erroneously recognized as being 'achiral' and 'prochiral' in spite of the local chirality of the C-3 atom.

sistent with Fujita's stereoisogram approach, where the two *p*'s are concluded to belong to a two-membered *RS*-enantiotropic $C_{\bar{2}}(/C_1)$ -orbit (cf. Eq. 14.3) under the action of the *RS*-permutation group $T_{\bar{2}}$, while they are concluded to belong separately to two one-membered hemispheric $C_1(/C_1)$ -orbits (cf. the type-II row of Fig. 13.3 on page 372) under the action of the point group T_d .

Exercise 14.8. By referring to the type-II row of Fig. 13.3 (page 372), try the following exercises:

- Confirm that the C-3 atom of **14-3** shown in Fig. 14.4(a) belongs to a one-membered $C_1(/C_1)$ -orbit under the point group T_d .
- Confirm that the C-3 atom of **14-3** belongs to a one-membered $C_{\bar{2}}(/C_{\bar{2}})$ -orbit under the *RS*-permutation group $T_{\bar{2}}$.
- Demonstrate the misleading characterization of 'Achiral and prochiral' at the C-3 atom of **14-3'** in Fig. 14.4(b).

14.4 Pro-*RS*-Stereogenicity Distinct From Prochirality

14.4.1 Simultaneity of Prochirality and Pro-*RS*-Stereogenicity in a Type-IV Promolecule

The promolecule **11-31** with the composition $A^2p\bar{p}$ in Fig. 14.1 is categorized into type IV, where its stereoisogram is shown in Fig. 14.5(a). The symmetry of **11-31** is characterized by the index: $[C_{s\tilde{\sigma}\hat{\sigma}}, C_s, C_{\tilde{\sigma}}; IV]$. Let us first examine **11-31** from a viewpoint of orbits.

As found in the upper type-IV row of Fig. 13.3 (page 372), the four positions of **11-31** are divided into two orbits, where two proligands A^2 construct a two-membered $C_{s\tilde{\sigma}\hat{\sigma}}(/C_{\tilde{\sigma}})$ -orbit and a pair of p and \bar{p} constructs a two-membered $C_{s\tilde{\sigma}\hat{\sigma}}(/C_s)$ -orbit. This mode of division is controlled by the subduction listed in the 14th row of Table 11.2 (page 326). The corresponding Young's tableau is shown at the intersection between the upper type-IV-row and the *RS*-stereoisogram-column in Fig. 13.3 (page 372).

Under the point group C_s , the four proligands of **11-31** are divided into one two-membered enantiospheric $C_s(/C_1)$ -orbit (accommodating a pair of p and \bar{p}) and two one-membered homospheric $C_s(/C_s)$ -orbits (accommodating two A 's separately). This mode of division is controlled by the subduction listed in the 5th row of of Table 11.2, which can be equalized to the subduction under the point group C_s . The presence of an enantiospheric $C_s(/C_1)$ -orbit indicates the prochirality of **11-31**. The corresponding Young's tableau is shown at the intersection between the upper type-IV-row and the chirality-column in Fig. 13.3.

Under the *RS*-permutation group $C_{\tilde{\sigma}}$, the four proligands of **11-31** are divided into one two-membered *RS*-enantiotropic $C_{\tilde{\sigma}}(/C_1)$ -orbit (accommodating two A 's) and two one-membered *RS*-homotropic $C_{\tilde{\sigma}}(/C_{\tilde{\sigma}})$ -orbits (accommodating p and \bar{p} separately). This mode of division is controlled by the subduction listed in the third row of of Table 11.2, which can be equalized to the subduction under the *RS*-permutation group $C_{\tilde{\sigma}}$. The presence of an *RS*-enantiotropic $C_{\tilde{\sigma}}(/C_1)$ -orbit indicates the pro-*RS*-stereogenicity of **11-31**. The corresponding Young's tableau is shown at the intersection between the upper type-IV-row and the *RS*-stereogenicity-column in Fig. 13.3.

It follows that **11-31** exhibits the simultaneous appearance of prochirality and pro-*RS*-stereogenicity, where the prochirality is concerned with the $C_s(/C_1)$ -orbit of p and \bar{p} , while the pro-*RS*-stereogenicity is concerned with the $C_{\tilde{\sigma}}(/C_1)$ -orbit of two A 's. Note that the assignability of *pro-R/pro-S*-descriptors depends on the *RS*-enantiotropic $C_{\tilde{\sigma}}(/C_1)$ -orbit of two A 's.

The conclusions described in the preceding paragraph can be confirmed by drawing probe stereoisograms shown in Fig. 14.5.

1. The probe stereoisogram shown in Fig. 14.5(b) aims at testifying prochirality, where a pair of proligands p and \bar{p} are differentiated by labelling α or β . The resulting probe stereoisogram belongs to type II. The vertical equality symbols in the original stereoisogram (Fig. 14.5(a)) are changed into vertical double-headed arrows in Fig. 14.5(b), so

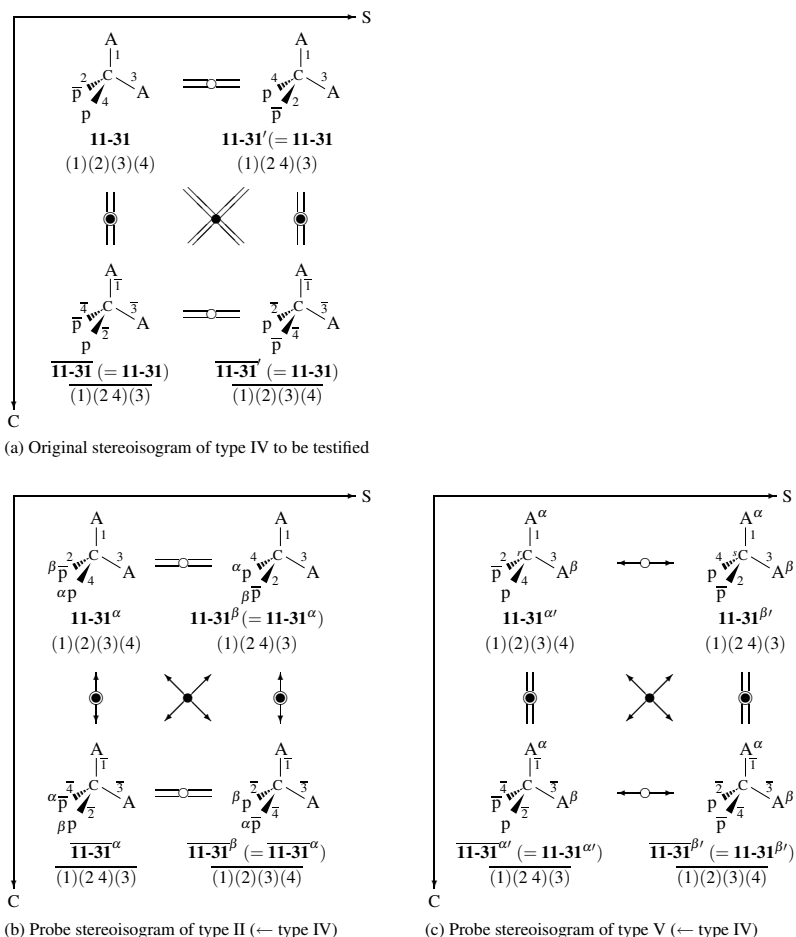


Fig. 14.5. Probe stereoisograms generated from a type-IV stereoisogram exhibiting simultaneity of prochirality and pro-*RS*-stereogenicity. (a) Original stereoisogram of Type IV. (b) Change from type IV to type II for testifying prochirality. (c) Change from type IV to type V for testifying pro-*RS*-stereogenicity. Tentative differentiations of appropriate proligands (labels α and β) in a promolecule of type IV (**11-31**) generate hypothetical promolecules of type II (left) and type V (right), which construct probe stereoisograms.

that the promolecule **11-31** is concluded to be prochiral. This type of prochirality is not a target of *pro-R/pro-S*-descriptors.

- The probe stereoisogram shown in Fig. 14.5(c) aims at testifying pro-*RS*-stereogenicity, where two A's are differentiated by labelling α or β . The resulting probe stereoisogram belongs to type V. The horizontal equality symbols in the original stereoisogram (Fig. 14.5(a)) are changed into horizontal double-headed arrows in Fig. 14.5(c), so that the promolecule **11-31** is concluded to be pro-*RS*-stereogenic. The proligand A^α in **11-31 $^{\alpha\prime}$**

is determined to have *pro-r*, while the proligand A^α in **11-31** ^{β'} is determined to have *pro-s* under a tentative priority sequence $A^\alpha > A^\beta > p > \bar{p}$. The lowercase labels '*pro-r*' and '*pro-s*' are used, because the probe stereoisogram (Fig. 14.5(c)) belongs to type V, where the lowercase labels '*r*' and '*s*' are assigned to the central atoms.

The probe stereoisograms shown in Figs. 14.5(b) and (c) demonstrate a simultaneous appearance of an enantiotopic relationship (prochirality) and an *RS*-diastereotopic relationship (pro-*RS*-stereogenicity) in the promolecule **11-31**. Note again that the enantiotopic relationship (prochirality due to enantiosphericity) is concerned with a pair of proligands p and \bar{p} as an orbit under the point group T_d , while the *RS*-diastereotopic relationship (pro-*RS*-stereogenicity due to *RS*-enantiotropicity) is concerned with a pair of proligands A 's of the same kinds as an orbit under the *RS*-permutation group $T_{\bar{\sigma}}$.

14.4.2 Coincidence of Prochirality and Pro-*RS*-stereogenicity

The promolecule **11-30** with the composition A^2BX (Fig. 14.1 on page 389) is characterized by a stereoisogram of type IV shown in Fig. 11.6 (page 320). The symmetry of **11-30** is characterized by the index: $[C_{s\bar{\sigma}\bar{I}}, C_s, C_{\bar{\sigma}}; IV]$. Let us examine **11-30** from a viewpoint of orbits.

As found in the lower type-IV-row of Fig. 13.3 (page 372), the four positions of **11-30** are divided into three orbits, where two proligands A^2 construct a two-membered $C_{s\bar{\sigma}\bar{I}}(/C_{\bar{\sigma}})$ -orbit, while a proligand B (or X) constructs a one-membered $C_{s\bar{\sigma}\bar{I}}(/C_{s\bar{\sigma}\bar{I}})$ -orbit. This mode of division is controlled by the subduction listed in the 16th row of Table 11.2 (page 326). The corresponding Young's tableau is shown at the intersection between the lower type-IV-row and the *RS*-stereoisogram-column in Fig. 13.3 (page 372).

Under the point group C_s , the four proligands of **11-30** are divided into three orbits, i.e., one two-membered enantiospheric $C_s(/C_1)$ -orbit (accommodating two A 's) and two one-membered homospheric $C_s(/C_s)$ -orbits (accommodating B or X separately). This mode of division is controlled by the subduction listed in the 5th row of of Table 11.2, which can be equalized to the subduction under the point group C_s . The presence of an enantiospheric $C_s(/C_1)$ -orbit indicates the prochirality of **11-30**. The corresponding Young's tableau is shown at the intersection between the lower type-IV-row and the chirality-column in Fig. 13.3.

Under the *RS*-permutation group $C_{\bar{\sigma}}$, the four proligands of **11-30** are divided into one two-membered *RS*-enantiotropic $C_{\bar{\sigma}}(/C_1)$ -orbit (accommodating two A 's) and two one-membered *RS*-homotropic $C_{\bar{\sigma}}(/C_{\bar{\sigma}})$ -orbits (accommodating B or X separately). This mode of division is controlled by the subduction listed in the third row of of Table 11.2, which can be equalized to the subduction under the *RS*-permutation group $C_{\bar{\sigma}}$. The presence of an *RS*-enantiotropic $C_{\bar{\sigma}}(/C_1)$ -orbit indicates the pro-*RS*-stereogenicity of **11-30**. The corresponding Young's tableau is shown at the intersection between the lower type-IV-row and the *RS*-stereogenicity-column in Fig. 13.3.

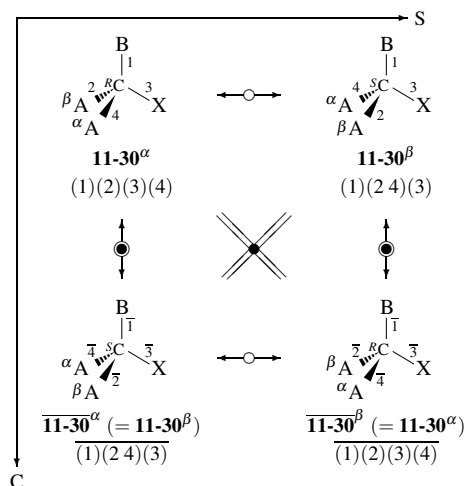


Fig. 14.6. Probe stereoisogram of type I produced from a type-IV stereoisogram for testing the coincidence of prochirality and pro-*RS*-stereogenicity.

It follows that prochirality and pro-*RS*-stereogenicity coincide with each other in **11-30**, where the orbit of two A's is characterized by the enantiospheric coset representation $C_s(/C_1)$ under the point-group symmetry as well as by the *RS*-enantiotropic coset representation $C_{\bar{\sigma}}(/C_1)$ under the *RS*-permutation-group symmetry. Note that the assignability of *pro-R/pro-S*-descriptors depends on the *RS*-enantiotropic $C_{\bar{\sigma}}(/C_1)$ -orbit of two A's.

The conclusions described in the preceding paragraph can be confirmed by drawing a probe stereoisogram shown in Fig. 14.6. By labelling two proligands A's with α and β , the promolecule **11-30** is converted into a hypothetical promolecule **11-30 $^{\alpha}$** , which generates a probe stereoisogram of type I as shown in Fig. 14.6.

The probe stereoisograms shown in Fig. 14.6 aims at testing both prochirality and pro-*RS*-stereogenicity, where two proligands A's are differentiated by labelling α or β . The resulting probe stereoisogram belongs to type I.

The vertical equality symbols in the original stereoisogram (Fig. 11.6 on page 320) are changed into vertical double-headed arrows in Fig. 14.6. At the same time, the horizontal equality symbols in the original stereoisogram (Fig. 11.6) are changed into horizontal double-headed arrows in Fig. 14.6. It follows that the promolecule **11-30** is concluded to be prochiral and pro-*RS*-stereogenic with respect to the two A's. In other words, the probe stereoisogram shown in Fig. 14.6 demonstrates the coincidence of an enantiotopic relationship (prochirality) and an *RS*-diastereotopic relationship (pro-*RS*-stereogenicity) in the promolecule **11-30**.

Because the tentative promolecule **11-30 $^{\alpha}$** has an *R*-configuration under the priority sequence $A^{\alpha} > A^{\beta} > B > X$, the precedent A^{α} is determined to be *pro-R*. Because the tentative promolecule **11-30 $^{\beta}$** has an *S*-configuration under the priority sequence $A^{\alpha} > A^{\beta} > B > X$, the precedent A^{α} is determined to be *pro-S*. Note that the tentative promolecules

11-30^α and **11-30^β** are *RS*-diastereomeric to each other in the probe stereoisogram of type I (Fig. 14.6), so that the two A's in the original stereoisogram of type IV (Fig. 11.6) can be labelled as *pro-R* and *pro-S*.

Although the labels *pro-R* and *pro-S* are originally assigned to a pair of *RS*-diastereotopic A's on the basis of pro-*RS*-stereogenicity, they are interpreted to be assigned to a pair of enantiotopic A's on the basis of prochirality in this case. It should be emphasized that a pair of *RS*-diastereotopic A's (due to pro-*RS*-stereogenicity) is conceptually distinct from a pair of enantiotopic A's (due to prochirality), although they coincide with each other in this case.

14.4.3 Prochiral (but Already *RS*-Stereogenic) Promolecules

The promolecule **11-32** with the composition ABp \bar{p} (Fig. 14.1 on page 389) is characterized by a type-V stereoisogram shown in Fig. 11.7 (page 321). The symmetry of **11-32** is characterized by the index: [$C_s, C_s, C_1; V$]. The examination of **11-32** from a viewpoint of orbits have been conducted in Section 13.3, where orbits to be examined are produced by the subductions shown in Eq. 13.6 (page 373) for the point group T_d and in Eq. 13.7 (page 374) for the *RS*-permutation group $T_{\bar{\sigma}}$.

The presence of an enantiospheric $C_s(/C_1)$ -orbit (cf. Eq. 13.6) indicates the prochirality of **11-32**. The corresponding Young's tableau is shown at the intersection between the type-V-row and the chirality-column in Fig. 13.3. On the other hand, the presence of four *RS*-hemitropic $C_1(/C_1)$ -orbits (cf. Eq. 13.7) indicates that **11-32** is already *RS*-stereogenic, so that *R/S*-stereodescriptors can be assigned. The corresponding Young's tableau is shown at the intersection between the type-V-row and the *RS*-stereogenicity-column in Fig. 13.3 (page 372).

It follows that the prochirality of **11-32** cannot be characterized by *pro-R/pro-S*-descriptors, because *pro-R/pro-S*-descriptors is concerned with pro-*RS*-stereogenicity, but not with prochirality.

The promolecule **11-32** of type V as a prochiral (but already *RS*-stereogenic) promolecule can be examined by drawing a probe stereoisogram shown in Fig. 14.7. By labelling two proligands p and \bar{p} with α and β , the type-V stereoisogram of **11-32** (Fig. 11.7 on page 321) is converted into a type-III probe stereoisogram (Fig. 14.7), which contains a tentative promolecule **11-32^α** as a reference.

The horizontal double-headed arrows in the original type-V stereoisogram (Fig. 11.7 on page 321) maintain in the corresponding type-III probe stereoisogram (Fig. 14.7), where they represent *RS*-diastereomeric relationships (and *RS*-stereogenicity). On the other hand, the vertical equality symbols (self-enantiomeric relationships and achirality) in the original type-V stereoisogram (Fig. 11.7) change into double-headed arrows (enantiomeric relationships and chirality) in the corresponding type-III probe stereoisogram (Fig. 14.7).

The prochirality of **11-32** corresponds to the conversion of **11-32** (or its *RS*-diastereomer of type V) into **11-20** (type III) or the conversion of **11-32** (type V) into **11-21** (type III),

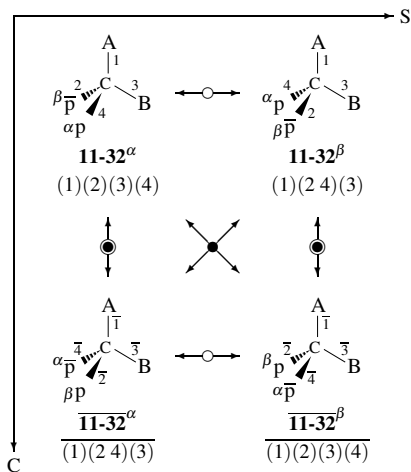


Fig. 14.7. Probe stereoisogram of type III generated by stereoisogram change from type V to type III for testifying prochirality.

where an achiral (and *RS*-stereogenic) promolecule is converted into a chiral (and *RS*-stereogenic) promolecule in a single desymmetrization step.

14.5 Pro-*RS*-Stereogenicity for *pro-R/pro-S*-Descriptors

Modern stereochemistry lays too much stress on coincident cases of prochirality and *pro-RS*-stereogenicity, where all of the four proligands are achiral in isolations. As discussed in Subsection 14.4.2, the two A's of the promolecule **11-30** with the composition A^2BX (Fig. 11.6 on page 320) are *enantiotopic* to each other; and, at the same time, they are *RS*-diastereotopic each other according to Fujita's stereoisogram approach. Modern stereochemistry lacks an *RS*-diastereotopic relationship as a pairwise relationship, so that a pair of *pro-R/pro-S*-descriptors is misleadingly presumed to be assigned directly to a pair of enantiomers in the case of **11-30**. As commented in Footnote 3, the coinage of the term 'stereoheterotopic' ('enantiotopic' + 'diastereotopic') conceals the misleading presumption of modern stereochemistry. Note that the term *RS*-diastereotopic is conceptually distinct from the term *enantiotopic* in Fujita's stereoisogram approach, whereas the term 'stereoheterotopic' contains the term 'enantiotopic' in modern stereochemistry.

The final conclusion of this chapter is that the terminology on 'prochirality' by Hanson [2] should be thoroughly abandoned and replaced by the terminology on *pro-RS*-stereogenicity due to Fujita's stereoisogram approach [3,8]. Moreover, the use of the term 'stereoheterotopic' should be abandoned and replaced by the term *RS*-diastereotopic due to Fujita's stereoisogram approach [3,8].



Remark 14.2. (Comments on the stereochemical terminology) [3]. Eliel (page 21 of [10]) has claimed that “Just as chiral centers can be labelled *R* or *S* not only in enantiomers but also in many diastereomers, so the designations *pro-R* and *pro-S* are not confined to enantiotopic ligands but may also be used for a number of diastereotopic ones (for exception, see below).” This claim is misleading and should be abandoned, so as to be replaced by the single criterion summarized in Table 14.1, which is derived from Rule 14.1 in Fujita’s stereoisogram approach. Thus, we should say that “Just as *RS*-stereogenic centers are labelled *R* or *S* in *RS*-diastereomers (not in enantiomers), so the designations *pro-R* and *pro-S* should be confined to *RS*-diastereotopic proligands.” Note that there are coincident cases between *RS*-diastereotopic relationships and enantiotopic ones (cf. **11-30**).

References

- [1] IUPAC Organic Chemistry Division, *Pure Appl. Chem.*, **68**, 2193–2222 (1996).
- [2] K. R. Hanson, *J. Am. Chem. Soc.*, **88**, 2731–2742 (1966).
- [3] S. Fujita, *Tetrahedron: Asymmetry*, **25**, 1190–1204 (2014).
- [4] S. Fujita, Prochirality and Pro-*RS*-Stereogenicity. Stereoisogram Approach Free from the Conventional “Prochirality” and “Prostereogenicity”, in “Carbon Bonding and Structures. Advances in Physics and Chemistry”, ed. by M. V. Putz, Springer-Verlag, Dordrecht Heidelberg London (2011) Vol. 5 of Carbon Materials: Chemistry and Physics Chapter 10, pp 227–271.
- [5] S. Fujita, *J. Math. Chem.*, **52**, 508–542 (2014).
- [6] S. Fujita, *Tetrahedron*, **62**, 691–705 (2006).
- [7] S. Fujita, *J. Math. Chem.*, **33**, 113–143 (2003).
- [8] S. Fujita, *J. Comput. Aided Chem.*, **10**, 76–95 (2009).
- [9] S. Fujita, *MATCH Commun. Math. Comput. Chem.*, **61**, 39–70 (2009).
- [10] E. L. Eliel, *Top. Curr. Chem.*, **105**, 1–76 (1982).
- [11] E. L. Eliel, S. H. Wilen, and M. P. Doyle, “Basic Organic Stereochemistry”, Wiley-Interscience, New York (2001).

15 Perspectives

15.1 Enumeration of Highly Symmetric Molecules

This book is devoted to the introduction of Fujita's USCI approach in Chapter 5 as well as Fujita's proligand method in Chapter 7. These approaches are versatile to combinatorial enumeration in general. The future task is to pursue further applications of these approaches to symmetry-interesting molecules, in particular, highly symmetric molecules.

Fujita's USCI approach [1,2] supports four methods of symmetry-itemized enumeration of three-dimensional (3D) structures, i.e.,

1. the fixed-point-matrix (FPM) method based on generating functions derived from subduced cycle indices (SCIs) and mark tables [3–5],
2. the partial-cycle-index (PCI) method based on generating functions derived from partial cycle indices (PCIs) [6,7],
3. the elementary-superposition method [8], and
4. the partial-superposition method [6,8].

Among the four methods of the USCI approach [1], the former three have been compared by starting from a common cubane skeleton of the point group O_h , i.e., symmetry-itemized enumeration of cubane derivatives as 3D entities by the FPM method [9], by the PCI method [10], and by the elementary-superposition method [11]. These articles would be templates for further investigations of highly symmetric molecules by means of Fujita's USCI approach.

Fujita's proligand method for enumerating 3D structures [12] is a substantial extension of Pólya's method for enumerating graphs [13]. Fujita's proligand method is accompanied with several related methods for gross enumeration of 3D structures, which have been also developed by Fujita [12]. They have been compared by starting from a common cubane skeleton of the point group O_h , i.e., gross enumeration of cubane derivatives by Fujita's proligand method [14], by the markaracter method [15], by the characteristic-monomial method [16], by the extended-superposition method [17], and by the double-coset-representation method [17]. These articles would be templates for further investigations of highly symmetric molecules by means of Fujita's proligand method and the related methods.

15.2 Interaction of Orbits of Different Kinds

This book emphasizes the importance of the concept of equivalence classes (orbits) derived from the concept of equivalence relationships. Although the discussions of this book aim mainly at the orbits of vertices (substitution positions, substituents, proligands, etc.), extended discussions on the orbits of edges (bonds etc.) are permitted under parallel theoretical foundations. For example, there have appeared the enumeration of organic reactions

by counting substructures of imaginary transition structures (ITS) [18,19], the sphericity concept for an orbit of bonds during the enumeration of fullerene C₆₀-adducts [20], the enumeration of edge configurations on a regular octahedron [21], and so on.

When Fujita's USCI approach is applied to enumeration of Kekulé structures, the selection of two adjacent edges (adjacent double bonds) is not permitted and should be excluded by reasonable procedures. For this purpose, a joint position of two adjacent edges should be detected to exclude adjacent edges. In other words, the methodology for enumerating edge configurations should be extended to take interaction of orbits of different kinds into consideration.

The restricted-subduced-cycle-index (RSCI) method has been developed by Fujita to accomplish symmetry-itemized enumeration of Kekulé structures and applied to fullerene C₆₀ [22]. The RSCI method has been applied to the counting of matchings of graphs, which are used to obtain Z-counting polynomials and the Hosoya index as well as to calculate matching polynomials [23]. By starting from the FPM method and the PCI method of Fujita's USCI approach, the restricted-fixed-point-matrix (RFPM) method [24] and the restricted-partial-cycle-index (RPCI) method [25], both of which are based on restricted subduced cycle indices, have been developed by Fujita and applied to enumeration of 3D structures derived from a dodecahedrane skeleton under a restriction condition. Recently, the RSCI method has been introduced in a series of review articles [26–29]. This series would be templates for further investigations of Kekulé structures and perfect matchings of graphs.

15.3 Correlation Diagrams of Stereoisograms

In this book, Fujita's stereoisogram approach is discussed by selecting skeletons of a single focused center (e.g., a tetrahedral skeleton and an allene skeleton) in the form of the proligand-promolecule model. The remaining task is to examine molecules characterized by multiple stereoisograms of *RS*-stereoisomeric centers in isolation. The concept of *correlation diagrams of stereoisograms* has been developed by Fujita to characterize a set of stereoisomers [30]. Correlation diagrams of stereoisograms are capable of solving most problems which have been left unsolved within the traditional terminology of stereochemistry and related chemoinformatics practices, e.g., over-simplified features of the conventional dichotomy between enantiomers and diastereomers, incomplete separation of *RS*-stereogenicity from chirality, unconscious disregard of local *RS*-stereogenicity and confusion of it with local chirality, implications of reflection-invariant cases of the CIP priority system, and others [31]. Correlation diagrams of stereoisograms for characterizing stereoisomers of cyclobutane derivatives have been discussed as more complicated cases [32]. Correlation diagrams of stereoisograms have been used to comprehend the global and local symmetries of oxirane derivatives [33]. Thereby, *R/S*-stereodescriptors of the CIP system have been found to specify local symmetries at respective positions of an oxirane

derivative, so that the global symmetry of the oxirane derivative requires the other types of descriptors (R_a/S_a -descriptors and Z/E -descriptors) proposed in [34].

Theory of organic stereoisomerism in harmony with molecular symmetry has been developed by starting from RS -stereoisomeric groups correlated to stereoisograms and their correlation diagrams, where a set of epimerizations at RS -stereogenic centers of a stereoskeleton is taken into consideration to formulate a stereoisomeric group [35]. This course would be one of promising formulations for rationalizing stereoisomerism.

15.4 Group Hierarchy

Group hierarchy stems from Fujita's stereoisogram approach for integrating geometric aspects and stereoisomerism in stereochemistry, where a quadruplet of RS -stereoisomers under an RS -stereoisomeric group, a set of stereoisomers under a stereoisomeric group, and a set of isoskeletomers under an isoskeletal group are recognized as respective equivalences classes (orbits) of molecular entities [34]. This group hierarchy is illustrated by a flowchart shown in Fig. 15.1(a) or by a simplified flowchart shown in Fig. 15.1(b). On the other hand, the revised flowchart shown in Fig. 2.4 (page 47) is redrawn to give Fig. 15.1(c) from a group-theoretical point of view.

The judgement due to an enantiomeric relationship in Fig. 2.4 (or due to a point group in Fig. 15.1(c)) is replaced by the successive judgements due to an RS -stereoisomeric group and due to stereoisograms in Fig. 15.1(a) or by the successive judgements due to an RS -stereoisomeric group and due to a point group in Fig. 15.1(b). Thereby, the final categories of Fig. 2.4 (or Fig. 15.1(c)) are pairs of enantiomers, while the final categories of Fig. 15.1(a) are type-I to type-V quadruplets. Even in Fig. 15.1(b), pairs of enantiomers as final categories are linked with type-I to type-V quadruplets because of the intervention of the judgement due to an RS -stereoisomeric group.

As found in Figs. 15.1(a) and (b), the concept of RS -stereoisomers mediates between enantiomers and stereoisomers, which have been directly linked with each other in the conventional flowchart of modern stereochemistry (even in a revised form shown in Fig. 15.1(c)). Such an intermediate concept as created by Fujita's stereoisogram approach has brought about a paradigm shift, so that modern stereochemistry has been restructured substantially on the basis of mathematical formulations, as described in this book. This fact is parallel to the historical event that Avogadro's theory has brought about a paradigm shift in chemistry by creating the intermediate concept of *molecule* (e.g., H_2O), which mediates between atoms (e.g., hydrogen atoms and oxygen atoms) and substances (e.g., water).

From an alternative point of view, Fujita's stereoisogram approach summarized by the flowchart of Fig. 15.1(a) can be regarded as an integration of van't Hoff's way and Le Bel's way (cf. Subsection 1.1.2). Note that modern stereochemistry lays stress on van't Hoff's way and treats inconsistent cases due to Le Bel's way (e.g., pseudoasymmetry, the CIP system, and the *pro-R/pro-S* system) as exceptions in an ad-hoc fashion.

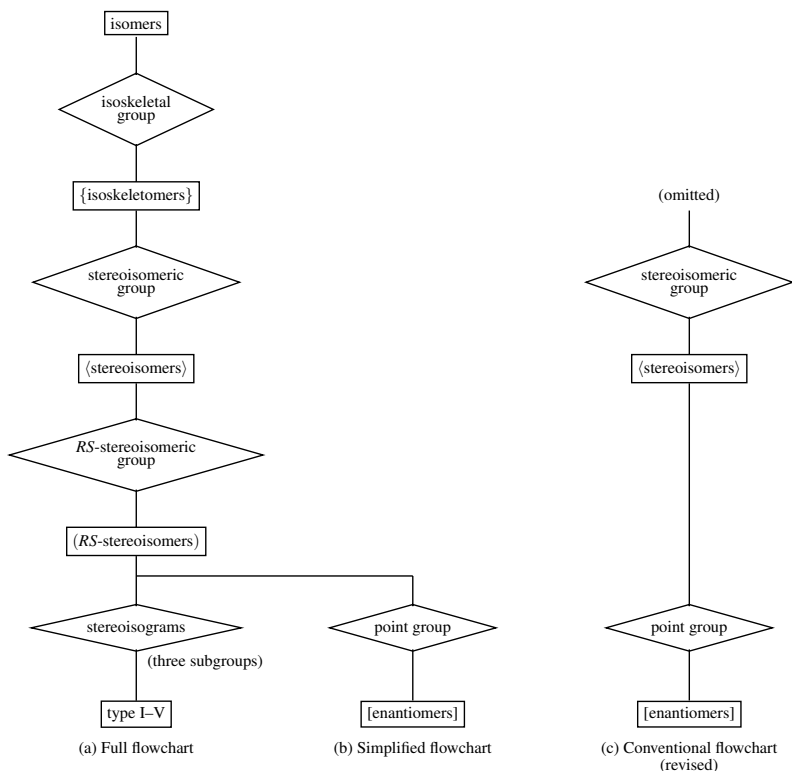


Fig. 15.1. Flowchart for classifying various kinds of isomers on the basis of equivalence classes [34]. (a) Full flowchart in which the lowest judgement based on stereoisograms uses the combination of equivalence classes due to three subgroups of the *RS*-stereoisomeric group, i.e., a point group, an *RS*-permutation group, and a ligand-reflection group. (b) Simplified flowchart in which the lowest judgement uses a point group. (c) Revised conventional flowchart with no *RS*-stereoisomeric group.

Fujita's proligand method, which was developed originally for combinatorial enumeration under point groups (Chapter 7) [36], has been extended to meet the group hierarchy (Fig. 15.1(b)) [34]. Combinatorial enumerations under respective levels of the group hierarchy have been conducted to count inequivalent pairs of (self-)enantiomers under a point group, inequivalent quadruplets of *RS*-stereoisomers under an *RS*-stereoisomeric group, inequivalent sets of stereoisomers under a stereoisomeric group, and inequivalent sets of isoskeletomers under an isoskeletal group [37]. Two kinds of compositions have been used for the purpose of representing molecular formulas in an abstract fashion, that is to say, the compositions for differentiating proligands having opposite chirality senses and the compositions for equalizing proligands having opposite chirality senses. Thereby, the classifications of isomers have been accomplished in a systematic fashion. Because stereoskeletons of ligancy 4 (i.e., a tetrahedral skeleton, an allene skeleton, an ethylene skeleton, an oxi-

rane skeleton, a square planar skeleton, and a square pyramidal skeleton) have been used as examples, we are able to have wider perspectives by examining other skeletons in general.

15.5 Non-Rigid Molecules and Conformations

The concept of *coronas* by Pólya [13,38] and a generalized wreath product method by Balasubramanian [39] have been applied to *gross* enumerations of non-rigid organic compounds, where inner ligands are considered to be graphs or structureless objects.

On the other hand, Fujita's USCI approach has provided powerful methods of *symmetry-itemized* enumerations, where the concept of *coronas* (equivalent to wreath products) are extended to support symmetry-itemized enumerations of non-rigid organic compounds [40–42]. Systematic enumerations of non-rigid compounds with given ligand symmetries have been investigated, where inner ligands are considered to have 3D structures [42,43]. Symmetry-itemized enumeration of flexible cyclohexane derivatives has been conducted according to Fujita's USCI approach [44].

The concept of *pseudo-point groups* has been proposed by Fujita for the purpose of symmetry characterization and combinatorial enumeration of non-rigid compounds [45–47]. The concept of *pseudo-point groups* has been applied to cyclohexane derivatives [48].

A group-theoretical framework for characterizing ring flipping and N-inversion has been developed on the basis of extended pseudo-point groups [49]. Thereby symmetry-itemized enumeration of piperidine derivatives has been conducted.

Flexibility in inorganic complexes can be treated on the basis of Fujita's stereoisogram approach. Thus, a revised interpretation of Berry's pseudorotation has been reported by examining stereoisograms of trigonal bipyramidal compounds [50]. Stereoisograms of octahedral complexes are examined to discuss *RS*-stereogenicity vs. stereogenicity as well as *RS*-stereoisomerism vs. stereoisomerism [51]. Thus, flexibility in octahedral complexes has been investigated within the scope of Fujita's stereoisogram approach.

Conformational change due to bond rotations around a single bond can be treated as an interconversion among two or more (rigid) conformers, which are governed by pseudo-point groups. This is open to future investigation.

15.6 Interdisciplinary Nature of Mathematical Stereochemistry

Before closing this book, the interdisciplinary nature of mathematical stereochemistry should be revisited in practical levels as well as in conceptual levels. Thereby, a motivation for pursuing further possibilities of mathematical stereochemistry would be enhanced in both chemistry and mathematics.

15.6.1 Mathematical and Stereochemical Barriers In Practical Levels

During the process of investigation and communication on mathematical stereochemistry, tools for drawing structural formulas and tools for typesetting mathematical equations are both important. From the viewpoint of chemistry, ChemDraw, ChemSketch, etc. are available as powerful tools for drawing structural formulas, whereas the typesetting of mathematical equations by Word is not so convenient as compared with the $\text{T}_{\text{E}}\text{X}/\text{L}^{\text{A}}\text{T}_{\text{E}}\text{X}$ utilities. From the viewpoint of mathematics, the $\text{T}_{\text{E}}\text{X}/\text{L}^{\text{A}}\text{T}_{\text{E}}\text{X}$ utilities are available as powerful tools for typesetting mathematical equations, whereas the original $\text{T}_{\text{E}}\text{X}/\text{L}^{\text{A}}\text{T}_{\text{E}}\text{X}$ system lacks tools for drawing structural formulas.

If the state-of-the-art situations in scientific software are taken into consideration, the selection of the $\text{T}_{\text{E}}\text{X}/\text{L}^{\text{A}}\text{T}_{\text{E}}\text{X}$ is inevitable for the purpose of satisfactory typesetting of mathematical equations. Although the $\text{T}_{\text{E}}\text{X}/\text{L}^{\text{A}}\text{T}_{\text{E}}\text{X}$ system is not so familiar to chemists (i.e., a mathematical barrier) and although tools for drawing structural formulas (such as ChemDraw and ChemSketch) are not so familiar to mathematicians (i.e., a stereochemical barrier), the combination of $\text{T}_{\text{E}}\text{X}/\text{L}^{\text{A}}\text{T}_{\text{E}}\text{X}$ with ChemDraw (or ChemSketch) would be the most promising selection to do well in investigation and communication on mathematical stereochemistry. However, switching between two different types of software would provide chemists and mathematicians with some troublesome feelings. These situations indicate that a $\text{L}^{\text{A}}\text{T}_{\text{E}}\text{X}$ utility for drawing structural formulas is highly desirable to be coupled with the original $\text{T}_{\text{E}}\text{X}/\text{L}^{\text{A}}\text{T}_{\text{E}}\text{X}$ system.

The $\text{X}^{\text{M}}\text{T}_{\text{E}}\text{X}$ system was developed by myself (Fujita) and released in 1993 as a $\text{L}^{\text{A}}\text{T}_{\text{E}}\text{X}$ utility for drawing structural formulas, the manual of which was published as a book in 1997 [52]. The PostScript-compatible mode supported by $\text{X}^{\text{M}}\text{T}_{\text{E}}\text{X}$ version 4.00 can be used to draw structural formulas of high printing quality [53], so that it enabled us to publish a book for surveying organic compounds for color photography in 2004 [54]. The book published in 2007 was concerned with a new concept of *mandalas*, which was proposed as a basis for rationalizing enumeration of 3D structures [2]. The book published in 2013 was concerned with the *proligand method* proposed by myself (Fujita) to enumerate 3D structures [12]. In addition, the present book, which will be published in 2015, is concerned mainly with *Fujita's stereoisogram approach*. These books contain many mathematical equations as well as structural formulas because of interdisciplinary nature, where the mathematical equations have been typeset by the original $\text{T}_{\text{E}}\text{X}/\text{L}^{\text{A}}\text{T}_{\text{E}}\text{X}$ utilities and the structural formulas have been drawn by the $\text{X}^{\text{M}}\text{T}_{\text{E}}\text{X}$ system. Moreover, the on-line manual [55] of the $\text{X}^{\text{M}}\text{T}_{\text{E}}\text{X}$ system Version 5.01 itself provides us with an illustrative example for publishing a book which contains both chemical structural formulas and mathematical equations.

In recent review articles [56,57], the merits of the $\text{X}^{\text{M}}\text{T}_{\text{E}}\text{X}$ system for publishing interdisciplinary chemistry/mathematics books were emphasized. It follows that the combination of the $\text{X}^{\text{M}}\text{T}_{\text{E}}\text{X}$ system with the $\text{T}_{\text{E}}\text{X}/\text{L}^{\text{A}}\text{T}_{\text{E}}\text{X}$ system would be promising as a practical tool for investigation and communication on mathematical stereochemistry, which is an interdisciplinary field of chemistry and mathematics [58].

15.6.2 Mathematical and Stereochemical Barriers In Conceptual Levels

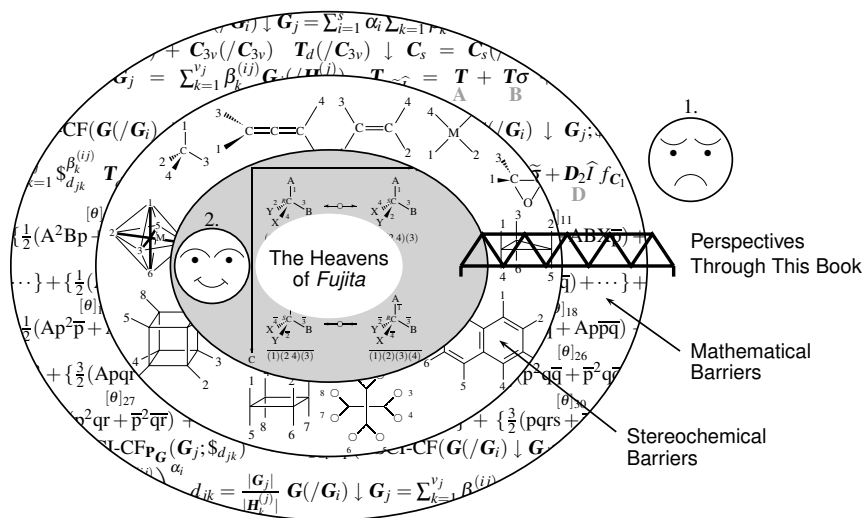
Fujita's USCI approach has been referred to as 'an organic chemistry paradox in Era of Fujita' by El-Basil in his review [59]. By keeping the monograph of 1991 [1] in mind, mathematical and stereochemical barriers against Fujita's USCI approach have been caricatured under the name of 'the Heavens of Fujita' [60, Fig. 35]. El-Basil has pointed out that such heavens can only be reached by mathematics, so long as an organic chemist (who is not interested in mathematics) is trying to make his way through such heavens.

Although a similar situation concerning mathematical and stereochemical barriers holds true for inorganic stereochemistry, von Zelewsky has maintained a different attitude in his textbook on inorganic stereochemistry [61, page 11], i.e., "It will be useful to put mathematics to work in order to develop some concepts of stereochemistry further, but the experimental chemist will always find well-defined simple concepts more useful than mathematical derivations." after the citation of Pólya's book [13], Fujita's book [1], and so on. However, Fujita's stereoisogram approach derived mathematically in the present book has clarified that a fundamental set of 'well-defined simple concepts more useful than mathematical derivations' is misleading. It should be noted that such 'simple concepts' would become truly 'well-defined' and 'more useful' only after mathematical derivations.

In order to bridge across the barriers to 'the Heavens of Fujita', diagrammatic devices have been introduced as the first remedy for avoiding mathematical barriers [2], where abstract mathematical concepts of Fujita's USCI approach are visualized diagrammatically. As the second remedy, Fujita's USCI approach has been simplified to develop Fujita's proligand method [12]. As the third remedy, Fujita's stereoisogram approach has been developed as a higher-level integration (the present book), so that it provides us with broader perspectives of mathematical stereochemistry. Thereby, mathematical and stereochemical barriers have become lower and lower to both chemists and mathematicians. Thus, the caricature of 'the Heavens of Fujita' is redrawn to give Fig. 15.2, where a bridge with broader perspectives is added as a new matter.

15.7 Reorganizing the Theoretical Foundations of Stereochemistry and Stereoisomerism

As formulated in Chapter 10, *RS*-stereoisomeric groups and their stereoisograms are capable of constructing a strict and succinct mathematical framework for reorganizing modern stereochemistry. The group-subgroup relationship concerned with an *RS*-stereoisomeric group, e.g., $T_{d\sigma\hat{1}}$ for a tetrahedral skeleton, permits us to accomplish qualitative and quantitative discussions on stereochemistry (concerning geometric properties) and stereoisomerism (concerning changes of configurations), as clarified by a review [62]. Thereby, misleading standpoints for *R/S*-stereodescriptors of the CIP system have been avoided rationally [63]. In a parallel way, related misleading standpoints for *pro-R/pro-S*-descriptors have been avoided rationally [64]. Although the traditional practices of assigning *R/S*-stereodescriptors



1. An organic chemist (or a mathematician) trying to make his way through!
2. He made it.

Fig. 15.2. Mathematical barriers and stereochemical barriers. This figure is a revision of El-Basil's caricature [60, Fig. 35].

and *pro-R/pro-S*-descriptors can be maintained, their theoretical foundations have been thoroughly revised by means of Fujita's stereoisogram approach. It follows that the descriptions of textbooks on organic chemistry and on stereochemistry should be thoroughly revised in conceptually deeper levels, but not in superficial verbal levels.

References

- [1] S. Fujita, "Symmetry and Combinatorial Enumeration in Chemistry", Springer-Verlag, Berlin-Heidelberg (1991).
- [2] S. Fujita, "Diagrammatical Approach to Molecular Symmetry and Enumeration of Stereoisomers", University of Kragujevac, Faculty of Science, Kragujevac (2007).
- [3] S. Fujita, *Theor. Chim. Acta*, **76**, 247–268 (1989).
- [4] S. Fujita, *J. Math. Chem.*, **5**, 121–156 (1990).
- [5] S. Fujita, *Bull. Chem. Soc. Jpn.*, **63**, 203–215 (1990).
- [6] S. Fujita, *J. Math. Chem.*, **12**, 173–195 (1993).
- [7] S. Fujita, *Bull. Chem. Soc. Jpn.*, **73**, 329–339 (2000).
- [8] S. Fujita, *Theor. Chim. Acta*, **82**, 473–498 (1992).
- [9] S. Fujita, *Bull. Chem. Soc. Jpn.*, **84**, 1192–1207 (2011).

- [10] S. Fujita, *Bull. Chem. Soc. Jpn.*, **85**, 793–810 (2012).
- [11] S. Fujita, *Bull. Chem. Soc. Jpn.*, **85**, 811–821 (2012).
- [12] S. Fujita, “Combinatorial Enumeration of Graphs, Three-Dimensional Structures, and Chemical Compounds”, University of Kragujevac, Faculty of Science, Kragujevac (2013).
- [13] G. Pólya and R. C. Read, “Combinatorial Enumeration of Groups, Graphs, and Chemical Compounds”, Springer-Verlag, New York (1987).
- [14] S. Fujita, *MATCH Commun. Math. Comput. Chem.*, **67**, 5–24 (2012).
- [15] S. Fujita, *MATCH Commun. Math. Comput. Chem.*, **67**, 25–54 (2012).
- [16] S. Fujita, *MATCH Commun. Math. Comput. Chem.*, **67**, 649–668 (2012).
- [17] S. Fujita, *MATCH Commun. Math. Comput. Chem.*, **67**, 669–686 (2012).
- [18] S. Fujita, *J. Math. Chem.*, **7**, 111–133 (1991).
- [19] S. Fujita, “Computer-Oriented Representation of Organic Reactions”, Yoshioka-Shoten, Kyoto (2001).
- [20] S. Fujita, *J. Chem. Inf. Comput. Sci.*, **36**, 270–285 (1996).
- [21] S. Fujita and N. Matsubara, *Internet Electronic Journal of Molecular Design*, **2**, 224–241 (2003).
- [22] S. Fujita, *Bull. Chem. Soc. Jpn.*, **85**, 282–304 (2012).
- [23] S. Fujita, *Bull. Chem. Soc. Jpn.*, **85**, 439–449 (2012).
- [24] S. Fujita, *J. Comput. Chem. Jpn.*, **11**, 131–139 (2012).
- [25] S. Fujita, *J. Comput. Chem. Jpn.*, **11**, 140–148 (2012).
- [26] S. Fujita, *MATCH Commun. Math. Comput. Chem.*, **69**, 263–290 (2013).
- [27] S. Fujita, *MATCH Commun. Math. Comput. Chem.*, **69**, 291–310 (2013).
- [28] S. Fujita, *MATCH Commun. Math. Comput. Chem.*, **69**, 311–332 (2013).
- [29] S. Fujita, *MATCH Commun. Math. Comput. Chem.*, **69**, 333–354 (2013).
- [30] S. Fujita, *MATCH Commun. Math. Comput. Chem.*, **63**, 3–24 (2010).
- [31] S. Fujita, *MATCH Commun. Math. Comput. Chem.*, **63**, 25–66 (2010).
- [32] S. Fujita, *J. Math. Chem.*, **47**, 145–166 (2010).
- [33] S. Fujita, *J. Math. Chem.*, **53**, 353–373 (2015).
- [34] S. Fujita, *J. Math. Chem.*, **53**, 305–352 (2015).
- [35] S. Fujita, *J. Math. Chem.*, **49**, 95–162 (2011).
- [36] S. Fujita, *Theor. Chem. Acc.*, **113**, 73–79 (2005).
- [37] S. Fujita, *J. Math. Chem.*, **53**, 1010–1053 (2015).
- [38] G. Pólya, *Acta Math.*, **68**, 145–254 (1937).

- [39] K. Balasubramanian, *Theor. Chim. Acta*, **51**, 37–54 (1979).
- [40] S. Fujita, *Theor. Chim. Acta*, **77**, 307–321 (1990).
- [41] S. Fujita, *Bull. Chem. Soc. Jpn.*, **63**, 2033–2043 (1990).
- [42] S. Fujita, *J. Chem. Inf. Comput. Sci.*, **40**, 135–146 (2000).
- [43] S. Fujita, *J. Chem. Inf. Comput. Sci.*, **40**, 426–437 (2000).
- [44] S. Fujita, *Bull. Chem. Soc. Jpn.*, **67**, 2935–2948 (1994).
- [45] S. Fujita, *Bull. Chem. Soc. Jpn.*, **67**, 2927–2934 (1994).
- [46] S. Fujita, *J. Chem. Soc. Faraday Trans.*, **94**, 2515–2523 (1998).
- [47] S. Fujita, *J. Chem. Soc. Faraday Trans.*, **94**, 3197–3205 (1998).
- [48] S. Fujita, *Proc. Japan Acad. Ser. B*, **77**, 197–202 (2001).
- [49] S. Fujita, *Bull. Chem. Soc. Jpn.*, **72**, 1759–1768 (1999).
- [50] S. Fujita, *J. Math. Chem.*, **50**, 1815–1860 (2012).
- [51] S. Fujita, *MATCH Commun. Math. Comput. Chem.*, **71**, 537–574 (2014).
- [52] S. Fujita, “ $\text{\X}\text{\M}\text{\T}\text{\E}\text{\X}$ —Typesetting Chemical Structural Formulas”, Addison-Wesley Japan, Tokyo (1997).
- [53] S. Fujita, *J. Comput. Chem. Jpn.*, **4**, 69–78 (2005).
- [54] S. Fujita, “Organic Chemistry of Photography”, Springer-Verlag, Berlin-Heidelberg (2004).
- [55] S. Fujita, “ $\text{\X}\text{\M}\text{\T}\text{\E}\text{\X}$: Reliable Tool for Drawing Chemical Structural Formulas”, Shonan Institute of Chemoinformatics and Mathematical Chemistry, Kanagawa (2013). <http://xymtex.com/fujitas3/xymtex/indexe.html>.
- [56] S. Fujita, *Asian J. T_EX*, **3**, 89–108 (2009).
- [57] S. Fujita, *TUGboat*, **34** (3), 325–328 (2013).
- [58] The $\text{\X}\text{\M}\text{\T}\text{\E}\text{\X}$ system Version 5.01 is available from Fujita’s homepage: <http://xymtex.com/fujitas3/xymtex/indexe.html>.
- [59] S. El-Basil, *MATCH Commun. Math. Comput. Chem.*, **46**, 7–23 (2002).
- [60] S. El-Basil, “Combinatorial Organic Chemistry: An Educational Approach”, Nova Science, Huntington (2000).
- [61] A. von Zelewsky, “Stereochemistry of Coordination Compounds”, John Wiley & Sons, Chichester (1996).
- [62] S. Fujita, *Tetrahedron: Asymmetry*, **25**, 1153–1168 (2014).
- [63] S. Fujita, *Tetrahedron: Asymmetry*, **25**, 1169–1189 (2014).
- [64] S. Fujita, *Tetrahedron: Asymmetry*, **25**, 1190–1204 (2014).

Index

Symbols

2D basis	45
3D basis	45
3D-skeleton	
– bicentroidal —	217
– centroidal —	214
3D-structural isomer	51, 187
3D-tree	
– achiral and chiral centroidal —	214
– achiral bicentroidal —	218
– achiral centroidal —	214
– chiral bicentroidal —	218
– chiral centroidal —	214

A

absolute configuration	365
– chiral aspect of —	377
– chirality-faithful —	382
– chirality-unfaithful —	382
– <i>RS</i> -stereogenic aspect of —	377
accent	
– hat —	290, 323, 354
– tilde —	290, 323, 354
achiral	369
achirality	16
— for type IV or V	335
– chirality/—	285
activity	
– optical —	2
acyclic	49
— molecule	109
adamantan-2-one	144
– dioxa derivative of —	126
– oxa derivative of —	126
– polyaza- —	144
– polyoxa- —	144
adamantane	22, 167
adamantane-2,6-dione	98
– dioxa derivative of —	126
adduct	
– C_{60} - —	168
alcohol	49

– aliphatic —	193
aldehyde	49
algebra system	
– computer —	141
alkane	22, 177
– bicentroidal —	218
– centroidal —	214
– enumeration of —	193
– monosubstituted —	177, 193, 195
alkanol	21, 22, 42, 195
alkyl	
– — as graph	209
– — of carbon content 5	200
– pseudoasymmetric —	205
alkyl ligand	242
– chiral —	207
alkylamine	42
allene	341
– — skeleton	190, 261, 341, 358
– stereochemical notation for —	384
– tetramethyl- —	165
allene promolecule	
– achiral and chiral —	190
alternating group	
– — $A^{[3]}$	206
– — $A^{[4]}$	236
– — $A^{[5]}$	168
– — $A^{[n]}$	233
– — of degree 3	206
ammonia	165
angle	58
– — of Cl—C—Cl	81
angle bracket	38, 228, 270
anisomeric	41
antipode	11
approach	
– Fujita's stereoisogram —	23, 158, 286, 313, 341
– Fujita's USCI —	22, 336
– USCI —	22
arrow	
– double-headed —	273
ascleral	369
asclerality	343
– sclerality/—	285
asymmetric	2, 15

- carbon 258
 - center 194
 - synthesis 95
 - atom
 - with valency 2 or more 145
 - with valency 3 or more 145
 - asymmetric — 365
 - asymmetric carbon — 233, 260
 - bromine — 87
 - carbon — 291
 - central — 375
 - chlorine — 78, 87
 - divalent oxygen — 148
 - fluorine — 96
 - hydrogen — 200
 - oxygen — 71
 - phosphorus — 85, 239
 - stereogenic — 233
 - attribute
 - geometric — 49
 - three pairs of — 366
 - three pairwise — 284
 - attributive term 16, 17, 98, 106
 - Avogadro 407
 - axial position 85
 - axis
 - chirality — 161
 - pseudoasymmetric — 351
 - rotation — 56, 59
 - rotoreflexion — 59
 - $S_{4(3)}$ — 58
 - stereogenic — 25
 - three-fold (rotation) — 56
 - three-fold — 59
 - two-fold — 60, 105
 - x - y -, or z - — 59
- B**
- barrier
 - mathematical — 410
 - stereochemical — 410
 - Bentley 94
 - benzene 44
 - dibromo- — 1, 43
 - symmetry-itemized enumeration of — 166
 - Berry 169
 - Berzelius 5
 - bicentroid 213
 - bicentroidal
 - 3D-tree 194, 213
 - bicentroidal alkane
 - as graph 228
 - as steric isomer 224
 - bicentroidal tree 109, 212, 228
 - three-dimensional — 177
 - bicyclo[1.1.1]pentane
 - 1-aza- — 245, 250
 - bidentate 168
 - Biggs 212
 - bijection 42
 - binuclear
 - promolecule 177
 - biphenyl
 - sterically-hindered — 53
 - bipyramidal
 - trigonal — complex 84
 - trigonal — skeleton 84
 - Blair 193
 - block
 - of G_C -symmetry 101
 - C_2 - — 103
 - C'_2 - — 102
 - D_2 - — 98
 - G_i - — 102
 - G_j - — 95
 - shadowed — 99
 - bond
 - multiplicity 38
 - rotation 165, 409
 - coordination — 72
 - delocalized double — 1
 - double — 12
 - oxime double — 13
 - single — 409
 - book
 - interdisciplinary — 410
 - brace 9
 - bracket
 - angle — 8, 38, 270
 - floor — 248
 - square — 10, 37, 248, 249
 - branch 212
 - branching
 - internal — 177, 194
 - bridge 144, 167, 411

- bridge position 75
 bridgehead 144, 167
 bridgehead position 75
 Brocas 84, 131
 bromine 78, 87
 Burnside 118, 173, 291
 butan-2-yl ligand 205
 butanol
 – isomeric — 6
- C**
- C/A*-convention 384
C/A-descriptor 384
 cage-shaped
 — molecule 167
 Cahn 93, 109
 Cahn-Ingold-Prelog (CIP) 239
 calculation
 – algebraic — 183
 – recursive — 204
 carbon
 – asymmetric — 2, 15
 caricature 411
 Cauchy 173
 Cayley 193
 center
 – asymmetric — 177, 194
 – asymmetric carbon — 158
 – chirality — 25, 158
 – pseudoasymmetric — 25, 177, 194
 – *RS*-stereogenic — 25
 – *RS*-stereoisomeric — 25
 – stereogenic — 25
 centroid 213
 centroidal
 — 3D-tree 194, 213
 centroidal alkane
 — as graph 227
 — as steric isomer 224
 — \hat{S}_k 224
 centroidal tree 109, 212, 227
 – three-dimensional — 177
 change
 – conformational — 409
 characteristic monomial 22
 characteristic-monomial method 405
 ChemDraw 410
 ChemSketch 410
 chiral 369
 chiral aspect
 — of absolute configuration 367, 377
 chiral center 112, 258
 chiral label 379
 — abandoned 379
 chiral labelling
 – hypothetical — 100
 chiral ligand
 – disregard of — 233
 chiral reagent 387
 chiral subgroup
 – maximum — 62, 90
 chiral synthesis 95
 – single-step — 100
 chirality 2, 16, 23
 — (un)faithfulness 25
 — and enantiomeric relationship 367
 — as purely-geometric concept 113
 — axis 161
 — center 158, 365
 — element 365
 — fittingness 22
 — for type I, II, or III 335
 — unit 365, 379
 —/achirality 285
 chirality faithfulness 127
 chirality fittingness 88, 107, 131, 151, 254,
 267, 387
 — of a hemispheric cycle 180
 — of a hemispheric orbit 92
 — of a homospheric cycle 178
 — of a homospheric orbit 89
 — of an enantiospheric cycle 178
 — of an enantiospheric orbit 91
 — of *d*-cycle 178
 — of $\hat{G}/(\hat{G}_i)$ -orbit 295
 — of orbit 178
 chirality rule
 — abandoned 378
 chirality sense
 – alternation of — 66
 – no alternation of — 65
 – no reverse of — 239
 – opposite — 54, 91, 275
 – reverse of — 236
 chirality unit

- abandoned 379
- chirality-faithful 380, 382
- type-III 381
- chirality-unfaithful 382
- type-III 383
- type-V 381
- chirality/achirality 366
- chirogenic 107
- chirogenic site 101
- C_2 - — 103, 106
- C'_2 - — 102
- enantiotopic — 105
- G_C - — 101, 102
- G_I - — 101, 102
- H - — 101
- homotopic — 105
- presence of — 101
- chirotopic 26, 106
- chlorine 78, 87
- Cl
 - for gross enumeration 257, 263
 - Cl-CF 181, 194
 - for achiral planted promolecules 198
 - for achiral promolecules 188
 - for $C_{3v\hat{\sigma}I}$ 302
 - for enantiomeric pairs 188
 - for enantiomeric planted promolecules 199
 - for five types 301
 - for gross enumeration 303, 334
 - for planted promolecule 196
 - for *RS*-stereoisomeric group 304
 - for steric isomers 187, 202
 - for T_d 183
 - for type-itemized enumeration 332, 361
 - under D_{2d} 190
 - under T_d 190
- CIP system 16, 24, 93, 239
- cis* site 233
- cis/trans*-isomeric 45
- class
 - equivalence — 17, 35
- classification
 - of organic reaction 169
- coalescence 249
- coefficient 132
- coincidence 25
- color photography 410
- comparison
 - between D_{2d} and $D_{2d\hat{\sigma}I}$ 363
 - between T_d and $T_{d\hat{\sigma}I}$ 334
 - between $T_{\hat{\sigma}}$ and $T_{d\hat{\sigma}I}$ 336
- complex
 - hexacoordinate — 233
 - inorganic — 168
 - octahedral — 22
 - square planar — 169
 - trigonal bipyramidal — 84, 169
- composition
 - A^2B^2 344
 - A^2BX 319, 400
 - $A^2p\bar{p}$ 375, 398
 - A^3 280
 - $A^3\bar{p}$ 258
 - A^3p 258
 - A^4 349
 - ABp 284
 - ABp^2 317, 345, 374, 396
 - $ABp\bar{p}$ 320
 - $ABp\bar{p}$ 162, 258, 264, 270, 351, 373, 402
 - ABX 248, 280
 - ABX^4 250
 - $ABX\bar{p}$ 258
 - $ABXp$ 158, 258, 318, 373, 381
 - $ABXp$ or $ABX\bar{p}$ 159
 - $ABXY$ 158, 258, 267, 270, 315, 343, 371
 - Ap^2 283
 - $Ap\bar{p}$ 249, 283
 - $C^kN^lO^m$ 164
 - \bar{p}^4 136
 - p^4 136
 - $p\bar{p}q\bar{q}$ 317, 360
 - PX^3YZ 84
 - W_{θ} 140, 150, 182, 298
 - X^2Y^2 133
 - X^3Y 132
 - X^4 132
 - $X^4p\bar{p}$ 250
 - $X^lY^mZ^n$ 169
 - $X^xY^yZ^z p^p\bar{p}^{\bar{p}}$ 148
 - two kinds of — 408
- compound
 - non-rigid — 409
- concept
 - 2D-based — 3
 - 3D-based — 3, 47
 - intermediate — 311

- ITS — 169
 - purely-geometric — 112
 - well-defined simple — 411
 configuration 51, 53, 365
 - absolute — 53, 365
 - edge — 168
 - relative — 53, 365
 configurational isomer 51
 conformation 53, 365
 - eclipsed — 291
 - staggered — 291
 confusion
 - — between T_d and $T_{\bar{\sigma}}$ 339
 - — in modern stereochemistry 2
 - — on 'prochirality' 25, 92
 - unconscious — 4
 conjugacy 116
 conjugate 81, 262
 connectivity 38, 53
 conservation
 - — of chirality/achirality 55
 - — of orbits 87
 constitution 6, 38, 53
 constitutional isomer 40, 51, 210, 228, 230
 - conventional definition of — 6
 constitutionally-anisomeric
 - — relationship 40, 45
 constitutionally-isomeric
 - — relationship 40, 45
 convention
 - misleading — 237
 corona 194
 correlation diagram
 - — of stereoisograms 28, 406
 correspondence
 - one-to-one — 42
 coset 62, 313
 - a set of — C_{2v}/C_2 117
 - double — 122
 coset decomposition 64, 115, 217, 313, 341
 - — C_{2v} by C_2 117
 - — of $C_{3v\bar{\sigma}\bar{I}}$ 278
 - — of $D_{2d\bar{\sigma}\bar{I}}$ 342
 - — of $T_{d\bar{\sigma}\bar{I}}$ 313
 coset representation 116, 174, 290
 - — $C_1(/C_1)$ 81
 - — C_{2v}/C_1 69, 96
 - — C_{2v}/C_2 117
 - — C_{2v}/C_{2v} 72
 - — C_{2v}/C'_s 71
 - — C_{3h}/C_s 277
 - — $C_{3\bar{I}}(/C_{\bar{I}})$ 275
 - — $C_{3\bar{\sigma}}(/C_1)$ 245
 - — $C_{3\bar{\sigma}}(/C_{\bar{\sigma}})$ 240
 - — C_{3v}/C_1 245
 - — C_{3v}/C_s 195, 240
 - — $C_{3v\bar{\sigma}\bar{I}}(/C_{s\bar{\sigma}\bar{I}})$ 294
 - — $C_s(/C_1)$ 81, 87, 108
 - — $C_s(/C_s)$ 87
 - — D_{2d}/C_1 74
 - — D_{2d}/C_{2v} 68
 - — D_{2d}/C_s 67, 88, 185, 261, 341
 - — D_{2d}/D_{2d} 68
 - — $D_{2d\bar{\sigma}\bar{I}}(/C_{s\bar{\sigma}\bar{I}})$ 342, 355
 - — D_{2h}/C_1 266
 - — D_{2h}/C'_{2v} 69
 - — D_{2h}/C'_h 265
 - — D_{2h}/C''_s 68, 186, 265
 - — $D_{2\bar{\sigma}}(/C_{\bar{\sigma}})$ 341
 - — D_{3h}/C_s 73
 - — D_{4h}/C'_{2v} 69, 169
 - — D_{4h}/C_s 74
 - — D_{6h}/C'_{2v} 73
 - — $D_{\infty h}/C_{\infty v}$ 109, 217
 - — $G(/G_i)$ 79, 89, 116, 118
 - — $G_j(/H_k^{(j)})$ 131
 - — $G_{\bar{\sigma}}(/G_{\bar{\sigma}(i)})$ 388
 - — $K(/K')$ 217
 - — $O(/C_4)$ 235
 - — of C_3 206
 - — $O_h(/C'_{2v})$ 168
 - — $O_h(/C_{3v})$ 73
 - — $O_h(/C_{4v})$ 72, 168, 235
 - — $O_h(/D_{3d})$ 313
 - — $T(/C_3)$ 236
 - — $T_d(/C_{3v})$ 60, 66, 67, 75, 78, 183, 236, 252
 - — $T_d(/C_s)$ 75
 - — $T_{d\bar{\sigma}\bar{I}}(/C_{3v\bar{\sigma}\bar{I}})$ 313, 326, 370
 - — $T_h(/C_2)$ 105, 106
 - — $T_h(/C_3)$ 105
 - — $T_{\bar{\sigma}}(/C_{3\bar{\sigma}})$ 253, 390
 - degree of — 67
 - enantiosphericity of — 95
 - set of — 116
 - set of — (SCR) 67, 82
 - subduction of — 22, 122, 131, 132
 - sum of — 123, 293

- counter-example 25
 Couper 1
 criterion
 — general — 102
 — membership — 98, 99
 — single — 404
 — single — for *pro-R/pro-S*-descriptor 393
 — single — for *R/S*-stereodescriptor 377
 — substitution — 99
 — symmetry — 98
 Crum Brown 1
 cubane 167
 — derivative 144, 152
 — skeleton 405
 cycle
 — 1- — 118, 291
 — 2- — 179
 — 3- — 57
 — 4- — 58
 — *d*- — 178
 — enantiospheric — 178
 — hemispheric — 178
 — homospheric — 178
 — product of — 56
 — sphericity of — 178, 194
 cycle index 241
 — with chirality fittingness (CI-CF) 194
 — Fujita's — with chirality fittingness (CI-CF) 181
 — partial — 405
 — partial — with chirality fittingness (PCI-CF) 150, 298
 — partial — without chirality fittingness (PCI) 151
 — Pólya's — 131, 176
 — subduced — 405
 — subduced — (SCI) 139
 — subduced — (SCI-CF) 139, 297
 — unit subduced — 127
 cycle structure 304
 — (2^2) 179
 cycle term 174, 241, 266, 269
 cyclic group 22
 cyclic subgroup 119
 cyclobutane 13
 — 1,3-dichloro- — 365
 — stereoisomer of — 406
 cyclohexane 165, 409
 — dibromo- — 3
 — cyclopentadienyl 169
 — cyclophane
 — $[2_6](1,2,3,4,5,6)$ - — 166
 — cyclopropane
 — — skeleton 277
 — cyclopropylidene- — 266
- ## D
- de Bruijn 233
 decomposition
 — coset — 115
 degree
 — of coset representation 67
 derivation
 — algebraic — 67
 — diagrammatic — 67
 — inductive — 167
 — subductive — 167
 derivative
 — sterically hindered — 168
 — trigonal pyramidal — 298
 desymmetrization step
 — single — 395
 diagonal direction 277
 diastereoisomer 11, 250
 diastereoisomerism 11, 250
 diastereomer 11, 40, 250, 404
 — conventional definition of — 11
 diastereomeric 45, 91
 — relationship 40
 diastereotopic 93, 404
 dichotomy
 — between enantiomers and diastereomers 11, 249, 368
 — misleading — 25
 difference
 — between prochirality and *pro-RS*-stereogenicity 388
 dimethyl ether 39
 dioxane
 — 1,3- — 166
 — 1,4- — 166
 diploid 200
 — hydrogen — 203
 diploid generator 204
 direction

- diagonal — 277
 - horizontal — 277
 - vertical — 277
 - dissymmetry 2
 - dodecahedrane 105, 167
 - double bond 12
 - delocalized — 1
 - oxime — 13
 - twist of — 269
 - double coset 122, 131
 - — representation 22
 - duality
 - — of the term 'isomeric' 50
 - dumbbell 217
 - — skeleton 169
- E**
- edge 168, 212
 - — substitution 170
 - orbit of — 405
 - edge configuration
 - enumeration of — 406
 - El-Basil 411
 - element
 - chirality — 365
 - symmetry — 59
 - elementary-superposition 405
 - — method 164
 - Eliel 11
 - enantiomer 11, 239, 366, 404
 - — and quadruplet 306
 - conventional definition of — 10
 - geometric — 12
 - enantiomeric 100, 236
 - — relationship 23, 36, 285, 369
 - — relationship (coalescence) 249
 - — relationship and chirality 367
 - enantiomerism 11, 250
 - geometric — 270
 - enantiomorph 233
 - enantiospheric 106
 - — as an attributive term 98
 - — $C_{2v}(/C_1)$ -orbit 132
 - — cycle 178
 - — $G(/G_i)$ -orbit 90
 - — orbit 89, 105, 107, 387, 398, 400
 - enantiospheric orbit
 - chirality fittingness of — 91
 - eight-membered — 98
 - four-membered — 96
 - two halves of — 95
 - two-membered — 91
 - enantiosphericity 89
 - — of coset representation 95
 - extended — 295
 - prochirality due to — 400
 - enantiotopic 93, 106, 404
 - — as a relational term 98
 - definition of — 98, 99
 - general definition of — 102
 - membership criterion of — 98
 - relational term — 387
 - symmetry criterion of — 98
 - enantiotopic relationship 100
 - entity
 - molecular — 36
 - enumeration
 - — of alkane 177, 193
 - — of edge configurations 406
 - — of Kekulé structures 406
 - — of monosubstituted alkane 177
 - — of organic reactions 405
 - — of quadruplets 28
 - — under point group 334, 362
 - — under *RS*-permutation group 336
 - graph — 22
 - gross — 22
 - itemized — 141
 - recursive — 200
 - symmetry-itemized — 22, 405
 - symmetry-itemized — under $T_{d\hat{\sigma}i}$ 329
 - symmetry-itemized — under $T_{\hat{\sigma}}$ 254
 - type-itemized — 301, 332, 361
 - epimerization 4, 26, 251
 - equality symbol
 - absence of — 284, 318
 - diagonal — 282, 315, 343
 - horizontal — 284, 317, 345
 - vertical — 283, 320, 350
 - equation
 - functional — 202
 - mathematical — 410
 - equatorial position 85
 - equivalence class 17, 35, 63, 78, 106, 368
 - — by $C_s(/C_s)$ 249

- by $C_{\bar{\sigma}}/C_1$ 249
 - of isomers 39
 - of isoskeletonomers 44
 - of stereoisomers 38
 - under D_2 or D_{2h} 267
 - under D_{2d} 264, 347
 - under $D_{2d}\hat{\sigma}_i$ 349
 - under D_{2h} 268
 - under $D_{2\bar{\sigma}}$ 264, 347
 - under T_d 261, 313
 - under $T_{\bar{\sigma}}$ 261, 313
 - importance of — 405
 - equivalence relationship 17, 35, 368, 405
 - Era of Fujita 411
 - ES method 22
 - ethane 291
 - ethanol 39
 - ether
 - cyclic — 48
 - dimethyl — 165
 - ethylene
 - skeleton 186, 265
 - face of — 166
 - *Z/E*-isomer of — 13
 - ex-achiral 295
 - ex-chiral 295
 - exponent 140
 - expression
 - diagrammatic — 235
 - extended superposition 22
 - extended-superposition method 405
- F**
- factor group 286
 - $C_{3v}\hat{\sigma}_i/C_3$ 286
 - K 217
 - factorization 112
 - ferrocene 169
 - Fischer 54
 - fixation 321
 - flexibility 409
 - flipping
 - ring — 165, 409
 - floor bracket 248
 - flowchart 17, 18, 407
 - revised — 46
 - fluorene
 - 9H — 44
 - fluorine 78, 96
 - Flurry 84
 - formation
 - mirror-image — 71, 379
 - formula
 - 2D-structural — 1, 42
 - 3D-structural — 2
 - condensed structural — 42
 - constitutional — 6
 - molecular — 38
 - rational — 42
 - stereochemical — 6
 - structural — 1, 410
 - four-group
 - Klein — 286
 - FPM 134
 - for itemized enumeration 142
 - alternative form of — 136
 - FPM method 22, 405
 - of Fujita's USCI approach 143
 - procedure of — 143
 - FPV 120, 123, 135, 291
 - framework group 83
 - Frankland 1
 - Frobenius 173
 - Fujita 21, 23, 84, 89, 95, 106, 107, 109, 116, 122, 131, 169, 174, 177, 193, 194, 206, 234, 239, 273, 366, 378, 396
 - fullerene
 - C_{60} 406
 - adduct of — 168
 - symmetry-itemized enumeration of — 168
 - function
 - for mode of derivation 132
 - generating — 132, 136
 - ligand-inventory — 142, 143, 145, 151, 153, 196, 242, 256, 257, 263, 299
 - orbital — 36
 - functional equation 202
 - $a(x)$ 203
 - $\hat{A}(x)$ 214
 - $\tilde{A}(x)$ 219
 - $\hat{B}(x)$ 214
 - $\tilde{B}(x)$ 219
 - $b(x)$ 206
 - $\hat{C}(x)$ 214
 - $\tilde{C}(x)$ 219

- $c(x^2)$ 204
 --- $\tilde{R}(x)$ 227
 --- $\tilde{R}(x)$ 229
 --- $r(x)$ 209
 --- $\hat{S}(x)$ 224
 --- $\tilde{S}(x)$ 226
 --- $s(x)$ 210
- G**
- general criterion
 --- for enantiotopic 102
 generating function 132, 136
 --- $\tilde{A}(x)$ 219
 --- $A(x)^{(\Gamma)}$ 222
 --- $\tilde{B}(x)$ 219
 --- $B(x)^{(\Gamma)}$ 222
 --- $\tilde{C}(x)$ 219
 --- $C(x)^{(\Gamma)}$ 222
 --- for achiral planted promolecules 199
 --- for adamantan-2-ones 163
 --- for allene derivatives 160
 --- for \hat{A}_{θ_i} 298
 --- for C_3 310
 --- for $C_{3\bar{\sigma}}$ 308
 --- for C_{3v} 305
 --- for $D_{2d\bar{\sigma}\hat{I}}$ 358
 --- for diploids 202
 --- for enantiomeric planted promolecules 199
 --- for five types 303
 --- for gross enumeration 184–186, 257, 263, 304
 --- for PCI-CF 150, 300
 --- for PCI-CFs of oxiranes 153
 --- for planted promolecules 197
 --- for SCl-CFs of adamantan-2-ones 145
 --- for $T_{d\bar{\sigma}\hat{I}}$ 329
 --- for tetrahedral derivatives 155
 --- for $T_{\bar{\sigma}}$ 256
 --- for $\hat{T}_{\theta K}$ 302
 --- for type-itemized enumeration 333, 361
 --- $\tilde{R}(x)$ 227
 --- $\tilde{R}(x)$ 229
 generator 292
 - achiral structure — 203
 - diploid — 204
 - graph — 209
 - steric-isomer — 206, 210
 geometric
 --- attribute 18, 49
 --- concept 93
 --- enantiomer 12, 270
 --- isomer 270
 global symmetry 26
 --- $T_{d\bar{\sigma}\hat{I}}$ 370
 glossary
 --- of IUPAC 365
 glutaric acid
 - 2,3,4-trihydroxy- — 78, 107
 - 2,4-dihydroxy- — 111
 - achiral 2,3,4-trihydroxy- — 320, 381
 - chiral 2,3,4-trihydroxy- — 317
 glyceraldehyde
 - D-(+)- — 93, 391
 glycerol 110
 graph 1, 41, 193, 209, 210
 --- theory 1, 21
 - matching of — 166
 - non-cyclic — 212
 - perfect matching of — 168, 406
 graph generator 209
 gross enumeration
 --- of cubanes 405
 --- under *RS*-permutation group 241
 --- under $T_{\bar{\sigma}}$ 257
 - generating function for — 184
 group 54
 --- hierarchy 23, 407
 --- theory 54
 - achiral — 98
 - automorphism — 131
 - chiral — 244
 - cyclic — 22
 - cyclic achiral — 178
 - cyclic chiral — 180
 - factor — 286
 - functional — 9
 - hydroxyl — 12
 - identity — 116
 - isoskeletal — 24, 407
 - ligand-reflection — 275, 341
 - maximum chiral — 90
 - permutation — 233
 - point — 56, 143
 - pseudo-point — 165, 409

– <i>RS</i> -astereogenic —	244
– <i>RS</i> -permutation —	235
– <i>RS</i> -stereogenic —	244
– <i>RS</i> -stereoisomeric —	23, 277

H

halogen	78
Hanson	92, 109
Harary	212
hardware	141
Hässelbarth	131
Heavens of Fujita	411
Helmchen	365, 378
hemispheric	
— cycle	178
— orbit	89
hemispheric orbit	
– chirality fittingness of —	92
hemisphericity	89
– extended —	295
Henze	193
hept-2-ene	
– bicyclo[2.2.1]- —	44
heptane	
– 3,4,5-trimethyl- —	223
heptane-3,5-dithiol	
– 4-(2-bromoethenylidene)- —	351
hexacoordinate	
— complex	233
hierarchy	311
— of subgraph	169
– group —	407
hindrance	
– steric —	168
Hirschmann	94
holantimer	23, 366
holantimeric	236
— relationship	23, 277, 285, 369
— relationship and sclerality	367
homomeric	56, 62
— relationship	62
— under ligand-reflection group	275
— under <i>RS</i> -permutation group	245
— under <i>RS</i> -stereoisomeric group	279
homospheric	
— cycle	178

— orbit	89, 398, 400
homospheric orbit	
– chirality fittingness of —	89
homosphericity	89
– extended —	295
homotopic	105
horizontal direction	277
Hosoya	166
— index	166, 406
hydroxymethyl	110

I

ICM	135, 141, 331
– alternative —	138
icosahedron	168
ICV	141
identity element	287
identity group	116
identity operation	276
Ihde	1
imaginary transition structure	169, 406
index	
– cycle —	176
– Hosoya —	166
– partial cycle —	150
– sphericity —	127, 180
– subduced cycle — (SCI)	139
– subduced cycle — (SCI-CF)	139, 297
– type —	286, 378
– unit subduced cycle —	22
Ingold	93, 109
inner structure	
— of type-I promolecule	371
— of type-II promolecule	374
— of type-III promolecule	373
— of type-IV promolecule	375
— of type-V promolecule	373
intransitive	140
inventory	
– ligand —	132, 135, 140, 153
inverse	
— element	64
— mark table	119
— matrix	119, 121
— of mark table	292
– lower-triangular — mark table	292

- inverse mark table
 — of $C_{3v\hat{\sigma}I}$ 292
 — of $D_{2d\hat{\sigma}I}$ 355
 — of $T_{d\hat{\sigma}I}$ 325
 inversion 2, 53
 – N- — 165
 irreducible representation
 – restriction of — 122
 isobutyl 5
 isomer 39, 187
 — number 21, 28
 – 3D-structural — 51, 187, 207
 – *cis*- — 4
 – configurational — 51
 – constitutional — 3, 40, 51
 – conventional definition of — 6
 – conventional definition of constitutional — 6
 – geometric — 270
 – geometrical — 11
 – positional — 3, 9, 42
 – steric — 51, 187
 – *trans*- — 4
 isomeric
 — relationship 38
 – constitutionally — 5
 isomerism 5, 365
 – permutational — 251
 isomerization
 – *cis/trans*- — 4, 13
 – *syn/anti*- — 12
 isometry 19
 isomorphic
 — $S^{[4]}$ and T_d 59
 isomorphism 5
 — between O_h and $T_{d\hat{\sigma}I}$ 325
 isopentyl 5
 isoskeletal group 24, 407
 isoskeletomer 43
 – set of — 407
 isoskeletomeric 344
 isotactic 5
 isotherm 5
 isotope 5
 isotropic 5
 ITS 169, 406
 — concept 169
 – subgroup of — 169
- J**
- Jordan 109, 212
- K**
- Kekulé 1, 42
 Kelvin 2
 ketone 49
 Klein 286
- L**
- label
 – chiral — 379
 – lowercase — 382
 – *RS*-stereogenic — 379
 – uppercase — 382
 labelling
 – hypothetical chiral — 100
 lattice
 – desymmetrization — 168
 Le Bel 2, 407
 lemma
 – Burnside's — 173
 – Cauchy-Frobenius — 173
 ligancy
 — 4 67
 — 6 72
 — 8 73
 ligand 54, 131
 — inventory 153
 – methyl — 165
 – mobile — 165
 – mono-valent — 200
 – phenyl — 165
 ligand inventory 132, 135, 140, 145, 176, 182, 280
 ligand reflection 196, 274, 278, 369
 – identity — 237
 ligand-inventory
 — function 151
 ligand-reflection group 275
 — $C_{3\hat{I}}$ 275, 277
 — $D_{2\hat{I}}$ 341

- $G_{\hat{f}}$ 278
 — $T_{\hat{f}}$ 313
 Lloyd 212
 LM-numbered skeleton 275, 277
 local symmetry 26
 — $C_{3v\hat{\sigma}\hat{t}}$ 370
 lone pair 239
 lowercase
 — label 381, 382
- ## M
- mandala 410
 manual
 — on-line — 410
 Maple 141, 183, 204, 219
 — programming code 167, 215, 219
 mark 118
 — tables of — 291
 mark matrix 120
 mark table 118, 131, 144, 291, 405
 — of C_{2v} 118
 — of $C_{3v\hat{\sigma}\hat{t}}$ 291
 — of D_{3d} 291
 — inverse — 144, 292
 — inverse — $M_{C_{2v}}^{-1}$ 122
 — inverse — $M_{D_{2d\hat{\sigma}\hat{t}}}^{-1}$ 355
 — inverse — M_{G}^{-1} 119, 143
 — inverse — $M_{G_j}^{-1}$ 124
 — inverse — M_T^{-1} 325
 — inverse — of C_{2v} 119
 — lower-triangular — 292
 markaracter method 22, 405
 matching
 — of graph 166
 — polynomial 166, 167, 406
 Mathematica 141
 matrix
 — fixed-point — (FPM) 134, 142
 — inverse — 121
 — isomer-counting — (ICM) 135, 141, 331
 — lower triangular — 120, 121
 — mark — 120
 — type-enumeration — 301
 maximum subgroup 277
 McCasland 233
- Mead 131
 membership criterion
 — for enantiotopic 98, 99
meta 1
 methane 44, 78
 — bromochloro- — 77, 81
 — bromochlorofluoro- — 81, 92
 — chloro- — 79
 — dichloro- — 81
 methanol 39
 method
 — characteristic-monomial — 22, 405
 — double-coset-representation — 22, 405
 — elementary-superposition (ES) — 22
 — elementary-superposition — 164, 405
 — extended-superposition — 22, 405
 — fixed-point-matrix (FPM) — 22, 28, 405
 — Fujita's prolignand — 22
 — markaracter — 22, 405
 — Otter's — 193
 — partial-cycle-index (PCI) — 22, 28, 405
 — partial-superposition — 165, 405
 — restricted-fixed-point-matrix (RFPM) — 167, 406
 — restricted-partial-cycle-index (RPCI) — 167, 168, 406
 — restricted-subduced-cycle-index (RSCI) — 166, 406
 — RSCI — 166
 methyl
 — ligand 165
 mirror image 2, 57, 91, 250
 — global — 57
 — local — 57
 mirror plane 27, 55, 57, 59, 81
 — $\sigma_{d(1)}$ 57
 — a pair of — 59
 — a perpendicular set of — 59
 mirror-image formation 71
 mirror-numbered
 — skeleton 57, 195, 273
 Mislow 11, 18, 94, 106, 233, 251
 mixture
 — racemic — 251
 model
 — prolignand-promolecule — 21, 53, 77, 165, 236
 molecular
 — entity 36

— formula	38
molecular symmetry	
— systematic classification of —	131
molecule	77
— CHFCIBr	96
— of G_j	131
— acyclic —	109
— cage-shaped —	167
— derivation of —	77
— highly symmetric —	405
— matched —	88
— mismatched —	56, 87
— non-rigid —	165
— symmetry-interesting —	405
monodentate	168
monograph	
— Fujita's —	119, 169, 182, 292
Morris	11
multiplication table	117
— of C_{2v}	71
— of T_d	60
multiplicity	120
— of coset representation	79
— of $G(/G_i)$ -orbit	141
— vector	121
— vector (MV)	124
— bond —	38
MV	124

N

N-inversion	165, 409
nitrogen	144
nomenclature	
— stereochemical —	286
non-redundant set	
— of subgroups	62
normal subgroup	
— maximum —	278
North	11
notation	
— graphic —	1
— SCR —	166, 169
— stereochemical —	384
number	
— of orbits	173
numbered skeleton	195, 236, 273

O

octahedral	
— skeleton	168, 235
octahedral complex	22
— enumeration of —	168
— inorganic —	72
— stereochemical notation for —	384
octahedron	
— regular —	406
OMV	145
operation	
— (roto)reflection —	56
— \hat{I}	274
— of $D_{2d\bar{\sigma}\hat{I}}$	342
— of T_d	60
— of $T_{d\bar{\sigma}\hat{I}}$	313
— symmetry —	56
optical activity	2
orbit	35, 63, 78, 106
— among promolecules	138
— Δ_i	173
— due to global and local symmetries	64
— of bonds	168
— of edges	405
— of vertices	405
— within a promolecule	138
— $C_1(/C_1)$ -	371, 402
— $C_j(/C_j)$ -	371
— conservation of —	87
— $C_s(/C_1)$ -	87, 96, 398, 400
— $C_s(/C_s)$ -	81, 87, 398, 400
— $C_{\bar{\sigma}}(/C_1)$ -	398, 400
— $C_{\bar{\sigma}}(/C_{\bar{\sigma}})$ -	398, 400
— $C_{s\bar{\sigma}\hat{I}}(/C_{\bar{\sigma}})$ -	400
— $C_{s\bar{\sigma}\hat{I}}(/C_{s\bar{\sigma}\hat{I}})$ -	400
— D_{2d}/C_1 -	98
— D_{3h}/C_{3v} -	85
— enantiospheric —	89, 105, 107
— hemispheric —	89
— homospheric —	89
— importance of —	405
— multiplicity of —	173
— number of —	173
— procedure for determining —	80
— RS -enantiotropic —	390, 391
— RS -hemitropic —	390, 402
— RS -homotropic —	390
— sphericity of —	178

- $-T_d(/C_{3v})-$ — 88
orbital 36
orbital function 36
order 254
organic reaction
— classification of — 169
— enumeration of — 405
ortho 1
Otter 193
overbar 66, 196, 236
oxathiane
— 1,4- — 166
oxetane 48
oxime
— *Z/E*-isomer of — 12
oxirane 48, 174, 179, 407
— ring 71
— skeleton 96, 132, 152
— 2,2-dimethyl- — 97
— *cis*-2,3-dimethyl- — 97
— stereochemical notation for — 384
oxygen 71, 144
- P**
- pair
— reaction — 170
Paquette 105
para 1
paradigm shift 311, 407
paradox
— organic chemistry — 411
parenthesis
— bold — 39
partial cycle index
— with chirality fittingness (PCI-CF) 150, 298
— without chirality fittingness (PCI) 151
partial-superposition 405
— method 165
partition 36, 140, 228, 230, 249
— $[\theta]$ 182, 298, 330
— seemingly parallel — 249
Pasteur 2
PCI 151, 405
— for $C_{3\bar{\sigma}}$ 307
— method 151
— for $T_{\bar{\sigma}}$ 256
PCI method 22, 405
— procedure of — 151
PCI-CF 150
— for adamantan-2-ones 163
— for allene derivatives 160
— for C_3 310
— for C_{3v} 305
— for $C_{3v\bar{\sigma}\hat{I}}$ 298
— for $D_{2d\bar{\sigma}\hat{I}}$ 355
— for *RS*-stereoisomeric group 298
— for $T_{d\bar{\sigma}\hat{I}}$ 327
— for tetrahedral derivatives 155
pentaerythritol 55, 87
pentan-3-ol
— 1-chloro-1-fluoro- — 381
pentane
— 2,3,4-trihydroxy- — 396
perfect matching
— of graph 168, 406
permutation 12, 56, 116, 134
— representation 134
permutation group 166, 174, 251
— of order 12 236
— of order 24 235
— without reflection 193
— enumeration under — 166
— *ZE*- — 269
permutation representation 174
— $\Lambda^{[\theta]}_{\mathbf{G}}$ 140
— $\mathbf{P}C_{2v}$ 76, 121
— $\mathbf{P}C_{3v}$ 79, 195
— $\mathbf{P}D_{2d}$ 76, 159, 185
— $\mathbf{P}D_{2h}$ 74
— $\mathbf{P}\hat{\mathbf{G}}$ 297
— $\mathbf{P}\mathbf{G}$ 79, 120, 139, 173, 176
— $\mathbf{P}T_d$ 75, 154, 183
— transitive — 66, 116
permutational isomerism 233, 251
phenyl
— ligand 165
philology
— chemical — 11
phosphine 239
— tertiary — 251
phosphorus 85, 239
photography
— color — 410
piperidine 166

- plane
 – a pair of mirror — 59
 – mirror — 55, 57, 59
 planted promolecule 195, 242
 – achiral — 200
 planted tree 194
 – three-dimensional — 177
 point
 – fixed — 57, 291
 point group 56, 143
 – — C_1 249, 315
 – — C_2 149
 – — C_{2v} 69, 149, 286
 – — C_3 149
 – — C_{3h} 149, 277
 – — C_{3i} 292
 – — C_{3v} 63, 149, 212
 – — C_5 149
 – — C_{5v} 149, 169
 – — C_s 55, 149
 – — D_2 149
 – — D_{2d} 55, 67, 74, 149, 261, 341, 347, 362
 – — D_{2h} 68, 149, 166, 265
 – — D_3 149
 – — D_{3d} 287
 – — D_{3h} 73, 149, 287
 – — D_{4h} 69, 74, 149, 342
 – — D_5 149
 – — D_{6h} 73, 149
 – — G 278
 – — I 149, 168
 – — I_h 105, 149, 167, 168
 – — integrated 273
 – — O_h 72, 73, 144, 149, 168, 235, 405
 – — S_4 149
 – — S_6 292
 – — T 63, 105, 149
 – — T_d 55, 149, 183, 236, 252, 313, 334, 370
 – — T_h 105, 149
 – maximum-chiral — 187, 309, 338
 – subgroup of — 60
 point-group symmetry
 – — of promolecule 55
 – global — 63, 89
 – local — 63, 89
 Pólya 21, 174, 193, 206
 Pólya's theorem 233
 – — of counting 174, 176
 polynomial
 – infinite — 203
 – matching — 166, 167, 406
 – Z-counting — 166, 167, 406
 Pople 83
 position
 – axial — 85
 – bridge — 75
 – bridgehead — 75
 – equatorial — 85
 – substitution — 54
 positional isomer 42
 Prelog 93, 109, 378
 Prelog's rule 98
 presumption
 – misleading — of modern stereochemistry 403
 primary 177
 priority sequence 378
 – tentative — 395
 prismane 22, 167
 – stereochemical notation for — 384
pro-R/pro-S-descriptor 25, 92, 93, 109, 388, 392
 – — by *pro-RS*-stereogenicity 393
 – assignability of — 398
pro-RS-stereogenicity 95, 388, 390, 396
 – — due to *RS*-enantiotropicity 400
 – — for textit*pro-R/pro-S*-descriptor 393
 probe stereoisogram 394
 – — of type I 401
 – — of type-III 402
 procedure
 – — for determining orbits 80
 – — for determining prochirality 95
 – — for Fujita's proligand method 183
 – — of FPM method 143
 – — of PCI method 151
 prochiral center 112
 prochirality 92, 387
 – — as geometric concept 95
 – — as purely-geometric concept 113
 – — due to enantiosphericity 400
 – — for faces of ethylene 166
 – — of *meso*-tartaric acid 108
 – global — 109
 – Hanson's — 93
 – local — 110
 – misleading interpretation of — 396

- polysemous definition of — 93
 - procedure for determining — 95
 - product
 - of cycles 56
 - of sphericity indices (PSI) 180
 - programming code
 - Maple — 167, 204, 215, 219
 - projection
 - Fischer-like — 54
 - proligand 22, 53, 77, 131, 195
 - inventory 256, 263
 - achiral — 77, 132
 - chiral — 135
 - disregard of chiral — 233
 - enantiomeric — 77
 - inner — 195
 - mirror-image — 237
 - proligand method 177, 410
 - for allene derivatives 184
 - for ethylene derivatives 186
 - for tetrahedral derivatives 183
 - Fujita's — 22, 174, 177, 194, 267, 304, 405
 - Fujita's — for achiral promolecules 189
 - Fujita's — for pairs of enantiomers 189
 - Fujita's — for steric isomers 187
 - Fujita's — of counting 182
 - promolecule 22, 54, 77
 - of G_j 131
 - binuclear — 177, 194
 - dumbbell-type — 110
 - planted — 195, 242
 - reference — 23
 - tentative — 395
 - tetrahedral — 313
 - trigonal pyramidal — 307
 - type-I, type-III, or type-V — 25
 - uninuclear — 177, 194
 - proof
 - for five types of stereoisograms 286
 - propane
 - 2,2-dimethyl- — 165
 - prototype
 - of a stereogenic atom 233
 - of permutational isomerism 251
 - pseudo-point group
 - \tilde{D}_{3h} 165
 - \tilde{D}_{6h} 165, 170
 - extended — 166
 - pseudoasymmetric 91, 379
 - alkyl ligand 205
 - axis 351
 - center 194, 259, 365
 - unit 365
 - pseudoasymmetry 16, 223
 - pseudorotation 2
 - Berry's — 169, 409
 - PSI 180, 304
 - construction of — 183, 185
 - pyrrolidine 44
- ## Q
- quadruplet 298
 - and enantiomer 306
 - and respective promolecule 310
 - and *RS*-diastereomer 308
 - of promolecules 23
 - of *RS*-stereoisomers 28, 366, 368, 370, 407
 - of type-III stereoisogram 347
 - enumeration of — 28
 - number of — \hat{A}_{θ_i} 298
 - type-I to type-V — 407
 - quantum chemistry 36
- ## R
- R/S*-stereodescriptor 16, 24, 93, 109, 239, 260, 365, 371
 - assigned by *RS*-stereogenicity 377
 - Raban 106
 - racemate group 251
 - racemic mixture 251
 - reaction
 - forward — 170
 - organic — 169
 - reverse — 170
 - reaction center graph
 - (RCG) 170
 - reaction graph
 - (RG) 170
 - basic — (BRG) 170
 - reaction pair 170
 - hexagonal — 170

- Rectus 378
 recursion 203
 recursive calculation 209
 – Maple code for — 204
 reflection 2, 56, 193, 236, 278, 369
 – global — 57
 – ligand — 196, 274, 278
 – local — 57
 reflection-invariant 382
 reflective
 – — nature 36
 regular representation 71, 102
 – — C_{2v}/C_1 71
 – — T_d/C_1 167
 relational term 17, 98, 106
 relationship
 – anisomeric — 47
 – constitutionally-anisomeric — 40, 47
 – constitutionally-isomeric — 40
 – diastereomeric — 40, 47
 – enantiomeric — 23, 36, 47, 249, 273, 285
 – enantiotopic — 100
 – equivalence — 17, 35
 – holantimeric — 23, 277, 285
 – homomeric — 62
 – isomeric — 38, 46
 – isoskeletal — 43, 46
 – *RS*-diastereomeric — 23, 239, 240, 249, 274, 285
 – skeletally-anisomeric — 43, 47
 – stereoisomeric — 38, 46
 – three — 284
 representation
 – coset — 116
 – irreducible — 122
 – permutation — 134
 – regular — 71
 – subduced — 122
 RFPM method 167, 406
 RG
 – hexagonal — 170
 ring
 – — flipping 165
 – benzene — 1
 – chair-form — 165
 – oxirane — 71
 rise
 – — from 2D to 3D 259
 Robinson 193
 root 200
 rotation 56
 – — axis 56, 59
 – bond — 165, 409
 – proper — 278
 – three-fold — 56
 rotoreflection 58
 – — $S_{4(3)}$ 58
 – four-fold — 58
 rotoreflection axis 59
 – four-fold — 60
 row vector
 – — of SCI-CF 152
 RPCI method 167, 168, 406
RS-astereogenic 244, 369
RS-astereogenic group 388
 – — $C_{3\bar{\sigma}}$ 390
 – — $T_{\bar{\sigma}}$ 390
RS-astereogenicity
 – *RS*-stereogenicity/— 285
RS-diastereomer 23, 239, 249, 366, 404
 – quadruplet and — 308
RS-diastereomeric 91, 236
 – — relationship 23, 239, 240, 285, 369
 – — relationship (coalescence) 249
 – — relationship and *RS*-stereogenicity 367
RS-diastereotopic
 – — proligand 404
 – — relationship 25, 392
RS-enantiotropic
 – — orbit 390, 391, 397, 398, 400
RS-enantiotropicity 390
 – pro-*RS*-stereogenicity due to — 400
RS-hemitropic
 – — orbit 390
RS-hemitropicity 390
RS-homotropic
 – — orbit 390, 398, 400
RS-homotropicity 390
RS-non-stereogenic 244
RS-numbered skeleton 240, 274
RS-permutation 237, 239, 240, 244, 278, 369, 379
RS-permutation group 235, 239, 244
 – — C_1 249, 317
 – — $C_{3\bar{\sigma}}$ 245
 – — $C_{3\bar{\sigma}}$ 240, 307
 – — D_{2h} 265, 266
 – — $D_{2\bar{\sigma}}$ 261, 341, 347

- $G_{\bar{\sigma}}$ 278, 388
 - integrated 273
 - $T_{\bar{\sigma}}$ 59, 252, 313, 336, 371
 - lack of — 251
 - *RS*-astereogenic — 244
 - *RS*-stereogenic — 244
 - RS*-permutation-group
 - symmetry 388
 - RS*-stereogenic 244, 369
 - carbon 261
 - center 25, 404
 - group 388
 - label 379
 - RS*-stereogenic aspect
 - of absolute configuration 367, 377
 - RS*-stereogenicity 23, 24, 234, 260
 - and *RS*-diastereomeric relationship 367
 - for type-I, type-III, or type-V 337
 - rule 378
 - /*RS*-astereogenicity 285, 366
 - RS*-stereoisomer 366
 - quadruplet of — 28
 - RS*-stereoisomeric
 - center 25, 406
 - term — 25
 - RS*-stereoisomeric group 23, 28, 235, 366
 - C_1 284
 - $C_{3v\bar{\sigma}\bar{I}}$ 277, 280, 287
 - $C_{\bar{I}}$ 282, 315
 - C_s 283
 - $C_{\bar{\sigma}}$ 284, 317
 - $D_{2d\bar{\sigma}\bar{I}}$ 341, 349
 - G 278
 - $T_{d\bar{\sigma}\bar{I}}$ 313, 370
 - RS*-stereoisomerism 235
 - RS*-tropicity 390
 - RSCI 166
 - RSCI method 166, 406
 - Ruch 131, 233
 - rule
 - Prelog's — 98
- S**
- sandwich 169
 - scheme
 - attributive — 17
 - relational — 17
 - Schönflies 84
 - Schönflies symbol 60
 - modified — 84
 - SCI 139, 405
 - SCI-CF 139, 144, 145, 297
 - for *RS*-stereoisomeric group 297
 - formal row vector of — 327
 - formal summation of — 149
 - scleral 369
 - scleral aspect
 - of absolute configuration 368
 - sclerality 23
 - and holantimeric relationship 367
 - /asclerality 285, 366
 - SCR 67, 82
 - SCR notation 166, 169
 - of Methodology 1 82, 84
 - of Methodology 2 83, 84
 - Fujita's — 84, 85
 - secondary 177
 - self-enantiomer 37
 - self-enantiomeric
 - (or achiral) 49
 - relationship 36, 369
 - self-holantimeric
 - relationship 369
 - self-isoskeletomeric 43
 - self-*RS*-diastereomeric
 - pair 258
 - relationship 369
 - set
 - Δ 173
 - Sheehan 131
 - SI
 - assignment of — 185
 - Siegel 18, 94, 106, 233, 251
 - single bond 409
 - single criterion
 - by *RS*-stereogenicity 377
 - single-step
 - conversion by *RS*-permutation 391
 - Sinister 378
 - site
 - symmetry 84
 - chirogenic — 101
 - skeletally-anisomeric 43
 - skeleton
 - of G 131

- of I_h 105
- of ligancy 4 67, 158
- of ligancy 6 72
- of ligancy 8 73
- 1-azabicyclo[1.1.1]pentane — 245
- adamantan-2-one — 75, 121
- adamantane — 75
- adamantane-2,6-dione — 75, 98
- allene — 67, 190, 261, 341, 358
- benzene — 43, 73
- bicentroidal — 228
- butene — 46
- centroidal — 228
- cubane — 73, 167, 405
- cyclobutane — 46, 74
- cyclopropane — 46, 73, 277, 291
- cyclopropylidencyclopropane — 266
- Dewar-benzene — 43
- dicyclopropylidenemethane — 74
- dodecahedrane — 105
- dumbbell — 108, 169, 217
- ethane — 291
- ethylene — 45, 68, 186, 265
- homomeric — 314
- ligand-mirror (LM)-numbered — 315, 343
- LM-numbered — 275, 277
- mirror-numbered — 57, 195, 236, 273, 314, 343
- molecular — 44
- naphthalene — 74
- numbered — 57, 132, 195, 236, 273
- octahedral — 72, 168, 235
- oxetane — 48
- oxirane — 48, 69, 96, 132, 152, 174
- phosphine — 239
- prismane — 43, 73, 167
- reference-numbered — 314, 343
- rigid — 53
- RS-numbered — 240, 274, 314, 343
- square planar — 69, 169
- square pyramidal — 409
- stereo- — 54
- tetrahedral — 23, 55, 67, 183, 190, 252, 313
- tetrahydrofuran — 48
- trigonal bipyramidal — 84
- trigonal pyramidal — 195, 239, 273
- software 141
- scientific — 410
- sphericity 22, 88, 131
 - of cycle 178, 194
 - of orbit 178
 - concept of — 131, 267
 - extended — 295
 - extended concept of — 294
 - sphericity index 127, 132, 254
 - for cycle 180
 - product of — 304
 - product of — (PSI) 180
 - spiro[5.5]undecane 166
 - square
 - planar complex 169
 - planar skeleton 169
 - pyramidal skeleton 409
 - square bracket 37, 248, 249
 - square matrix 119
 - SSG 116, 123
 - of $C_{3\bar{\sigma}}$ 241
 - of C_{3v} 241
 - of $C_{3v\bar{\sigma}\hat{l}}$ 289
 - of $D_{2d\bar{\sigma}\hat{l}}$ 352
 - of $D_{2\bar{\sigma}}$ 262
 - of D_{3d} 289
 - of D_{3h} 289
 - of D_{4h} 352
 - of G 62
 - of O_h 322
 - of $S^{[4]}$ 253
 - of T_d 62
 - of $T_{d\bar{\sigma}\hat{l}}$ 322
 - of $T_{\bar{\sigma}}$ 252
 - stabilization 321
 - stabilizer 64, 115, 279
 - stereochemical notation
 - for allene 384
 - stereochemistry
 - beginning of — 2
 - development of — 5
 - history of — 2
 - inorganic — 385, 411
 - intra- and intermolecular — 28
 - mathematical — 29
 - modern — 2
 - organic — 385
 - traditional terminology of — 406
 - stereodescriptor
 - R/S — 16, 24
 - stereogenic 233, 365

- atom 260
- center 258
- unit 26, 260, 365
- stereogenicity 16, 24, 260
- stereoheterotopic 93
 - abandoned 394, 403
 - relationship 25
- stereoisogram 23, 235, 236, 366, 368
 - of five types 323
 - of type I 23, 282, 380
 - of type II 284, 396
 - of type III 284
 - of type IV 280, 400
 - of type V 283
 - type 317
 - correlation diagram of — 28, 406
 - elementary — 277, 315, 343, 370
 - five types of — 23, 286
 - multiple — 406
 - probe — 394
 - probe — for pro-*RS*-stereogenicity 399
 - probe — for prochirality 398
 - tentative type-III — 394
 - type-I — 315, 343, 360
 - type-II — 317, 345, 360
 - type-III — 318, 347, 360
 - type-IV — 319, 349, 360
 - type-V — 320, 350, 360, 402
- stereoisogram approach
 - by Fujita 95
 - Fujita's — 23, 91, 113, 158, 234, 286, 313, 341, 366, 379, 404
- stereoisomer 53, 228, 230, 250, 365
 - conventional definition of — 6
 - set of — 406
- stereoisomeric
 - relationship 38
- stereoisomerism 5, 11, 131, 250, 251
 - *cis/trans*- — 259
 - theory of organic — 407
- stereoisomerization 2
- stereoskeleton 54, 109
 - of G 131
 - of I_h 105
 - of ligancy 4 67, 158, 408
 - of ligancy 6 72
 - of ligancy 8 73
- steric hindrance 168
- steric isomer 51, 187
 - steric-isomer
 - generator 206, 210
 - structure
 - 2D — 259
 - 3D — 1, 194
 - cycle — 304
 - imaginary transition — (ITS) 169
 - inner — 110
 - Kekulé — 168
 - sandwich — 169
 - structure generator
 - achiral — 203
 - subduced cycle index
 - with chirality fittingness 139, 297
 - without chirality fittingness 139
 - unit — 127
 - subduced representation
 - $\hat{G}(/G_i) \downarrow \hat{G}_j$ 293
 - subduction 100, 122
 - $C_{2v}(/C_1) \downarrow C_1$ 132
 - $C_{2v}(/C_1) \downarrow C_s$ 132
 - $C_{3v\sigma\bar{I}}(/C_{s\sigma\bar{I}}) \downarrow \hat{G}_j$ 293
 - for \hat{G} 292
 - for *RS*-stereoisomeric group 292
 - of coset representation 79, 122
 - of $D_{2d\sigma\bar{I}}(/C_{s\sigma\bar{I}})$ 355
 - of $D_{\infty h}(/C_{\infty v})$ 109
 - of $T_{d\sigma\bar{I}}(/C_{3v\sigma\bar{I}})$ 326, 371
 - table 124, 294
 - $T_d(/C_{3v}) \downarrow C_1$ 371
 - $T_{d\sigma\bar{I}}(/C_{3v\sigma\bar{I}}) \downarrow C_1$ 373
 - $T_{d\sigma\bar{I}}(/C_{3v\sigma\bar{I}}) \downarrow C_{\bar{I}}$ 371
 - $T_{d\sigma\bar{I}}(/C_{3v\sigma\bar{I}}) \downarrow C_s$ 373
 - $T_{d\sigma\bar{I}}(/C_{3v\sigma\bar{I}}) \downarrow C_{\bar{\sigma}}$ 374, 391
 - $T_{d\sigma\bar{I}}(/C_{3v\sigma\bar{I}}) \downarrow C_{s\bar{\sigma}\bar{\sigma}}$ 375
 - $T_{\bar{\sigma}}(/C_{3\bar{\sigma}}) \downarrow C_1$ 371, 374
 - $T_{\bar{\sigma}}(/C_{3\bar{\sigma}}) \downarrow C_{\bar{\sigma}}$ 374, 376
 - under *RS*-permutation group 398
 - $T_d(/C_{3v}) \downarrow C_s$ 373
 - subduction table
 - of C_{2v} 124, 125
 - of $C_{3v\sigma\bar{I}}$ 294
 - of D_{3h} 294
 - of G 124
 - subgraph
 - of ITS 169
 - hierarchy of — 169
 - subgroup
 - of O_h 322

- of T_d 60
 - of $T_{d\bar{\sigma}i}$ 322
 - $S_9^{[4]}$ 262
 - conjugate — 60, 73, 123, 293
 - cyclic — 119, 292
 - five types of — 290
 - maximum — 277
 - maximum chiral — 62, 90
 - maximum chiral — G_C 278
 - maximum normal — 278
 - maximum *RS*-stereogenic — 244
 - non-cyclic — 119, 292
 - non-redundant set of — (SSG) 62, 116, 241, 252, 262, 289, 322, 352
 - normal — 286
 - type-I — 324, 354
 - type-II — 323, 353
 - type-III — 323, 353
 - type-IV — 324, 354
 - type-V — 323, 353
 - suborbit 85
 - C_s ($/C_1$)- — 110
 - enantiospheric — 110
 - sum of — 131
 - substituent 132
 - achiral — 105
 - achiral and chiral — 166
 - dummy — 195
 - monovalent — 211
 - substitution
 - — position 54
 - chiral — 99
 - edge — 170
 - substitution criterion 106
 - — for enantiotopic 99
 - succinic acid 110
 - switching
 - — between 2D- and 3D-based concepts 50
 - arbitrary — 4
 - Sylvester 1
 - symmetric group
 - — of degree 3 208, 240
 - — of degree 4 59, 236, 253
 - — of degree 6 235, 247
 - — $S^{[3]}$ 240
 - — $S^{[4]}$ 59, 236, 253
 - — $S^{[5]}$ 149
 - — $S^{[6]}$ 235, 247
 - — $S^{[n]}$ 233
 - symmetry
 - — element 59
 - — operation 56
 - $D_{\infty h}$ - — 109
 - global — 22, 26
 - global point-group — 63, 89
 - highest-attainable — 55, 87, 110
 - local — 22, 26
 - local point-group — 63, 89
 - point-group — 55
 - site — 84
 - term — 26
 - T_h - — 105
 - symmetry criterion 106
 - — for enantiotopic 98
 - synthesis
 - asymmetric — 95
 - chiral — 95, 100
 - single-step — 95
 - system
 - Cahn-Ingold-Prelog (CIP) — 239
 - computer algebra — 141
 - Maple — 183
 - *pro-R/pro-S* — 393
- ## T
- table
 - — of marks 118
 - mark — 118
 - multiplication — 60
 - subduction — 124, 294
 - USCI-CF — 127, 144
 - tableau
 - Young's — 94, 371, 398
 - tartaric acid 222
 - chiral — 94
 - *meso*- — 94, 108, 222
 - set of — 230
 - tautomerism
 - valence — 53
 - taxonomy
 - — of organic compounds 42
 - TEM 301, 332, 361
 - terdentate 168
 - term
 - attributive — 16, 17, 98, 106

- relational — 17, 98, 106
 - tertiary 177
 - tetradecane
 - 3,6,9,12-tetraoxa- — 44
 - tetrahedral
 - skeleton 23, 67, 183, 190, 252, 313
 - tetrahedral promolecule 313
 - of type I, III, or V 377
 - achiral and chiral — 190
 - enumeration of — 336
 - four positions of — 378
 - tetrahydrofuran 48
 - tetrahydropyran 166
 - $\text{T}_{\text{E}}\text{X}/\text{L}_{\text{A}}\text{T}_{\text{E}}\text{X}$ 410
 - theorem 42, 55, 102, 142, 173, 189, 306, 308, 310
 - for chirality fittingness 89, 91, 92, 178, 180, 295
 - for chirogenic site 101
 - for conservation of orbit 87
 - for enumerating quadruplets 298
 - for Fujita's proligand method 182, 187
 - for homomeric relationship 62, 245, 275, 279
 - for orbit 64
 - for regular representation 102
 - for single-step synthesis 95
 - for single-step conversion 391
 - for the PCI method 150
 - for types of quadruplets 302
 - of conservation of chirality/achirality 55
 - Cauchy-Frobenius — 173
 - Pólya's — 21, 193, 267
 - theory
 - graph — 1, 21
 - group — 54
 - Le Bel's — 21
 - permutation-group — 131
 - point-group — 131
 - van't Hoff's — 14
 - topicity 131
 - total number
 - of achiral 3D-trees 222
 - of alkanes (3D-trees) 222, 226
 - of alkanes (trees) 231
 - transition structure
 - imaginary — 406
 - transitive 116, 123, 135
 - tree 109, 193
 - 3D- — 194
 - balanced 3D- — 194
 - bicentroidal — 109, 212, 228
 - bicentroidal 3D- — 194, 213
 - centroidal — 109, 212, 227
 - centroidal 3D- — 194, 213
 - planted — 177, 194
 - planted 3D — 194
 - unbalanced 3D- — 194
 - triangular matrix
 - lower — $M_{\mathbf{G}}$ 120
 - lower — $M_{\mathbf{G}}^{-1}$ 121
 - trigonal bipyramidal
 - complex 84, 169
 - skeleton 84
 - stereochemical notation for — compound 384
 - trigonal pyramidal
 - derivative 298
 - promolecule 307
 - skeleton 195, 239, 273
 - trioxane
 - 1,3,5- — 165
 - twist
 - of double bond 269
 - type index 286, 378
- ## U
- Ugi 233, 251
 - uninuclear
 - promolecule 177
 - unit
 - chirality — 365, 379
 - pseudoasymmetric — 365
 - stereogenic — 26, 365
 - unit subduced cycle index 22, 127
 - uppercase
 - label 382
 - USCI 128
 - Fujita's — (unit-subduced-cycle-index) approach 370
 - USCI approach 22
 - Fujita's — 22, 131, 256, 287, 336, 368, 405
 - USCI table
 - of C_{2v} 129

— of G	129
USCI-CF	127, 131, 327
— for RS -stereoisomeric group	295
USCI-CF table	144
— of C_{2v}	128
— of $C_{3v\hat{\sigma}h}$	296
— of D_{3h}	296
— of G	127

V

valence tautomerism	53
valency	
— obligatory minimum — (OMV)	145
van't Hoff	2, 258, 407
variable	309
— dummy —	128, 139, 151, 200, 212, 254
vector	
— fixed-point —	291
— fixed-point — (FPV)	120, 123, 135
— isomer-counting — (ICV)	141
— multiplicity —	121, 124
vertex	212
— orbit of —	405
vertical direction	277

W

Wilson	212
Word	410
wreath product	194

X

$\hat{X}\text{M}\text{T}\text{E}\text{X}$	410
---	-----

Y

Young	94
Young's tableau	371, 398

Z

Z/E -descriptor	260, 270
Z/E -isomer	270
ZE -permutation group	269
— \tilde{D}_2	269
Zelewsky	11, 233, 411

